Stable Cyclopropenium-Based Radicals

Zack M. Strater

Submitted in partial fulfillment of the
requirements for the degree of Doctor of Philosophy
in the Graduate School of Arts and Science

Columbia University

2019

© 2019

Zack M. Strater

All rights reserved

ABSTRACT

Stable Cyclopropenium-Based Radicals

Zack M. Strater

Stable radicals have enjoyed widespread use in a variety of fields including synthetic chemistry, materials chemistry, energy storage, and biochemistry. This thesis outlines our investigations of cyclopropenium-based stable radicals and their application as redox mediators, redox-active ligands, catalysts, and materials for energy storage.

The first chapter gives a brief overview of the use of radicals in synthetic chemistry. The principles that govern the stability of radicals is discussed and notable examples are highlighted. The second section of the first chapter reviews the aromatic platforms that have been developed by the Lambert group and how they might be converted into stable radical species.

The second chapter details our study of 2,3-diaminocyclpropenones as stable radicals. These electron rich cyclopropenium derivatives undergo facile oxidation to yield a radical cation species. The origin of the stability of this oxygen-centered radical was elucidated by density functional theory calculations and analysis of the crystal structure. Diaminocyclopropenones were also found to be effective neutral L-type ligands in Ce(IV) complexes. EPR and UV-VIS experiments revealed that these complexes exhibited reversible homolytic dissociation of their diaminocyclopropenone ligands.

The third chapter describes the use of trisaminocyclopropeniums as catholytes for nonaqueous redox flow batteries. A newly designed trisaminocyclopropenium structure could be accessed in large quantities and showed long lasting stability in its oxidized state. A new composite polyionic material was developed for use as a membrane suitable for organic solvent and high voltages. Cycling in combination with a perylenediimide anolyte yielded a 1.7 V

battery that exhibited excellent coulombic efficiency and capacity retention. Using a spiro-bis(phthalimido) anolyte afforded a battery with an open circuit voltage of 2.8 V.

The fourth chapter details how our battery studies with trisaminocyclopropenium radical dications led us to discover their photoinduced reactivity. We developed an electrophotocatalytic platform using trisaminocyclopropeniums as a species capable of being activated by both photochemical and electrochemical energy. The excited state oxidation potential of the doubly activated species was found to be +3.33 V, which was capable of effecting oxidative coupling reactions using both arenes and ethers as substrates. Density functional theory calculations and spectroscopic experiments revealed that the photoreactivity was due to a SOMO-inversion event. The trisaminocyclopropenium radical dication could be prepared on scale via direct electrolysis and subsequently used in high throughput screening.

TABLE OF CONTENTS

List of Figures iii

List of Schemes v

List of Tables vi

Acknowledgements vii

Chapter 1 1

Section A: Approach to Stable Radicals 1

(1.1) A Brief Overview of Radicals 1

(1.2) Accessing Radical Species 2

(1.3) Principles of Radical Stability 4

Section B: Aromatic Ions as Radicals 9

(1.4) Review of Reactivity of Aromatic Ions 9

(1.5) Trisaminocyclopropenium Radical Cation 13

Chapter 2: Stable Radial Cations from Diaminocyclopropenones 15

(2.1) Conceptualizing the Diaminocyclopropenone Radical 15

(2.2) Synthesis and Electrochemical Measurement of Diaminocyclopropenones 18

(2.3) Chemical Oxidation of Diaminocyclopropenones 20

(2.4) Analysis of the DACO radical 23

(2.5) Cerium Complexes with Diaminocyclopropenone Ligands 26

(2.6) Reversible Homolytic Dissociation of Diaminocyclopropenone Ligands 28

Chapter 3: Trisaminocyclopropeniums in Nonaqueous Redox Flow Batteries 36

(3.1) Redox Flow Battery Overview 36

(3.2) Advantages and Challenges of Nonaqueous Redox Flow Batteries 38

(3.3) Designing a Trisaminocyclopropenium Catholyte 40

(3.4) Issues with Commercially Available Membranes 43

(3.5) Designing a Membrane for NARFBs 44

(3.6) Crossover and Cycling Studies 48

Chapter 4: Photoelectrocatalysis with Trisaminocyclopropeniums 54

(4.1) Variations in Battery Cycling Data 54

(4.2) Combining Photoredox and Electrocatalysis 56

(4.3) Electrophotocatalyic Oxidations of Arenes and Ethers 60

(4.4) Insights into Photoexcitation of the TAC Radical Dication 65

(4.5) Highthroughput Reaction Screening with the TAC Radical Dication 73

References 77

Appendix I: Experimental, NMR Spectra, and other Data (Chapter 2) 90

Appendix II: Experimental, NMR Spectra, and other Data (Chapter 3) 147

Appendix III: Experimental, NMR Spectra, and other Data (Chapter 4) 166

LIST OF FIGURES

Figure 1-1. (a) Triphenylmethyl Radical and Dimer, (b) Triarylaminium Radical Cation 5

Figure 1-2. Delocalization in the (a) Phenalenyl Radical and (b) PDI Radical Anion 7

Figure 1-3. Resonance Forms of Nitroxyl Radical 8

Figure 1-4. Aromatic Ions: Cyclopropenium, Cyclopentadienyl, and Tropylium Ions 9

Figure 1-5. Pentacarboxy-Functionalized Cyclopentadienyl Brønsted Acid 10

Figure 1-6. Applications of Cyclopropenimines and Trisaminocyclopropeniums 12

Figure 2-1. Resonance forms of 2,3-Diaminocyclopropenones 16

Figure 2-2. Reversible Oxidation of 2,3-Diaminocyclopropenone (1) 20

Figure 2-3. X-Ray Crystal Structure of $SbCl_5$-diaminocyclopropenone (1) Adduct 21

Figure 2-4. X-Ray Crystal Structure of DACO Radical Cation (1) 23

Figure 2-5. DFT Calculated SOMO (left) and Spin Density Plot (right) 24

Figure 2-6. Experimental EPR Spectrum of DACO Radical (1) in DCM (black) and Simulated Spectrum (red) 25

Figure 2-7. Cerium Complexes (1) and (2) with Diaminocyclopropenone Ligands 26

Figure 2-8. Dicationic Cerium Complex (3) with Diaminocyclopropenone Ligands 27

Figure 2-9. EPR Spectra of Diaminocyclopropenone-Cerium Complexes and DACO Radical (1) 28

Figure 2-10. Variable Temperature EPR Spectrum of complex (3) 30

Figure 2-11. UV-VIS of Successive Dilution of Complex (3) (dark blue to light blue) 31

Figure 2-12. (a) UV-VIS of Addition of Complex (2) to DACO radical (1), (b) Visualization of Addition of Complex (2) to DACO radical (1) 32

Figure 2-13. (a) Complex (1), (b) After Addition of Hydroquinone, (c) Reoxidation by Oxygen 35

Figure 3-1. General Schematic of a Redox Flow Battery 37

Figure 3-2. PDI Anolyte and Ferrocenyl Tetramer Catholyte by Nuckolls et. al. 40

Figure 3-3. TAC (1) Radical Dication after 3 Months 43

Figure 3-4. Electrochemical Window of Model Monomer 45

Figure 3-5. Polymerizing Ionic Monomer within Microporous Scaffold 47

Figure 3-6. Electron Microscope Image of (a) Microporous Daramic and (b) after Polymerization with Quaternary Ammonium Functionalized Styrene 48

Figure 3-7. Crossover Experiment with PDI (1) in an H-cell 48

Figure 3-8. Crossover of PDI (1) after 16 Days 49

Figure 3-9. Crossover of Anilino-Substituted TAC over Time. 49

Figure 3-10. (a) Discharge Capacity and Coulombic Efficiency of PDI/TAC Battery (b) Voltage Profiles During Cycling 50

Figure 3-11. Cyclic Voltammogram of the PDI/TAC Redox Couple 51

Figure 3-12. Spiro-bis(phthalimido) Anolyte 52

Figure 3-13. Open Circuit Voltage of TAC/Spiro Battery with TBATFSI 53

Figure 4-1. Cyclical Performance Loss of TAC Battery in DME 54

Figure 4-2. Introducing Light to TAC Battery in DME 55

Figure 4-3. Comparison of (a) Photocatalysis, (b) Electrocatalysis, and (c) Electrophotocatalysis 58

Figure 4-4. Comparison of (a) Direct Electrolysis, (b) Electrocatalysis, (c) Electrophotocatalysis 59

Figure 4-5. Comparing the Results of Direct Electrolysis and Electrophotocatalysis 60

Figure 4-6. Electrophotocatalysis in Divided (left) and Undivided (right) Cells 62

Figure 4-7. X-ray Crystal Structure of TAC (1) Radical Dication 66

Figure 4-8. Molecular Orbitals of Simplified (NMe2) TAC 68

Figure 4-9. UV-VIS Spectra of TAC (1) Radical Dication with Various Anions 69

Figure 4-10. Comparing Doublet and Triplet Photocatalysts 70

Figure 4-11. TAC (1) Radical Dication Fluorescence Data in HClO4 (a) UV-VIS (298 K), (b) Fluorescence Emission (Excitation: 500 nm, 298 K), (c) Fluorescence Emission (Excitation: 500 nm, 77 K), (d) Fluorescence Excitation (Emission: 650 nm, 77K) 72

Figure 4-12. Fluorescence Lifetime of TAC (1) Radical Dication in Concentrated HClO4 at 77 K 72

Figure 4-13. Bulk Electrolysis of TAC (1), (a) Before Electrolysis, (b) Electrolysis Initiated, (c) Isolated TAC (1) Radical Dication 74

Figure 4-14. Highthroughput Screening Using Isolate TAC (1) Radical Dication 75

LIST OF SCHEMES

Scheme 1-1. Example of Electrolytic Kolbe Dimerization Reaction 1

Scheme 1-2. Methods of Generating Radicals 3

Scheme 1-3. Utilizing Cyclopentadienyl Anion as a Leaving Group 10

Scheme 1-4. Chlorodehydration of Alcohols via Cyclopropenium Activation 11

Scheme 1-5. Single Electron Oxidation of Trisaminocyclopropeniums 13

Scheme 2-1. Comparison of Redox Couple of (a) TEMPO and (b) Diaminocyclopropenone 17

Scheme 2-2. Synthesis of 2,3-Diaminocyclopropenones 18

Scheme 2-3. Single Electron Oxidation of Diaminocyclopropenone (1) by $NOPF_6$ 22

Scheme 2-4. Dissociative Equilibrium of Complex (3) 29

Scheme 3-1. One Pot Synthesis of TAC (1) 42

Scheme 3-2. Synthesis of Organic Soluble or Unproccessable Polymers 46

Scheme 4-1. SET and HAT Mechanisms Involved in Electrophotocatalysis with TAC (1) 65

LIST OF TABLES

Table 2-1. Oxidation Potentials of 2,3-Diaminocyclopropenones 19

Table 4-1. Oxidative Coupling of Heterocycles to Arenes via Electrophotocatalysis with TAC (1) 61

Table 4-2. Oxidative Coupling Reaction of Ethers via Electrophotocatalysis with TAC (1) 63

Table 4-3. Optimization of Conditions for Oxidative Arene Coupling 67

ACKNOWLEDGEMENTS

I'd first like to thank my committee members, Tristan Lambert, Jon Owen, Colin Nuckolls, Jim Leighton, and Christian Rojas for giving me the opportunity to defend my thesis. Each member brings a unique perspective to chemistry and I look forward to your insightful comments and questions. A special thank you to Colin for his role as a collaborator in our joint investigation of radicals in energy storage.

It is a difficult thing for a boss to sustain their grad students' interest in chemistry throughout an entire PhD, but Tristan Lambert has done exactly that for me. You have been a great boss to work under, always seeming to know when I was in need of some inspiration. I will always admire the curiosity and creativity you bring to chemistry. I am especially grateful that you always gave me the freedom to pursue the ideas and research that excited me most.

I owe a huge debt of gratitude to all of my collaborators. None of the projects I have worked on would have been nearly as successful without their help. To Tom Sisto, thank you for teaching me the ropes of battery chemistry and for being the catalyst that brought me to study radicals in the first place. I'd like to thank Mike Rauch for allowing me to endlessly torture him with a slew of difficult crystal structures, James Shee for his crucial computational work, and Steffen Jockusch for his help with many of my spectroscopic studies. Lastly, I'd like to give a huge thank you to He Huang at Cornell; you are an outstanding chemist and it has been a joy to collaborate with you, even from afar.

Lastly and most importantly, I'd like to thank my incredible girlfriend Faith, without whom I wouldn't have made it through grad school. You have been the most loving and supportive partner I could ever hope for. I love the life we've built together and couldn't imagine it any other way. Also thank you Peanut and Porter for being the best cats that ever lived.

Chapter 1 Section A: Approach to Stable Radicals

(1.1) A Brief Overview of Radicals

Radical reactions are one of the fundamental ways in which molecules can be transformed. As such, these open-shelled species govern many important processes in both nature and in chemical synthesis. In our environment, radicals mediate processes such as combustion, the ozone cycle, photosynthesis, and cell signaling.[1–4] As well, we have found great utility in radical species, using them in a wide variety of applications including synthetic chemistry, fabrication of polymers, and energy storage.[5–7] Despite this, we have only known about their existence for around a century.[8] Even once radical species were well known, it was commonly thought that their reactivity was uncontrollable and therefore of little use.[9] Only in the modern era of chemical research have we begun to more fully realize the synthetic potential of radical species.

The development of radical-mediated reactions actually predate our knowledge of their existence.[9] Early examples that unknowingly used radical processes are the Kolbe electrochemical decarboxylation (**Scheme 1-1**) and the Hofmann-Loffler-Freytage C-H functionalization.[10,11]

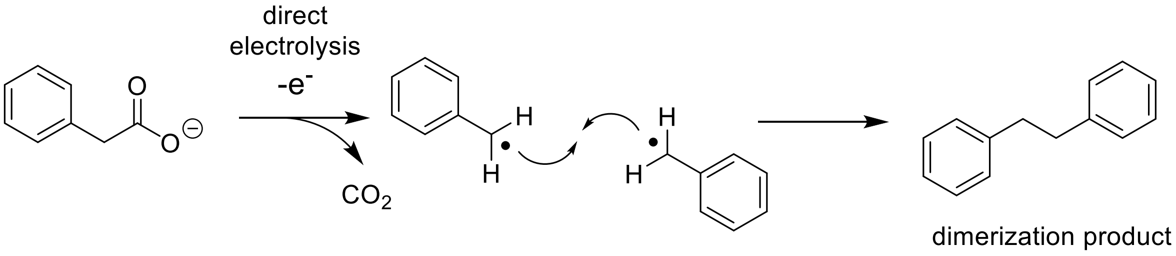

Scheme 1-1. Example of Electrolytic Kolbe Dimerization Reaction

The first radical species to be observed was the triphenylmethyl radical by Gomberg in 1900.[8] Although this landmark report was initially met with great skepticism, it began the "rational" era of research into the property and reactivity of radicals.[9] Some notable historical developments in radical chemistry include Kharasch's discovery that peroxides could yield anti-

Markovnikov selectivity in atom transfer reactions,[12,13] the Birch reduction of arenes,[14] the use of stannanes to yield carbon centered radicals under mild conditions,[15–17] the development of the theory of radical stability and radical clocks by Ingold, Griller, and Newcomb,[18–20] the development of electron paramagnetic resonance (EPR) spectroscopy by Yevgeny Zavoisky,[21] elucidation of the persistent radical effect (PRE) by Perkins,[22,23] and the development of atom transfer radical polymerization (ATRP).[24] More recently, radical processes have undergirded the fruitful areas of electrocatalysis,[25,26] photoredox catalysis,[27–29] and its merger in cross coupling reactions with transition metals.[30] Since radical species were first discovered by Gomberg in 1900, research in this field has increasingly accerlerated and has granted access to a trove of new materials, reactions, and reactivity.

(1.2) Accessing Radical Species

There are a variety of methods to access radical species (**Scheme 1-2**).[31] One of the most fundamental approaches is thermolysis, in which a molecule is heated with sufficient energy to rupture a covalent bond under the stress of excessive vibrational energy. The temperature at which this fragmentation occurs depends on the bond strength, with typical covalent bonds requiring temperature in excess of 800 ℃. However, there are several classes of molecules with much weaker bonds that can undergo homolytic cleavage with temperature below 150 ℃, such as azo compounds, peroxides, and nitrite esters, which have been used to great effect as radical initiators for polymerizations.[31] Photolysis is a related approach that involves using electromagnetic radiation to enact bond homolysis. This process can be used with many radical initiators as well and it also governs important processes in photosynthesis and atmospheric chemistry.[2,3]

Atom abstraction is another method of generating radicals, although this type of reaction can essentially be considered a reagent-controlled homolysis reaction. In this case, an existing or in situ generated radical species can abstract an atom from another molecule. This process relies on the fact that the abstractor radical has a greater bond dissociation energy (BDE) than that of the substrate, thus facilitating the exchange of the atom. Well known atom abstraction reagents include tributyltin hydride, nitroxyl radicals, peroxides, and silyl radicals. Halogen, sulfur, and hydrogen atoms are the most common elements for abstraction, with the latter being known as hydrogen atom transfer (HAT).[32,33]

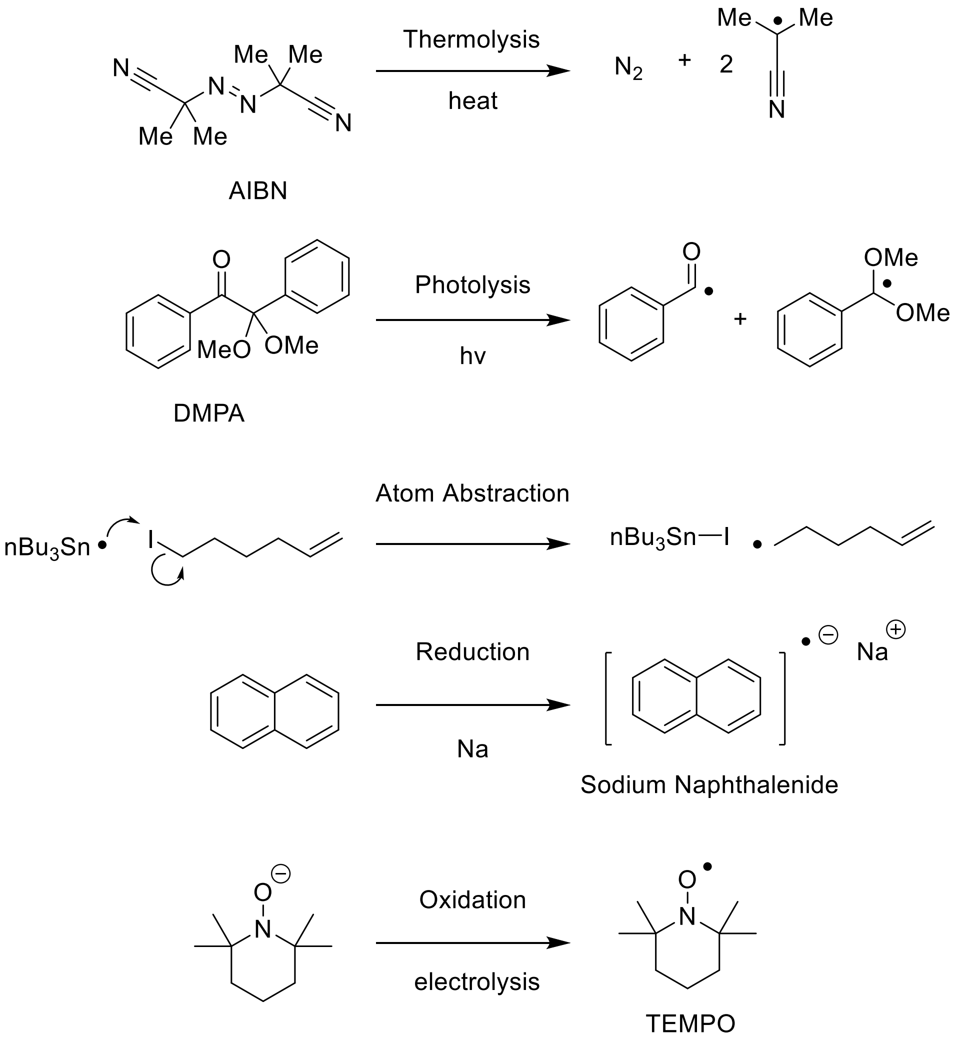
AIBN
Thermolysis
heat
N_2 + 2
DMPA
Photolysis
hv
Atom Abstraction
nBu₃Sn
nBu₃Sn—I
Reduction
Na
Sodium Naphthalenide
Oxidation
electrolysis
TEMPO

Scheme 1-2. Methods of Generating Radicals

The last major category of radical generation is from redox events. Since most organic molecules have a singlet HOMO, a radical species can be generated either by either single electron oxidation or reduction. The two primary methods of enacting a redox event are either by reducing or oxidizing chemical reagents or through direct electrolysis.[34–36] Common examples of single electron oxidants include cerium ammonium nitrate (CAN), persulfate, and nitrosonium salts while common single electron reductants include sodium naphthalenide and samarium iodide.[36] Electrochemical redox events can be effected by applying a voltage, typically through a pair of electrodes.[25,26] At the anodic electrode, if the voltage applied is greater than the inherent oxidation potential of a substrate, an electron will transfer from that substrate to the anode. Similarly, molecules can undergo single electron reduction if sufficient negative potential is applied to the cathode.

One related type of redox promoter that has garnered much attention recently is photoredox catalysis.[27–29] In this regime, a strongly absorbing molecule can utilize light energy to promote one of its electron to a higher orbital in either an excited singlet or triplet state, which can be thought of as a biradical species in that it now possesses two half-filled orbitals. If the excited state is sufficiently long lived, the photocatalysts can participate in a redox event with a substrate molecule given the redox potentials are correctly matched.

(1.3) Principles of Radical Stability

While there are many ways to generate radicals, most compounds are not stable as a radical species. Most radicals that can be generated are intrinsically high energy species and are additionally prone to many facile degradation pathways.[9] Despite this, a variety of stable radical species have been identified throughout history.[37,38] Of course, the term "stable" is a relative term and the length of time of a radical's persistence can depend heavily on the context. Some "stable" radicals only have a half-life of minutes, while others, such as those used in energy storage, can have a half-life of months or even years. Furthermore, some radicals are only present in small quantities in equilibrium with their dimeric form and therefore cannot be isolated. It is therefore helpful to adopting Ingold's practical convention of defining stable radicals as those that can be isolated, persistent radicals as those that can be measured spectroscopically but not isolated, and transient radicals as those that cannot be directly observed through conventional spectroscopy.[18] With these parameters in mind, I will review a few notable discoveries of persistent and stable radicals and what factors lead to their stability.

In 1900, Moses Gomberg identified the first radical species, triphenylmethyl radical (**Figure 1-1**).[8] This seminal discovery occurred during Gomberg's attempts to prepare hexaphenylethane from triphenylmethyl chloride and zinc metal. The resulting yellow material unexpectedly reacted with oxygen to form a peroxide and iodine to form triphenylmethyl iodide. He concluded that this reactivity could only be explained by a trivalent radical species, an assertion that was met with much skepticism from the scientific community. Nonetheless, this important discovery inspired a great deal of research on radical species in the coming years, much to the chagrin of Gomberg who ended his seminal report by stating "this work will be continued and I wish to reserve the field for myself".[8]

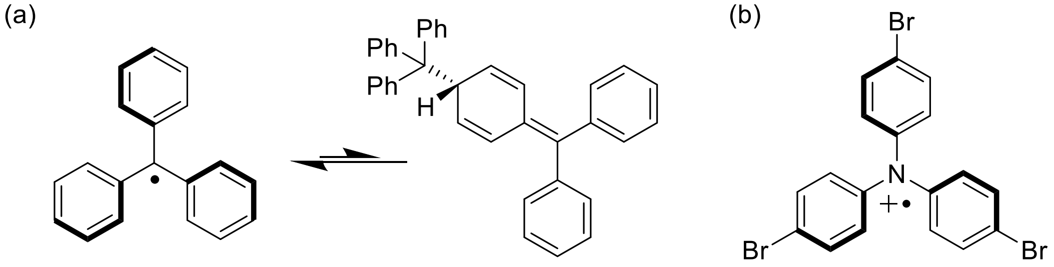

Figure 1-1. (a) Triphenylmethyl Radical and Dimer, (b) Triarylaminium Radical Cation

At a first glance, one might assume that the triphenylmethyl radical owes its persistence to delocalization of the radical amongst the three phenyl rings. In reality, the relative stability of this radical is primarily attributable to the fact that the phenyl rings are geared ~30° out of plane.[39–41] The twisted nature of the phenyl substituents offers steric shielding to the central carbon where most of the spin density is held. This shielding effect prevents direct dimerization between the central carbons of two triphenylmethyl radicals, which explains why Gomberg was unsuccessful in synthesizing triphenylethylene. However, this radical species is in equilibrium with a dimer formed by connecting the central carbon to the para position of another triphenylmethyl radical (**Figure 1-1**). Capping the phenyl rings with chlorine atoms prevents all dimerization and further gears the phenyl rings out of plane. The increased steric bulk and twisting of the phenyl rings renders these species essentially inert despite the radical being essentially exclusively located on the central carbon.[42,43]

A related isoelectronic species, triarylaminium radical cations, similarly takes advantage of the geared nature of its phenyl substituents (**Figure 1-1**).[44] The para-brominated version of this molecule, known as "magic blue",[45] is a stable radical that has enjoyed widespread use in both organometallic and organic chemistry.[36,46] Notably, Bauld and Ledwith pioneered the use of the oxidizing nature of this reagent (+1.05 V vs SCE) to promote cyclization reactions, rearrangements, and oxidations. Recent examples by Jia use catalytic triarylaminium radical cation to promote heterocyclization reactions.[47–49]

Perhaps the most intuitive principle of radical stabilization is through pi-delocalization. Almost every radical that exhibits some degree of stability does so because of delocalization through a pi system. Even Gomberg's triphenylmethyl radical shows some spin density on the phenyl rings despite being twisted out of planarity as evidenced by its EPR spectrum.[50] This strategy relies on spreading the spin density throughout each atom participating in the pi system such that no atom shares much of the overall spin density. Thus, any given atom in the pi system is less likely to participate in dimerization or degradation processes. Phenalenyl radicals are a prime example of radical stability through pi delocalization (**Figure 1-2**). These tricyclic aromatic radicals were first prepared and characterized by Reid and Calvin in the 1950s.[51,52] The SOMO of the phenalenyl radical distributes the spin density among six of peripheral carbon atoms. Notably, no spin density is housed in the central carbon as the remaining pi orbitals would form a 12 pi electron antiaromatic system.

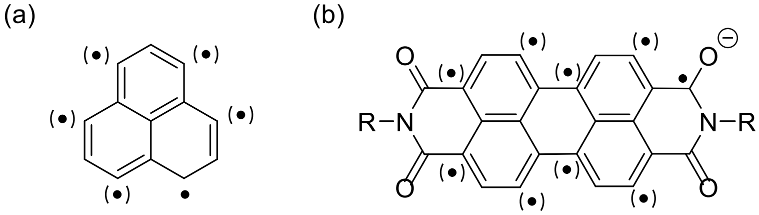

Figure 1-2. Delocalization in the (a) Phenalenyl Radical and (b) PDI Radical Anion

An extension of this principle can be observed in the radical anion of perylenediimide (PDI) (**Figure 1-2**). As the name implies, this molecule is made up of a perylene core conjugated with two imide groups at either end. Reduction of the neutral molecule leads to a supremely stabilized radical anion, with the imide group bearing the majority of the negative charge and the radical being distributed throughout the pi system.[53] Their stability in their radical anion form has made these molecules attractive building blocks for materials and energy storage applications.[54–57] König has also recently discovered that the PDI radical anion can act as a photocatalyst in the reduction of aryl halides.[58,59]

A third common motif in stable radicals is housing the majority of the spin density on heteroatoms. This strategy encompasses a large variety of classes of stable radicals including phenoxyl, aminyl, thiyl, and pyridyl radicals among others. This effect can be rationalized by the electronegativity of nitrogen, oxygen, and sulfur atoms. Heteroatoms can bear a large amount of the negative charge in electron-rich radicals (i.e. radical anions) due to their electronegativity. Electron poor radicals (i.e. radical cations) are stabilized by heteroatoms due to participation from their electron-rich lone pairs. Additionally, radicals situated on heteroatoms tend to resist dimerization due to the fact that bonding between two electronegative atoms usually results in a weak bond.

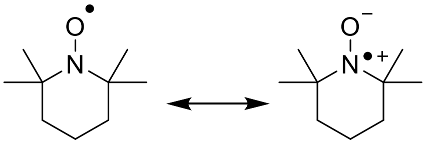

Figure 1-3. Resonance Forms of Nitroxyl Radical

Nitroxyl radicals are primarily stabilized by housing the majority of the spin density on the nitrogen and oxygen atoms. Both heteroatoms share an equal load of spin density in most nitroxyl structures, which is clearly reflected in its two resonance forms (**Figure 1-3**). 2,2,6,6-tetramethylpiperidin-1-yl oxyl (TEMPO) is the most well-known and widely used of this class of radicals. It bears four methyl groups alpha to the nitroxyl moiety, which provide both steric protection and prevent degradation at the alpha carbon. Due in part to its extraordinary stability, TEMPO has seen widespread use in a variety of fields.[5–7,60,61] Of particular note are the studies conducted by Studer that elucidated the use of TEMPO for cyclization reactions and for radical mediated polymerizations.[62–65]

The development of stable radicals has expanded greatly since Gomberg's discovery of the triphenylmethyl radical. Radicals have proved to be invaluable tools for synthetic methodology, materials chemistry, and energy storage among other fields. While the structures of stable radicals are diverse in nature, their stabilities are commonly governed by three main principles: (1) steric protection, (2) pi-delocalization, and (3) stabilization through heteroatoms. These fundamental principles of organic radical stability underscore the properties of the radical studied herein.

Chapter 1 Section B: Aromatic Ions as Radicals

(1.4) Review of Reactivity of Aromatic Ions

A common theme in much of the Lambert lab's chemistry is utilizing the unique nature of aromatic ions. These molecules consist of a cyclic conjugated pi system that follows the Huckel's 4n+2 pi electron rule for aromaticity while also being persistent anions or cations (**Figure 1-4**). The studies detailed in this thesis pertain to radicals generated from these aromatic ions, but it is useful to first have an understanding of the properties and reactivity of the parent compounds. Therefore, a brief overview of the chemistry of the closed-shell aromatic ions will be reviewed. Aromatic ion species are conveniently drawn as either a carbon-centered cation or anion, but the positive or negative charge is actually distributed throughout the aromatic system, stabilizing what would otherwise be an unstable species (**Figure 1-4**).

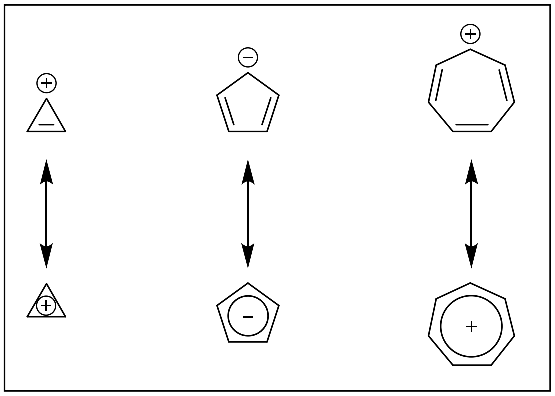

Figure 1-4. Aromatic Ions: Cyclopropenium, Cyclopentadienyl, and Tropylium Ions

This unique configuration leads to a host of intriguing species and reactivity. In particular, aromatic ions are ripe for catalytic transformations due to the fact that they derive reactivity from their overall charge, yet are capable of existing in dynamic equilibria due to the stabilizing effects of the aromatic system. The Lambert group has been inspired by these unique structures and has sought to take advantage of the reactivity they offer.

The first example of our group's exploration of aromatic ions was using the cyclopentadienyl anion as a leaving group in palladium-catalyzed allylation reactions (**Scheme 1-3**). It is atypical to have a carbon serve as a leaving group, but the stabilization of the resulting carbanion by the cyclopentadienyl system allows the allylation of amines to occur by heterolytic C-C bond cleavage.[66]

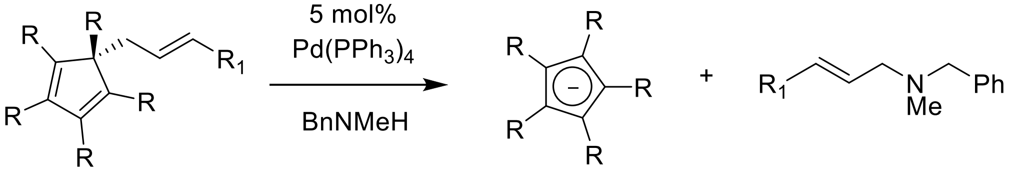

Scheme 1-3. Utilizing Cyclopentadienyl Anion as a Leaving Group

Later, we explored cyclopentadienyl anions as strong Brønsted acids, which can be accomplished by outfitting all five carbon positions with electron withdrawing groups such as esters and amides (**Figure 1-5**).[67,68]

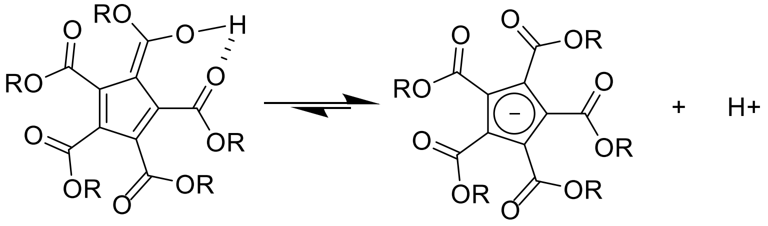

Figure 1-5. Pentacarboxy-Functionalized Cyclopentadienyl Brønsted Acid

Chiral derivatives of these aromatic ion acids were able to effectively catalyze enantioselective Mukiyama-Mannich, oxocarbenium aldol, and inverse electron-demand Diels-Alder cycloaddition reactions.[69,70] We also showed that these highly stabilized anions could be coupled with silicon species to form strong Lewis acid complexes capable of promoting allylation and benzylation reactions.[71]

Additionally, our group has also been interested in investigating the properties and reactivity of cationic cyclopropenium species. The bare cyclopropenium ring is the smallest member of the aromatic family and it was first isolated by Breslow in 1957.[72] Since its discovery, a variety of cyclopropenium derivatives have been synthesized and the study of their reactivity and properties has been the subject of a great deal of research.[73] Our first venture in this area involved using dichlorodiphenylcyclopropenes as dehydrating reagents (**Scheme 1-4**). These species are in equilibrium with the cyclopropenium chloride, which allows attack from a nucleophile at the cationic carbon center. The resulting adduct is activated via proximity to the cationic cyclopropenium and can undergo further reaction, usually resulting in a cyclopropenone byproduct (**Scheme 1-4**). This strategy was shown to be effective in converting alcohols to alkyl chlorides, generating acyl chlorides from carboxylic acids, enabling self-propagating Beckmann rearrangements, and cyclodehydration of alcohols all under mild reaction conditions.[74–77] This platform was eventually made catalytic with respect to the cyclopropenone species and was applied to chlorodehydration and a Mitsunobu-type reaction.[78,79]

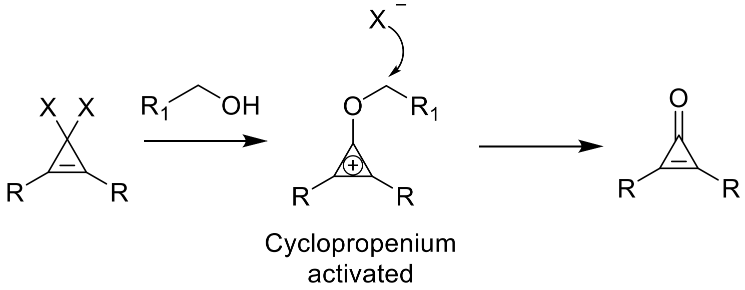

Scheme 1-4. Chlorodehydration of Alcohols via Cyclopropenium Activation

We have also extensively investigated the reactivity of aminocyclopropeniums, which represent a class of cyclopropeniums that are highly stabilized by electron-rich amino substituents (**Figure 1-6**). Cyclopropenimines (CPIs) are Brönsted basic members of this class of aromatic ions that typically bear two donating amino groups in the 2 and 3 positions and a highly polarized imine moiety. CPIs can be thought of as higher-order analogues of guanidines, with the central carbon being expanded to a cyclopropenium core.[80] While guanidines and CPI's possess the same number of nitrogen substituents, CPIs were found to be more than three order of magnitude more basic than the corresponding guanidines due to the fact that the protonated form is stabilized by the latent cyclopropenium core.[81,82] We found CPIs to be efficient base catalysts in asymmetric Michael and Mannich reactions as well as being useful components in organic superbases.[83–87] Trisaminocyclopropeniums (TACs) are a related class of amino stabilized cyclopropeniums that exists as persistent cations. The three nitrogen atoms help to form a highly stabilized organic salt, which has an estimated pKr+ of 13, 10 order of magnitude greater than that of the trisarylated cyclopropenium.[81] We found these salts to have applications as phase transfer catalysts, as "macrosteres" of guanidinium ions, and, in collaboration with the Campos lab, as building blocks for cationic polyelectrolyte materials.[80,88–90] Aminocyclopropenium compounds have also found use as transition metal ligands and as ionic liquids.[91–95]

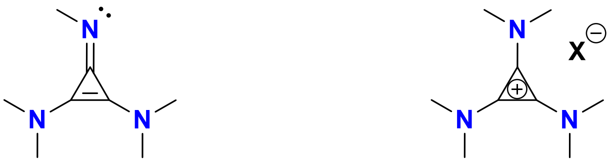

Cyclopropenimine (CPI):
- Brønsted Base
- Chiral Organocatalyst
- Transition Metal Ligand

Trisaminocyclopropenium (TAC):
- Phase-Transfer Catalyst
- Ionic Liquid
- Polyelectrolyte Building Block

Figure 1-6. Applications of Cyclopropenimines and Trisaminocyclopropeniums

Other notable examples of aromatic ions are the tropylium ion, a seven membered cationic species that was actually the first of the non-benzenoid aromatic ions to be discovered.[96,97] It's derivatives have also seen use as catalysts and as stoichiometric reagents, but it's reactivity is quite similar to that of analogous cyclopropenium compounds.[98] Also of note is cyclooctatetraene, which can remarkably undergo a double reduction in the presence of alkali metals to yield an aromatic 10 pi electron dianionic species.[99] N-heterocyclic carbenes are another related class of aromatic compounds that, while not ionic, exhibit a similar mix of reactivity and stability and have an empty p-orbital similar to cyclopropeniums and tropyliums.[100]

(1.5) Trisaminocyclopropenium Radical Cation

The study of aromatic ions has given rise to a variety of interesting compounds and wealth of novel chemistry, in part due to their balance between stability and reactivity. However, most if not all of the reactions developed with these species have utilized two-electron processes.[98] As outlined earlier, one-electron processes enable synthetic translations that would not be possible otherwise. We wondered if the aromatic ion platforms that the Lambert group has developed would lend themselves to being stable radical species as a result of a single-electron oxidation or reduction. Presumably, the same factors that lead to stabilization of an anion or cation (steric protection, pi-delocalization, electronic effects) could also serve to stabilize a radical entity. Additionally, we wondered what properties and reactivity the radicals generated from these aromatic ions would offer.

In this domain, there is precedent for both cyclopentadienyl and cyclopropenium ions being converted into radical species, the latter of which will be detailed here.[101–104] In the same year, the Yoshida group reported the first synthesis of a TAC and that these species could undergo a one electron oxidation to furnish a stable radical dication species (**Scheme 1-5**).[105,106] Using the iodide salt, they found that oxidation could be effected either by dissolving the TAC in concentrated sulfuric acid or by electrolysis using tetraethylammonium perchlorate as a supporting electrolyte.

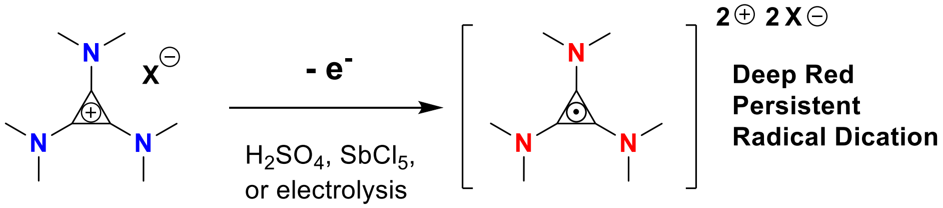

Scheme 1-5. Single Electron Oxidation of Trisaminocyclopropeniums

This species was unable to be isolated, but they found the “red-violet” solutions of the TAC radical dication in sulfuric acid to be stable for several hours. The EPR spectrum of this solution was collected, which demonstrated coupling to all three of the nitrogen atoms. A few years later, Weiss also reported a similar oxidation by using the TAC chloride salt in conjunction with $SbCl_5$, yielding the TAC radical dication with two $SbCl_6$ counteranions in >90% yield as brick red microcrystals.[107] The oxidation could also be carried out using Br_2, $NOBF_4$, or NO_2BF_4. The resulting TAC radical dication solid was found to be air stable for several hours, degrading slowly over the course of weeks. This report also suggested that the red color of this species is due to an electronic transition from a lower set of degenerate orbitals to the SOMO.[106,107] In the same year as Weiss's publication, Johnson reported more detailed experiments on the electrochemistry of TACs and related heteroatom, alkyl, and aryl substituted analogues.[108] The trisamino-substituted cyclopropenium was found to undergo a reversible oxidation at +1.2 V vs. SCE and a second irreversible oxidation at +2.1 V vs. SCE. The TAC was found to be quite resistant to reduction, requiring -2.6 V of potential to effect reduction. Interestingly, this irreversible reduction led to recovery of hexaminobenzene, presumably due to a dimerization of the neutral radical species followed by a rearrangement. Weiss and Pairs later reported that TACs bearing hexahalogeno-selenide and telluride anions exhibited a visible light promoted electronic transition that corresponds to an excitation of an electron from the dianion to the SOMO of the TAC.[109]

More recently, Sanford found that bulkier tris(diisopropylamino)-cyclopropeniums were exceptionally stable in their oxidized state.[110] These sterically encumbered TACs could be cycled in an electrochemical cell with minimal degradation. Notably, TACs with less steric protection or anilino substituents were found to be much less stable under these conditions. In a later report, the Sanford group also prepared oligomeric TACs and implemented them in a proof of concept battery.[111] Both of these reports were important steps in utilizing TACs for the purpose of energy storage, a topic that will be revisited in chapter three.

Despite these reports detailing the interesting spectroscopic and physical qualities of TAC radical dications, there have been essentially no reports on the reactivity or synthetic applications of this peculiar species. Due to our experience in developing these aromatic ion species as valuable reagents and catalysts, we wondered if they also might be a suitable platform for one-electron chemistry. Herein, I report our recent findings concerning cyclopropeniums and their derivatives as radical species, a chemical space we found to be especially fertile for scientific discovery.

Chapter 2: Diaminocyclopropenones as Stable Radical Cations

(2.1) Conceptualizing the Diaminocyclopropenone Radical

The previous reports of the stability of the TAC radical dication made us wonder if other cyclopropenium-based structures could undergo oxidation to yield stable organic radicals. One species we felt would be interesting is the radical that would result from the single electron oxidation of cyclopropenones.

The reactivity and properties of cyclopropenones have been studied extensively, although it has primarily been utilized as a synthetic intermediate in reactions where the cyclopropene core is not conserved.[73,112] The chemical behavior of these species mostly results from their ambiphilicity, derived from the polarized nature of the carbonyl moiety. Cyclopropenones have been found to participate in reactions as a nucleophile, an electrophile, and as a coupling partner in cycloaddition reactions.[73,112] The Lewis-basicity of the carbonyl moiety also allows them to participate as sigma-donor ligands in metal complexes.[113]

Cyclopropenone species have a significant resonance contributor in which the cyclopropenium core bears a positive charge and the oxygen atom is anionic (**Figure 2-1**). This resonance form can further be accentuated by installing donating amino substituents at the 2 and 3 positions of the cyclopropene core.

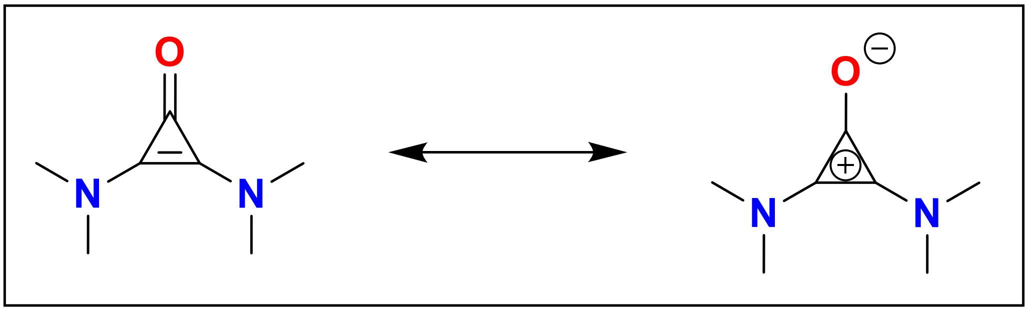

Figure 2-1. Resonance forms of 2,3-Diaminocyclopropenones

These 2,3-Diaminocyclopropenones have mainly been used as synthetic intermediates in accessing various TAC compounds, but we hypothesized that these electron rich molecules might be amenable to reversible oxidation.[89,92,114]

Due to the build-up of electron density on the carbonyl oxygen, we speculated that these species would house much of the spin density on the oxygen atom after single electron oxidation, thereby providing a new class of oxygen-centered radicals. Stable oxygen-centered radicals such TEMPO are an important class of molecules that have found use as catalysts,[65,115,116] polymerization mediators,[6] radical probes,[117–119] spin labels,[120] biochemical agents,[121–124] and energy storage materials.[7,125–129] Interestingly, a diaminocyclopropenone derived radical would be possess a certain orthogonality to aminoxyl radicals (**Scheme 2-1**). TEMPO is an open-shell neutral species that can be oxidized to the corresponding oxoammonium, which is a closed-shell cationic species.[115] On the other hand, the cyclopropenone is a closed shell neutral species that would undergo single electron oxidation to give an open-shell cationic species.

(a) Aminoxyl redox couple

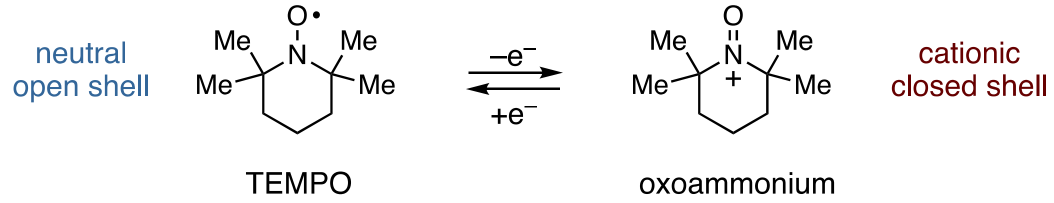
neutral
open shell
Me
Me
Me
Me
O•
N
−e⁻
+e⁻
O
N
+
cationic
closed shell
TEMPO
oxoammonium

(b) Diaminocyclopropenone redox couple

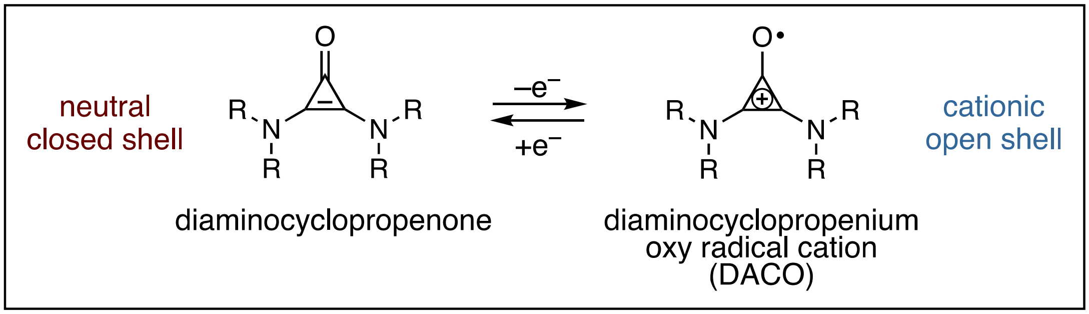
neutral
closed shell
O
R
N
R
R
N
R
−
−e⁻
+e⁻
O•
+
cationic
open shell
diaminocyclopropenone
diaminocyclopropenium
oxy radical cation
(DACO)

Scheme 2-1. Comparison of Redox Couple of (a) TEMPO and (b) Diaminocyclopropenone

We were intrigued by how the difference between these two oxidation regimes might be reflected in their reactivity. Since only a few classes of stable oxygen-centered radical species are known,[130–133] we believed that developing a structurally distinct type of radical from cyclopropenones might yield new and interesting properties and reactivity.

We hypothesized that single-electron oxidation of 2,3-diaminocyclopropenones would yield an open-shell diaminocyclopropenium oxy (DACO) radical cation, with much of the spin density being localized on the oxygen atom. Furthermore, we predicted that this oxidation would be relatively facile due to the electron rich nature of the diaminocyclopropenone precursor. However, oxidations of carbonyl species typically result in very unstable species and it was not immediately clear that the DACO radical would have the necessary electronic or steric structural features to exist as a long-lived open-shelled species.

(2.2) Synthesis and Electrochemical Measurement of Diaminocyclopropenones

We first set out to prepare a variety of diaminocyclopropenones with varying steric and electronic properties. 2,3-Diaminocyclopropenones can readily be prepared from pentachlorocyclopropane, which can either be purchased or prepared on a kilogram scale from trichloroethylene and sodium trichloroacetate.[134] Addition of three equivalents of amine to pentachlorocyclopropane under basic conditions leads to the corresponding TAC in high yields, while bulkier amines such as dicyclohexylamine and diisopropylamine only add twice to produce the corresponding diaminochlorocyclopropeniums.[135]

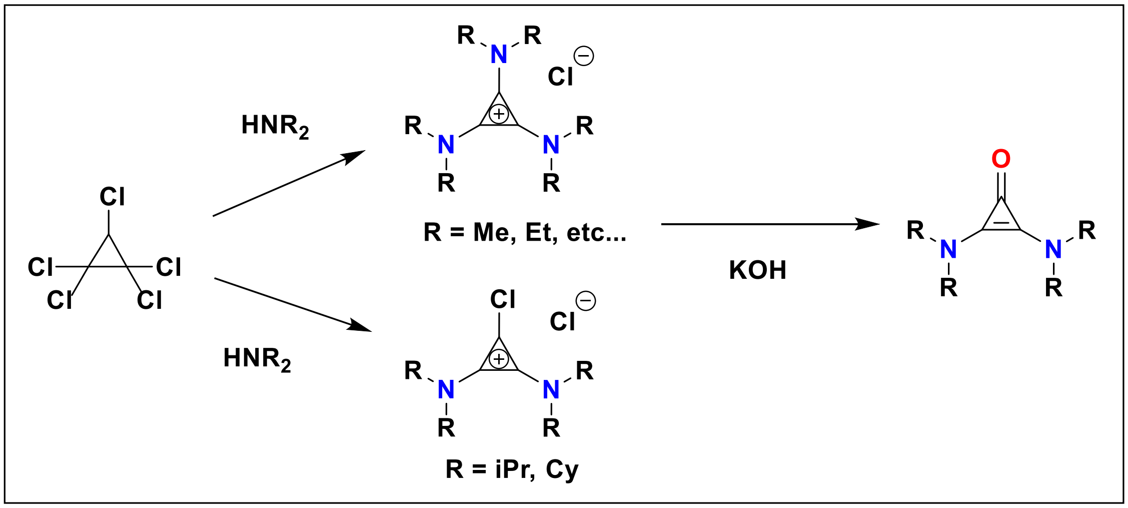

Scheme 2-2. Synthesis of 2,3-Diaminocyclopropenones

Both of these intermediates can then be hydrolyzed to yield the corresponding cyclopropenone in high yield.[136] This two-step synthesis enables access to a diversity of 2,3-diaminocyclopropenones on a multigram scale (**Scheme 2-2**).

With these diaminocyclopropenones in hand, we next sought to evaluate their electrochemical oxidations (**Table 2-1**). Using cyclic voltammetry (CV), we found the oxidations of the prepared diaminocyclopropenones were fully reversible (**Figure 2-2**) with potentials ranging between +0.74 and +1.10 V vs SCE. This oxidation potential is quite low for a carbonyl species, which clearly reflects the stabilizing nature of the diamino cyclopropenium moiety.[116]

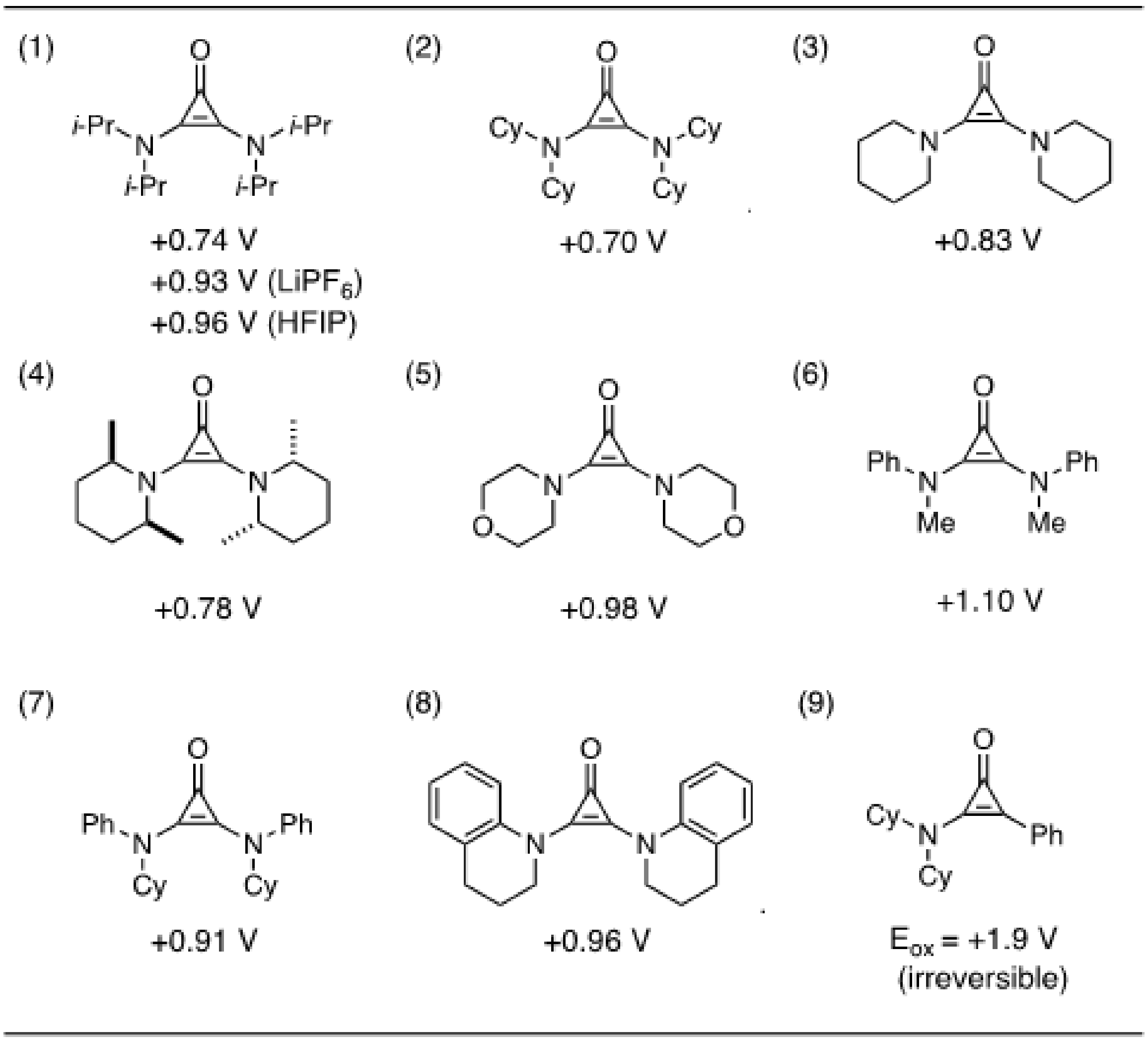
(1)
O
i-Pr
N
i-Pr
N
i-Pr
i-Pr
+0.74 V
+0.93 V (LiPF6)
+0.96 V (HFIP)
(2)
O
Cy
N
Cy
N
Cy
Cy
+0.70 V
(3)
O
N
N
+0.83 V
(4)
O
N
N
+0.78 V
(5)
O
N
N
O
O
+0.98 V
(6)
O
Ph
N
Me
Ph
N
Me
+1.10 V
(7)
O
Ph
N
Cy
Ph
N
Cy
+0.91 V
(8)
O
N
N
+0.96 V
(9)
O
Cy
N
Cy
Ph
Eox = +1.9 V
(irreversible)

Table 2-1. Oxidation Potentials of 2,3-Diaminocyclopropenones

A pertinent comparison is to tetramethyl urea, which is a lower homologue of the diaminocyclopropenone.[80,137] It contains the same heteroatoms and conjugated pi system, but is missing the latent cyclopropenium ion. As a result, tetramethyl urea was found to irreversibly oxidize at a much greater potential, +2.4 V vs SCE. We found that increased steric encumbrance on the amino substituents only had a small impact on the oxidation potential (**Table 2-1** entries **1-4**), while electronic effects significantly altered the oxidation potential. The weaker donating morphlino and anilino substituents led to diaminocyclopropenones with significantly higher oxidation potentials (**Table 2-1** entries **5-8**).

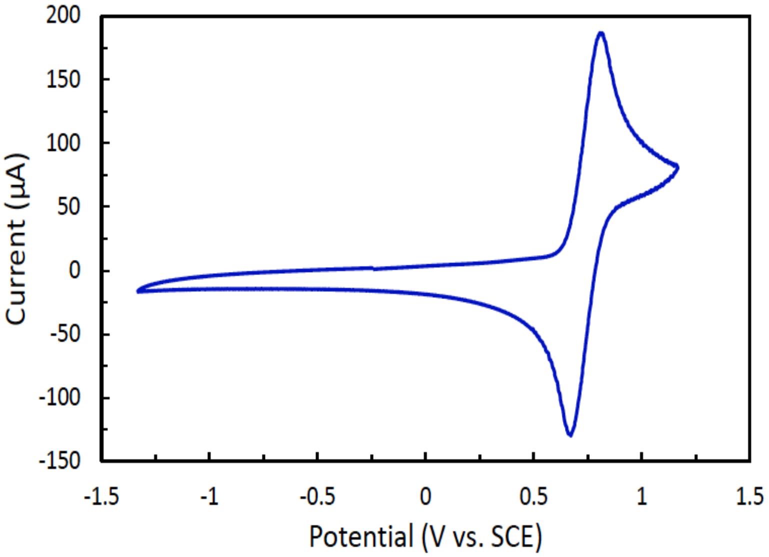

Figure 2-2. Reversible Oxidation of 2,3-Diaminocyclopropenone **(1)**

We also measured the oxidation potential of a cyclopropenone with one of the amino substituents replaced with a phenyl ring and found that this cyclopropenone was irreversibly oxidized at a far higher potential (**Table 2-1** entry 9), demonstrating that both amino substituents are required for the stability of the oxidized species. Finally, we found that the oxidation potential can be increased further by the addition of Brønsted or Lewis acids. $LiPF_6$ and Hexafluoroisopropanol (HFIP) both increased the oxidation potential of diaminocyclopropenone **(1)** by several hundred millivolts. We believe that the ability to modify the electronic properties of these species by simply exchanging the amine substituents will be a significant advantage compared to other radical species such as TEMPO, which requires extensive synthetic efforts to functionalize.[61,138]

(2.3) Chemical Oxidation of Diaminocyclopropenones

With the knowledge that diaminocyclopropenones could undergo reversible oxidation, we sought to effect a single electron oxidation and isolate the resulting radical cation species. We first attempted to oxidize diisopropylamino-cyclopropenone **(1)** chemically using pentachloroantimony ($SbCl_5$) as an oxidant. This reagent has previously been shown to achieve single electron oxidation for both the TAC and for triarylamine species.[45,107] We found that adding $SbCl_5$ to diaminocyclopropenone (**1**) resulted in DCM resulted in a dark red solution. Crystallization via vapor diffusion produced dark red crystals, which were examined by X-ray crystallography. The solved structure revealed that, in fact, a single electron oxidation had not occurred and instead the cyclopropenone had directly complexed to $SbCl_5$ in a 1:1 fashion (**Figure 2-3**). These types of adducts are well known and have been developed as part of the Guttman scale of Lewis basicity.[139]

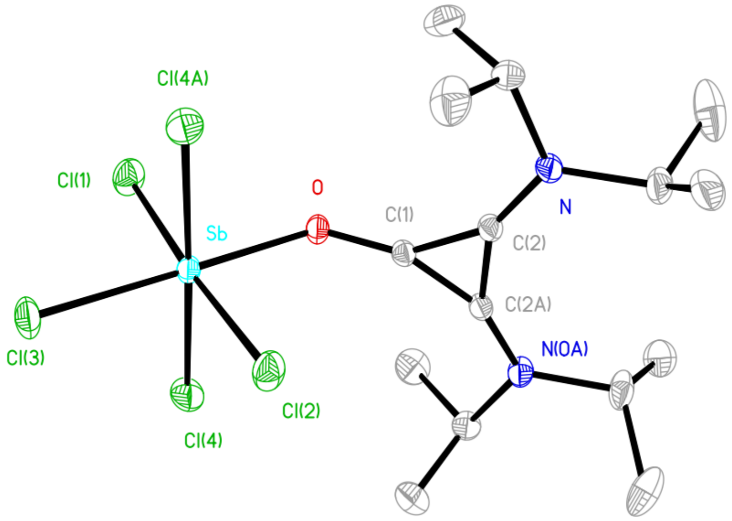

Figure 2-3. X-Ray Crystal Structure of $SbCl_5$-diaminocyclopropenone **(1)** Adduct

Still, it is interesting to note that triarylamines are oxidized by $SbCl_5$ while diaminocyclopropenones form an adduct. This result can be rationalized by the fact that oxygen atom of the diaminocyclopropenone is more Lewis basic and less sterically hindered than the nitrogen of a triarylamine. Thus, complexation between the diaminocyclopropenone and $SbCl_5$ can kinetically outcompete oxidation, despite $SbCl_5$ being a potent oxidant.

We next attempted the oxidation with cerium ammonium nitrate (CAN), which is a potent one electron oxidant capable of oxidizing various organic molecules.[35] Stoichiometric addition of CAN to cyclopropenone **(1)** in DCM led to a dark blue solution. EPR measurements on this blue solution showed the presence of an organic radical that displayed a spectrum that looked similar to what we might expect from the diaminocyclopropenone radical. Dark blue crystals were isolated from this solution after vapor diffusion with ether. To our surprise, the crystals were not the DACO radical, but a monocationic Ce(IV) complex with three cyclopropenone ligands. We will return to this topic and this cerium complex later in this chapter.

Our next attempt at oxidation involved the use of nitrosonium salts, which are powerful one electron oxidants that are typically used in inorganic and organometallic chemistry.[140,141] This reagent possesses a unique property as an oxidant in that it can potentially leave no byproducts. After reduction of the nitrosonium salt, nitric oxide (NO) gas is produced and bubbles off from the solution, leaving only a counterion behind to balance the charge of the oxidized species. Addition of nitrosonium tetrafluoroborate ($NOBF_4$) to diaminocyclopropenone **(1)** in DCM was found to lead to a dark red solution accompanied by vigorous bubbling. However, the solution discolored at room temperature within an hour, which was the result of decomposition of the diaminocyclopropenone. Addition of $NOPF_6$ was found to similarly lead to a dark red solution, but this solution retained its color for over 24 hours at room temperature (**Scheme 2-3**).

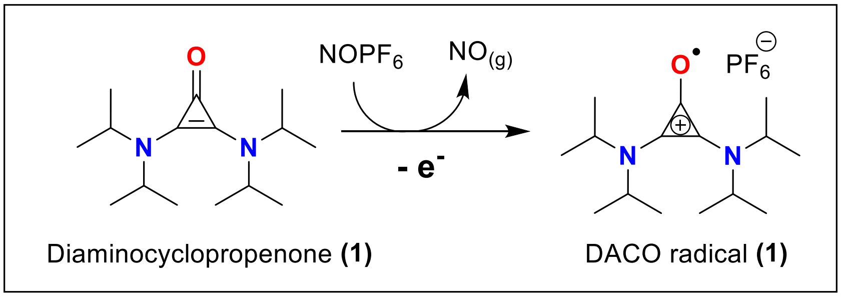

Scheme 2-3. Single Electron Oxidation of Diaminocyclopropenone **(1)** by $NOPF_6$

Crystallization of this solution via vapor diffusion produced long dark red rods that were stable to ambient conditions. X-ray analysis showed that the DACO radical cation had indeed been formed, with the diaminocyclopropenone and PF_6 anion present in a one-to-one ratio.

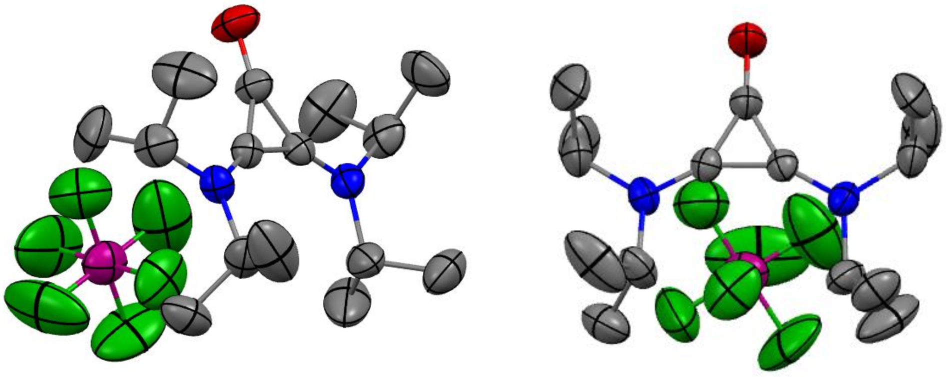

Figure 2-4. X-Ray Crystal Structure of DACO Radical Cation (**1**)

As shown in the crystal structure, the PF_6 anion associates facially with the cyclopropenyl ring (**Figure 2-4**). One notable feature of the structure is that all three cyclopropenium C-C bond lengths (1.407-1.408) are essentially identical and all the internal bond angles of the cyclopropenium ring (59.97-60.01) are also equivalent, which we believe is indicative of the aromatic character of the cyclopropenyl ring. We also furnished a crystal structure of the neutral diiscopropylamino-cyclopropenone **(1)** as a comparison. Notably, the bonds between the heteroatoms and the cyclopropenyl ring in its oxidized state were appreciably shorter than in its neutral state.

(2.4) Analysis of the DACO radical

To better understand the differences between the neutral cyclopropenone and the DACO radical cation, we performed density functional theory (DFT) calculations on both species. These computational studies revealed that the SOMO is made up of the conjugated p-orbitals of the cyclopropenium and the three heteroatom substituents (**Figure 2-5**). In this molecular orbital, all of the cyclopropenium pi orbitals are in-phase and have antibonding interactions with all of the heteroatom pi orbitals. The calculations also predicted the same contraction in bond length between the heteroatoms and cyclopropenium that was found experimentally. This effect can be rationalized by the fact that taking an electron out of the HOMO would minimize this antibonding interaction, thus shortening these bonds.

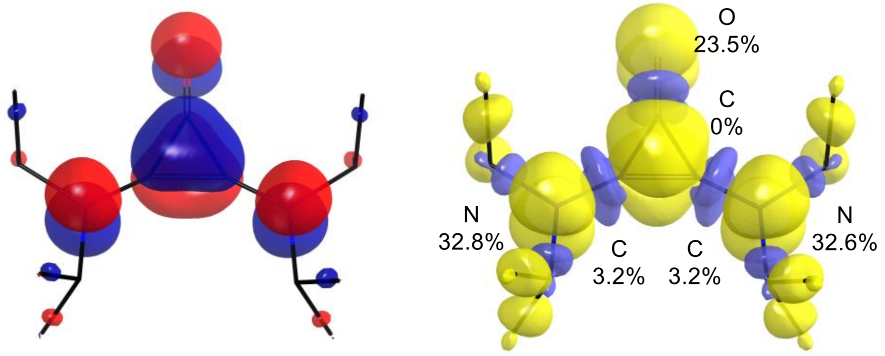

Figure 2-5. DFT Calculated SOMO (left) and Spin Density Plot (right)

DFT calculations were also used to predict how the spin density was distributed across the DACO radical. We found that the nitrogen atoms each carried ~33% of the spin density while the oxygen atom possesses ~24%. Only ~6% of the spin density was located in the cyclopropenium ring, with the carbon proximal to the oxygen containing no spin density, which reflects the polarized nature of the carbonyl bond (**Figure 2-5**). The remaining spin density (<5%) was located in the aliphatic region of the molecule. Although a significant amount of spin density does lie on the oxygen atom, the majority of the spin density is housed within the nitrogen atoms, which implies that our Lewis representation of the radical cation is only a partial resonance contributor (**Scheme 2-3**). It would seem that the oxygen atom only bearing around 24% of the total spin density might contradict our hypothesis that this species would be an oxygen-centered radical. However, it is important to keep in mind that the "oxygen-centered" radical TEMPO only possess around 40% of its total spin on the oxygen. Clearly, having less than a majority of the spin density on the oxygen atom does not preclude the oxygen atom from participating in radical processes.[142]

The large share of spin density housed in the nitrogen atoms helps rationalize why this species can be a stable radical cation; the electron-rich nitrogens help to stabilize the positive charge and also house much of the radical character in a sterically encumbered site of the molecule. This rationalization is further supported by our observations that diaminocyclopropenones with more sterically hindered amino groups formed more stable radical cation species (stability: NCy2>NiPR2>piperidnyl).

The EPR spectrum of DACO radical **(1)** displays a 1:2:3:2:1 quintuplet that is representative of coupling to two equivalent nitrogen atoms (A value = 8.11 G), which demonstrates that the radical is delocalized in the diaminocyclopropenone pi system (there is no splitting from oxygen as O^{16} is EPR silent) (**Figure 2-6**). There is some smaller splitting present which is presumably due to coupling to the protons alpha to the nitrogen atoms. The EPR spectrum could be effectively simulated using these parameters.

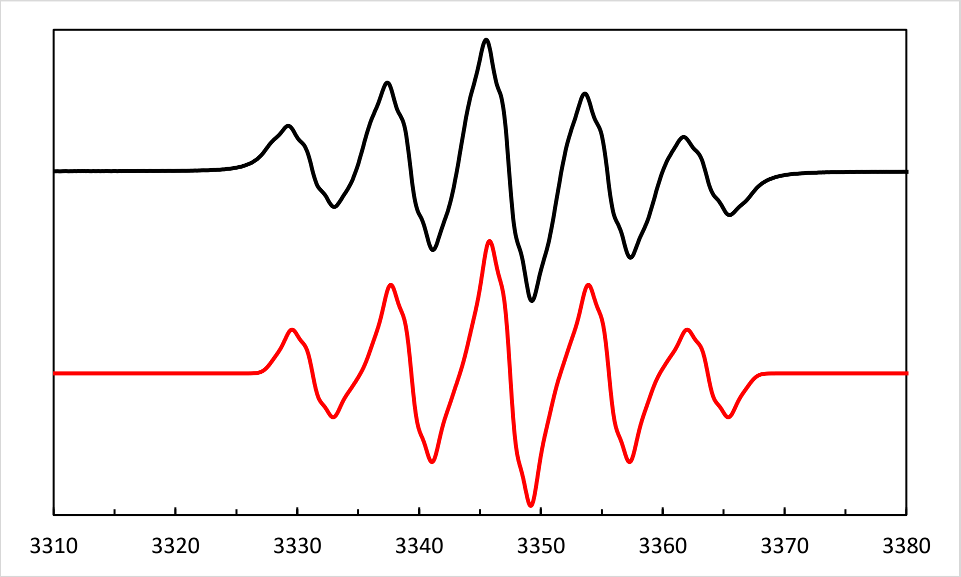

Figure 2-6. Experimental EPR Spectrum of DACO Radical **(1)** in DCM (black) and Simulated Spectrum (red)

We also measured both the pK_a of the protonated cyclopropenone, which we found to be 11.38 in acetonitrile, which is only slightly less basic than pyridine (pK_{BH+} = 12.53 in acetonitrile).[82] From this value and the oxidation potential we calculated the BDE (O-H) to be 82.9 kcal/mol, which is considerably higher than the BDE (O-H) of TEMPO-H (70.6 kcal mol).[143] In this regard, we thought the diaminocyclopropenone radical cation might also be a useful H-atom abstractor. To test this hypothesis, we added the DACO radical **(1)** to thiophenol (BDE S-H = ~79 kcal/mol), which resulted in phenyl disulfide and the protonated diaminocyclopropenone.[144] We believe this process is facilitated through H-atom abstraction (or perhaps proton-coupled electron transfer) and not through direct oxidation because the oxidation potential of thiophenol (+1.51 V vs SCE) is much greater than that of the diaminocyclopropenone (**1**) (+0.74 V vs SCE).[116] This result demonstrates that even though a minority of the spin density is located at the oxygen atom, it can still be the site of useful chemistry, which may be in part due to the fact that the oxygen atom is the most exposed part of the pi system.

(2.5) Cerium Complexes with Diaminocyclopropenone Ligands

As mentioned earlier, cyclopropenones have seen use as ligands in metal complexes due to the Lewis basicity of the carbonyl group. However, we were still surprised when treatment of diisopropylamino-cyclopropenone with CAN did not undergo one-electron oxidation but instead produced cerium complex **(1)** (**Figure 2-7**).

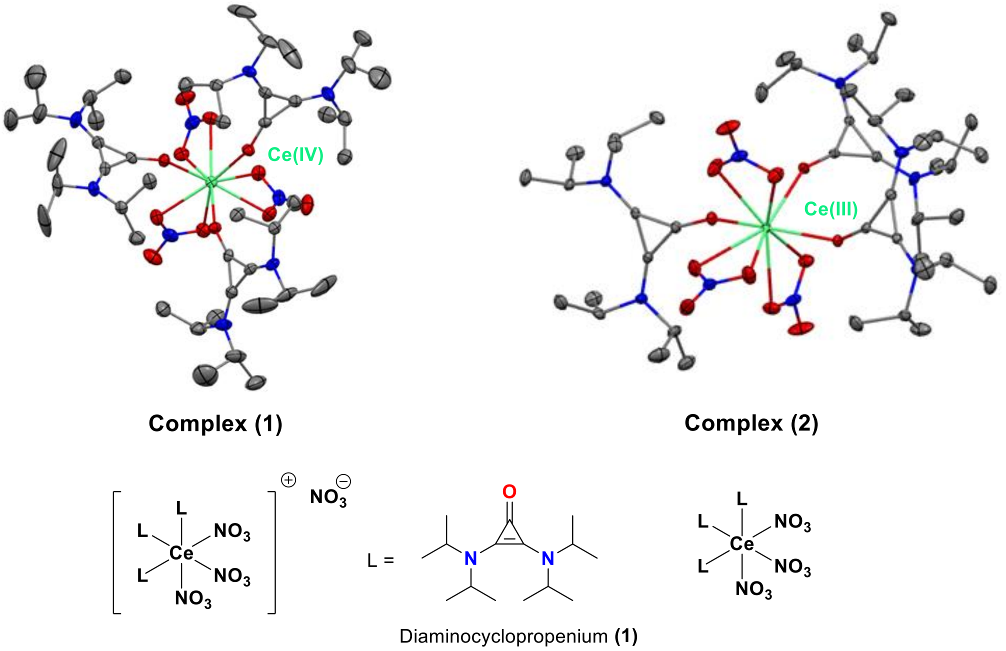

Complex (1)

Complex (2)

Figure 2-7. Cerium Complexes **(1)** and **(2)** with Diaminocyclopropenone Ligands

Complex **(1)** appeared to be a monocationic Ce(IV) complex with 3 nitrate ligands and 3 cyclopropenone ligands and a nitrate counterion. It should be noted that the nitrate counterion of complex **(1)** could never be fully resolved in the crystal structure because it was located on a high-symmetry special position. We also prepared and furnished an X-ray crystal structure of the corresponding neutral Ce(III) complex **(2)** from Ce(III)$(NO_3)_3$ (**Figure 2-7**). The Oxygen-cerium bond distances for both the nitrate and cyclopropenone ligands in the Ce(IV) complex **(1)** are significantly shorter than those in the Ce(III) complex **(2)**, which is consistent with a change in oxidation state. Furthermore, we found that salt metathesis with LiBARF on the Ce(IV) complex **(1)** produced the dicationic complex **(3)** that unmistakably had a tetravalent cerium metal center (**Figure 2-8**).

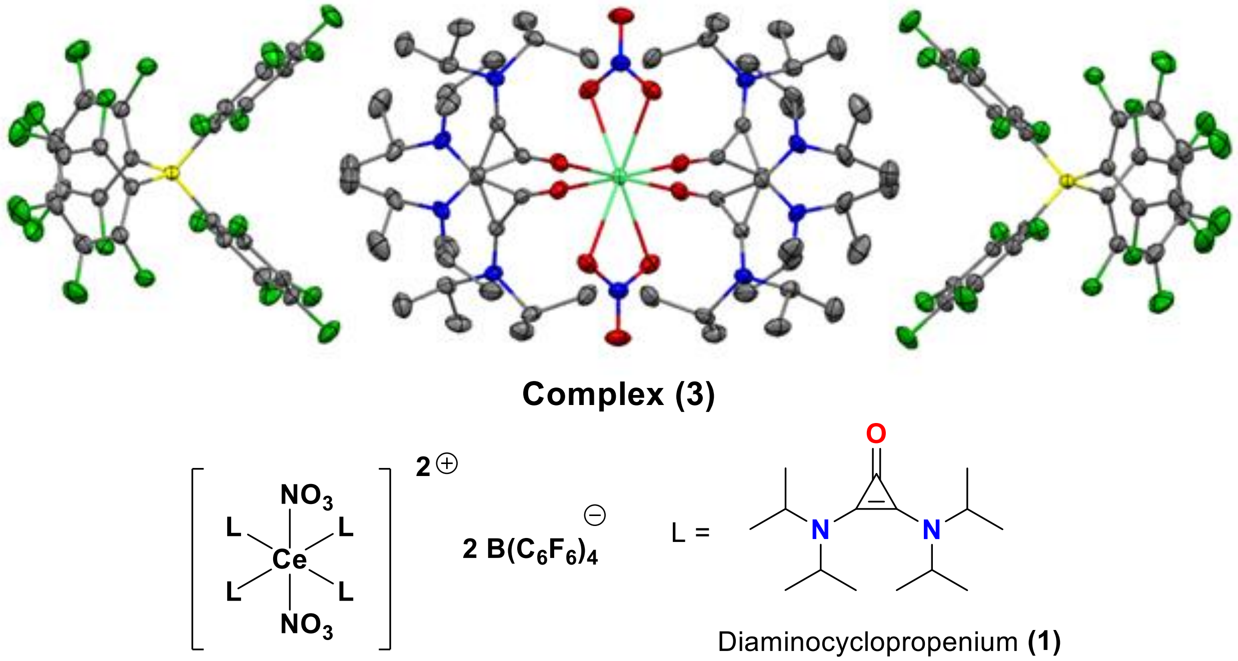

Figure 2-8. Dicationic Cerium Complex **(3)** with Diaminocyclopropenone Ligands

One of the more peculiar aspects of the Ce(IV) complexes **(1)** and **(3)** was that they produced EPR spectra that were similar to that of the cyclopropenone radical (identical in the case of complex **(3)**) in solution (**Figure 2-9**). This result was surprising to us because the crystal structures of these complexes did not indicate that there should be any unpaired spin. Additionally, we found that Ce(III) complex **(2)** was EPR silent.

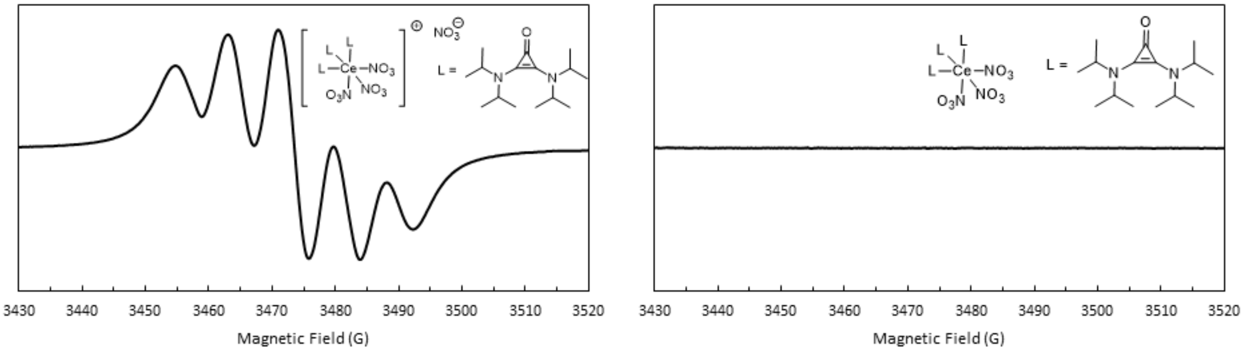

Complex (1) **Complex (2)**

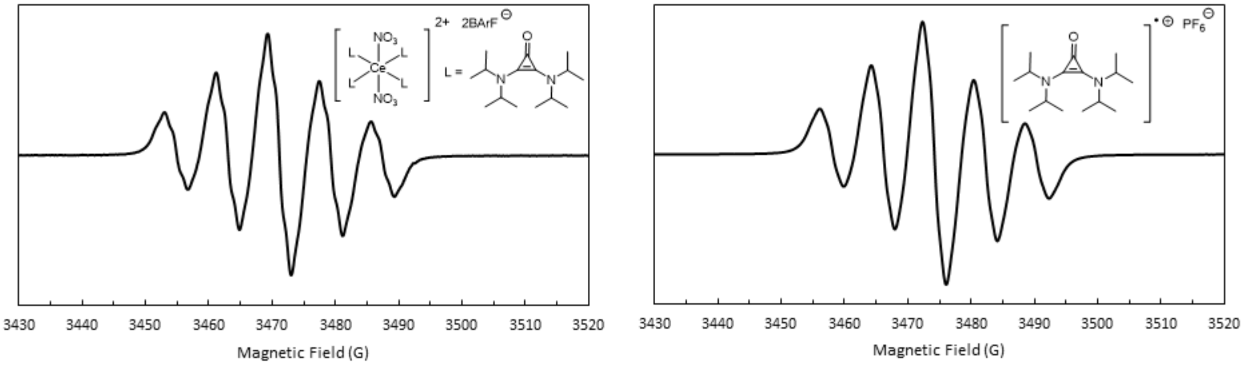

Complex (3) **DACO Radical (1)**

Figure 2-9. EPR Spectra of Diaminocyclopropenone-Cerium Complexes and DACO Radical **(1)**

(2.6) Reversible Homolytic Dissociation of Diaminocyclopropenone Ligands

We considered whether this EPR signal was due to the complexes having an oxidized ligand shell (as with non-innocent ligands),[145–147] some sort of dynamic process, or from an impurity. We felt we could reasonably rule out the possibility of the signal arising from an impurity due to the fact that we used single crystals of all of the complexes to prepare solutions for EPR measurement. Furthermore, we found that samples from different crystallization batches produced the same EPR intensity. The diaminocyclopropenones acting as non-innocent ligands seemed like a plausible explanation due to the fact that Ce(IV) is quite oxidizing (for example

CAN has an oxidation potential of +1.37 V vs SCE)[148] and the diaminocyclopropenone ligands are capable of facile oxidation. However, it is unlikely that an oxidized ligand shell would produce an identical EPR spectrum to that of the DACO radical as the EPR signal would be distorted by the environment of the metal complex. Due to the similarity in the EPR spectra of the DACO radical **(1)** and complex **(3)**, we thought it might be possible that some sort of dynamic process was responsible for the presence of DACO radical cation in solution. With the experiments described below, we concluded that complex **(3)** was involved in an equilibrium process in which it reversibly dissociates to form DACO radical cation **(1)** and, by inference, a Ce(III) complex (**Scheme 2-4**).

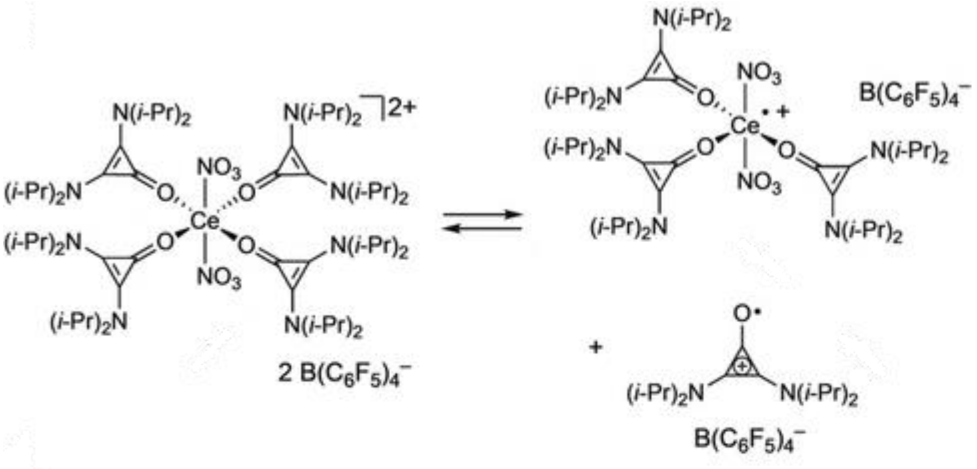
N(i-Pr)2
N(i-Pr)2
2+
NO3
(i-Pr)2N
O
O
N(i-Pr)2
Ce
(i-Pr)2N
O
O
N(i-Pr)2
NO3
(i-Pr)2N
N(i-Pr)2
2 B(C6F5)4−
N(i-Pr)2
NO3
B(C6F5)4−
(i-Pr)2N
O
• +
Ce
(i-Pr)2N
O
O
N(i-Pr)2
NO3
(i-Pr)2N
N(i-Pr)2
+
O•
(i-Pr)2N
N(i-Pr)2
B(C6F5)4−

Scheme 2-4. Dissociative Equilibrium of Complex **(3)**

We first found that temperature had a stark effect on the EPR signal intensity of complex **(3)**. Cooling the sample from 300 K to 270 K resulted in a decrease of over half of the signal intensity (**Figure 2-10**). As a control, we also measured the effect of temperature on the signal intensity of the DACO radical (**1**), but found that the signal intensity was much less affected by the same decrease in temperature. We thus attributed the majority of the temperature dependence on the effect it has on the dissociation of complex **(3)** and the DACO radical **(1)**.

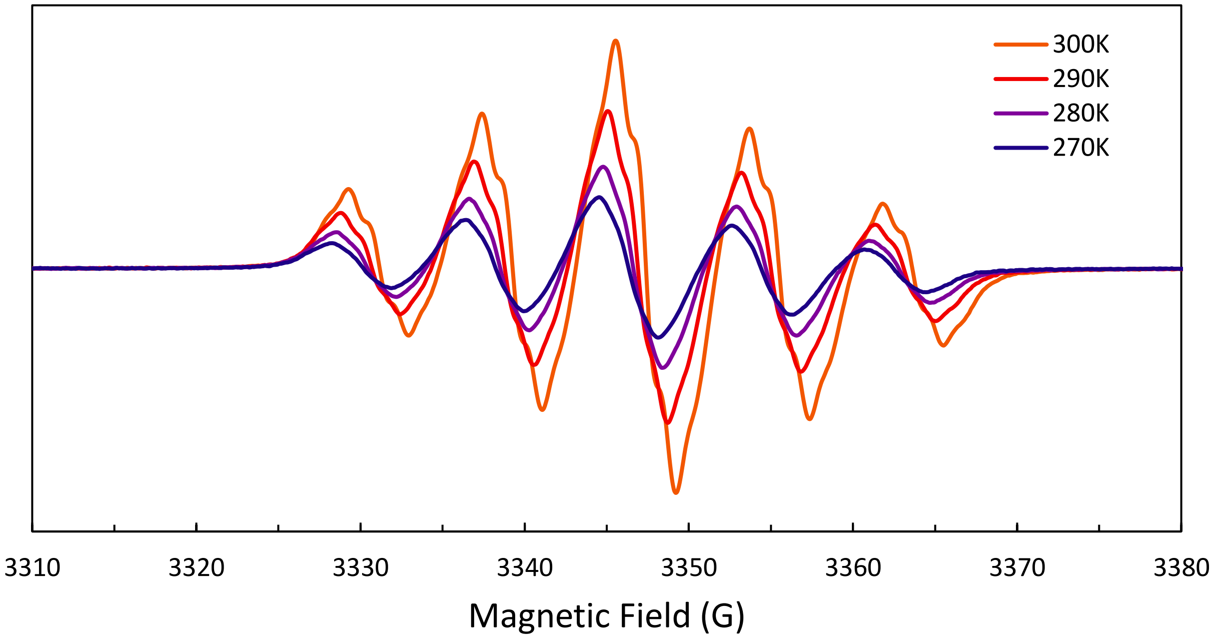

Figure 2-10. Variable Temperature EPR Spectrum of complex **(3)**

This effect can be rationalized by the fact that the dissociation of complex **(3)** to form DACO radical **(1)** and the corresponding Ce(III) complex will presumably have a positive entropy term and thus decreasing temperature will drive the equilibrium towards complex **(3)**. As a result, there will be less DACO radical **(1)** in solution and the EPR signal will decrease.

Like temperature, concentration should also be able to drive this equilibrium. Our investigation of the effect of concentration on this equilibrium very clearly shows the interchange between complex **(3)** and the DACO radical **(1)** because both species have clearly identifiable UV-VIS signatures. Complex **(3)** has a diagnostic broad peak with a maximum at 650 nm that presumably corresponds to an LMCT band from the diaminocyclopropenone ligands to the cerium center while the DACO radical **(1)** cation shows diagnostic peaks at 475 and 515 nm. At higher concentrations of complex **(3)**, essentially only the LMCT band is present. As the sample is successively diluted, the LMCT band weakens in intensity and the diagnostic peaks of the DACO radical (**1**) appear and grow in intensity (**Figure 2-11**).

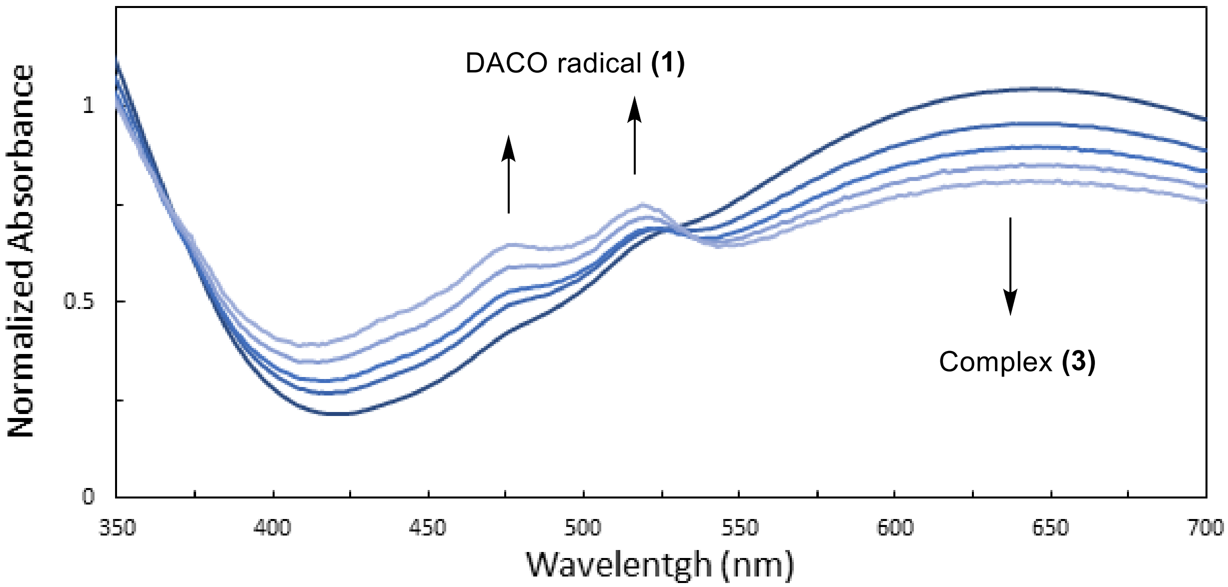

Figure 2-11. UV-VIS of Successive Dilution of Complex **(3)** (dark blue to light blue)

Finally, we wanted to see if we could drive the equilibrium the opposite direction, starting from a Ce(III) complex and forming a Ce(IV) complex by addition of DACO radical. For this purpose, we used the Ce(III) complex **(2)** **(**Figure **2-8**) that we had prepared earlier as a model complex for the Ce(III) complex that we inferred should also be in solution after dissociation of complex **(3)** (**Scheme 2-4**). When complex **(2)** was added to DACO radical **(1)**, the diagnostic peaks of the diaminocyclopropenone radical began to diminish and a broad LMCT band at 650 nm (similar to the one exhibited by Ce(IV) complex **(3)**) began to emerge (**Figure 2-12**). With 4 equivalents of complex **(2)** added, the peaks of DACO radical **(1)** were almost entirely gone, indicating that nearly all of the DACO radical in solution had been consumed to form a blue Ce(IV) complex. It should be noted that the isosbestic points are clearly visible in this experiment, which is further proof of a dynamic equilibrium.

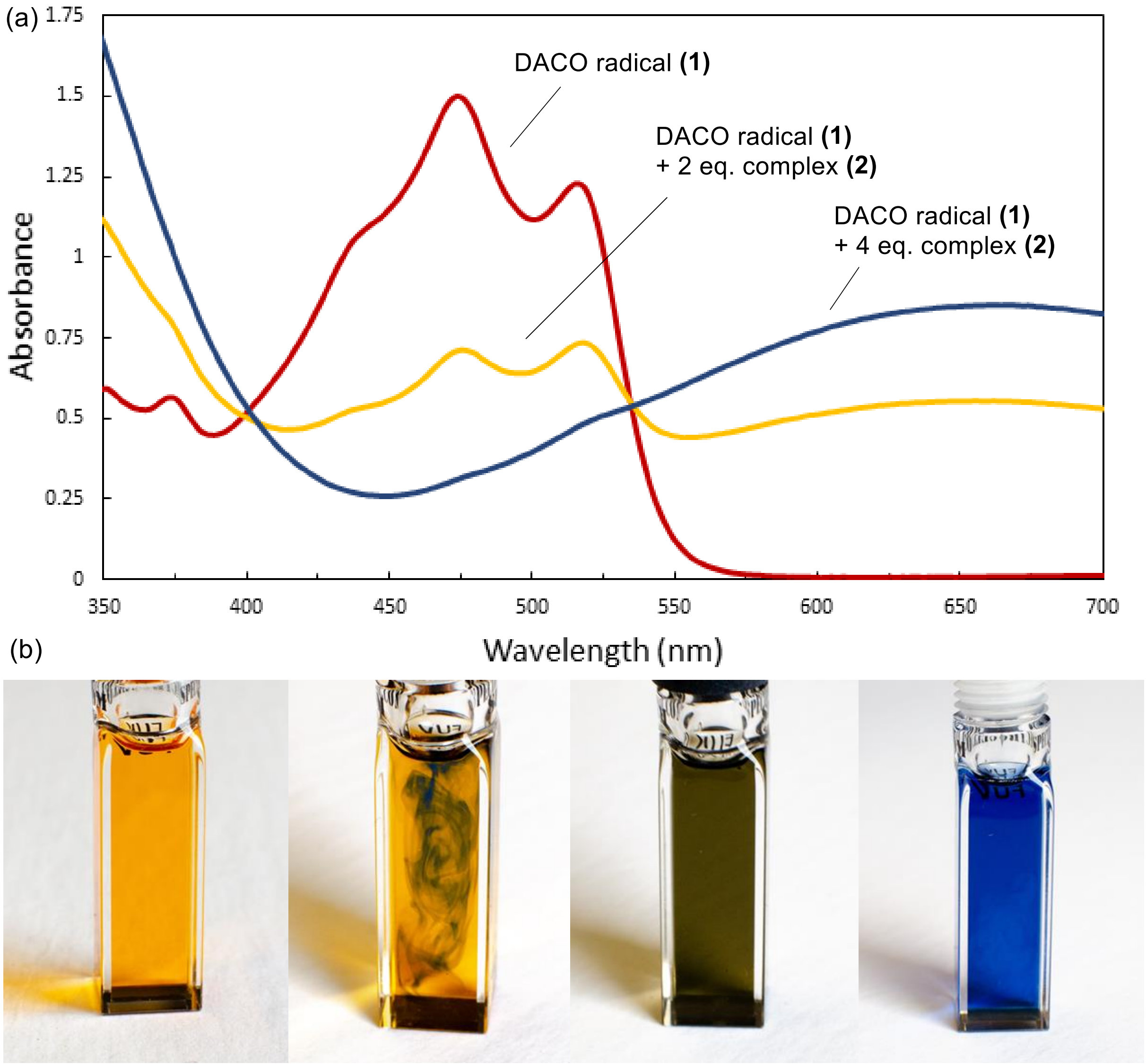

Figure 2-12. (a) UV-VIS of Addition of Complex **(2)** to DACO radical **(1)**, (b) Visualization of Addition of Complex **(2)** to DACO radical **(1)**

We believe that these experiments strongly support the hypothesis that the Ce(IV) complex **(3)** can homolytically dissociate one of its diaminocyclopropenone ligands as a radical cation and form the corresponding Ce(III) complex. Although metal-oxygen homolytic ligand dissociation has been observed in complexes with aminoxyl ligands,[149,150] we believe this is the first example of a reversible homolytic dissociation of a neutral oxygen ligand to a free radical cation. This unusual behavior can be attributed to the unique structure of 2,3-diaminocyclopropenones in that they are proficient L-type donors, but can also be oxidized to form a stable radical species. In contrast, common types of neutral L-type donor ligands such as amines and phosphines are typically not stable under highly oxidizing conditions. Thus, we believe that diaminocyclopropenones can be a useful new entry in the library of ligands, especially for highly oxidizing metal centers.

With evidence of this equilibrium established we were still left with one question: Why does a Ce(IV) complex form (complexes **(1)** and **(3)**) when CAN is added to the diaminocyclopropenone and not simply a single electron oxidation event? CAN has an oxidation potential that should more than sufficient to oxidize a diaminocyclopropenone so why don't we see this oxidation in the first place? Our hypothesis is that oxidation does occur and that it is the first step that in the formation of the Ce(IV) complexes. This effect can be observed by adding only a small amount of cyclopropenone to a solution of CAN, which results in a solution that has mostly DACO radical cation UV-VIS peaks and almost none of the LMCT band of the Ce(IV) complexes. At this point the DACO radical cation is either balanced by a nitrate anion or by an anionic Ce(III) complex.

In a typical preparation of these complexes, the ratio of diaminocyclopropenone to cerium salt is 3:1. Thus, after the initial oxidation of a diaminocyclopropenone, the remaining neutral diaminocyclopropenones in solution can complex to the Ce(III) species, making it increasingly electron rich. At some point, enough diaminocyclopropenones have coordinated to the Ce(III) metal center that it is now capable of being reoxidized by the free DACO radical cation in solution. Therefore, the last step involves the oxidative addition of the DACO to the Ce(III) metal center, resulting in a Ce(IV) complex. Presumably, now the metal center and the ligands are of similar oxidation potentials, which allows the last step of oxidative addition of the DACO radical to be reversible. As a result, we can observe these complexes homolytically dissociating one of their diaminocyclopropenone ligands.

It should also be noted that the counterion plays a significant role in the extent to which this dissociation occurs. By comparing the EPR intensity of DACO radical **(1)** to complex **(3)**, We estimated the dissociation constant of complex **(3)** to be: **K_d = 8.4*10^{-3}**, which corresponds to about 10% of the complex being dissociated at 0.76 mM concentration in DCM. The EPR signal of complex **(1)**, which only has a nitrate counterion, was several orders of magnitude less intense at the same concentration. We suspect that it is far more energetically unfavorable for this dissociation to occur if the DACO radical cation can only be balanced by either a nitrate anion or an anionic Ce(III) complex, whereas complex **(3)** can utilize one of its noncoordinating BARF anions to balance the DACO radical. It should be noted that the EPR spectrum of complex **(1)** in solution does look somewhat different than that of the DACO radical **(1)**, although it does still possess the same splitting pattern (Figure **2-9**). This difference could be due to the fact that when complex **(1)** homolytically dissociates, the resulting DACO radical is associated with a Ce(III) species or a nitrate counterion.

Similar to the diaminocyclopropenone radical cation, we found that complex **(1)** could be used to oxidize aryl thiols to the corresponding disulfides and hydroquinones to quinones. Due to the fact that the resulting Ce(III) complex can be aerobically reoxidized, we found that these complexes could be used catalytically to promote the oxidation of a variety of aryl thiols and hydroquinones under oxygen atmosphere (**Figure 2-13**).

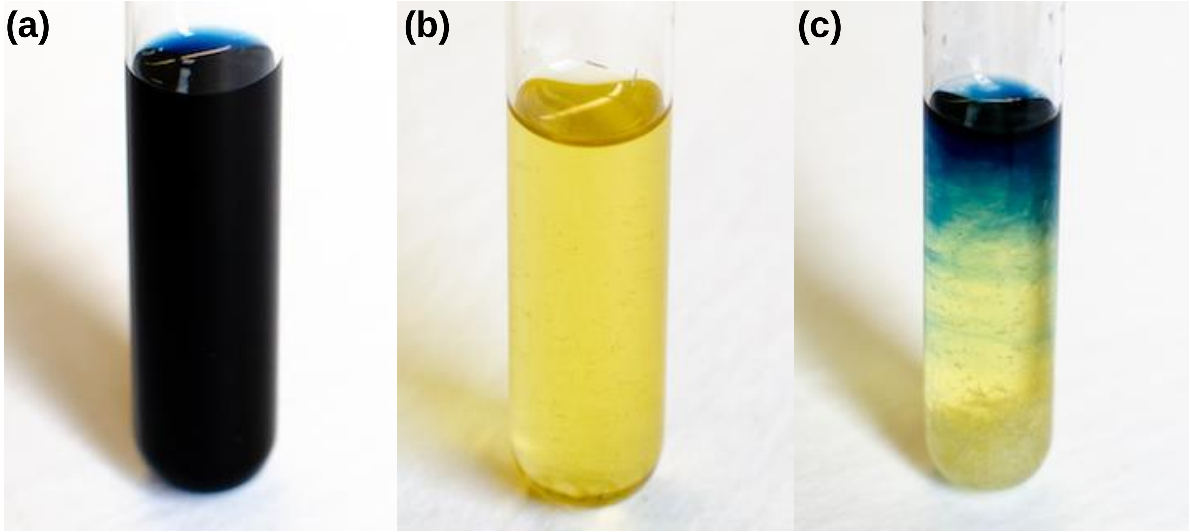

Figure 2-13. (a) Complex **(1)**, (b) After Addition of Hydroquinone, (c) Reoxidation by Oxygen

In conclusion, we have found that 2,3-diaminocyclopropenones can undergo oxidation to form stable radical cations. These DACO radicals possess an appreciable amount of spin density on the oxygen atom, but the majority of the spin density is located on the sterically encumbered nitrogen substituents. Notably, these molecules have a greater oxidation potential and a higher BDE (O-H) than the most commonly used oxygen-centered radical, TEMPO. In addition, we have shown that this class of molecule can be prepared on scale with a variety of amino substituents, which can significantly alter the electronic properties of these molecules. We also found that the diaminocyclopropenones are competent neutral L-type donors that possess the unusual ability to reversibly and homolytically dissociate from Ce(IV) complexes. We believe that given their ease of synthesis and intriguing properties, diaminocyclopropenones will be a useful addition to the arsenal of redox mediators, redox active ligands, and catalysts.

Chapter 3: Trisaminocyclopropeniums in Nonaqueous Redox Flow Batteries

(3.1) Redox Flow Battery Overview

Another area of research that seeks to take advantage of the stability of organic radicals is energy storage.[7] Rechargeable batteries have historically utilized the various oxidation states of metals such as lithium and lead (Pb) as a way to store electrical energy as chemical energy.[151,152] Similarly, if an organic molecule has multiple oxidation states and both charge states are stable, then the molecule can also be used as an active electrolyte for energy storage in a battery.[7]

The need for new technologies to store energy could not be more evident. Global energy demands have steadily increased are projected to continue growing.[153] Currently this growing demand is being met by increased carbon fuel consumption. To avoid the worst effects of climate change, we must begin a transition away from carbon-based fuel sources to renewable energy sources.[154] However, one of the greatest challenges to such a transition is that renewable energy from wind and solar are intermittent in nature.[155] Additionally, these renewable energy sources typically produce the least amount of energy when energy demand is at its greatest, a phenomenon referred to as the “duck curve”.[156] Both of these effects necessitate the implementation of large-scale energy storage to facilitate the effective use of renewable energy.[157] Lack of practical energy storage technology has been one of the greatest barriers to wide-scale adoption of renewable energy sources.

Currently, The U.S. only has 25 GW of energy storage capability, which is only 0.2% of the total daily demand.[158–160] The vast majority of the U.S.’s energy storage capability is in the form of pumped hydroelectric storage.[159] This technology entails physically pumping water to an elevated location and then using the kinetic energy of the water as it is released to ground level to power turbines and generate electric energy.[161] This method of energy storage is highly region limited and also poses a threat to the surrounding areas if the integrity of the water storage area falters. Lithium ion batteries have emerged as a possible solution to energy storage, although they only currently account for a miniscule percentage of the U.S.'s total energy storage capacity.[151,159] Additionally, lithium ion batteries still face the unresolved issues of high cost, insufficient lithium supply, unsatisfactory lifetimes, and safety.[162–165]

Redox flow batteries have emerged as a promising candidate for large-scale energy storage.[166–169] This technology utilizes the architecture of an electrochemical cell to store electrical energy as chemical energy (**Figure 3-1**).

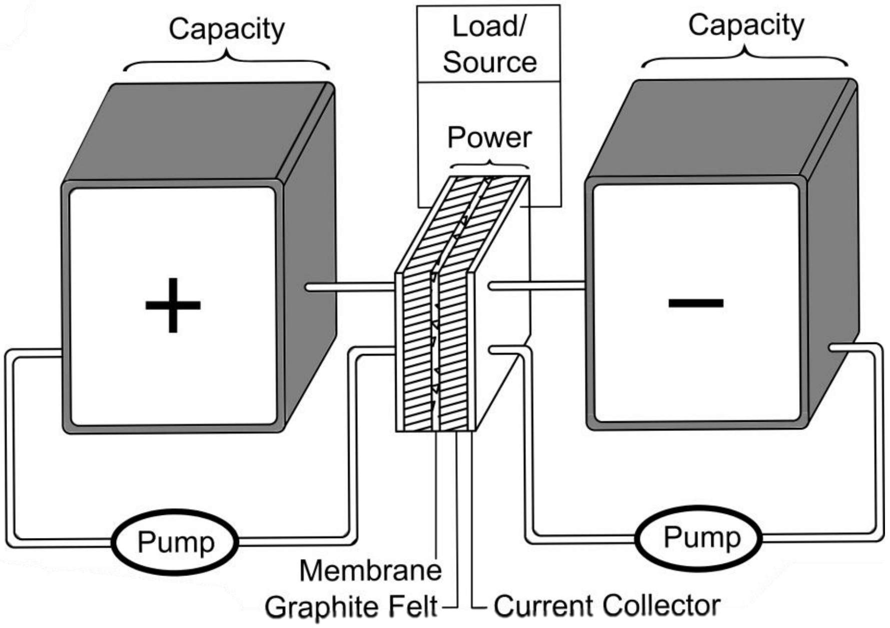

Figure 3-1. General Schematic of a Redox Flow Battery

Typically, two tanks are filled with a medium (water or an organic solvent) and connected by half of an electrical circuit with an electrode in each tank. A membrane is typically situated at the site of intersection between the two tanks. Ideally, this membrane only allows flow of solvent and the supporting electrolyte, which effectively completes the other half of the circuit. When the appropriate voltage is applied across the cell, active electrolyte molecules are oxidized at the anode and concomitantly active electrolyte molecules are reduced at the cathode. The active electrolytes, which are typically either metal complexes or organic molecules, effectively house this chemical energy. The stored energy can later be released by reactivating the circuit and allowing electrons to flow in the opposite direction, returning the active electrolytes to their original charge state. The voltage of the battery is equal to the additive absolute value of the oxidation potential of the catholyte and the reduction potential of the anolyte.

One interesting property of these batteries in contrast to solid-state batteries is that the power and capacity are decoupled.[168] The capacity, and thus power density, is determined by how much charged active electrolyte can be dissolved in solution while the power (current*voltage) is governed by the flux of the battery medium through the electrodes. Thus, the battery medium is typically pumped through the electrodes to increase charge and discharge rates. The flexibility of capacity and power operating independently makes redox flow batteries a prime candidate for grid energy storage. Additional advantages of flow batteries also include flexibility of their architecture, rapid charging and discharging rates, and potentially longer battery lifetimes and lower costs.[166]

(3.2) Advantages and Challenges of Nonaqueous Redox Flow Batteries

While significant progress has been made in the area of water-based flow batteries,[170–174] the development of nonaqueous flow batteries (NARFBs) has lagged.[111,175–184] Although aqueous flow batteries have the advantage of having an inexpensive solvent and supporting electrolytes, they can only operate within the electrochemical window of water, which is effectively 1.23 V.[165,185] Outside this range, water itself begins to undergo redox events, which generally leads to downstream degradation of the active electrolyte as well as gas generation.

Organic solvents can have a solvent window in the range of ~4-6 V,[186] which theoretically allows NARFBs to operate at much higher potentials, have greater energy densities, and a lower physical footprint.[187,188] However, the development of long-lasting organic flow batteries have been plagued by two main issues: active electrolyte instability[38] and lack of suitable membranes.[111,186,189–191]

The greatly expanded electrochemical window of organic solvents can only be utilized if there are molecules that can maintain stability at higher voltages. As such, there has been much effort to find active electrolytes that possess high redox potentials and still remain stable after change in oxidation state.[179] However, identification of such species has proved to be quite challenging, evidenced in part by the many reports in which the charged active electrolytes used have a half-life on the order of hours.[38,181,192] Of course, such short-lived charged species are wholly insufficient for the purposes of constructing a long lifetime battery.

Designing a suitable membrane for NARFBs represents another difficult challenge in that the material must be electrochemically inert, insoluble in organic solvents, and it must limit the transport of the active electrolytes across the membrane. As with the solvent, any membrane present in a flow battery will come in contact to both the charged catholyte and anolyte. In this sense, the membrane must be comprised of a material that is inert to the voltages of the molecules that are present on both sides of the cell, which can be difficult considering that most functional groups are prone to either oxidation or reduction.[116] Preventing crossover of the active electrolytes is achieved in two main fashions: (1) using a size-exclusion membrane and active electrolytes that are large enough that they can’t pass through the pores of the membrane,[111,189,193] or (2) by using an ion-exclusion (a.k.a. ion-exchange) membrane which can prevent the crossover of active electrolytes if they are functionalized to be ionic.[191,194] Unfortunately, most commercially available membranes of either type are designed to work in aqueous conditions and are not suitable for high potential or organic solvents.[194,195] Thus, identification of a broadly effective membrane for use in NARFBs has remained an outstanding challenge in the field.[175,177,186,192,196]

One of the first examples of a long lasting NARFB was reported by the Nuckolls et. al.[57] This battery utilized a ferrocene tetramer as the catholyte and quaternized ammonium-functionalized PDI (PDI **(1)**) as the anolyte (**Figure 3-2**).

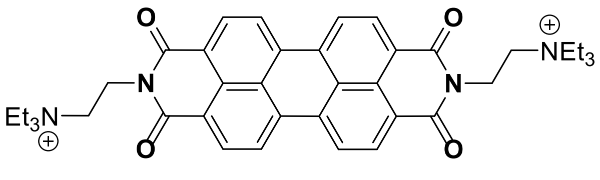

PDI **(1)**

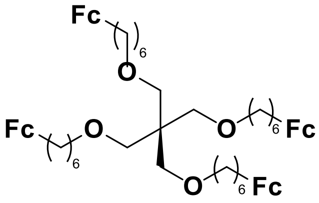

Fc = Ferrocene

Figure 3-2. PDI Anolyte and Ferrocenyl Tetramer Catholyte by Nuckolls et. al.

A cellulose membrane, typically used for purifying proteins and polymers, was used as a size-exclusion membrane. Because both active electrolytes were specifically designed to be macromolecular, the cellulose membrane could effectively preclude crossover of the active electrolytes. The battery showed a remarkable coulombic efficiency of >99.95% (the percentage of electrons returned upon discharge) and a capacity retention of 99.994% per cycle (a measure of how much of the total capacity is maintained from cycle to cycle). However, one of the main drawbacks of this system is that it only had voltage of 0.85 V, which doesn't make use of the wide electrochemical window of the solvent being used (acetonitrile). Thus, the logical next step was to build off of the precedent of this system by replacing the active electrolytes with those with greater redox potentials.

(3.3) Designing a Trisaminocyclopropenium Catholyte

One candidate that seemed promising for a higher voltage catholyte was the trisaminocyclopropenium (TAC). As mentioned previously, these molecules have been shown to have a reversible oxidation that would be +0.8 V greater than ferrocene.[108,175] While these molecules have been cycled in a half cell and a proof of concept battery by the Sanford group, they had never been applied in a functioning battery.[111,175] Due to our experience in synthesizing TACs and related species, the Lambert lab was enlisted to help realize this high-voltage NARFB.[88,134]

Previous reports of oxidations of TACs indicated that the nitrogen substituents had a large effect of the stability of the TAC in its radical dication form.[175] The two most important factors were that increased steric bulk produced more stable TACs and dialkyl (as opposed to aryl) amino substituents also led to greater stability. We also found these trends were mirrored in our investigations of DACO radicals. This effect can be rationalized by the fact the nitrogen atoms presumably possess the overwhelming majority of the spin density of the radical dication and thus sterically protecting the nitrogen atoms will serve to shield the radical. Additionally, more steric hindrance could also lead to stability by shielding the protons alpha to the nitrogen, whose abstraction or deprotonation is the most likely form of degradation or the radical dication species.[197,198] While aryl substituents increase the oxidation potential of the TACs, they lead to less stable radical dication species, presumably because the radical can delocalize around the exposed phenyl rings where it is subject to dimerization and other degradation pathways. One last concern was that the trisaminocyclopropenium that had been tested in battery-like conditions was the tris(diisopropylamino)cyclopropenium, which is difficult to synthesize on scale. The original report on this molecule showed only an 8% yield and subsequent reports by the Sanford group did not bother reporting a yield.[199,200] Our own attempts at synthesizing this molecule produced a similarly unsatisfactory yield and as such we decided that a new structure was required.

With these structural constraints in mind, we sought to design a new TAC structure that would be similarly stable in its oxidized form, but could be synthesized on a scale large enough to support a multitude of battery tests. We similarly found that TACs that were not alpha-branched such as those with piperidinyl and pyrrolidinyl amino substituents were less stable. We eventually landed on using cis-2,6-dimethyl piperidine for the amino substituents, which is an inexpensive starting material produced from the hydrogenation of 2,6-lutidine.[201] We found that the corresponding TAC could be synthesized in 50-60% yield in one step on a multigram scale with no chromatography.

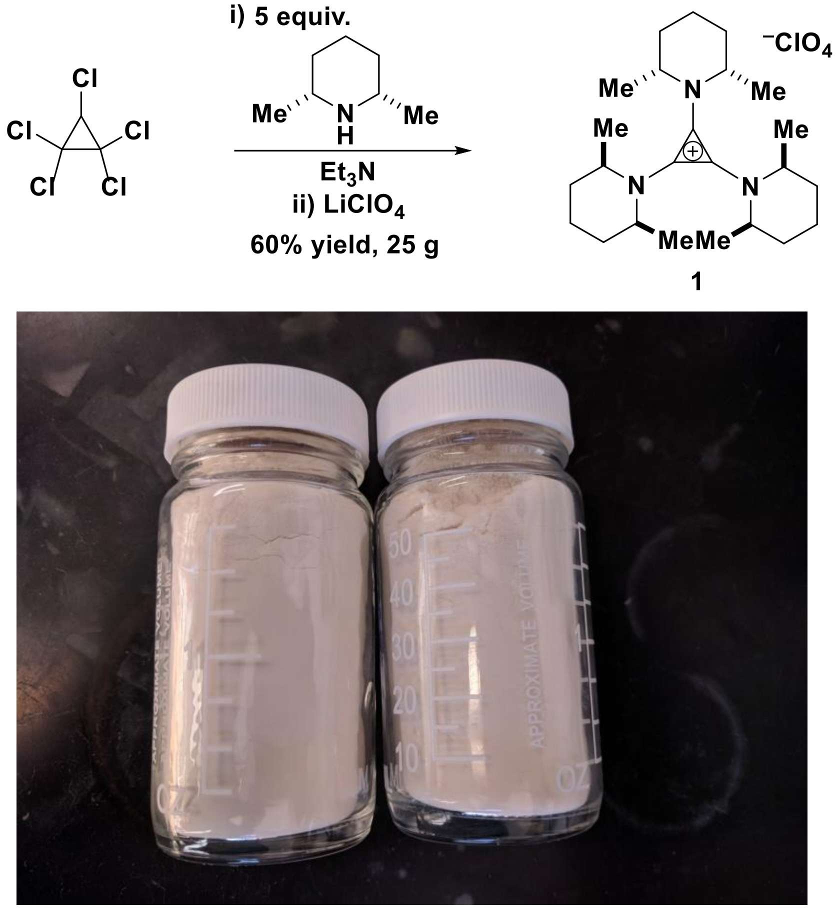

Scheme 3-1. One Pot Synthesis of TAC **(1)**

Notably, this TAC maintained a similar steric encumbrance to the tris(diisopropylamino)cyclopropenium provided by the alpha branching of the amino groups. We found that solutions of the charged TAC with bis(trifluoromethane)sulfonimide (TFSI) counterions retained the red color of its oxidized form for months, even in ambient conditions (**Figure 3-3**). Additionally, we found this TAC to have greater solubility than the tris(diisoprylamino)cyclopropenium in acetonitrile.

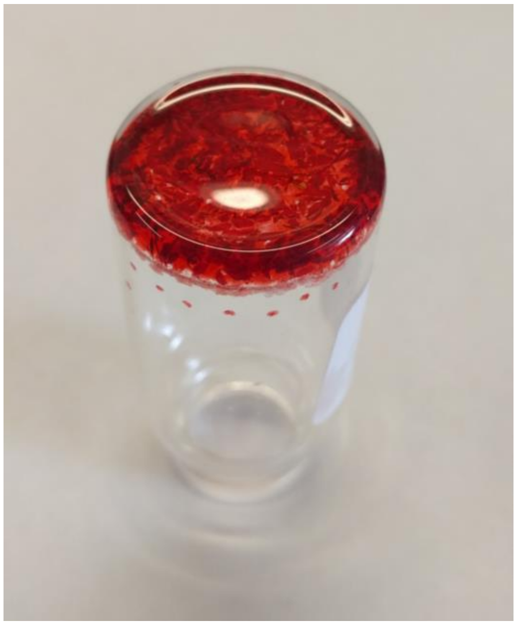

Figure 3-3. TAC **(1)** Radical Dication after 3 Months

(3.4) Issues with Commercially Available Membranes

With this new TAC in hand as our new catholyte, we set out to construct a battery system using PDI **(1)** as the anolyte (**Figure 3-2**). The first issue we discovered was that the cellulose membrane that had been utilized as a membrane in the battery system developed by Nuckolls et. al. was not stable to the TAC radical dication. When the cellulose membrane was soaked in a solution of TAC radical dication, we found that it could no longer prevent the crossover of the PDI anolyte, which is a crucial aspect that gave the previous system its high coulombic efficiency and capacity retention. This result was not entirely unexpected as this cellulose membrane was previously found to be unstable under highly oxidizing conditions, specifically in the presence of $NOBF_4$.[57] Presumably, the hydroxyl functionality of the cellulose membrane is susceptible to oxidation by either the TAC radical dication or $NOBF_4$ and the ensuing degradation eliminates its size exclusion properties.

Due to the lack of other available size-exclusion membranes, we turned to ion-exclusion membranes as a feasible alternative. These membranes are usually composed of ionic polymers that can block transport of either anions or cations across the membrane. Cation-exclusion membranes were a natural fit due to the fact that the quaternary ammonium functionalized PDI (**1**) anolyte was doubly cationic and TACs are monocationic in their neutral state and becomes doubly cationic in their oxidized state. We first attempted to construct a cell using the commercially available membrane Fumasep, one of the most common cation-exclusion membranes used for aqueous batteries.[202] However, we found this membrane was incompatible with multiple elements in our system. First, we found that Fumasep was electrochemically unstable to the charged species in our battery. While the exact chemical makeup of Fumasep has not been disclosed, it most likely achieves its cation-exclusion properties with permethylated quaternary ammoniums.[203] It is well documented that quaternary ammonium salts are more susceptible to redox mediated rearrangements and degradation than those with longer alkyl chains.[204] As such, we found that exposing Fumasep to both charged species led to brown discoloration of the membrane and the detection of amine due to degradation of the ammonium salts. In addition, Fumasep most likely bears chloride counterions due to its use in water-based systems, which are unstable to oxidative conditions. Attempts to convert the chloride salt to the more electrochemically stable TFSI salt resulted in the membrane partially dissolving in acetonitrile, causing it tear under the gentlest handling. Due to the lack of available commercial membrane designed for NARFBs, we decided to fabricate a membrane that would be suitable for a high voltage system.

(3.5) Designing a Membrane for NARFBs

We hypothesized that polystyrene would be a versatile monomer building block for constructing a viable membrane for NARFBs. Styrene monomers are easy to derivatize, undergo facile polymerization, and result in a hydrocarbon polymer that is electrochemically inert. We also predicting that outfitting the styrene monomer with a quaternary ammonium with ethyl or longer alkyl chains would provide the membrane with cation exclusion properties while remaining electrochemically inert. To probe the electrochemical stability of such a polymer, we measured the cyclic voltammogram of a model repeating unit of the polymer, bearing a perethylated quaternary ammonium TFSI salt (**Figure 3-4**). The electrochemical analysis showed that the model monomer had a wide electrochemical window and would be suitable for the voltages present in the cell.

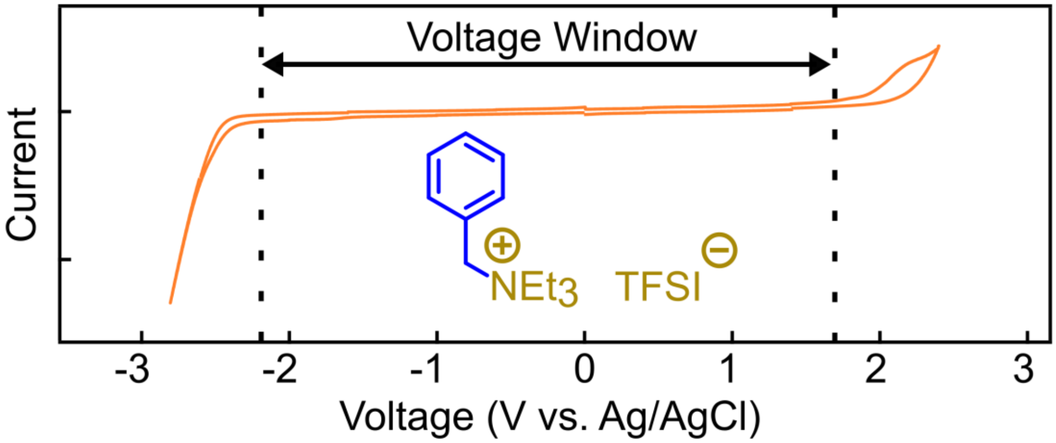

Figure 3-4. Electrochemical Window of Model Monomer

With this information in hand we prepared the corresponding styrenyl monomer from commercially available chloromethyl styrene and triethylamine. Subsequent salt metathesis of the chloride salt with LiTFSI prevented the need for post-polymerization salt exchange and potentially avoided oxidation of the chloride salt by the initiator. Typical conditions for radical-initiated polymerization of styrene with AIBN were implemented, resulting a clear gel-like polymer. Unfortunately, this polymer was soluble in acetonitrile, even at low initiator loadings. To prevent solubility, 1,4-divinyl benzene was added as a crosslinker in varying amounts. We found that the polymer was soluble in acetonitrile until it contained greater than 35% of crosslinker loadings (**Scheme 3-2**). Perhaps unsurprisingly, such a high crosslinker content produced a polymer solid that could not be melted and thus was not able to be processed. Differential scanning calorimetry measurements showed that the polymer did not have a glassification temperature before degradation.

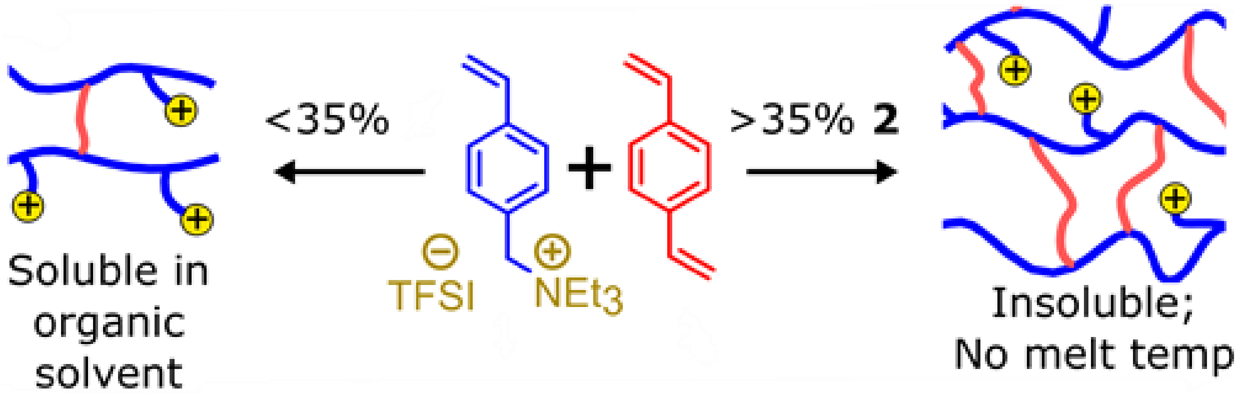

Scheme 3-2. Synthesis of Organic Soluble or Unproccessable Polymers

This situation appeared to be an impasse due to the fact high crosslinker content caused the polymer to be unprocessable, while lower crosslinker content caused the polymer to be soluble in acetonitrile. We proposed that the highly crosslinked polymer could be utilized if it was housed in a solid support (**Figure 3-5**). This arrangement would thus obviate the need to process the ionic polymer into a suitable membrane. A somewhat similar strategies for composite membranes has previously been applied to fabricating membranes designed for aqueous systems.[205–208]

For a solid support, we used Daramic, which is a commercially produced membrane that is commonly used in lead acid batteries.[209,210] It consists of a thin sheet of polyethylene, which should be completely inert to our battery conditions, with 0.6 µm pores. In order to house our ionic polymer in the solid support, the Daramic sheet was first soaked thoroughly in the monomer/ /crosslinker/AIBN/acetonitrile solution (**Figure 3-5**).

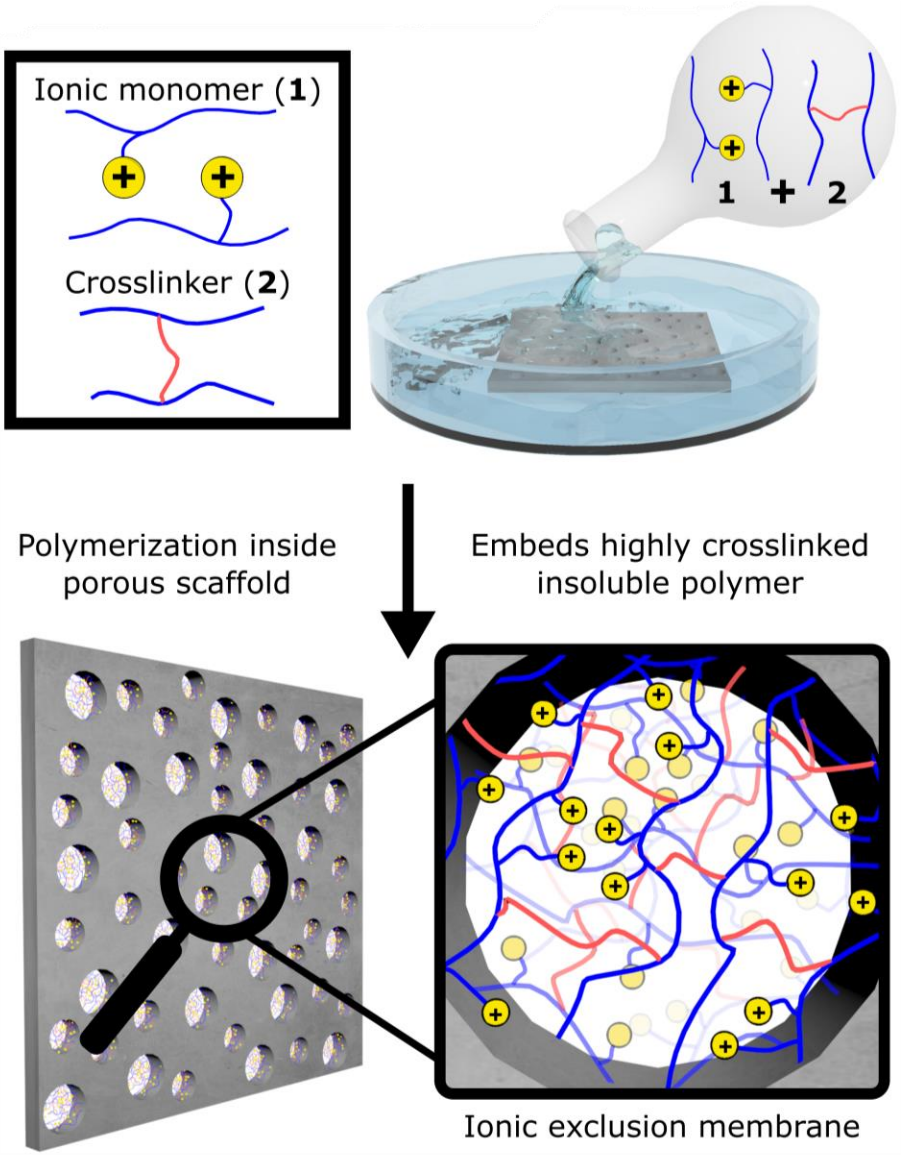
Ionic monomer (1)
+
+
Crosslinker (2)
+
+
1 + 2
Polymerization inside porous scaffold
Embeds highly crosslinked insoluble polymer
Ionic exclusion membrane

Figure 3-5. Polymerizing Ionic Monomer within Microporous Scaffold

Polymerization was thermally initiated, resulting in the Daramic membrane with a thin layer of polymerized material on both surfaces, indicating that the ionic polymer was distributed throughout the membrane. The change in the material could also be viewed by electron microscopy (**Figure 3-6**). The mixed polymer material was considerably more inflexible than the initial Daramic sheet, but could be manipulated easily after soaking in organic solvent.

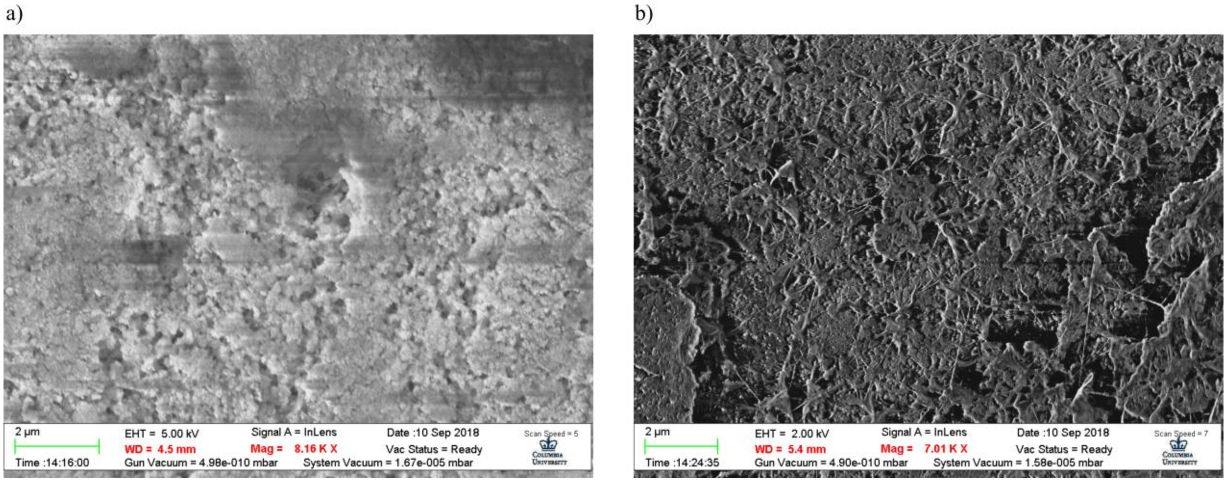
a)
b)
2 µm
EHT = 5.00 kV
Signal A = InLens
Date :10 Sep 2018
Scan Speed = 5
WD = 4.5 mm
Mag = 8.16 K X
Vac Status = Ready
Time :14:16:00
Gun Vacuum = 4.98e-010 mbar
System Vacuum = 1.67e-005 mbar
Columbia University
2 µm
EHT = 2.00 kV
Signal A = InLens
Date :10 Sep 2018
Scan Speed = 7
WD = 5.4 mm
Mag = 7.01 K X
Vac Status = Ready
Time :14:24:35
Gun Vacuum = 4.90e-010 mbar
System Vacuum = 1.58e-005 mbar
Columbia University

Figure 3-6. Electron Microscope Image of (a) Microporous Daramic and (b) after Polymerization with Quaternary Ammonium Functionalized Styrene

(**3.6**) **Crossover and Cycling Studies**

The circular membranes could be situated between two Teflon cutouts in an H-cell for conducting cross over studies and running battery tests. We first tested the crossover of the PDI (**1)** anolyte in acetonitrile/LiTFSI solution (**Figure 3-7**).

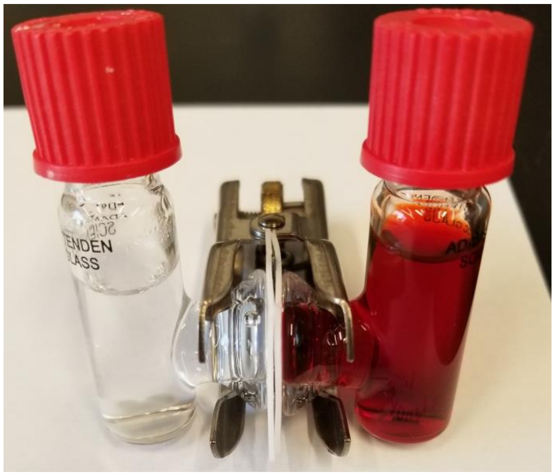

Figure 3-7. Crossover Experiment with PDI (**1**) in an H-cell

Adding the anolyte to one side of the H-cell, we found that there was no detectable crossover of the PDI compound after 16 days (**Figure 3-8**).

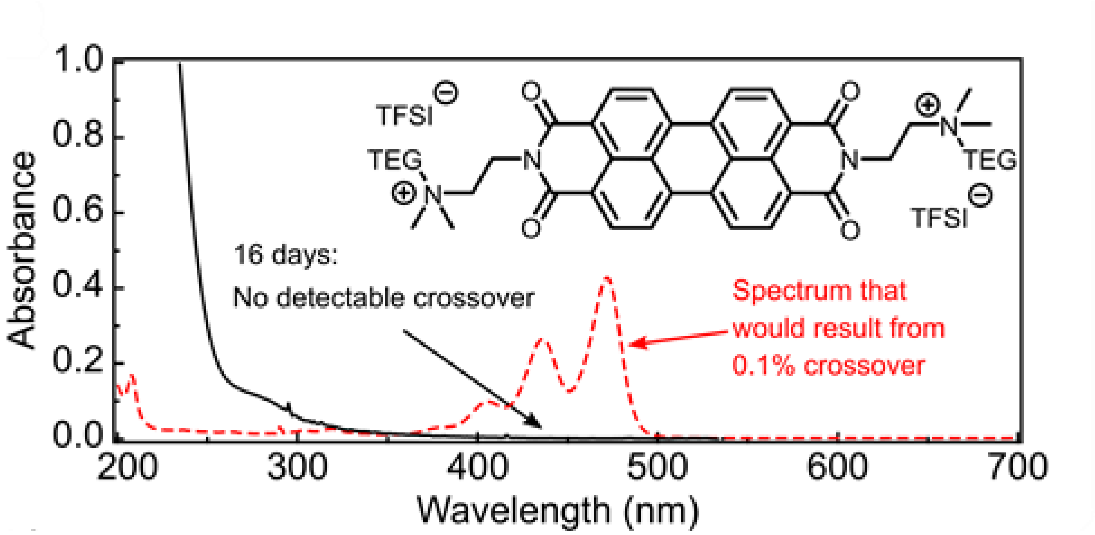

Figure 3-8. Crossover of PDI **(1)** after 16 Days

We found this result to be remarkable given that other examples of ion exclusion membranes are found to have at least some amount of observable crossover.[196,211–213] We also tested a membrane where the ionic monomer was excluded from the polymerization mixture and found that there was considerable crossover of the PDI in only 24 hours.

We next tested the crossover of a UV-VIS detectable TAC with anilino substituents and found that there was 0.08% crossover of this compound per day (**Figure 3-9**).

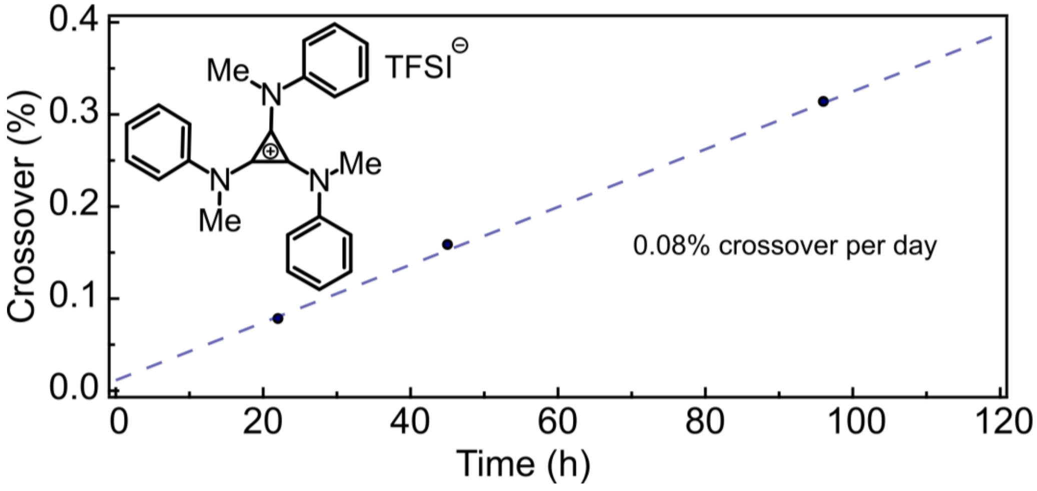

Figure 3-9. Crossover of Anilino-Substituted TAC over Time.

The difference in crossover rates between the TAC and the PDI molecules may be attributable to two factors. Firstly, the PDI bears two discrete positive charges in its quaternary ammonium tails while the TAC has only one positive charge (in its unoxidized state) that is distributed amongst its pi system. The distributed nature of this positive charge may lead to less coulombic repulsion by the ionic polymer and thus lead to greater crossover. Secondly, the TAC is significantly smaller in size compared to the PDI (**1**), which suggests that this membrane may also have size-exclusion properties.

Crucially, we also found this membrane to be conductive. Applying 1.7 V of potential across an H-cell fitted with the membrane was able to begin charging using TAC (**1**) and PDI (**1**) as active electrolytes. With the knowledge that this membrane was both conductive and possessed ion exclusion properties, we proceeded to testing the battery performance.

We prepared a battery using the PDI (**1**) as an anolyte and the TAC (**1**) as a catholyte in 0.5M LiTFSI/acetonitrile solution using the composite membrane we fabricated (**Figure 3-10**).

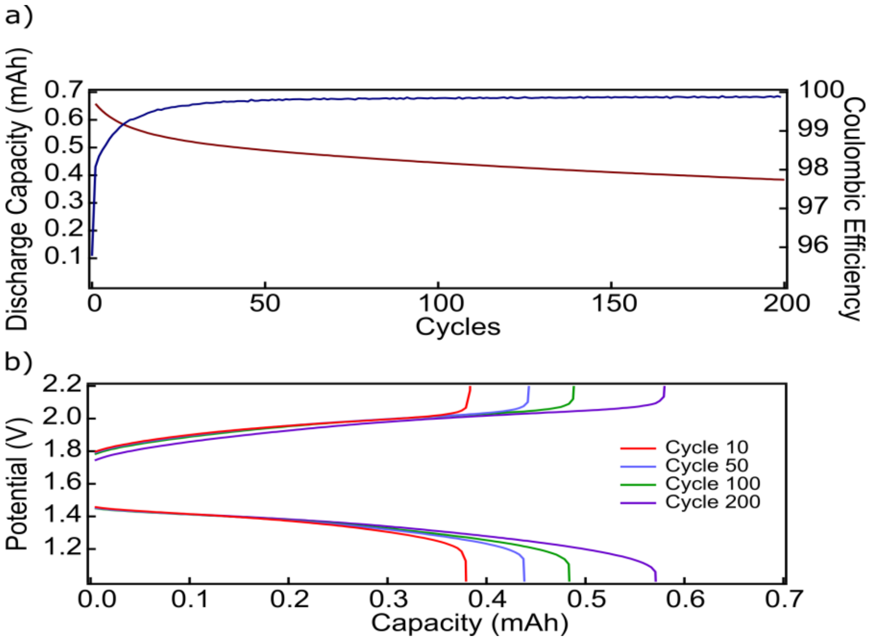

Figure 3-10. (a) Discharge Capacity and Coulombic Efficiency of PDI/TAC Battery (b) Voltage Profiles During Cycling

The current was set to 0.5 mA/cm^2 and cycling proceeded under galvanostatic conditions for more than two weeks, completing 200 cycles. The cycling data showed this battery had >99.5% coulombic efficiency and capacity retention, displaying very little loss of charge over time. The slight amount of fade could be due to crossover of the TAC, which may increase under the osmotic pressure of the running battery. However, this experiment demonstrates that this membrane is still highly effective for retaining charge in a NARFBs.

The open circuit voltage of this battery was 1.7 V, which is 0.8 V greater than the battery originally reported by Nuckolls et. al.[57] (**Figure 3-11**). This increase in potential is due to the much greater oxidation potential of TAC (**1**) compared to the ferrocenyl tetramer that was originally used (**Figure 3-2**).

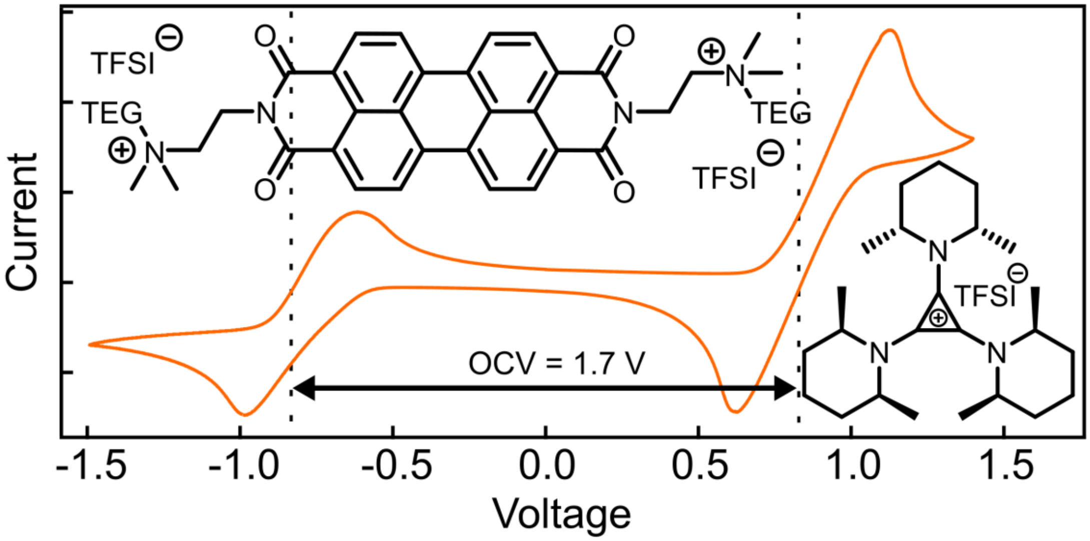

Figure 3-11. Cyclic Voltammogram of the PDI/TAC Redox Couple

We wondered if we could further increase the voltage of the cell by swapping the PDI anolyte for one that is reduced at a higher potential. Towards this end, the Nuckolls group prepared a spiro-bis(phthalimido) compound (Spiro **(1)**) (**Figure 3-12**). This molecule has a reduction potential that is around -0.75 V lower than PDI (**1**).

Spiro **(1)**

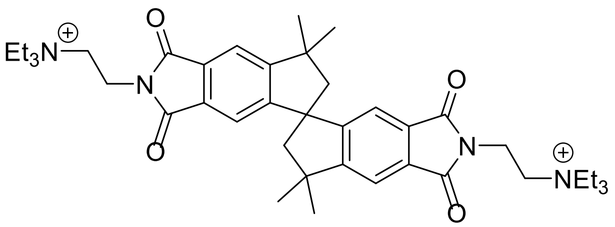

Figure 3-12. Spiro-bis(phthalimido) Anolyte

We thus set out to find conditions the would be suitable for both of these active electrolytes. Applying both active electrolytes to the same conditions as the previous cell, we quickly learned that the Spiro (**1**) anolyte was incompatible with acetonitrile, indicated by the lack of coloration upon charging (Spiro (**1**) is typically green when charged). We suspect that this charged anolyte is involved in some degradation pathway with acetonitrile, either by a reduction, HAT, or a deprotonation pathway. Due to this result, we screened several potential solvents and supporting electrolytes for this system. To our displeasure, we found that the vast majority of solvents were unworkable, due to reaction with one or both of the charged active electrolytes. One promising solvent was dimethoxyethane (DME), which appeared to be stable to both the charged TAC (**1**) and Spiro (**1**). We found that cycling in DME with LiTFSI afforded a capacity retention of ~98% over several days with an open circuit voltage of 2.5 V. Switching the supporting electrolyte to tetrabutylammonium TFSI further increased the voltage to an astonishing 2.8 V (**Figure 3-13**), which is the highest voltages reported for NARFBs.[186,191]

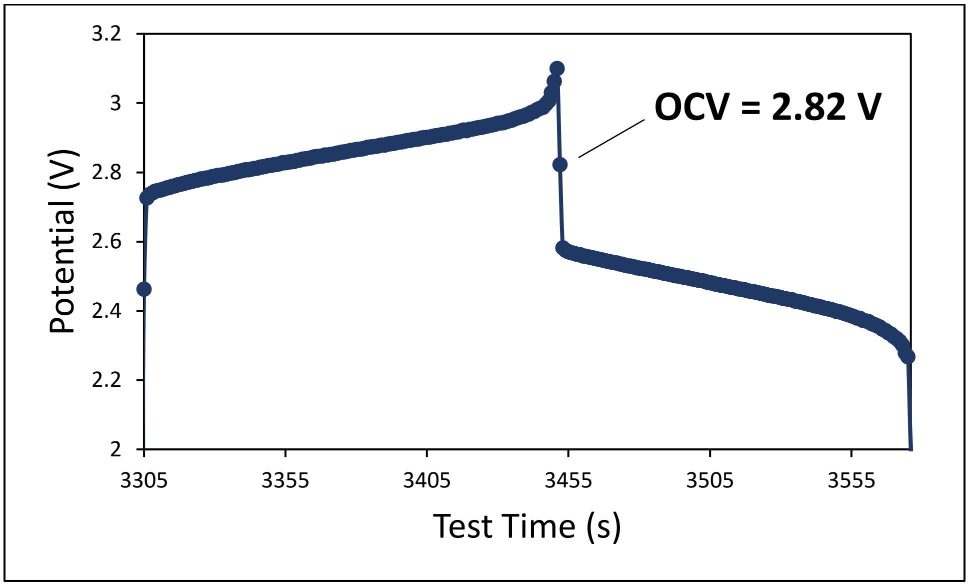

Figure 3-13. Open Circuit Voltage of TAC/Spiro Battery with TBATFSI

The capacity loss in this battery could come from a variety of sources including interaction between the charged TAC and DME, between the charged Spiro (**1**) compound and the membrane, or instability of the charged Spiro (**1**) compound.

It should be noted here that while organic solvents do possess a much higher electrochemical window than water, our studies in this field made us wonder if it is actually possible to access voltages much higher than 3 V without significant capacity loss over time. Not only is it difficult to identify active electrolytes that are stable upon oxidation or reduction at high potential, it is also difficult to identify organic solvents or membrane materials that can withstand such high electrochemical potentials as well.

In conclusion, we have successfully designed a new type of ion-exclusion polymer that is fabricated by polymerizing quaternary ammonium-adorned styrene inside a microporous polyethylene support. We implemented this membrane using the newly synthesized TAC (**1**) and PDI (**1**) to produce a battery with an open circuit voltage of 1.7 V and capacity retention and coulombic efficiency >99.5%. Using a spiro-bis(phthalimido) anolyte with TAC (**1**), we were able to prepare a battery with an open circuit voltage greater than 2.8 V, which is an exceptional potential for NARFBs. We believe that both the active electrolytes and the membrane will serve as important benchmarks for this field and will be aid in further development of new high voltage NARFB’s in the future.

Chapter 4: Electrophotocatalysis with Trisaminocyclopropeniums

(4.1) Variations in Battery Cycling Data

While testing various battery conditions, we noticed a very perplexing result: batteries that contained DME and TAC (**1**) would occasionally exhibit a cyclic depreciation of performance. During these several hour periods, the coulombic efficiency would drop from ~99% to ~80% before recovering back to ~99% (**Figure 4-1**). When a battery exhibits a loss in performance, it is typically a sign of degradation or crossover of active electrolyte. However, these factors would not explain the recovery in performance nor the cyclical nature of the variance.

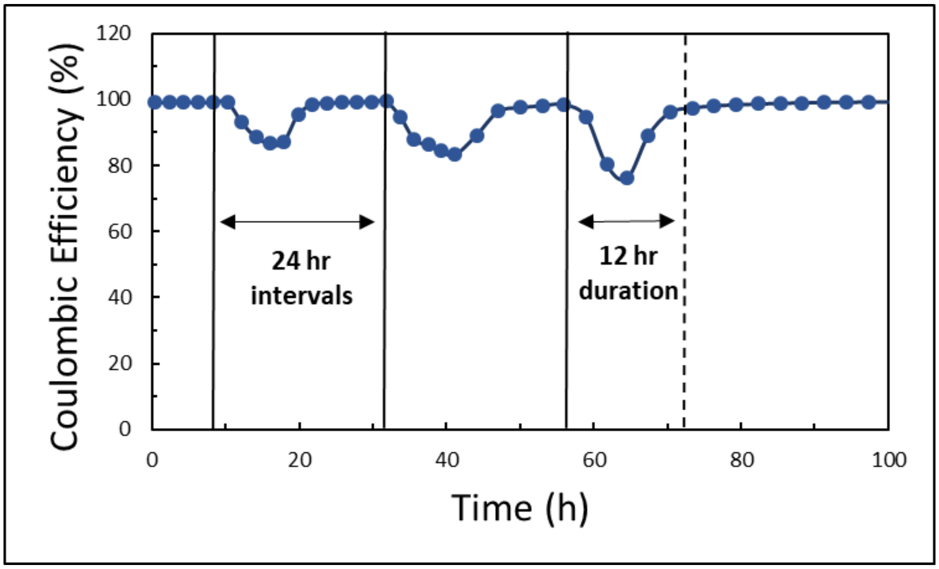

Figure 4-1. Cyclical Performance Loss of TAC Battery in DME

Our first clue in uncovering the origin of this cyclic performance loss was that the cycles repeated roughly every 24 hours and that the duration of the performance loss lasted around 12 hours. This pattern reflected the roughly 12 hours each day we were working in the room that housed our battery experiments.

We "put on our tinfoil hats" and considered many potential factors ranging from the contaminants in the glovebox atmosphere to electrical surges. Eventually the lightbulb both metaphorically and literally went off above our heads: the lights! We considered that the ambient light in the room and glovebox could be interacting with the active electrolyte molecules in our battery. This hypothesis seemed plausible given the fact that both of the active electrolytes are strongly colored when charged and could thus absorb visible light. Furthermore, PDI has been shown to undergo photoinduced reactions in both its neutral and reduced states.[58,59] Perhaps a similar type of photoinduced reactivity was responsible for the missing electrons in our battery.

To test this hypothesis, we brought a bright compact fluorescent light (CFL) into the glovebox and illuminated it directly next to a running battery containing DME as a solvent. Indeed, after direct stimulation by the bright light source the coulombic efficiency fell to near 0% within two cycles (**Figure 4-2**). This result indicates that 0% of charge was recovered upon discharging while the battery was exposed to light

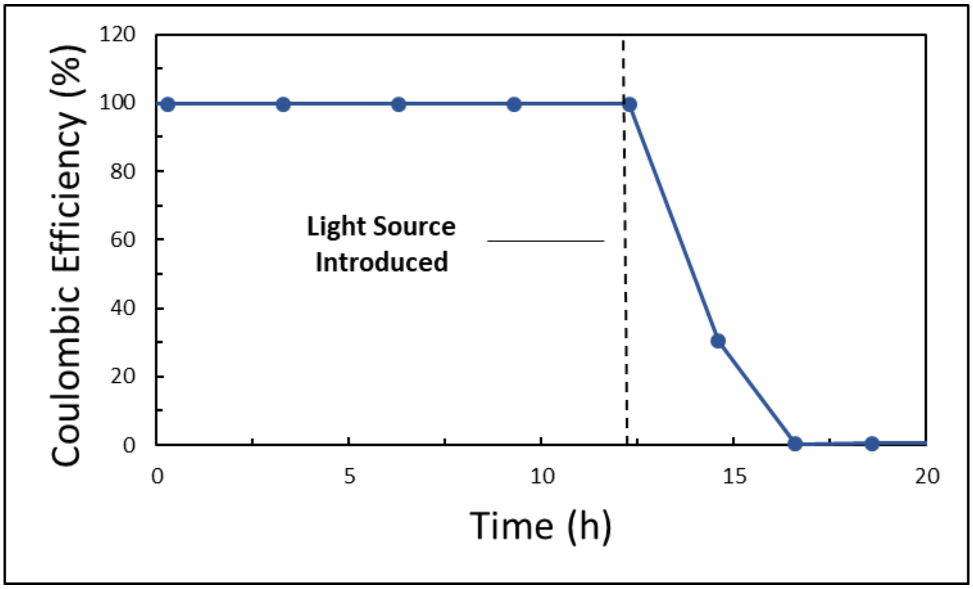

Figure 4-2. Introducing Light to TAC Battery in DME

The most likely explanation for this phenomenon is that the active electrolytes were either degrading or undergoing a redox reaction and could therefore not hold charge. By looking at the cell we could clearly see that the TAC was the culprit in this case. At full charge, the half-cell containing TAC radical dication is usually a dark red solution. After fully charging in the presence of the bright CFL light, the half-cell was only faintly red, suggesting that that the TAC was no longer in a charged state. Thus, discharging the battery resulted in no energy output because the TAC had already either reduced or had degraded. We also found this result to be mirrored when tetrahydrofuran (THF) was used as a solvent.

The first implication of this finding was that all further batteries would be run in complete darkness. However, we also wondered if this unexpected photoinduced reactivity of the oxidized TAC could be harnessed in a productive way. We had already considered that the TAC radical dication might serve as a useful oxidant. We found the idea that its reactivity could be further augmented by light to be especially intriguing.

(4.2) Combining Photoredox and Electrocatalysis

In evaluating the use of this photoinduced reactivity, we first needed to ascertain whether the lack of discharging in the illuminated battery was due to degradation or reduction of the charged TAC. If the TAC was photodegrading in this process then any useful reactivity could not be translated into a catalytic system. As a test, we isolated charged TAC (**1**) from a fully charged battery and dissolved it in both DME and THF. Stirring these solutions while exposed to bright light caused decolorization in minutes. NMR analysis of the solutions showed that this decolorization was indeed a result of the reduction of the TAC (**1**) radical dication, suggesting that THF and DME had been oxidized in the process. This result indicated to us that we had potentially discovered a new type of photocatalyst, and an odd one at that. Most known photocatalysts are either transition metal complexes or organic dyes, but have a closed-shelled ground state in either case.[27,28] Conversely, the TAC radical dication would represent a photocatalyst with an open-shelled ground state.

The first step in conceptualizing how this reactivity could be translated into a catalytic system was finding a method of reoxidizing the TAC. Typically, oxidative photocatalytic reactions must either have a stoichiometric oxidant, a photocatalyst that can be reoxidized by molecular oxygen, or the reaction must be engineered to be net redox-neutral.[28] Our unusual photocatalyst gave us an opportunity to rethink the turnover step in such a catalytic reaction. Given our familiarity with electrochemistry, we wondered if we could simply reoxidize the TAC electrochemically. Of course, the idea of using direct electrolysis to regenerate a catalyst is a key part of the well-established field of electrocatalysis.[25,26] However, the idea of combining electrochemical energy and photochemical energy in one molecule is a concept that has been little explored.[26]

The advantages that this type of electrophotocatalysis would provide can be understood both through the lens of photoredox catalysis and through electrocatalysis. In a photoredox regime, the effect of "stacking" both electrochemical and light energy into a catalyst would theoretically allow access to energies aren't available to traditional photocatalysts (**Figure 4-3**). Since the ground state of most conventional photocatalysts are generally redox-neutral, all of the energy that contributes to the excited state oxidation potential comes from excitation by visible light. In the case of the TAC, the excited potential would be effectively increased by the +1.2 V of "extra" energy that it requires to access the TAC radical dication, which can then become further energized by absorbing visible light. Based on long wavelength absorption tail (600 nm) of TAC (**1**) radical dication, the photoexcited state is expected to have a remarkable excited state oxidation potential of $E^*_{1/2}$ = 3.33 V vs SCE.

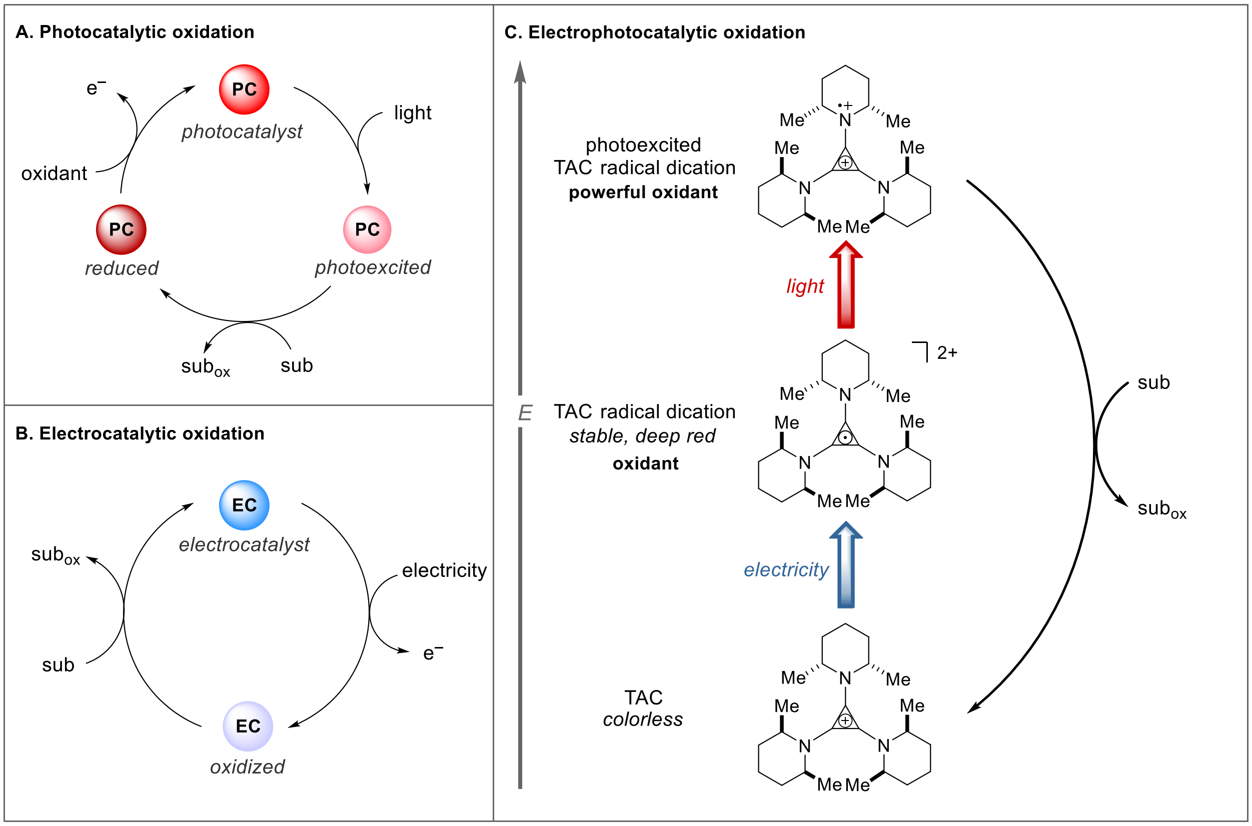
A. Photocatalytic oxidation
e⁻
PC
photocatalyst
light
oxidant
PC
reduced
PC
photoexcited
sub$_{ox}$
sub
B. Electrocatalytic oxidation
EC
electrocatalyst
sub$_{ox}$
electricity
sub
e⁻
EC
oxidized
C. Electrophotocatalytic oxidation
E
photoexcited
TAC radical dication
powerful oxidant
Me
Me
N
Me
Me
N
N
Me
Me
light
2+
TAC radical dication
stable, deep red
oxidant
electricity
sub
sub$_{ox}$
TAC
colorless

Figure 4-3. Comparison of (a) Photocatalysis, (b) Electrocatalysis, and (c) Electrophotocatalysis

In an electrochemical sense, this effect can be viewed as a way to overcome the shortcomings of both direct electrolysis and of electrocatalysts. In theory, direct electrolysis can be used to exert any amount of positive or negative potential on a substrate in order to enable a redox event.[25] However, in practice this is unfeasible for molecules with high redox potentials due to overreaction, electrode deposition, solvent and supporting electrolyte degradation, and poor chemoselectivity.[26] Redox mediators can serve as a catalyst to solve many of these problems in that they enable faster kinetics, reduction in passivation of the electrode, and catalyst control of the reaction pathway.[26] However, there are few classes of well-established redox mediators and the range of potentials they inhabit is still quite limited. Furthermore, for reactions involving outer-sphere electron transfer, the redox potentials of the electrode, mediator, and substrate must all exist in a narrow and finely tuned window to allow the correct electrochemical equilibrium. As such, electrolysis procedures can be difficult to reproduce and additionally often call for highly specialized electrodes and equipment. Requiring the redox mediator to undergo the additional step of photoexcitation could conceivably ameliorate both of these issues. Cooperatively adding electrochemical and photochemical light in one molecule could allow access potentials that are unavailable to traditional redox mediators. Additionally, requiring light input for the catalyst to react means that the electrode potential can be set far below the redox potential of the substrate. As a result, the catalyst could exert exclusive control over the redox event without competing with direct electrolysis (**Figure 4-4**).

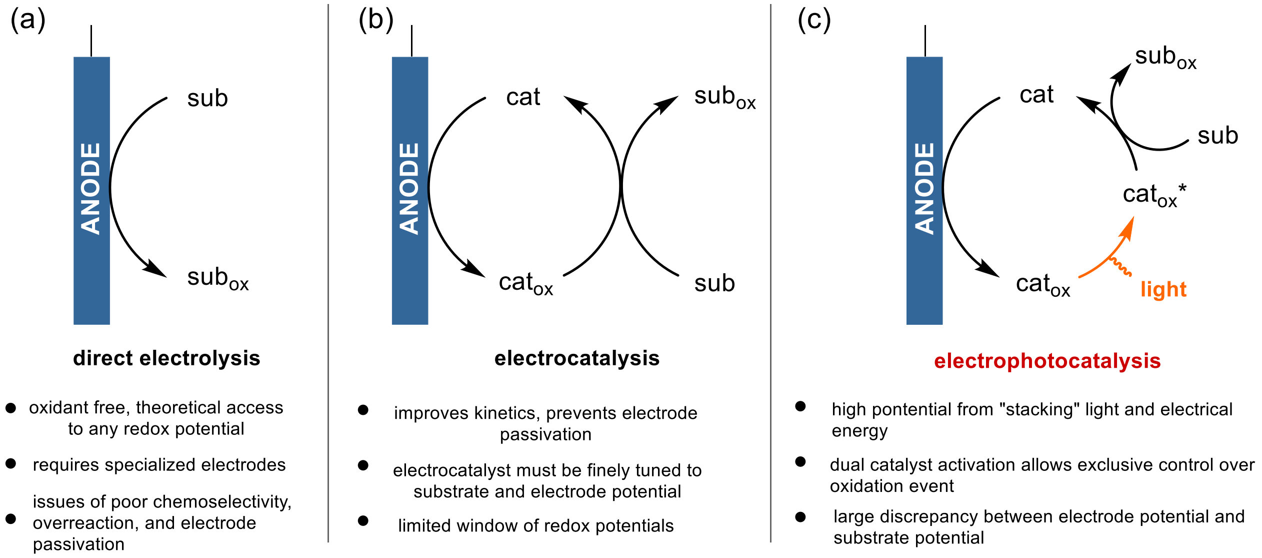
(a)
ANODE
sub
sub_{ox}
direct electrolysis
oxidant free, theoretical access to any redox potential
requires specialized electrodes
issues of poor chemoselectivity, overreaction, and electrode passivation
(b)
ANODE
cat
cat_{ox}
sub_{ox}
sub
electrocatalysis
improves kinetics, prevents electrode passivation
electrocatalyst must be finely tuned to substrate and electrode potential
limited window of redox potentials
(c)
ANODE
cat
cat_{ox}
cat_{ox}*
light
sub_{ox}
sub
electrophotocatalysis
high pontential from "stacking" light and electrical energy
dual catalyst activation allows exclusive control over oxidation event
large discrepancy between electrode potential and substrate potential

Figure 4-4. Comparison of (a) Direct Electrolysis, (b) Electrocatalysis, (c) Electrophotocatalysis

However, despite these advantages, combining photo- and electrocatalysis is an area that has been rarely reported.[214–218] Perhaps this is partly due to the fact that such an electrophotocatalyst would need to (1) undergo a facile and reversible redox event, (2) absorb visible light once it has undergone that redox event, (3) have a sufficiently long-lived excited state to interact with a substrate, and (4) survive the catalytic cycle. We believed that TAC radical dication did meet all of these requirements and as such we continued on to testing its ability to effect catalytic oxidations.

(4.3) Electrophotocatalyic Oxidations of Arenes and Ethers

Because we suspected that our catalyst would be highly oxidizing, we first targeted the oxidation of benzene, which has been a difficult substrate for both electrocatalysis and photocatalysis.[218–222] These methods have typically used electron rich arenes such as anisoles due to the fact that benzene has such a high oxidation potential (+2.48 V vs SCE). We found that we could catalytically effect the oxidative coupling of benzene and pyrazole in 65% yield using 8 mol% TAC with a cell voltage of 1.5 V (E_{anode} = +1.4 V) and irradiation from a 23 W compact fluorescent light (CFL) (**Table 4-1**). The reduction of the acetic acid to hydrogen gas at the cathode was used as an electron sink, although the overall reaction is net proton neutral. Crucially, control experiments showed that no reaction occurred without the catalyst, light, or current. Furthermore, direct electrolysis at higher potentials up to 3.0 V resulted in very low yield and the visible formation of polymeric material. The stark difference between direct electrolysis and the electrophotocatalytic approach can be appreciated by the visual comparison in **Figure 4-5**.

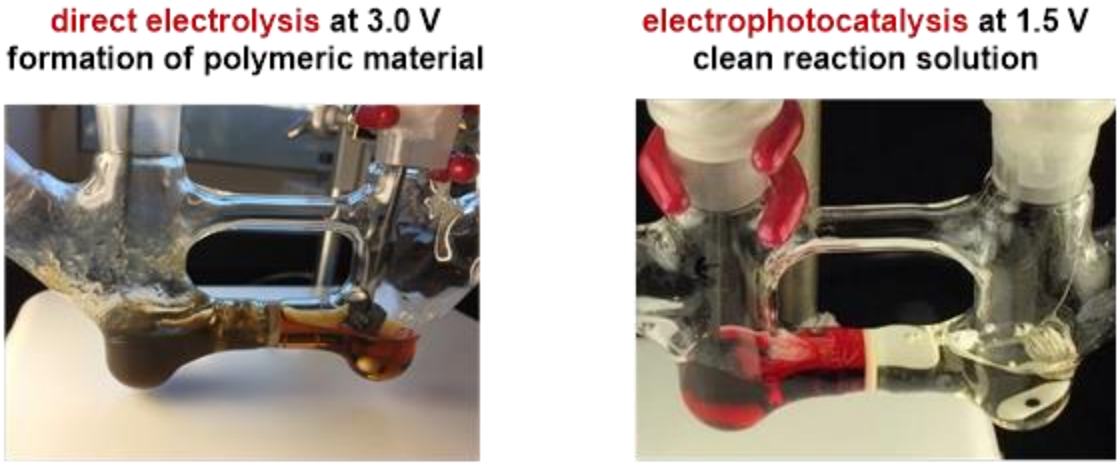

direct electrolysis at 3.0 V
formation of polymeric material

electrophotocatalysis at 1.5 V
clean reaction solution

Figure 4-5. Comparing the Results of Direct Electrolysis and Electrophotocatalysis

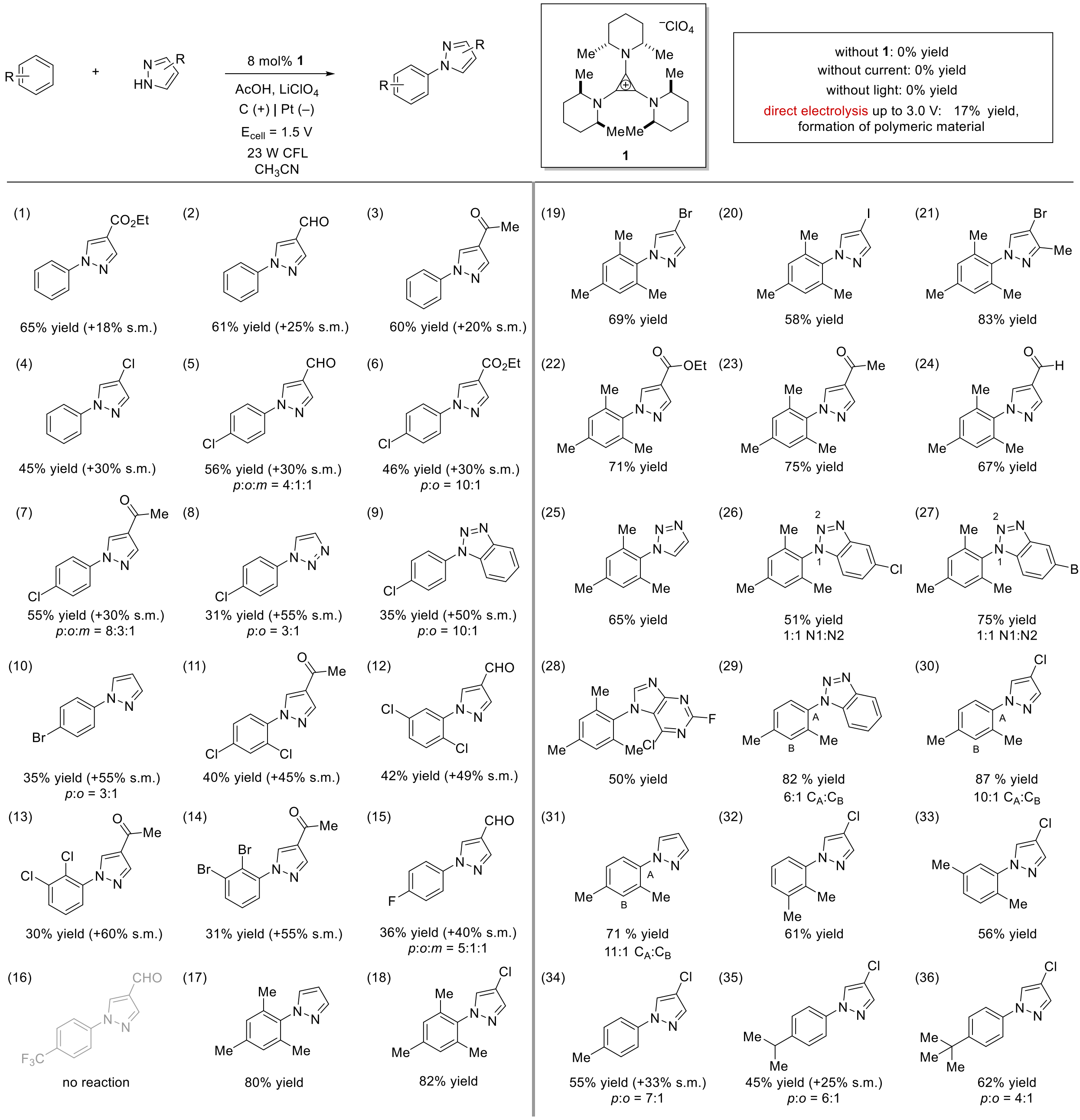
8 mol% 1
AcOH, LiClO4
C (+) | Pt (–)
Ecell = 1.5 V
23 W CFL
CH3CN
–ClO4
1
without 1: 0% yield
without current: 0% yield
without light: 0% yield
direct electrolysis up to 3.0 V: 17% yield, formation of polymeric material
(1) 65% yield (+18% s.m.)
(2) 61% yield (+25% s.m.)
(3) 60% yield (+20% s.m.)
(4) 45% yield (+30% s.m.)
(5) 56% yield (+30% s.m.) p:o:m = 4:1:1
(6) 46% yield (+30% s.m.) p:o = 10:1
(7) 55% yield (+30% s.m.) p:o:m = 8:3:1
(8) 31% yield (+55% s.m.) p:o = 3:1
(9) 35% yield (+50% s.m.) p:o = 10:1
(10) 35% yield (+55% s.m.) p:o = 3:1
(11) 40% yield (+45% s.m.)
(12) 42% yield (+49% s.m.)
(13) 30% yield (+60% s.m.)
(14) 31% yield (+55% s.m.)
(15) 36% yield (+40% s.m.) p:o:m = 5:1:1
(16) no reaction
(17) 80% yield
(18) 82% yield
(19) 69% yield
(20) 58% yield
(21) 83% yield
(22) 71% yield
(23) 75% yield
(24) 67% yield
(25) 65% yield
(26) 51% yield 1:1 N1:N2
(27) 75% yield 1:1 N1:N2
(28) 50% yield
(29) 82 % yield 6:1 CA:CB
(30) 87 % yield 10:1 CA:CB
(31) 71 % yield 11:1 CA:CB
(32) 61% yield
(33) 56% yield
(34) 55% yield (+33% s.m.) p:o = 7:1
(35) 45% yield (+25% s.m.) p:o = 6:1
(36) 62% yield p:o = 4:1

Table 4-1. Oxidative Coupling of Heterocycles to Arenes via Electrophotocatalysis with TAC **(1)**

A variety of pyrazoles were tolerated in this reaction, including those bearing esters, aldehydes, and ketones as well as halogenated pyrazoles (**Table 4-1**). Additionally, triazoles, benzotriazoles, and purines were found to be suitable coupling partners. We found that the catalyst was also capable of the oxidative functionalization of chlorobenzene, bromobenzene, as well as various dihalobenzenes. Even fluorobenzene was amenable to oxidative coupling (**Table 4-1** entry 15). However, trifluorotoluene was inert to these reaction conditions, suggesting that the arene is too deactivated to be oxidized by the photoexcited TAC radical cation. In addition to these challenging arenes, this method also works with more easily oxidized substrates such as mesitylene. However, anisole did not undergo coupling to any extent, which is unexpected given its electron-rich nature. However, other reports[221,222] have also found oxygen bearing arenes to be unreactive to photocatalysis and this phenomenon may be the result of facile back-electron transfer.[28]

It should be noted that for the reaction of benzene and the halobenzenes, the use of a divided H-cell, in which the electrodes were separated by a fine glass filter, resulted in higher yields (**Figure 4-6**). The divided cell likely allows all of the TAC in solution to be converted to its radical dication form, which can otherwise be reduced at the cathode. The depletion of unoxidized TAC in solution may be necessary for more difficult oxidations as the unoxidized TAC can presumably be “self”-oxidized by the photoexcited TAC radical dication. Therefore, limiting the concentration of unoxidized TAC in solution prevents competition with the substrate. For the more easily oxidized arenes such as mesitylene, an undivided cell was sufficient.

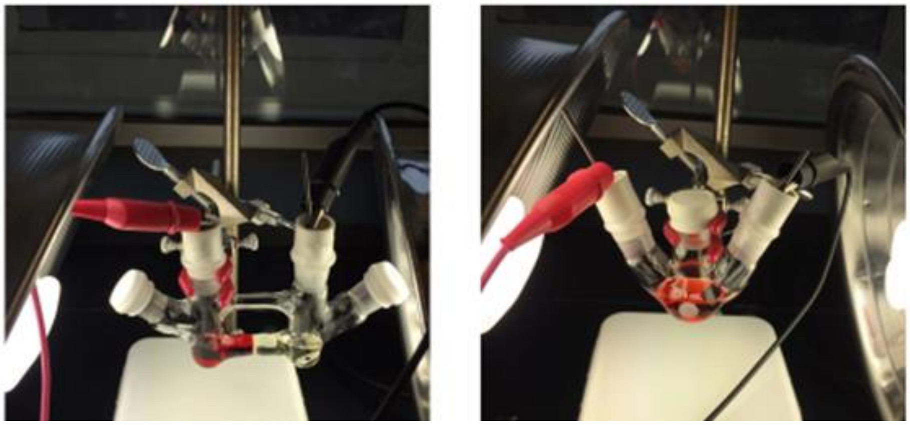

Figure 4-6. Electrophotocatalysis in Divided (left) and Undivided (right) Cells

From our battery experiments, we had identified THF and DME as potentially oxidizable substrates. As such, we predicted that oxidative electrophotocatalysis could also be employed with ethers as well. We found that the tetrhydorfuran (THF) and tetrahydropyran (THP) could undergo oxidative coupling with a variety of pyrazoles in good yields (**Table 4-2** entries 1-6) using electrophotocatlaysis with TAC (**1**). For this reaction, the ether was used as a cosolvent and the potential was increased to 2.0 V. In addition to pyrazoles, benzyl alcohol and acetates were found to be suitable coupling partners (entries 7-9). These oxidative coupling reactions presumably entail nucleophilic addition to an oxocarbenium intermediate. We considered that an alpha-oxy radical might be a precursor to the oxocarbenium intermediate and hypothesized that it might be possible to trap this radical with a suitable electrophile. In this case, we found that electrophotocatalysis with TAC (**1**) furnished the radical-mediated coupling of THF and 4-bromoisoquinoline in 75% yield (**Table 4-2** entry 10).

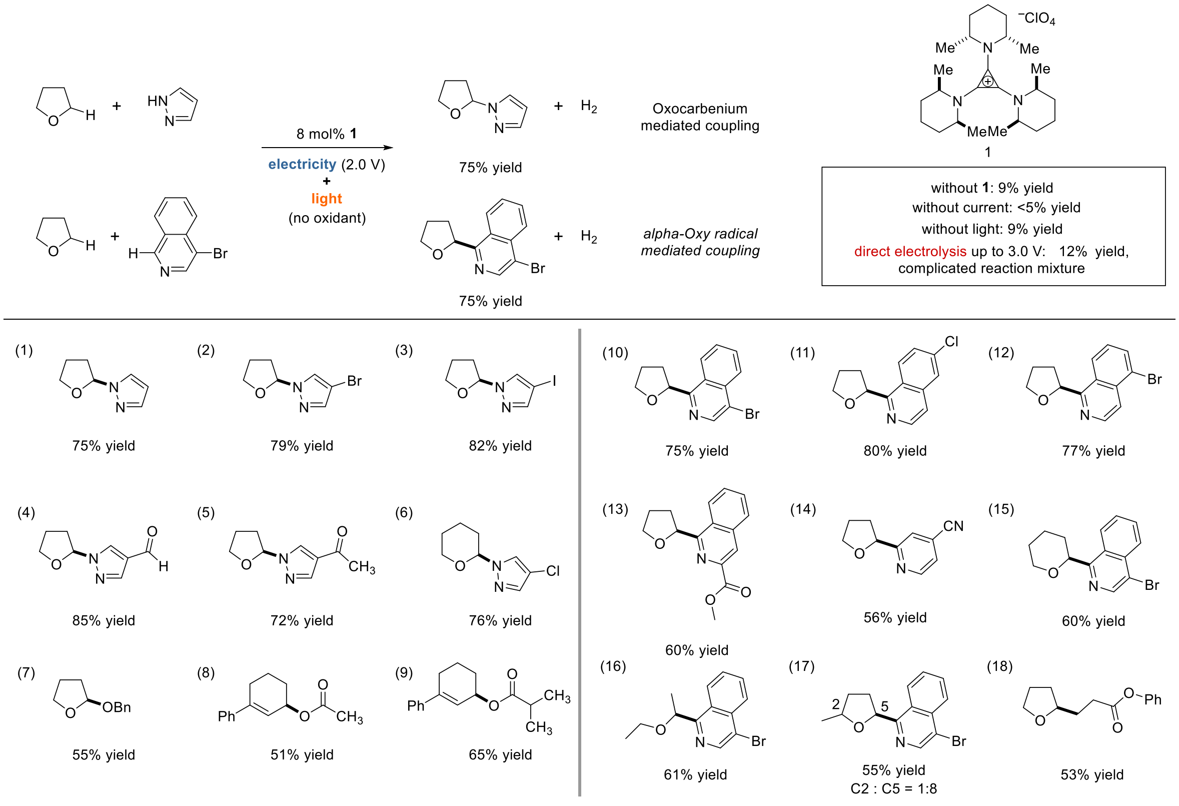
8 mol% 1
electricity (2.0 V)
+
light
(no oxidant)
+ H2
Oxocarbenium mediated coupling
alpha-Oxy radical mediated coupling
75% yield
75% yield
−ClO4
Me
1
without 1: 9% yield
without current: <5% yield
without light: 9% yield
direct electrolysis up to 3.0 V: 12% yield, complicated reaction mixture
(1) 75% yield
(2) 79% yield
(3) 82% yield
(4) 85% yield
(5) 72% yield
(6) 76% yield
(7) 55% yield
(8) 51% yield
(9) 65% yield
(10) 75% yield
(11) 80% yield
(12) 77% yield
(13) 60% yield
(14) 56% yield
(15) 60% yield
(16) 61% yield
(17) 55% yield
C2 : C5 = 1:8
(18) 53% yield
OBn
Ph
CH3
Br
Cl
I
CN
N

Table 4-2. Oxidative Coupling Reaction of Ethers via Electrophotocatalysis with TAC (**1**)

Once again, exclusion of the TAC, the light, or the current resulted in no more than trace conversion (<10%), while direct electrolysis led to minimal product formation and a complex mixture of products. A variety of isoquinoline partners were tolerated as well as 4-cyanopyridine (**Table 4-2** entry 14) and phenyl acrylate (**Table 4-2** entry 18).

A mechanistic rationale for these electrophotocatalytic reactions is shown in **Scheme 4-1**. Electrochemical oxidation of the TAC (**1)** generates the corresponding radical dication. Photoexcitation then leads to a highly reactive species that can oxidize an arene via SET, resulting in the reduced TAC. The arene radical cation can then undergo nucleophilic trapping by pyrazole with a concomitant loss of a proton. The resulting neutral radical adduct can undergo facile oxidation by either TAC (**1**), oxygen, or via the anode. Rearomatization via deprotonation then affords the coupled product. This mechanistic rationale is in agreement with previous reports of this type of arene-azole coupling.[219,220] However, it is plausible that in some cases the pyrazole substrates can also be oxidized given that they exist in a similar oxidation potential regime to some of the more difficult to oxidize arenes. This possibility seems unlikely because the arene is used in excess, the chemistry works even with strongly deactivated pyrazoles, and the reaction is run in the presence of both lithium cations and acid, both of which serve to prevent oxidation of the mildly basic pyrazoles. Alternatively, it is possible that oxidation of pyrazole occurs, but the back-electron transfer process is fast enough to prevent any observable reactivity.

Ethers can undergo H-atom transfer (HAT) by the photoexcited TAC (**1**) radical cation to furnish an alpha-oxy radical (**Scheme 4-1**). This radical can then add to a suitable electrophile (such as isoquinoline) or be further oxidized to the oxocarbenium and act as an electrophile for pyazole or other nucleophiles.

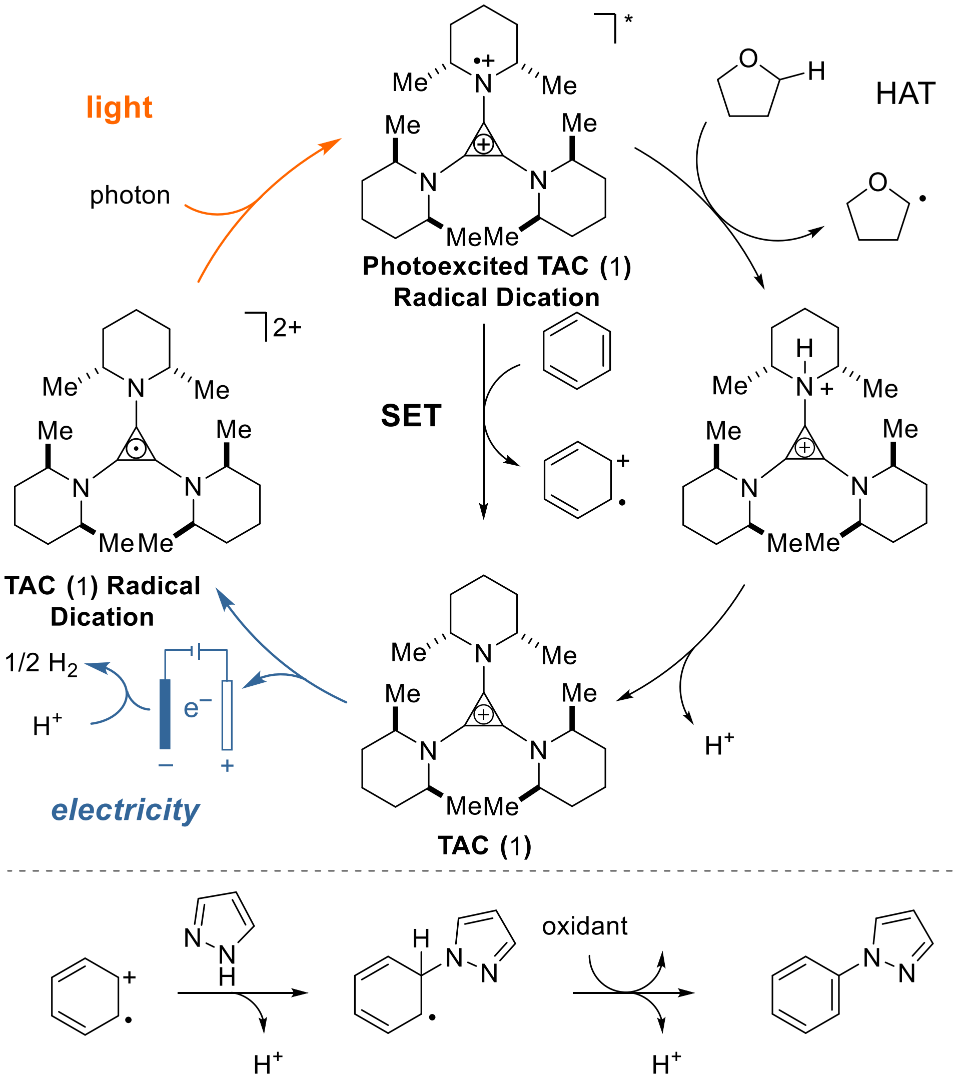
light
photon
Photoexcited TAC (1)
Radical Dication
HAT
SET
TAC (1) Radical
Dication
2+
*
1/2 H2
H+
e−
−
+
electricity
TAC (1)
H+
oxidant
H+
H+

Scheme 4-1. SET and HAT Mechanisms Involved in Electrophotocatalysis with TAC **(1)**

(4.4) Insights into Photoexcitation of the TAC Radical Dication

Despite such a strongly oxidizing character, TAC (**1**) is remarkably stable, with >95% of the catalyst remaining intact after a typical electrophotocatalytic reaction. To investigate this stability, we prepared X-ray quality crystals of the TAC (**1**) radical dication as the bis-perchlorate salt (**Figure 4-7**). Surprisingly, the crystal structure revealed that this molecule adopts a conformation that places all six methyl substituents in the axial position. This orientation presumably avoids what would otherwise be a severe allylic-type strain caused by the rigidity of the cyclopropenium ring. Notably, this conformation also places the piperidinyl alpha hydrogens in a sterically protected pocket adjacent to the plane of the cyclopropenium ring. The steric shielding of these protons renders them unavailable for deprotonation or H-atom abstraction, which is the primary degradation pathway of aminyl radical cations.

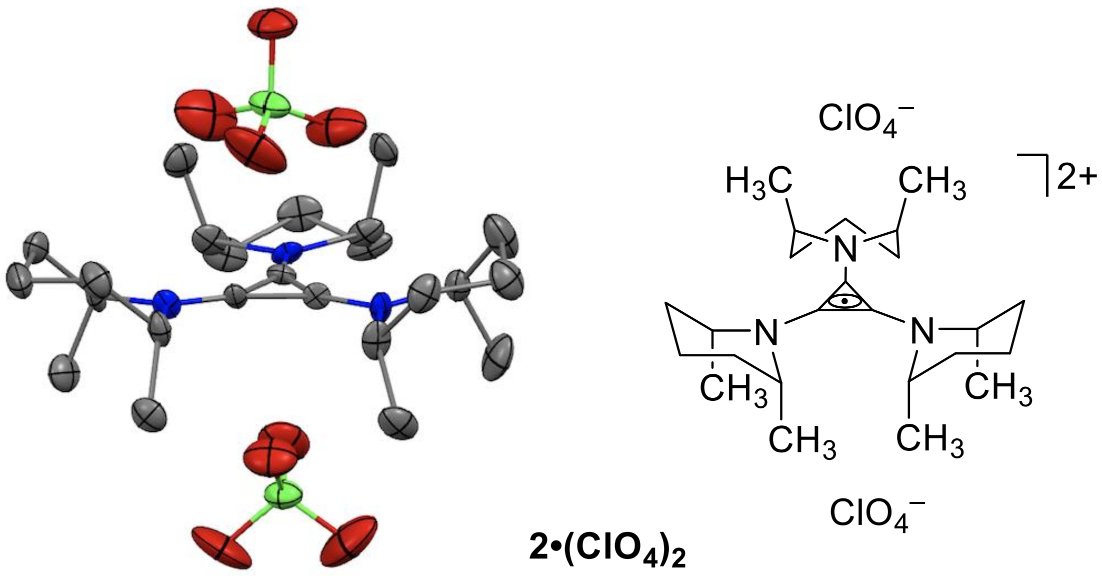

2•(ClO4)2

Figure 4-7. X-ray Crystal Structure of TAC **(1)** Radical Dication

Our optimization of these electrophotocatalytic reactions gave us many key insights into what conditions were important for reactivity (**Table 4-3**). We found that using a platinum cathode increased the yield of the reaction, presumably because it lowers the potential necessary for the reduction of acid. Acetonitrile was the best choice of solvent, with DMF and DCM both giving essentially no conversion. Acetonitrile has one of the widest redox windows of common solvents and is clearly the ideal choice for reaction with high redox potentials.[186] We found that 10 eq of acid gave the best yield, with 1 eq only giving 8% yield, which may be further evidence that acid prevents the oxidation of pyrazole in the reaction. Greater amounts of acid decreased the yield and stronger acid was also found to be deleterious to the reaction. We also found $LiClO_4$ to be the best choice of supporting electrolyte, with LiTFSI giving much worse yields, which could be in part due to the stability of the TAC radical dication with perchlorate counterions. Lastly, we found that simply using a white CFL light gave better yields than a green LED. We found this result perplexing given the fact that the catalyst absorbs most strongly in the green portion of visible spectrum. However, this effect may simply be due to the fact that the CFL was significantly brighter than the green LEDs that were used and that the TAC radical dication absorbs over a large portion of the visible spectrum (~380-600 nm).

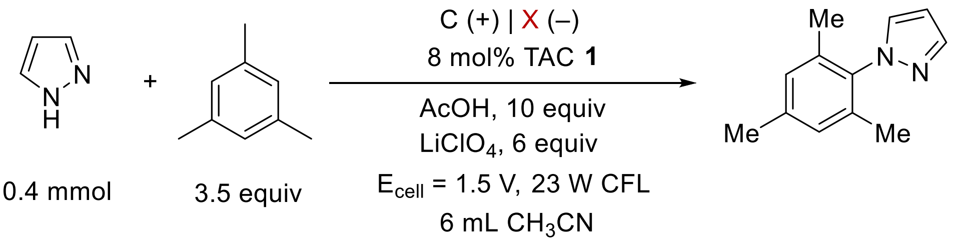

electrode material	**yield**
Pt	**80%**
C	**50%**

solvent	**yield**
CH_3CN	**80%**
DMF	**0%**
DCM	**trace**

light	**yield**
CFL	**80%**
green LED	**26%**

electrolyte	**yield**
$LiClO_4$	**80%**
LiTFSI	**<5%**
none	**0**

acid	**yield**
CH_3COOH, 1 equiv	**8%**
CH_3COOH, 10 equiv	**80%**
CH_3COOH, 100 equiv	**56%**
CF_3COOH, 10 equiv	**<5%**

Yields determined by ^1H NMR against CH_2Br_2

Table 4-3. Optimization of Conditions for Oxidative Arene Coupling

The TAC radical dication photocatalyst belongs to a unique class of photocatalyst in that its ground state is a doublet. Almost every traditional photocatalyst, whether it be a metal complex or an organic molecule, has a singlet ground state and undergoes photoexcitation to yield a triplet or singlet excited state.[27,28]

While a few recent publications have described radical anions that can behave as photocatalysts[58,59,223], we believe the TAC radical cation to be one of the first doublet species that operates as an oxidative photocatalyst. As such, we were intrigued by what potential mechanism would explain its photocatalytic activity. We used time-dependent density functional theory (TD-DFT) calculations to examine the frontier orbitals of a simplified TAC radical dication with dimethylamino substituents (**Figure 4-8**).

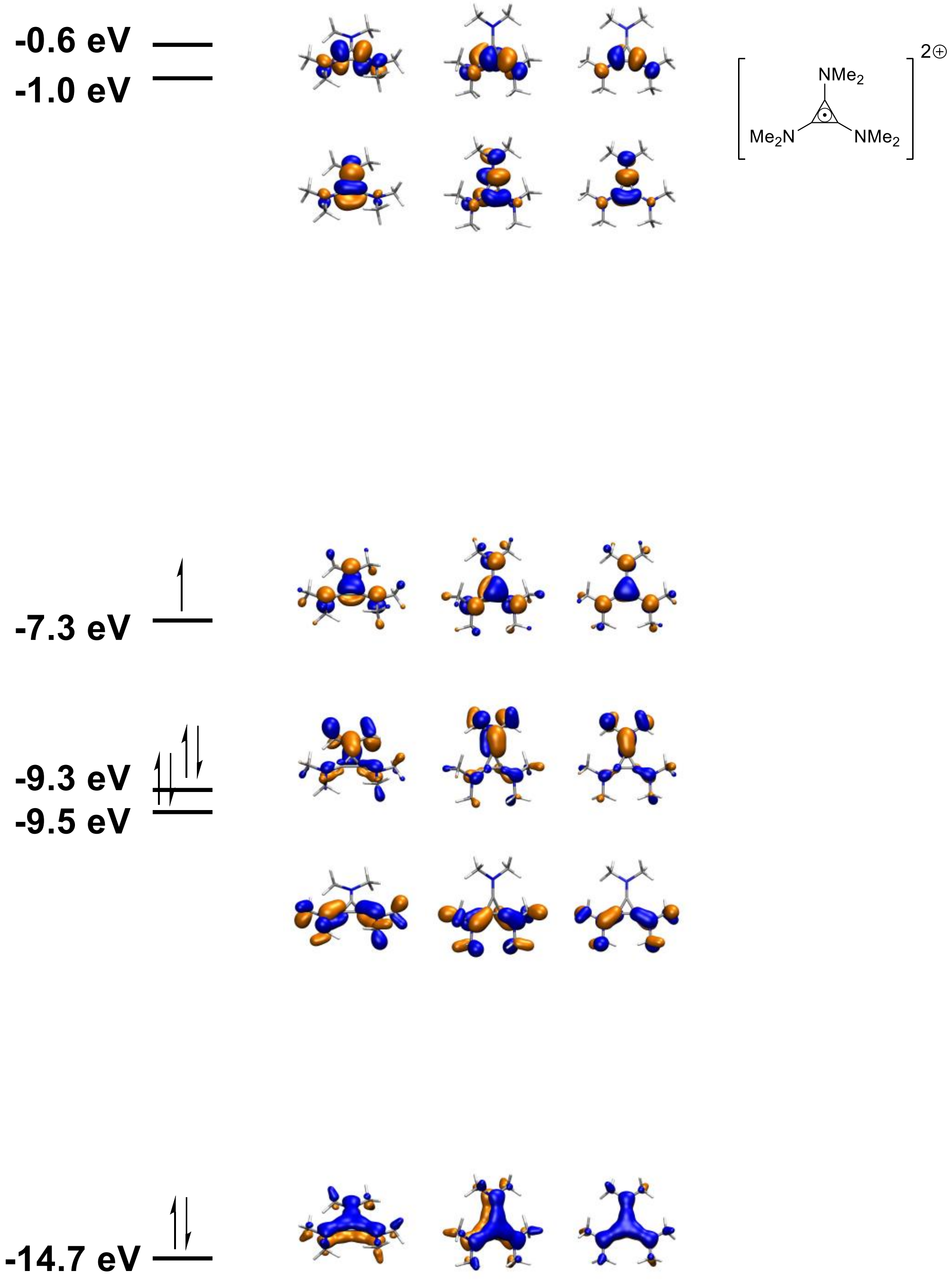
-0.6 eV
-1.0 eV
-7.3 eV
-9.3 eV
-9.5 eV
-14.7 eV
NMe2
Me2N
NMe2
2⊕

Figure 4-8. Molecular Orbitals of Simplified (NMe_2) TAC

These calculations revealed that the frontier molecular orbitals are composed of pi orbitals, which is perhaps unsurprising given that oxidation of the TAC would be most likely to occur in the molecular orbitals containing the three electron-rich nitrogen atoms. The SOMO is highly symmetric and contains an antibonding interaction between the cyclopropenium pi orbitals and the nitrogen pi orbitals. The LUMO and LUMO +1 are two degenerate orbitals composed of several antibonding interactions between pi orbitals that exists more than +6.0 V above the SOMO. The HOMO-1 and HOMO-2 are estimated to be around 2.0 V below the SOMO.

We considered three possible explanations for photoexcitation of the TAC radical dication: (1) excitation of the SOMO to one of the LUMOs, (2) excitation of one of the HOMO-1 and HOMO-2 orbitals to the SOMO, or (3) excitation of the counteranion to the SOMO. While a transition from the counteranion to the SOMO may seem unlikley, this behavior was seen in oxidized TACs with electron rich counteranions such as $SeCl_6^{2-}$.[109] To probe this, we prepared the oxidized TAC with various counteranions, but found that all had the same UV-VIS spectrum profile (**Figure 4-9**).

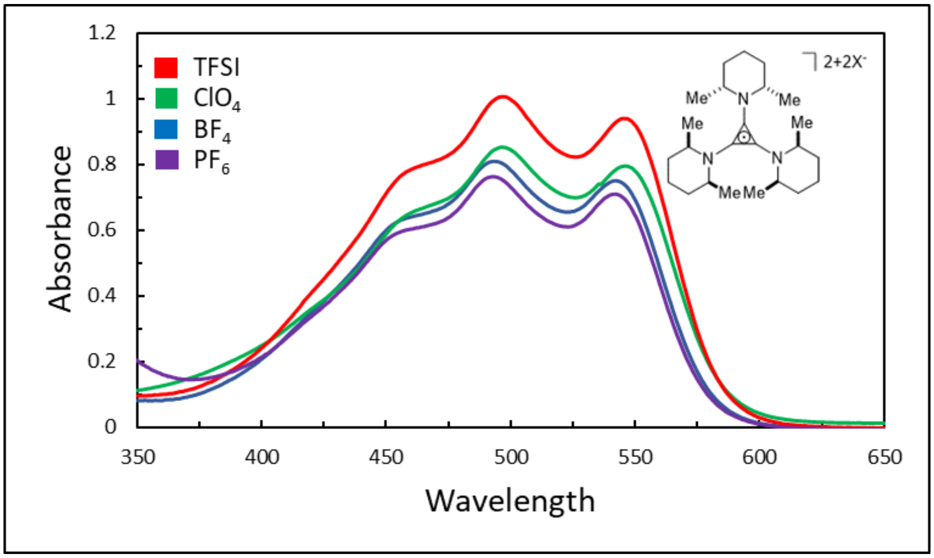

Figure 4-9. UV-VIS Spectra of TAC **(1)** Radical Dication with Various Anions

If the excitation were originating from the counterion, we would expect that changing the counterion would result in some change in the UV-VIS spectrum. While excitation of the SOMO to the LUMO seemed like a likely explanation as this is how traditional and radical anion photocatalysts work,[28,58,59,223] the gap between the SOMO and LUMO was predicted to be greater than 6.0 V apart. This large energy gap makes such a transition extremely unlikely and the energy required would correspond to wavelengths deep within the ultraviolet spectrum of light. Thus, excitation from the degenerate HOMO-1 and HOMO-2 orbitals to the SOMO seemed like the most likely explanation, a hypothesis that was also echoed in one of the earliest reports of the TAC radical dication by Weiss.[107] This phenomenon is rare, but has been reported under the term SOMO-inversion,[224] in which the promotion of an electron to the SOMO transfers the electron hole to a lower energy molecular orbital (**Figure 4-10**). The TD-DFT calculations predicted that the transitions from both the degenerate HOMO-1 and HOMO-2 orbitals to the SOMO had a large transition dipole moment, signifying a likely transition. The calculation also predicted the energy of this transition to be about 2.0 V, which is approximately where the TAC radical cation absorbs in the visible region (I_{max} = 500 nm).

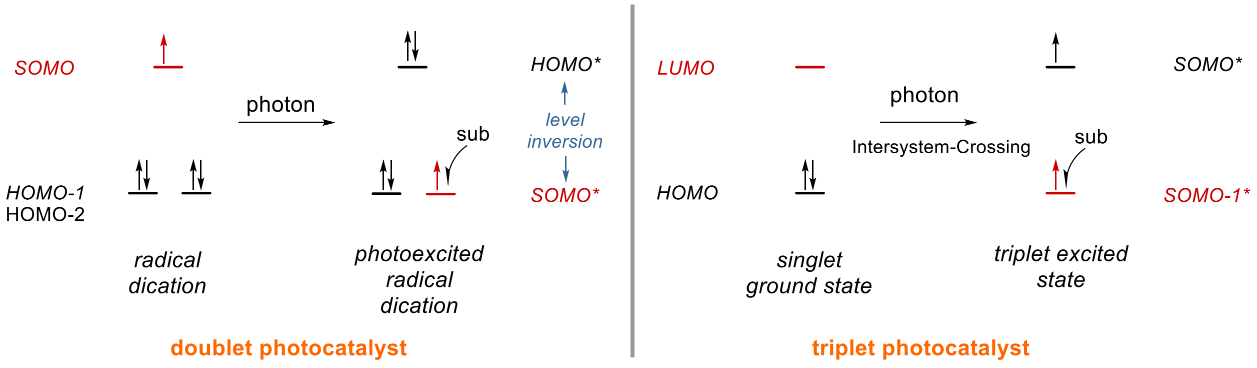
SOMO
HOMO-1
HOMO-2
photon
sub
HOMO*
level inversion
SOMO*
radical dication
photoexcited radical dication
doublet photocatalyst
LUMO
HOMO
photon
Intersystem-Crossing
sub
SOMO*
SOMO-1*
singlet ground state
triplet excited state
triplet photocatalyst

Figure 4-10. Comparing Doublet and Triplet Photocatalysts

One last piece of evidence that also suggests that this transition is responsible for the photoactivity is the shape of the absorption spectrum. Noticeably, the TAC radical cation absorbs from 380 nm to around 600 nm, which is almost the entirety of the visible spectrum. It also possesses three distinct maxima that occur at 50 nm intervals, which is indicative of vibronic coupling to the electronic transition (**Figure 4-9**). The IR spectra of this molecule did not reveal any prominent peaks at the correct energy for 50 nm. However, a Raman spectrum of the TAC radical dication did reveal a peak at 1870 wavenumbers, which matches the 50 nm spacing observed in the UV-VIS spectrum. DFT calculation revealed that this vibrational frequency corresponds to the expansion and contraction of cycloporpenium ring.[80] Due to the fact that there are significant interactions between the nitrogen pi orbitals and the cyclopropenium pi orbitals in the HOMO-1, HOMO-2, and SOMO, it follows that this vibrational mode would be coupled to an electronic transition between these orbitals.

Another notably odd feature the TAC radial dication photocatlayst is that it exhibits almost no fluorescence. Most traditional photocatalysts are typically quite fluorescent, which is due to the fact that the radiative relaxation pathway occurs faster than nonradiative pathways, which can be an indicator of a long-lived excited state. Due to the fact that the TAC is a very flexible molecule, including several active vibrational and rotational modes, it is perhaps unsurprising that the TAC's primary relaxation pathway occurs via internal conversion. We found that fluorescence measurements were nearly impossible due to the fact that intensity of the fluorescence was barely detectable above the background noise. However, the TAC became much more fluorescent at cryogenic temperatures (**Figure 4-11**), indicating that decreasing the availability of the TAC's vibrational modes led to partial deactivation of the nonradiative decay pathway. Using a perchloric acid as a cryogenic glassing solvent, we were able to more reliably measure the fluorescence lifetime at 2 ns at 77 K (**Figure 4-12**).

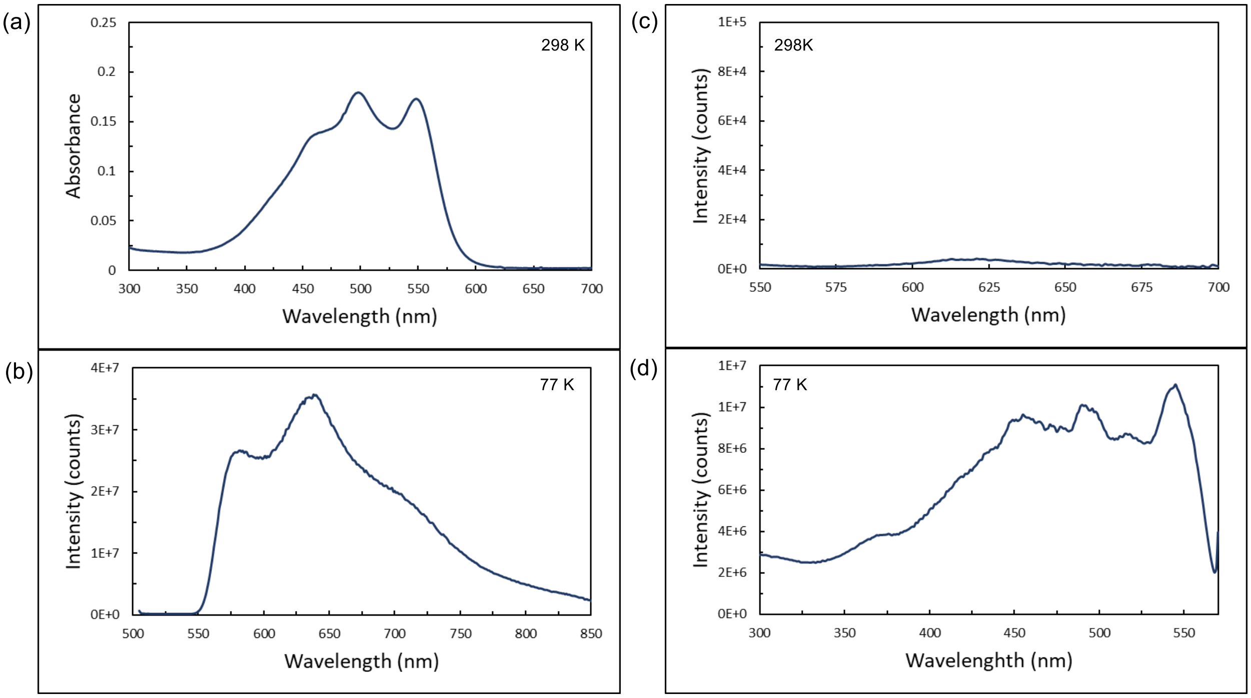

Figure 4-11. TAC **(1)** Radical Dication Fluorescence Data in $HClO_4$ (a) UV-VIS (298 K), (b) Fluorescence Emission (Excitation: 500 nm, 298 K), (c) Fluorescence Emission (Excitation: 500 nm, 77 K), (d) Fluorescence Excitation (Emission: 650 nm, 77K)

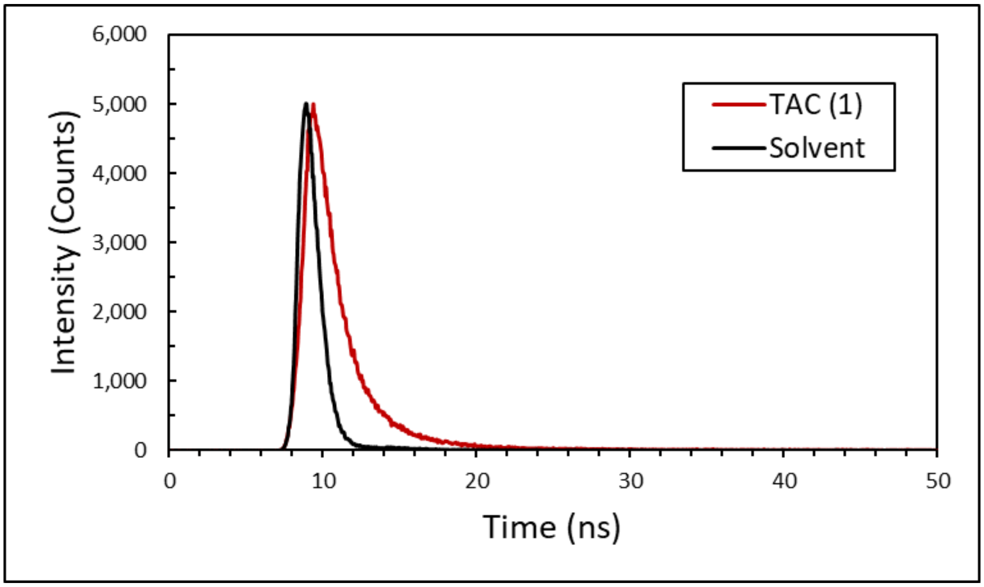

Figure 4-12. Fluorescence Lifetime of TAC **(1)** Radical Dication in Concentrated $HClO_4$ at 77 K

We also found that excitation at multiple wavelengths in the absorbance region of the TAC led to the same fluorescence profile, indicating that the excited electron relaxes to the same vibrational mode before radiatively decaying to the ground electronic state.

It should be noted that since nonradiative decay is the predominant relaxation pathway for the TAC at room temperature, the average excited-state lifetime of the catalysts is most likely far below 2 ns. The short excited-state lifetime is one potential factor that explains why several of the reactions require such a protracted reaction time. It has been noted that lifetimes below 1 ns are unlikely to undergo photoinduced electron transfer because it approaches the diffusion limit.[28] However, there are other examples of photocatalysts have been shown to function on sub-nanosecond excited state lifetimes and still promote light-induced reactions.[59] One possible explanation is that the substrates preassociate with the TAC radical dication before oxidation occurs. Thus, the photoinduced electron transfer would not be limited by diffusion of the excited state catalyst. Conceivably, substrates such as benzene, mesitylene, and THF could associate with the hydrophobic region of the TAC N-alkyl groups. This effect would be further exacerbated in the highly polar medium in which these reactions take place ($LiClO_4$/AcOH/acetonitrile solution). Further study is clearly required to elaborate how this catalyst is able to interact substrates and effect the reactions that have been shown given its presumably short-lived excited state. One also wonders whether the kinetics of these reactions could be increased by further sterically immobilizing the TAC structure, thus deactivating the rapid relaxation caused through internal conversion.

(4.5) Highthroughput Reaction Screening with the TAC Radical Dication

Lastly, one disadvantage of electrochemical reactions is their incompatibility with high throughput screening (HTS). HTS has been proved to be an immensely powerful technique in a variety of fields such as method development, enzymatic mutation, and finding pharmaceutical leads.[225–228] Due to the stability of the TAC radical cation, we considered the possibility of isolating large quantities of the charged species to enable HTS methodology in order to quickly evaluate the scope of a method or to find new reactivity. We found that the TAC (**1**) radical dication could be produced via direct electrolysis of the TAC (**1**) in $LiClO_4$/ACN solution with 10 eq of AcOH at 2.0 V using a Daramic separator (**Figure 4-13**). Electrolysis was allowed to maintain until the current dropped to 0.1 mA, at which point the solution was concentrated and the charged TAC was separated from the salts in solution via extraction into DCM.

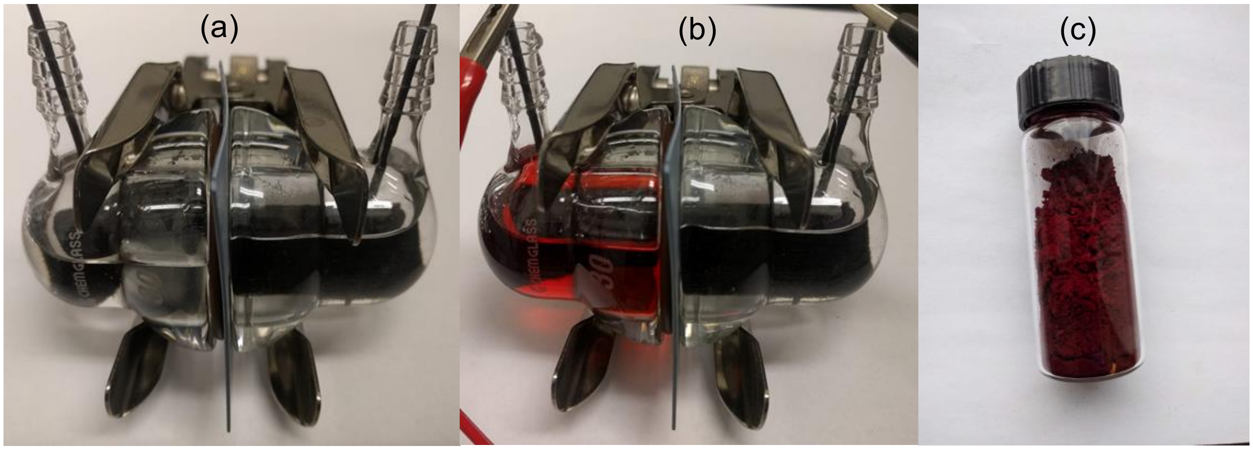

Figure 4-13. Bulk Electrolysis of TAC **(1)**, (a) Before Electrolysis, (b) Electrolysis Initiated, (c) Isolated TAC **(1)** Radical Dication

UV-VIS analysis of the red powder showed that it was around 90% purity, with the remaining weight presumably being made up of uncharged TAC (**1**), $LiClO_4$, and acetic acid. The charged TAC could then be dosed into 96 well plates with various reactants and illuminated by a CFL in order to simulate the conditions that would be present in our typical reaction setup (**Figure 4-14**).

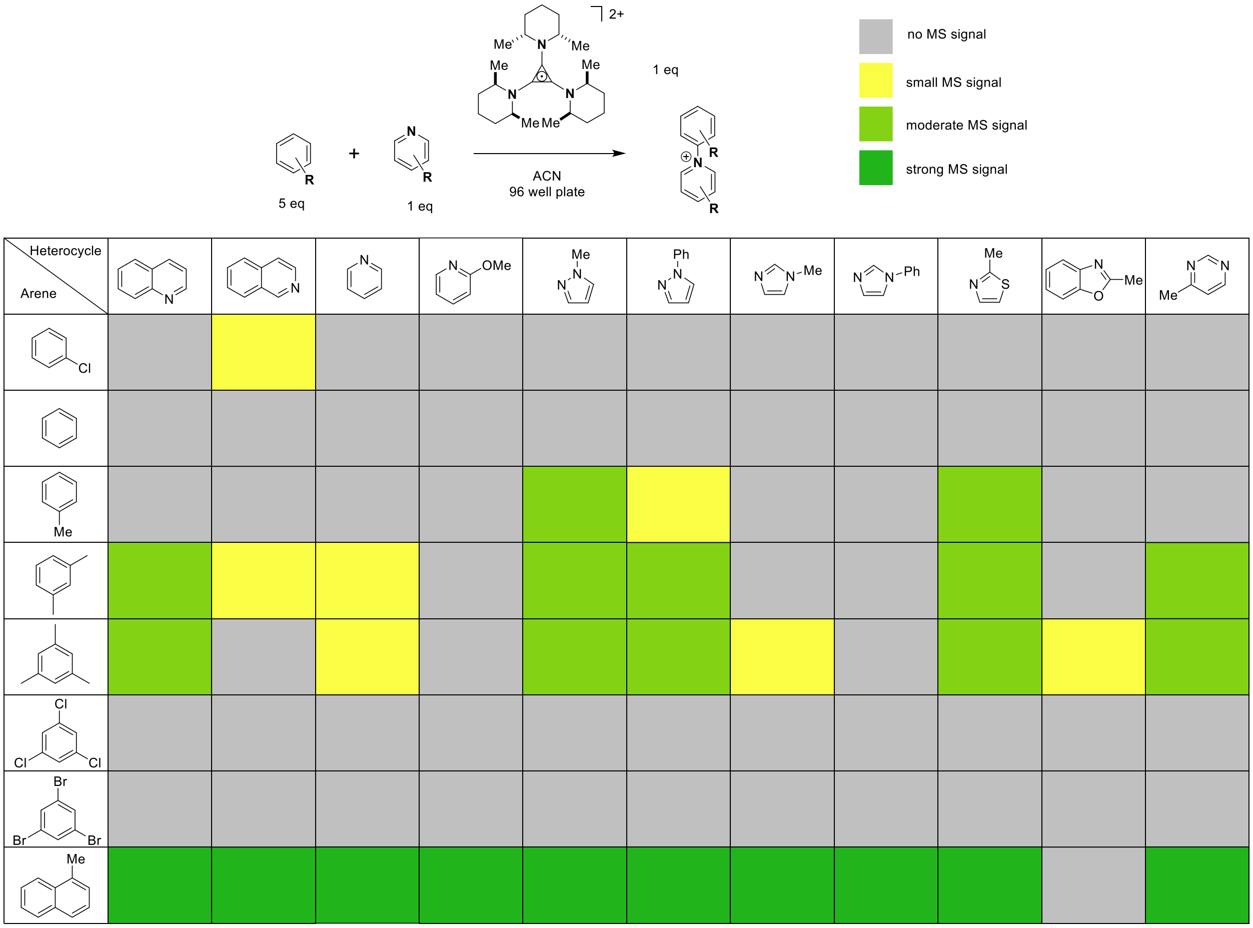
2+
Me
N
1 eq
R
5 eq
+
ACN
96 well plate
no MS signal
small MS signal
moderate MS signal
strong MS signal
Heterocycle
Arene
OMe
Ph
S
O
Cl
Br

Figure 4-14. Highthroughput Screening Using Isolate TAC **(1)** Radical Dication

We found this to be an effective method to quickly screen reactions, using LCMS to analyze the products of the reactions. One reaction we discovered using this method was the coupling of aprotic nitrogenous heterocycles with arenes, resulting in cationic NHC-precursor type products (**Figure 4-14**). We found that this reaction works with a variety of heterocycles and arenes.

In conclusion, we have found the TAC to be an effective electrophotocatalyst, capable of bearing both electrochemical and photochemical energy to yield a highly oxidizing catalyst. We found that this catalyst was capable of oxidizing inert arenes such as toluene, benzene, and fluorobenzene and could affect their coupling to a variety of N-heterocycles. Furthermore, the TAC was also found to promote oxidative reaction of ethers, both through SET and HAT mechanisms. The photoreactivity of this catalyst stems from a photoinduced SOMO inversion, producing a excited-state oxidation potential of +3.3 V. As this catalyst can be simply prepared on a multigram scale from commercially available starting materials, we believe that it will be a broadly useful photo- and electrocatalyst.

REFERENCES

(1) Walker, R. W. *Sci. Prog.* **1990**, *74* (2), 163.

(2) Stone, D.; Whalley, L. K.; Heard, D. E. *Chem. Soc. Rev.* **2012**, *41* (19), 6348.

(3) Lubitz, W.; Lendzian, F.; Bittl, R. *Acc. Chem. Res.* **2002**, *35* (5), 313.

(4) Cadenas, E. *Mol. Aspects Med.* **2004**, *25* (1-2), 17.

(5) Romero, K. J.; Galliher, M. S.; Pratt, D. a.; Stephenson, C. R. J. *Chem. Soc. Rev.* **2018**, *47* (21), 7851.

(6) Grubbs, R. B. *Polym. Rev.* **2011**, *51* (2), 104.

(7) Wilcox, D. a.; Agarkar, V.; Mukherjee, S.; Boudouris, B. W. *Annu. Rev. Chem. Biomol. Eng.* **2018**, *9* (1), 83.

(8) Gomberg, M. *J. Am. Chem. Soc.* **1900**, *22* (11), 757.

(9) Yan, M.; Lo, J. C.; Edwards, J. T.; Baran, P. S. **2016**.

(10) Kolbe, H. *Ann. Chem. Pharma.* **1848**, *64*, 339.

(11) Hofmann, A. W. *Ber. Dtsch. Chem. Ges.* **1885**, *18*, 5.

(12) Kharasch, M. S.; McNab, M. C.; Mayo, F. R. *J. Am. Chem. Soc.* **1933**, *55* (6), 2521.

(13) Kharasch, M. S.; Engelmann, H.; Mayo, F. R. *J. Org. Chem.* **1937**, *2* (3), 288.

(14) Birch, A. J. *Online* **1942**, No. 430, 430.

(15) KERK, G. J. M. VAN DER; LUIJTEN, J. G. A. *J. appl. Chem.* **1956**, *6*, 49.

(16) Kuivila, H. G. *Acc. Chem. Res.* **1968**, *1* (10), 299.

(17) Kulvlla, H. G. *Adv. Organomet. Chem.* **1964**, *1*, 47.

(18) Griller, D.; Ingold, K. U. *Acc. Chem. Res.* **1976**, *9* (1), 13.

(19) Griller, D.; Ingold, K. U. *Acc. Chem. Res.* **1980**, *13* (9), 317.

(20) Newcomb, M. *Tetrahedron* **1993**, *49* (6), 1151.

(21) Roessler, M. M.; Salvadori, E. *Chem. Soc. Rev.* **2018**, *47* (8), 2534.

(22) Hey, D. H.; Perkins, M. J. *Tetrahedron Lett.* **1963**, *9* (7), 445.

(23) Perkins, M. J. *J. Chem. Soc.* **1964**, No. 0, 5932.

(24) Matyjaszewski, K. *Macromolecules* **2012**, *45* (10), 4015.

(25) Yan, M.; Kawamata, Y.; Baran, P. S. *Chem. Rev.* **2017**, *117* (21), 13230.

(26) Francke, R.; Little, R. D. *Chem. Soc. Rev.* **2014**, *43* (8), 2492.

(27) Prier, C. K.; Rankic, D. a.; MacMillan, D. W. C. *Chem. Rev.* **2013**, *113* (7), 5322.

(28) Romero, N. a.; Nicewicz, D. a. *Chem. Rev.* **2016**, *116* (17), 10075.

(29) Shaw, M. H.; Twilton, J.; MacMillan, D. W. C. *J. Org. Chem.* **2016**, *81* (16), 6898.

(30) Twilton, J.; Le, C. C.; Zhang, P.; Shaw, M. H.; Evans, R. W.; MacMillan, D. W. C. *Nat. Rev. Chem.* **2017**, *1*.

(31) Renaud, P.; Sibi, M. P. *Radicals in Organic Synthesis*; WILEY-VCH Verlag GmbH, 2001.

(32) Danen, W. C.; Saunders, D. G. *J. Am. Chem. Soc.* **2005**, *91* (21), 5924.

(33) Capaldo, L.; Ravelli, D. *European J. Org. Chem.* **2017**, *2017* (15), 2056.

(34) Broggi, J.; Terme, T.; Vanelle, P. *Angew. Chemie - Int. Ed.* **2014**, *53* (2), 384.

(35) Nair, V.; Deepthi, A. *Chem. Rev.* **2007**, *107* (5), 1862.

(36) Connelly, N. G.; Geiger, W. E. *Chem. Rev.* **1996**, *96* (2), 877.

(37) Hicks, R. G. *Org. Biomol. Chem.* **2007**, *5* (9), 1321.

(38) Armstrong, C. G.; Toghill, K. E. *Electrochem. commun.* **2018**, *91* (April), 19.

(39) Andersen, P. *Acta. Chem. Scand.* **1965**, *19*, 629.

(40) Andersen, P.; Klewe, B. *Acta Crystallogr. Sect. D Biol. Crystallogr.* **1967**, *21*, 2599.

(41) Kahr, B.; Van Engen, D.; Gopalan, P. *Chem. Mater.* **1993**, *5* (5), 729.

(42) Falle, H. R.; Luckhurst, G. R.; Horsfield, a.; Ballester, M. *J. Chem. Phys.* **2004**, *50* (1), 258.

(43) Veciana, J.; Carilla, J.; Miravitlles, C.; Molins, E. *J. Chem. Soc. Chem. Commun.* **1987**, No. 11, 812.

(44) Quiroz-Guzman, M.; Brown, S. N. *Acta Crystallogr. Sect. C Cryst. Struct. Commun.* **2010**, *66* (7).

(45) Bell, A.; Ledwith, A.; Laboratories, D. *J. Chem. Soc.* **1969**, 2719.

(46) Earle, M. J.; Vibert, A.; Jahn, U. *Encycl. Reag. Org. Synth.* **2011**.

(47) Jia, X.; Lü, S.; Yuan, Y.; Zhang, X.; Zhang, L.; Luo, L. *Org. Biomol. Chem.* **2017**, *15* (14), 2931.

(48) Liu, J.; Liu, F.; Zhu, Y.; Ma, X.; Jia, X. *Org. Lett.* **2015**, *17* (6), 1409.

(49) Wang, Y.; Peng, F.; Liu, J.; Huo, C.; Wang, X.; Jia, X. *J. Org. Chem.* **2015**, *80* (1), 609.

(50) Neumann, W. P.; Uzick, W.; Zarkadis, A. K. *J. Am. Chem. Soc.* **1986**, *108* (13), 3762.

(51) Reid, D. H. *Tetrahedron* **1958**, *3* (3), 339.

(52) Sogo, P. B.; Nakazaki, M.; Calvin, M. *J. Chem. Phys.* **1957**, *26* (5), 1343.

(53) Shirman, E.; Ustinov, A.; Ben-shitrit, N.; Weissman, H.; Iron, M. a. *J. Phys. Chem. B* **2008**, *16* (Figure 1), 1.

(54) Peurifoy, S. R.; Castro, E.; Liu, F.; Zhu, X. Y.; Ng, F.; Jockusch, S.; Steigerwald, M. L.; Echegoyen, L.; Nuckolls, C.; Sisto, T. J. *J. Am. Chem. Soc.* **2018**, *140* (30), 9341.

(55) Lü, B.; Chen, Y.; Li, P.; Wang, B.; Müllen, K.; Yin, M. *Nat. Commun.* **2019**, *10* (1), 1.

(56) Wang, Z.; Zheng, N.; Zhang, W.; Yan, H.; Xie, Z.; Ma, Y.; Huang, F.; Cao, Y. *Adv. Energy Mater.* **2017**, *7* (15), 1.

(57) Milton, M.; Cheng, Q.; Yang, Y.; Nuckolls, C.; Hernández Sánchez, R.; Sisto, T. J. *Nano Lett.* **2017**, *17* (12), 7859.

(58) Ghosh, I.; Ghosh, T.; Bardagi, J. I.; König, B. *Science (80-.).* **2014**, *346* (6210), 725 LP.

(59) Marchini, M.; Gualandi, A.; Mengozzi, L.; Franchi, P.; Lucarini, M.; Cozzi, P. G.; Balzani, V.; Ceroni, P. *Phys. Chem. Chem. Phys.* **2018**, *20* (12), 8071.

(60) Nutting, J. E.; Rafiee, M.; Stahl, S. S. *Chem. Rev.* **2018**, *118* (9), 4834.

(61) Zhou, Z.; Liu, L. *Curr. Org. Chem.* **2014**, *18* (4), 459.

(62) Studer, A. *Angew. Chemie Int. Ed.* **2000**, *39* (6), 1108.

(63) Schulte, T.; Studer, A. *Macromolecules* **2003**, *36* (9), 3078.

(64) Studer, A.; Harms, K.; Knoop, C.; Müller, C.; Schulte, T. *Macromolecules* **2004**, *37* (1), 27.

(65) Tebben, L.; Studer, A. *Angew. Chemie - Int. Ed.* **2011**, *50* (22), 5034.

(66) Fisher, E. L.; Lambert, T. H. *Org. Lett.* **2009**, *11* (18), 4108.

(67) Gheewala, C. D.; Radtke, M. A.; Hui, J.; Hon, A. B.; Lambert, T. H. *Org. Lett.* **2017**, *19* (16), 4227.

(68) Radtke, M. A.; Dudley, C. C.; O'Leary, J. M.; Lambert, T. H. *Synth.* **2019**, *51* (5), 1135.

(69) Gheewala, C. D.; Collins, B. E.; Lambert, T. H. *Science (80-.).* **2016**, *351* (6276), 961 LP.

(70) Gheewala, C. D.; Hirschi, J. S.; Lee, W. H.; Paley, D. W.; Vetticatt, M. J.; Lambert, T. H. *J. Am. Chem. Soc.* **2018**, *140* (10), 3523.

(71) Radtke, M. A.; Lambert, T. H. *Chem. Sci.* **2018**, *9* (30), 6406.

(72) Breslow, R. *J. Am. Chem. Soc.* **1957**, *79* (19), 5318.

(73) Komatsu, K.; Kitagawa, T. *Chem. Rev.* **2003**, *103* (4), 1371.

(74) Kelly, B. D.; Lambert, T. H. *J. Am. Chem. Soc.* **2009**, *131* (39), 13930.

(75) Hardee, D. J.; Kovalchuke, L.; Lambert, T. H. *J. Am. Chem. Soc.* **2010**, *132* (14), 5002.

(76) Vanos, C. M.; Lambert, T. H. *Chem. Sci.* **2010**, *1* (6), 705.

(77) Kelly, B. D.; Lambert, T. H. *Org. Lett.* **2011**, *13* (4), 740.

(78) Vanos, C. M.; Lambert, T. H. *Angew. Chemie - Int. Ed.* **2011**, *50* (51), 12222.

(79) Nacsa, E. D.; Lambert, T. H. *Org. Lett.* **2013**, *15* (1), 38.

(80) Mishiro, K.; Hu, F.; Paley, D. W.; Min, W.; Lambert, T. H. *European J. Org. Chem.* **2016**, *2016* (9), 1655.

(81) Bandar, J.; Lambert, T. *Synth.* **2013**, *45* (18), 2485.

(82) Kaljurand, I.; Kütt, A.; Sooväli, L.; Rodima, T.; Mäemets, V.; Leito, I.; Koppel, I. a. *J. Org. Chem.* **2005**, *70* (3), 1019.

(83) Bandar, J. S.; Lambert, T. H. *J. Am. Chem. Soc.* **2012**, *134* (12), 5552.

(84) Bandar, J. S.; Lambert, T. H. *J. Am. Chem. Soc.* **2013**, *135* (32), 11799.

(85) Bandar, J. S.; Sauer, G. S.; Wulff, W. D.; Lambert, T. H.; Vetticatt, M. J. *J. Am. Chem. Soc.* **2014**, *136* (30), 10700.

(86) Bandar, J. S.; Barthelme, A.; Mazori, A. Y.; Lambert, T. H. *Chem. Sci.* **2015**, *6* (2), 1537.

(87) Nacsa, E. D.; Lambert, T. H. *J. Am. Chem. Soc.* **2015**, *137* (32), 10246.

(88) Bandar, J. S.; Tanaset, A.; Lambert, T. H. *Chem. - A Eur. J.* **2015**, *21* (20), 7365.

(89) Jiang, Y.; Freyer, J. L.; Cotanda, P.; Brucks, S. D.; Killops, K. L.; Bandar, J. S.; Torsitano, C.; Balsara, N. P.; Lambert, T. H.; Campos, L. M. *Nat. Commun.* **2015**, *6*, 1.

(90) Paren, B. a.; Raghunathan, R.; Knudson, I. J.; Freyer, J. L.; Campos, L. M.; Winey, K. I. *Polym. Chem.* **2019**.

(91) Bruns, H.; Patil, M.; Carreras, J.; Vázquez, A.; Thiel, W.; Goddard, R.; Alcarazo, M. *Angew. Chemie - Int. Ed.* **2010**, *49* (21), 3680.

(92) Kozma, Á.; Gopakumar, G.; Farès, C.; Thiel, W.; Alcarazo, M. *Chem. - A Eur. J.* **2013**, *19* (11), 3542.

(93) Curnow, O. J.; MacFarlane, D. R.; Walst, K. J. *Chem. Commun. (Cambridge, United Kingdom)* **2011**, *47* (37), 10248.

(94) Litterscheidt, J.; Judge, P.; Bühlmeyer, A.; Bader, K.; Bandar, J. S.; Lambert, T.; Laschat, S. *Liq. Cryst.* **2018**, *45* (8), 1250.

(95) Walst, K. J.; Yunis, R.; Bayley, P. M.; MacFarlane, D. R.; Ward, C. J.; Wang, R.; Curnow, O. J. *RSC Adv.* **2015**, *5* (49), 39565.

(96) Merling, G. *Berichte der Dtsch. Chem. Gesellschaft* **1891**, *24* (2), 3108.

(97) Doering, W. V. E.; Knox, L. H. *J. Am. Chem. Soc.* **1954**, *76* (12), 3203.

(98) Lyons, D. J. M.; Crocker, R. D.; Blümel, M.; Nguyen, T. V. *Angew. Chemie - Int. Ed.* **2017**, *56* (6), 1466.

(99) Katz, T. J. *J. Am. Chem. Soc.* **1960**, *82* (14), 3784.

(100) Flanigan, D. M.; Romanov-Michailidis, F.; White, N. a.; Rovis, T. *Chem. Rev.* **2015**, *115* (17), 9307.

(101) Culshaw, P. N.; Walton, J. C.; Hughes, L.; Ingold, K. U. *J. Chem. Soc. Perkin Trans. 2* **2004**, *4* (5), 879.

(102) Kieslich, W.; Kurreck, H. *J. Am. Chem. Soc.* **2005**, *106* (16), 4328.

(103) Thépot, J. Y.; Lapinte, C. *J. Organomet. Chem.* **2002**, *656* (1-2), 146.

(104) Sitzmann, H.; Dezember, T.; Bock, H.; Havlas, Z.; Zanathy, L.; Boese, R.; Kaim, W.; Moscherosch, M. *J. Am. Chem. Soc.* **1993**, *115* (25), 12003.

(105) Yoshida, Z. I.; Tawara, Y. *J. Am. Chem. Soc.* **1971**, *93* (10), 2573.

(106) Gerson, F.; Plattner, G.; Yoshida, Z. *Mol. Phys.* **2006**, *21* (6), 1027.

(107) Weiss, R. *Tetrahedron Lett.* **1975**, No. 40, 3491.

(108) Johnson, R. *Tetrahedron Lett.* **1976**, No. 8, 589.

(109) Pairs, O. O. I.; Weiss, R. **2013**, No. Iv.

(110) Sevov, C. S.; Samaroo, S. K.; Sanford, M. S. *Adv. Energy Mater.* **2017**, *7* (5).

(111) Hendriks, K. H.; Robinson, S. G.; Braten, M. N.; Sevov, C. S.; Helms, B. a.; Sigman, M. S.; Minteer, S. D.; Sanford, M. S. *ACS Cent. Sci.* **2018**, *4* (2), 189.

(112) Potts, K. T.; Baum, J. S. *Chem. Rev.* **1974**, *74* (2), 189.

(113) Baird, M. S.; Bushby, R. J.; Butenschön, H.; Hopf, H. *Houben-Weyl Methods of Organic Chemistry Vol. E 17d, 4th Edition Supplement: Carbocyclic Three-Membered Ring Compounds, Cyclopropenes, Author Index, Compound Index*, 4th ed.; Meijere, A. de, Ed.; Georg Thieme Verlag, 2014.

(114) Maas, G.; Stang, P. J. *J. Org. Chem.* **1983**, *48* (18), 3038.

(115) Nutting, J. E.; Rafiee, M.; Stahl, S. S. *Chem. Rev.* **2018**, *118* (9), 4834.

(116) Roth, H. G.; Romero, N. a.; Nicewicz, D. a. *Synlett* **2016**, *27* (5), 714.

(117) Barton, D. H. R.; Le Gloahec, V. N. *Tetrahedron* **1998**, *54* (51), 15457.

(118) Gentilini, C.; Franchi, P.; Mileo, E.; Polizzi, S.; Lucarini, M.; Pasquato, L. *Angew. Chemie - Int. Ed.* **2009**, *48* (17), 3060.

(119) Acton, A.; Allen, A. D.; Fedorov, A. V.; Henry-Riyad, H.; Tidwell, T. T. *J. Phys. Org. Chem.* **2006**, *19* (12), 841.

(120) Clore, G. M.; Iwahara, J. *Chem. Rev.* **2009**, *109* (9), 4108.

(121) Nilssonsj, U. a; Olssonti, L.; Carlinfi, G. *Biochemistry* **1989**, 0.

(122) Mitchell, J. B.; Samuni, A.; Krishna, M. C.; DeGraff, W. G.; Ahn, M. S.; Samuni, U.; Russo, A. *Biochemistry* **1990**, *29* (11), 2802.

(123) Lafon-Cazal, M.; Pietri, S.; Culcasi, M.; Bockaert, J. *Nature* **1993**, *364* (6437), 535.

(124) Venditti, E.; Scirè, A.; Tanfani, F.; Greci, L.; Damiani, E. *Biochim. Biophys. Acta - Gen. Subj.* **2008**, *1780* (1), 58.

(125) Zhang, Z.; Chen, P.; Murakami, T. N.; Zakeeruddin, S. M.; Grätzel, M. *Adv. Funct. Mater.* **2008**, *18* (2), 341.

(126) Nakahara, K.; Oyaizu, K.; Nishide, H. *Chem. Lett.* **2011**, *40* (3), 222.

(127) Kato, F.; Kikuchi, A.; Okuyama, T.; Oyaizu, K.; Nishide, H. *Angew. Chemie - Int. Ed.* **2012**, *51* (40), 10177.

(128) Bergner, B. J.; Schürmann, A.; Peppler, K.; Garsuch, A.; Janek, J. *J. Am. Chem. Soc.* **2014**, *136* (42), 15054.

(129) Janoschka, T.; Martin, N.; Hager, M. D.; Schubert, U. S. *Angew. Chemie - Int. Ed.* **2016**, *55* (46), 14427.

(130) Foti, M.; Ingold, K. U.; Lusztyk, J. *J. Am. Chem. Soc.* **1994**, *116* (21), 9440.

(131) Altwicker, E. R. *Chem. Rev.* **1967**, *67* (5), 475.

(132) Von Sonntag, C.; Schuchmann, H.-P. *ChemInform* **2010**, *22* (50), no.

(133) Ingold, K. U. *Acc. Chem. Res.* **1969**, *2* (1), 1.

(134) Nacsa, E. D.; Lambert, T. H. *J. Am. Chem. Soc.* **2015**, *137* (32), 10246.

(135) Taylor, M. J.; Surman, P. W.; Clark, G. R. *J. Chem. Soc. D Chem. Commun.* **1994**, *375* (2), 2517.

(136) Yoshida, Z.; Konishi, H.; Tawara, Y.; Nishikawa, K.; Ogoshi, H. *Tetrahedron Lett.* **1973**, *14* (28), 2619.

(137) Yoshida, Z.; Konishi, H.; Tawara, Y.; Ogoshi, H. *J. Am. Chem. Soc.* **1973**, *95* (9), 3043.

(138) Hamada, S.; Wada, Y.; Sasamori, T.; Tokitoh, N.; Furura, T.; Kawabata, T. *Tetrahedron Lett.* **2014**, *55* (11), 1943.

(139) Stouffer, S. A.; Guttman, L.; Suchman, E. A.; Lazarsfeld, P. F.; Star, S. A.; Clausen, J. A. *Measurement and prediction. [Studies in social psychology in World War II. Vol.4.]*; Princeton University Press: Princeton, NJ, US, 1950.

(140) Connelly, N. G.; Geiger, W. E. *Chem. Rev.* **1996**, *96* (2), 877.

(141) Mocella, M. T.; Okamoto, M. S.; Barefield, E. K. *Synth. React. Inorg. Met. Chem.* **1974**, *4* (1), 69.

(142) Pontillon, Y.; Grand, A.; Ishida, T.; Lelièvre-Berna, E.; Nogami, T.; Ressouche, E.; Schweizer, J. *J. Mater. Chem.* **2000**, *10* (7), 1539.

(143) Warren, J. J.; Tronic, T. a; Mayer, J. M. *Chem. Rev.* **2011**, *110* (12), 6961.

(144) Bordwell, F. G.; Cheng, J. P.; Harrelson, J. a. *J. Am. Chem. Soc.* **1988**, *110* (4), 1229.

(145) Luca, O. R.; Crabtree, R. H. *Chem. Soc. Rev.* **2013**, *42* (4), 1440.

(146) Lyaskovskyy, V.; De Bruin, B. *ACS Catal.* **2012**, *2* (2), 270.

(147) Butin, K. P.; Beloglazkina, E. K.; Zyk, N. V. *Russ. Chem. Rev.* **2005**, *74* (6), 531.

(148) Piro, N. a.; Robinson, J. R.; Walsh, P. J.; Schelter, E. J. *Coord. Chem. Rev.* **2014**, *260* (1), 21.

(149) Huang, K. W.; Waymouth, R. M. *J. Am. Chem. Soc.* **2002**, *124* (28), 8200.

(150) Porter, T. R.; Mayer, J. M. *Chem. Sci.* **2014**, *5* (1), 372.

(151) Li, M.; Lu, J.; Chen, Z.; Amine, K. *Adv. Mater.* **2018**, *30* (33), 1.

(152) May, G. J.; Davidson, A.; Monahov, B. *J. Energy Storage* **2018**, *15*, 145.

(153) International Energy Agency. *Global Energy and CO2 Status Report*; 2018.

(154) Intergovernmental Panel on Climate Change. *Global Warming of 1.5°C. An IPCC Special Report on the impacts of global warming of 1.5°C above pre-industrial levels and related global greenhouse gas emission pathways, in the context of strengthening the global response to the threat of climate change,*; 2018.

(155) Yang, Z.; Zhang, J.; Kintner-Meyer, M. C. W.; Lu, X.; Choi, D.; Lemmon, J. P.; Liu, J. *Chem. Rev.* **2011**, *111* (5), 3577.

(156) Denholm, P.; Margolis, R.; Milford, J. *Production Cost Modeling for High Levels of Photovoltaics Penetration*; 2008.

(157) Denholm, P.; Ela, E.; Kirby, B.; Milligan, M. *Role of Energy Storage with Renewable Electricity Generation*; 2010.

(158) U.S. Energy Information Administration. *Electric power monthly*; 2019.

(159) Department of Energy. DOE Global Energy Storage Database https://www.energystorageexchange.org/projects/data_visualization.

(160) Gyuk, I. P. *EPRI-DOE Handbook of Energy Storage for Transmission &amp; Distribution Applications DISCLAIMER OF WARRANTIES AND LIMITATION OF LIABILITIES*; 2003.

(161) Barbour, E.; Wilson, I. A. G.; Radcliffe, J.; Ding, Y.; Li, Y. *Renew. Sustain. Energy Rev.* **2016**, *61*, 421.

(162) Palacín, M. R. *Chem. Soc. Rev.* **2018**, *47* (13), 4924.

(163) Sonoc, A.; Jeswiet, J. *Procedia CIRP* **2014**, *15*, 289.

(164) Lu, L.; Han, X.; Li, J.; Hua, J.; Ouyang, M. *J. Power Sources* **2013**, *226*, 272.

(165) Suo, L.; Borodin, O.; Gao, T.; Olguin, M.; Ho, J.; Fan, X.; Luo, C.; Wang, C.; Xu, K. *Science (80-.).* **2015**, *350* (6263), 938 LP.

(166) Winsberg, J.; Hagemann, T.; Janoschka, T.; Hager, M. D.; Schubert, U. S. *Angew. Chemie - Int. Ed.* **2017**, *56* (3), 686.

(167) Weber, A. Z.; Mench, M. M.; Meyers, J. P.; Ross, P. N.; Gostick, J. T.; Liu, Q. *J. Appl. Electrochem.* **2011**, *41* (10), 1137.

(168) Soloveichik, G. L. *Chem. Rev.* **2015**, *115* (20), 11533.

(169) Ye, R.; Henkensmeier, D.; Yoon, S. J.; Huang, Z.; Kim, D. K.; Chang, Z.; Kim, S.; Chen, R. *J. Electrochem. Energy Convers. Storage* **2017**, *15* (1), 010801.

(170) Ding, Y.; Li, Y.; Yu, G. *Chem* **2016**, *1* (5), 790.

(171) Huskinson, B.; Marshak, M. P.; Suh, C.; Er, S.; Gerhardt, M. R.; Galvin, C. J.; Chen, X.; Aspuru-Guzik, A.; Gordon, R. G.; Aziz, M. J. *Nature* **2014**, *505* (7482), 195.

(172) Kwabi, D. G.; Lin, K.; Ji, Y.; Kerr, E. F.; Goulet, M. A.; De Porcellinis, D.; Tabor, D. P.; Pollack, D. a.; Aspuru-Guzik, A.; Gordon, R. G.; Aziz, M. J. *Joule* **2018**, *2* (9), 1894.

(173) Beh, E. S.; De Porcellinis, D.; Gracia, R. L.; Xia, K. T.; Gordon, R. G.; Aziz, M. J. *ACS Energy Lett.* **2017**, *2* (3), 639.

(174) Hardee, D.; Chen, Q.; Gordon, R. G.; Kim, S. B.; Marshak, M. P.; Tong, L.; Aziz, M. J.; Eisenach, L.; Lin, K.; Valle, a. W.; Gerhardt, M. R. *Science (80-.).* **2015**, *349* (6255), 1529.

(175) Sevov, C. S.; Samaroo, S. K.; Sanford, M. S. *Adv. Energy Mater.* **2017**, *7* (5).

(176) Hendriks, K. H.; Sevov, C. S.; Cook, M. E.; Sanford, M. S. *ACS Energy Lett.* **2017**, *2* (10), 2430.

(177) Sevov, C. S.; Hickey, D. P.; Cook, M. E.; Robinson, S. G.; Barnett, S.; Minteer, S. D.; Sigman, M. S.; Sanford, M. S. *J. Am. Chem. Soc.* **2017**, *139* (8), 2924.

(178) Friedl, J.; Lebedeva, M. a.; Porfyrakis, K.; Stimming, U.; Chamberlain, T. W. *J. Am. Chem. Soc.* **2018**, *140* (1), 401.

(179) Kowalski, J. a.; Su, L.; Milshtein, J. D.; Brushett, F. R. *Curr. Opin. Chem. Eng.* **2016**, *13*, 45.

(180) Milshtein, J. D.; Fisher, S. L.; Breault, T. M.; Thompson, L. T.; Brushett, F. R. *ChemSusChem* **2017**, *10* (9), 2080.

(181) Duan, W.; Huang, J.; Kowalski, J. a.; Shkrob, I. a.; Vijayakumar, M.; Walter, E.; Pan, B.; Yang, Z.; Milshtein, J. D.; Li, B.; Liao, C.; Zhang, Z.; Wang, W.; Liu, J.; Moore, J. S.; Brushett, F. R.; Zhang, L.; Wei, X. *ACS Energy Lett.* **2017**, *2* (5), 1156.

(182) Kowalski, J. a.; Casselman, M. D.; Kaur, A. P.; Milshtein, J. D.; Elliott, C. F.; Modekrutti, S.; Attanayake, N. H.; Zhang, N.; Parkin, S. R.; Risko, C.; Brushett, F. R.; Odom, S. a. *J. Mater. Chem. A* **2017**, *5* (46), 24371.

(183) Hagemann, T.; Winsberg, J.; Häupler, B.; Janoschka, T.; Gruber, J. J.; Wild, A.; Schubert, U. S. *NPG Asia Mater.* **2017**, *9* (1).

(184) Wang, W.; Xu, W.; Cosimbescu, L.; Choi, D.; Li, L.; Yang, Z. *Chem. Commun.* **2012**, *48* (53), 6669.

(185) AJ, B.; LR, F. *Electrochemical Methods: Fundamentals and Applications*, 2nd ed.; John Wiley & Sons: New York, 2001.

(186) Gong, K.; Fang, Q.; Gu, S.; Li, S. F. Y.; Yan, Y. *Energy Environ. Sci.* **2015**, *8* (12), 3515.

(187) Darling, R. M.; Gallagher, K. G.; Kowalski, J. a.; Ha, S.; Brushett, F. R. *Energy Environ. Sci.* **2014**, *7* (11), 3459.

(188) Milshtein, J. D.; Barton, J. L.; Carney, T. J.; Kowalski, J. a.; Darling, R. M.; Brushett, F. R. *J. Electrochem. Soc.* **2017**, *164* (12), A2487.

(189) Doris, S. E.; Ward, A. L.; Baskin, A.; Frischmann, P. D.; Gavvalapalli, N.; Chénard, E.; Sevov, C. S.; Prendergast, D.; Moore, J. S.; Helms, B. a. *Angew. Chemie - Int. Ed.* **2017**, *56* (6), 1595.

(190) Ma, T.; Pan, Z.; Miao, L.; Chen, C.; Han, M.; Shang, Z.; Chen, J. *Angew. Chemie - Int. Ed.* **2018**, *57* (12), 3158.

(191) Shin, S. H.; Yun, S. H.; Moon, S. H. *RSC Adv.* **2013**, *3* (24), 9095.

(192) Kaur, A. P.; Holubowitch, N. E.; Ergun, S.; Elliott, C. F.; Odom, S. a. *Energy Technol.* **2015**, *3* (5), 476.

(193) Montoto, E. C.; Nagarjuna, G.; Moore, J. S.; Rodríguez-López, J. *J. Electrochem. Soc.* **2017**, *164* (7), A1688.

(194) Yuan, Z.; Zhang, H.; Li, X. *Chem. Commun.* **2018**, *54* (55), 7570.

(195) Prifti, H.; Parasuraman, A.; Winardi, S.; Lim, T. M.; Skyllas-Kazacos, M. *Membranes (Basel).* **2012**, *2* (2), 275.

(196) Hu, B.; Liu, T. L. *J. Energy Chem.* **2018**, *27* (5), 1326.

(197) Hioe, J.; Šakić, D.; Vrček, V.; Zipse, H. *Org. Biomol. Chem.* **2015**, *13* (1), 157.

(198) Hu, J.; Wang, J.; Nguyen, T. H.; Zheng, N. *Beilstein J. Org. Chem.* **2013**, *9*, 1977.

(199) Butchard, J. R.; Curnow, O. J.; Garrett, D. J.; Maclagan, R. G. a. R. *Angew. Chemie - Int. Ed.* **2006**, *45* (45), 7550.

(200) Butchard, J. R.; Curnow, O. J.; Pipal, R. J.; Robinson, W. T.; Shang, R. *J. Phys. Org. Chem.* **2008**, *21* (2), 127.

(201) Adkins, H.; Kuick, L. F.; Farlow, M.; Wojcik, B. *J. Am. Chem. Soc.* **1934**, *56* (11), 2425.

(202) Toshikatsu Sata. *Ann. N. Y. Acad. Sci.* **2002**, *57* (3), 177.

(203) Arges, C. G.; Zhang, L. *ACS Appl. Energy Mater.* **2018**, *1* (7), 2991.

(204) Mousavi, M. P. S.; Kashefolgheta, S.; Stein, A.; Bühlmann, P. *J. Electrochem. Soc.* **2016**, *163* (2), H74.

(205) Arora, P.; Zhang, Z. *Chem. Rev.* **2004**, *104* (10), 4419.

(206) Chieng, S. C.; Kazacos, M.; Skyllas-Kazacos, M. *J. Memb. Sci.* **1992**, *75* (1-2), 81.

(207) Mohammadi, T.; Skyllas-Kazacos, M. *J. Memb. Sci.* **1995**, *107* (1-2), 35.

(208) Mohammadi, T.; Skyllas-Kazacos, M. *J. Memb. Sci.* **1995**, *98* (1-2), 77.

(209) Radel, C.; Hanauerstrasse; Kung, J. K.-J.; Choi, W. M. Lead/sulphuric acid storage battery, 1992.

(210) Reitz, J. W. **1987**, *19*, 181.

(211) DeBruler, C.; Hu, B.; Moss, J.; Liu, X.; Luo, J.; Sun, Y.; Liu, T. L. *Chem* **2017**, *3* (6), 961.

(212) Debruler, C.; Hu, B.; Moss, J.; Luo, J.; Liu, T. L. *ACS Energy Lett.* **2018**, *3* (3), 663.

(213) Luo, J.; Wu, W.; Debruler, C.; Hu, B.; Hu, M.; Liu, T. L. *J. Mater. Chem. A* **2019**, *7* (15), 9130.

(214) Moutet, J. C.; Reverdy, G. *J. Chem. Soc. - Ser. Chem. Commun.* **1982**, No. 12, 654.

(215) Scheffold, R.; Orlinski, R. *J. Am. Chem. Soc.* **2005**, *105* (24), 7200.

(216) Yan, H.; Hou, Z. W.; Xu, H. C. *Angew. Chemie - Int. Ed.* **2019**, *58* (14), 4592.

(217) Wang, F.; Rafiee, M.; Stahl, S. S. *Angew. Chemie - Int. Ed.* **2018**, *57* (22), 6686.

(218) Zhang, L.; Liardet, L.; Luo, J.; Ren, D.; Grätzel, M.; Hu, X. *Nat. Catal.* **2019**, *2* (4), 366.

(219) Romero, N. A.; Margrey, K. A.; Tay, N. E.; Nicewicz, D. A. *Science (80-.).* **2015**, *349* (6254), 1326 LP.

(220) Margrey, K. a.; Levens, A.; Nicewicz, D. a. *Angew. Chemie - Int. Ed.* **2017**, *56* (49), 15644.

(221) Ohkubo, K.; Fujimoto, A.; Fukuzumi, S. *J. Am. Chem. Soc.* **2013**, *135* (14), 5368.

(222) Das, S.; Natarajan, P.; König, B. *Chem. - A Eur. J.* **2017**, *23* (72), 18161.

(223) Bardagi, J. I.; Ghosh, I.; Schmalzbauer, M.; Ghosh, T.; König, B. *European J. Org. Chem.* **2018**, *2018* (1), 34.

(224) Kumar, A.; Sevilla, M. D. *J. Phys. Chem. B* **2018**, *122* (1), 98.

(225) Goddard, J. P.; Reymond, J. L. *Curr. Opin. Biotechnol.* **2004**, *15* (4), 314.

(226) Jäkel, C.; Paciello, R. *Chem. Rev.* **2006**, *106* (7), 2912.

(227) Macarron, R.; Banks, M. N.; Bojanic, D.; Burns, D. J.; Cirovic, D. A.; Garyantes, T.; Green, D. V. S.; Hertzberg, R. P.; Janzen, W. P.; Paslay, J. W.; Schopfer, U. *Nature* **2011**, *10* (March 2011), 188.

(228) Shevlin, M. *ACS Med. Chem. Lett.* **2017**, *8* (6), 601.

(229) Sheldrick, G. M. SHELXTL, An Integrated System for Solving, Refining, and Displaying Crystal Structures from Diffraction Data; University of Göttingen, Göttingen, Federal Republic of Germany, 1981. **1981**.

(230) Sheldrick, G. M. *Acta Crystallogr. Sect. A Found. Crystallogr.* **2015**, *71* (1), 112.

(231) Sheldrick, G. M. *Acta Crystallogr. Sect. A Found. Crystallogr.* **2015**, *71* (1), 3.

(232) Jaguar, version 8.9, Schrodinger, Inc., New York, NY, 2015. .

(233) Bochevarov, A. D.; Harder, E.; Hughes, T. F.; Greenwood, J. R.; Braden, D. a.; Philipp, D. M.; Rinaldo, D.; Halls, M. D.; Zhang, J.; Friesner, R. a. *Int. J. Quantum Chem.* **2013**, *113* (18), 2110.

(234) Becke, a. D. *Phys. Rev. A* **1988**, *38* (6), 3098.

(235) Becke, A. D. *J. Chem. Phys.* **1993**, *98* (7), 5648.

(236) Lee, C.; Yang, W.; Parr, R. G. *Phys. Rev. B* **1988**, *37* (2), 785.

(237) Vosko, S. H.; Wilk, L.; Nusair, M. *Can. J. Phys.* **1980**, *58* (8), 1200.

(238) Slater, J. C. Quantum Theory of Molecules and Solids, Vol. 4: The Self-Consistent Field for Molecules and Solids; McGraw-Hill: New York, 1974. .

(239) Bordwell, F. G.; Cheng, J. P.; Harrelson, J. a. *J. Am. Chem. Soc.* **1988**, *110* (4), 1229.

(240) Wayner, D. D. M.; Parker, V. D. *Acc. Chem. Res.* **1993**, *26* (5), 287.

(241) Oba, M.; Tanaka, K.; Nishiyama, K.; Ando, W. *J. Org. Chem.* **2011**, *76* (10), 4173.

1. General Information

All reactions were performed open to atmosphere with magnetic stirring, unless otherwise noted. Pentachlorocyclopropane and tetrachlorocyclopropene were prepared as previously described. (1) All other commercial reagents were used as provided. Organic solutions were concentrated using a Buchi rotary evaporator. Flash column chromatography was performed employing 32-63 µm silica gel (Dynamic Adsorbents Inc). Thin-layer chromatography (TLC) was performed on silica gel 60 F_{254} plates (SiliCycle). ^{1}H and ^{13}C NMR were recorded on Bruker DRX spectrometers in deuterated solvents and at frequencies as noted. Data for ^{1}H NMR are reported as follows: chemical shift (δ, in ppm), multiplicity (s = singlet, d = doublet, t = triplet, tt = triplet of triplets, quart = quartet, quint = quintet, sept = septet, m = multiplet, br = broad), coupling constant (J, in Hz), and integration. Data for ^{13}C NMR are reported in terms of chemical shift. The chemical shifts were referenced to the corresponding residual solvent signals ($CDCl_3$: δ H = 7.26, δ C = 77.16). Infrared spectra were recorded on a Perkin Elmer Paragon 1000 FT-IR spectrometer. High-resolution mass spectra were obtained from the Columbia University Mass Spectrometry Facility on a Waters XEVO G2XS QToF mass spectrometer with an electrospray ionization (ESI) probe. Cyclic voltammograms were recorded on a CH166 electrochemical workstation using 0.1M solutions of tetrabutylammonium hexafluorophosphate as the supporting electrolyte with ferrocene used as an internal standard (Fc/Fc^+ = 0.40 V). (2) EPR spectroscopy was performed on samples dissolved in DCM using 3-mm inner diameter quartz tubes. EPR spectra were recorded on a Bruker EMX spectrometer equipped with a variable temperature accessory (ER413VT) using a modulation amplitude of 1.00 G and a modulation frequency of 100.00 kHz. X-ray diffraction data were collected on a Bruker Apex II diffractometer. EPR spectra were simulated using WINEPR SimFonia (Bruker). Crystal data, data collection, and refinement parameters are summarized on pages S44-S46. The structures were solved by using direct methods and standard difference map techniques, and were refined by full-matrix least-squares procedures on F^2 with SHELXTL (Version 2014/7). (3-5) Calculations were carried out using DFT as implemented in the Jaguar 8.9 (release 15) suite of *ab initio* quantum chemistry programs. (6-7) Geometry optimizations were performed with the B3LYP density functional (8-12) using the LACVP** basis sets.

2. Experimental Details and Characterization of Compounds.

2.1 Synthesis and Characterization of Cyclopropenones

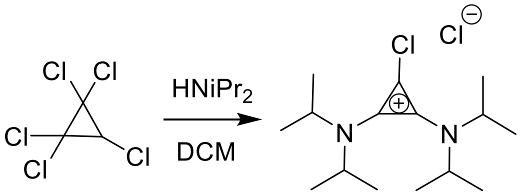

1,2-bis(diisopropylamino)-3-chlorocyclopropenium chloride (S1). A 1L roundbottom flask was charged with DCM (500 mL) and pentachlorocyclopropane (10.0 mL, 70.0 mmol). The flask was cooled to 0 °C and diisopropylamine (78.5 ml, 560 mmol) was added slowly. The reaction was stirred for 4 h at 0 °C, then the DCM layer was washed with 1M HCl (100 mL). The organic layer was concentrated *in vacuo* and the solids were triturated with Et_2O, collected via filtration and washed twice more with Et_2O to give **S1** as white crystals (13.8 g, 44.9 mmol, 64% yield). ^{1}H NMR (500 MHz, $CDCl_3$) δ 4.50-4.41 (sept, J = 6.5 Hz, 2H), 3.92-3.84 (sept, J = 6.7 Hz, 2H), 1.48-

1.38 (dd, *J* = 20.8, 6.7 Hz, 24H). ^{13}C NMR (126 MHz, $CDCl_3$) δ 132.3, 58.3, 48.3, 22.80, 21.2. FTIR (film) 3380 (br), 2979, 2936, 2875, 1912, 1584, 1460, 1418, 1376, 1348 cm^{-1}. HRMS (ESI, m/z) calcd for [M-Cl]$^+$: 271.1941; found 271.1940.

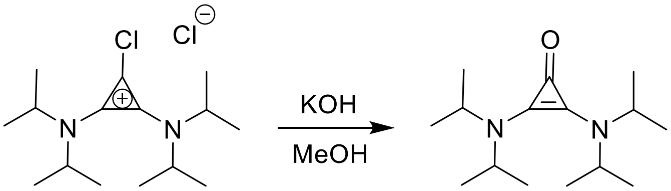

Bis-2,3-(diisopropylamino)-cycloprop-2-en-1-one (1). S1 (10.0 g, 32.5 mmol) was dissolved in 150 mL MeOH, and KOH (18.2 g, 325 mmol) was added in one portion and the reaction was stirred for 4 h at rt. The reaction was concentrated *in vacuo* and subsequently partitioned between H_2O (150 mL) and DCM (150 mL). The organic layer was separated and the water layer was washed twice more with DCM (50 mL). The organic layers were combined, dried with anhydrous Na_2SO_4 and concentrated *in vacuo*. The solids were triturated with Et_2O, collected via filtration and washed twice more with Et_2O to give **1** as white crystals (6.74 g, 26.7 mmol, 82% yield). ^{1}H NMR (500 MHz, $CDCl_3$) δ 3.59-3.49 (sept, *J* = 6.7 Hz, 4H), 1.28-1.14 (d, *J* = 6.9 Hz, 24H). ^{13}C NMR (126 MHz, $CDCl_3$) δ 133.9, 117.4, 49.5, 22.5. FTIR (film) 2975, 2932, 2873, 1900, 1578, 1471, 1385, 1367, 1351 cm^{-1}. HRMS (ESI, m/z) calcd for [M+H]$^+$: 253.2280; found 253.2278.

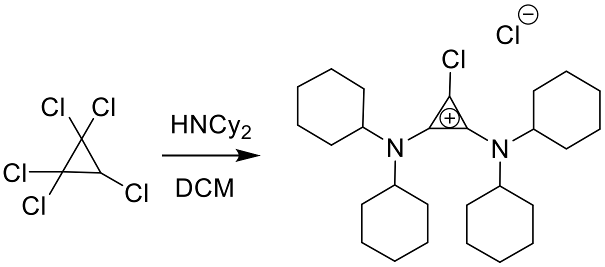

1,2-bis(dicyclohexylamino)-3-chlorocyclopropenium chloride (S2). A 1L roundbottom flask was charged with DCM (500 mL) and pentachlorocyclopropane (10.0 mL, 70.0 mmol). The flask was cooled to 0 °C and dicyclohexylamine (111 mL, 560 mmol) was added slowly. The reaction was stirred for 24 h at rt, at which time concd HCl (20 mL) was added to precipitate the excess dicyclohexylamine. The reaction was filtered and the solids were washed with DCM. The filtrate was transferred to a separatory funnel and washed 1M HCl (3 x 100 mL) and brine. The organic layer was dried over anhydrous Na_2SO_4 and concentrated *in vacuo*. The solids were triturated with hot EtOAc and collected via filtration to give **S2** as an off-white solid (29.1 g, 62.2 mmol, 89% yield). ^{1}H NMR (500 MHz, $CDCl_3$) δ 3.62-3.51 (m, 2H), 3.40-3.30 (m, 2H), 2.03-1.95 (d, *J* = 11.3 Hz, 4H), 1.92-1.78 (quart, *J* = 11.6 Hz, 12H), 1.69-1.60 (d, *J* = 13.0 Hz, 4H), 1.60-1.40 (m, 8H), 1.36-1.18 (m, 8H), 1.17-1.04 (m, 4H). ^{13}C NMR (126 MHz, $CDCl_3$) δ 132.5, 93.7, 66.0, 57.1, 32.9, 31.0, 25.7, 25.5, 24.8, 24.7. FTIR (film) 3260, 3184, 2929, 2852, 1932, 1585, 1452, 1416, 1377, 1320 cm^{-1}. HRMS (ESI, m/z) calcd for [M-Cl]$^+$: 431.3193; found 431.3193.

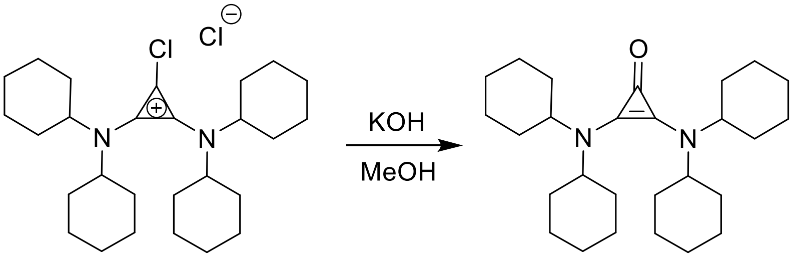

Bis-2,3-(dicyclohexylamino)-cycloprop-2-en-1-one (2). S2 (10.0 g, 21.4 mmol) was dissolved in 100 mL MeOH, and KOH (12.0 g, 214 mmol) was added in one portion and the reaction was stirred for 4 h at rt. The reaction was concentrated *in vacuo* and the residue was subsequently partitioned between H_2O (100 mL) and DCM (100 mL) and transferred to a separatory funnel. The organic layer was separated and the water layer was washed twice more with DCM (50 mL). The organic layers were combined, dried over anhydrous Na_2SO_4 and concentrated *in vacuo*. The solids were suspended in EtOAc, collected via filtration, and washed twice more with EtOAc to give **2** as a pale-yellow solid (8.30 g, 20.1 mmol, 94% yield). ^{1}H NMR (500 MHz, $CDCl_3$) δ 3.12-3.01 (m, 4H), 1.88-1.76 (m, 8H), 1.75-1.54 (m, 20H), 1.31-1.16 (m, 12H). ^{13}C NMR (126 MHz, $CDCl_3$) δ 133.7, 117.6, 58.5, 33.2, 26.4, 25.3. FTIR (film) 2926, 2856, 1894, 1573, 1450, 1426, 1347 cm^{-1}. HRMS (ESI, m/z) calcd for $[M+H]^+$: 413.3532; found 413.3528.

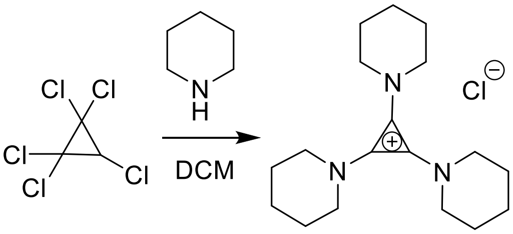

Tris(piperidino)cyclopropenium chloride (S3). A roundbottom flask was charged with 40 mL of DCM and pentachlorocyclopropane (1.00 mL, 7.00 mmol). The flask was cooled to 0 °C and piperidine (5.53 mL, 56 mmol) was added dropwise. The reaction was stirred for 1 h at 0 °C and then for 24 h at rt. The reaction was transferred to a separatory funnel and washed with twice with 1M HCl (20 mL) and brine (20 mL). The organic layer was dried over anhydrous Na_2SO_4 and concentrated *in vacuo* to give **S3** as a yellow solid, which was carried to the next step without further purification (2.13 g, 6.58 mmol, 94% yield). ^{1}H NMR (500 MHz, $CDCl_3$) δ 3.50-3.42 (t, J = 5.2Hz, 12H), 1.73-1.60 (m, 18H). ^{13}C NMR (126 MHz, $CDCl_3$) δ 117.2, 51.9, 25.39, 23.0. FTIR (film) 3380 (br), 2927, 2849, 1537, 1445, 1374 cm^{-1}. HRMS (ESI, m/z) calcd for $[M\text{-}Cl]^+$: 288.2440; found 288.2432.

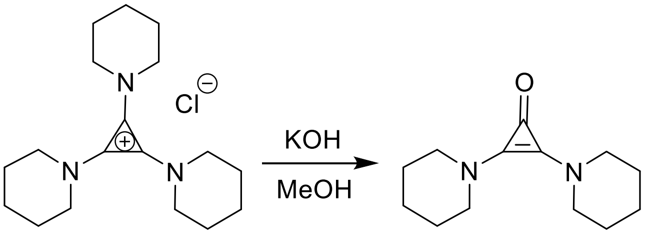

Bis-2,3-(piperidino)-cycloprop-2-en-1-one (3). S3 (2.00 g, 6.17 mmol) was dissolved in MeOH (50 mL), and KOH (3.40 g, 61.0 mmol) was added in one portion and the reaction was heated to 60 °C for 4 h. The reaction was then concentrated *in vacuo* and partitioned between DCM (50 mL) and H_2O (50 mL). The organic layer was separated and the water layer was washed twice with DCM (25 mL). The combined organic layers were dried over anhydrous Na_2SO_4 and concentrated *in vacuo*. The resulting solid was recrystallized from EtOAc to give **3** as light brown crystals (0.97g, 4.40mmol, 71% yield). ^{1}H NMR (500 MHz, $CDCl_3$) δ 3.30-3.10 (t, *J* = 5.3 Hz, 8H), 1.61-1.38 (m, 12H). ^{13}C NMR (126 MHz, $CDCl_3$) δ 134.9, 120.5, 50.8, 25.6, 23.8. FTIR (film) 2932.78, 2851.27, 1901, 1567, 1472, 1433, 1379 cm^{-1}. HRMS (ESI, m/z) calcd for $[M+H]^+$: 221.1654; found 221.1650.

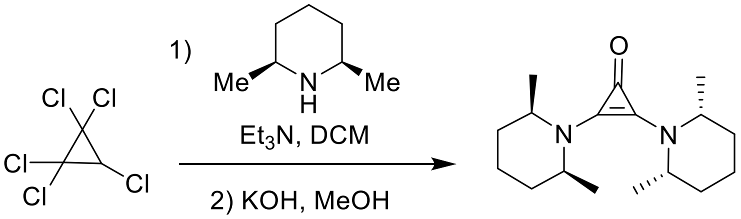

Bis-2,3-(2,6-dimethylpiperidino)-cycloprop-2-en-1-one (4). A roundbottom flask was charged with 40 mL of DCM and pentachlorocyclopropane (1.00 mL, 7.00 mmol). The flask was cooled to 0 °C, and 2,6-dimethylpiperidine (1.89 mL, 14.0 mmol) and Et_3N (2.93mL, 21 mmol) were added in succession. The reaction was stirred at 0 °C for 4 h, then the reaction was filtered and the filtrate was subsequently concentrated *in vacuo*. The residue was dissolved in MeOH (50 mL), then KOH (3.92 g, 70.0 mmol) was added in one portion and the reaction was stirred at rt for 24 h. The reaction was then concentrated *in vacuo* and subsequently partitioned between H_2O (50 mL) and DCM (50 mL). The water layer was washed twice more with DCM (25 mL) and the combined organic extracts were dried over anhydrous Na_2SO_4 and concentrated *in vacuo*. The resulting solids were triturated with Et_2O and filtered to give **4** as a white solid (0.62 g, 2.24 mmol, 32% yield). ^{1}H NMR (500 MHz, $CDCl_3$) δ 3.76-3.67 (m, 4H), 1.75-1.65 (m, 6H), 1.54-1.43 (m, 6H), 1.29-1.22 (d, *J* = 7.0 Hz, 12H). ^{13}C NMR (126 MHz, $CDCl_3$) δ 136.1, 120.6, 52.4, 30.2, 21.8, 14.2. FTIR (film) 2933, 2865, 1899, 1580, 1394, 1315 cm^{-1}. HRMS (ESI, m/z) calcd for $[M+H]^+$: 277.2280; found 277.2274.

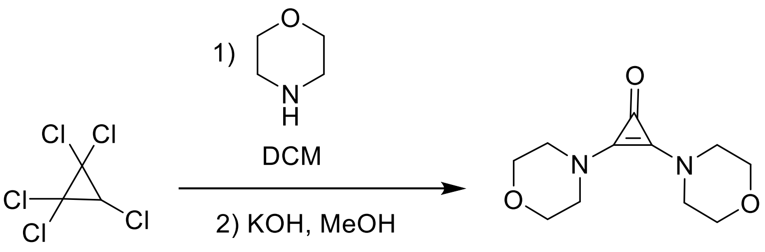

Bis-2,3-(morpholino)-cycloprop-2-en-1-one (5). A roundbottom flask was charged with 40 mL of DCM and pentachlorocyclopropane (1.00 mL, 7.00 mmol). The flask was cooled to 0 °C and morpholine (4.83 mL, 56.0 mmol) was added slowly. The reaction was stirred for 1 h at 0 °C and then for 24 h at rt. The reaction was filtered and concentrated *in vacuo*. The residue was dissolved in MeOH (50 mL) and KOH (3.92g, 70.0mmol) was added in one portion and the reaction was stirred at RT for 24 hr. The reaction was then concentrated *in vacuo* and the solids were triturated with DCM and filtered, washing the solids several times with DCM. The filtrate was then concentrated *in vacuo* and resulting solids were triturated with EtOAc and filtered to give **5** as an off-white solid (0.53 g, 2.38 mmol, 34% yield). ^{1}H NMR (500 MHz, CDCl$_3$) δ 3.77-3.60 (d, *J* = 4.7 Hz, 8H), 3.35-3.24 (t, *J* = 4.7 Hz, 8H). ^{13}C NMR (126 MHz, CDCl$_3$) δ 135.0, 120.5, 66.4, 49.5. FTIR (film) 2969, 2903, 2856, 1910, 1568, 1472, 1432, 1371 cm^{-1}. HRMS (ESI, m/z) calcd for [M+H]$^+$: 225.1239; found 225.1242.

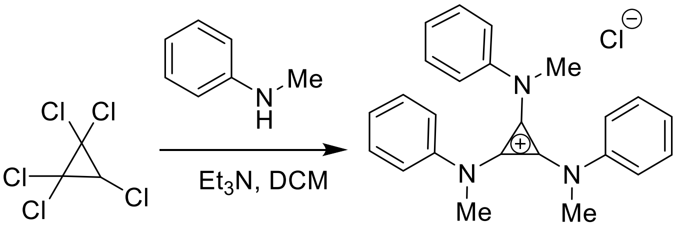

Tris(N-methylanilino)cyclopropenium chloride (S4). A roundbottom flask was charged with 40 mL DCM and pentachlorocyclopropane (1.00 mL, 7.00 mmol). The flask was cooled to 0 °C and N-methylaniline (2.28 mL, 21.0 mmol) and Et$_3$N (4.88ml, 35.0 mmol) were added in succession. The reaction was stirred for 1 h at 0 °C and then for 24 h at rt. The reaction was transferred to a separatory funnel and washed twice with 1M HCl (25 mL). The organic layer was dried over anhydrous Na$_2$SO$_4$ and concentrated *in vacuo*. The solids were triturated with EtOAc and collected via filtration to give **S4** as a light brown solid that was used without further purification (2.67 g, 6.86 mmol, 98% yield). ^{1}H NMR (500 MHz, CDCl$_3$) δ 7.40-7.33 (d, *J* = 7.8 Hz, 6H), 7.21-7.13 (t, *J* = 7.7 Hz, 6H) 7.09-7.03 (t, *J* = 7.4 Hz, 3H), 3.39 (s, 9H). ^{13}C NMR (126 MHz, CDCl$_3$) δ 143.5, 129.5, 127.0, 123.3, 122.7, 117.8, 42.5. FTIR (film) 3380 (br), 3047, 2944, 1631, 1592, 1517, 1454, 1406, 1288 cm^{-1}. HRMS (ESI, m/z) calcd for [M-Cl]$^+$: 354.1970; found 354.1967.

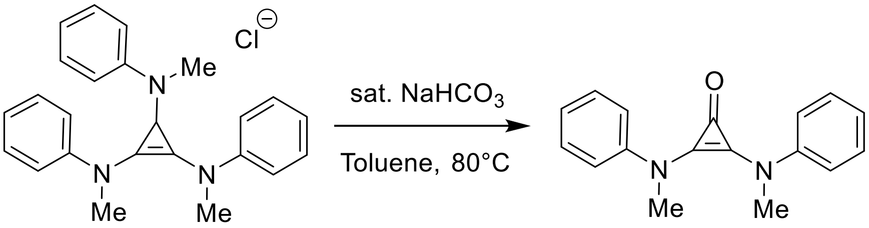

Bis-2,3-(N-methylanilino)-cycloprop-2-en-1-one (6). S4 (2.50g, 6.41mmol) was suspended in 30 mL toluene in a roundbottom flask. An equal volume of saturated $NaHCO_3$ solution was added and the reaction was heated at 80 ℃ for 16 h. The reaction was allowed to cool to rt, and the organic layer was separated, washed twice with 1M HCl, and concentrated. The resulting solids were recrystallized from acetone to give **6** as light brown crystals (1.29 g, 4.87 mmol, 76% yield). ^{1}H NMR (500 MHz, $CDCl_3$) δ 7.42-7.36 (m, 4H), 7.36-7.32 (m, 4H), 7.10-7.05 (m, 2H), 3.43 (s, 6H). ^{13}C NMR (126 MHz, $CDCl_3$) δ 143.8, 134.7, 129.7, 123.1, 118.9, 116.9, 39.1. FTIR (film) 3059, 2919, 1923, 1903, 1599, 1581, 1504, 1482, 1431, 1377, 1345, 1300. HRMS (ESI, m/z) calcd for $[M+H]^+$: 265.1341; found 265.1335.

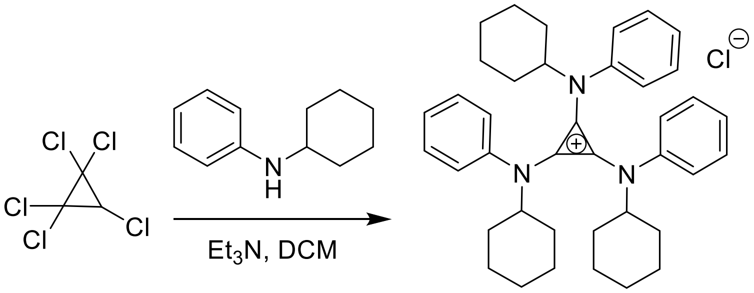

Tris(N-cyclohexylanilino)cyclopropenium dichloride (S5). A roundbottom flask was charged with 40 mL of DCM and pentachlorocyclopropane (1.00 mL, 7.00 mmol). The flask was cooled to 0 ℃, and N-cyclohexylaniline (3.70 mL, 21.0 mmol) and Et_3N (4.88 mL, 35.0 mmol) were added in succession. The reaction was stirred for 1 h at 0°C and then for 24 h at rt. The reaction was transferred to a separatory funnel and washed with twice with 1M HCl. The organic layer was dried over anhydrous Na_2SO_4 and concentrated *in vacuo*. The resulting solids were triturated with EtOAc and filtered to give **S5** as a white powder, which was used without further purification (4.08 g, 6.86 mmol, 98% yield). ^{1}H NMR (300 MHz, $CDCl_3$) δ 7.41 (s, 15H), 2.27-2.12 (t, *J* = 11.8 Hz, 3H), 1.69-1.57 (d, *J* = 11.1 Hz, 6H), 1.48-1.35 (d, *J* = 12.8 Hz, 6H), 1.27-1.17 (d, *J* = 11.4 Hz, 3H), 0.94-0.77 (quart, *J* = 11.1 Hz, 6H), 0.66-0.35 (m, 9H). ^{13}C NMR (126 MHz, $CDCl_3$) δ 144.9, 134.6, 128.6, 124.5, 122.4, 118.4, 63.5, 32.5, 26.1, 25.2. FTIR (film) 3380 (br), 2930, 2857, 1490, 1451, 1338. HRMS (ESI, m/z) calcd for $[M-Cl]^+$: 558.3848; found 558.3856.

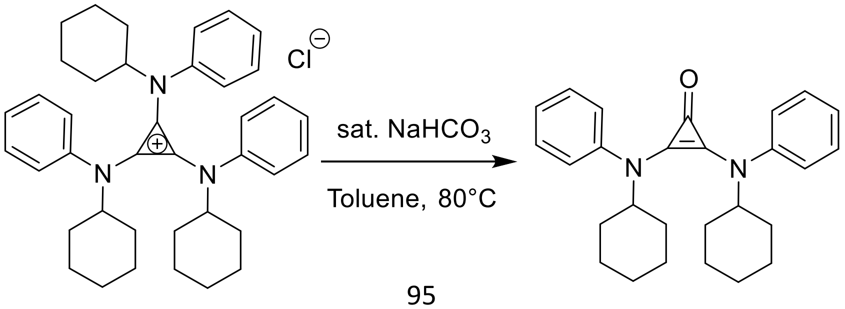

Bis-2,3-(N-cyclohexylanilino)-cycloprop-2-en-1-one (7). S5 (3.00 g, 6.41 mmol) was suspended in 30 mL toluene in a roundbottom flask. An equal volume of saturated $NaHCO_3$ solution was added and the reaction was heated at 80 °C for 16 h. The reaction was allowed to cool to rt and the organic layer was separated. The aqueous layer was extracted twice with DCM (25 mL) and the combined organic layers were washed twice with 1M HCl, dried over anhydrous Na_2SO_4 and concentrated *in vacuo*. The resulting solids were recrystallized from acetone to give **7** as light tan crystals (2.18 g, 5.44 mmol, 85% yield). ^1H NMR (500 MHz, $CDCl_3$) δ 6.89-6.81 (m, 8H), 6.73-6.69 (m, 2H), 3.46-3.38 (tt, $J = 11.3, 3.8$ Hz, 2H), 2.00-1.93 (m, 4H), 1.90-1.81 (m, 8H), 1.67-1.60 (m, 2H), 1.35-1.20 (m, 6H). ^{13}C NMR (126 MHz, $CDCl_3$) δ 144.9, 134.6, 128.6, 124.5, 122.4, 118.4, 63.5, 32.5, 26.1, 25.2. FTIR (film) 2924, 2856, 1908, 1578, 1495, 1453, 1292 cm^{-1}. HRMS (ESI, m/z) calcd for $[M+H]^+$: 401.2593; found 401.2596.

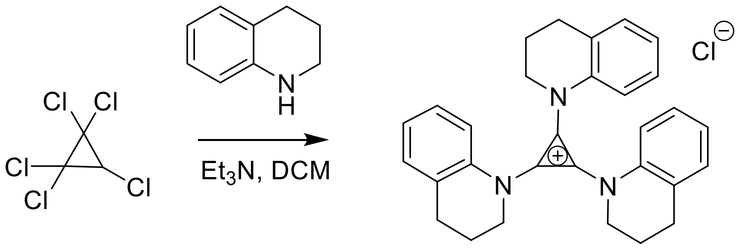

Tris(1,2,3,4-tetrahydroquinolino)cyclopropenium chloride (S6). A roundbottom flask was charged with 40 mL of DCM and pentachlorocyclopropane (1.00 mL, 7.00mmol). The flask was cooled to 0 °C and 1,2,3,4-tetrahydroquinoline (2.64 mL, 21 mmol) and Et_3N (4.88 mL, 35.0 mmol) were added in succession. The reaction was stirred for 1 h at 0 ºC and then for 24 h at rt. The reaction was transferred to a separatory funnel and washed twice with 1M HCl (25 mL). The organic layer was dried over Na_2SO_4 and concentrated *in vacuo*. The solids were triturated with EtOAc and collected via filtration to give **S6** as a light brown solid that was used without further purification. (3.21 g, 6.86 mmol, 98% yield.). ^1H NMR (500 MHz, $CDCl_3$) δ 7.15-7.06 (m, 6H), 7.04-6.96 (m, 6H), 3.90-3.79 (t, $J = 5.7$ Hz, 6H) 2.90-2.82 (t, $J = 6.5$ Hz, 6H), 2.27-2.16 (m, 6H). ^{13}C NMR (126 MHz, $CDCl_3$) δ 137.8, 137.8, 130.2, 128.1, 126.8, 125.0, 119.0, 52.2, 26.3, 22.2. FTIR (film) 3380 (br), 2937, 2854, 1499, 1449, 1390, 1343 cm^{-1}. HRMS (ESI, m/z) calcd for $[M-Cl]^+$: 432.2240; found 432.2240.

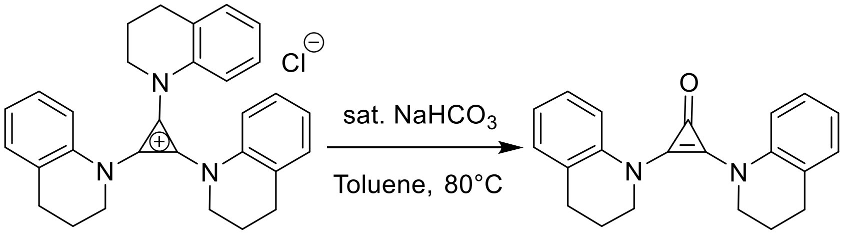

Bis-2,3-(1,2,3,4-tetrahydroquinolino)-cycloprop-2-en-1-one (8). **S6** (3.00 g, 6.41 mmol) was suspended in 30 mL toluene in a roundbottom flask. An equal volume of saturated $NaHCO_3$ solution was added and the reaction was heated at 80 °C for 16 h. The reaction was allowed to cool to rt and the organic layer was separated. The aqueous layer was extracted twice with DCM (25 mL) and the combined organic layers were washed twice with 1M HCl, dried over anhydrous Na_2SO_4, and concentrated *in vacuo*. The resulting solids were recrystallized from acetone to give **8** as light brown crystals (1.74 g, 5.51 mmol, 86% yield). ^1H NMR (500 MHz, $CDCl_3$) δ 7.86-7.79 (d, *J* = 8.3 Hz, 2H), 7.33-7.27 (t, *J* = 7.8 Hz, 2H), 7.08-7.03 (d, *J* = 7.4 Hz, 2H), 6.96-6.90 (t, *J* = 7.4 Hz, 2H), 3.89-3.81 (t, *J* = 5.8 Hz, 4H), 2.86-2.78 (t, *J* = 6.2 Hz, 4H), 2.12-2.04 (quint, *J* = 6.2 Hz, 4H). ^{13}C NMR (126 MHz, $CDCl_3$) δ 134.8, 120.4, 50.7, 25.4, 23.6. FTIR (film) 2957, 2936, 2862, 1898, 1610, 1574, 1495, 1370, 1310 cm^{-1}. HRMS (ESI, m/z) calcd for $[M+H]^+$: 317.1654; found 317.1649.

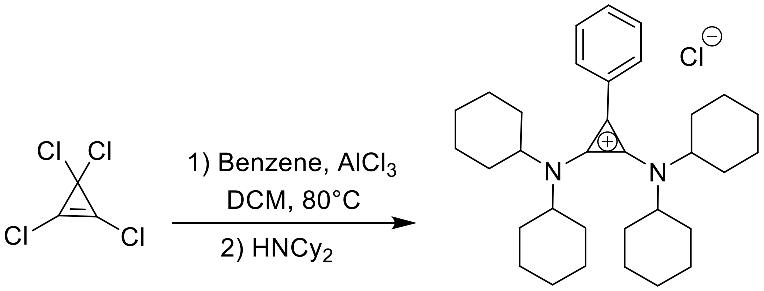

Bis-1,2-(dicyclohexylamino)-3-phenyl-cyclopropenium chloride (S7) A flame-dried flask was flushed with argon and charged with 50 mL DCM, tetrachlorocyclopropene (1.00 mL, 8.15 mmol), and benzene (0.78 mL, 8.97 mmol). The flask was cooled to 0 °C and anhydrous $AlCl_3$ (1.3 g, 9.78 mmol) was added portion-wise, producing a red solution. The reaction was heated to 40 °C for 20 min, then subsequently cooled to 0 °C and charged with dicyclohexylamine (6.5 mL, 32.7 mmol). The reaction was filtered and the precipitate was washed 3 times with DCM. The filtrate was washed 3 times with 1M HCl (25 mL) and once with brine. The organic layer was dried over anhydrous Na_2SO_4 and concentrated *in vacuo*. The resulting solids were triturated with EtOAc and collected via filtration to yield **S7** as a white powder that was used without further purification (2.91 g, 57.1 mmol, 70% yield). ^1H NMR (500 MHz, $CDCl_3$) δ 7.59-7.49 (m, 5H), 3.75-3.65 (m, 2H), 3.39-3.28 (m, 2H), 2.21-2.11 (d, *J* = 10.7 Hz, 4H), 2.03-1.94 (d, *J* = 13.3 Hz, 4H), 1.89-1.81 (d, *J* = 11.4 Hz, 4H), 1.80-1.58 (m, 12H), 1.54-1.42 (m, 6H), 1.42-1.31 (m, 4H) 1.29-1.16 (m, 6H). ^{13}C NMR (126 MHz, $CDCl_3$) δ 134.2, 130.9, 129.7, 128.9, 108.9, 65.6, 57.5, 31.7, 31.4, 25.9, 25.5, 24.9, 24.7. FTIR (film) 3380 (br), 2929, 2854, 1906, 1545, 1447, 1319. HRMS (ESI, m/z) calcd for $[M-Cl]^+$: 473.3896; found 473.3890.

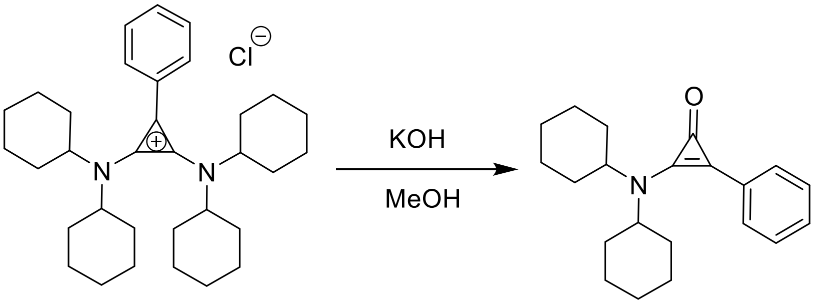

2-dicyclohexylamino-3-phenyl-cycloprop-2-en-1-one (9). S7 (2.50 g, 4.91 mmol) was dissolved in MeOH (30 mL), and KOH (2.75 g, 49.1 mmol) dissolved in MeOH (10 mL) was added. The reaction was stirred at rt for 30 min, at which point DCM (50 mL) and 1M HCl (50 mL) was added and transferred to a separatory funnel. The organic layer was separated and washed twice with 1M HCl, washed with brine, dried over anhydrous Na_2SO_4 and concentrated in vacuo. The resulting solid was triturated with hot Et_2O and collected via filtration giving **9** as a yellow solid (1.31 g, 4.23 mmol, 86% yield). ^1H NMR (500 MHz, $CDCl_3$) δ 7.61-7.56 (m, 2H), 7.45-7.39 (t, *J* = 7.3 Hz, 2H), 7.38-7.32 (tt, *J* = 7.5, 1.3 Hz, 1H), 3.78-3.67 (m, 1H), 3.16-3.05 (m, 1H), 1.99-1.13 (m, 20H). ^{13}C NMR (126 MHz, $CDCl_3$) δ 146.5, 141.5, 129.0, 128.9, 128.7, 125.3, 109.7, 63.6, 56.6, 34.2, 31.7, 26.0, 25.9, 25.1, 24.9. HRMS (ESI, m/z) calcd for $[M+H]^+$: 310.2171; found 310.2173.

2.2 NMR Spectra

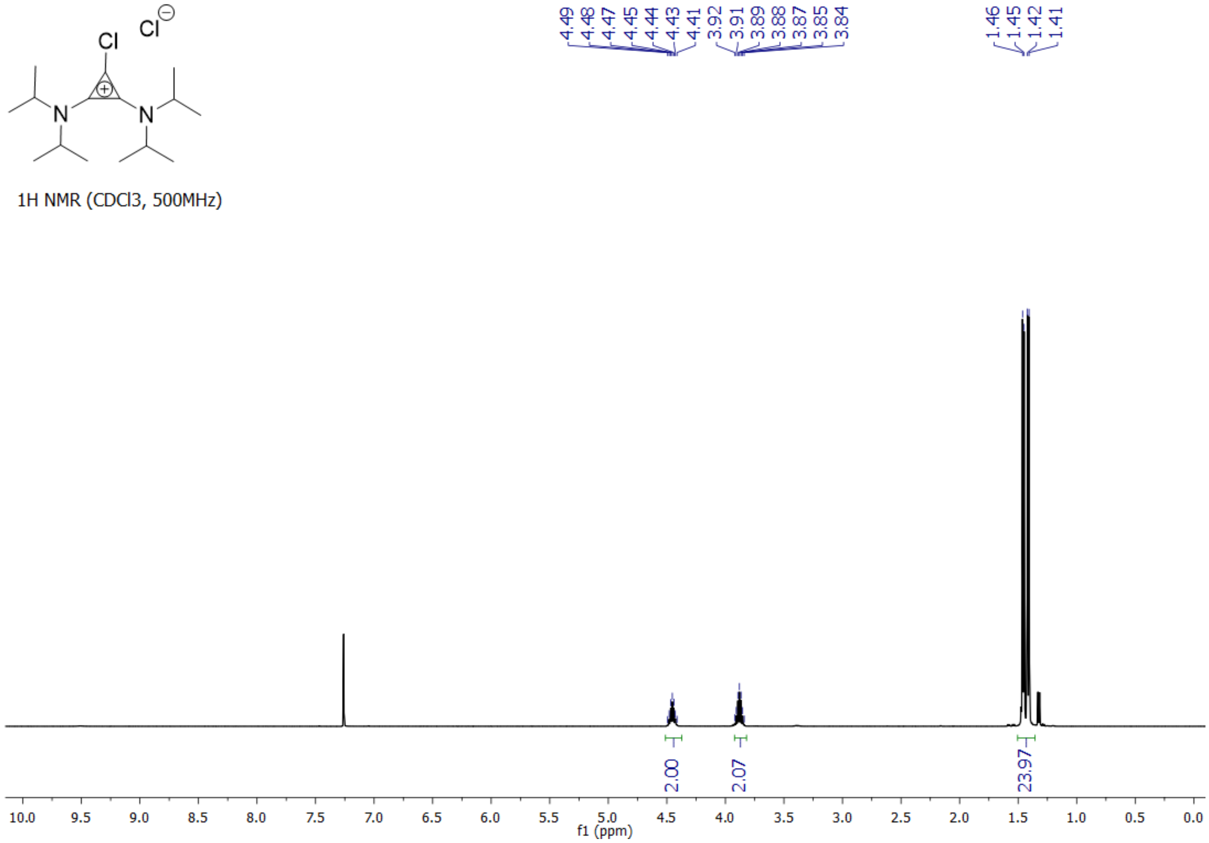

1H NMR (CDCl3, 500MHz)

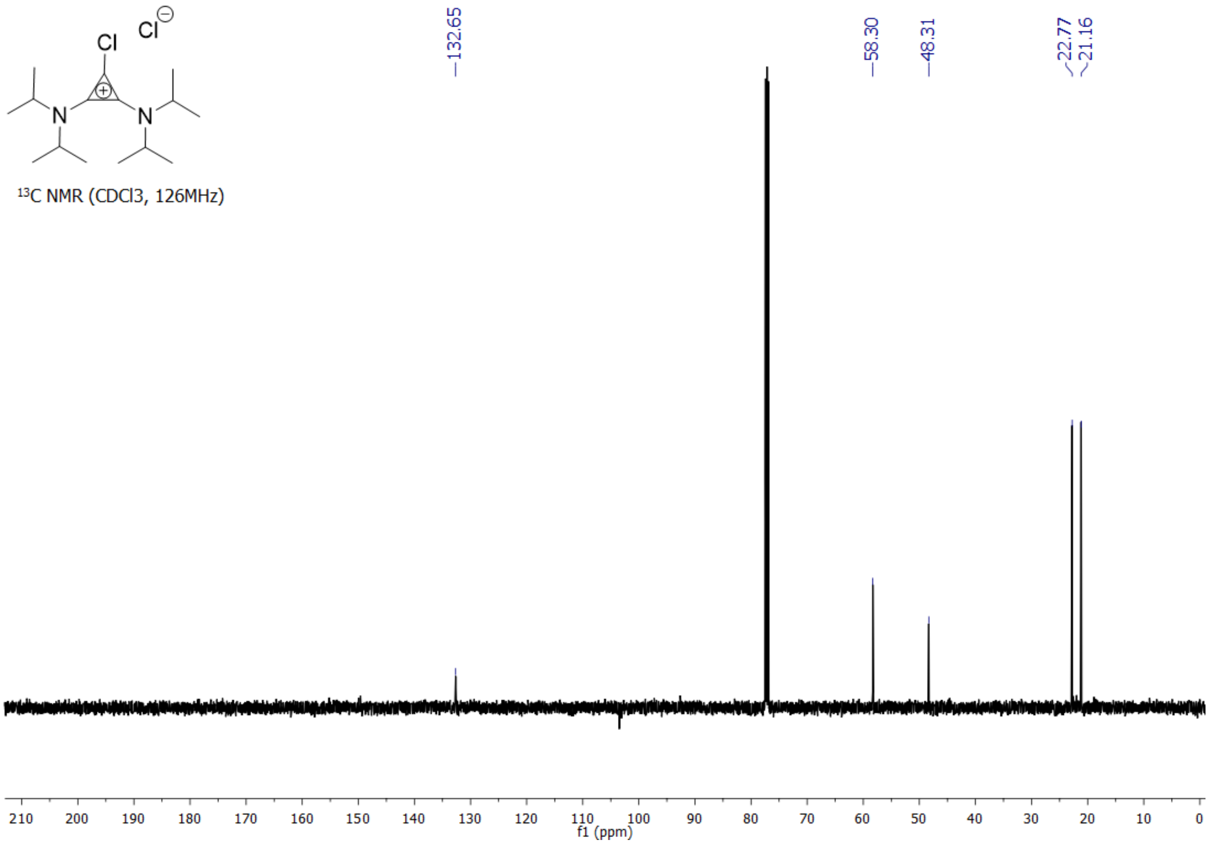

13C NMR (CDCl3, 126MHz)

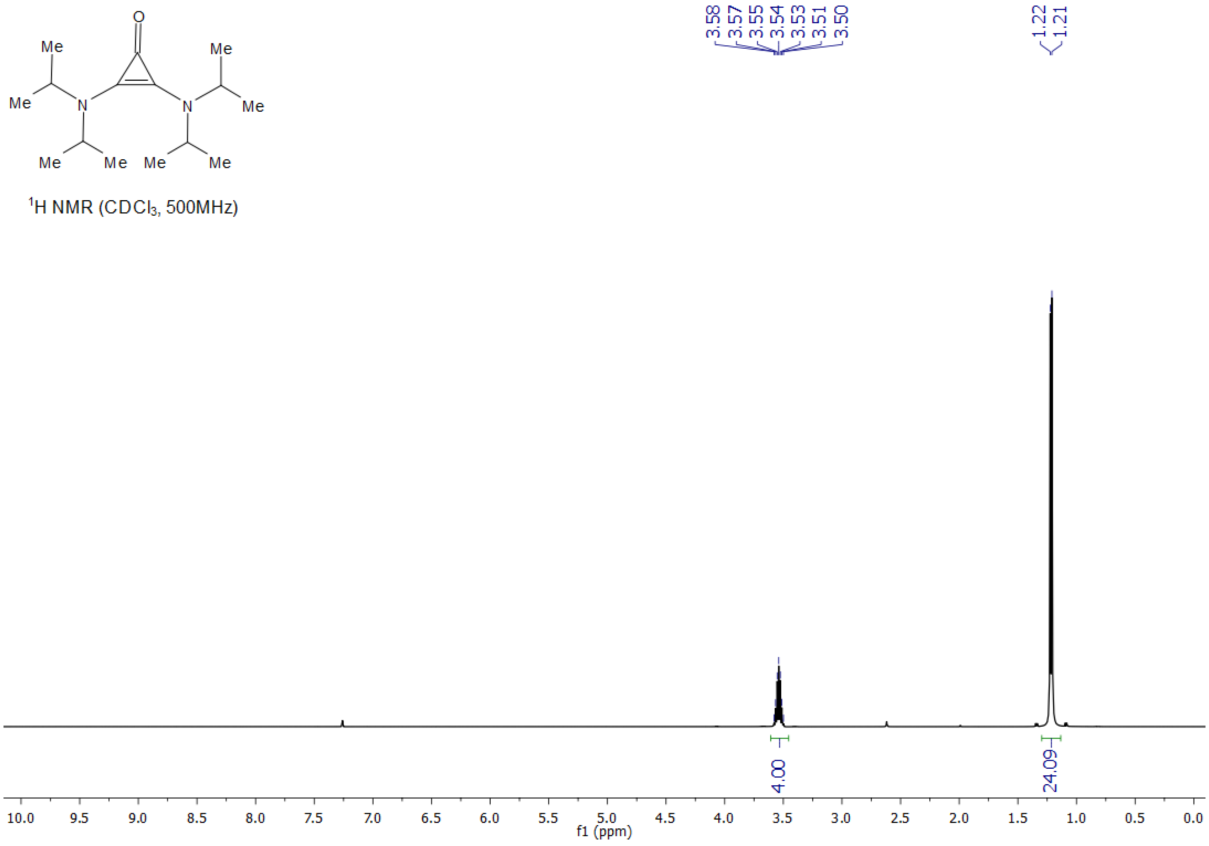

^{1}H NMR ($CDCl_3$, 500MHz)

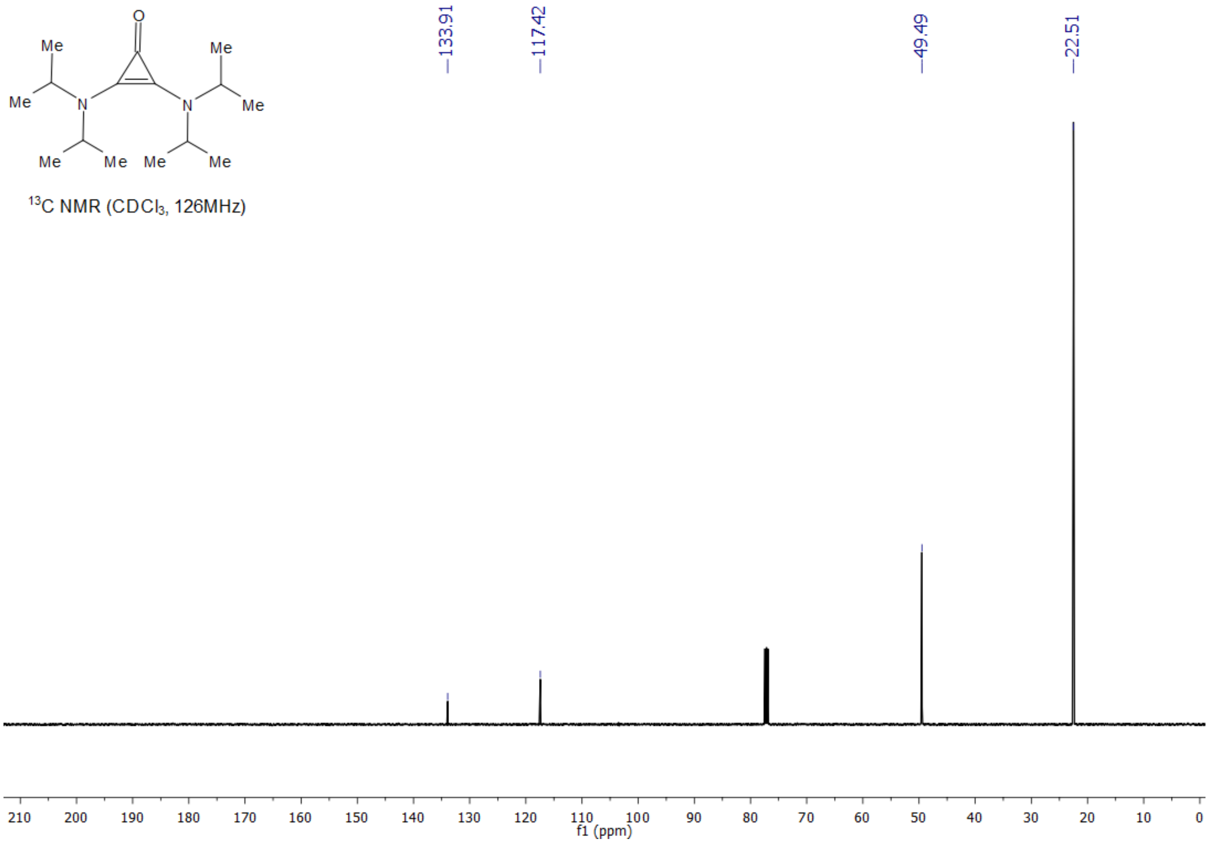

^{13}C NMR ($CDCl_3$, 126MHz)

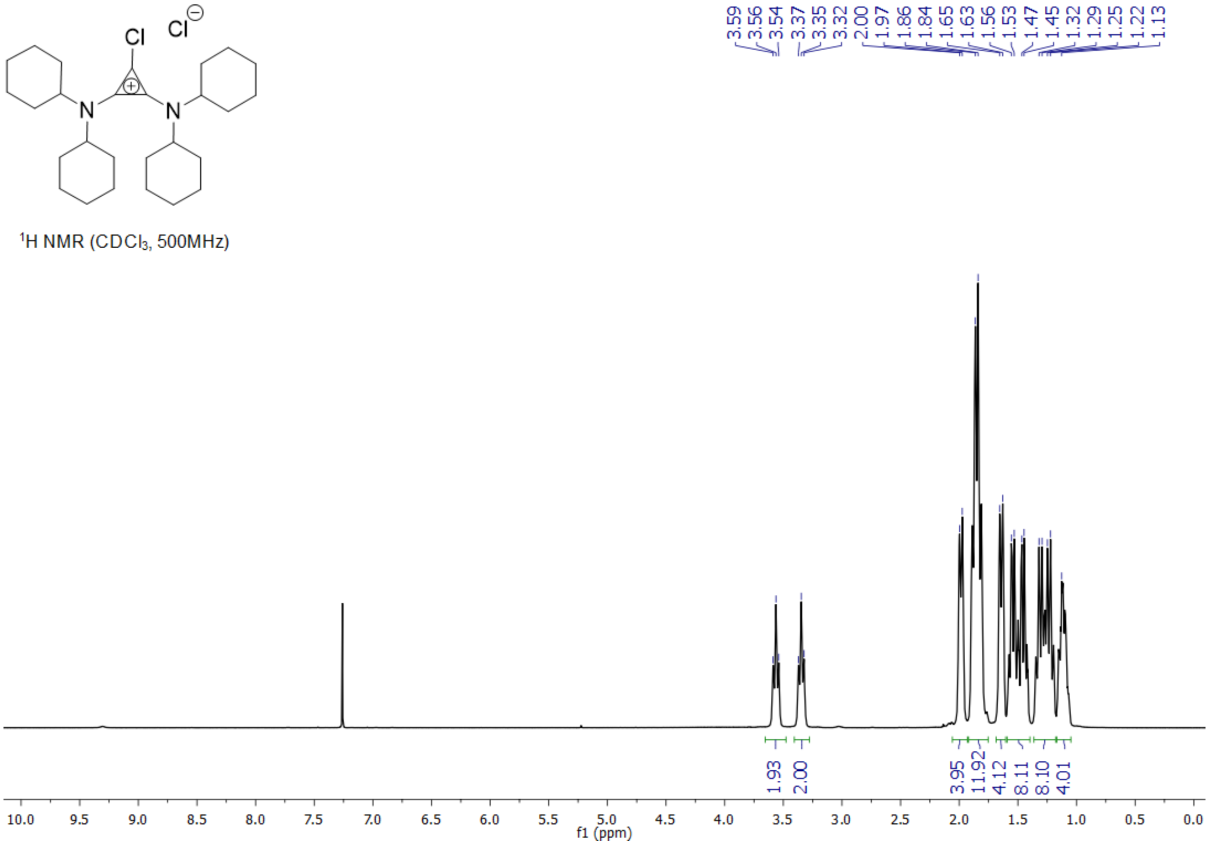

^{1}H NMR (CDCl$_3$, 500MHz)

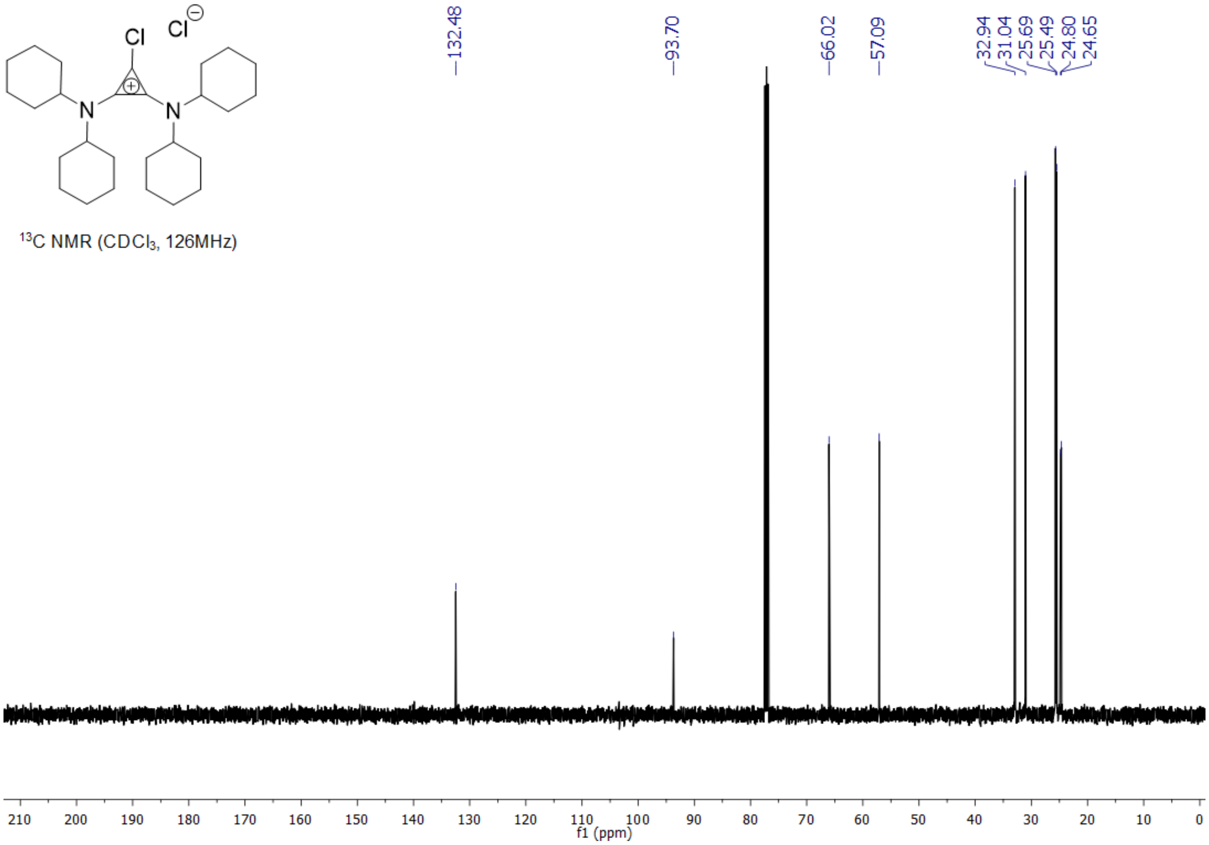

^{13}C NMR (CDCl$_3$, 126MHz)

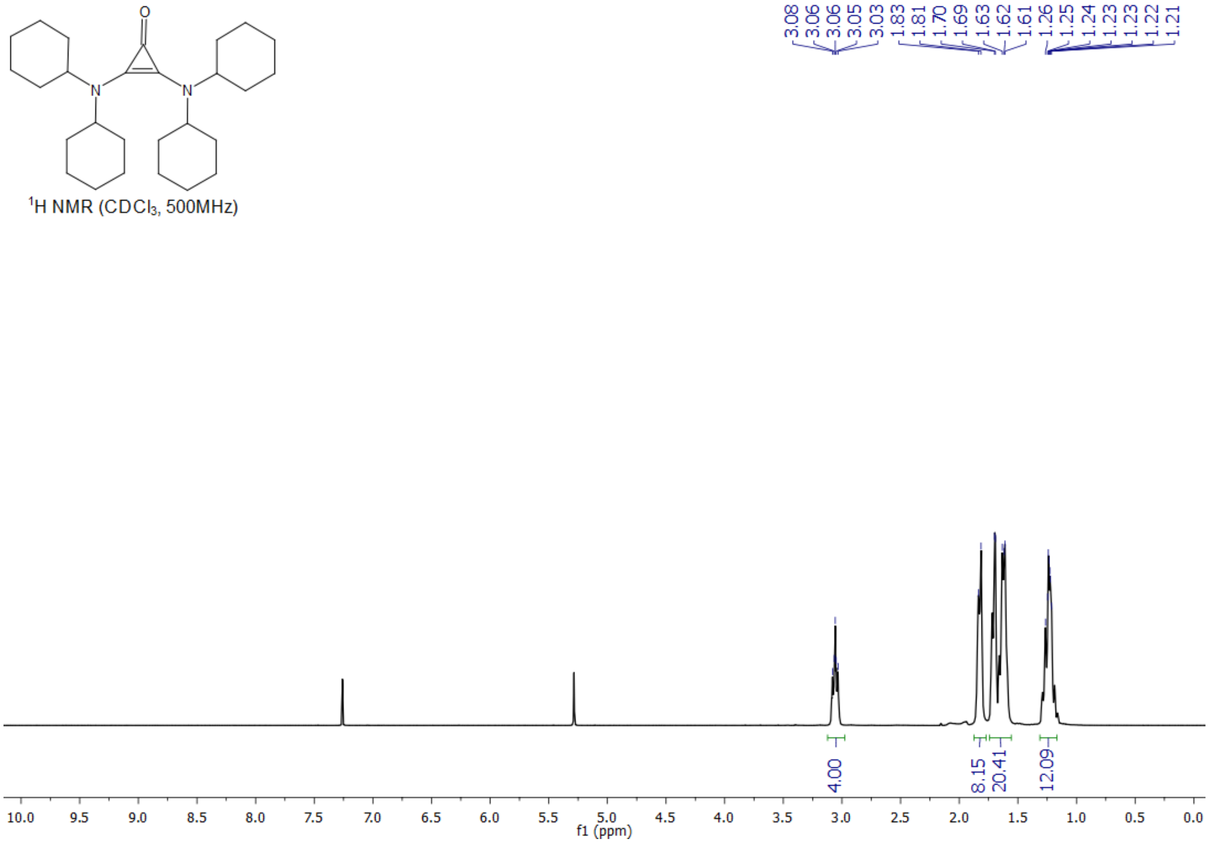

^{1}H NMR ($CDCl_3$, 500MHz)

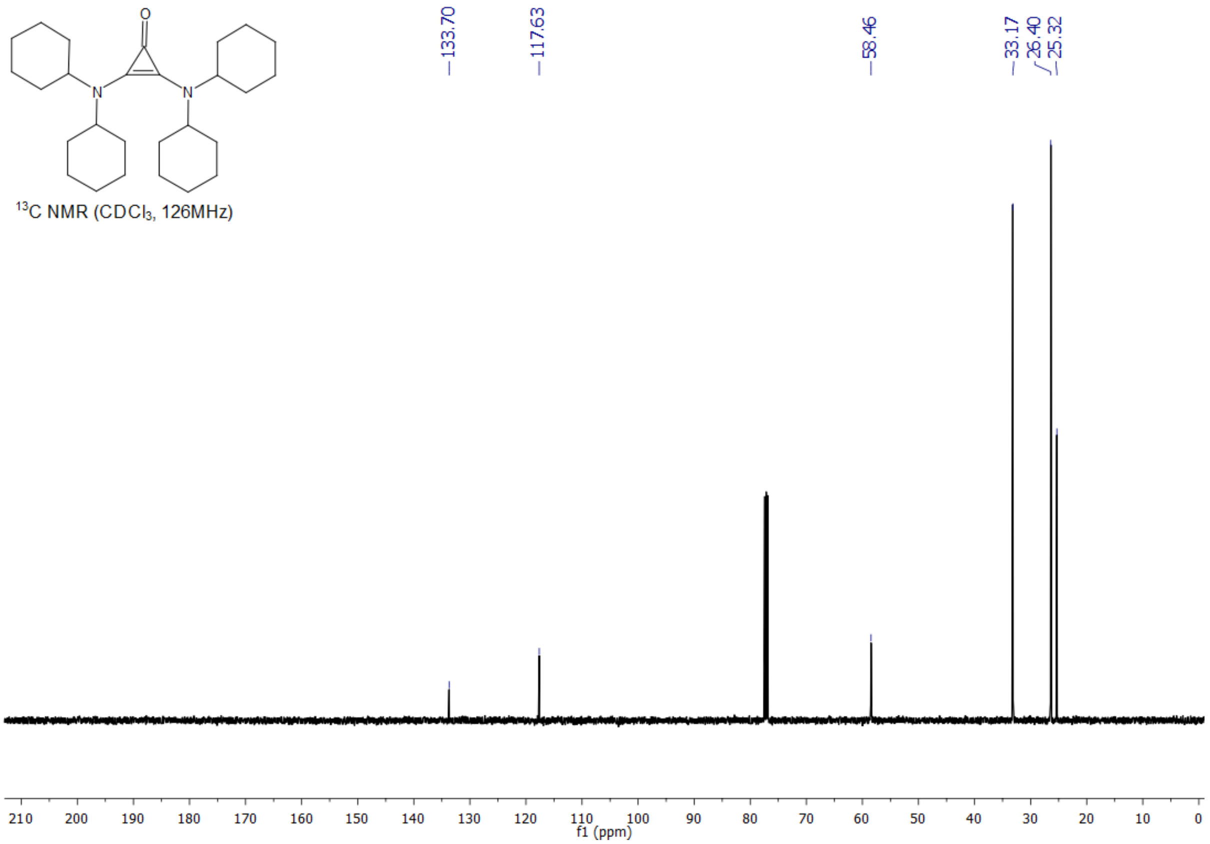

^{13}C NMR ($CDCl_3$, 126MHz)

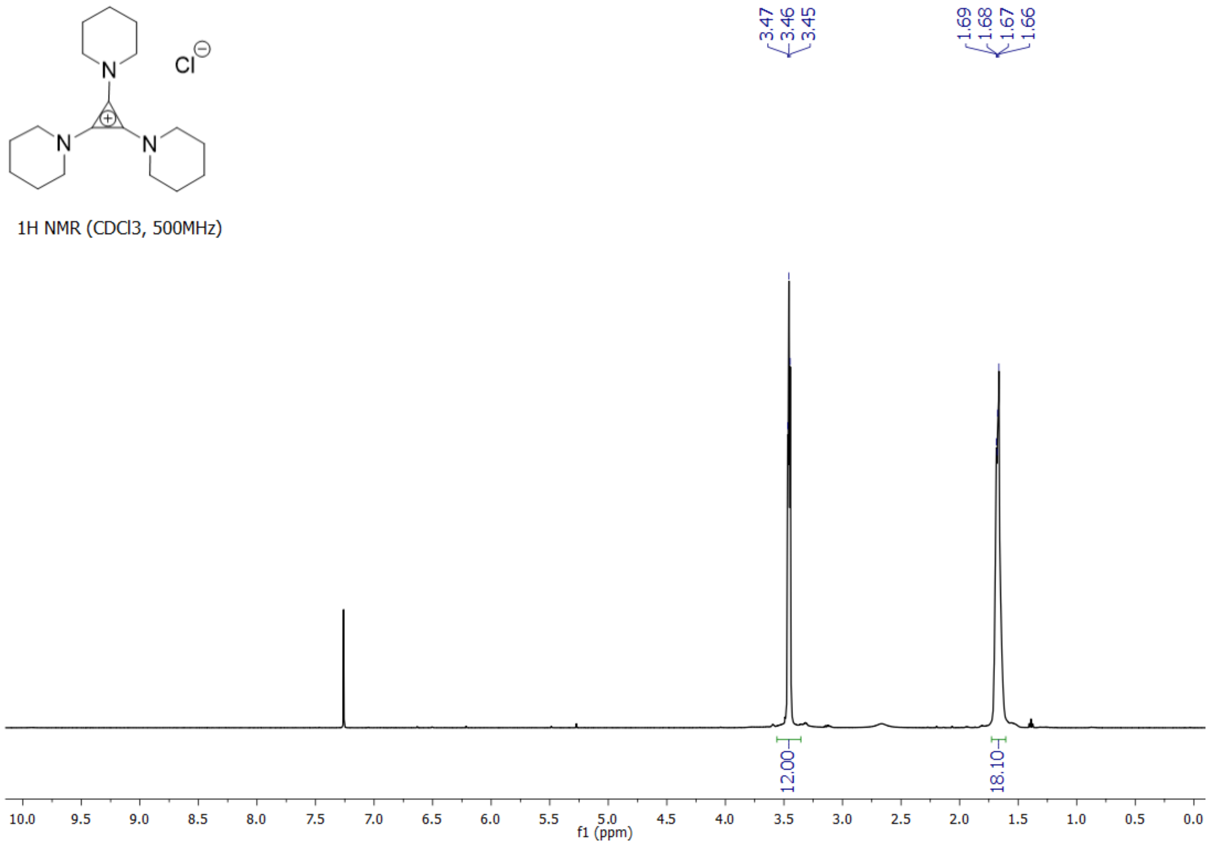

1H NMR (CDCl3, 500MHz)

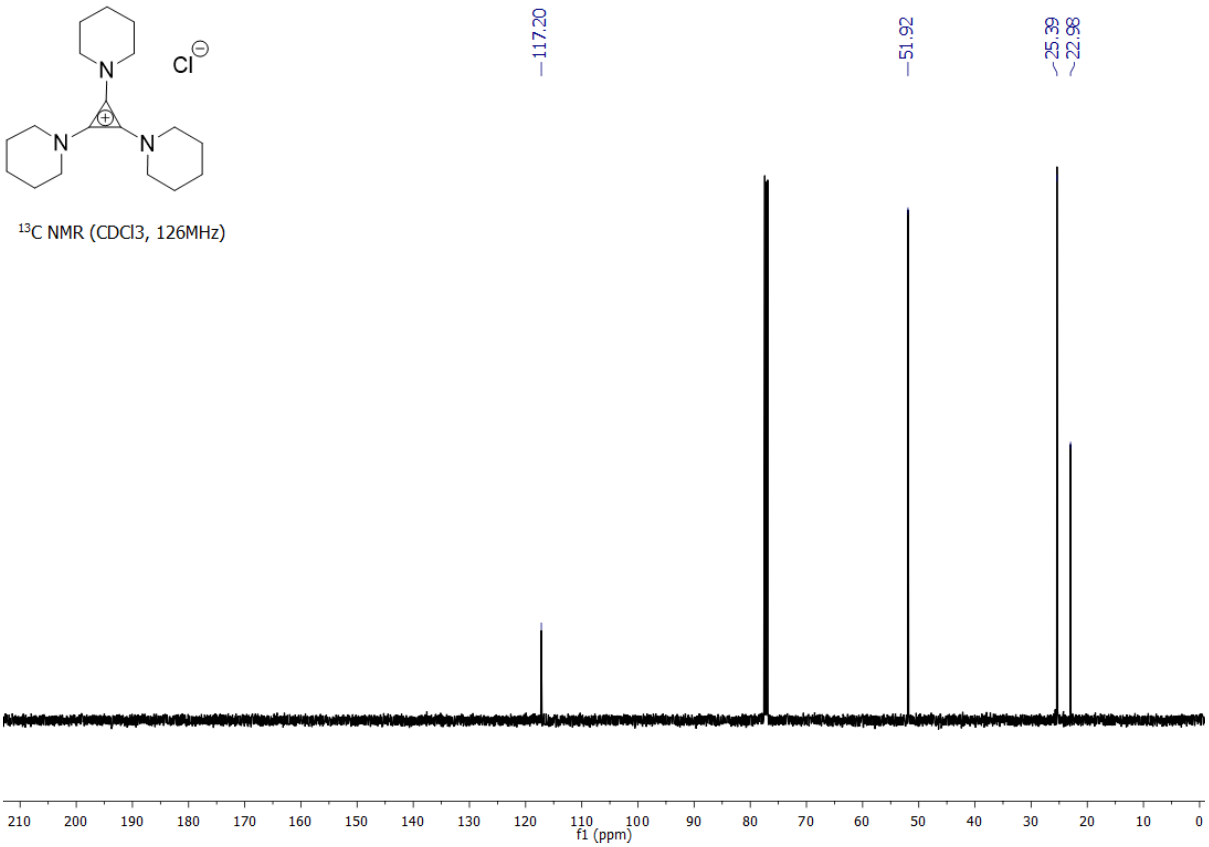

^{13}C NMR (CDCl3, 126MHz)

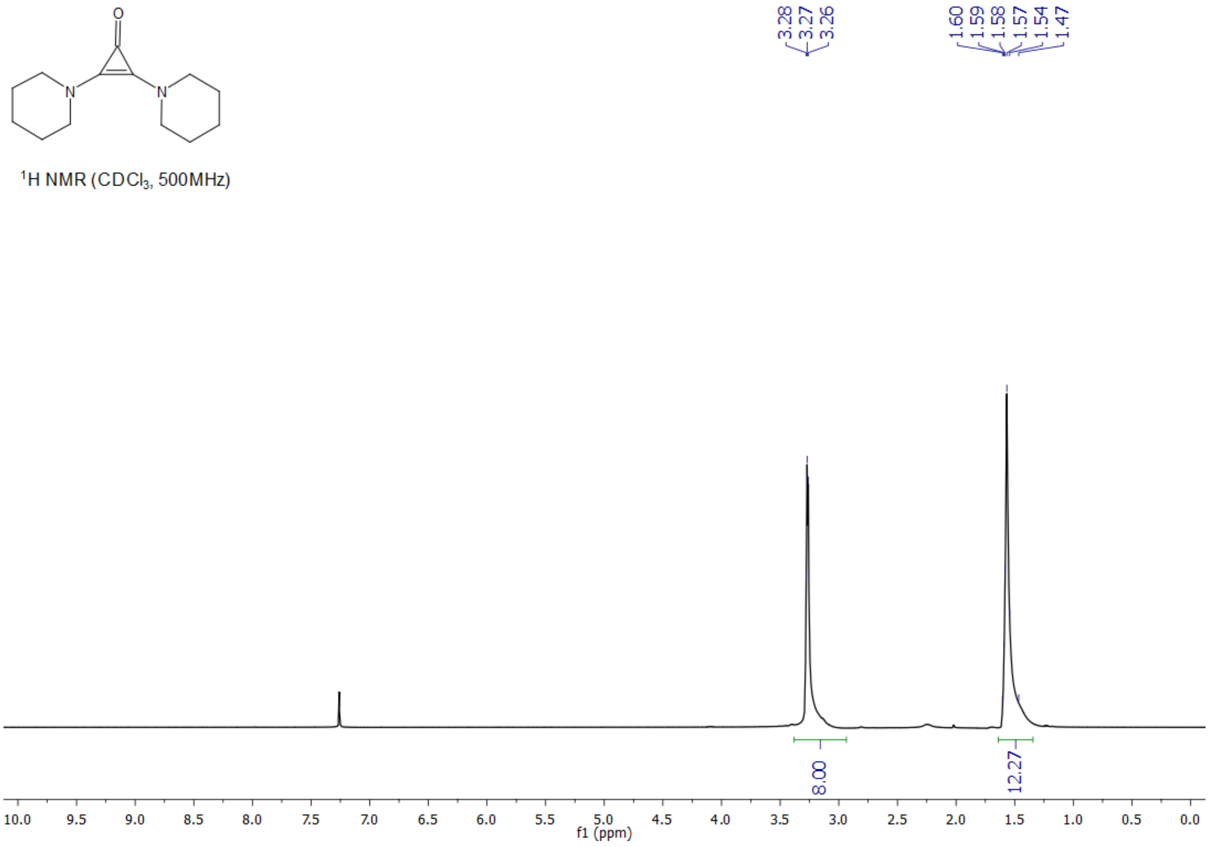

^1H NMR ($CDCl_3$, 500MHz)

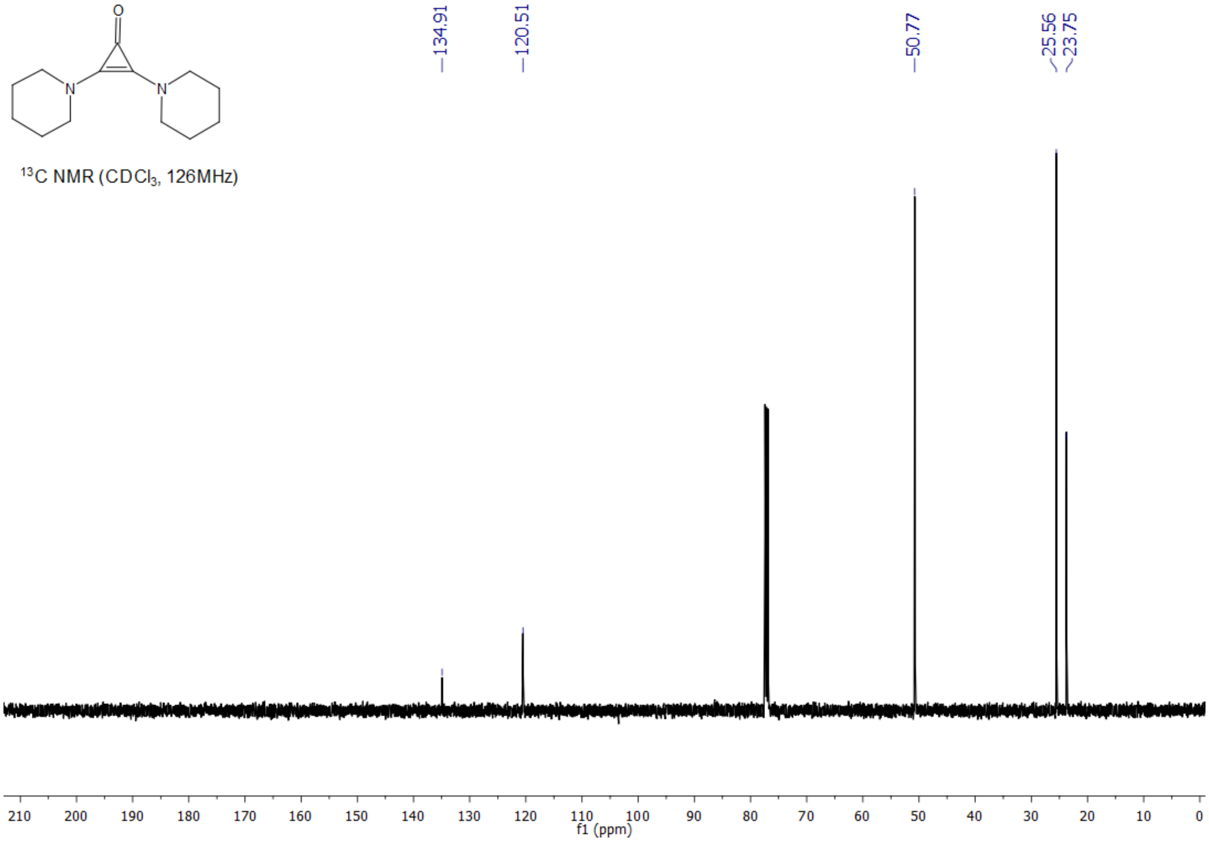

^{13}C NMR ($CDCl_3$, 126MHz)

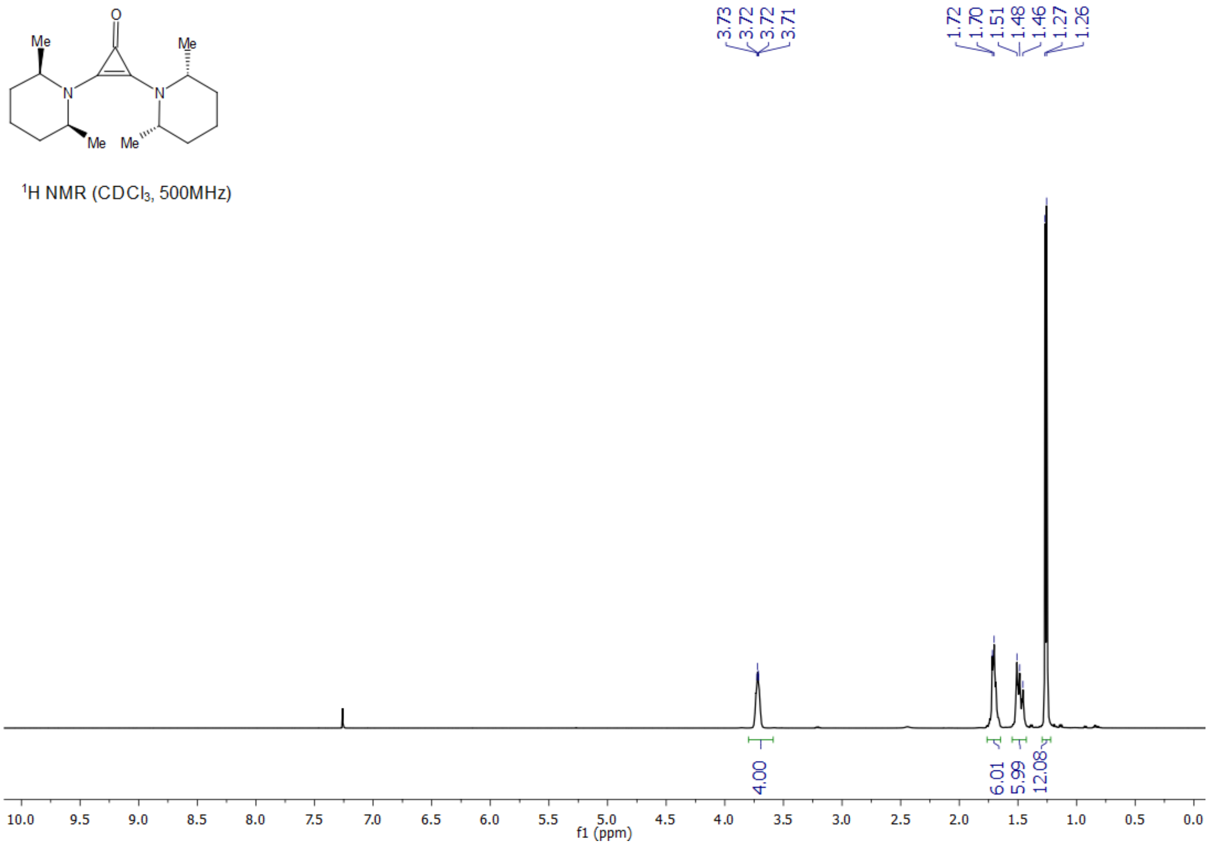

^{1}H NMR (CDCl$_3$, 500MHz)

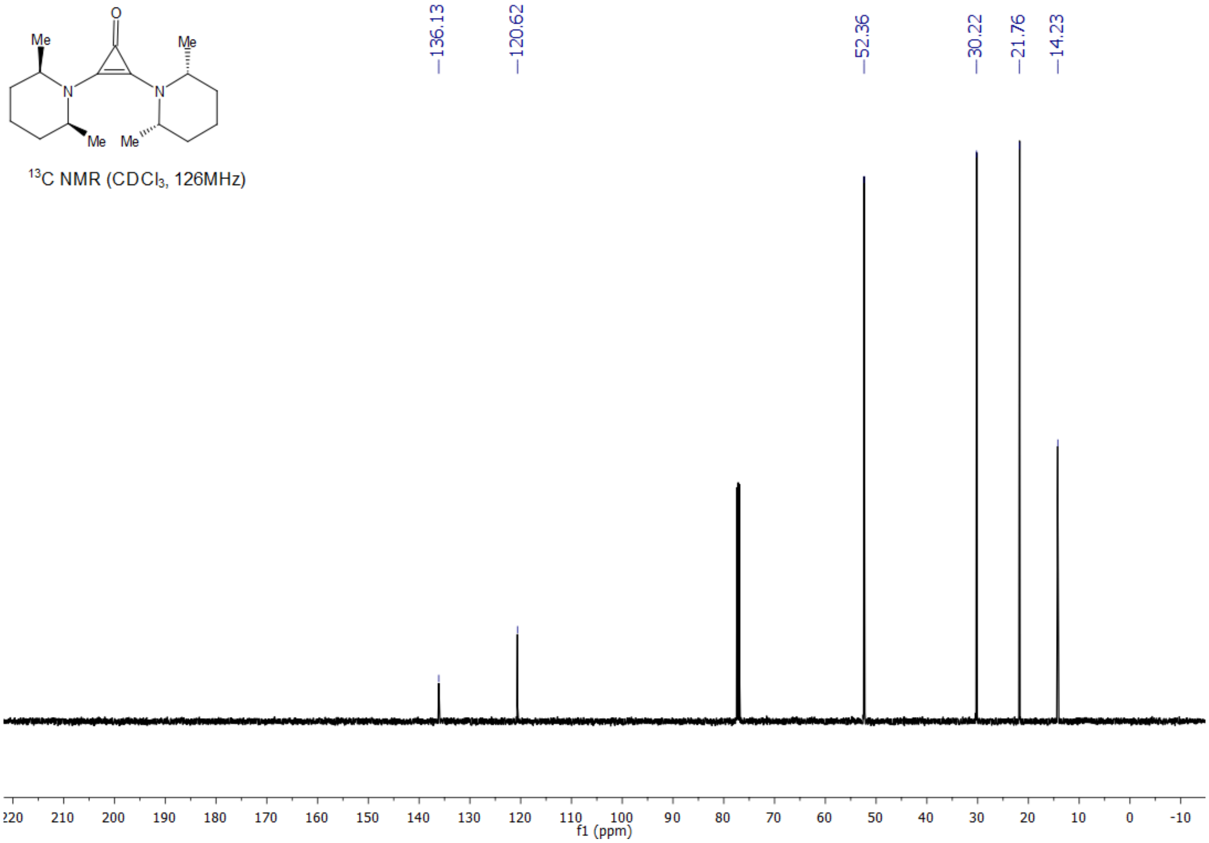

^{13}C NMR (CDCl$_3$, 126MHz)

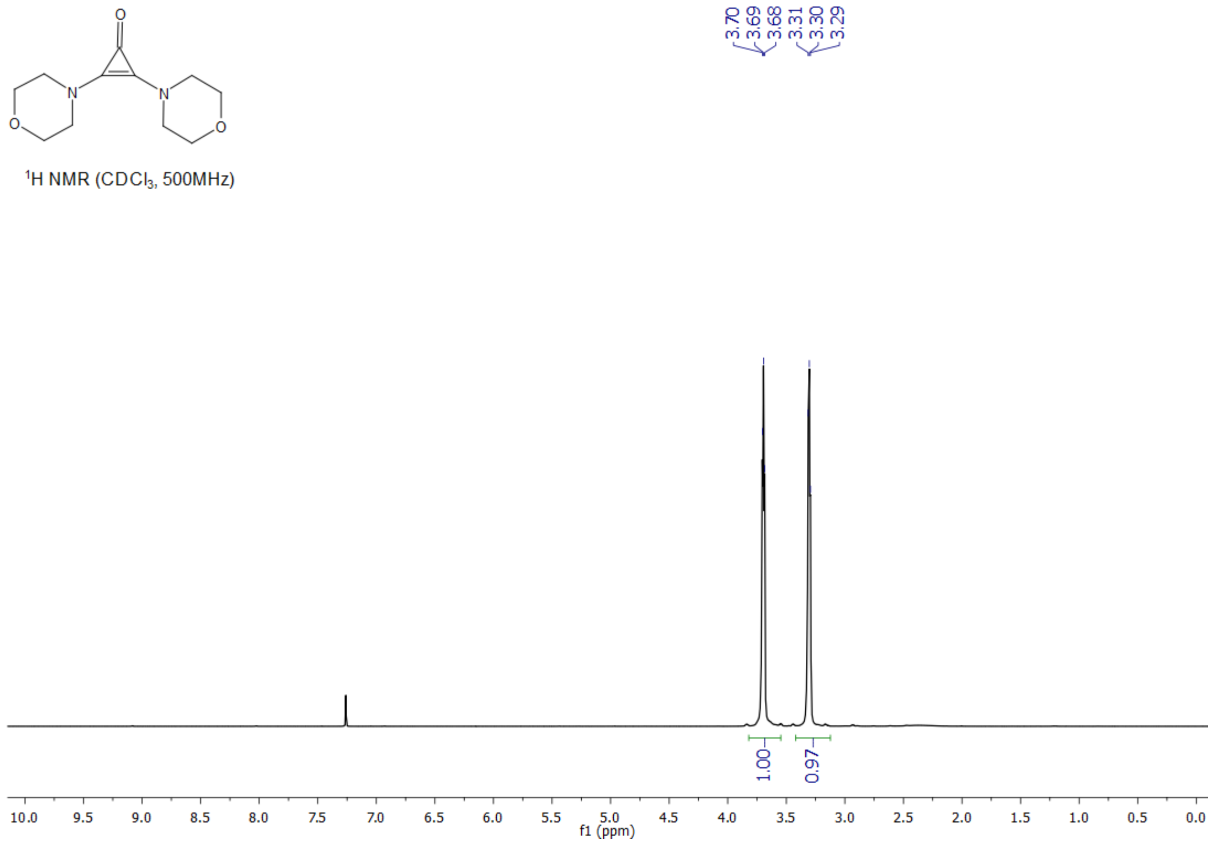

^{1}H NMR ($CDCl_3$, 500MHz)

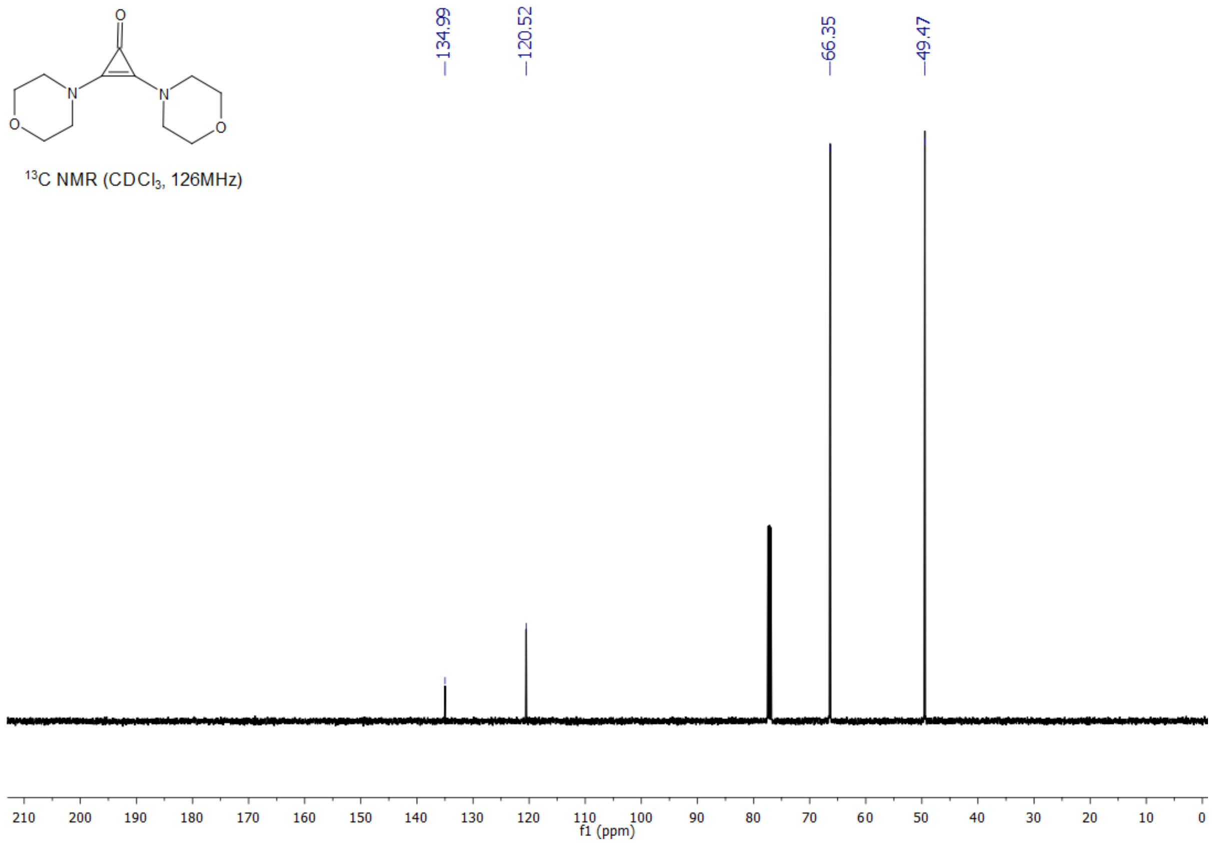

^{13}C NMR ($CDCl_3$, 126MHz)

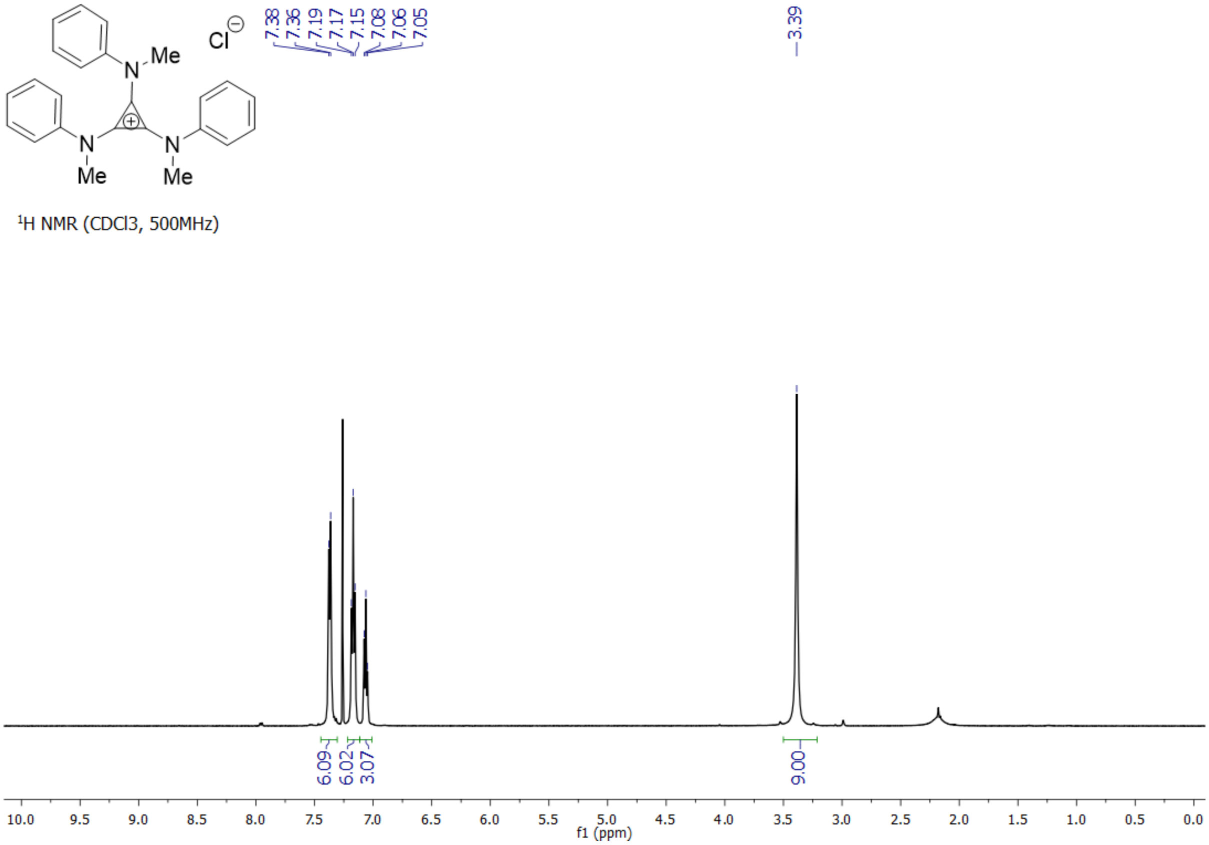

^{1}H NMR (CDCl3, 500MHz)

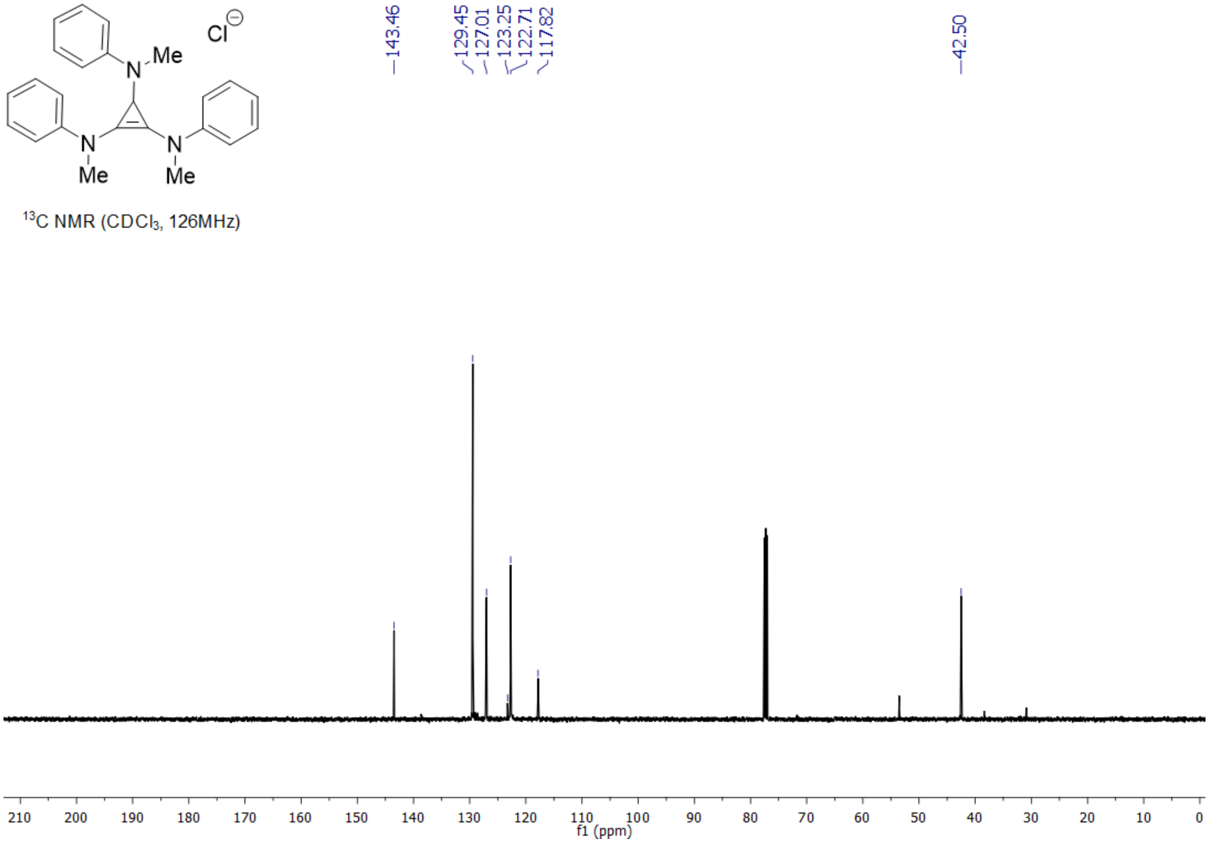

^{13}C NMR (CDCl$_3$, 126MHz)

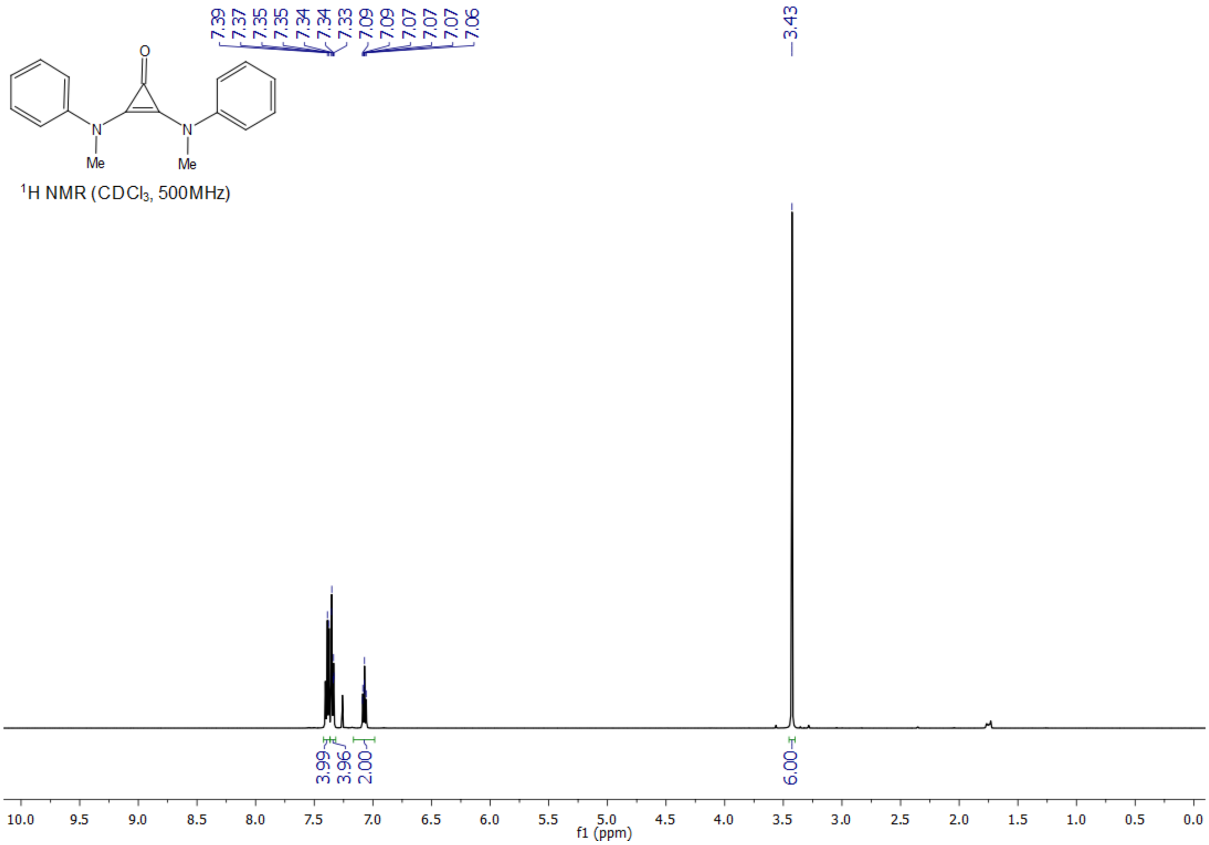
7.39
7.37
7.35
7.35
7.34
7.34
7.33
7.09
7.09
7.07
7.07
7.07
7.06
3.43
O
N
N
Me
Me
¹H NMR (CDCl₃, 500MHz)
3.99
3.96
2.00
6.00
10.0
9.5
9.0
8.5
8.0
7.5
7.0
6.5
6.0
5.5
5.0
4.5
4.0
3.5
3.0
2.5
2.0
1.5
1.0
0.5
0.0
f1 (ppm)

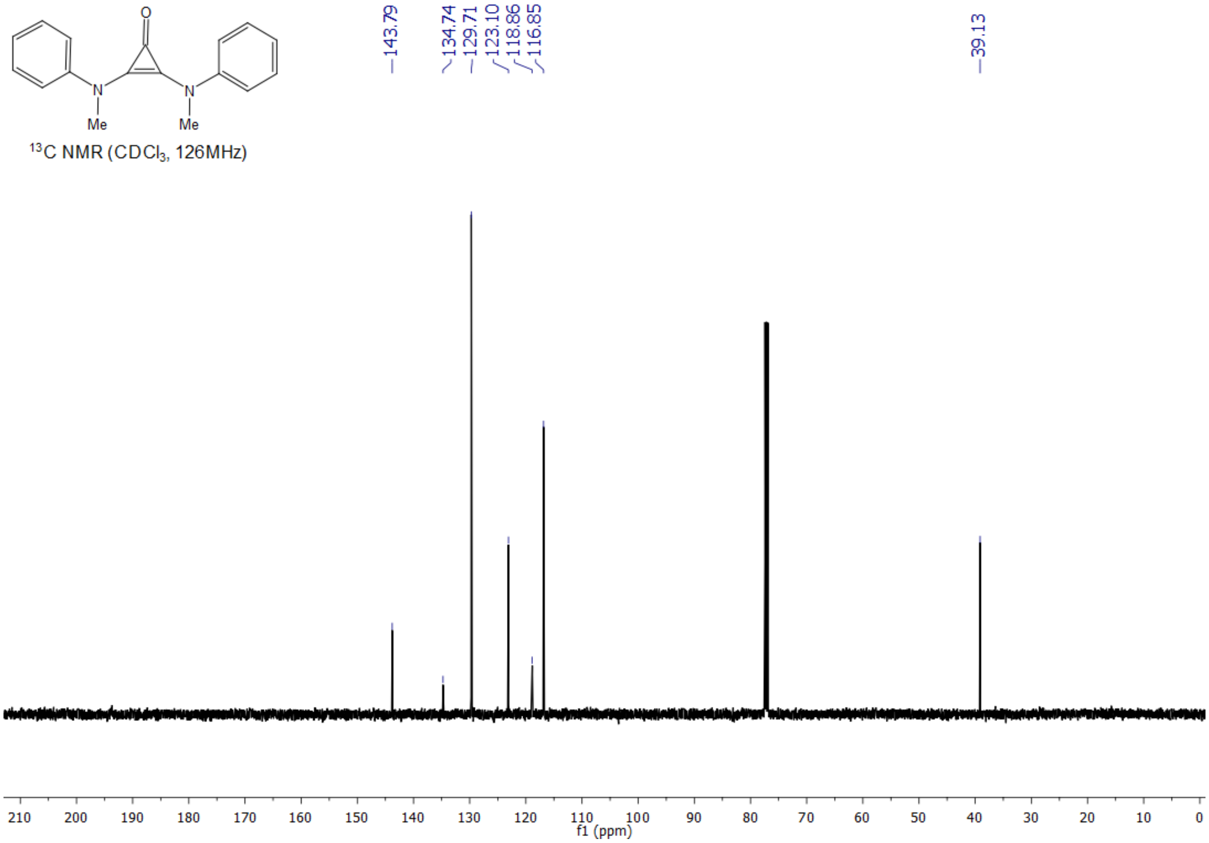
143.79
134.74
129.71
123.10
118.86
116.85
39.13
O
N
N
Me
Me
¹³C NMR (CDCl₃, 126MHz)
210
200
190
180
170
160
150
140
130
120
110
100
90
80
70
60
50
40
30
20
10
0
f1 (ppm)

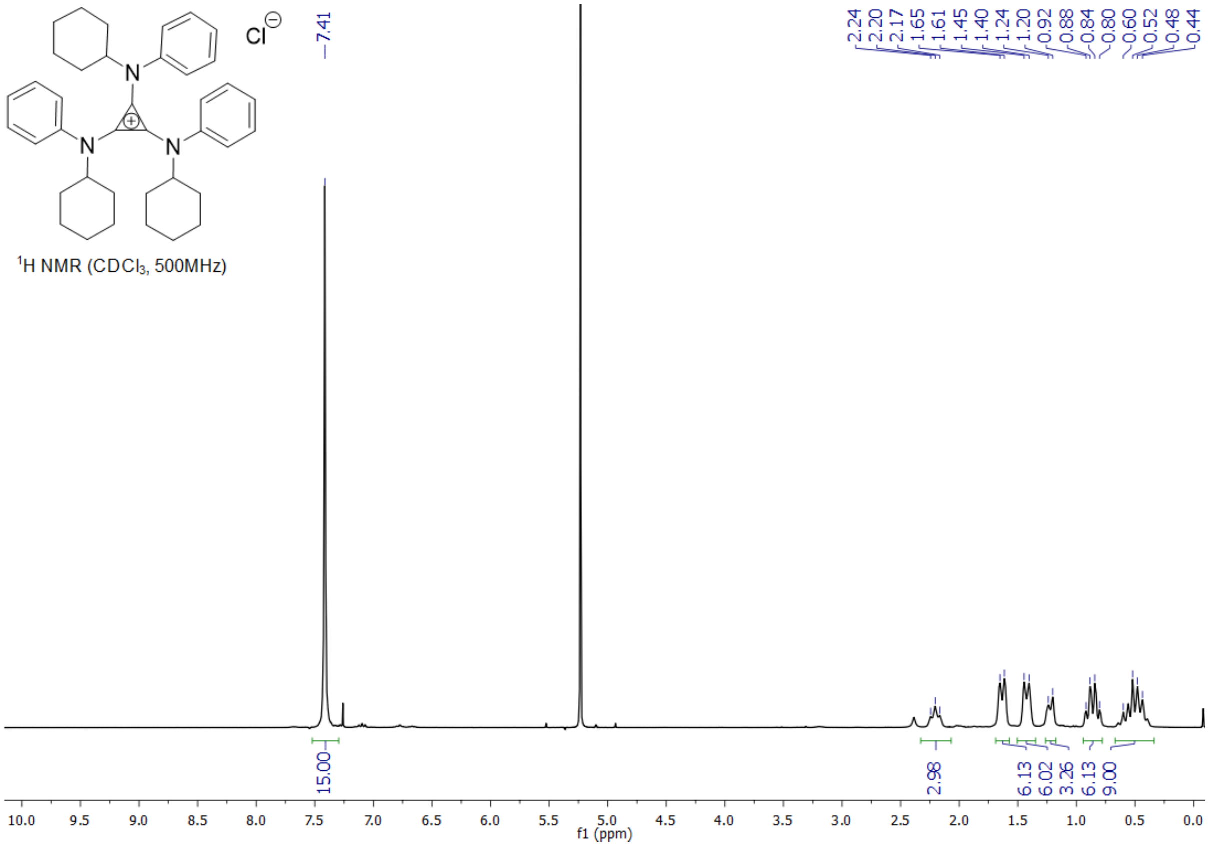
Cl⊖
N
N
N
+
^{1}H NMR (CDCl$_3$, 500MHz)
7.41
2.24
2.20
2.17
1.65
1.61
1.45
1.40
1.24
1.20
0.92
0.88
0.84
0.80
0.60
0.52
0.48
0.44
15.00
2.98
6.13
6.02
3.26
6.13
9.00
10.0 9.5 9.0 8.5 8.0 7.5 7.0 6.5 6.0 5.5 5.0 4.5 4.0 3.5 3.0 2.5 2.0 1.5 1.0 0.5 0.0
f1 (ppm)

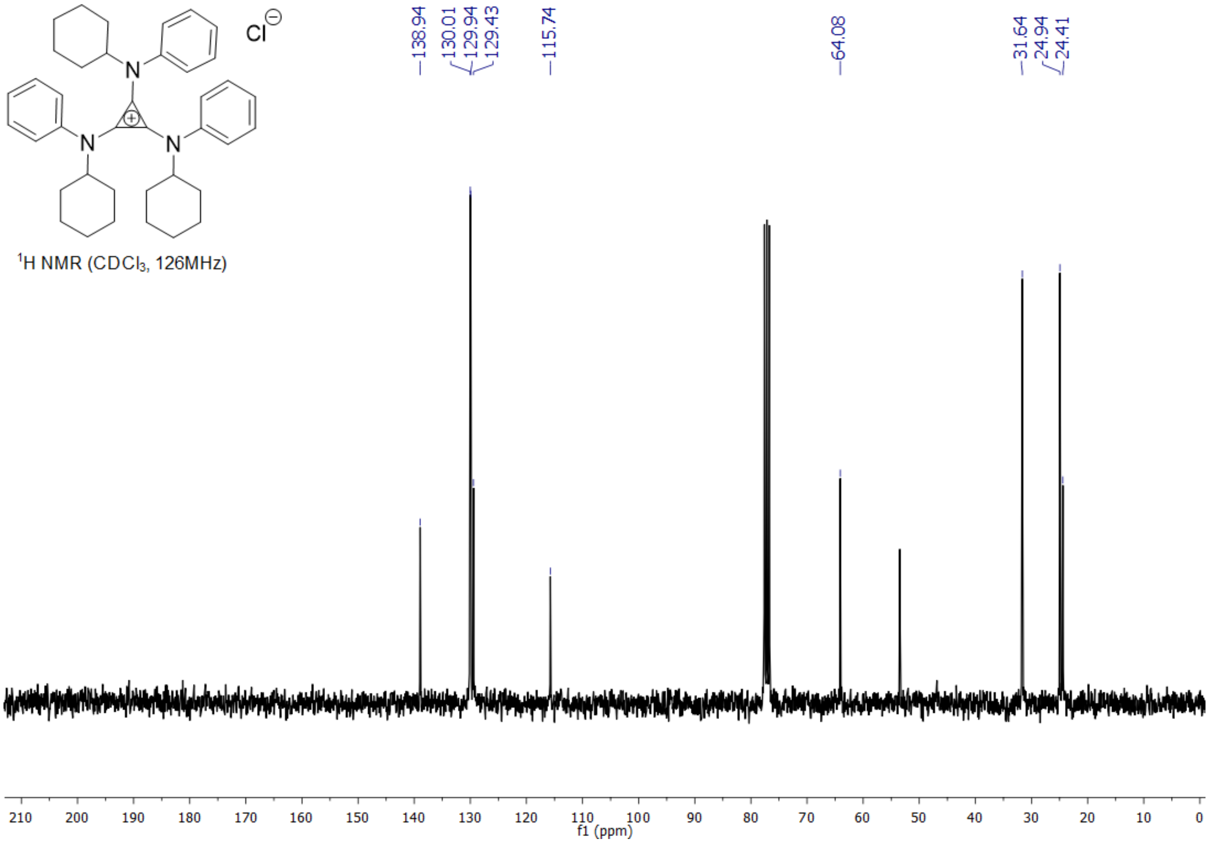
Cl⊖
N
N
N
+
^{1}H NMR (CDCl$_3$, 126MHz)
138.94
130.01
129.94
129.43
115.74
64.08
31.64
24.94
24.41
210 200 190 180 170 160 150 140 130 120 110 100 90 80 70 60 50 40 30 20 10 0
f1 (ppm)

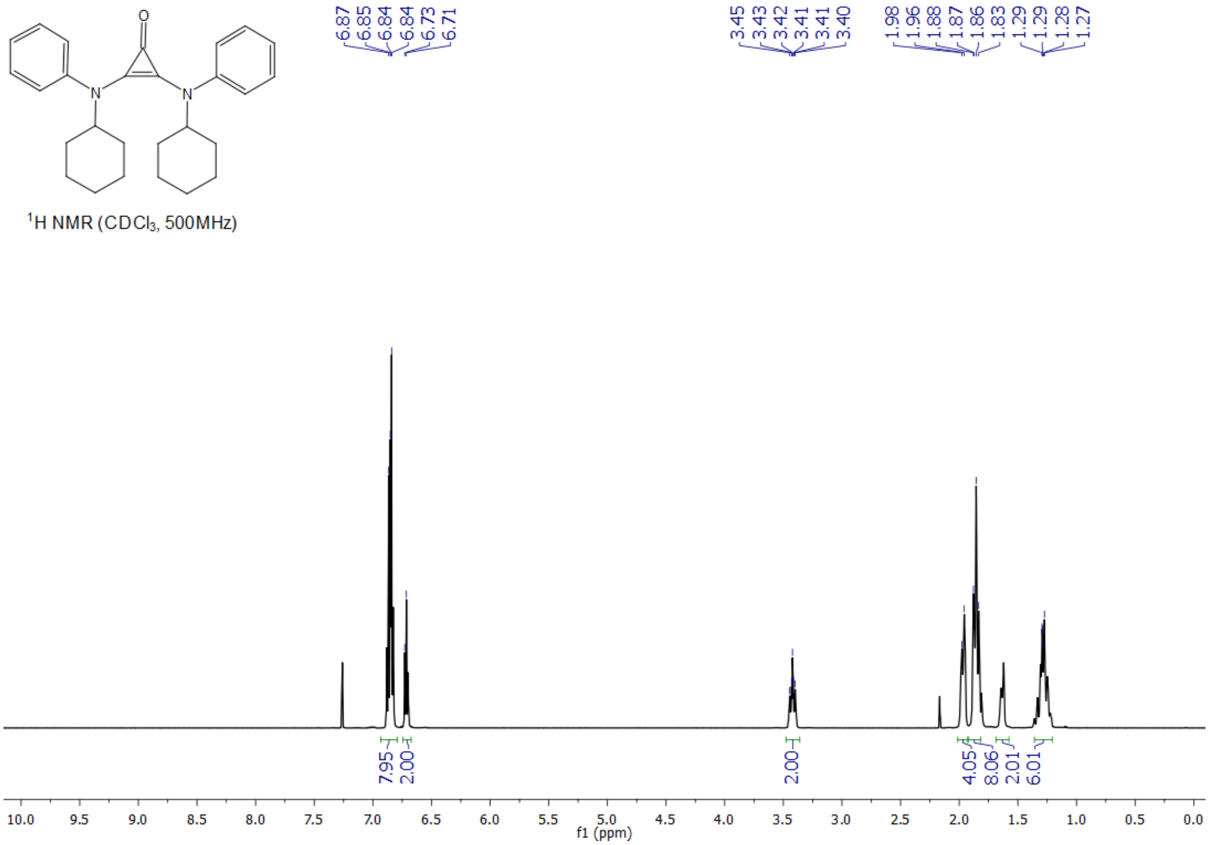

^{1}H NMR (CDCl$_3$, 500MHz)

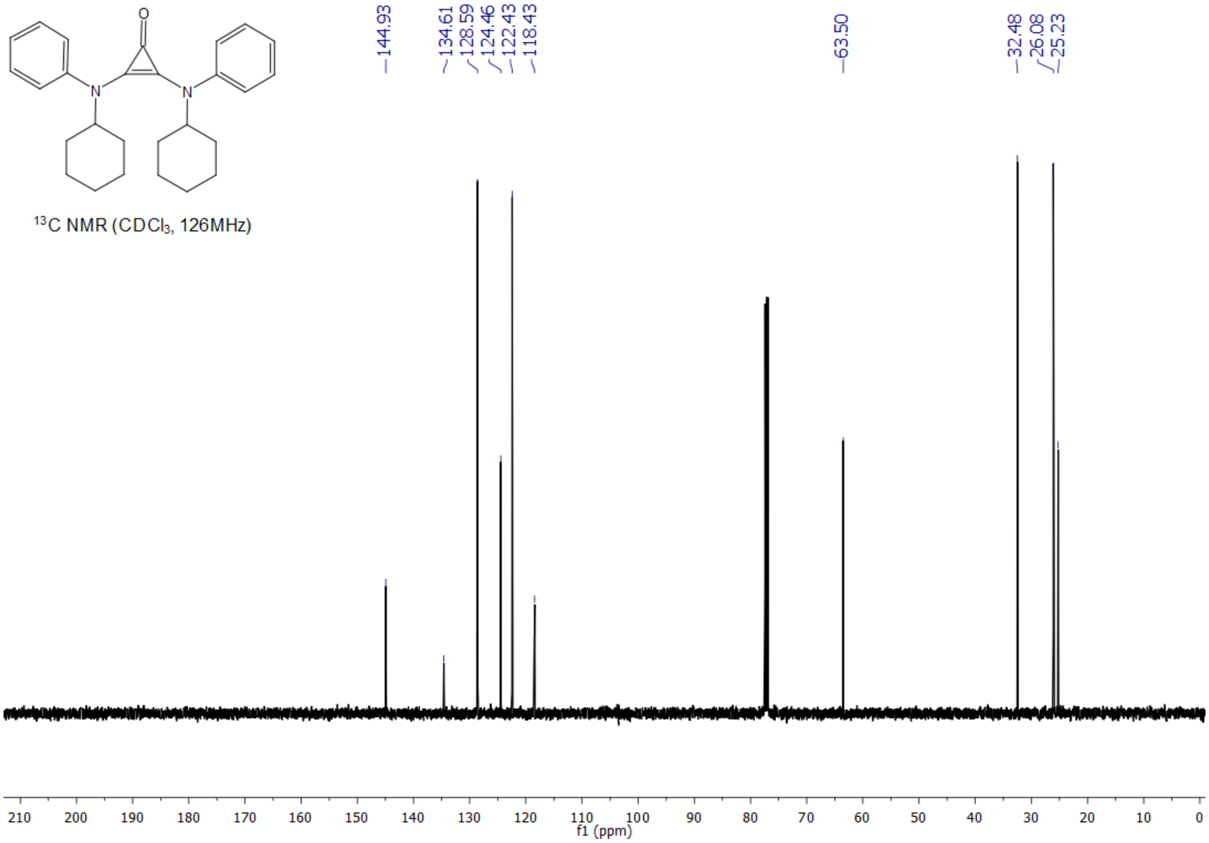

^{13}C NMR (CDCl$_3$, 126MHz)

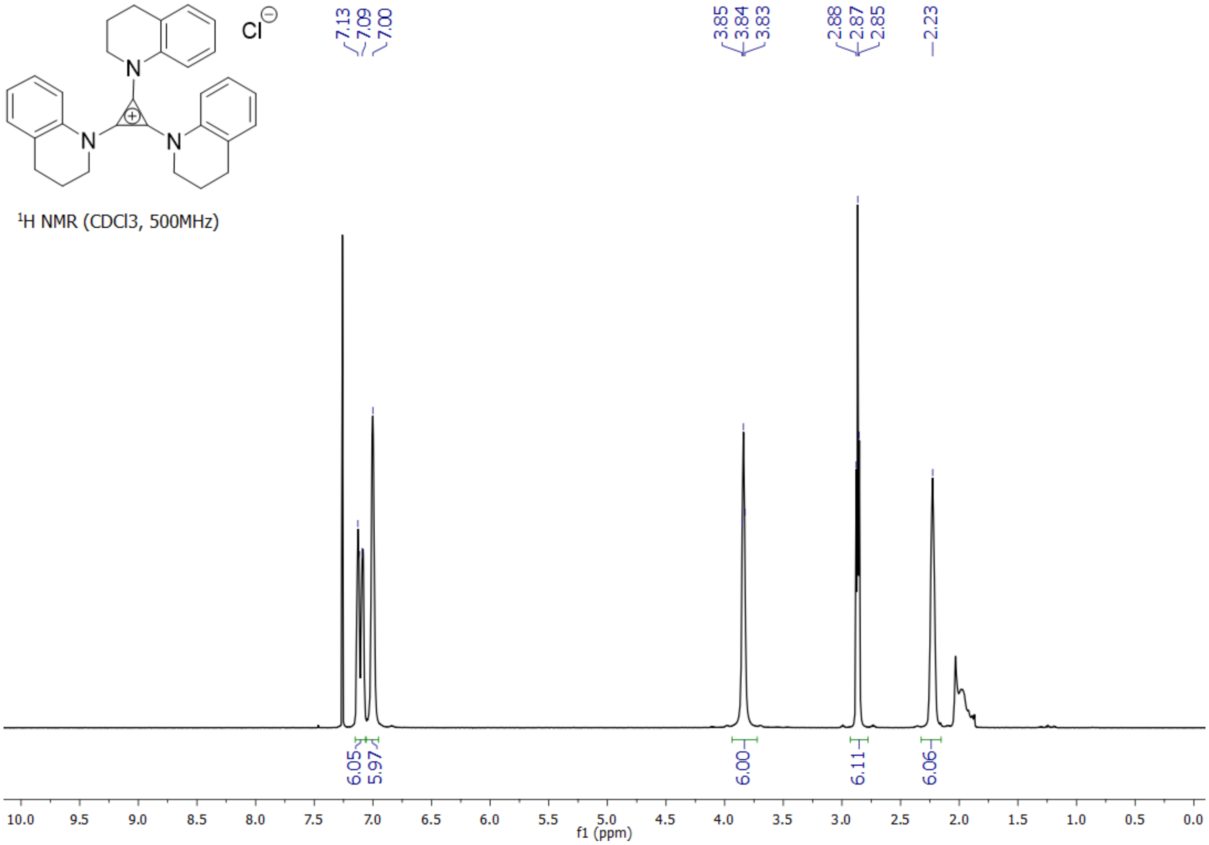
Cl⊖
N
N
N
+
¹H NMR (CDCl3, 500MHz)
7.13
7.09
7.00
3.85
3.84
3.83
2.88
2.87
2.85
2.23
6.05
5.97
6.00
6.11
6.06
10.0 9.5 9.0 8.5 8.0 7.5 7.0 6.5 6.0 5.5 5.0 4.5 4.0 3.5 3.0 2.5 2.0 1.5 1.0 0.5 0.0
f1 (ppm)

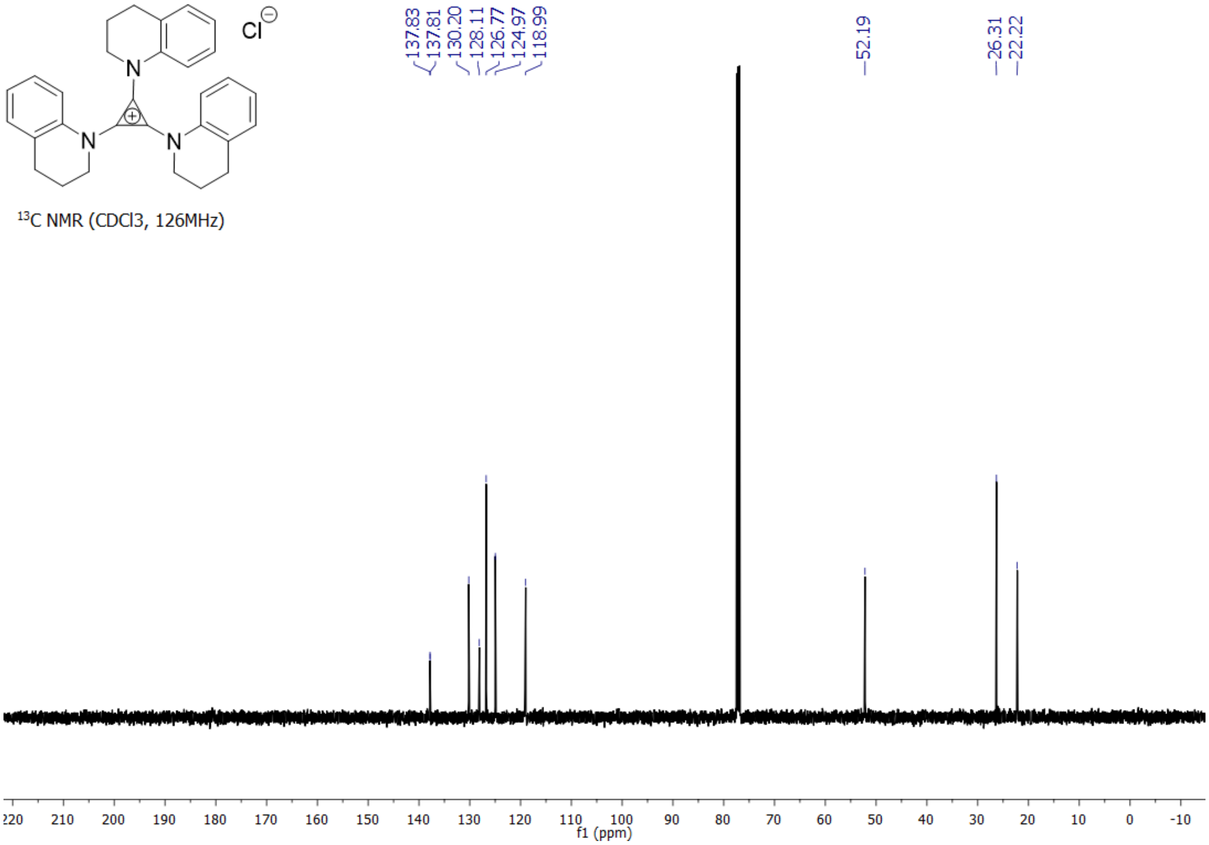
Cl⊖
N
N
N
+
¹³C NMR (CDCl3, 126MHz)
137.83
137.81
130.20
128.11
126.77
124.97
118.99
52.19
26.31
22.22
220 210 200 190 180 170 160 150 140 130 120 110 100 90 80 70 60 50 40 30 20 10 0 -10
f1 (ppm)

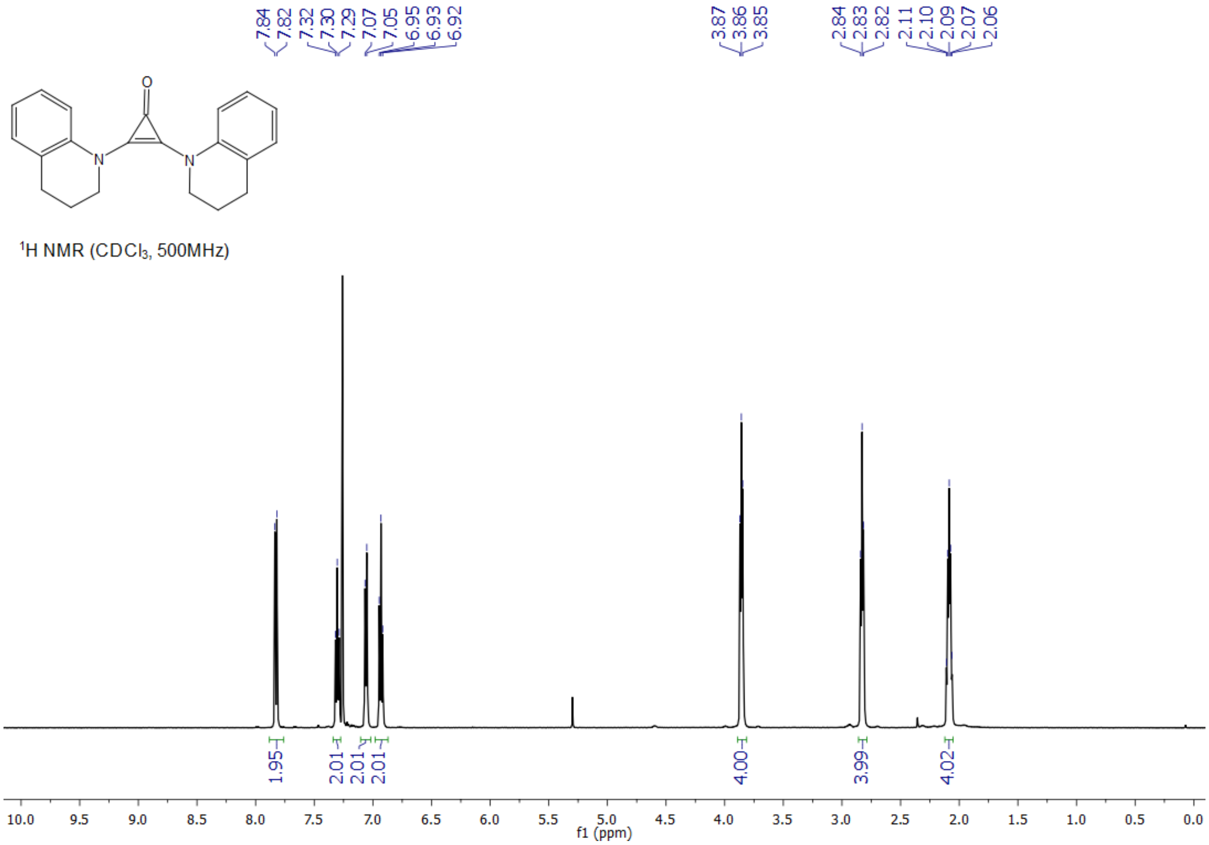

^{1}H NMR (CDCl$_3$, 500MHz)

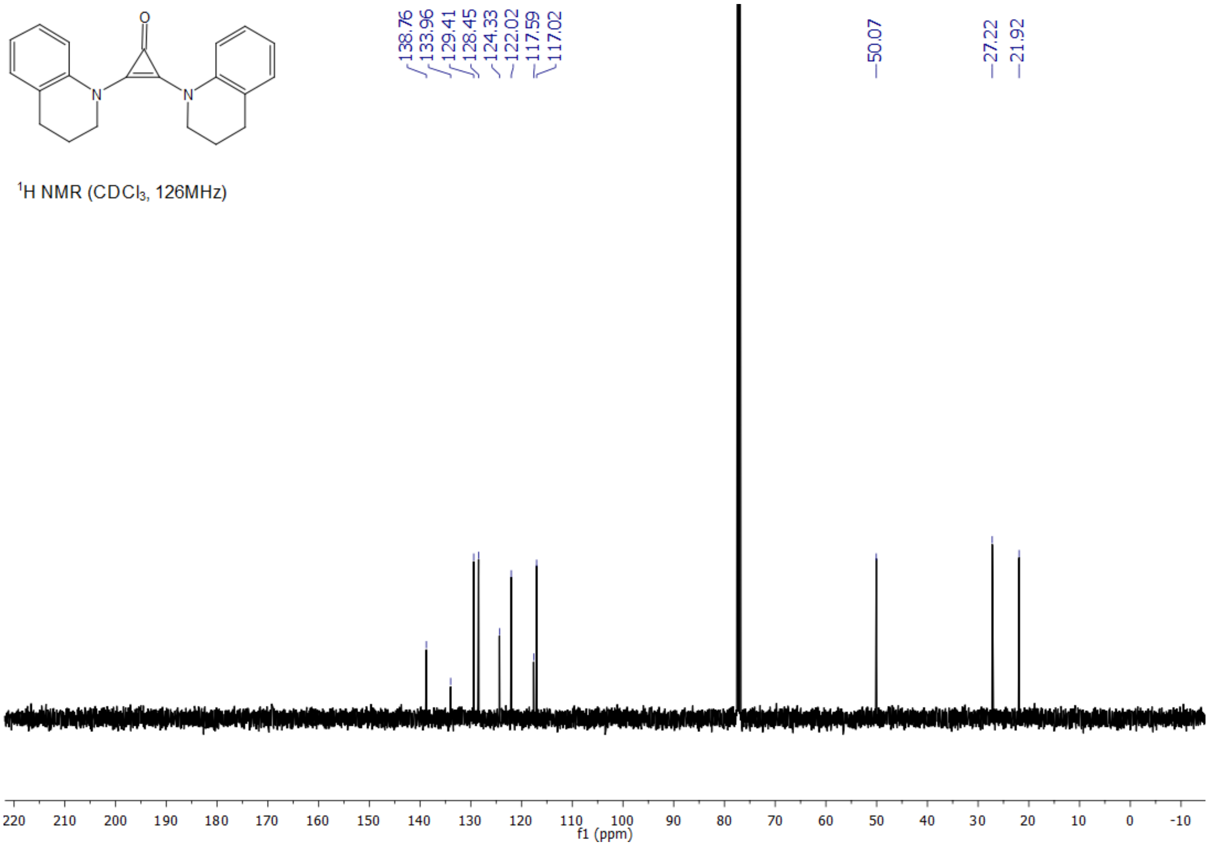

^{1}H NMR (CDCl$_3$, 126MHz)

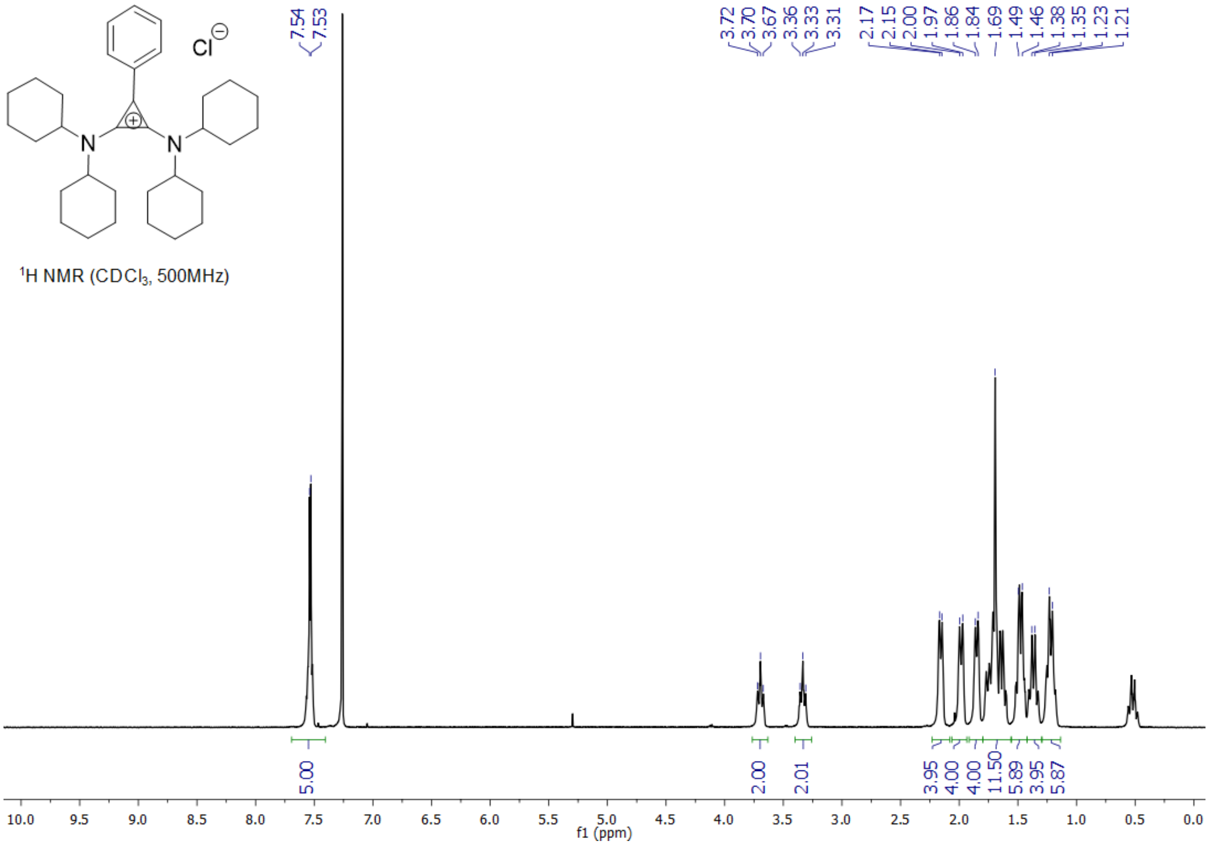
^{1}H NMR (CDCl$_3$, 500MHz)

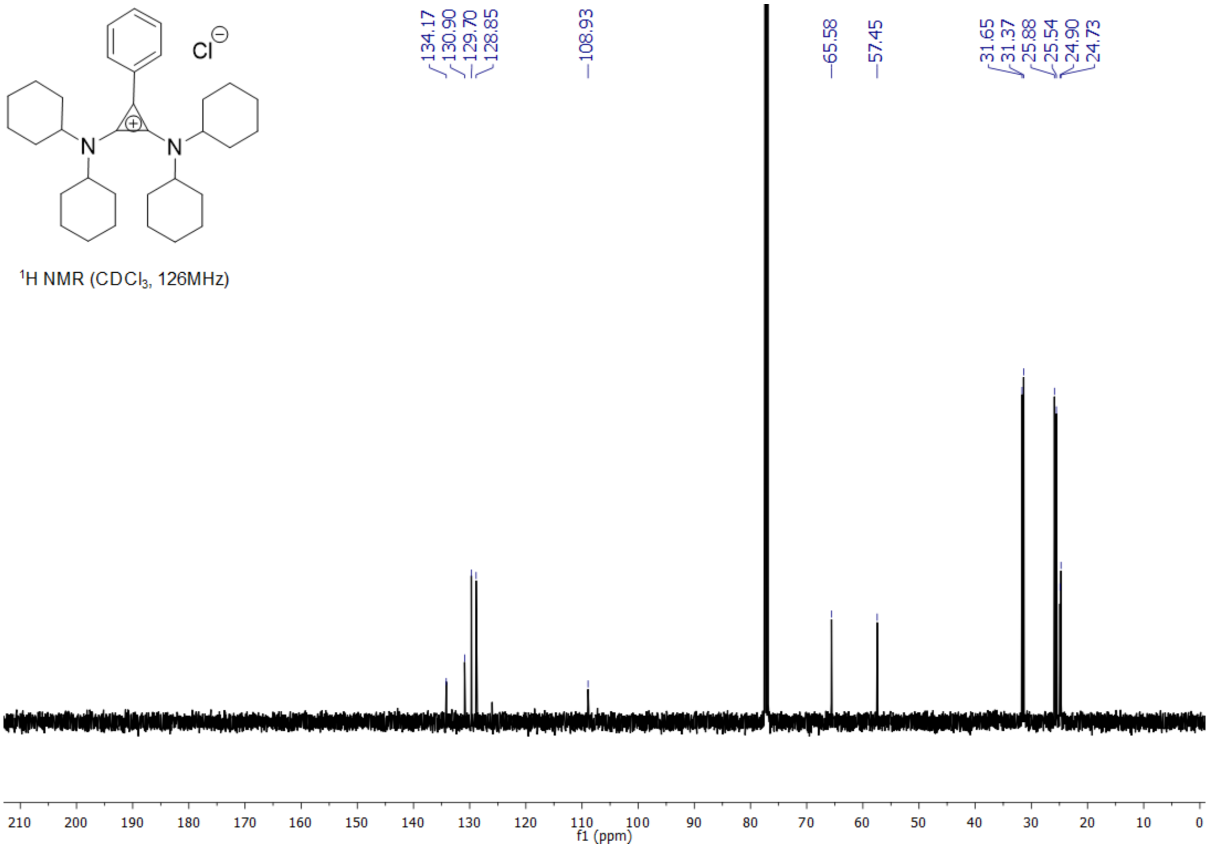
^{1}H NMR (CDCl$_3$, 126MHz)

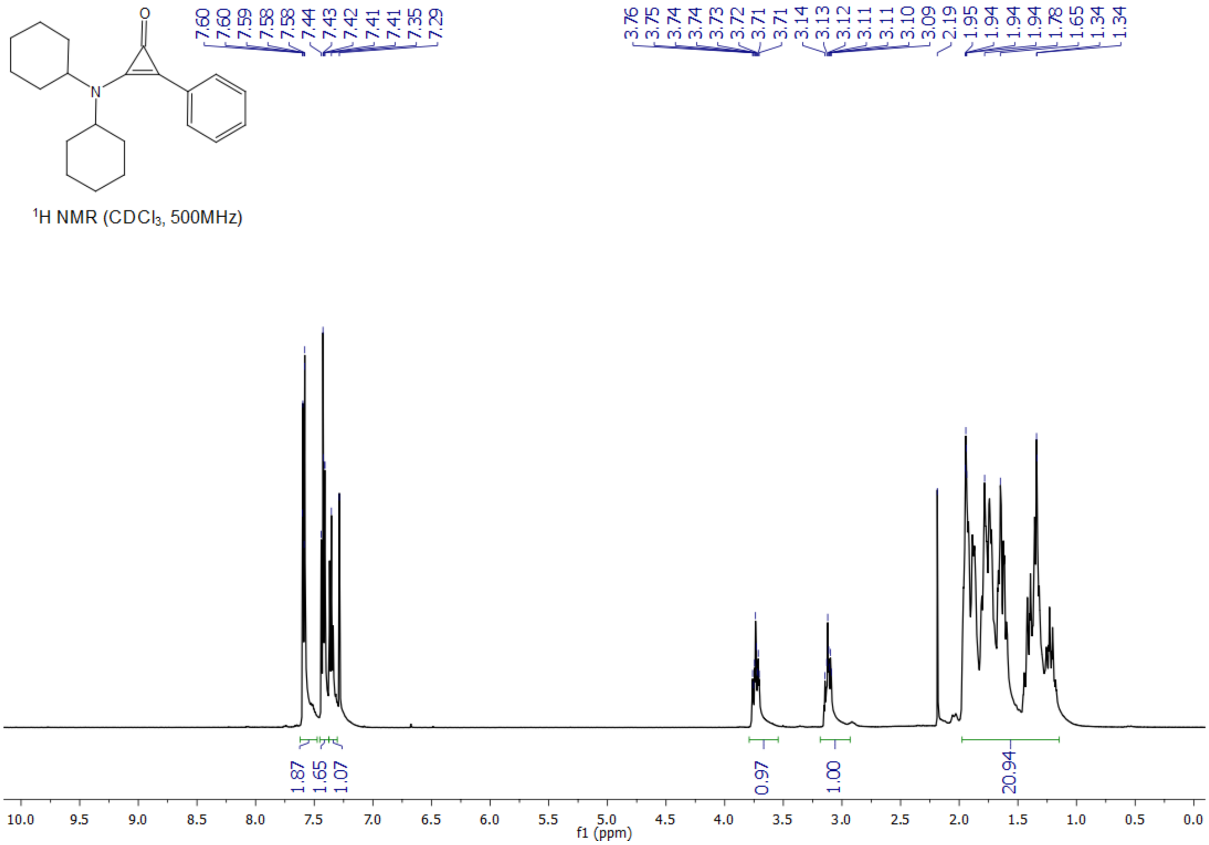

^{1}H NMR (CDCl$_3$, 500MHz)

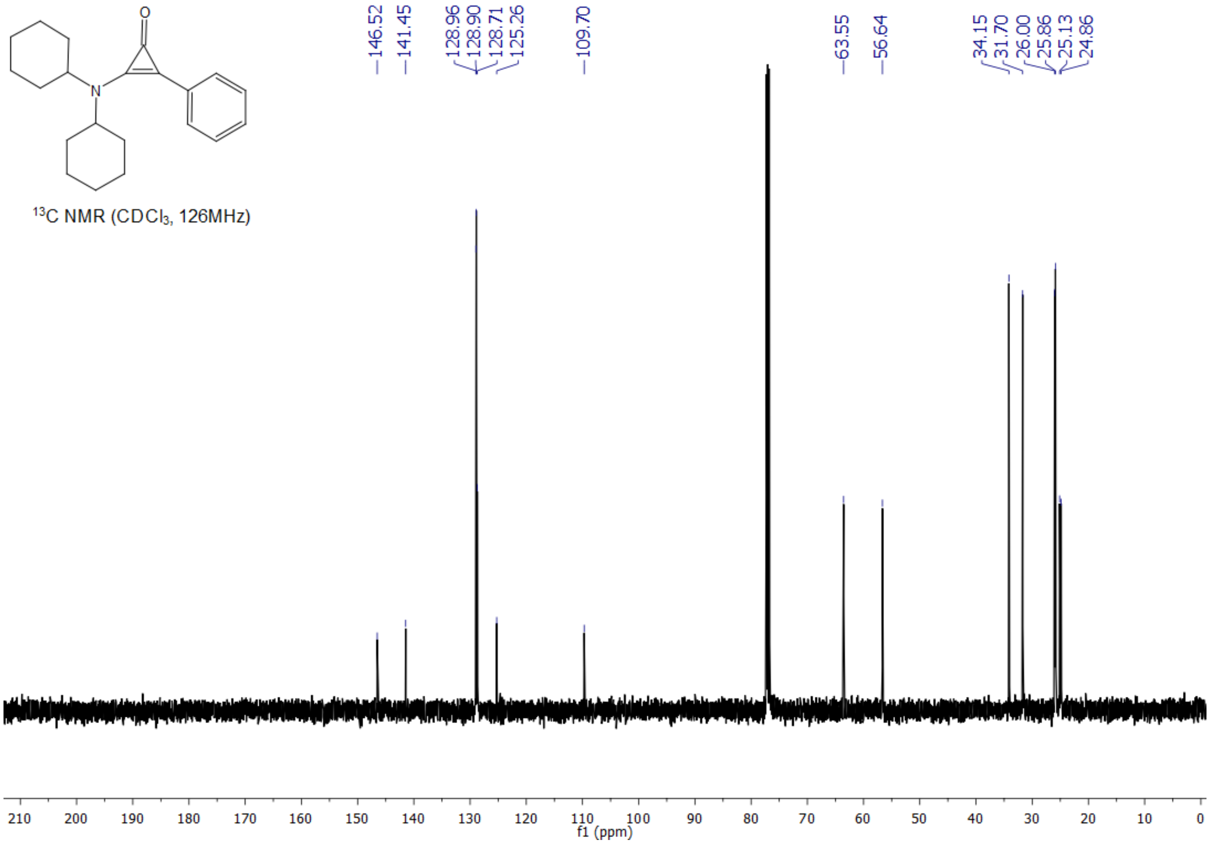

^{13}C NMR (CDCl$_3$, 126MHz)

3. Cyclic Voltammograms of Cyclopropenones

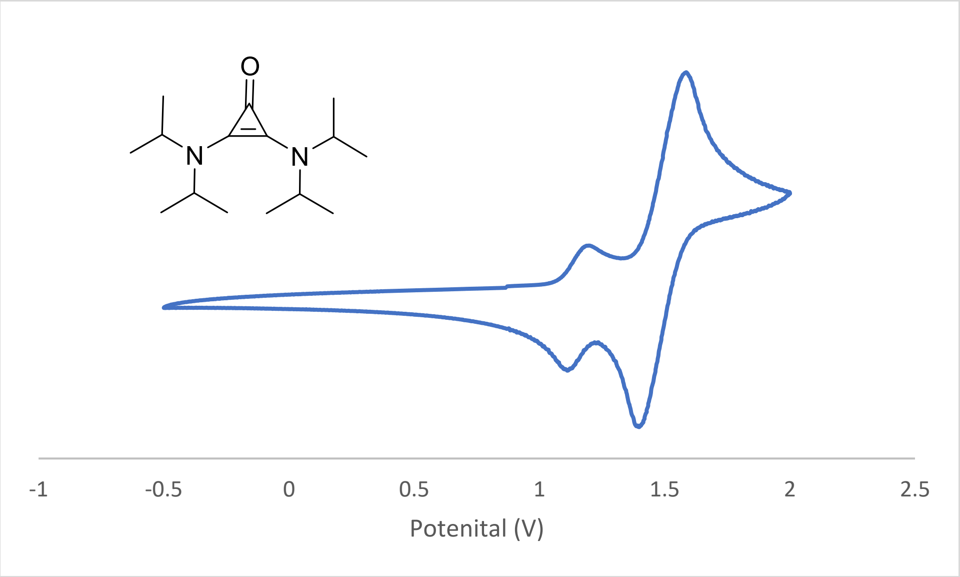

Fc $E_{1/2}$ = 1.15 V, $E_{1/2}$ **(1)** = 1.49 V, Corrected value = 0.74 V

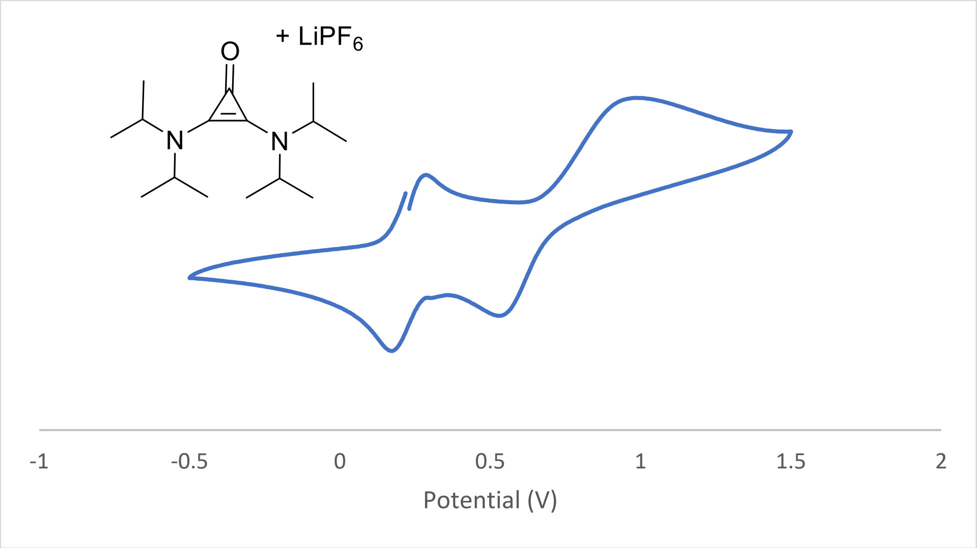

Fc $E_{1/2}$ = 0.23 V, $E_{1/2}$ **(1)** = 0.76 V, Corrected value = 0.93 V

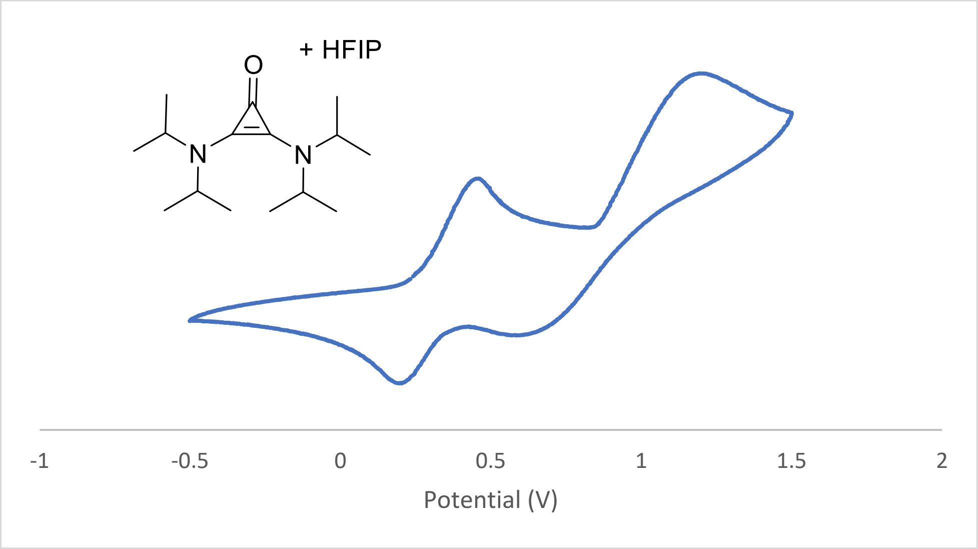

Fc $E_{1/2}$ = 0.33 V, $E_{1/2}$ **(1)** = 0.88 V, Corrected value = 0.96 V

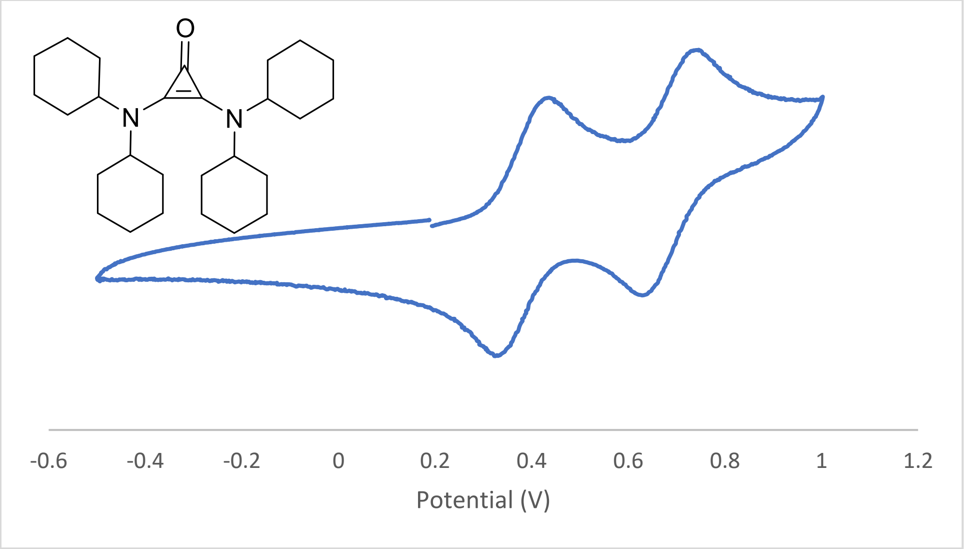

Fc $E_{1/2}$ = 0.38 V, $E_{1/2}$ **(2)** = 0.69 V, Corrected value = 0.70 V

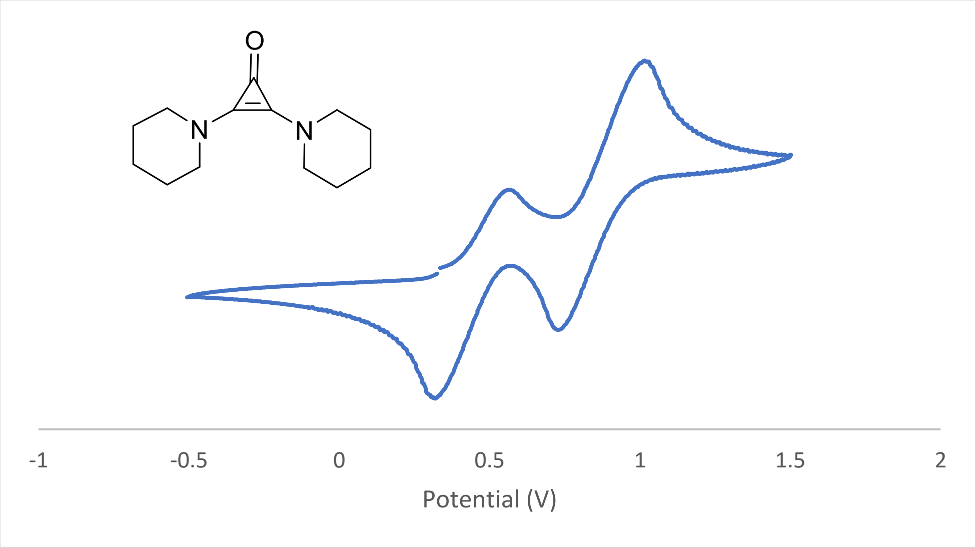

Fc $E_{1/2}$ = 0.44 V, $E_{1/2}$ **(3)** = 0.87 V, Corrected value = 0.83 V

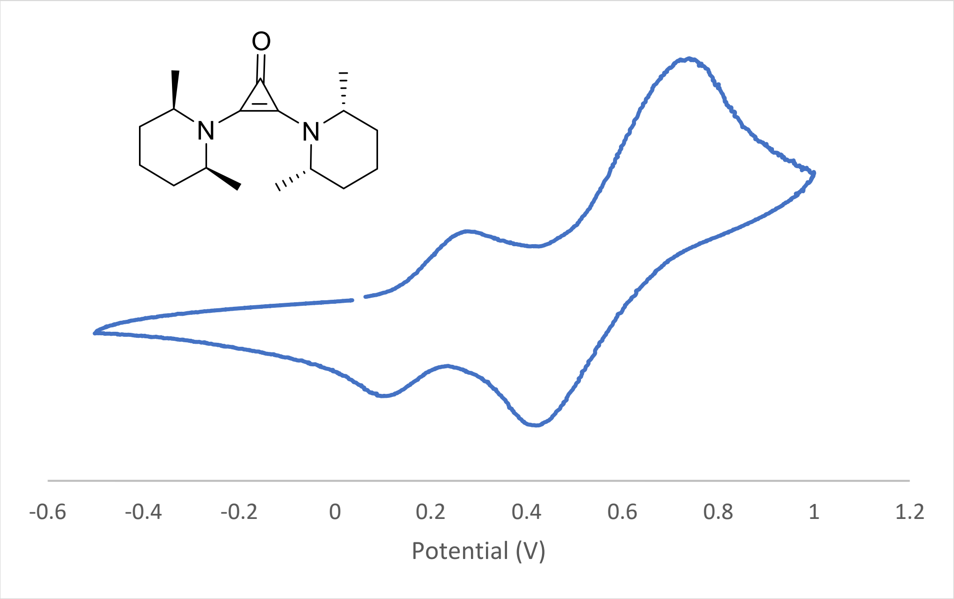

Fc $E_{1/2}$ = 0.19 V, $E_{1/2}$ **(4)** = 0.0.57 V, Corrected value = 0.78 V

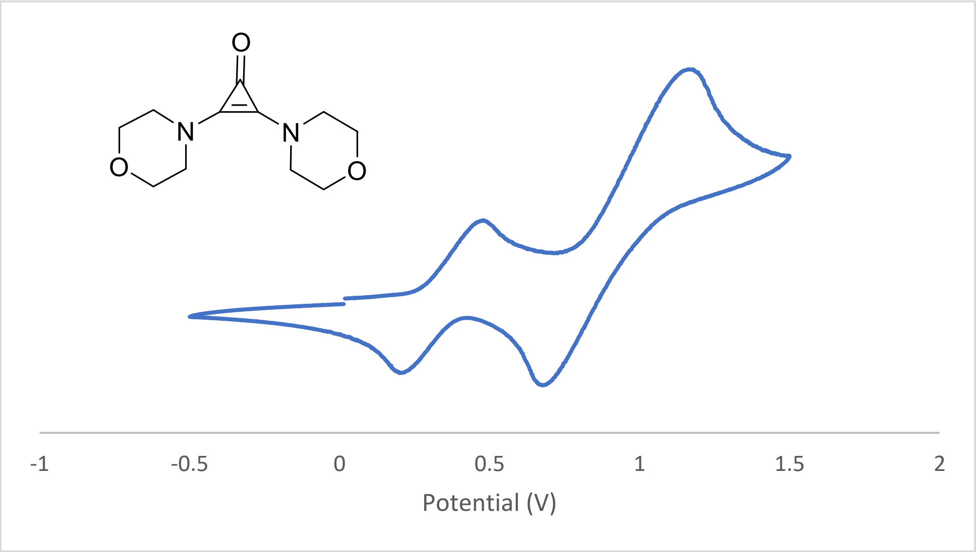

Fc $E_{1/2}$ = 0.34 V, $E_{1/2}$ **(5)** = 0.92 V, Corrected value = 0.98 V

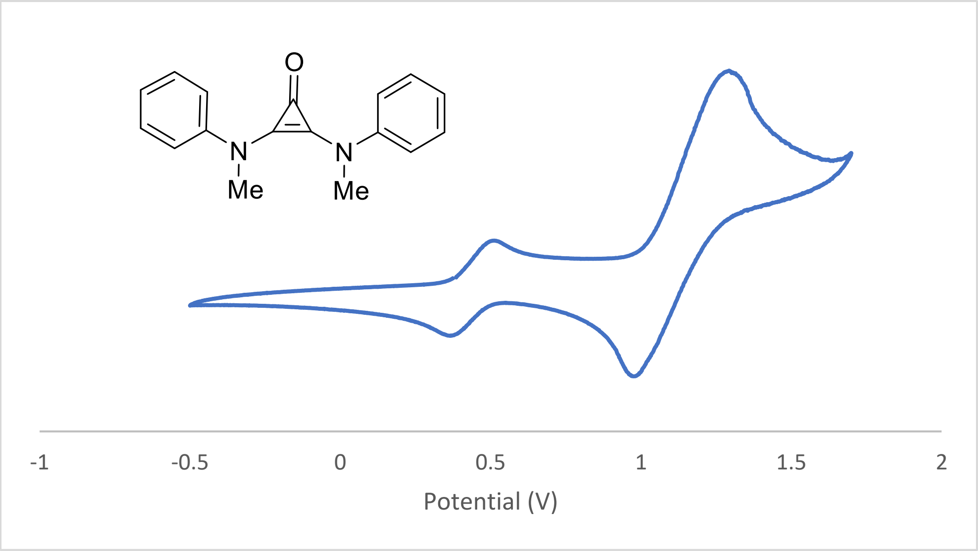

Fc $E_{1/2}$ = 0.44 V, $E_{1/2}$ **(6)** = 1.13 V, Corrected value = 1.10 V

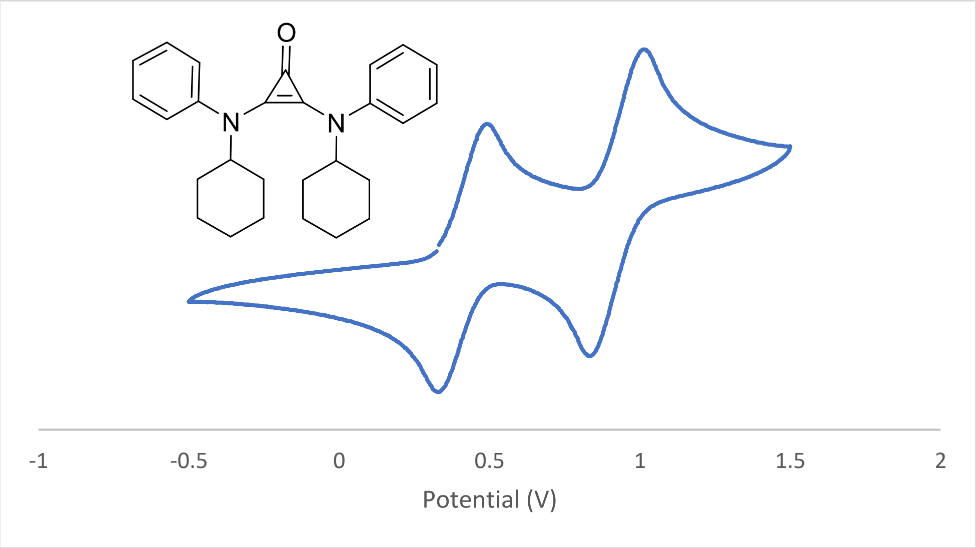

Fc $E_{1/2}$ = 0.41 V, $E_{1/2}$ **(7)** = 0.92 V, Corrected value = 0.91 V

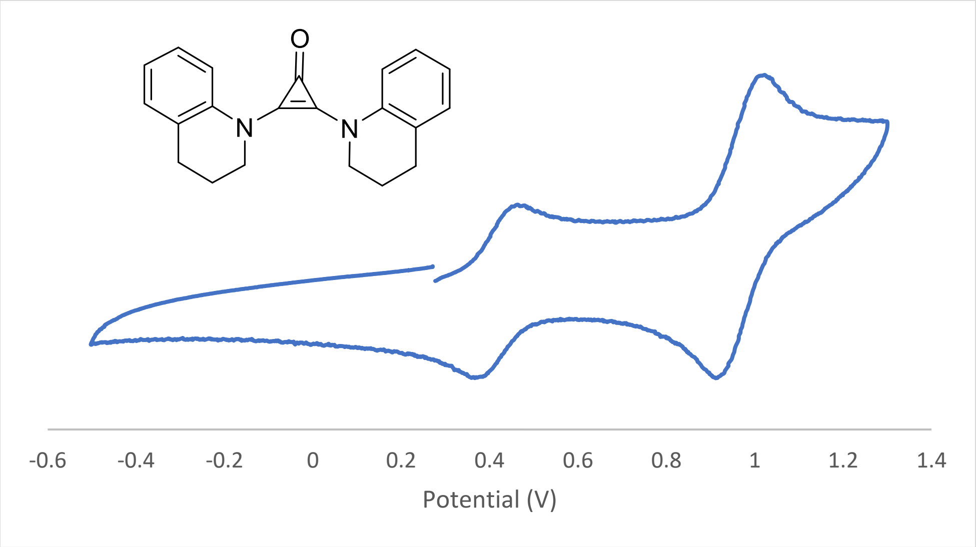

Fc $E_{1/2}$ = 0.41 V, $E_{1/2}$ **(8)** = 0.97 V, Corrected value = 0.96 V

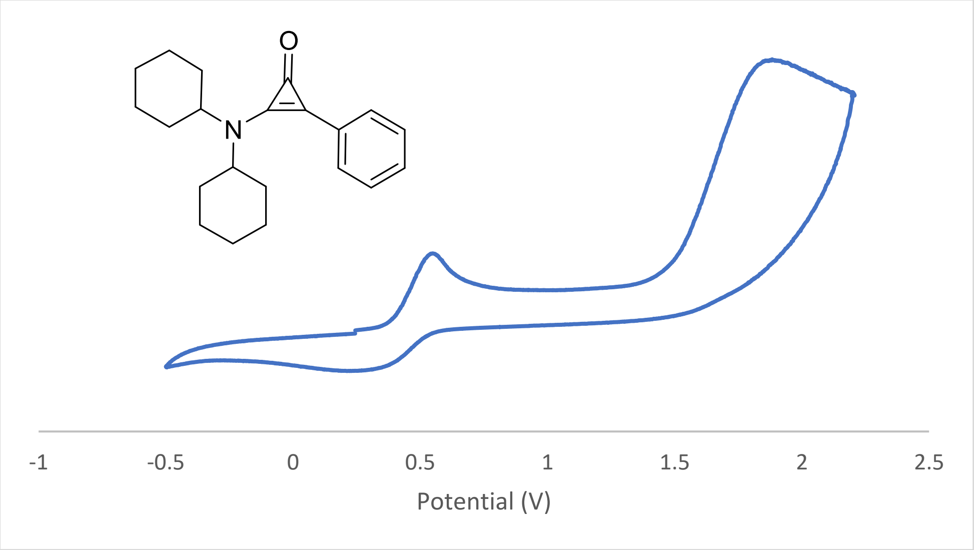

Fc $E_{1/2}$ = 0.38 V, E_{pc} **(9)** = 1.88 V, Corrected value = 1.90 V

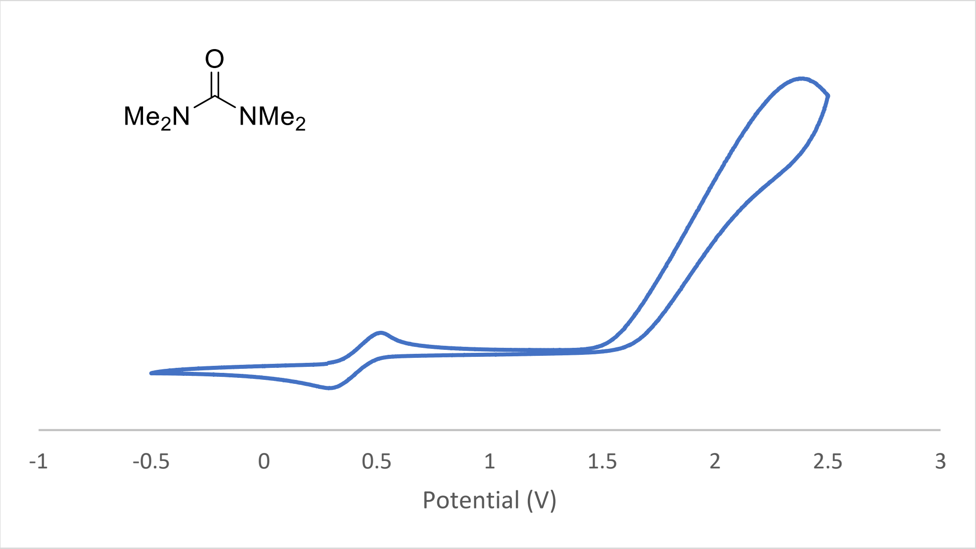

Fc $E_{1/2}$ = 0.40 V, E_{pc} **(Tetramethylurea)** = 2.40 V, Corrected value = 2.40 V

4. X-Ray Crystallography

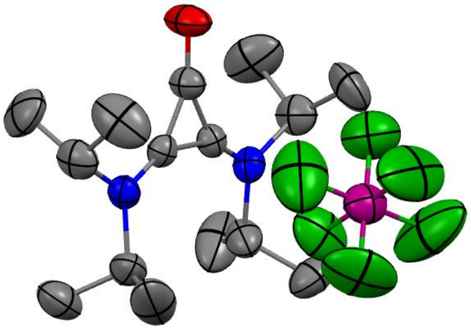

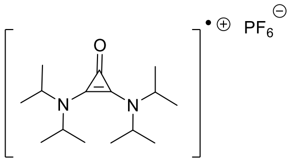

Synthesis of DACO Radical Cation (1): Cyclopropenone **1** (100 mg, 0.40 mmol) was dissolved in 1 mL of dry DCM in a glovebox. This solution was then transferred to a vial containing $NOPF_6$ (87.5 mg, 0.50 mmol), which immediately turned a dark red color and rapidly evolved gas. After 20 min of vigorous stirring, the solution was filtered and Et_2O was allowed to diffuse into the dark red solution at –20 °C for 2 days, giving **DACO Radical Cation (1)** as long, thin, dark red needles suitable for X-ray diffraction. ^1H NMR (500 MHz, $CDCl_3$) δ 1.37 (br s). No carbon peaks visible. FTIR (film) 2991, 2940, 2879, 1858, 1828, 1611, 1546, 1461, 1377, 1352 cm^{-1}. HRMS (ESI, m/z) calcd for $[M+H\cdot]^+$: 253.2280; found 253.2290. UV-VIS (DCM) 516, 474, 373, 350 nm.

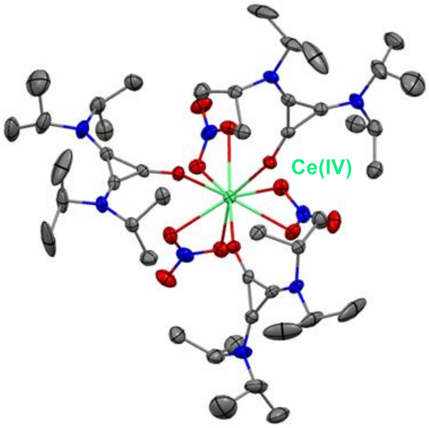

Complex (1)

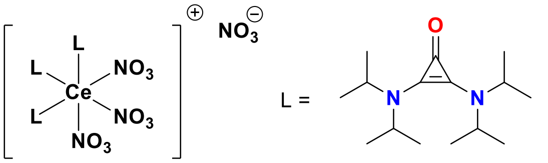

Diaminocyclopropenium **(1)**

Synthesis of complex (1): Diaminocyclopropenone **1** (252 mg, 1.00 mmol) was dissolved in 20 mL of DCM. CAN (0.458 g, 1.00 mmol) was added, and the reaction was stirred for 1 h, resulting in a dark blue solution that was subsequently filtered. Et_2O was then allowed to diffuse into the resulting solution over 2 days at rt and 1 week at –20 °C, giving complex **(1) as** dark blue crystals suitable for X-ray diffraction. Due to its location on a special position in the high-symmetry space group, the nature of the anion could not be conclusively assigned, and was removed from the structure as a contributing void by the PLATON SQUEEZE procedure. ^1H NMR (500 MHz, $CDCl_3$) δ 1.43 (br s). No carbon peaks visible. FTIR (film) 2977, 2936, 2980, 1478, 1452, 1391, 1333, 1297 cm^{-1}. HRMS (ESI, m/z) calcd for $[M-NO_3]^+$: 1082.5294; found 1082.5288. UV-VIS (DCM) 690, 342 nm.

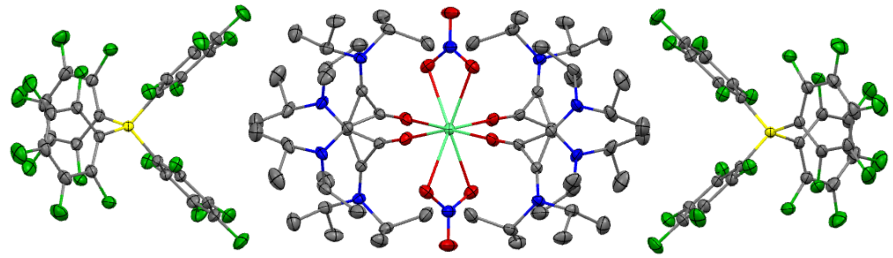

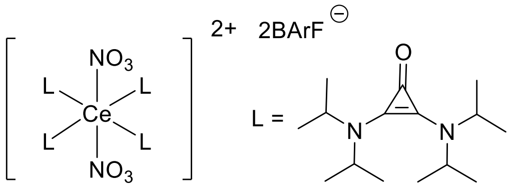

Synthesis of complex (3): Cyclopropenone **1** (504 mg, 2.00 mmol) was dissolved in 20 mL DCM. To this was added CAN (916 mg, 2.00 mmol) and the reaction was stirred for 1 h, resulting in a dark blue solution that was subsequently filtered. To the resulting solution was added a solution of lithium tetrakis(pentafluorophenyl)borate ethyl etherate (1.16 g, 1.33 mmol) in 1 mL DCM. The resulting mixture was stirred for 1 h, at which point the solids were filtered and the resulting solution was layered with hexanes and allowed to diffuse at 0 °C for 1 week, giving complex **(3)** as large dark-blue plates suitable for X-ray diffraction. ^{1}H NMR (500 MHz, CDCl$_3$) δ 3.69 (br s, 16H), 1.39,1.21 (two br s, 96H). No carbon peaks visible. FTIR (film) 2981, 2940, 2882, 1642, 1510, 1485, 1459, 1375, 1338 cm^{-1}. HRMS (ESI, m/z) calcd for [M-L$^{\cdot+}$, 2BArF$^-$]$^+$: 1020.5416; found 1020.5439. UV-VIS (DCM) 647, 517, 476, 325 nm.

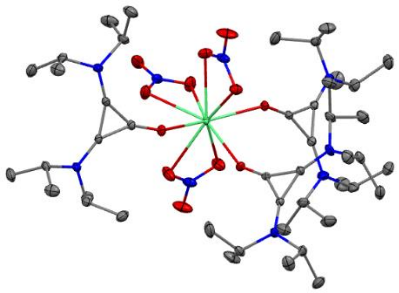

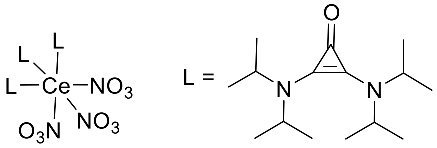

Synthesis of complex (2): Cyclopropenone **1** (252 mg, 1.00 mmol) was dissolved in 3 mL ACN in a vial. Cerium (III) nitrate hexahydrate (143 mg, 0.33 mmol) was added and the solution was stirred until all of the cerium nitrate hexahydrate was dissolved in solution. Et$_2$O was allowed to diffuse into the resulting solution over one week, giving complex **(2)** as clear plates suitable for X-ray diffraction. ^{1}H NMR (500 MHz, CDCl$_3$) δ 4.55 (br s, 12H), 1.88 (br s, 72H). ^{13}C NMR (126 MHz, CDCl$_3$) δ 23.02. FTIR (film) 2973, 2934, 2878, 1920, 1525, 1476, 1449, 1371, 1325, 1305 cm^{-1}. HRMS (ESI, m/z) calcd for [M-NO$_3$]$^+$: 1020.5416; found 1020.5410. UV-VIS (DCM) 338 nm.

Synthesis of Diaminocyclopropenone **(1)** described eariler. Recrystallization from EtOAc gave crystals stuiable for X-ray diffraction.

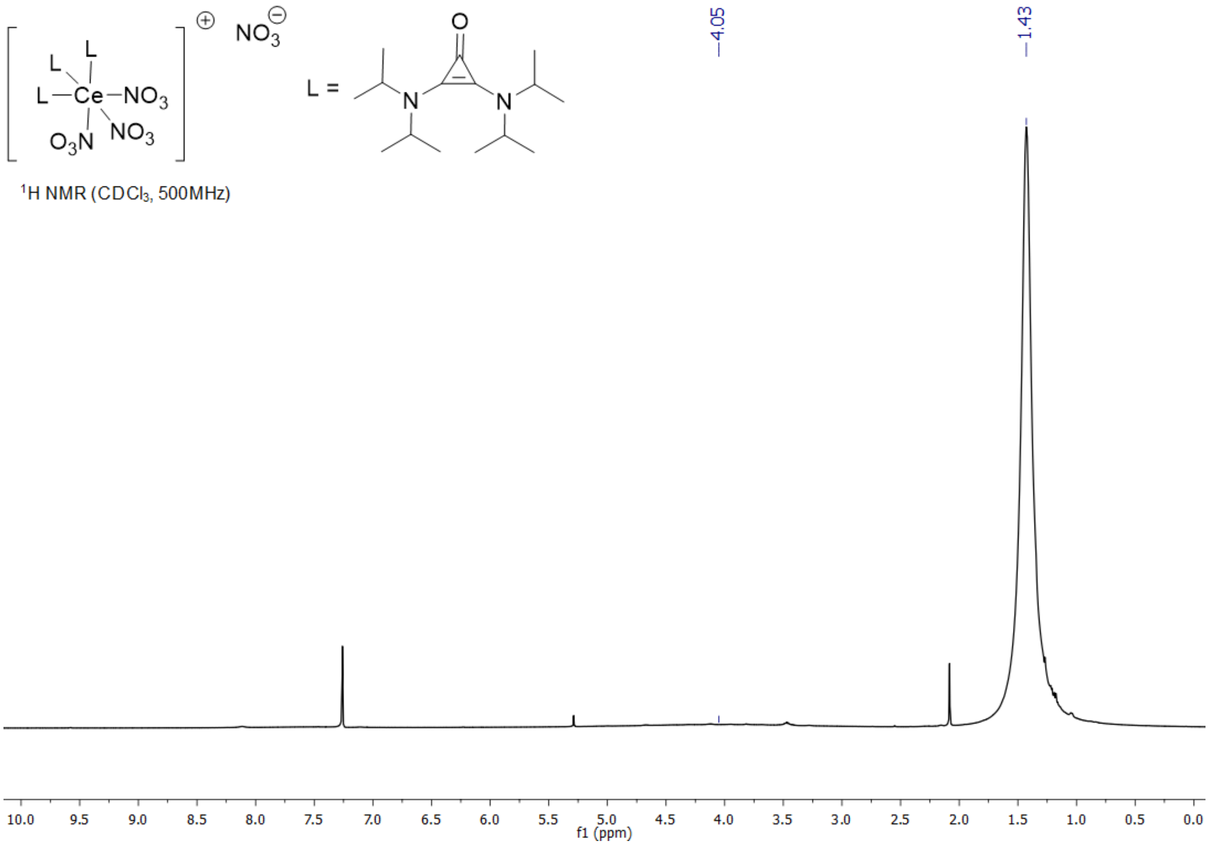
L
L
L—Ce—NO3
O3N
NO3
NO3
L =
O
N
N
1H NMR (CDCl3, 500MHz)
4.05
1.43
10.0
9.5
9.0
8.5
8.0
7.5
7.0
6.5
6.0
5.5
5.0
4.5
4.0
3.5
3.0
2.5
2.0
1.5
1.0
0.5
0.0
f1 (ppm)

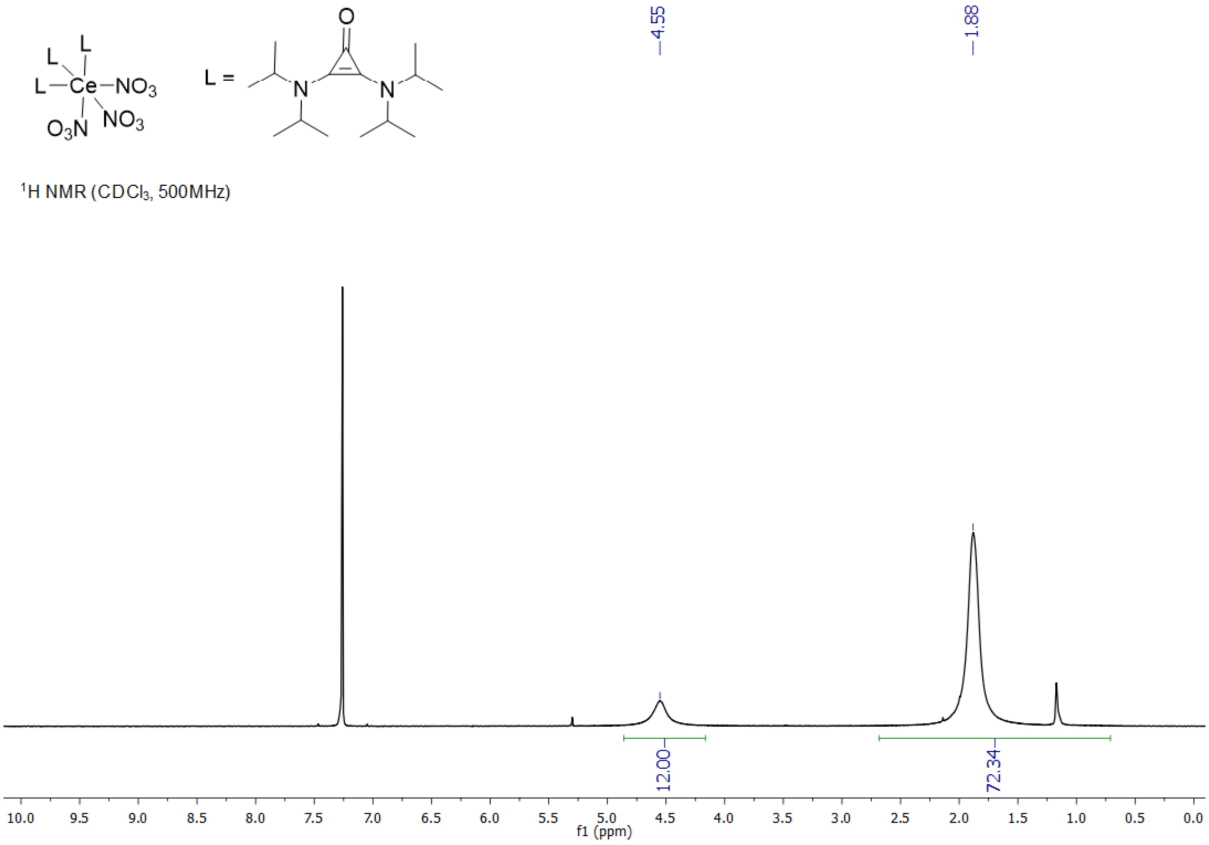
L
L
L—Ce—NO3
O3N
NO3
L =
O
N
N
1H NMR (CDCl3, 500MHz)
4.55
1.88
12.00
72.34
10.0
9.5
9.0
8.5
8.0
7.5
7.0
6.5
6.0
5.5
5.0
4.5
4.0
3.5
3.0
2.5
2.0
1.5
1.0
0.5
0.0
f1 (ppm)

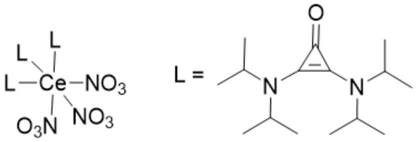
L
L
L
Ce
NO_3
O_3N
NO_3
L =
O
N
N

^{1}H NMR ($CDCl_3$, 126MHz)

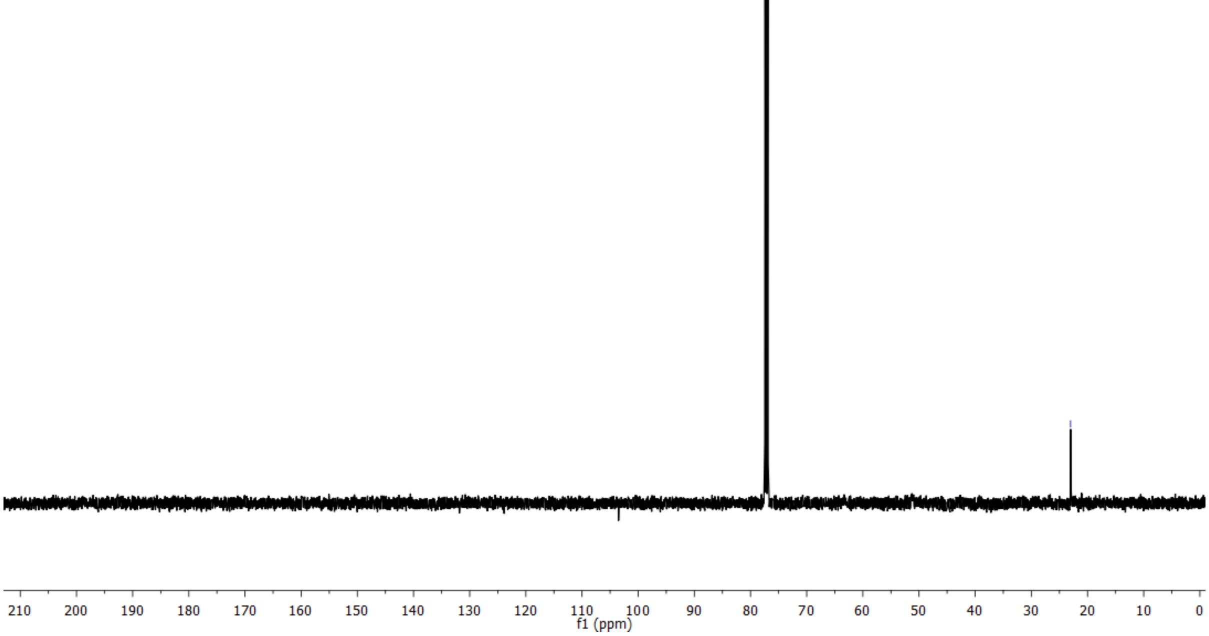

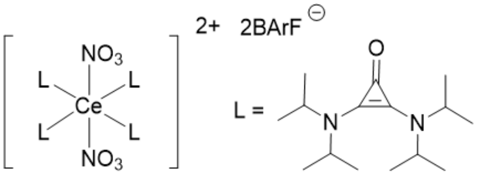
2+ 2BArF ⊖
NO_3
L
L
Ce
L
L
NO_3
L =
O
N
N

^{1}H NMR ($CDCl_3$, 500MHz)

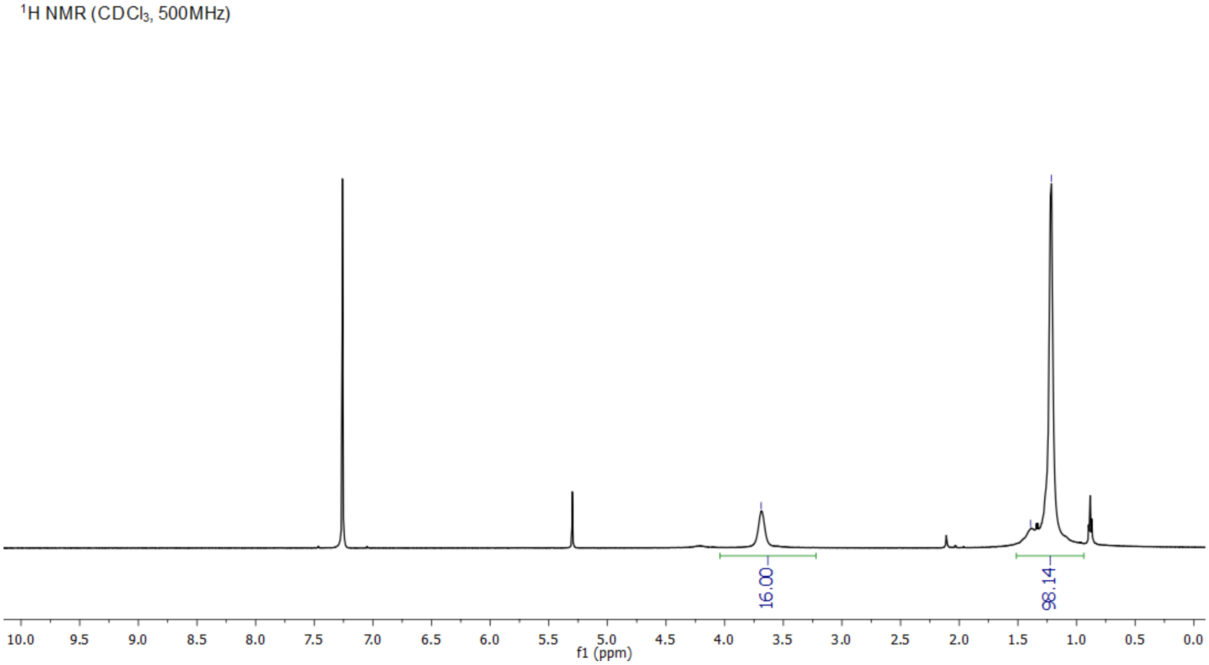

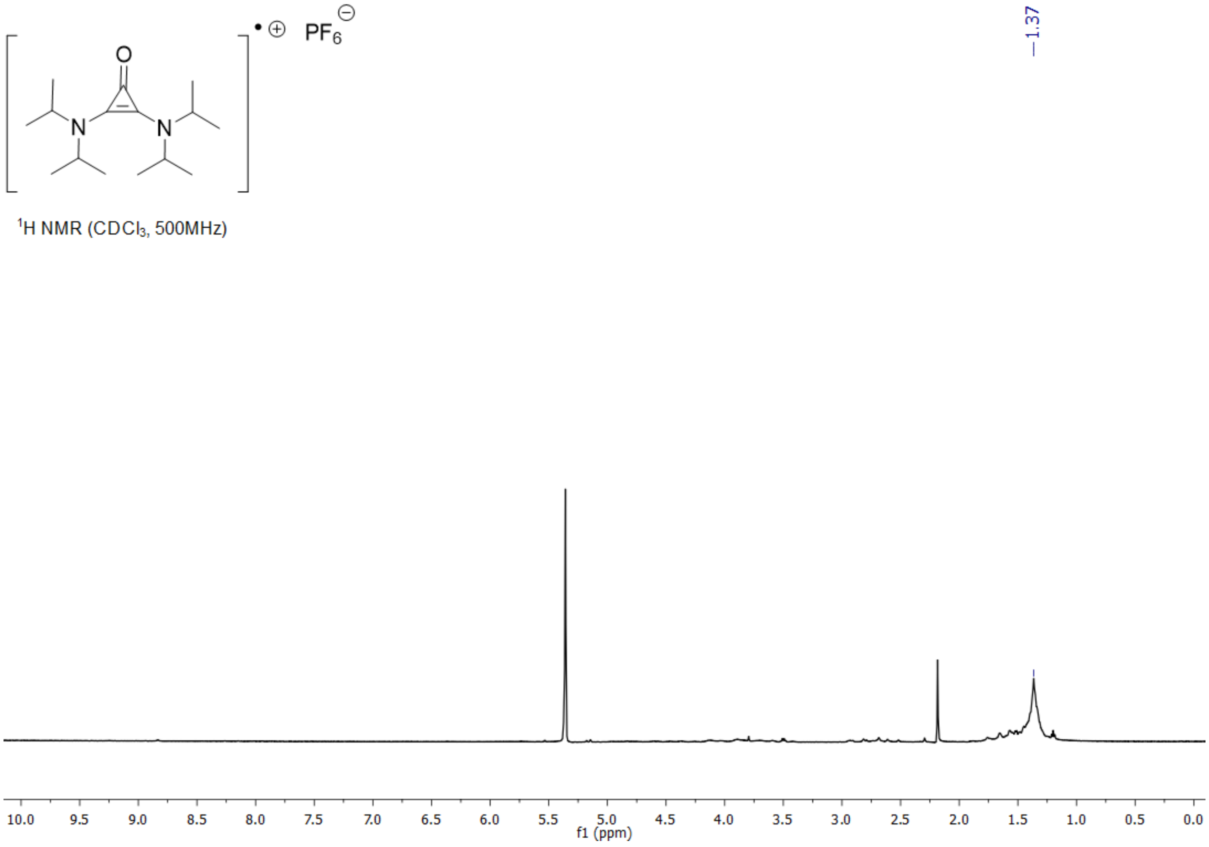
PF$_6^{\ominus}$
O
N
N
^{1}H NMR (CDCl$_3$, 500MHz)
1.37
10.0
9.5
9.0
8.5
8.0
7.5
7.0
6.5
6.0
5.5
5.0
4.5
4.0
3.5
3.0
2.5
2.0
1.5
1.0
0.5
0.0
f1 (ppm)

Crystal, intensity collection, and refinement data.

	Complex (3)	**Complex (1)**
lattice	Monoclinic	Hexagonal
formula	$C_{45}H_{84}CeN_9O_{12}$	$C_{45}H_{84}CeN_9O_{12}$
formula weight	1083.33	1083.33
space group	*Pc*	*P(6)3*
a/Å	11.0722(11)	20.154(3)
b/Å	21.321(2)	20.154(3)
c/Å	12.5992(13)	9.6263(12)
α/°	90	90
β/°	109.8922(13)	90
γ/°	90	120
V/Å^3	2796.8(5)	3386.1(9)
Z	2	2
temperature (K)	190(2)	190(2)
radiation (λ, Å)	0.71073	0.71073
ρ (calcd.) g cm^{-3}	1.286	1.063
μ (Mo Kα), mm^{-1}	0.875	0.723
θ max, deg.	30.591	30.560
no. of data collected	45486	53685
no. of data	17028	6902
no. of parameters	629	211
R_1 [$I > 2\sigma(I)$]	0.0492	0.0506
wR_2 [$I > 2\sigma(I)$]	0.1282	0.1260
R_1 [all data]	0.0526	0.0629
wR_2 [all data]	0.1319	0.1353
GOF	1.110	1.005
R_{int}	0.0416	0.1129

	Complex (2)	**Diaminocyclcopropenone 1**
lattice	Orthorhombic	Monoclinic
formula	$C_{108}H_{112}B_2CeF_{40}N_{10}O_{10}$	$C_{15}H_{28}N_2O$
formula weight	2631.81	252.39
space group	*Fddd*	*P21*
a/Å	19.786(2)	14.348(8)
b/Å	33.486(4)	7.878(5)
c/Å	37.223(4)	14.354(8)
α/°	90	90
β/°	90	98.360(9)
γ/°	90	90
V/Å^3	24663(5)	1605.3(16)
Z	8	4
temperature (K)	230(2)	230(2)
radiation (λ, Å)	0.71073	0.71073
ρ (calcd.) g cm^{-3}	1.418	1.044
μ (Mo Kα), mm^{-1}	0.487	0.065
θ max, deg.	30.521	26.371
no. of data collected	49363	21195
no. of data	9407	6548
no. of parameters	396	330
R_1 [$I > 2\sigma(I)$]	0.0302	0.0732
wR_2 [$I > 2\sigma(I)$]	0.0760	0.1897
R_1 [all data]	0.0381	0.1222
wR_2 [all data]	0.0821	0.2300
GOF	1.014	1.039
R_{int}	0.0426	0.0668

	DACO (1)
lattice	Tetragonal
formula	$C_{15}H_{28}F_6N_2OP$
formula weight	397.36
space group	$P4_32_12$
a/Å	11.031(3)
b/Å	11.031(3)
c/Å	16.623(5)
α/°	90
β/°	90
γ/°	90
V/Å^3	2022.7(14)
Z	4
temperature (K)	230(2)
radiation (λ, Å)	0.71073
ρ (calcd.) g cm^{-3}	1.305
μ (Mo Kα), mm^{-1}	0.194
θ max, deg.	26.366
no. of data collected	24784
no. of data	2071
no. of parameters	148
R_1 [$I > 2\sigma(I)$]	0.0699
wR_2 [$I > 2\sigma(I)$]	0.1932
R_1 [all data]	0.0880
wR_2 [all data]	0.2119
GOF	1.137
R_{int}	0.0644

UV-VIS spectra

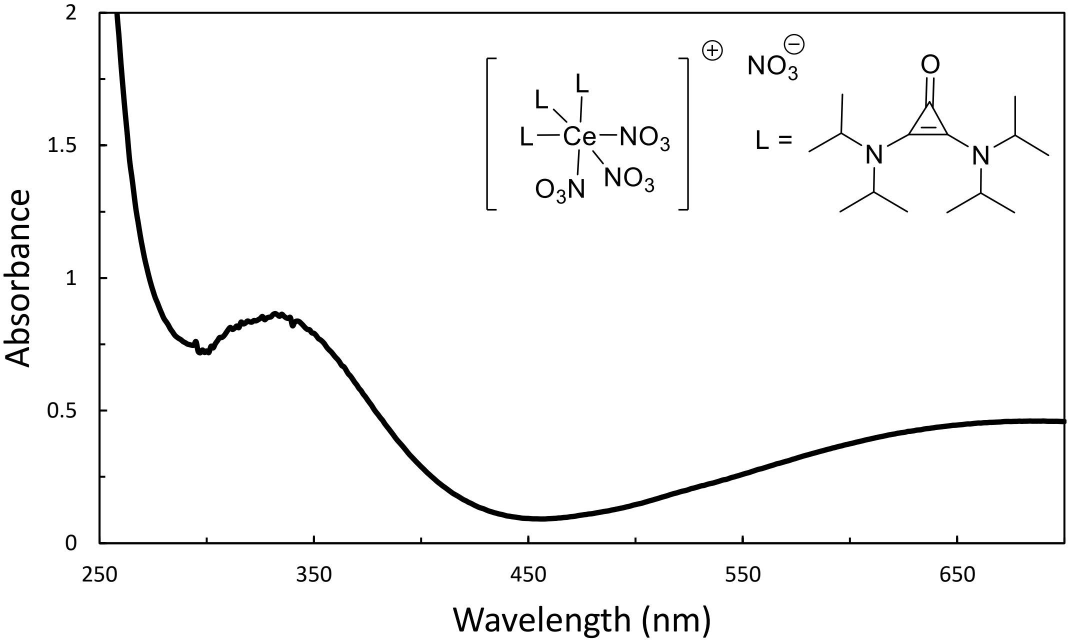

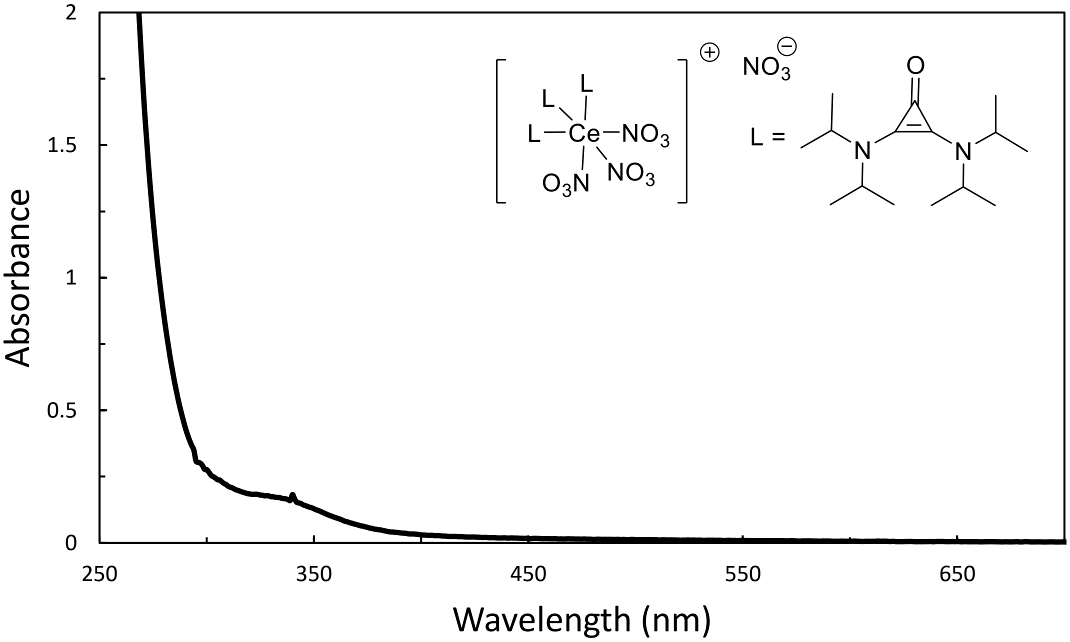

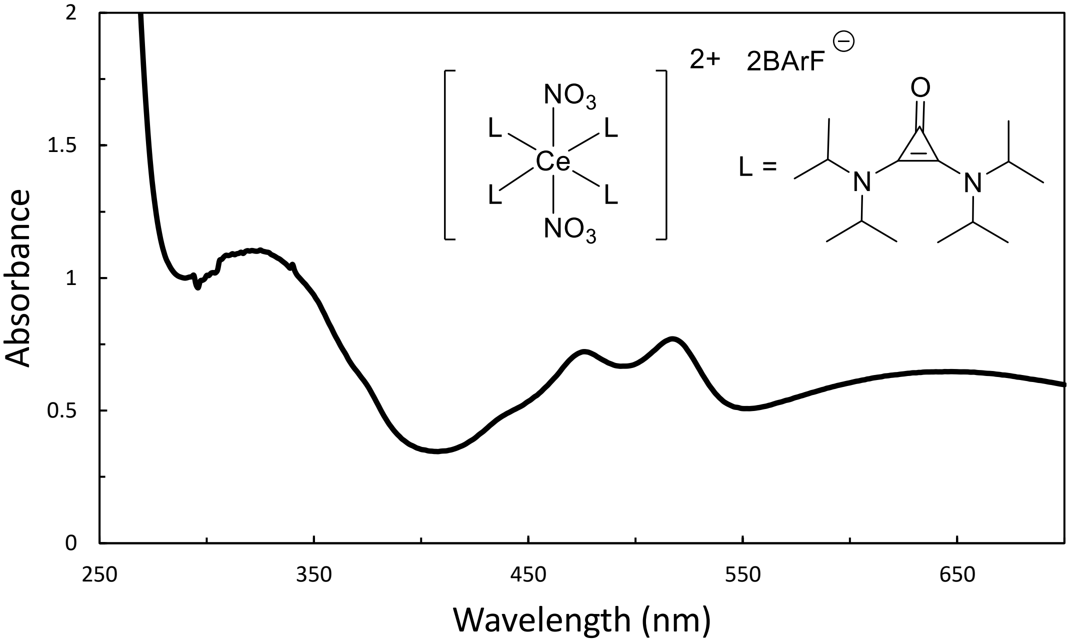

2
1.5
1
0.5
0
250
350
450
550
650
Absorbance
Wavelength (nm)
NO_3
L
L
Ce
L
L
NO_3
2+
2BArF ⊖
L =
O
N
N

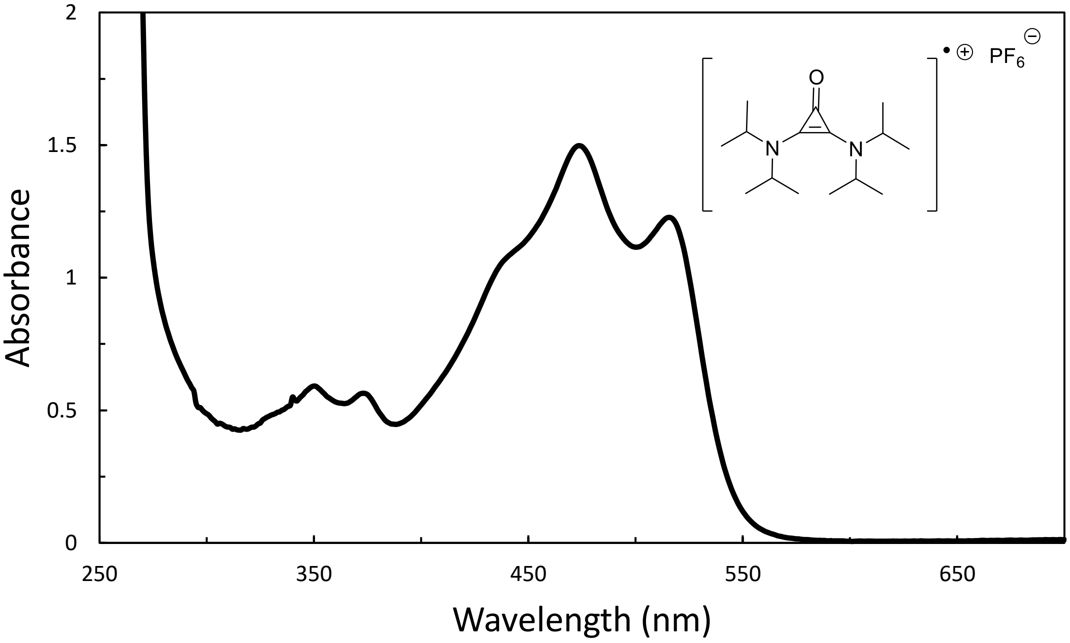

2
1.5
1
0.5
0
250
350
450
550
650
Absorbance
Wavelength (nm)
O
N
N
•⊕ PF_6 ⊖

5. EPR Spectra and Studies

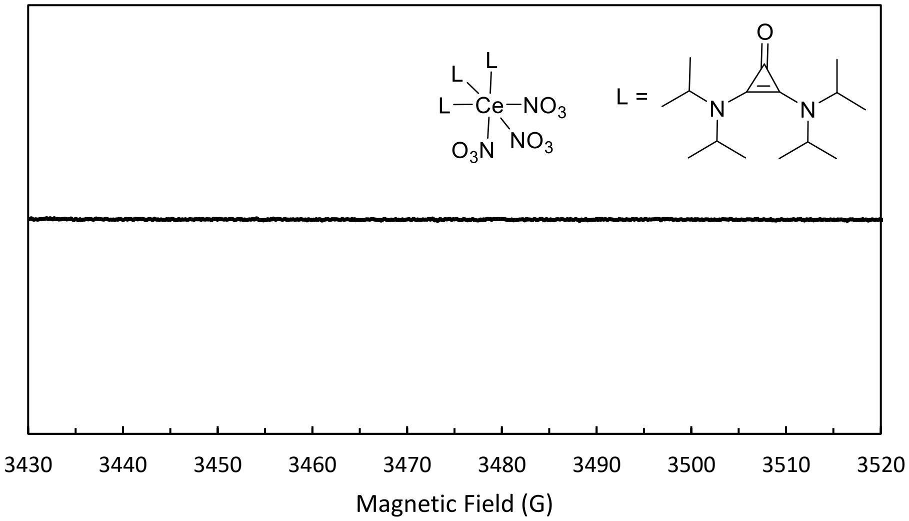

Frequency = 9.741 GHz, Power = 20 mW, Receiver gain = 1.00e+6, Mod. Frequency = 100.00 kHz, Mod. Amplitude = 1.00G, 0.15M in DCM

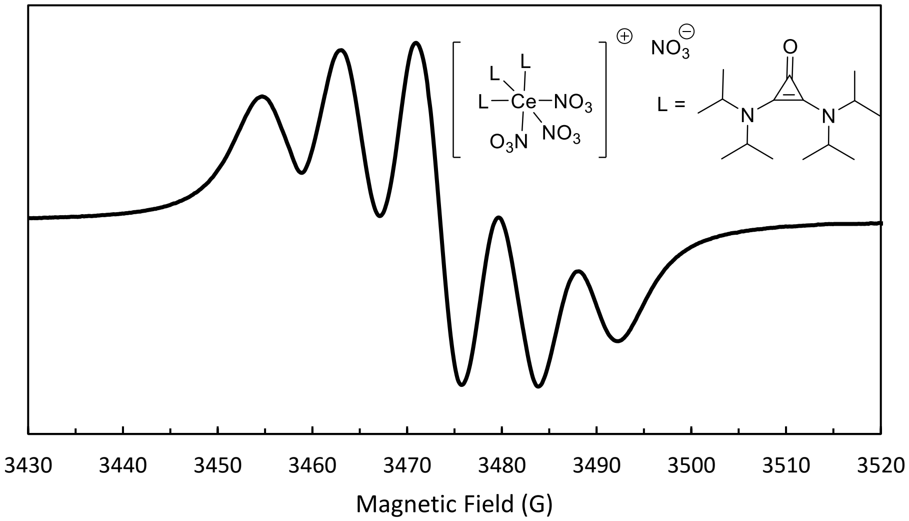

Frequency = 9.751 GHz, Power = 20 mW, Receiver gain = 1.00e+4, Mod. Frequency = 100.00 kHz, Mod. Amplitude = 1.00G, 0.15M in DCM.

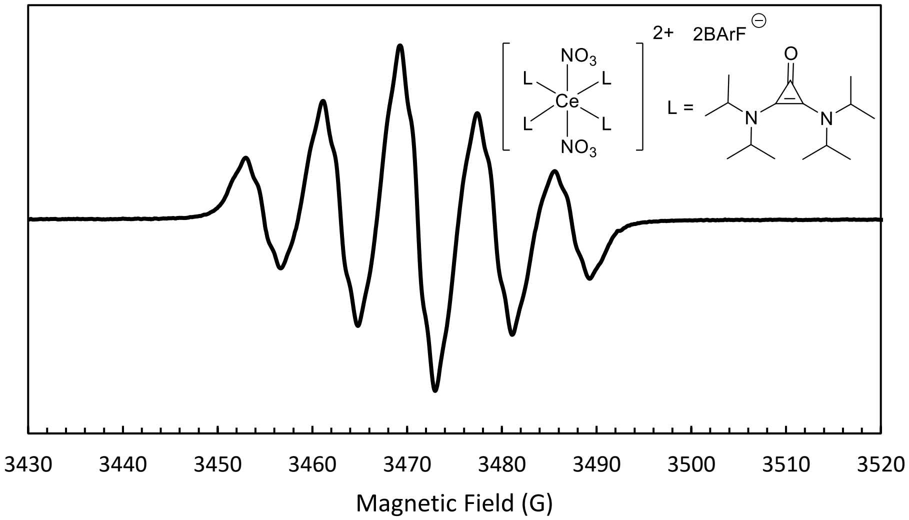

Frequency = 9.736 GHz, Power = 20 mW, Receiver gain = 5.02e+3, Mod. Frequency = 100.00 kHz, Mod. Amplitude = 1.00G, 0.76 mM in DCM.

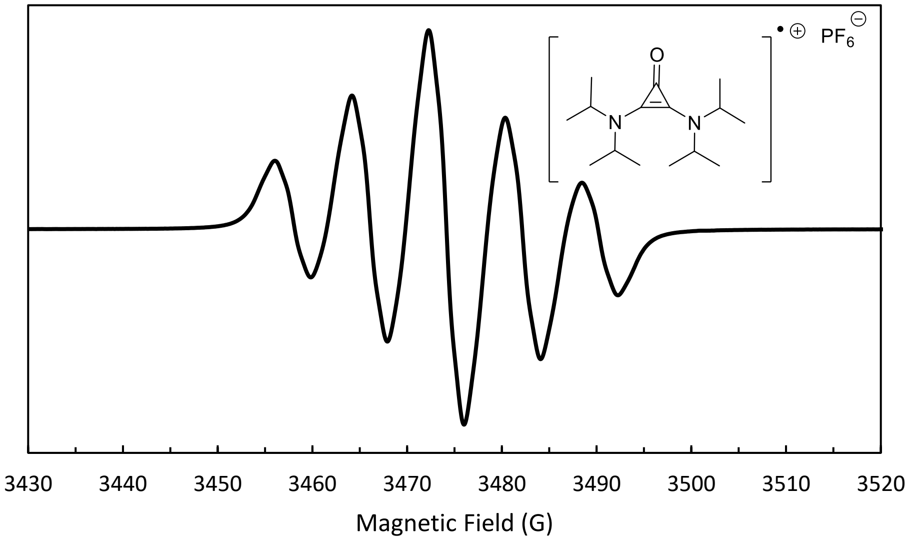

Frequency = 9.741 GHz, Power = 20 mW, Receiver gain = 5.02e+3, Mod. Frequency = 100.00 kHz, Mod. Amplitude = 1.00G, 0.76 mM in DCM.

Estimating the Dissociative Equilibrium Constant for Complex (3)

The dissociative equilibrium for complex **(3)** was estimated using the following equilibrium equation:

$$[\mathbf{A}] \rightleftharpoons [\mathbf{B}] + [\mathbf{C}] \tag{1}$$

Where [**A**] = [Complex **(3)**] = [Ce(IV))(**1**)$_4$(NO$_3$)$_2$(BArF)$_2$], [**B**] = [**DACO (1) (**BArF$^-$)], [**C**] = [Ce(III)(2)$_3$(NO$_3$)$_2$(BArF)].

This gives rise to the following expression of the equilibrium constant:

$$\mathrm{K_{eq}} = \frac{[\mathbf{B}][\mathbf{C}]}{[\mathbf{A}]} \tag{2}$$

In order to estimate the equilibrium constant (K$_{\mathrm{eq}}$), we measured the EPR signal of a sample of **A** at a known concentration [$\mathbf{A_{init.}}$] in DCM and double integrated the resulting spectrum. The obtained integration value ($\mathbf{I_1}$) was used as an estimation for the concentration of dissociated **B** in solution, as neither **A** nor **C** produce a detectable EPR signal. Next, we measured the EPR spectrum of a sample of **DACO (1)** at the same concentration as the first sample ([$\mathbf{A_{init.}}$]) in DCM and using the same instrument parameters. The integration value of this spectrum ($\mathbf{I_2}$) was used as an estimation of intensity of the signal that would result from a sample of **A** at concentration [$\mathbf{A_{init.}}$] that had 100% dissociated to **B** + **C**. Correlation of the two integration values allows for the determination of the concentration of **B** using the following equation:

$$\frac{\mathbf{I_1}}{\mathbf{I_2}} = \frac{[\mathbf{B}]}{[\mathbf{DACO\ (1)}]} \tag{3}$$

The Concentration of **A** was determined by subtracting the concentration of **B** from the initial concentration of **A**:

$$[\mathbf{A}] = [\mathbf{A_{init.}}] - [\mathbf{B}] \tag{4}$$

The following assumptions were made in estimating the value of the equilibrium constant:

i) The concentration of **B** and **C** are equal, resulting from the dissociation of **A**

ii) The counterion of **DACO (1)** (PF$_6^-$ or BArF$^-$) does not significantly change the intensity of the EPR signal

iii) The EPR signal intensity of **B** is linear with respect to concentration

The following values were obtained using this method:

$\mathbf{I_2}$ = 5.011e+8 (0.76 mM **5a**, Receiver Gain = 5.02e+3, Mod. Frequency = 100.00 kHz, Mod. Amplitude = 1.00 G)

$\mathbf{I_1}$ = 5.014e+7 (0.76 mM **A**, Receiver Gain = 5.02e+3, Mod. Frequency = 100.00 kHz, Mod. Amplitude = 1.00 G)

[**B**] = [**C**] = 0.076mM (from equation 3)

[**A] =** 0.68 mM (from equation 4)

K_{eq} = $8.4*10^{-3}$ (from equation 2)

VT EPR experiment data:

Instrument parameters for all measurements: Receiver Gain = 1.00e+4, Mod. Frequency = 100.00 kHz, Mod. Amplitude 1.00G.

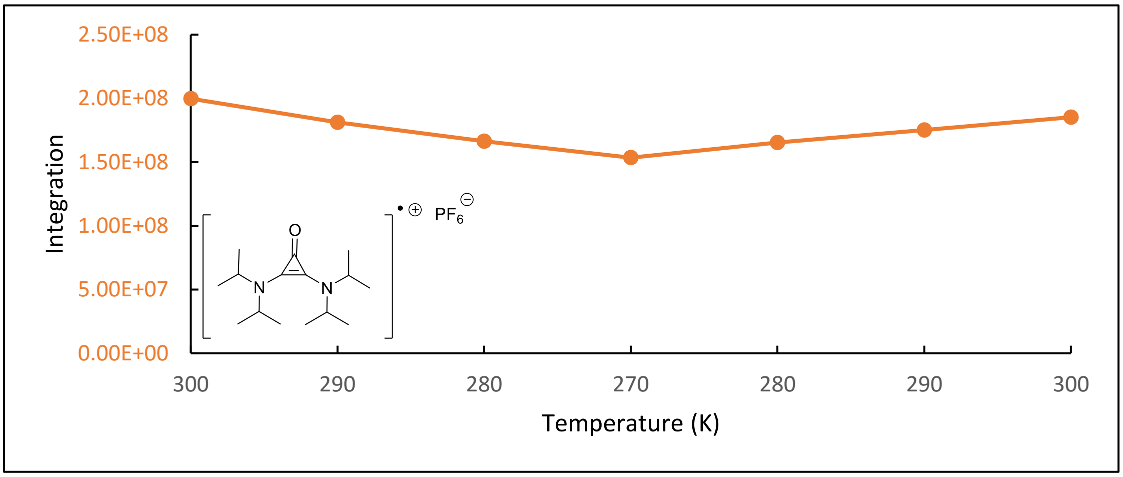

Sample: 0.76M **DACO (1)** in DCM

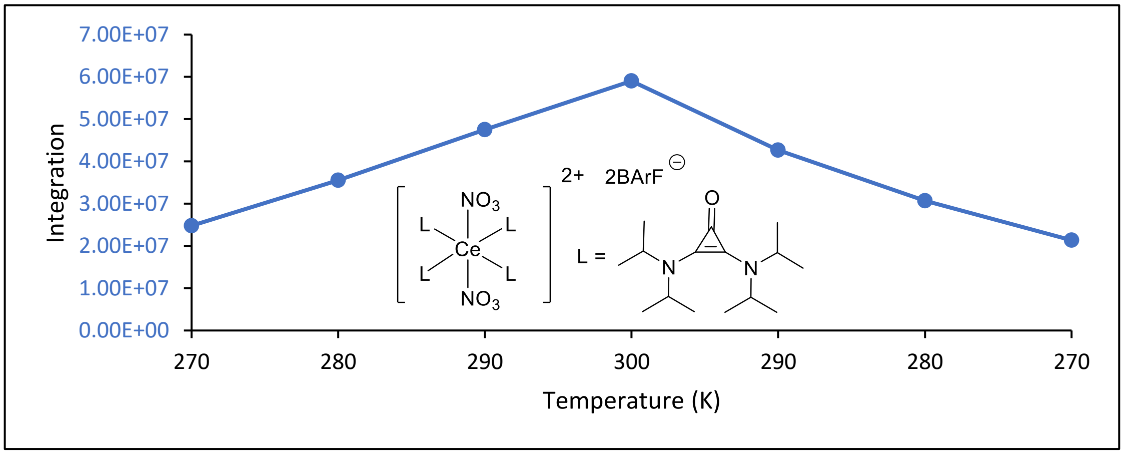

Sample: 0.76M complex **(3)** DCM

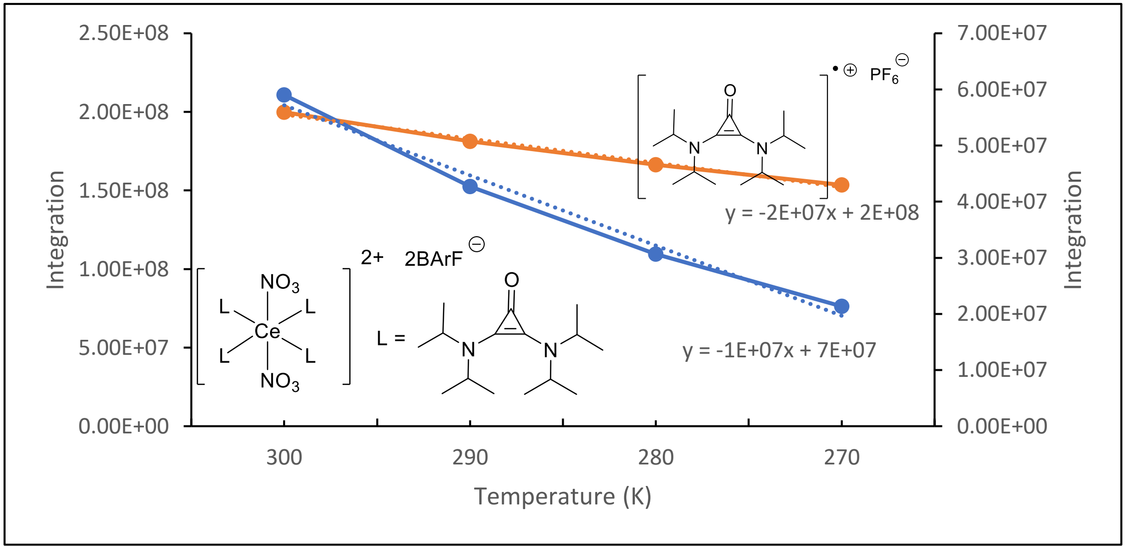

Comparison temp. effect on EPR signal of **DACO (1)** (orange) and complex **(3)** (blue).

6. Computational Data

Cartesian Coordinates for Geometry Optimized Compounds

Diaminocyclopropenone (1)

atom	**x**	**y**	**z**
O	8.182634212	5.539891255	8.106971608
N	6.180096554	7.178781144	5.557983323
N	4.615358713	4.853191158	8.097160764
C	6.252645445	6.337748206	6.617070399
C	4.885267001	6.934658032	3.436899729
C	4.544198986	8.961759925	4.946715138
C	8.107898276	8.642897436	6.158863251
C	4.908826471	7.470146274	4.877751125
C	8.427274522	6.682152362	4.587661866
C	5.67971875	5.483697962	7.546087909
C	7.455094512	7.765469543	5.07975117
C	2.754557491	3.627104019	6.970381295
C	5.437060224	4.78777821	10.45044724
C	5.823624364	2.819948409	8.903394824
C	2.270660344	5.589586369	8.525494549
C	7.074850538	5.724350217	7.593823862
C	3.261965908	4.965688946	7.53061703
C	4.884305226	3.980880257	9.265792404
H	3.900836229	7.095351247	2.984180093
H	5.623929308	7.44217966	2.807576741
H	5.102108538	5.862438799	3.418663696
H	5.256694764	9.579118339	4.389621092
H	3.553423543	9.131273225	4.511575901

H	4.529433789	9.308925902	5.983891732
H	8.421882044	8.032502637	7.011625916
H	8.996928571	9.138721851	5.754516881
H	7.416144737	9.413412082	6.512384532
H	4.150463219	6.923969543	5.445208936
H	9.321385924	7.145046064	4.156433535
H	8.746519377	6.047248638	5.420297551
H	7.964455412	6.052237072	3.821819277
H	7.184803935	8.401885177	4.230872827
H	2.63066679	2.881002501	7.76234671
H	1.780599444	3.758580283	6.486799517
H	3.454597802	3.226003229	6.231534428
H	5.540276563	4.143660562	11.33025053
H	6.426235461	5.191259546	10.21165837
H	4.771197844	5.616954431	10.70810433
H	5.435186283	2.245341571	8.057096574
H	6.818149215	3.198126272	8.645887707
H	5.932752659	2.142081618	9.756812027
H	1.295381791	5.738514016	8.049720945
H	2.115289643	4.94639688	9.397982366
H	2.634659472	6.55915796	8.877625603
H	3.361441969	5.657512591	6.689504755
H	3.912350294	3.56612892	9.552020583

DACO Radical Cation (1)

atom	x	y	z
O	8.174060514	5.531084672	8.094363164
N	6.186248745	7.147698726	5.554948987
N	4.633087215	4.840790189	8.075526216
C	6.25832068	6.333168239	6.588439771

C	4.903996923	6.962740391	3.428060908
C	4.566299292	8.957998056	4.999069378
C	8.07206678	8.68156311	6.137785491
C	4.895315659	7.464434269	4.877805984
C	8.443954678	6.693960832	4.583328779
C	5.667613237	5.466904546	7.551397189
C	7.465006526	7.77260278	5.062196308
C	2.749212212	3.608264956	7.007369476
C	5.400488345	4.799259751	10.45430678
C	5.809079374	2.802829347	8.920888218
C	2.311934661	5.622937942	8.527692139
C	7.082530057	5.713754055	7.58914016
C	3.256545742	4.964779013	7.513471289
C	4.876532412	3.966758858	9.27798185
H	3.915350338	7.124912471	2.989975796
H	5.628370066	7.502058049	2.811409768
H	5.12955868	5.894115	3.377105626
H	5.274433503	9.581861701	4.446817201
H	3.573490833	9.137499614	4.577666973
H	4.557230101	9.280857843	6.043591467
H	8.423275336	8.10197847	6.996411238
H	8.934891562	9.203150968	5.714648867
H	7.356533453	9.433408992	6.480956348
H	4.141245775	6.902451816	5.432849809
H	9.31364521	7.179989795	4.132814238
H	8.801345962	6.082746116	5.417210588
H	7.990821298	6.044012004	3.830190159
H	7.160891181	8.382282479	4.209545922
H	2.6019896	2.893949122	7.822110132
H	1.781574179	3.751875329	6.518875156
H	3.437550354	3.170997012	6.279170468
H	5.461910657	4.160904092	11.33995079

H	6.404406134	5.184469471	10.25346693
H	4.734703203	5.635136673	10.68487164
H	5.430601798	2.228655541	8.071232784
H	6.818448783	3.157790613	8.693379702
H	5.880414873	2.129948727	9.779778727
H	1.338406467	5.782156038	8.056027537
H	2.150838567	4.99296721	9.406908293
H	2.694402918	6.592283641	8.858599667
H	3.361568613	5.632427432	6.655341366
H	3.891933684	3.570553844	9.53241189

7. Miscellaneous

Calculation of the bond dissociation energy (BDE) of diaminocyclopropenone **1**H+

The BDE of the O-H bond of **1**H^+ was calculated using the Bordwell method of measuring the pK_a of the protonated species (**1**H+) in acetonitrile and $E_{1/2}$ of the deprotonated species (**1**) in acetonitrile vs Fc/Fc^+. (13-14)

The approximation is given by the equation:

$$\mathrm{BDE(M\text{-}H)(kcal\ mol^{-1})} = 1.37\ (pK_a) + 23.06(E_{1/2}) + 59.5 \qquad (5)$$

The $E_{1/2}$ for **1** vs Fc/Fc^+ was measured earlier as 0.34 V (see S33).

The pKa of **1**H^+ was measured by ^{1}H NMR in CAN-d6 using pyridine as a reference (pK_a = 12.53). (15) The multiplet at δ 7.73 was used as the diagnostic signal for pyridine, the multiplet at δ 8.50 was used as the diagnostic signal for pyridine·HCl, and the position of this multiplet between those two ppm values was used as an approximation of the relative concentration of pyridine and pyridine·HCl in solution. The pK_a of **1**H+ was obtained by averaging the results of three trials, using roughly 0.5, 1, and 1.5 equivalent of pyridine·HCl respectively. ^{1}H NMR spectra were referenced using the acetonitrile residual solvent peak at δ 1.94. In the following derivation of pK_a, concentration and number of moles for each species are used interchangeably as the volume is constant across all species. The effects of homoconjugation were not included. Pyr = pyridine, pyrH+ = pyridine·HCl.

The equilibrium can be represented by the following equation:

$$[\mathbf{1}\mathrm{H+}][\mathrm{pyr}] \rightleftharpoons [\mathbf{1}][\mathrm{pyrH+}] \qquad (6)$$

This equilibrium constant can thus be expressed as:

$$K_{eq} = \frac{[\mathbf{4}][\mathrm{pyrH+}]}{[\mathbf{4}\mathrm{H+}][\mathrm{pyr}]} \qquad (7)$$

The total moles of **1** + **1**H+ was arbitrarily set to 1:

$$1 = [\mathbf{1}] + [\mathbf{1}\mathrm{H+}] \qquad (8)$$

The total moles of pyr + pyrH+ was obtained from the integration of the ^{1}H NMR spectrum.

$$T_{pyr} = [\mathrm{pyr}] + [\mathrm{pyrH+}] \qquad (9)$$

The ratio of [pyrH+] to [pyr] was determined by measuring the relative position of the diagnostic multiplet of pyridine/pyridine·HCl between the location of the diagnostic peak of pyridine at δ 7.73 and of pyridine·HCl at δ 8.50. The ratio of [pyrH+] to [pyr] is equal the ppm difference between the measured peak from the pyridine peak at δ 7.73 divided by the total ppm difference for the diagnostic signals of pyridine and pyridine·HCl as shown in the following equation:

$$\frac{[\mathrm{pyrH+}]}{[\mathrm{pyr}]} = \frac{\delta(\mathrm{measured}) - \delta(\mathrm{pyr})}{\delta(\mathrm{pyrH+}) - \delta(\mathrm{pyr})} \qquad (10)$$

Finally, we can assume that the concentration of pyridine in solution will be equal to the concentration of **1**H+ as any pyridine present in solution will have resulted in the protonation of an equal amount of **1**:

$$[\mathrm{pyr}] = [\mathbf{4a}\mathrm{H+}] \qquad (11)$$

Equations (8), (9), (10), and (11) can then be used to solve for the four values in the equilibrium constant expression [**1**], [**1**H+], [pyr], and [pyrH+]. K_{eq} can then be determined using equation (7). The value of the pK_a of **1**H+ can then be determined from K_{eq} and the pK_a of pyridine in acetonitrile by the following equation:

$$pK_a(\mathbf{1}H+) = pK_a(pyrH+) + \log(K_{eq}) \tag{12}$$

The values of the pK_a(**1**H+) for each trial were:

(~0.5 eq pyridine·HCl) $pK_{a1} = 11.50$

(~1.0 eq pyridine·HCl) $pK_{a2} = 11.38$

(~1.5 eq pyridine·HCl) $pK_{a3} = 11.25$

Averaging the results of these trials gives the value:

pK_a(**1**H+) = 11.38

The BDE of the O-H bond of **1**H+ can thus be calculated using equation (5)

$E_{1/2}$ of **1** = 0.34 V (vs Fc/Fc^+ in ACN)

BDE of **1**H^+ = **83.7 kcal mol^{-1}**

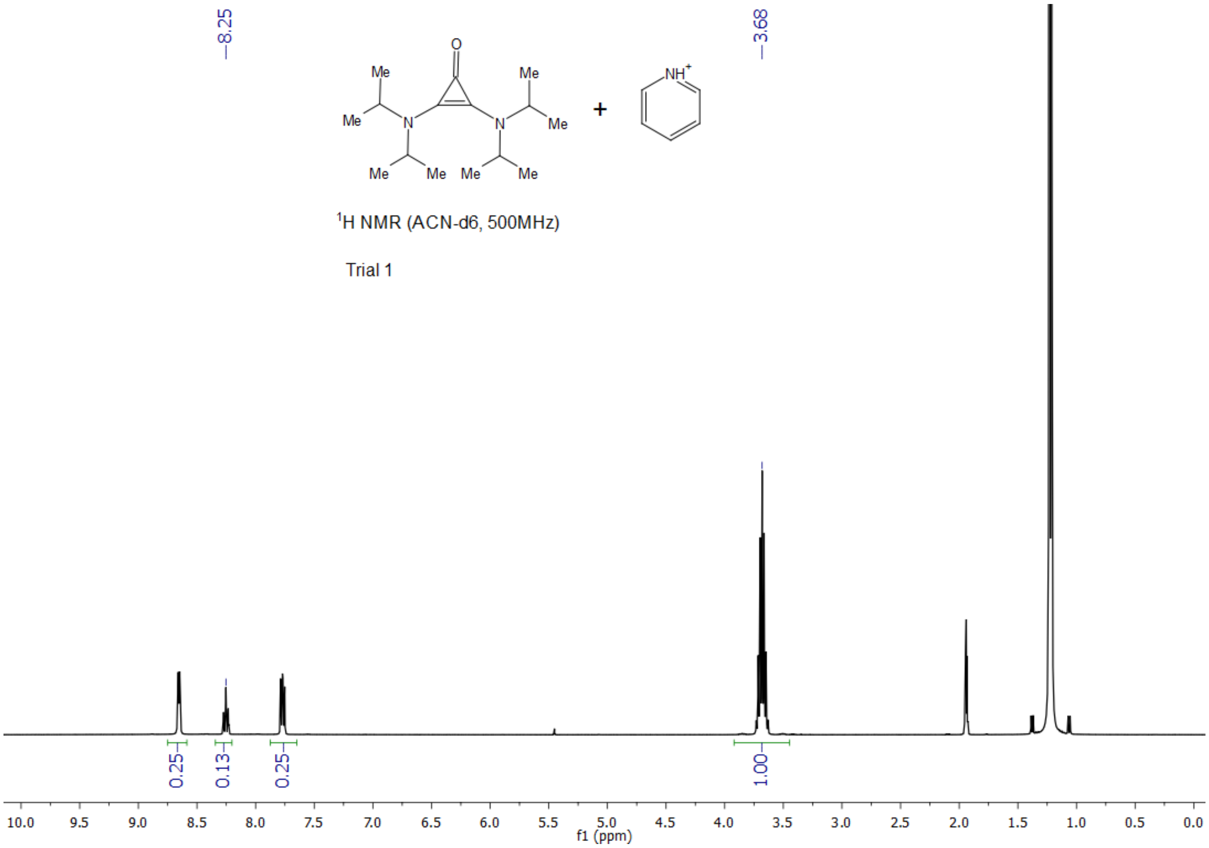
8.25
3.68
O
Me
Me
N
N
Me
Me
Me
Me
Me
Me
+
NH+
^{1}H NMR (ACN-d6, 500MHz)
Trial 1
0.25
0.13
0.25
1.00
10.0
9.5
9.0
8.5
8.0
7.5
7.0
6.5
6.0
5.5
5.0
4.5
4.0
3.5
3.0
2.5
2.0
1.5
1.0
0.5
0.0
f1 (ppm)

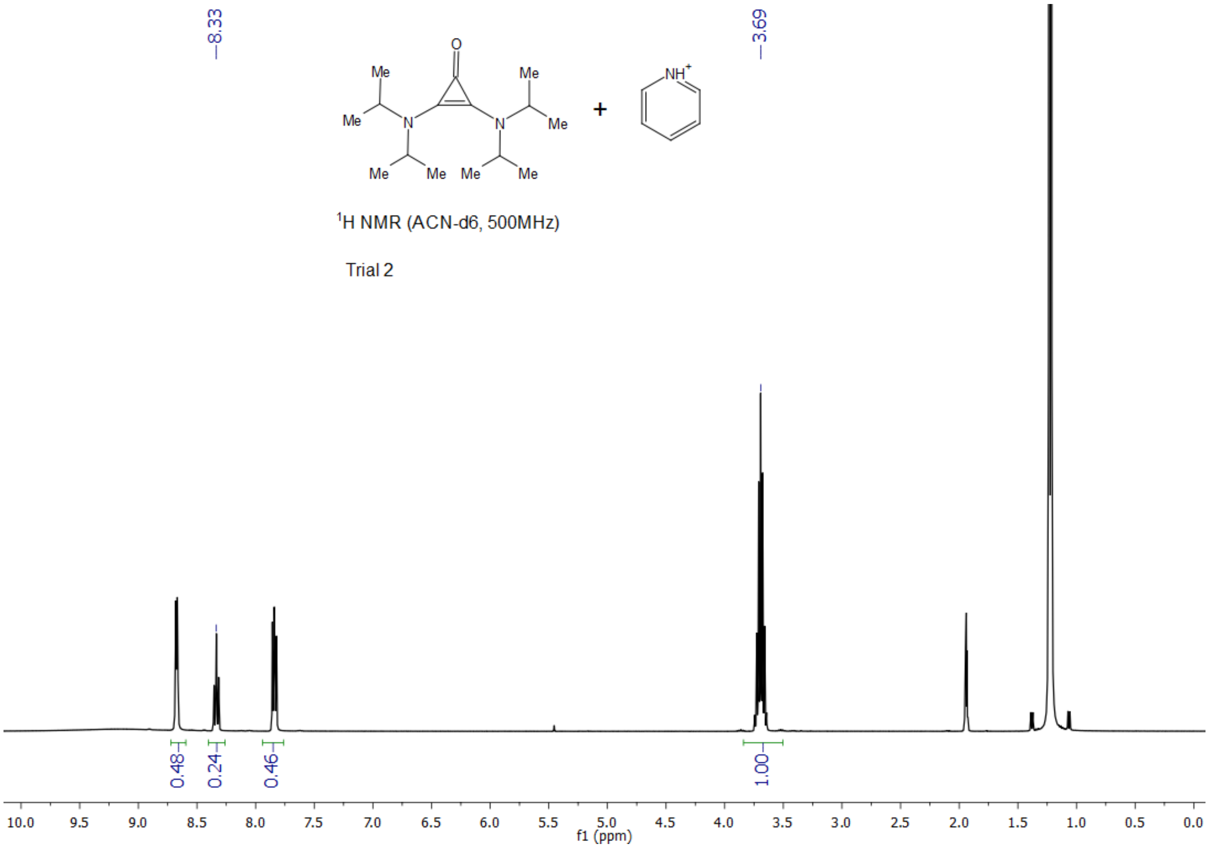
8.33
3.69
O
Me
Me
N
N
Me
Me
Me
Me
Me
Me
+
NH+
^{1}H NMR (ACN-d6, 500MHz)
Trial 2
0.48
0.24
0.46
1.00
10.0
9.5
9.0
8.5
8.0
7.5
7.0
6.5
6.0
5.5
5.0
4.5
4.0
3.5
3.0
2.5
2.0
1.5
1.0
0.5
0.0
f1 (ppm)

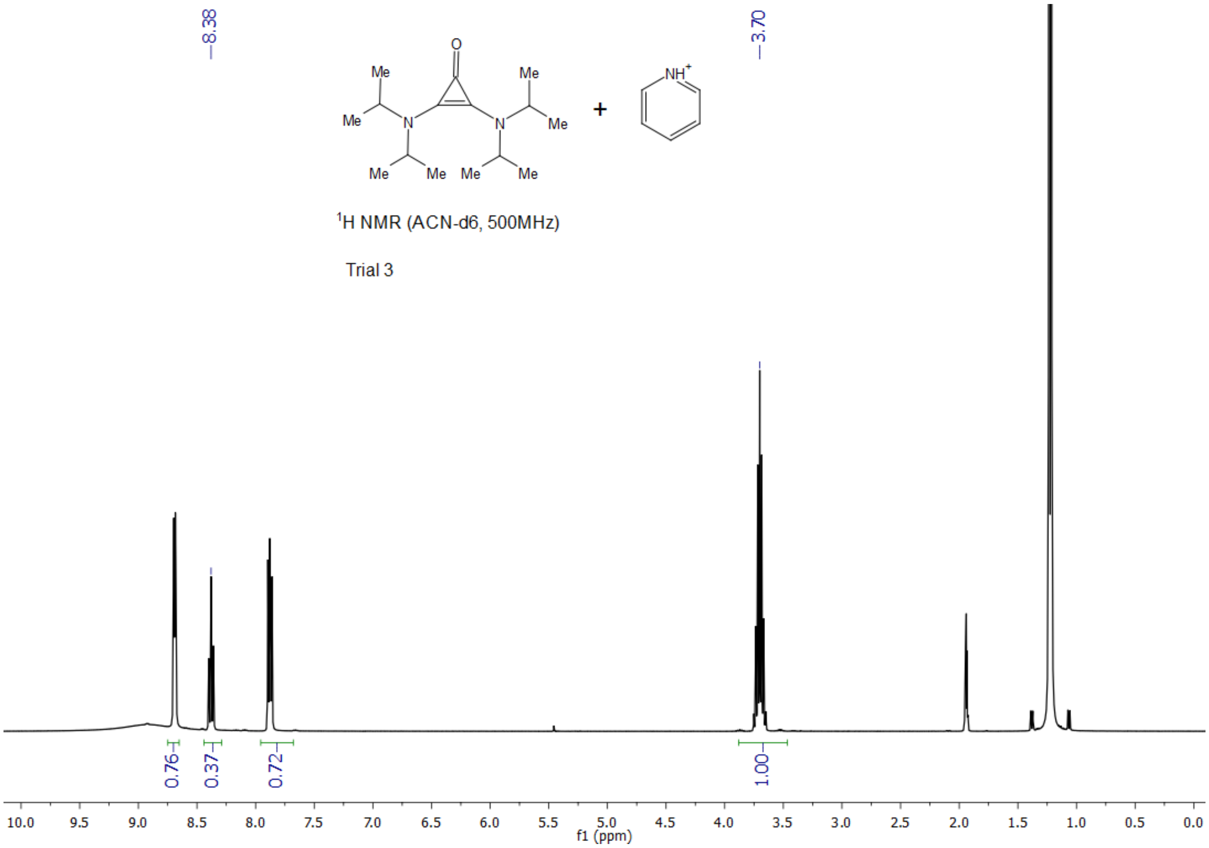
—8.38
—3.70
O
Me
Me
N
N
Me
Me
Me
Me
Me
Me
+
NH+
¹H NMR (ACN-d6, 500MHz)
Trial 3
0.76
0.37
0.72
1.00
10.0 9.5 9.0 8.5 8.0 7.5 7.0 6.5 6.0 5.5 5.0 4.5 4.0 3.5 3.0 2.5 2.0 1.5 1.0 0.5 0.0
f1 (ppm)

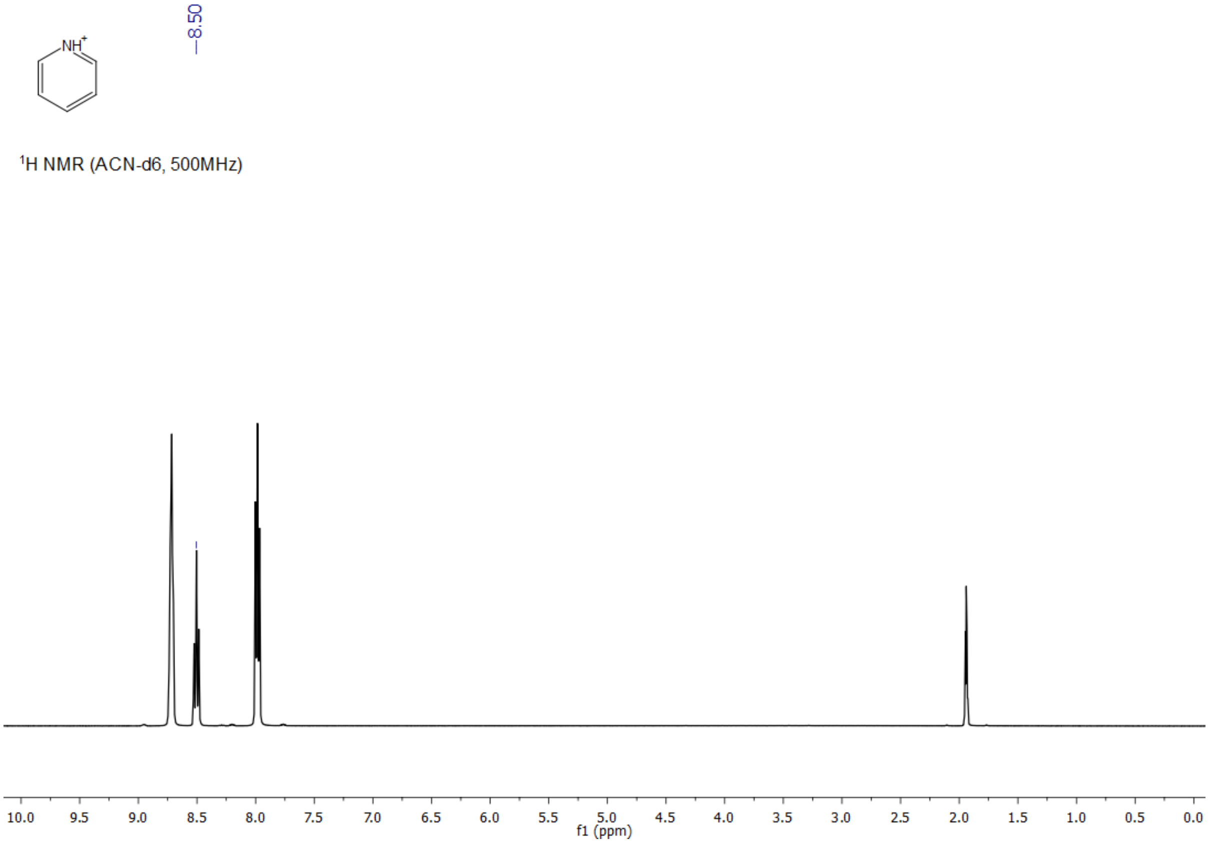
NH+
—8.50
¹H NMR (ACN-d6, 500MHz)
10.0 9.5 9.0 8.5 8.0 7.5 7.0 6.5 6.0 5.5 5.0 4.5 4.0 3.5 3.0 2.5 2.0 1.5 1.0 0.5 0.0
f1 (ppm)

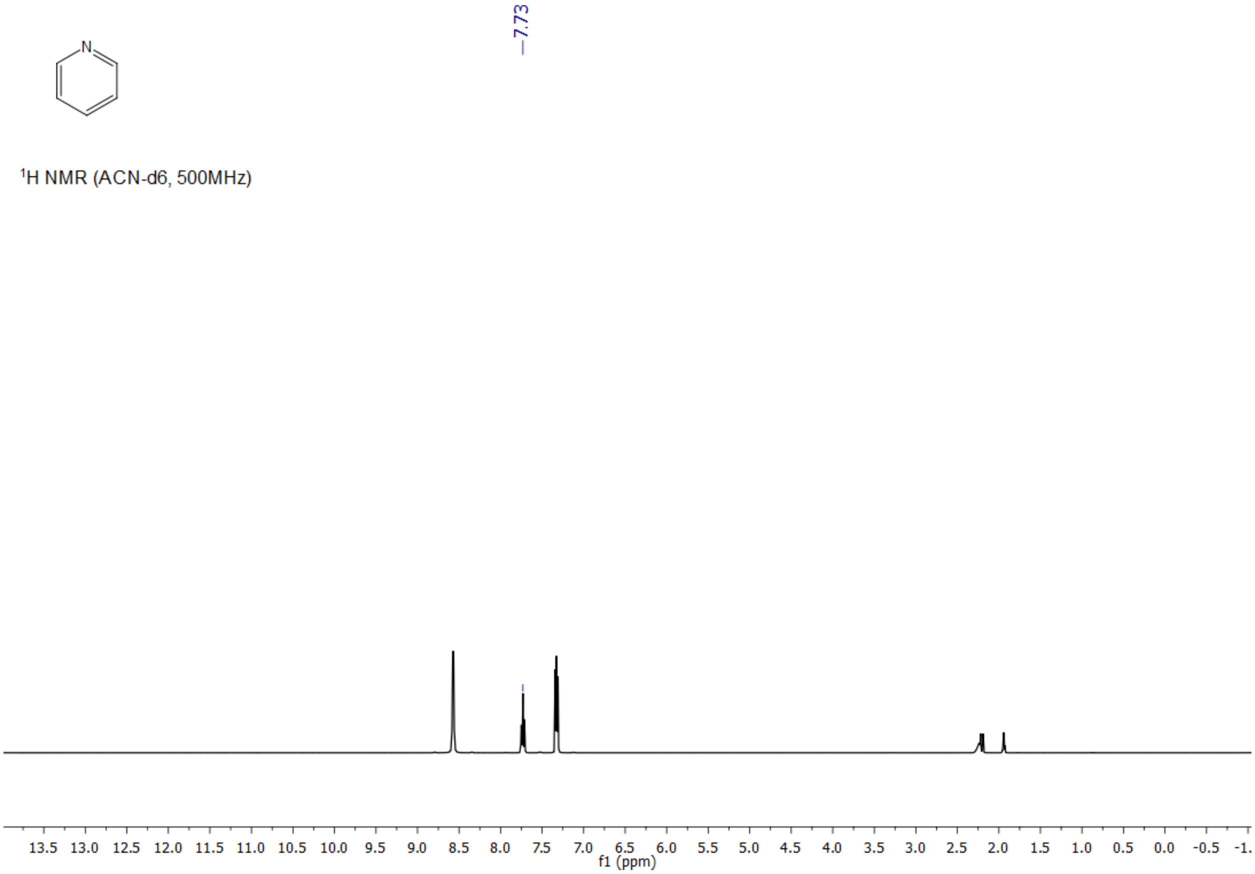

To test our measurement of the BDE of **1**H+, we subjected **DACO (1)** radical cation to thiophenol, which has a S-H bond strength of 78.5 kcal mol^{-1}. (13) We found that this indeed did result in the formation of phenyl disulfide, which we believe occurs through H atom abstraction rather than by oxidation due to the fact that the oxidation potential of thiophenol (1.51 V) is well beyond that of **1** (0.74 V). (16)

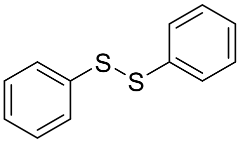

Phenyl disulfide (S8). diaminocyclopropenone **1** (265 mg, 1.05 mmol) was dissolved in 4 mL of DCM. $NOPF_6$ (175 mg, 1.00 mmol) was dissolved in 1 mL ACN and subsequently added dropwise to the solution of **1**, which immediately evolved gas and turned dark red. The solution was stirred for 20 minutes at which point there was no further gas evolution. The dark red solution of the cyclopropenone radical cation **DACO (1)** radical cation was cooled to 0°C and thiophenol (51 µL, 0.5 mmol) was added. The reaction was stirred at 0°C for 20 minutes and subsequently concentrated *in vacuo*. Column chromatography (5% EtOAc/Hexanes) gave the product as a white solid (53 mg, 0.49 mmol, 97% yield). The spectra are consistent with previous reports. (17) ^{1}H NMR (500 MHz, $CDCl_3$) δ 7.56-7.51 (m, 4H), 7.37-7.30 (t, *J* = 7.3 Hz, 4H), 7.29-7.24 (t, *J* = 7.5 Hz, 2H). ^{13}C NMR (126 MHz, $CDCl_3$) δ 137.2, 129.2, 127.6, 127.3.

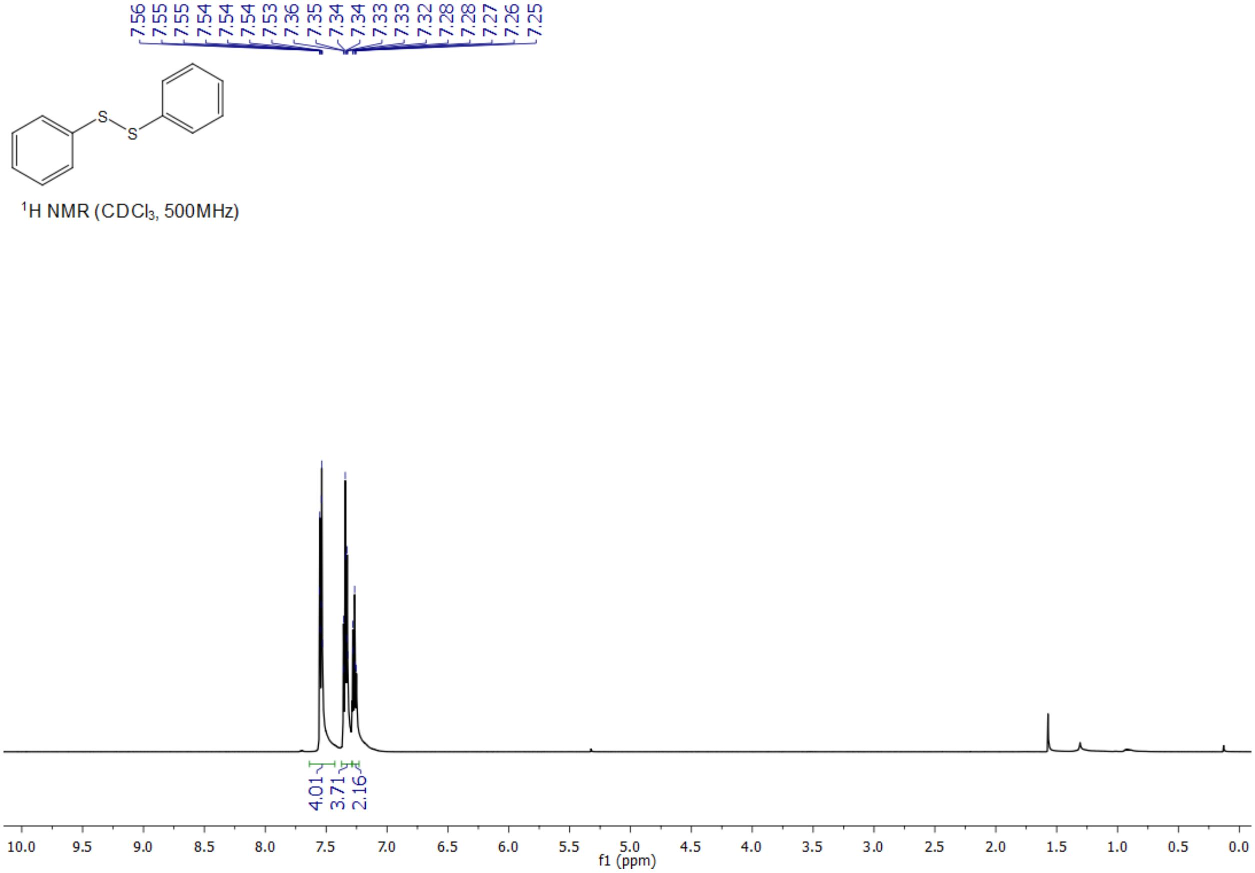

^{1}H NMR (CDCl$_3$, 500MHz)

8. References

(1) Nacsa, E. D.; Lambert, T. H. J. Am. Chem. Soc. 2015, 137 (32), 10246.

(2) Connelly, N. G.; Geiger, W. E. Chem. Rev. 1996, 96 (2), 877.

(3) Sheldrick, G. M. SHELXTL, An Integrated System for Solving, Refining, and Displaying Crystal Structures from Diffraction Data; University of Göttingen, Göttingen, Federal Republic of Germany, 1981. 1981.

(4) Sheldrick, G. M. Acta Crystallogr. Sect. A Found. Crystallogr. 2015, 71 (1), 112.

(5) Sheldrick, G. M. Acta Crystallogr. Sect. A Found. Crystallogr. 2015, 71 (1), 3.

(6) Jaguar, version 8.9, Schrodinger, Inc., New York, NY, 2015. .

(7) Bochevarov, A. D.; Harder, E.; Hughes, T. F.; Greenwood, J. R.; Braden, D. a.; Philipp, D. M.; Rinaldo, D.; Halls, M. D.; Zhang, J.; Friesner, R. a. Int. J. Quantum Chem. 2013, 113 (18), 2110.

(8) Becke, a. D. Phys. Rev. A 1988, 38 (6), 3098.

(9) Becke, A. D. J. Chem. Phys. 1993, 98 (7), 5648.

(10) Lee, C.; Yang, W.; Parr, R. G. Phys. Rev. B 1988, 37 (2), 785.

(11) Vosko, S. H.; Wilk, L.; Nusair, M. Can. J. Phys. 1980, 58 (8), 1200.

(12) Slater, J. C. Quantum Theory of Molecules and Solids, Vol. 4: The Self-Consistent Field for Molecules and Solids; McGraw-Hill: New York, 1974. .

(13) Bordwell, F. G.; Cheng, J. P.; Harrelson, J. a. J. Am. Chem. Soc. 1988, 110 (4), 1229.

(14) Wayner, D. D. M.; Parker, V. D. Acc. Chem. Res. 1993, 26 (5), 287.

(15) Kaljurand, I.; Kütt, A.; Sooväli, L.; Rodima, T.; Mäemets, V.; Leito, I.; Koppel, I. a. J. Org. Chem. 2005, 70 (3), 1019.

(16) Roth, H. G.; Romero, N. a.; Nicewicz, D. a. Synlett 2016, 27 (5), 714.

(17) Oba, M.; Tanaka, K.; Nishiyama, K.; Ando, W. J. Org. Chem. 2011, 76 (10), 4173.

APPENDIX II: Experimental, NMR Spectra, and other Data (Chapter 3)

General Experimental Details: All reactions were performed in oven-dried or flame-dried round bottom flasks or vials fitted with PTFE septa caps, unless otherwise noted. All reactions, unless noted, were conducted under a positive pressure of nitrogen using standard air-free technique. Anhydrous solvents were obtained from a Schlenk manifold with purification columns packed with activated alumina and supported copper catalyst (Glass Contour, Irvine, CA) or as Sure-Seal bottles from vendors. Automated flash chromatography was performed using a Teledyne Isco Combiflash Rf200 and Redisep Rf silica columns.

Materials: [PDI][TFSI]$_2$ was synthesized according to our reported procedures.[1] All chemical reagents were purchased from commercial sources and used without purification unless noted. All compounds and salts put into the battery were dissolved in anhydrous acetonitrile and dried overnight on molecular sieves (4A beads 8-12 mesh, Sigma-Aldrich) inside an inert, dry glovebox (N_2). H-Cells were purchased from Adams and Chittenden. PTFE sheets were purchased from Alfa Aesar (0.125-inch thickness). Daramic 0.6 was graciously provided by Daramic. AvCarb G100 Soft Graphite Battery Felt (3.2-mm thickness) was purchased from Fuel Cell Store.

Instrumentation: ^{1}H and ^{13}C NMR spectra were recorded on a Bruker DRX400 (400 MHz) or a Bruker DMX500 (500 MHz) spectrometer. Chemical shifts for protons are reported in parts per million downfield from tetramethylsilane and are referenced to residual protium within the NMR solvent ($CHCl_3$: δ 7.26 or $C_2H_2Cl_4$: 6.00). Chemical shifts for carbon are reported in parts per million downfield from tetramethylsilane and are referenced to the carbon resonances of the solvent ($CDCl_3$: δ 77.0). Data are represented as follows: chemical shift, multiplicity, (s = singlet, d = doublet, t = triplet, m = multiplet, b = broad), coupling constants in hertz, and integration. The mass spectroscopic data were obtained at the Columbia University mass spectrometry facility using a Bruker ultrafleXtreme MALDI TOF. IR spectra were recorded using Perkin Elmer Spectrum 400 FT-IR. Absorption spectra were obtained on a Shimadzu UV 1800 UV-Vis spectrophotometer. Scanning electron micrographs were collected using a ZEISS Sigma FE-SEM. Battery cycling was performed using an Arbin Battery Tester BT2000.

Procedures and Characterization:

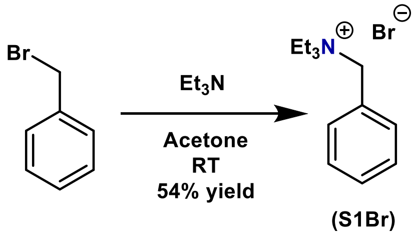

Benzyltriethylammonium bromide (S1Br):

A 20 mL vial was charged with acetone (10 mL), triethylamine (7.00 ml, 50.0 mmol), and benzyl bromide (2.00 mL, 16.8 mmol). The reaction was stirred at RT for 4 hours during which time a white precipitate formed. The reaction was diluted with diethyl ether and the precipitate was collected by filtration, giving **S1Br** as white crystals (2.46 g, 9.04 mmol, 54% yield) that were carried forward for salt metathesis.

^{1}H NMR (500 MHz, $CDCl_3$, 323 K): δ 7.52 (d, *J* = 6.7 Hz, 2H), 7.44-7.34 (m, 2H), 4.74 (s, 2H), 3.40 (q, *J* = 7.3 Hz, 6H), 1.42 (t, *J* = 7.3 Hz, 9H).

^{13}C NMR (126 MHz, $CDCl_3$, 323 K): δ 132.6, 130.8, 129.4, 127.2, 61.4, 53.1, 8.7.

IR (ATR) [cm^{-1}]: 3403, 2985, 1625, 1480, 1456, 1396, 1155, 1008, 756, 707, 539.

HRMS (ESI+) m/z [M]$^+$ calculated for $C_{13}H_{22}N^+$ = 192.1752; found 192.1746.

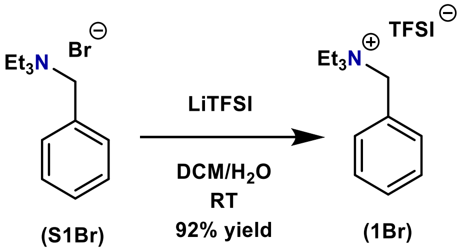

Benzyltriethylammonium Bis(trifluoromethane)sulfonimide (S1):

A 20 mL vial was charged with **1Br** (1.00 g, 3.67 mmol) and subsequently dissolved in dichloromethane (8 mL). To this mixture was added a solution of LiTFSi (2.11 g, 7.34 mmol) in deionized water (8 mL). This biphasic reaction mixture was stirred vigorously via magnetic stir bar for 16 hours, after which the stirring was halted and the layers were separated. The organic layer was washed with fresh LiTFSI solution (1M, 2X), and subsequently deionized water (3x). The organic layer was concentrated in vacuo to give **S1** as a clear oil the slowly crystallized (1.60 g, 3.39 mmol, 92% yield).

^{1}H NMR (500 MHz, $CDCl_3$, 323 K): δ 7.55-7.46 (m, 3H), 7.40 (d, *J* = 6.6 Hz, 2H), 4.34 (s, 2H), 3.22 (q, *J* = 6.9 Hz, 6H), 1.44 (t, *J* = 6.9 Hz, 9H).

^{13}C NMR (126 MHz, $CDCl_3$, 323 K): δ 132.2, 131.2, 129.8, 126.4, 60.9, 52.8, 7.8.

^{19}F NMR (282 MHz, $CDCl_3$, 323 K): δ 77.9

IR (ATR) [cm^{-1}]: 2920, 2851, 1459, 1348, 1183, 1136, 1054, 789, 755, 705, 616, 513.

HRMS (ESI+) m/z [M]$^+$ calculated for $C_{13}H_{22}N^+$ = 192.1752; found 192.1747.

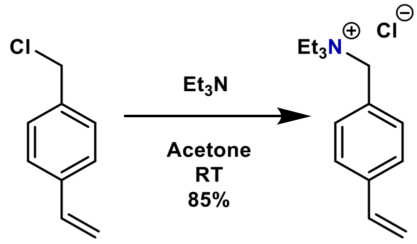

(1Cl)

(4-vinylbenzyl)triethylammonium chloride (1Cl):

A dry 20 mL vial was charged with a stir bar, stryrene chloride (18.75 mg, 0.125 mmol, 1 eq.), triethylamine (315 mg, 0.386 mmol, 3.1 eq.), and acetonitrile (360 mg, 3.13 mmol, 25 eq.). The charged vial was sparged with nitrogen to degass (20 min), at which point the mixture was heated to 67 degrees Celsius and stirred for 16 hours. The solution was then cooled to room temperature and the solid product was filtered. The crude solid was recrystallized in acetonitrile to afford styrene triethylammonium chloride (**1Cl**) (26 mg, 85%), which was carried forward for salt metathesis.

^{1}H NMR (500 MHz, $CDCl_3$, 323 K): δ 7.55-7.49 (m, 2H), 7.45-7.38 (m, 2H), 6.68 (dd, *J* = 17.6, 10.9 Hz, 1H), 5.79 (d, *J* = 17.6 Hz, 1H), 5.34 (d, *J* = 10.8 Hz, 1H), 4.85 (s, 2H), 3.51-3.39 (m, 6H), 1.45 (t, *J* = 7.0 Hz, 9H).

^{13}C NMR (126 MHz, $CDCl_3$, 323 K): δ 140.0, 135.6, 132.9, 127.1, 126.6, 116.5, 61.5, 53.1, 8.7.

IR (ATR) [cm^{-1}]: 3375, 2987, 2924, 2850, 1629, 1480, 1397, 1155, 1008, 910, 856, 786, 615.

HRMS (ESI+) m/z [M]$^+$ calculated for $C_{15}H_{24}N^+$ = 218.1909; found 218.1901.

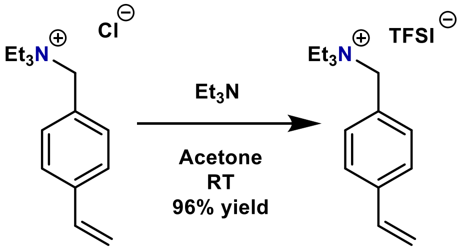

(1Cl)

(1)

(4-vinylbenzyl)triethylammonium bis(trifluoromethane)sulfonimide (1):

Styrene triethylammonium chloride **(1Cl)** (1 g, 3.95 mmol, 1 eq.) was charged into a 20 mL vial and subsequently dissolved in dichloromethane (10 mL). To this mixture was added a solution of LiTFSI (1.198 g, 4.175 mmol, 1.05 eq.) in deionized water (10 mL). This biphasic reaction mixture was stirred vigorously via magnetic stir bar for 16 hours, after which the stirring was halted and the layers were separated. The organic layer was washed with fresh LiTFSI solution (0.5 M, 3x), and subsequently deionized water (6x) to remove any trace chloride salts. The organic layer was not dried with any drying agent in order to avoid salt contamination. Once washed, the organic layer was evaporated under reduced pressure and vigorously dried under high vacuum for 24 hours to yield 1.9 g (96%) of **1** as a clear, colorless oil.

^{1}H NMR (500 MHz, $CDCl_3$, 323 K): δ 7.49 (d, *J* = 8.2 Hz, 2H), 7.36 (d, *J* = 8.3 Hz), 6.72 (dd, *J* = 17.6, 10.9 Hz, 1H), 5.84 (d, *J* = 17.6, 1H), 5.39 (d, *J* = 10.9 Hz, 1H), 4.32 (s, 2H), 3.22 (q, *J* = 7.2 Hz, 6H), 1.43 (t, *J* = 7.2 Hz, 9H).

^{13}C NMR (126 MHz, $CDCl_3$, 323 K): δ 140.5, 135.5, 132.5, 127.5, 125.4, 121.3, 116.9, 60.8, 52.8, 7.9.

^{19}F NMR (282 MHz, $CDCl_3$, 323 K): δ 77.9

IR (ATR) [cm^{-1}]: 2998, 2920, 2850, 1479, 1348, 1184, 1137, 1054, 787, 616, 513.

HRMS (ESI+) m/z [M]$^+$ calculated for $C_{15}H_{24}N^+$ = 218.909; found 218.909.

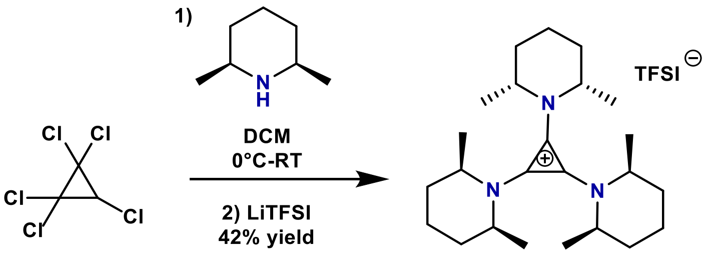

TAC (1)

Tris(2,6-dimethylpiperidnyl)-cyclopropenium bis(trifluoromethane)sulfonimide (TAC (1)):

A 250 mL roundbottom flask was charged with dichloromethane (100 mL) and pentachlorocyclopropane (2.00 mL, 14.0 mmol). The flask was cooled to 0 C and 2,6-dimethylipiperidine (15.1 mL, 112 mmol) was added slowly while vigorously stirring. The reaction was kept at 0°C for 1 hr and then allowed to stir for 16 hours at RT. The reaction was then transferred to a separatory funnel and washed with 1M HCl (3x), water (1x), and LiTFSI solution (1M, 3x). The organic layer was concentrated in vacuo and the solids were recrystallized twice from isopropyl alcohol to give **TAC (1)** as white crystals (3.84 g, 5.88 mmol, 42% yield).

^{1}H NMR (500 MHz, $CDCl_3$, 323 K): δ 3.86 (quint, *J* = 6.9 Hz, 4H), 1.96-1.84 (m, 4H), 1.84-1.73 (m, 2H), 1.71-1.63 (m, 4H), 1.63-1.55 (m, 2H), 1.36 (d, *J* = 7.2 Hz, 12H).

^{13}C NMR (126 MHz, $CDCl_3$, 323 K): δ 117.0, 53.6, 29.6, 21.9, 12.6.

^{19}F NMR (282 MHz, $CDCl_3$, 323 K): δ 77.9.

IR (ATR) [cm^{-1}]: 2981, 2946, 2867, 1479, 1352, 1175, 1043, 738, 614, 511 cm^{-1}.

HRMS (ESI+) m/z [M]$^+$ calculated for $C_{24}H_{42}N_3^+$ = 372.2279; found 372.3389.

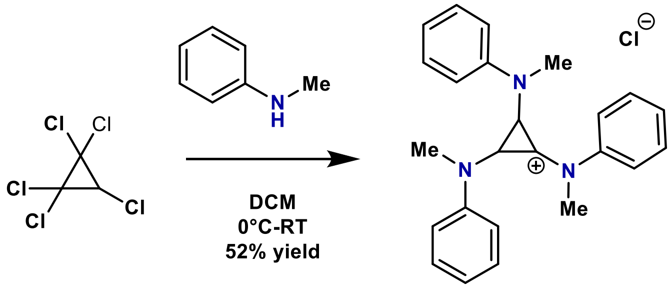

(5Cl)

Tris(N-methylanilino)-cyclopropenium chloride (5Cl):

A 250 mL roundbottom flask was charged with dichloromethane (100 mL) and pentachlorocyclopropane (1.00 mL, 7.00 mmol). The flask was cooled to 0°C and N-methylaniline (2.28 mL, 21 mmol) and triethylamine (4.88 mL, 35 mmol) were added slowly while vigorously stirring. The reaction was kept at 0°C for 1 hour and then allowed to stir for 16 hours at RT. The reaction was then transferred to a separatory funnel and washed with 1M HCl (3x) and water (1x). The organic layer was concentrated in vacuo and the solids were recrystallized from IPA:Hexanes (~1:10) to give **5Cl** as white crystals (1.45 g, 3.72 mmol, 53% yield).

^{1}H NMR (500 MHz, $CDCl_3$, 323 K): 7.28 (d, *J* = 7.9 Hz, 6H), 7.11 (t, *J* = 7.6 Hz, 6H), 7.00 (t, *J* = 7.4 Hz, 3H), 3.31 (s, 9H).

^{13}C NMR (126 MHz, $CDCl_3$, 323 K): δ 143.6, 129.5, 127.1, 122.9, 118.0, 42.6.

IR (ATR) [cm^{-1}]: 3374, 3042, 2920, 1591, 1516, 1492, 1407, 1287, 1176, 1110, 754, 734, 697.

HRMS (ESI+) m/z [M]$^+$ calculated for $C_{24}H_{24}N_3^+$ = 354.1970; found 354.1969.

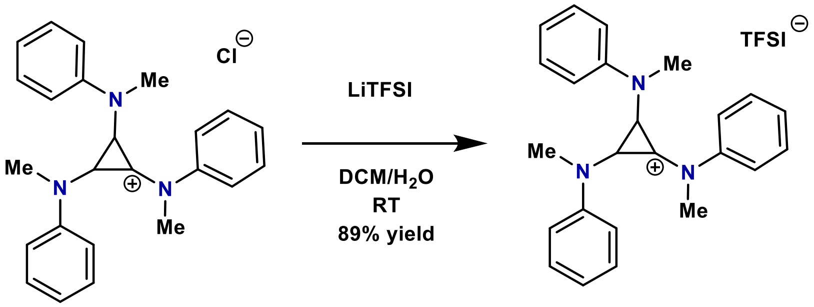

(5Cl) (5)

Tris(N-methylanilino)-cyclopropenium Bis(trifluoromethane)sulfonimide (MAD-CP; 5):

A 20 mL vial was charged with **6Cl** (0.5 g, 1.28 mmol) and subsequently dissolved in dichloromethane (5 mL). To this mixture was added a solution of LiTFSi (0.74 g, 2.56 mmol) in deionized water (5 mL). This biphasic reaction mixture was stirred vigorously via magnetic stir bar for 16 hours, after which the stirring was halted and the layers were separated. The organic layer was wash with fresh LiTFSI solution (1M, 2X), and subsequently deionized water (3x). The organic layer was concentrated in vacuo to give **5** as a slowly crystallizing clear oil (0.73 g, 1.15 mmol, 90% yield)

^{1}H NMR (500 MHz, CDCl$_3$, 323 K): 7.27-7.14 (m, 12H), 7.10 (t, *J* = 7.0 Hz, 3H), 3.27 (s, 9H).

^{13}C NMR (126 MHz, CDCl$_3$, 323 K): δ 143.6, 129.7, 127.4, 122.9, 118.9, 117.7, 42.4.

^{19}F NMR (282 MHz, CDCl$_3$, 323 K): δ 77.8.

IR (ATR) [cm^{-1}]: 3063, 2920, 1517, 1493, 1407, 1349, 1181, 1136, 1055, 753, 695, 615, 513.

HRMS (ESI+) m/z [M]$^+$ calculated for C$_{24}$H$_{24}$N$_3^+$ = 354.1970; found 354.1978.

^{1}H and ^{13}C NMR Spectra:

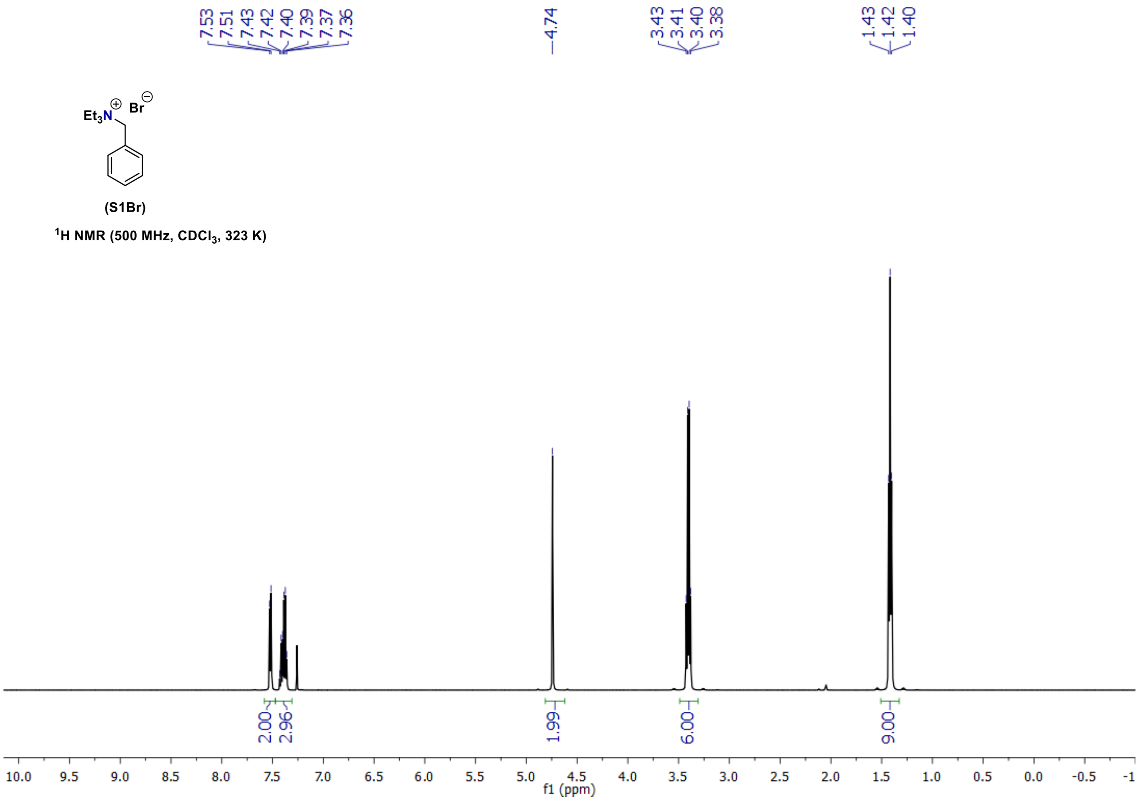

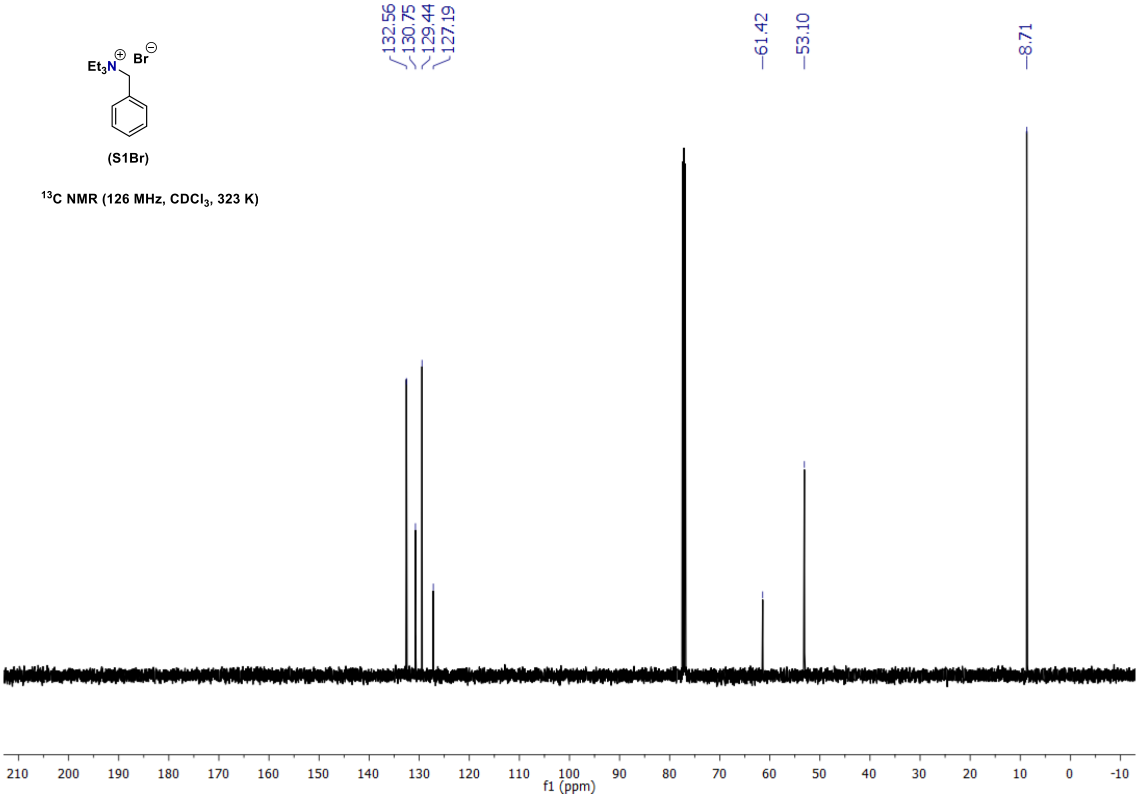

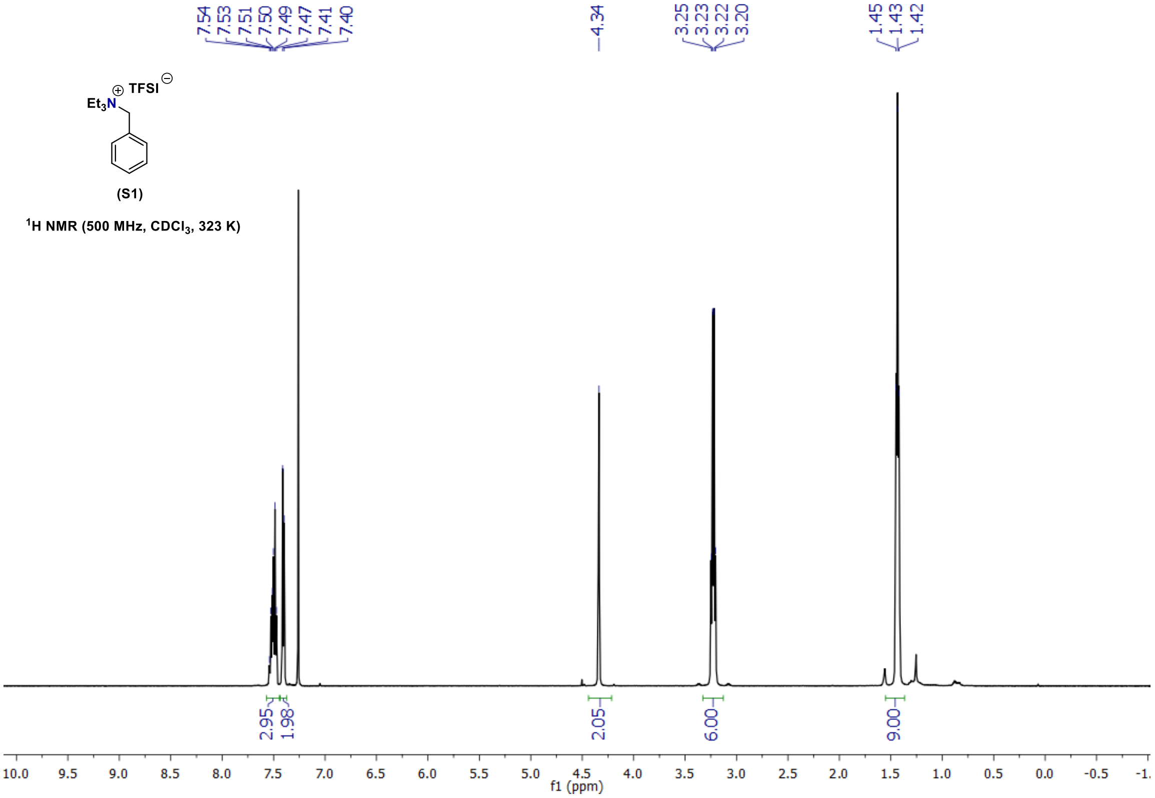

(S1)

^{1}H NMR (500 MHz, CDCl$_3$, 323 K)

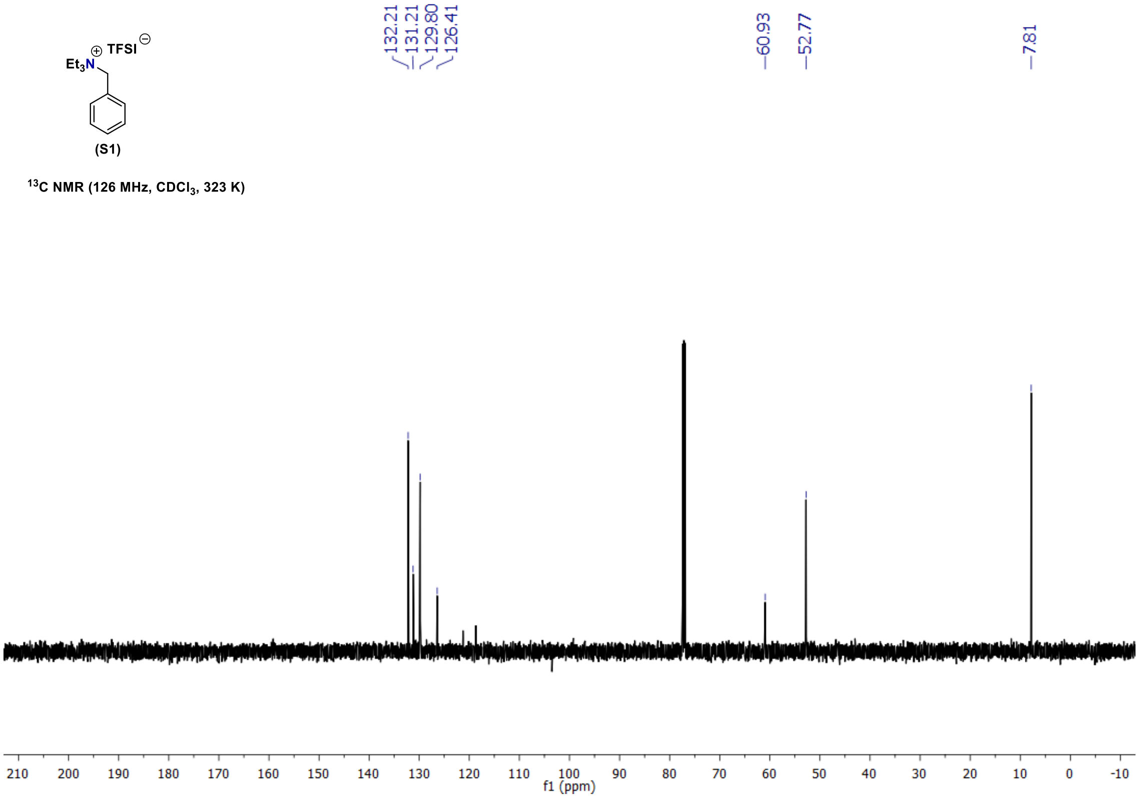

(S1)

^{13}C NMR (126 MHz, CDCl$_3$, 323 K)

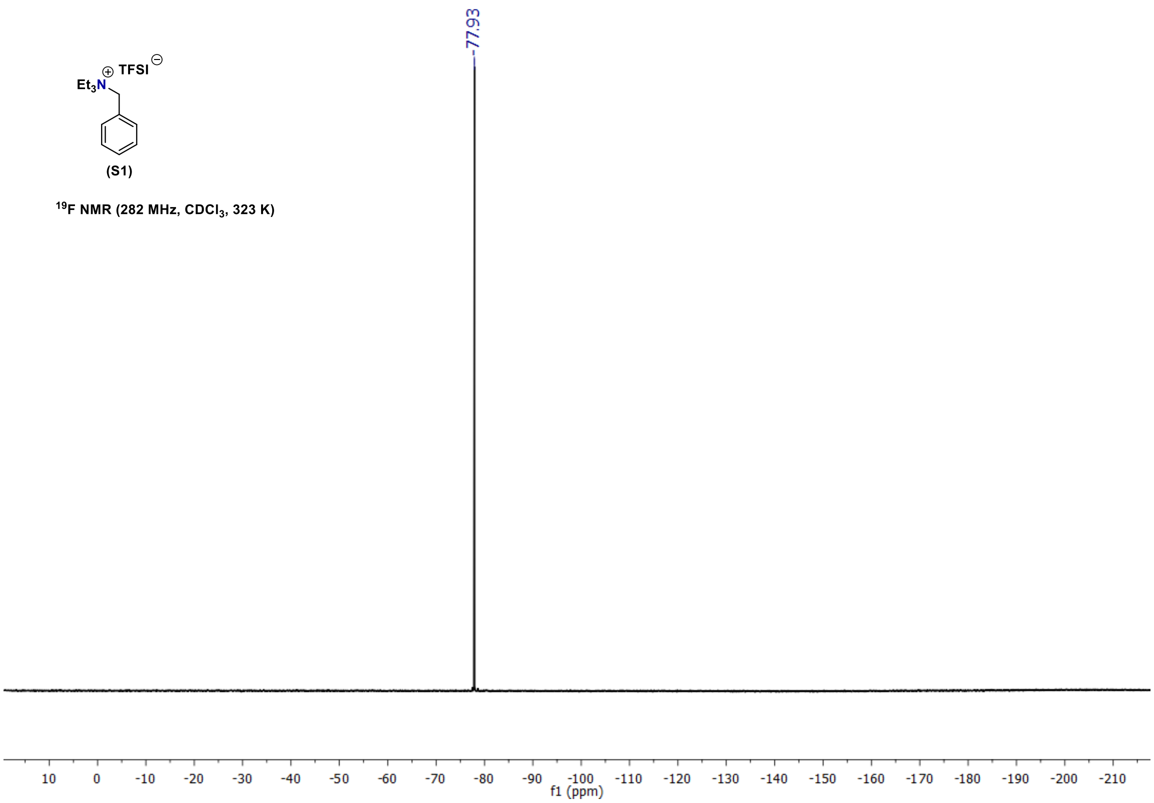

(S1)

^{19}F NMR (282 MHz, $CDCl_3$, 323 K)

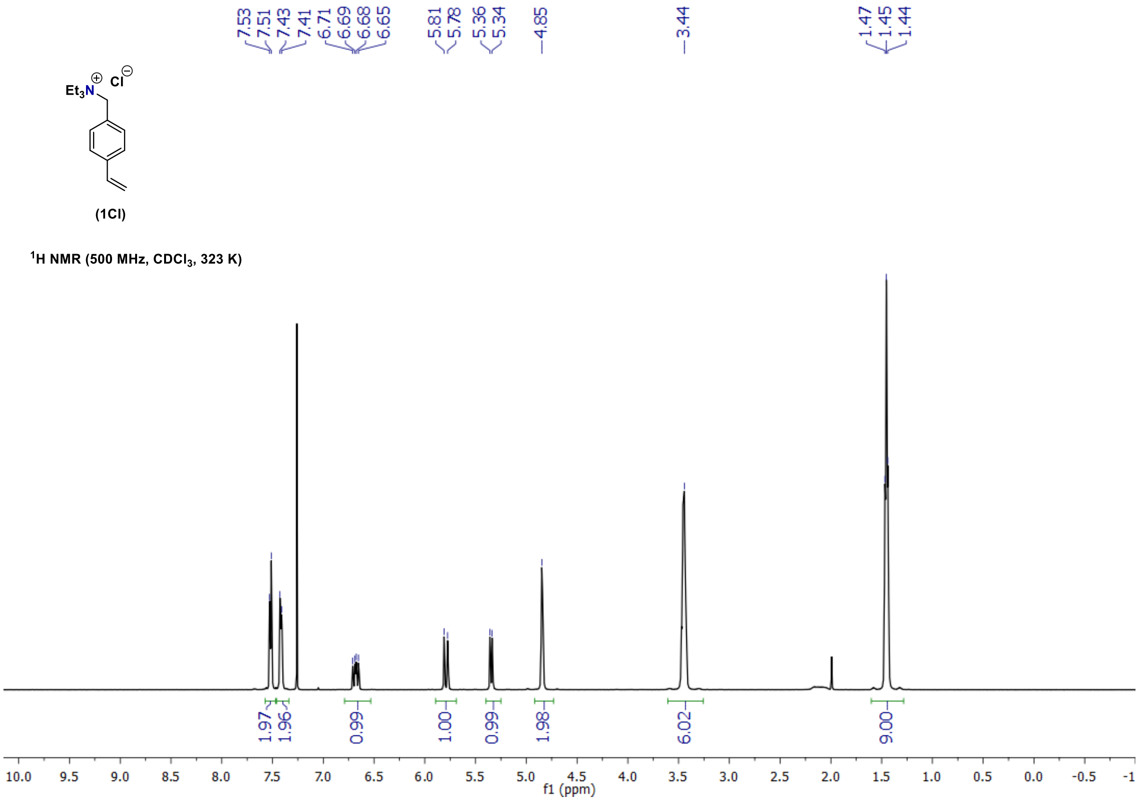

(1Cl)

^{1}H NMR (500 MHz, $CDCl_3$, 323 K)

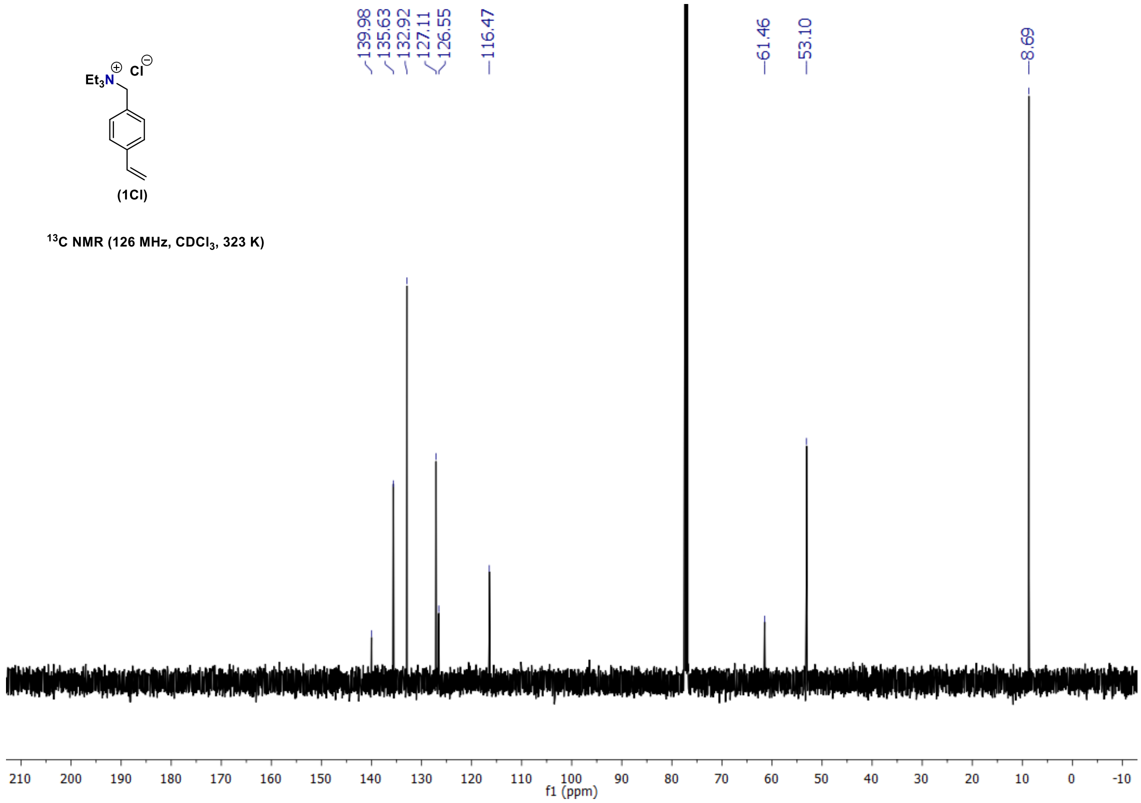

(1Cl)

^{13}C NMR (126 MHz, CDCl$_3$, 323 K)

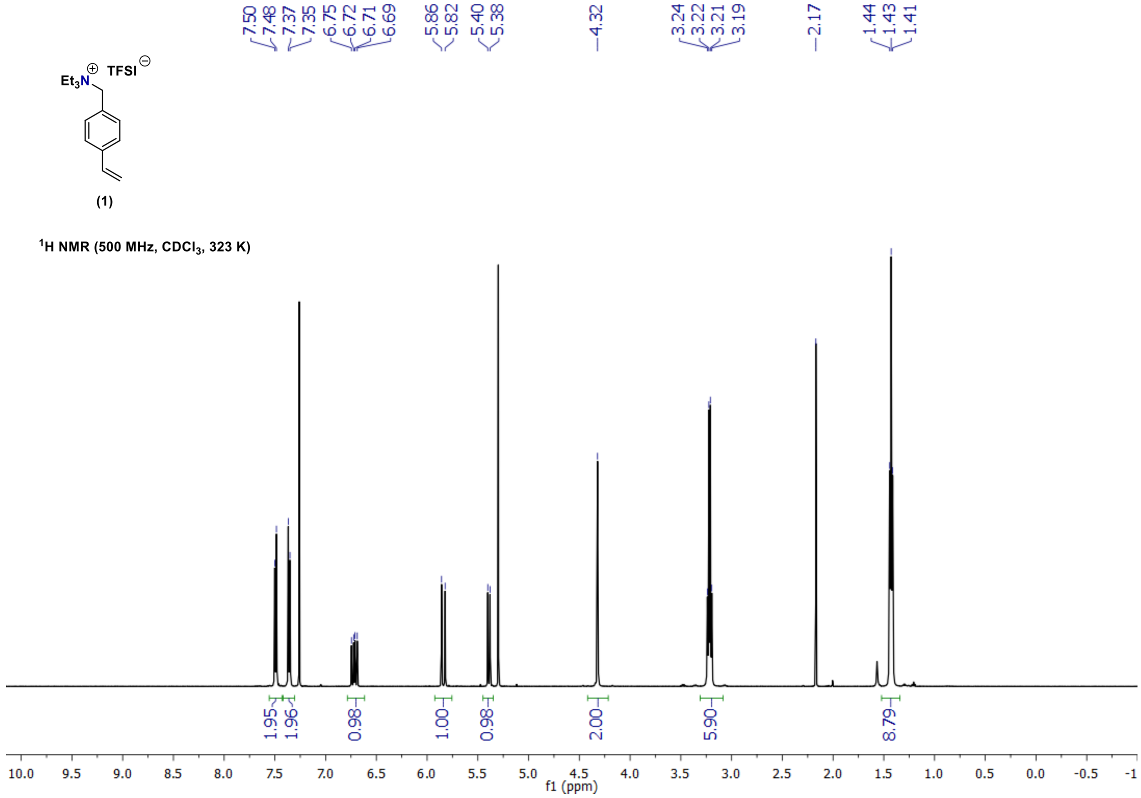

(1)

^{1}H NMR (500 MHz, CDCl$_3$, 323 K)

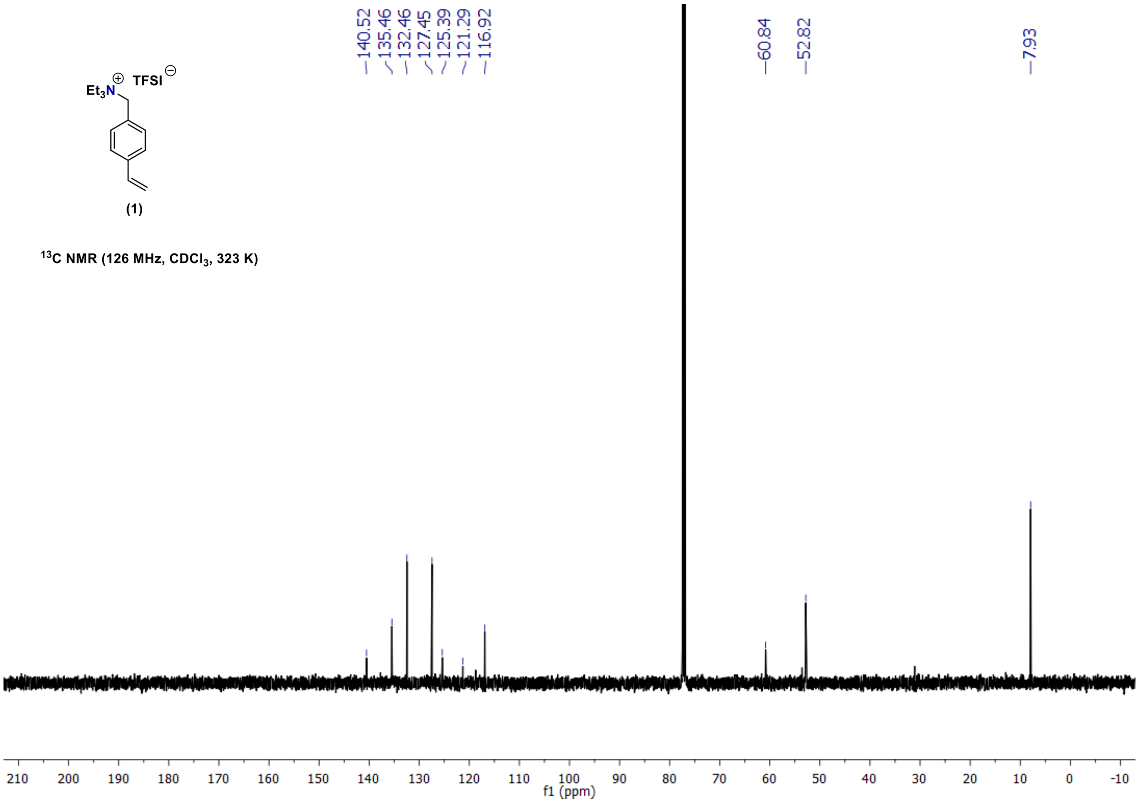

(1)

^{13}C NMR (126 MHz, CDCl$_3$, 323 K)

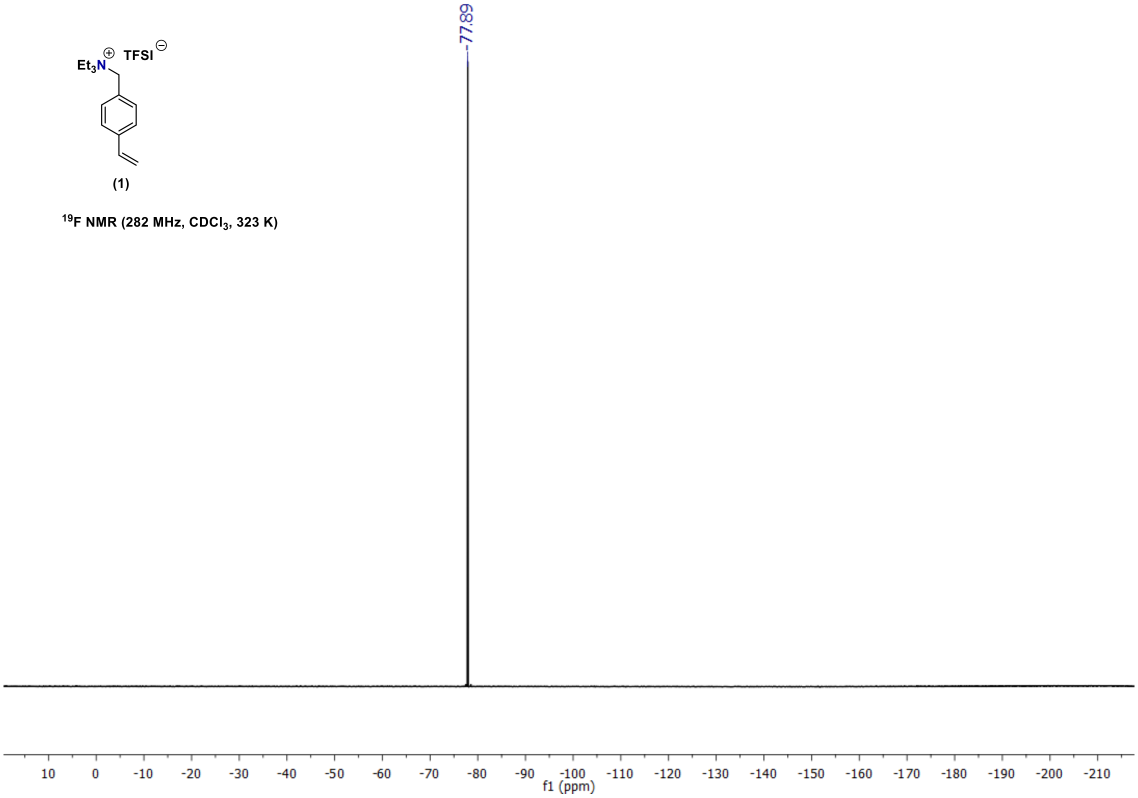

(1)

^{19}F NMR (282 MHz, CDCl$_3$, 323 K)

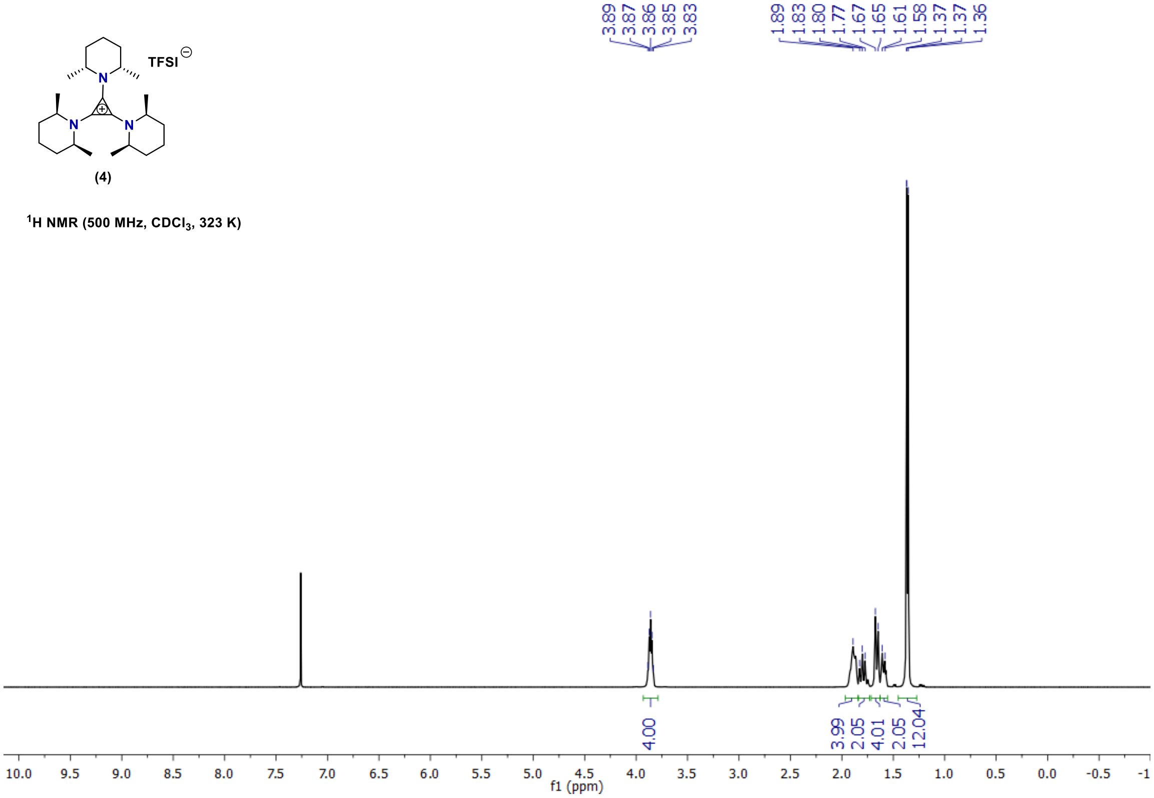

(4)

^{1}H NMR (500 MHz, CDCl$_3$, 323 K)

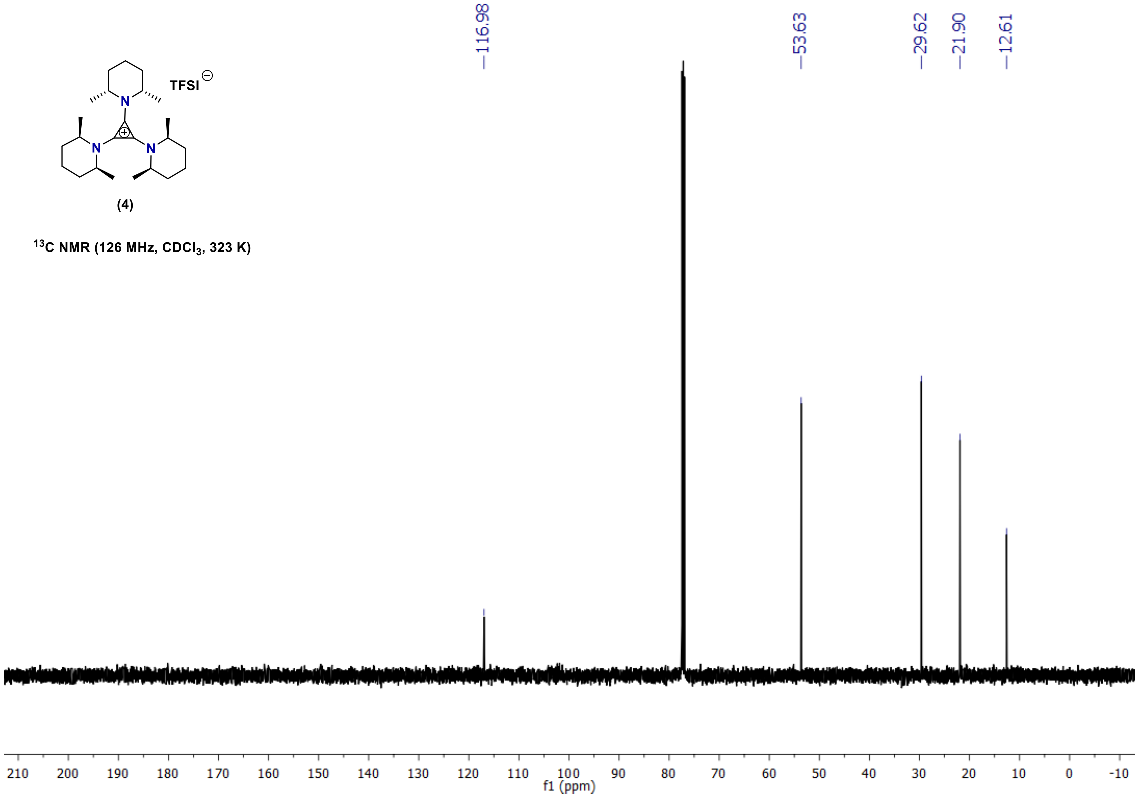

(4)

^{13}C NMR (126 MHz, CDCl$_3$, 323 K)

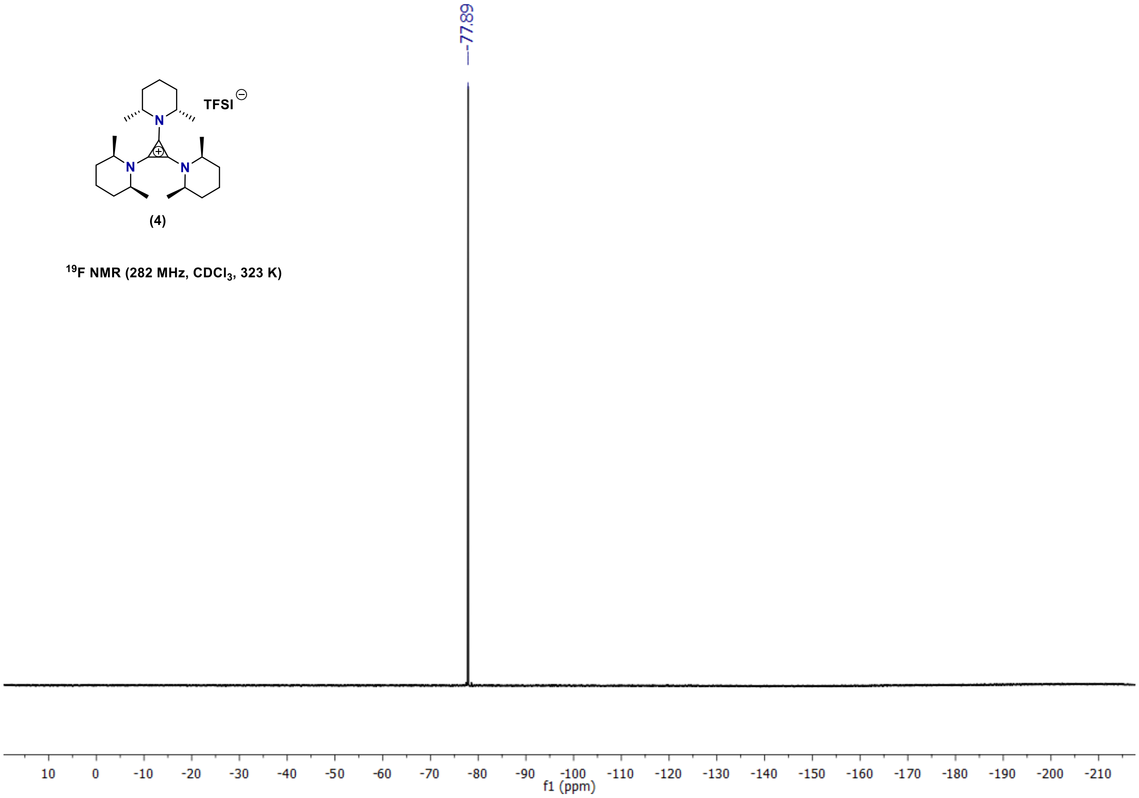

(4)

^{19}F NMR (282 MHz, CDCl$_3$, 323 K)

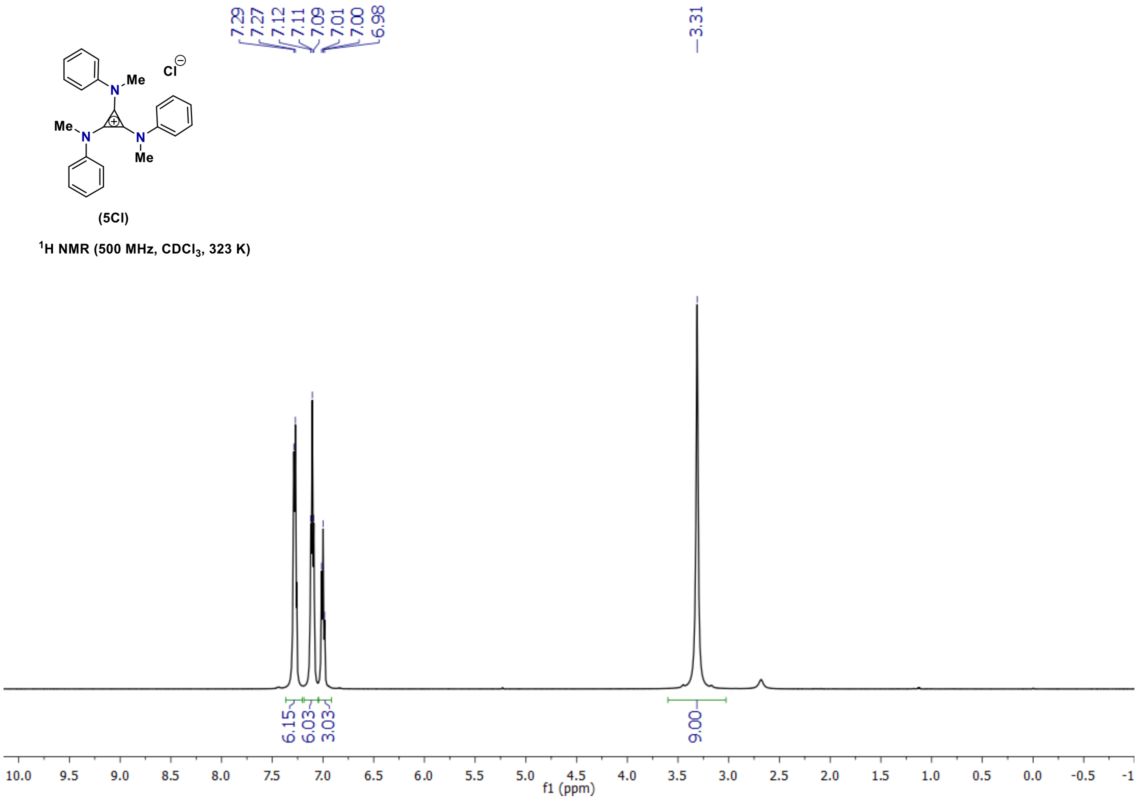

(5Cl)

^{1}H NMR (500 MHz, CDCl$_3$, 323 K)

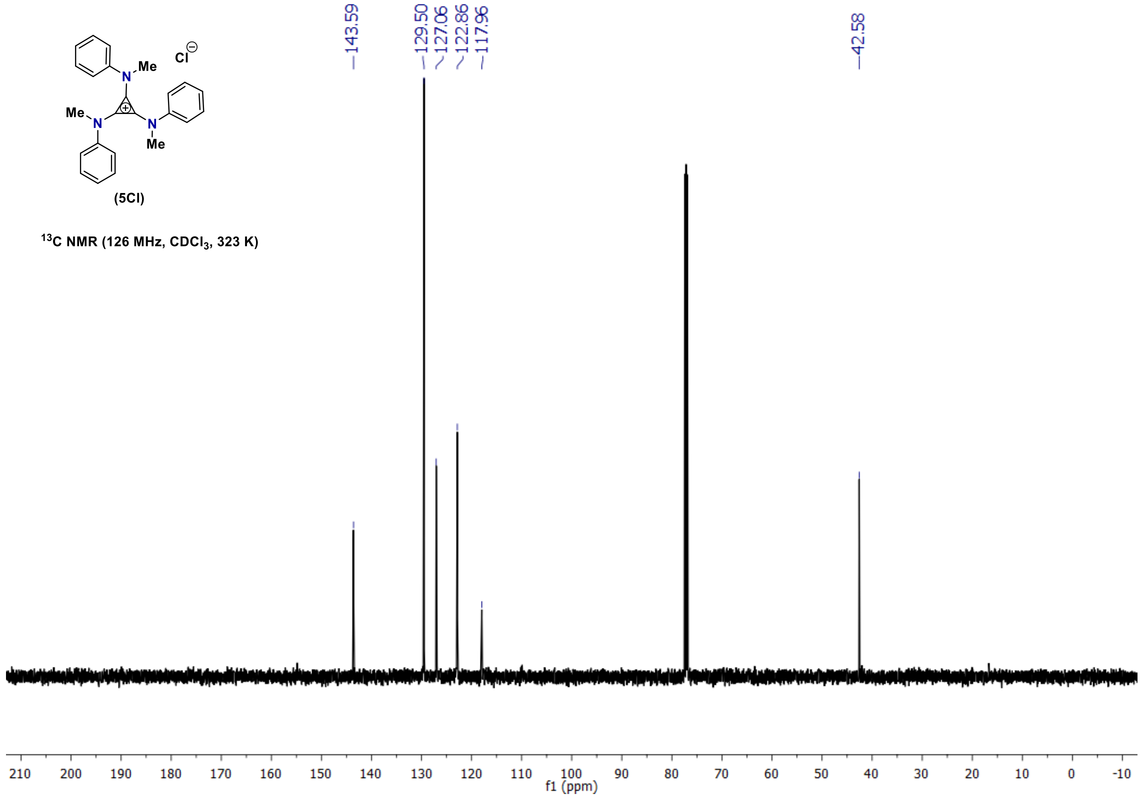

(5Cl)

^{13}C NMR (126 MHz, CDCl$_3$, 323 K)

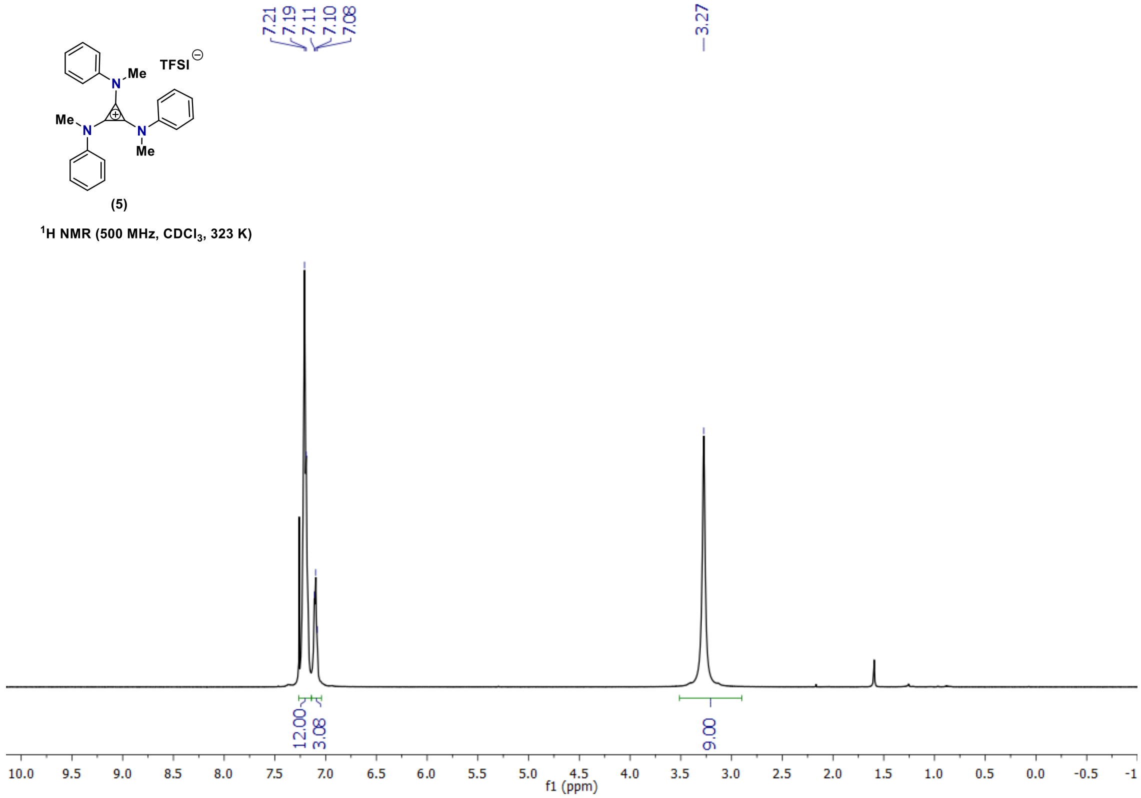

(5)

^{1}H NMR (500 MHz, CDCl$_3$, 323 K)

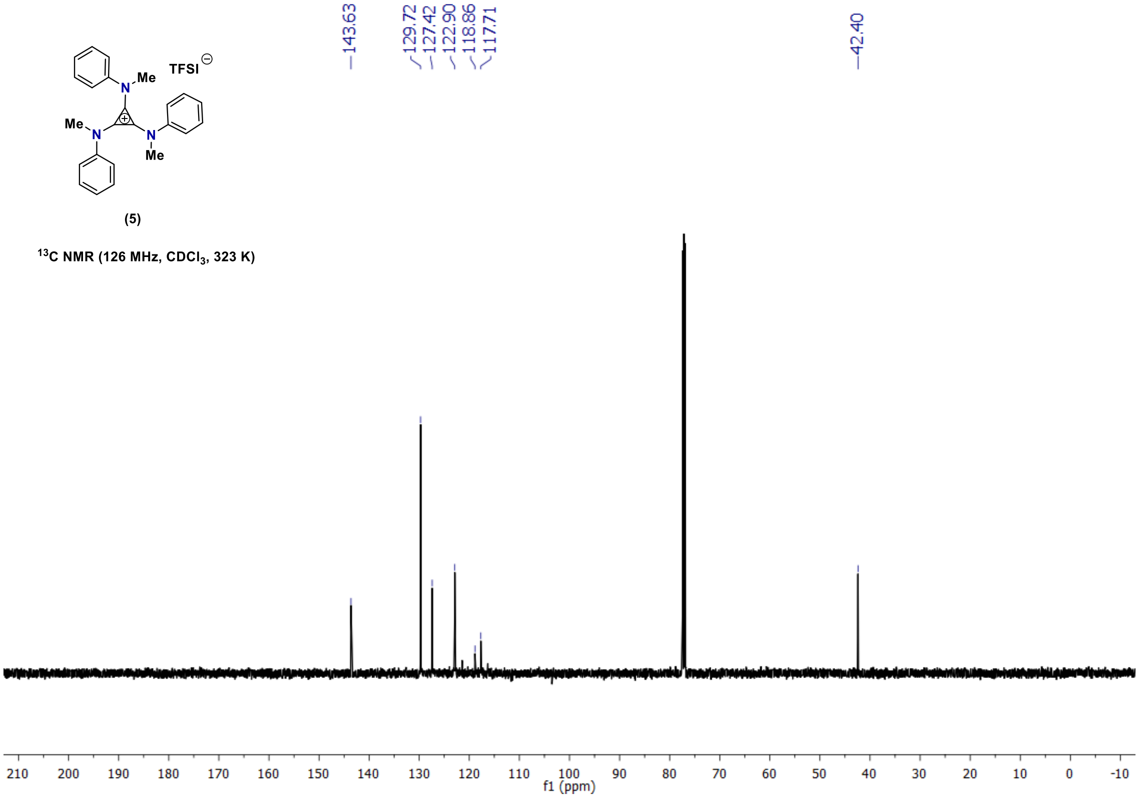

(5)

^{13}C NMR (126 MHz, $CDCl_3$, 323 K)

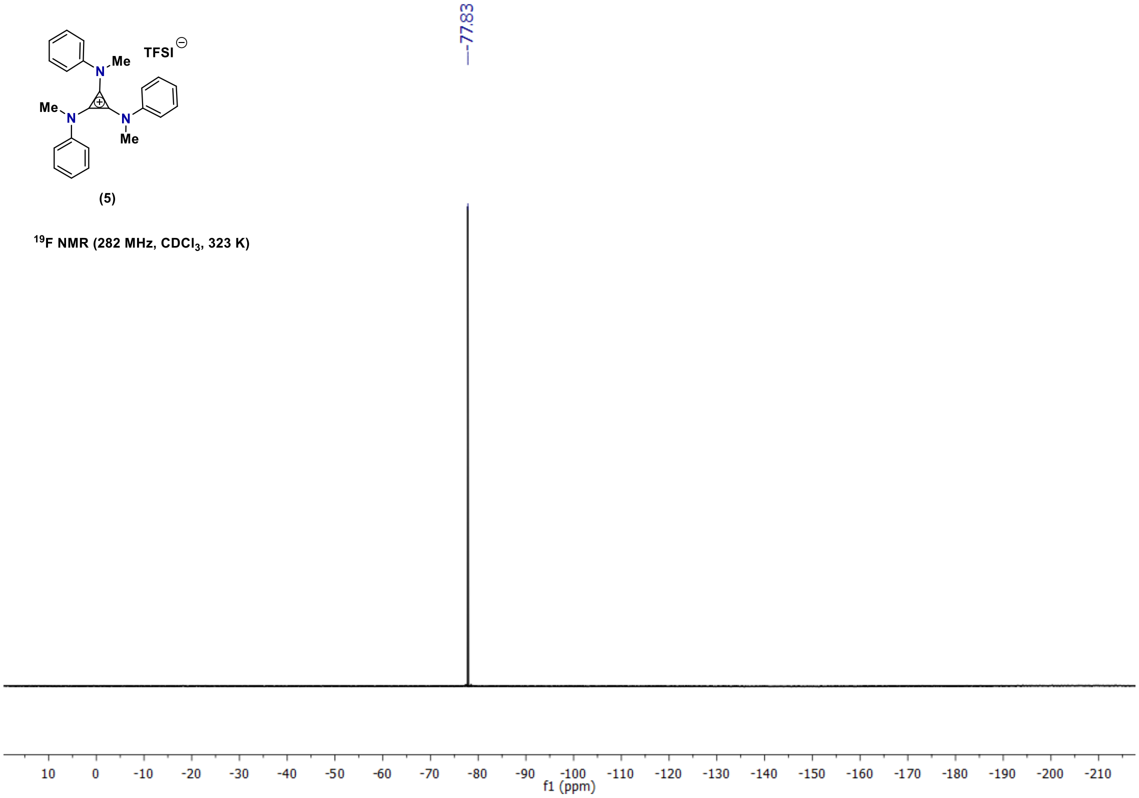

(5)

^{19}F NMR (282 MHz, $CDCl_3$, 323 K)

Membrane Fabrication:

A vial was charged with **STEA-TFSI** (**1**) (66 wt%), divinylbenzene (33 wt%), AIBN (10 mg), and dimethylformamide (0.25 mL). The mixture was degassed via sparging (30 min, N_2).

Separately, 12 individual membranes were cut as disks from Daramic. These disks were washed with dimethoxyethane (3x), allowed to dry overnight, and subsequently placed in 12 separate 20 mL vials fitted with PTFE septa caps. The vials and disks were evacuated with vacuum to remove oxygen, and backfilled with nitrogen (3x).

Once the Daramic disks are air-free and under positive nitrogen pressure, the degassed reaction mixture was syringed evenly onto the disks. These disks were subsequently allowed to soak for 45 minutes. After soaking, the membranes were formed by initiating thermal polymerization at 75 °C for 16 hours. After polymerization, the membranes were removed from the reaction vials and soaked (3x) and stored in the solvent to be utilized.

Cyclic Voltammetry:

Cyclic voltammograms (CVs) were recorded on a CH166 electrochemical workstation using Ag/$AgNO_3$ (0.01 M) electrode as the reference electrode. 0.1 M lithium bistrifluoromethanesulfonimide (LiTFSI) in acetonitrile was used as the supporting electrolyte. All sweep speeds were 100 mV/s.

To create Figure 2a, two separate cyclic voltammograms, one sweeping <0 V and one sweeping >0 V, were combined. This was done since both the oxidation and reduction of benzyltriethylammonium TFSI (**S1**) are irreversible, as expected, and lead to coating of the electrode. This does not allow for both a reducing and oxidizing sweep in the same experiment due to electrochemical oxidation and reduction of this impurity.

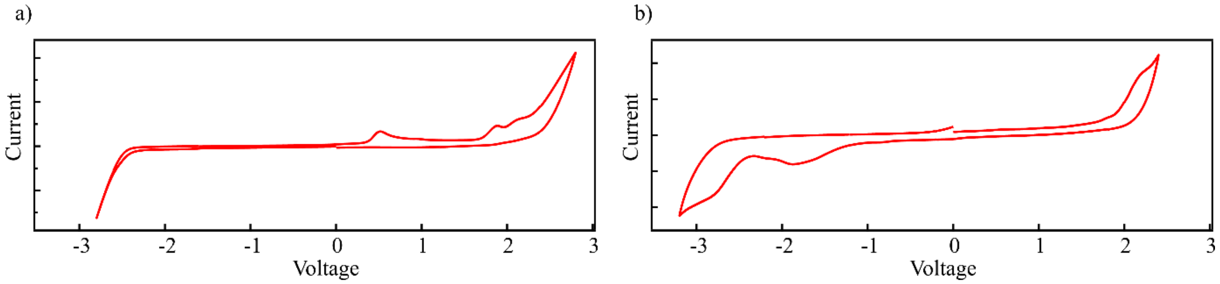

Figure S1 – CV of benzyltriethylammonium TFSI (**S1**) first sweeping a) >0 V and b) <0 V. These CVs are spliced together to form Figure 2a.

Differential Scanning Calorimetry:

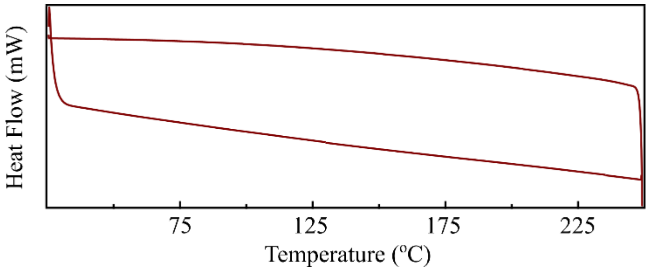

Figure S2 – Differential scanning calorimetry curve showing no glass transition prior to the decomposition temperature at around 250 °C.

Membrane Crossover Experiments:

Crossover experiments were conducted with H-Cells from Adam's and Chittenden. Membranes were mounted in the H-cells between two PTFE gaskets (PTFE sheet with 0.8 cm diameter hole in center) and tightened for leaks with a pinch clamp.

A typical experiment was conducted by charging one side of the H-cell with 25 mg of active material to be tested for crossover. The H-cell was then filled on both sides with a stock solution of 6 mL of 0.1 M LiTFSI in acetonitrile. Each chamber of the H-cell was then stirred for the duration of the experiment via magnetic stirbar. At timepoints throughout the experiment, the chamber containing the blank salt solution was measured for volume as well as for absorbance via UV-Vis spectroscopy. From this data concentration was calculated using the molar absorptivity of the active material being studied at λ_{max} (280 nm for **MAD-CP** and 465 nm for **[PDI][TFSI]$_2$**).

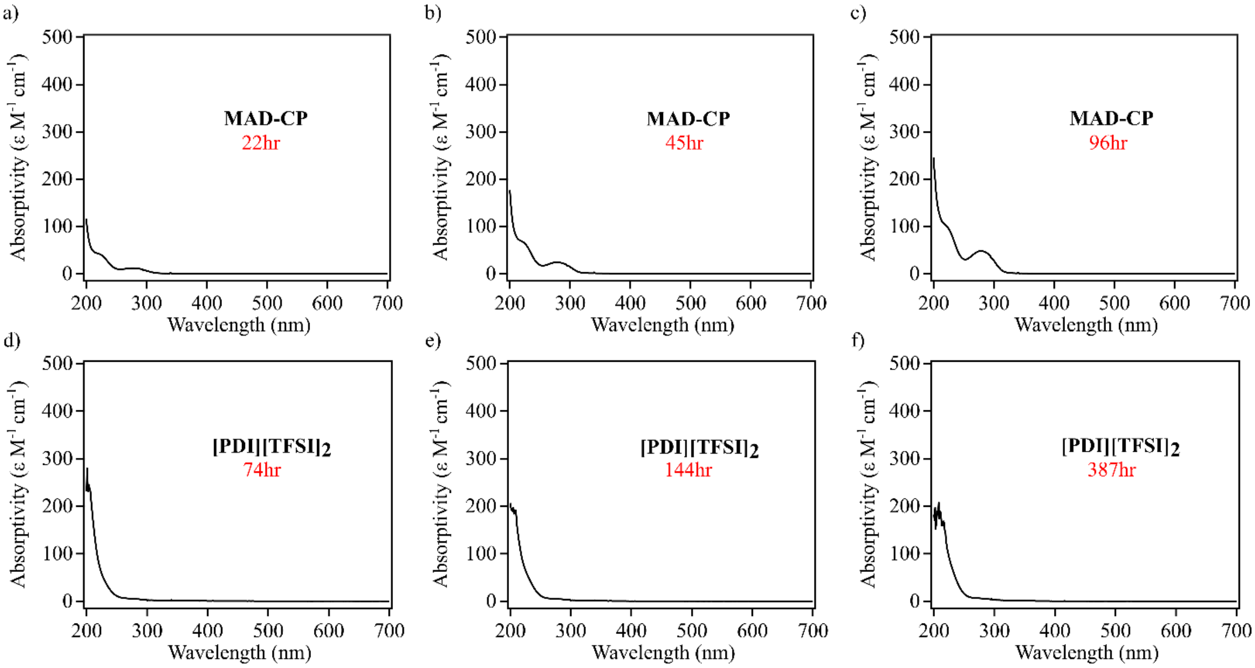

Figure S3 – UV-vis spectra used to determine crossover of a) **MAD-CP** at 22 hrs, b) **MAD-CP** at 45 hrs, c) **MAD-CP** at 96 hrs, d) **[PDI][TFSI]$_2$** at 74 hrs, e) **[PDI][TFSI]$_2$** at 144 hrs, and f) **[PDI][TFSI]$_2$** at 387 hours.

Scanning Electron Microscopy:

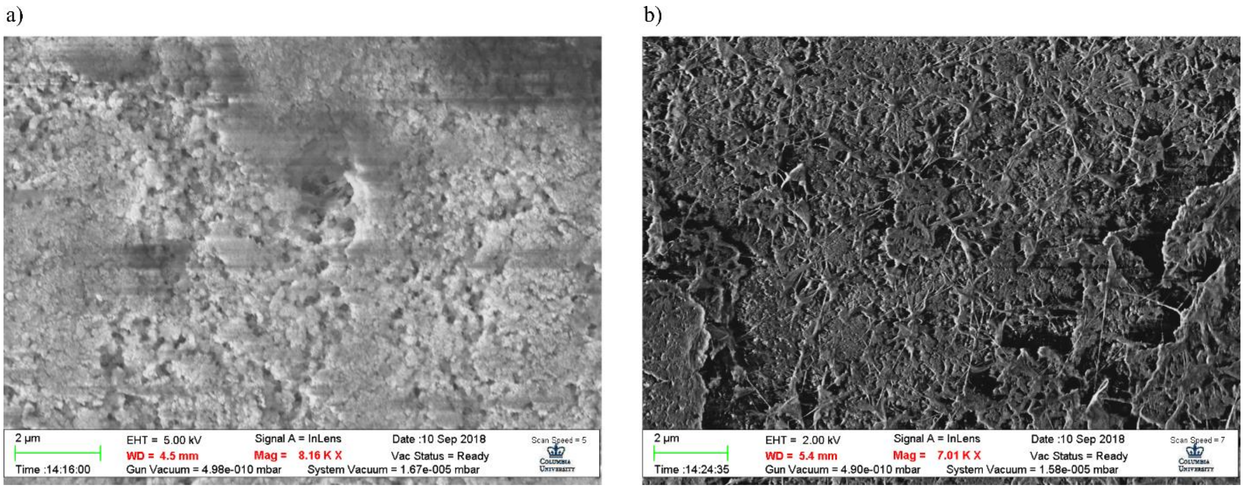
a)
2 µm
EHT = 5.00 kV
Signal A = InLens
Date :10 Sep 2018
Scan Speed = 5
WD = 4.5 mm
Mag = 8.16 K X
Vac Status = Ready
Time :14:16:00
Gun Vacuum = 4.98e-010 mbar
System Vacuum = 1.67e-005 mbar
Columbia University
b)
2 µm
EHT = 2.00 kV
Signal A = InLens
Date :10 Sep 2018
Scan Speed = 7
WD = 5.4 mm
Mag = 7.01 K X
Vac Status = Ready
Time :14:24:35
Gun Vacuum = 4.90e-010 mbar
System Vacuum = 1.58e-005 mbar
Columbia University

Figure S4 – Scanning electron micrographs of Daramic taken before polymerization (a) clearly showing the porous nature of the material and after polymerization (b), showing incorporation of the plastic-like polymer into the pores.

Battery Fabrication and Cycling:

The battery was fabricated in an inert, dry glovebox (nitrogen) The device was fabricated using an H-Cell from Adams and Chittenden. The membrane was mounted in the H-cell between two PTFE gaskets (PTFE sheet with 1 cm diameter hole in center) and tightened for leaks with a pinch clamp. Carbon felt electrodes were dried in a 200 °C oven overnight, at which point they were brought into the glovebox while hot. Electrodes were connected through a platinum wire threaded through the septa cap of the H-cell. Active materials were dissolved in acetonitrile and dried on molecular sieves overnight. Each chamber was filled with 6 mL of stock solution of 0.5 M LiTFSI in acetonitrile that was dried overnight on molecular sieves. The chambers were stirred via magnetic stir bar for the duration of the experiment. Cycling was conducted under galvanostatic conditions at a current of 0.5 mA/cm^2.

References

1. Milton, M.; Cheng, Q.; Yang, Y.; Nuckolls, C.; Hernández Sánchez, R.; Sisto T.J., Molecular Materials for Nonaqueous Flow Batteries with a High Coulombic Efficiency and Stable Cycling. *Nano Lett.* **2017**, *17*, 7859-7863.

APPENDIX III: Experimental, NMR Spectra, and other Data (Chapter 4)

1. General Information

Commercially available reagents were purchased from Sigma Aldrich, Matrix Chemical, AKSci, Alfa Aesar, Oakwood chemical or TCI, and used as received unless otherwise noted. Silica gel 60 (230-400 mesh) from SiliCycle was used for chromatography, and Merck silica gel plates with a fluorescence F_{254} indicator were used for thin-layer chromatography (TLC) analysis. ^{1}H and ^{13}C NMR spectra were recorded on Mercury-300 (300 MHz), Inova-400 (400 MHz), and Inova-500 (500 MHz) spectrometers. Chemical shifts in ^{1}H NMR spectra are reported in parts per million (ppm) relative to residual chloroform (7.26 ppm) or dimethyl sulfoxide (2.50 ppm) as internal standards. ^{1}H NMR data are reported as follows: chemical shift, multiplicity (s = singlet, d = doublet, t = triplet, q = quartet, dd = doublet of doublets, m = multiplet), coupling constant in Hertz (Hz) and number of hydrogen atoms based on integration intensities. ^{13}C NMR chemical shifts are reported in ppm relative to the central peak of $CDCl_3$ (77.16 ppm) CD_3OD (49.00 ppm) or $(CD_3)_2SO$ (39.52 ppm) as internal standards. ^{19}F NMR chemical shifts are reported in ppm relative to the central peak of $C_6H_5CF_3$ (-63.72 ppm) as an internal standard. Cyclic voltammetry was performed at 25 °C on a BASi Epsilon potentiostat using a glassy carbon working electrode, a platinum wire counter electrode, and a Ag/AgCl reference electrodes which were obtained from CH Instruments. The mass spectral (MS) data were obtained on a Thermo Fisher Scientific Exactive series DART Mass Spectrometer. Anhydrous tetrahydrofuran and acetonitrile were purchased as Sure/Seal™ bottles from Sigma-Aldrich.

2. General Procedures

Electrode preparation

Materials used for set-up:

Platinum wire (13039-BU from Alfa Aesar, 25 cm). Woods clamp lamp light with aluminum reflector (Amazon, 150 Watt 8.5 inch). Compact fluorescent light bulb (Amazon, 5000K daylight, 23W). Holmes Lil' Blizzard 8-inch oscillating table fan (Amazon). June gold 2.0 mm 2B pencil lead refills (Amazon). GW Instek bench power supply (Newark Element14 Electronics, gps-3030d). Carbon felt (cut around 7 mm x 7 mm x 7 mm) from AvCarb C200 Soft Carbon Battery Felt (fuelcellstore, Product Code: 1595010).

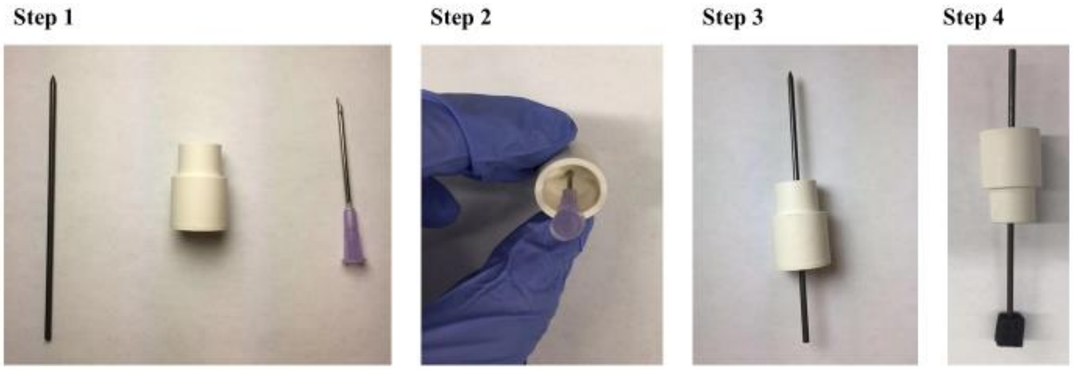

Fig. S1. Anode set up

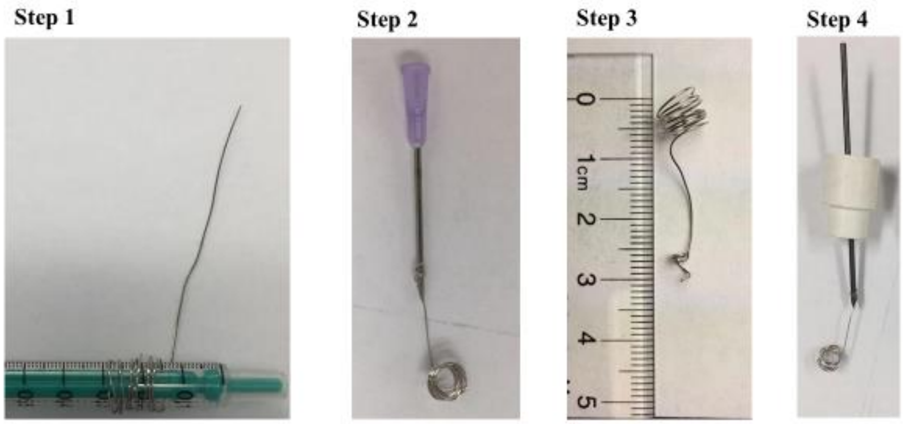

Fig. S2. Cathode set up

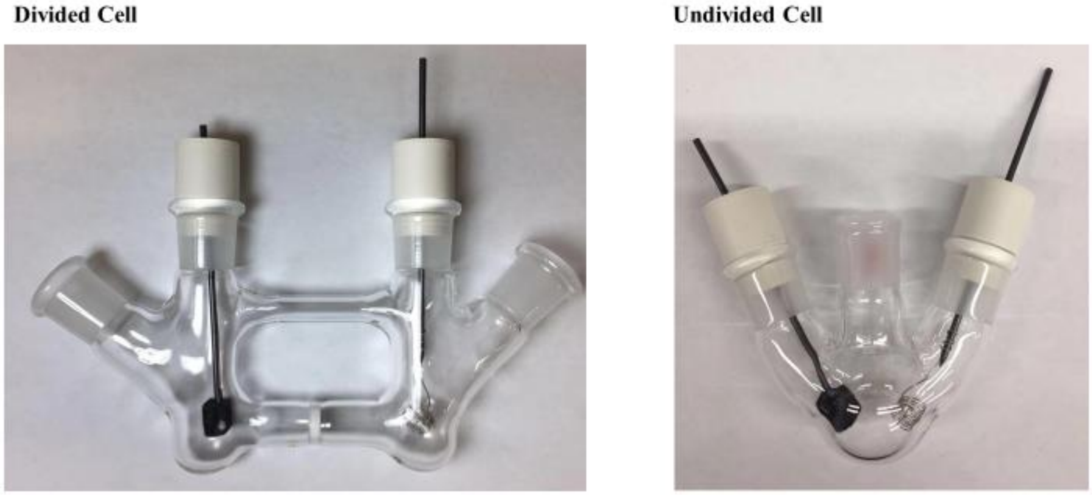

Fig. S3. Divided cell and undivided cell set up

Anode set-up: A septum was pierced with a needle, and a 2B pencil lead was inserted through the hole. A small square (~7 mm x 7 mm) of carbon felt was cut from the sheet, and this square was impaled onto the pencil lead.

Cathode set-up: A second septum was pierced with a needle, and a 2B pencil lead was inserted through the hole. Approximately 20 cm of the 25 cm platinum wire was coiled by wrapping it around a 1 mL syringe or other similarly sized object. At the other end of the wire, a smaller coil was made, and this coil was wrapped around the pencil lead.

Divided cell: The H-type divided cell with a fine glass filter was custom made by the Cornell chemistry glass shop.

Undivided cell: A simple 10 mL three-neck flask was used.

Procedure A for arene coupling

An oven-dried custom-made H-type divided cell was equipped with a stir bar on both sides, a carbon felt anode, and a platinum wire cathode. TAC **1** (15.2 mg, 0.032 mmol), nitrogen heterocycle (0.4 mmol), $LiClO_4$ (255.3 mg, 2.4 mmol) and arene (if it is solid) were added in the anodic chamber. The cathodic chamber was charged with $LiClO_4$ (255.3 mg, 2.4 mmol). The cell was sealed using a rubber septum and parafilm then flushed with nitrogen gas for 5 min. The anodic chamber was then sequentially charged with CH_3CN (2.0 mL) and arene (2.0 mL) via syringe. The cathodic chamber was then charged with CH_3CN (4 mL) and acetic acid (229 µL, 4.0 mmol, 10 equiv.) via syringe. Each chamber was then purged with nitrogen gas for an additional 5 min. The solution was stirred at room temperature under the irradiation from two 23W CFL bulbs, and electrolysis was initiated at a constant voltage of 1.5 V for the specified amount of time. The system was kept cool using a fan throughout the duration of the reaction. After completion of the reaction (as determined by TLC), the reaction mixture was subsequently poured into a saturated sodium bicarbonate solution (ca. 20 mL). The carbon felt anode was washed with EtOAc (3×5 mL) in an ultrasonic bath. The aqueous layer was separated and extracted with EtOAc (3×10 mL), and the combined organic layers were washed with brine and dried over anhydrous Na_2SO_4. Following concentration *in vacuo*, the crude residue was subjected to flash column chromatography on silica gel to yield the desired product.

Procedure B for radical-mediated ether coupling

To an oven-dried 10-mL three-neck flask equipped with a stir bar, a carbon felt anode and, a platinum wire cathode was added TAC **1** (15.2 mg, 0.032 mmol), 4-bromoisoquinoline (83.2 mg, 0.4 mmol), and $LiClO_4$ (255.3 mg, 2.4 mmol). The cell was sealed using a rubber septum and parafilm then flushed with nitrogen gas for 5 min, followed by the sequential addition via syringe of CH_3CN (3 mL), tetrahydrofuran (3.0 mL), trifluoroacetic acid (61.4 µL, 0.8 mmol) and acetic acid (72 µL, 1.2 mmol). The reaction mixture was then purged with nitrogen gas for an additional 5 min. The solution was then stirred at room temperature under the irradiation from two 23W CFL bulbs and electrolysis was initiated at a constant voltage of 2.0 V for 48h. After completion of the reaction (as determined by TLC), the reaction mixture was subsequently poured into a saturated sodium bicarbonate solution (ca. 20 mL). The carbon felt anode was washed with EtOAc (3×5 mL) in an ultrasonic bath. The aqueous layer was separated and extracted with EtOAc (3×10 mL), and the combined organic layers were washed with brine and dried over anhydrous Na_2SO_4. Following concentration *in vacuo*, the crude residue was subjected to flash column chromatography on silica gel to yield the desired product.

Procedure C for oxocarbenium-mediated ether coupling

To an oven-dried 10 mL three neck flask equipped with a stir bar, a carbon felt anode, and a platinum wire cathode was added TAC **1** (15.2 mg, 0.032 mmol), nitrogen heterocycle (0.4 mmol), and $LiClO_4$ (255.3 mg, 2.4 mmol). The cell was sealed using a rubber septum and parafilm then flushed with nitrogen gas for 5 min, followed by the sequential addition via syringe of CH_3CN (4 mL), tetrahydrofuran or tetrahydropyran (2.0 mL), nitrogen heterocycle (0.4 mmol) or benzyl alcohol (41.6 µL, 0.4 mmol), and acetic acid (229 µL, 4.0 mmol). The reaction mixture was then purged with nitrogen gas for an additional 5 min. The solution was then stirred at room temperature under the irradiation from two 23W CFL bulbs and electrolysis was initiated at a constant voltage of 2.0 V for the specified amount of time. The system was kept cool using a fan throughout the duration of the reaction. After completion of the reaction (as determined by TLC), the reaction mixture was subsequently poured into a saturated sodium bicarbonate solution (ca. 20 mL). The carbon felt anode was washed with EtOAc (3×5 mL) in an ultrasonic bath. The aqueous layer was separated and extracted with EtOAc (3×10 mL), and the combined organic layers were washed with brine and dried over anhydrous Na_2SO_4. Following concentration *in vacuo*, the crude residue was subjected to flash column chromatography on silica gel to yield the desired product.

Procedure D for 1-phenylcyclohexene coupling

To an oven-dried 10 mL three neck flask equipped with a stir bar, a carbon felt anode and a platinum wire cathode, was added TAC **1** (15.2 mg, 0.032 mmol), 1-phenyl-1-cyclohexene (0.4 mmol, 63.3 mg, 63.7 µL), and $LiClO_4$ (255.3 mg, 2.4 mmol). The cell was sealed using a rubber septum and parafilm then flushed with nitrogen gas for 5 min, followed by the sequential addition via syringe of CH_3CN (6 mL) and acid (4.0 mmol). The reaction mixture was then purged with nitrogen gas for additional 5 min. The solution was then stirred at room temperature under the irradiation from two 23W CFL bulbs and electrolysis was initiated at a constant voltage of 2.0 V for 10h. The system was kept cool using a fan throughout the duration of the reaction. After completion of the reaction (as determined by TLC), the reaction mixture was subsequently poured into a saturated sodium bicarbonate solution (ca. 20 mL). The carbon felt anode was washed with EtOAc (3×5 mL) in an ultrasonic bath. The aqueous layer was separated and extracted with EtOAc (3×10 mL), and the combined organic layers were washed with brine and dried over anhydrous Na_2SO_4. Following concentration *in vacuo*, the crude residue was subjected to flash column chromatography on silica gel to yield the desired product.

Procedure E for mesitylene coupling

To an oven-dried 10-mL three-neck flask equipped with a stir bar, a carbon felt anode, and a platinum wire cathode was added TAC **1** (15.2 mg, 0.032 mmol), nitrogen heterocycle (0.4 mmol), and $LiClO_4$ (255.3 mg, 2.4 mmol). The cell was sealed using a rubber septum and parafilm then flushed with nitrogen gas for 5 min, followed by the sequential addition via syringe of CH_3CN (6 mL), arene (195 µL – 2.0 mL) and acetic acid (229 µL, 4.0 mmol). The reaction mixture was then purged with nitrogen gas for an additional 5 min. The solution was then stirred at room temperature under the irradiation from two 23W CFL bulbs and electrolysis was initiated at a constant voltage of 1.5 V for the specified amount of time. The system was kept cool using a fan throughout the duration of the reaction. After completion of the reaction (as determined by TLC), the reaction mixture was subsequently poured into a saturated sodium bicarbonate solution (ca. 20 mL). The carbon felt anode was washed with EtOAc (3×5 mL) in an ultrasonic bath. The aqueous layer was separated and extracted with EtOAc (3×10 mL), and the combined organic layers were washed with brine and dried over anhydrous Na_2SO_4. Following concentration *in vacuo*, the crude residue was subjected to flash column chromatography on silica gel to yield the desired product.

Procedure F, reaction by 1.5 V battery

To an oven-dried 10 mL three neck flask equipped with a stir bar, a carbon felt anode and a platinum wire cathode, was added TAC **1** (15.2 mg, 0.032 mmol), 4-chloro-1H-pyrazole (0.4 mmol, 41.0 mg), and $LiClO_4$ (255.3 mg, 2.4 mmol). The cell was sealed using a rubber septum and parafilm then flushed with nitrogen gas for 5 min, followed by the sequential addition via syringe of CH_3CN (6 mL), mesitylene (1.4 mmol, 195 µL), and acetic acid (229 µL, 4.0 mmol). The reaction mixture was then purged with nitrogen gas for additional 5 min. The solution was then stirred at room temperature under the irradiation from two 23W

CFL bulbs and electrolysis was initiated by using a 1.5 V battery for 48 h. The system was kept cool using a fan throughout the duration of the reaction. After completion of the reaction (as determined by TLC), the reaction mixture was subsequently poured into a saturated sodium bicarbonate solution (ca. 20 mL). The carbon felt anode was washed with EtOAc (3×5 mL) in an ultrasonic bath. The aqueous layer was separated and extracted with EtOAc (3×10 mL), and the combined organic layers were washed with brine and dried over anhydrous Na_2SO_4. Following concentration *in vacuo*, the crude residue was subjected to flash column chromatography on silica gel to yield the desired product in 55% yield.

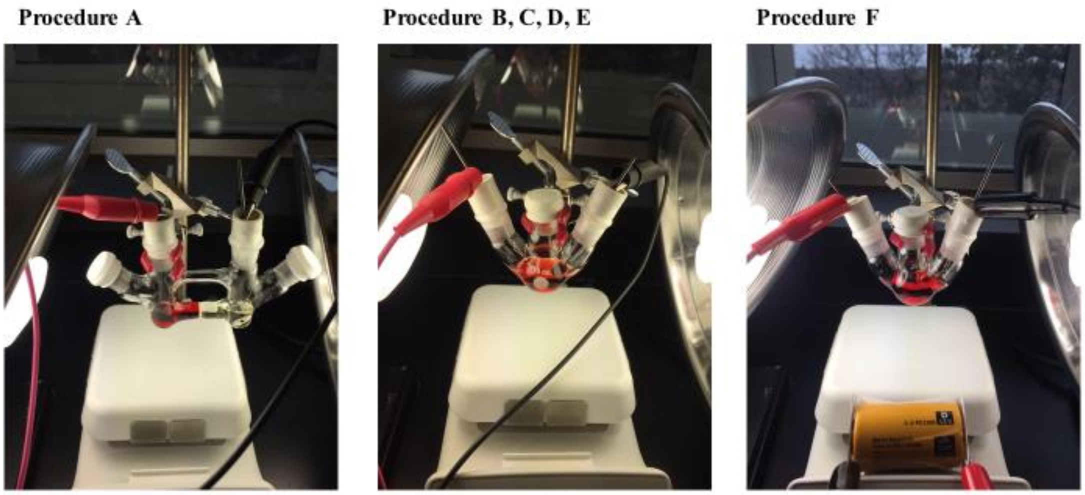

Fig. S4. Reaction set up

Notes for procedure:

1. Even though this reaction has not been found to be sensitive to water, anhydrous lithium perchlorate and anhydrous acetonitrile were used.

2. Because the carbon felt can absorb a significant amount of reaction solution, it should be rinsed in an ultrasonic bath for 5 min or more to obtain optimal product yields.

3. In the undivided cell, it is best to keep the anode and cathode relatively close (~0.5-1.0 cm) to one another; however they should not touch.

4. For the cathode, the platinum wire should be immersed in the solution, but not the pencil lead to which it is attached.

5. The carbon felt should be replaced for each reaction.

6. After the reaction, care should be taken when removing the septum in case of pressure build up from hydrogen gas generation.

Preparation of TAC 1 Catalysts

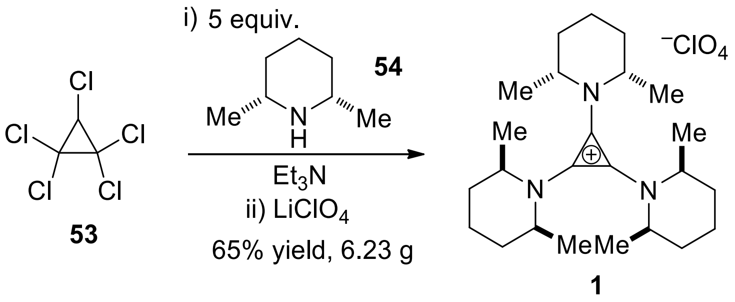

Fig. S5. TAC 1 synthesis

A round bottom flask was charged with 150 mL of DCM and pentachlorocyclopropane (2.86 mL, 20 mmol). The flask was cooled to 0 ºC, and the mixture of *cis*-2,6-dimethylpiperidine (13.5 mL, 100 mmol) and Et$_3$N (13.9 mL, 100 mmol) was added in slowly. The reaction was stirred for 3 h at 0 ºC and then for 24 h at rt. The reaction was transferred to a separatory funnel and washed sequentially with 1M HCl (100 mL), water (200 mL), and brine (200 mL). The organic layer was dried over anhydrous Na$_2$SO$_4$ and concentrated *in vacuo*. The resulting solids were washed with EtOAc to give **TAC 1•Cl** as a white powder. The resulting solids were recrystallized from isopropanol to give **TAC 1•Cl** as white crystals. The resulting crystals were dissolved in DCM (20 mL) and LiClO$_4$ solution (20 mL, 5.0 M) was added. The solution was stirred for 8 h and the biphasic solution was transferred to a separatory funnel. The aqueous layer was separated and extracted with DCM (20 mL). Then the combined organic layers were washed twice with LiClO$_4$ solution (20 mL, 5.0 M). The organic layer was separated, dried over anhydrous Na$_2$SO$_4$ and concentrated *in vacuo* to produce **1** in 6.23 g (13.1 mmol, 65% yield for two steps) as a white solid.

^{1}H NMR (500 MHz, Chloroform-*d*) δ 3.91 – 3.81 (m, 6H), 1.93 – 1.87 (m, 6H), 1.79 – 1.76 (m, 3H), 1.68 – 1.64 (m, 6H), 1.61 – 1.54 (m, 3H), 1.37 (d, *J* = 7.1 Hz, 18H). ^{13}C NMR (126 MHz, Chloroform-*d*) δ 117.0, 53.5, 29.6, 21.8, 12.6.

3. Optimization of Reaction Conditions

We chose mesitylene and pyrazole as our model reaction to probe reaction conditions. A typical reaction procedure is: to an oven-dried 10 mL three neck flask equipped with a stir bar, an anode and a cathode, was added **1** (15.2 mg, 0.032 mmol), pyrazole (0.4 mmol, 27.2 mg), and LiClO$_4$ (255.3 mg, 2.4 mmol). The cell was sealed using a rubber septum and parafilm and was then flushed with nitrogen gas for 5 min, followed by the sequential addition via syringe of solvent (6 mL), mesitylene (1.4 mmol, 195 µL, 3.5 equiv), and acid. The reaction mixture was then purged with nitrogen gas for an additional 5 min. The solution was then stirred at room temperature under the irradiation of light and electrolysis was initiated at a constant voltage of 1.5 V for the specified amount of time. The system was kept cool using a fan throughout the duration of the reaction. After completion of the reaction (as determined by TLC), the reaction mixture was subsequently poured into a saturated sodium bicarbonate solution (ca. 20 mL). The carbon felt anode was washed with EtOAc (3×5 mL) in an ultrasonic bath. The aqueous layer was separated and extracted with EtOAc (3×10 mL), and the combined organic layers were washed with brine and dried over anhydrous Na$_2$SO$_4$. Following concentration *in vacuo*, to the crude residue was added 0.7 mL CDCl$_3$ followed by dibromomethane (13.9 µL, 0.2 mmol) as internal standard, which was subsequently submitted for 1H NMR analysis.

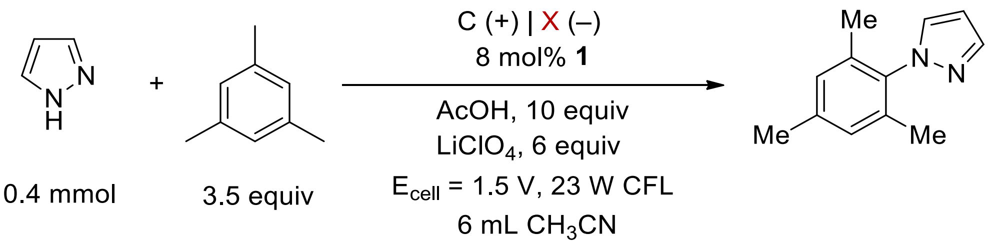
N
N
H
+
0.4 mmol
3.5 equiv
C (+) | X (–)
8 mol% 1
AcOH, 10 equiv
LiClO$_4$, 6 equiv
E$_{cell}$ = 1.5 V, 23 W CFL
6 mL CH$_3$CN
Me
N
N
Me
Me

electrode material	**yield**
Pt	**80% (80%)**
C	**50%**

Yields determined by ^{1}H NMR against CH_2Br_2
Isolated yield was in brackets

Fig. S6. Evaluation of electrode material

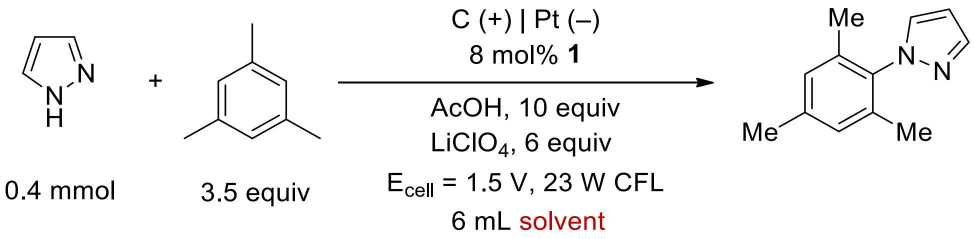
N
N
H
+
0.4 mmol
3.5 equiv
C (+) | Pt (–)
8 mol% 1
AcOH, 10 equiv
LiClO$_4$, 6 equiv
E$_{cell}$ = 1.5 V, 23 W CFL
6 mL solvent
Me
N
N
Me
Me

solvent	**yield**
CH_3CN	**80%**
DMF	**0%**
DCM	**trace**

Yields determined by ^{1}H NMR against CH_2Br_2

Fig. S7. Evaluation of solvent

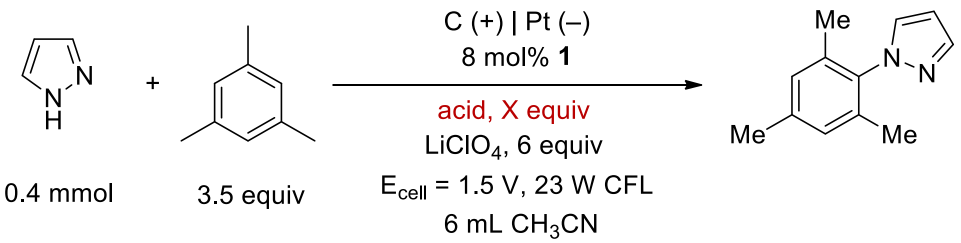
C (+) | Pt (–)
8 mol% **1**
acid, X equiv
LiClO$_4$, 6 equiv
E$_{cell}$ = 1.5 V, 23 W CFL
6 mL CH$_3$CN
0.4 mmol
3.5 equiv
N
N
H
Me
Me
Me

acid	yield
CH_3COOH, 1 equiv	**8%**
CH_3COOH, 10 equiv	**80%**
CH_3COOH, 100 equiv	**56%**
CF_3COOH, 10 equiv	**<5%**

Yields determined by ^1H NMR against CH_2Br_2

Fig. S8. Evaluation of acid

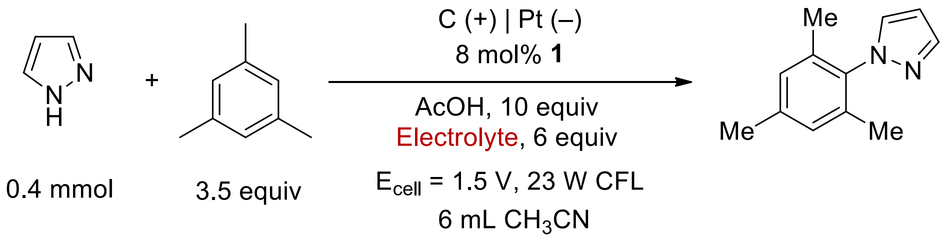
C (+) | Pt (–)
8 mol% **1**
AcOH, 10 equiv
Electrolyte, 6 equiv
E$_{cell}$ = 1.5 V, 23 W CFL
6 mL CH$_3$CN
0.4 mmol
3.5 equiv
N
N
H
Me
Me
Me

electrolyte	yield
$LiClO_4$	**80%**
LiTFSI	**<5%**
none	**0**

Yields determined by ^1H NMR against CH_2Br_2

Fig. S9. Evaluation of electrolyte

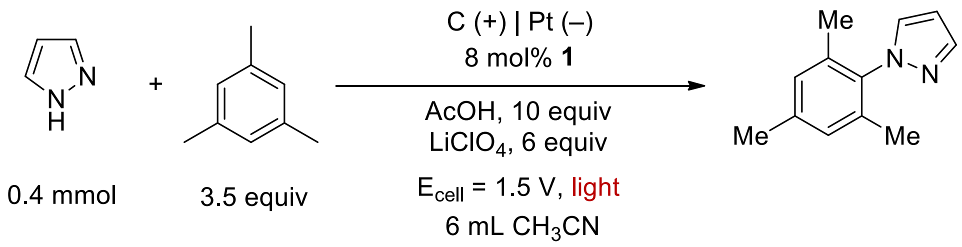
C (+) | Pt (–)
8 mol% **1**
AcOH, 10 equiv
LiClO$_4$, 6 equiv
E$_{cell}$ = 1.5 V, light
6 mL CH$_3$CN
0.4 mmol
3.5 equiv
Me
Me
Me
N
N
H

light	yield
CFL	**80%**
green LED	**26%**

Yields determined by ^{1}H NMR against CH$_2$Br$_2$

Fig. S10. Evaluation of light

4. Control Experiments

Control experiment without **TAC 1** catalyst:

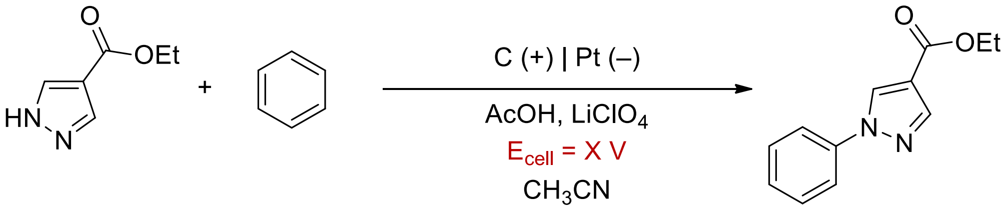
O
OEt
HN
N
+
C (+) | Pt (–)
AcOH, LiClO$_4$
E_{cell} = X V
CH$_3$CN
O
OEt
N
N

E_{cell}	**isolated yield**
E_{cell} = 1.5 V	**0%**
E_{cell} = 2.0 V	**<5%**
E_{cell} = 2.5 V	**10%**
E_{cell} = 3.0 V	**17%**

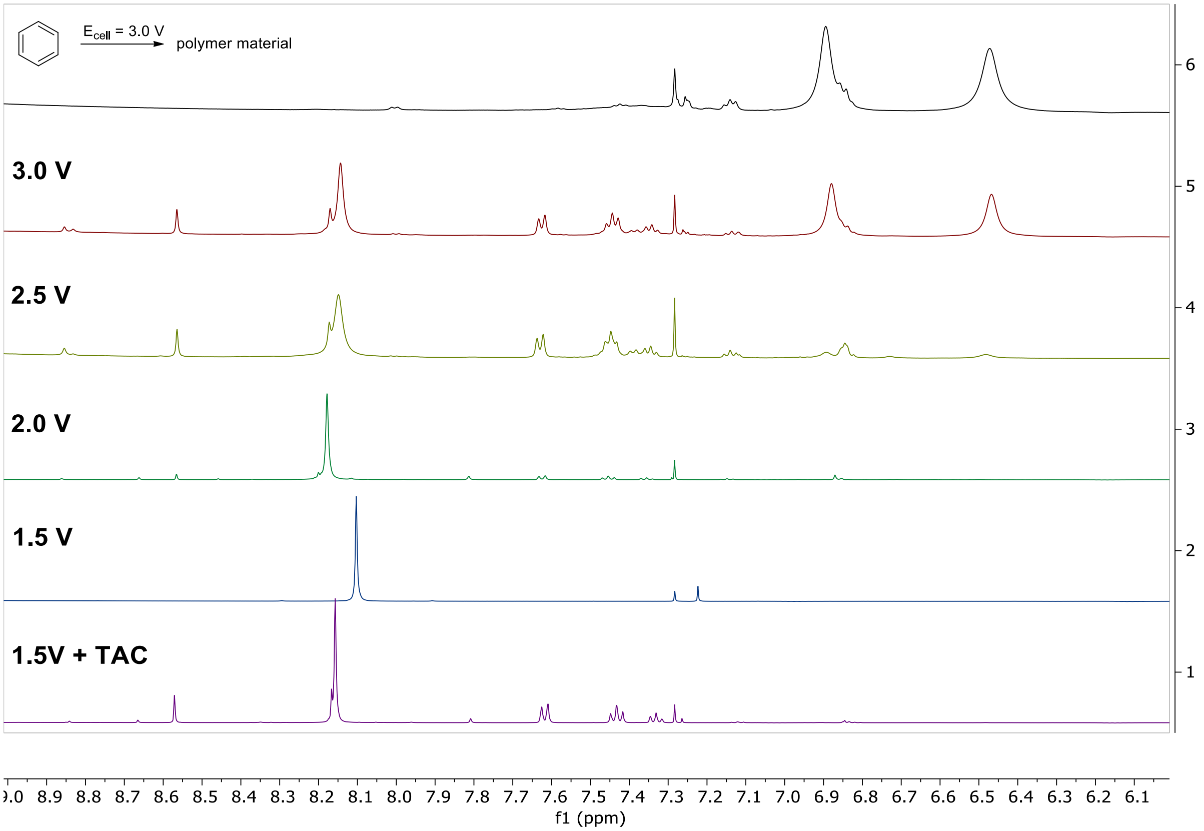

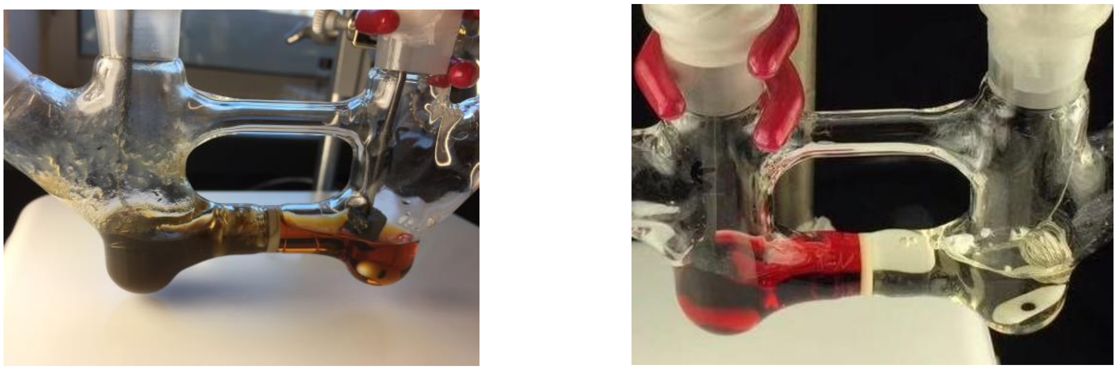

direct electrolysis at 3.0 V
formation of polymeric material

electrophotocatalysis at 1.5 V
clean reaction solution

Fig. S12. Control experiment of benzene oxidative functionalization

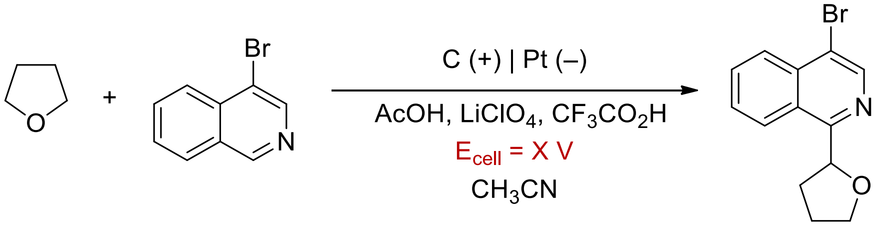
Br
+
Br
N
C (+) | Pt (–)
AcOH, LiClO$_4$, CF$_3$CO$_2$H
E$_{cell}$ = X V
CH$_3$CN
Br
N
O
O

E$_{cell}$	**isolated yield**
E$_{cell}$ = 2.0 V	**10%**
E$_{cell}$ = 2.5 V	**12%**
E$_{cell}$ = 3.0 V	**<5%**

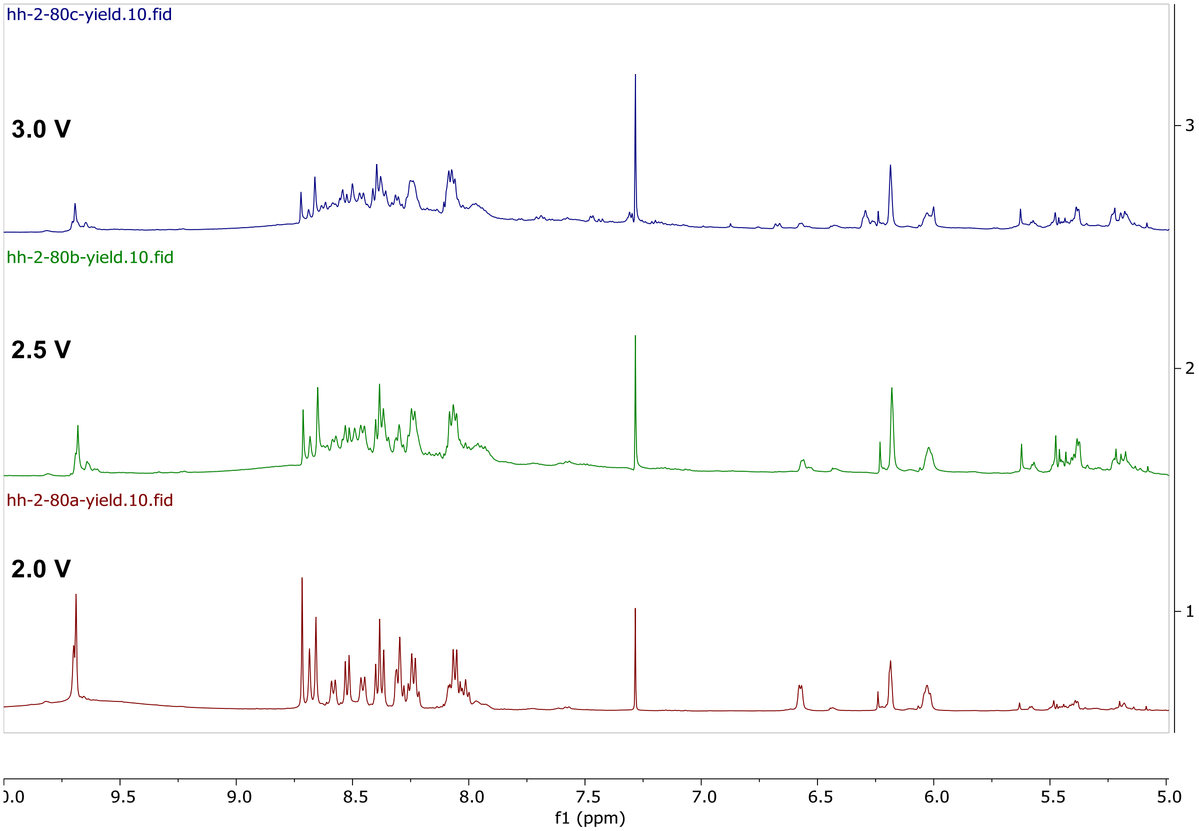

Fig. S13. Control experiment of C–H bonds functionalization

5. Catalyst Stability Study

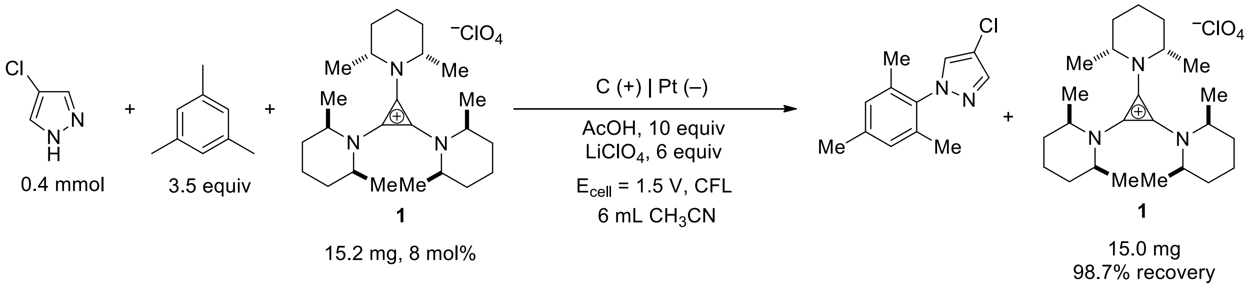

0.4 mmol
3.5 equiv
15.2 mg, 8 mol%
C (+) | Pt (–)
AcOH, 10 equiv
LiClO$_4$, 6 equiv
E$_{cell}$ = 1.5 V, CFL
6 mL CH$_3$CN
1
15.0 mg
98.7% recovery

Fig. S14. Catalyst recovery experiment

In situ NMR analysis:

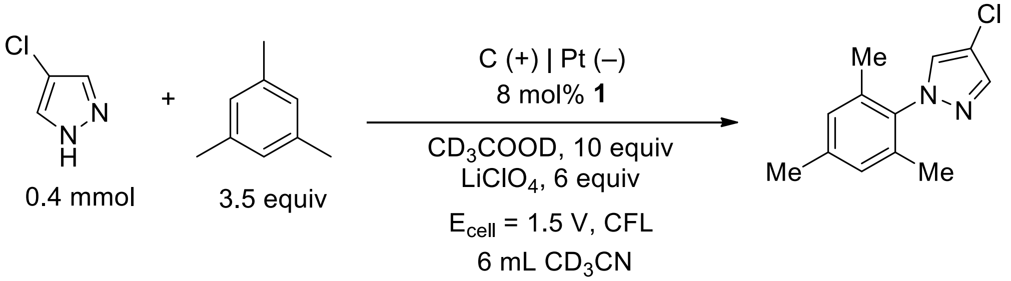

0.4 mmol
3.5 equiv
C (+) | Pt (–)
8 mol% **1**
CD$_3$COOD, 10 equiv
LiClO$_4$, 6 equiv
E$_{cell}$ = 1.5 V, CFL
6 mL CD$_3$CN

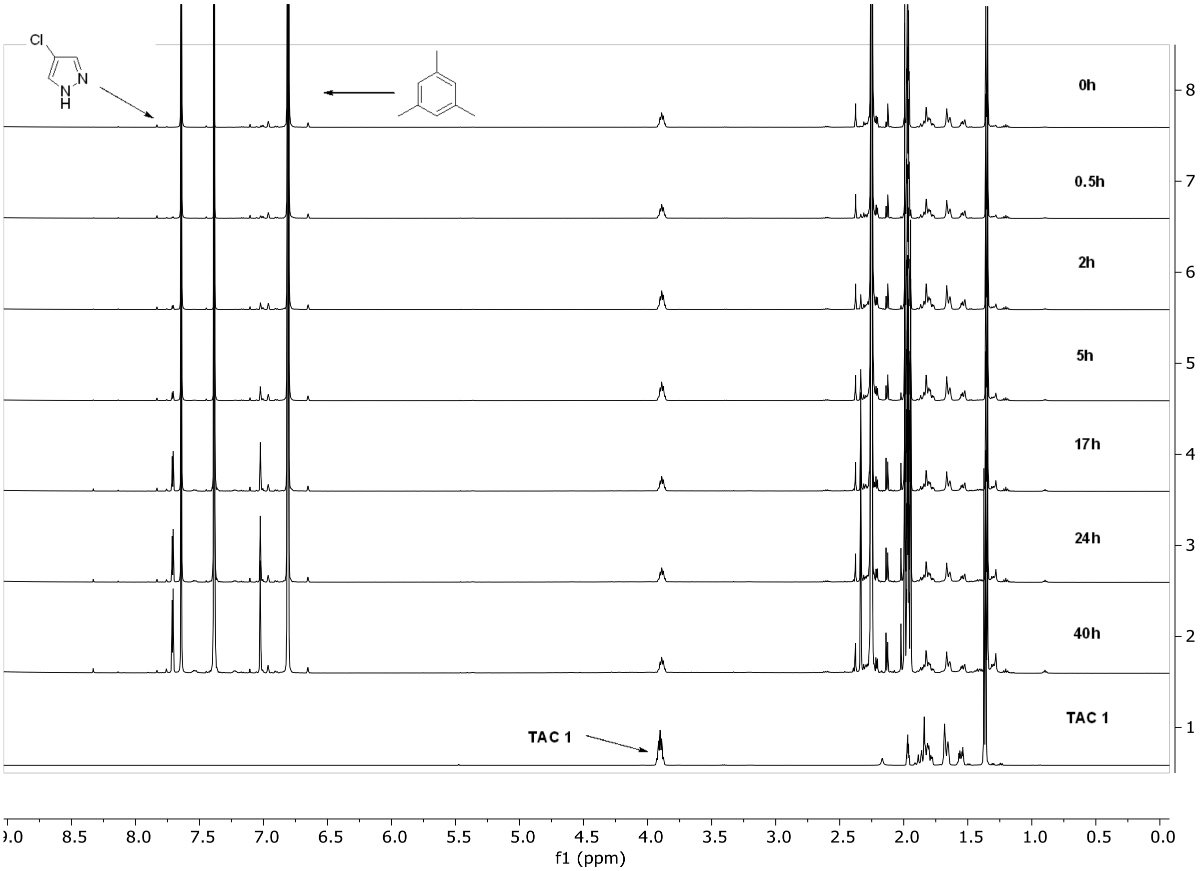

Fig S15. *in situ* ^{1}H NMR analysis of **TAC 1**

6. Cyclic Voltammetry Studies

General information: Cyclic voltammetry (CV) experiments were conducted in a 10 mL glass vial fitted with a glassy carbon working electrode, a Ag/AgCl reference electrode, and a platinum wire counter electrode. The solution of interest was purged with nitrogen for 3 minutes before data collection. Current was reported in µA. Scan rate: 100 mV/s, Bu_4NPF_6 as supporting electrolyte (0.1 M).

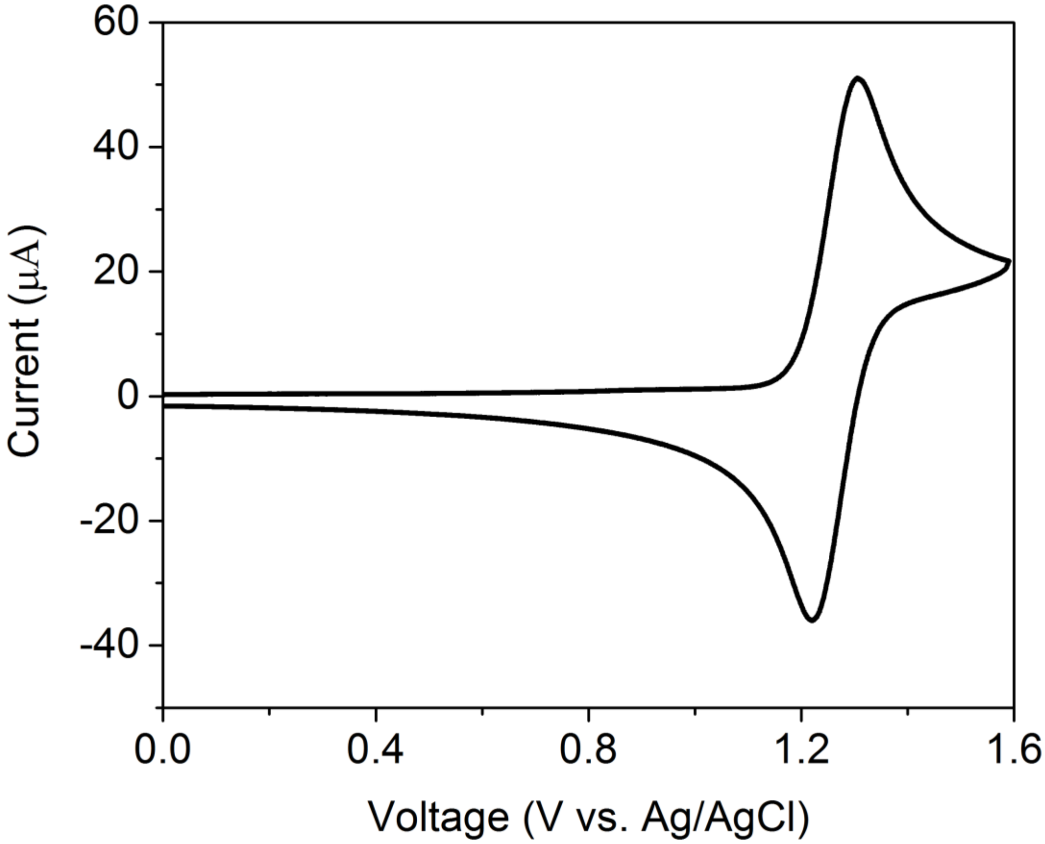

Figure S16. Cyclic voltammogram of TAC **1** [5.0 mM] in [0.1 M] Bu_4NPF_6 in CH_3CN. Scan rate: 100 mV/s. $E_{1/2}$(TAC **1**) = +1.26 V vs SCE

7. Absorption Spectra

UV-Vis Spectrum of **TAC (1) Radical Dication·$(ClO_4)_2$** was tested in a 1 cm path length quartz and analyzed using a Perkin Elmer Lambda 35 UV/Vis Spectrophotometer. **TAC (1) Radical Dication·$(ClO_4)_2$** was prepared by direct electrolysis the solution of TAC **1** (50 mg), $LiClO_4$ (100 mg), CH_3COOH (0.1 mL) in CH_3CN (6.0 mL).

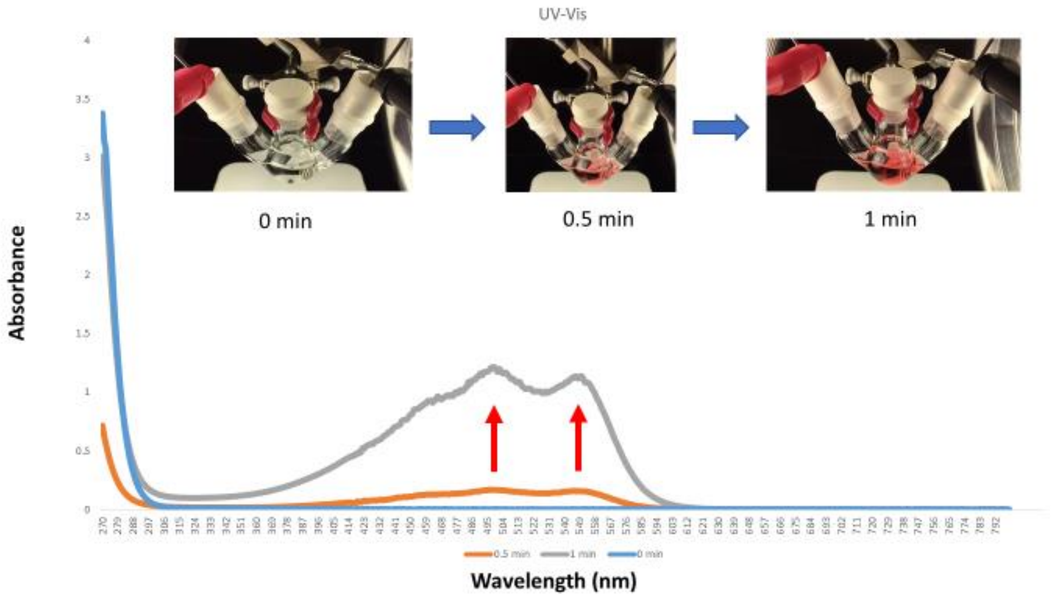

Fig. S17. UV-vis spectrum of **TAC (1) Radical Dication·$(ClO_4)_2$**

8. Evaluation of the Excited State Potential (*1*)

Using the data collected from the cyclic voltammetry studies (Fig. S16) and from the absorption spectra (Fig. S17) of the **TAC (1) Radical Dication·$(ClO_4)_2$ (TRD 1)**, we could estimate the redox potential of the excited of **TAC (1) Radical Dication·$(ClO_4)_2$** employing the following Equation 1:

$$E(\mathbf{TRD\ 1}^*/\mathbf{1}) = E(\mathbf{TRD\ 1}/\mathbf{1}) + E_{0\text{-}0}(\mathbf{2}^*/\mathbf{2}) \quad \text{Eq. 1}$$

E(**2**/**1**) is +1.26 V vs SCE (Fig. S16), while $E_{0\text{-}0}$(**TRD***/**TRD**) was determined using the position of the tail of the peak with the longest wavelength in the absorption spectrum. This wavelength was found to be 600 nm (Fig. S17), which translates to an $E_{0\text{-}0}$(**TRD 1***/**TRD 1**) of 2.07 eV. E(**TRD 1***/**1**) = +1.26 + 2.07 = +3.33 V (vs SCE)

9. Kinetic Isotope Effect Experiments (KIE) (*2*)

The KIE value was determined from an intermolecular competition reaction. Reaction was run in 0.4 mmol scale in undivided cell.

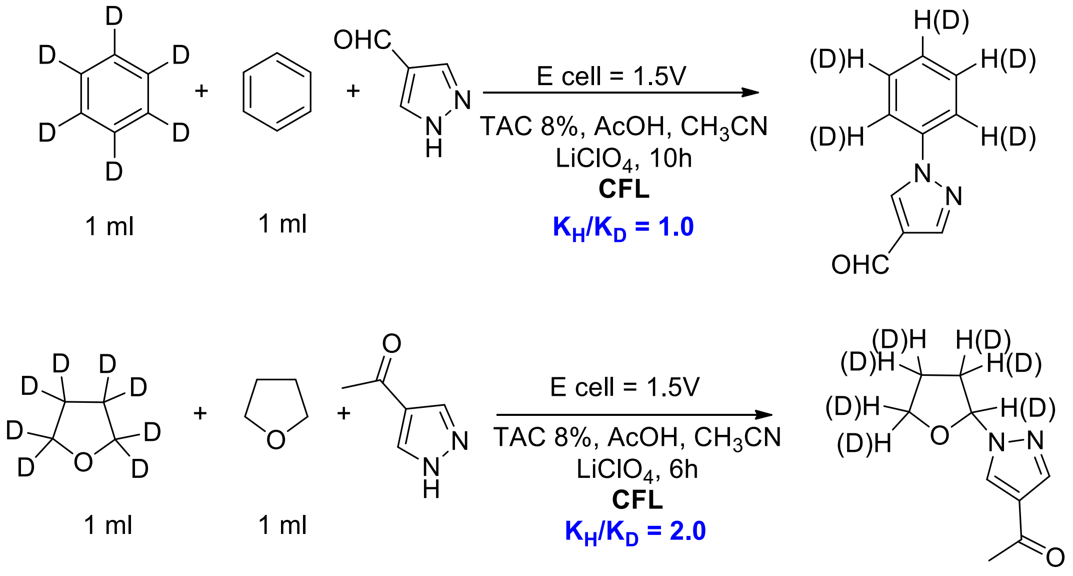
D
D
D
D
D
D
+
+
OHC
N
N
H
1 ml
1 ml
E cell = 1.5V
TAC 8%, AcOH, CH$_3$CN
LiClO$_4$, 10h
CFL
K$_H$/K$_D$ = 1.0
H(D)
(D)H
H(D)
(D)H
H(D)
N
N
OHC
D
D
D
D
D
D
D
D
O
+
O
+
O
N
N
H
1 ml
1 ml
E cell = 1.5V
TAC 8%, AcOH, CH$_3$CN
LiClO$_4$, 6h
CFL
K$_H$/K$_D$ = 2.0
(D)H
H(D)
(D)H
H(D)
(D)H
H(D)
(D)H
O
N–N
O

Fig S18. Kinetic isotope effect experiments

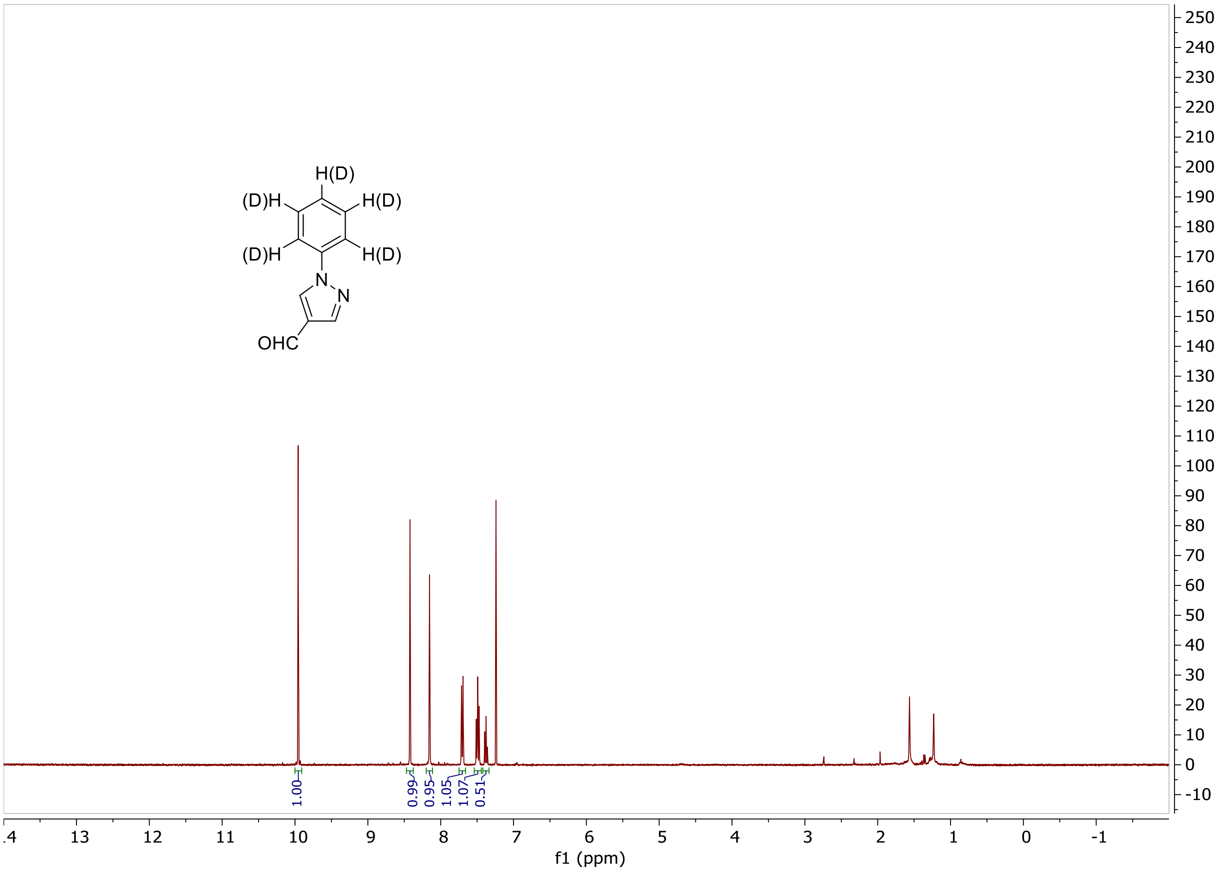

Fig. S19. NMR Spectral Data of Deuterated 4-Chloro-1-mesityl-1H-pyrazole

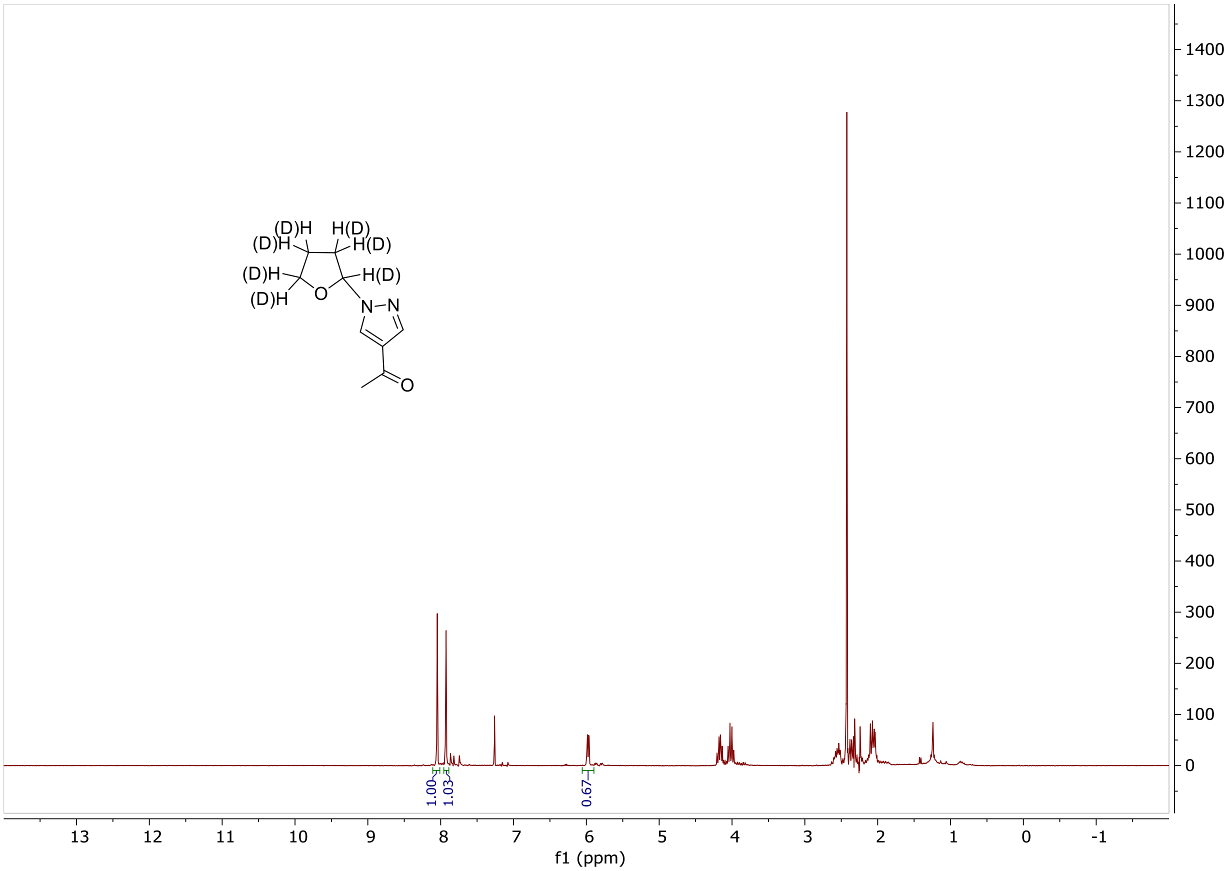

Fig. S20. NMR Spectral Data of Deuterated 1-(1-(Tetrahydrofuran-2-yl)-1H-pyrazol-4-yl)ethanone

10. X-ray Crystallography Data

X-ray diffraction data was collected on a Bruker Apex II diffractometer. Crystal data, data collection and refinement parameters are summarized in Fig. S23. The structures were solved by using direct methods and standard difference map techniques, and were refined by full-matrix least-squares procedures on F^2 with SHELXTL (Version 2014/7) (*3*-*5*).

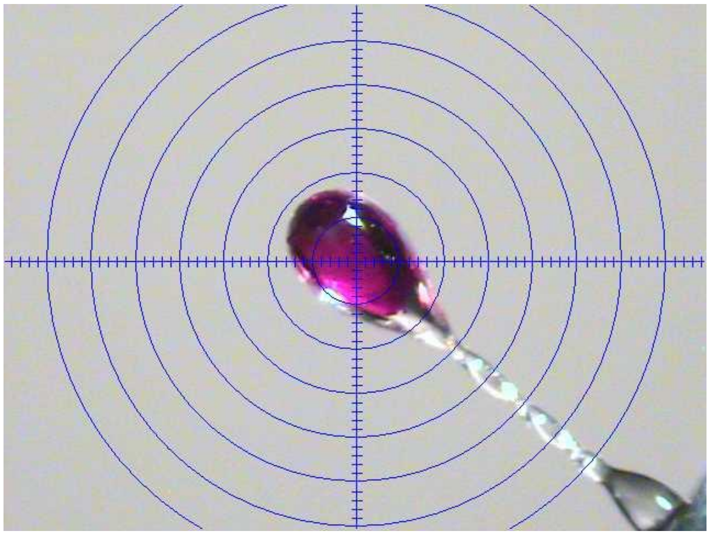

Fig. S21. Picture of Crystal

Synthesis of Crystal:

An electrochemical cell with a microporous polyethylene divider was equipped with a stir bar on each side and a carbon felt electrode on each side. The cell was charged with 20 mL of 0.5M solution of $LiClO_4$ in acetonitrile. **TAC 1·ClO_4** (1.00 g, 2.12 mmol) was added to the cathodic side in 1 mL of acetonitrile and AcOH (1.14 mL, 20 mmol) was added to the anodic side. Electrolysis was then initiated at 2.0V while stirring, which was maintained until the current dropped to 1 mA (roughly 8 hr). The solution from the cathodic side was transferred to a flask and concentrated *in vacuo*. The resulting solid was stirred in DCM (20 mL) for 1 hr and subsequently filtered through a cotton plug. The solution was concentrated *in vacuo* to give **TAC (1) Radical Dication·$(ClO_4)_2$** as a dark red powder (0.53 g, 0.93 mmol, 44% yield). **TAC (1) Radical Dication·$(ClO_4)_2$** (100 mg, 0.18 mmol) was dissolved in 1 mL of acetonitrile and Et_2O was allowed to diffuse into the solution at–14 °C for 1 week, resulting in dark red columns suitable for X-ray diffraction.

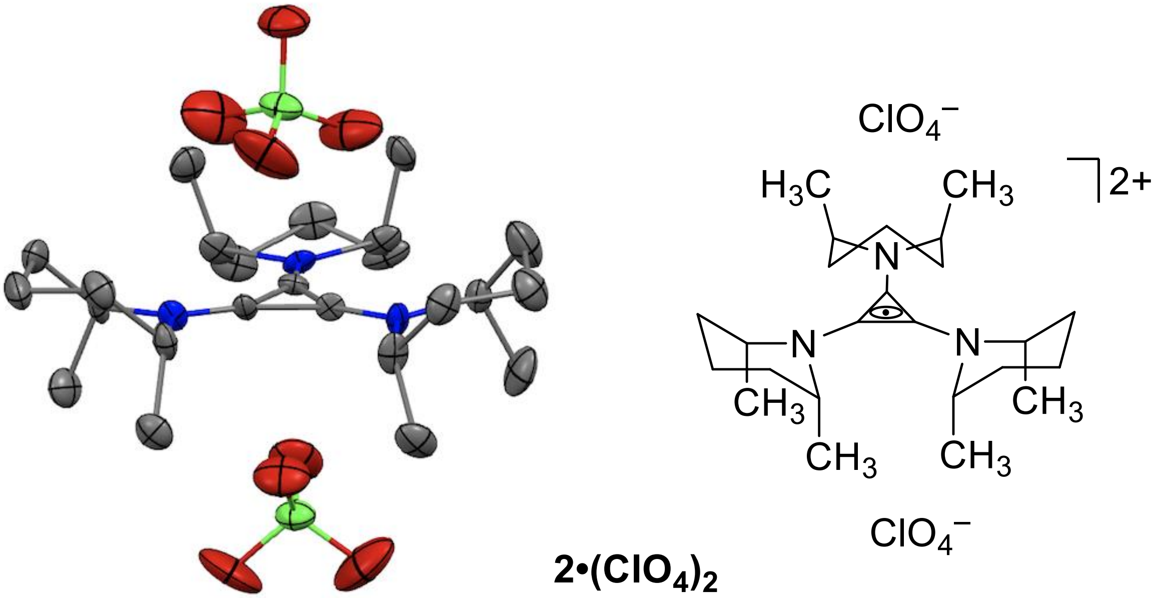
ClO4−
H3C
CH3
2+
N
N
N
CH3
CH3
CH3
CH3
ClO4−

2•(ClO$_4$)$_2$

Fig. S22. X-ray Structure Determination of **2·(ClO$_4$)$_2$**

	TRD 1·(ClO$_4$)$_2$ (CSD#: 1892753)
lattice	Monoclinic
formula	$C_{24}H_{42}Cl_2N_3O_8$
formula weight	571.50
space group	*P2$_1$/c*
a/Å	19.5306(16)
b/Å	11.7733(9)
c/Å	57.147(5)
α/°	90
β/°	90.0835(13)
γ/°	90
V/Å^3	13140.3(18)
Z	16
temperature (K)	210(2)
radiation (λ, Å)	0.71073

ρ (calcd.) g cm^{-3}	1.156
μ (Mo Kα), mm^{-1}	0.241
θ max, deg.	26.371
no. of data collected	162493
no. of data	26900
no. of parameters	1359
R_1 [$I > 2$□(I)]	0.1064
wR_2 [$I > 2$□(I)]	0.2695
R_1 [all data]	0.1951
wR_2 [all data]	0.3234
GOF	1.024
R_{int}	0.1502

Fig S23. Crystal data and structure refinement for **TRD 1·(ClO_4)$_2$**

11. Computational Data

All calculations were performed with ORCA (*6*), an open-source quantum chemistry package.

Cartesian coordinates of the atoms in TAC radical dication were extracted from the crystal structure, having added hydrogen atoms in the expected configurations. These atomic positions were then used to initialize a geometry optimization, using the B3LYP exchange-correlation functional, the cc-pVDZ basis set, and an implicit solvation model for acetonitrile. With the resulting geometry, the unrestricted Kohn-Sham equations were solved. The molecular orbitals in Fig. 4 were generated using an iso-surface value of 0.06, with the VMD program (*7*).

Time-Dependent Density Functional Theory (TD-DFT) (*8*) is a computational technique to calculate excited electronic states, which are assumed to be (linear combinations of) single-particle excitations from the ground-state. The physical result we wish to emphasize is that the first and second excited states of TAC radical dication are energetically separated by ~5 nm, and correspond predominately to excitations from the ground-state HOMO-1 and HOMO-2 to the SOMO.

We have verified that using a larger basis set (cc-pVTZ) does not change the energetics and orbital characters of the relevant lowest-energy excited states. As additional checks, we ran the original calculation but with the ωB97x exchange-correlation functional, and also the more systematic Equation of Motion Coupled Cluster method with Single and Double excitations (EOM-CCSD) with localized orbitals (*9*). In both cases, while the excitation energies were shifted from the original B3LYP/cc-pVDZ calculation, the first and second excited states were again separated by ~5 nm. In the former calculation, the relevant excited states were characterized by identical orbital transitions.

Cartesian Coordinates for Geometry Optimized Structure of **TRD 1**

Atom	**X**	**Y**	**Z**
N	25.197507	9.8133958	-1.03502
N	21.637893	8.8464044	-1.09876

N	23.522327	8.8377518	2.097436
C	24.121849	9.3947121	-0.40714
C	22.747953	9.0404926	-0.42326
C	23.470129	9.0325176	0.799183
H	24.408603	10.548619	4.263632
H	26.097558	10.442766	3.712552
C	19.578484	9.7332976	0.013938
H	20.217892	10.473675	0.518326
H	19.105999	10.214077	-0.85369
H	18.783093	9.4321991	0.712945
C	21.248362	10.524999	-2.91879
H	21.838996	11.244308	-2.33107
H	21.455569	10.695959	-3.98652
H	20.182931	10.725795	-2.74196
C	25.576357	8.7395331	-3.26287
H	25.017699	7.8637704	-2.89798
H	25.353467	8.8727891	-4.3329
H	26.650309	8.5308897	-3.15991
C	27.327839	8.7338384	-0.28355
H	26.738759	7.8492537	0.003613
H	27.77605	8.5460491	-1.26875
H	28.143621	8.8584275	0.444885
C	22.511894	7.4306616	3.888353
H	21.605417	7.3443438	4.507461
H	22.626749	6.4786012	3.343715
C	23.754112	7.6770767	4.746708
H	23.902205	6.831629	5.436379
H	23.624935	8.5753807	5.373232
C	24.977387	7.8163669	3.839618
H	25.134743	6.8700327	3.295292
H	25.89161	8.0124483	4.420905
C	27.21274	11.260919	-0.76283
H	26.660987	12.15356	-0.42347
H	28.1935	11.276862	-0.26387
C	27.35326	11.304535	-2.28432
H	27.974261	10.468441	-2.64673
H	27.86881	12.231045	-2.58162
C	25.962527	11.265698	-2.91763
H	26.017986	11.282596	-4.01688
H	25.397803	12.160955	-2.60676
C	25.155819	10.017519	-2.52373
H	24.102036	10.221786	-2.74706
C	26.473478	10.008613	-0.26492
H	26.149333	10.202284	0.764267
C	19.568725	7.4509145	-1.18217
H	20.089818	6.4804476	-1.13438
H	18.599262	7.3250019	-0.67608
C	19.390654	7.8520978	-2.64677

H	18.799175	8.7785653	-2.73387
H	18.828407	7.0690225	-3.17881
C	20.767803	8.0202981	-3.28906
H	20.68988	8.3171373	-4.34615
H	21.299829	7.0543848	-3.26131
C	21.633916	9.0772139	-2.585
H	22.6728	8.9110516	-2.89387
C	20.373881	8.4788297	-0.37137
H	20.713558	7.9832778	0.544902
C	22.264396	8.5528386	2.867078
H	21.556004	8.1824713	2.119094
C	21.689212	9.8375185	3.481698
H	21.622205	10.644757	2.73646
H	20.672853	9.6130504	3.839579
H	22.278632	10.19661	4.336327
C	24.841323	8.9521819	2.810595
H	25.593902	8.7812509	2.031594
C	25.04794	10.356789	3.391901
H	24.850991	11.135901	2.639457

Frontier Orbital Energies from DFT Calculation:

	Alpha			**Beta**		
	Orbital #	**Occupancy**	**Energy (eV)**	**Orbital #**	**Occupancy**	**Energy (eV)**
HOMO-5	97	1	-9.18	97	1	-9.17
HOMO-4	98	1	-9.08	98	1	-9.07
HOMO-3	99	1	-9.02	99	1	-9.00
HOMO-2	100	1	-8.91	100	1	-8.61
HOMO-1	101	1	-8.88	101	1	-8.58
SOMO	102	1	-7.09	102	0	-5.11
LUMO	103	0	-0.72	103	0	-0.33
LUMO+1	104	0	-0.70	104	0	-0.30
LUMO+2	105	0	0.34	105	0	0.38

Lowest Energy Excited States from TD-DFT Calculation:

	Energy (eV)	**Wavelength (nm)**	**Transition Orbitals**	**% Composition (c^2)**
State 1	2.70	460	102a -> 104a	0.03
			101b -> 102b	0.94
State 2	2.73	454	102a -> 103a	0.03
			100b -> 102b	0.94
State 3	2.90	427	99a -> 102a	0.98
State 4	3.03	410	95b -> 102b	0.01
			96b -> 102b	0.01
			98b -> 102b	0.97

State 5	3.148	394	97b -> 102b	0.98

12. Characterization

Substratres for Table 4-1 (entries 1-36):

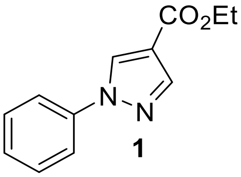

1

***Ethyl 1-phenyl-1H-pyrazole-4-carboxylate* (1):** The title compound was prepared from benzene (2.0 mL) and ethyl 1H-pyrazole-4-carboxylate (0.4 mmol, 56.0 mg) according to general procedure A with an irradiation/electrolysis time of 60 hours. The crude residue was purified by column chromatography on silica gel with an eluent of hexanes to 10% EtOAc/hexanes to yield a white solid in 65% yield (56.2 mg).

1: ^{1}H NMR (500 MHz, Chloroform-*d*) δ 8.43 (s, 1H), 8.12 (s, 1H), 7.74 – 7.72 (m, 2H), 7.52 – 7.49 (m, 2H), 7.39 – 7.36 (m, 1H), 4.36 (q, *J* = 7.1 Hz, 2H), 1.40 (t, *J* = 7.1 Hz, 3H). ^{13}C NMR (126 MHz, Chloroform-*d*) δ 162.9, 142.2, 139.4, 130.0, 129.6, 127.6, 119.6, 117.0, 60.5, 14.4. MS (DART) exact mass: calculated for $(M+H)^+$: 217.0972; found: 217.0979.

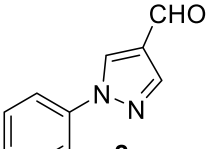

2

***1-Phenyl-1H-pyrazole-4-carbaldehyde* (2):** The title compound was prepared from benzene (2.0 mL) and 1H-pyrazole-4-carbaldehyde (0.4 mmol, 38.4 mg) according to general procedure A with an irradiation/electrolysis time of 60 hours. The crude residue was purified by column chromatography on silica gel with an eluent of hexanes to 10% EtOAc/hexanes to yield a white solid in 61% yield (42.0 mg).

2: ^{1}H NMR (500 MHz, Chloroform-*d*) δ 9.97 (s, 1H), 8.44 (s, 1H), 8.17 (s, 1H), 7.73 – 7.71 (m, 2H), 7.56 – 7.46 (m, 2H), 7.44 – 7.35 (m, 1H). ^{13}C NMR (126 MHz, Chloroform-*d*) δ 184.1, 141.7, 139.2, 130.0, 129.7, 128.1, 125.7, 119.8. MS (DART) exact mass: calculated for $(M+H)^+$: 173.0709; found: 173.0719

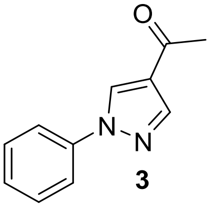

3

1-(1-Phenyl-1H-pyrazol-4-yl)ethanone **(3):** The title compound was prepared from benzene (2.0 mL) and 1-(1H-pyrazol-4-yl)ethanone (0.4 mmol, 44.0 mg) according to general procedure A with an irradiation/electrolysis time of 60 hours. The crude residue was purified by column chromatography on silica gel with an eluent of hexanes to 10% EtOAc/hexanes to yield a white solid in 60% yield (44.7 mg).

3: ^{1}H NMR (500 MHz, Chloroform-*d*) δ 8.39 (d, *J* = 0.6 Hz, 1H), 8.10 (s, 1H), 7.76 – 7.65 (m, 2H), 7.53 – 7.45 (m, 2H), 7.41 – 7.33 (m, 1H), 2.50 (s, 3H). ^{13}C NMR (126 MHz, Chloroform-*d*) δ 192.08, 141.56, 139.32, 129.67, 129.08, 127.77, 125.64, 119.74, 28.07. MS (DART) exact mass: calculated for $(M+H)^+$: 187.0866; found: 187.0876.

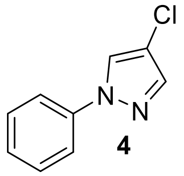

4

4-Chloro-1-phenyl-1H-pyrazole **(4):** The title compound was prepared from benzene (2.0 mL) and 4-chloro-1H-pyrazole (0.4 mmol, 41.0 mg) according to general procedure A with an irradiation/electrolysis time of 60 hours. The crude residue was purified by column chromatography on silica gel with an eluent of hexanes to 10% EtOAc/hexanes to yield a white solid in 45% yield (32.1 mg).

4: ^{1}H NMR (500 MHz, Chloroform-*d*) δ 7.91 (s, 1H), 7.64-7.63 (m, 3H), 7.48-7.45 (m, 2H), 7.33-7.30 (m, 1H). ^{13}C NMR (126 MHz, Chloroform-*d*) δ 139.8, 139.5, 129.6, 127.0, 124.8, 119.0, 112.4. MS (DART) exact mass: calculated for $(M+H)^+$: 179.0371; found: 179.0377.

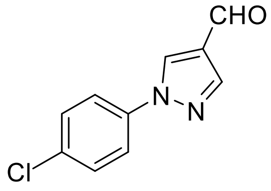

5a

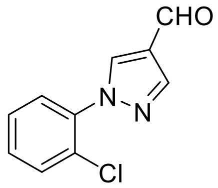

5b

1-(4-chlorophenyl)-1H-pyrazole-4-carbaldehyde **(5a)** **and** ***1-(2-chlorophenyl)-1H-pyrazole-4-carbaldehyde*** **(5b):** The title compounds were prepared from chlorobenzene (2.0 mL) and 1H-pyrazole-4-carbaldehyde (0.4 mmol, 38.4 mg) according to general procedure A with an irradiation/electrolysis time of 72 hours. The crude residue was purified by column chromatography on silica gel with an eluent of hexanes to 15% EtOAc/hexanes to yield a white solid in 56% yield (46.3 mg) as a mixture of para and ortho isomers. The crude isomer ratio of the mixture was 4:1:1 (*p*:*m*:*o*) as determined by ^{1}H NMR of reaction solution.

5a: ^{1}H NMR (500 MHz, Chloroform-d) δ 9.96 (s, 1H), 8.41 (s, 1H), 8.15 (s, 1H), 7.67 (d, *J* = 8.8 Hz, 2H), 7.47 (d, *J* = 8.8 Hz, 2H); ^{13}C NMR (126 MHz, Chloroform-d) δ 183.9, 141.9, 137.7, 133.7, 129.9, 129.9, 125.9, 121.0.

5b: ^{1}H NMR (500 MHz, Chloroform-d) δ 9.97 (s, 1H), 8.41 (s, 1H), 8.16 (s, 1H), 7.68-7.67 (m, 2H), 7.49-7.47 (m, 2H); ^{13}C NMR (126 MHz, Chloroform-*d*) δ 184.0, 141.3, 135.1, 130.9, 130.2, 129.9, 129.9, 128.4, 128.0, 127.7.

MS (DART) exact mass: calculated for $(M+H)^+$: 187.1235; found: 187.1228.

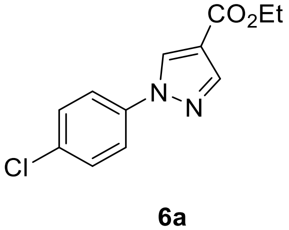

6a

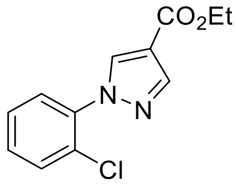

6b

ethyl 1-(4-chlorophenyl)-1H-pyrazole-4-carboxylate **(6a) and ethyl 1-(2-chlorophenyl)-1H-pyrazole-4-carboxylate (6b):** The title compounds were prepared from chlorobenzene (2.0 ml), ethyl 1H-pyrazole-4-carboxylate (0.4 mmol, 56.0 mg) according to general procedure A with an irradiation time of 72 hours. The crude residue was purified by column chromatography on silica gel with an eluent of hexanes to 20% EtOAc/hexanes to yield a white solid in 46% (46.1 mg). The ratio of the mixture was 10:1 (*p*:*o*) as determined by ^{1}H NMR of reaction solution.

6a: ^{1}H NMR (500 MHz, DMSO-d_6) δ 9.14 (s, 1H), 8.16 (s, 1H), 8.04 – 7.87 (m, 2H), 7.67 – 7.52 (m, 2H), 4.28 (q, *J* = 7.1 Hz, 2H), 1.31 (t, *J* = 7.2 Hz, 3H); ^{13}C NMR (126 MHz, DMSO-d_6) δ 162.5, 142.5, 138.2, 132.0, 130.0, 121.2, 117.0, 60.5, 17.3, 14.8.

6b: ^{1}H NMR (500 MHz, DMSO-d_6) δ 9.14 (s, 1H), 8.16 (s, 1H), 8.04 – 7.87 (m, 2H), 7.67 – 7.52 (m, 2H), 4.28 (q, *J* = 7.1 Hz, 2H), 1.31 (t, *J* = 7.2 Hz, 3H); ^{13}C NMR (126 MHz, DMSO-d_6) δ 162.5, 142.5, 138.2, 132.0, 131.9, 130.0, 129.1, 121.2, 117.0, 60.5, 17.3, 14.8.

MS (DART) exact mass: calculated for $(M+H)^+$:251.0582; found: 251.0593.

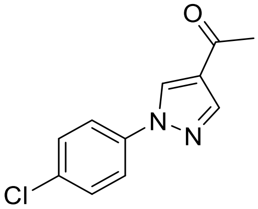

7a

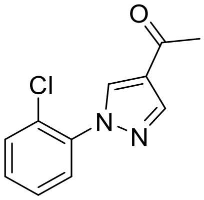

7b

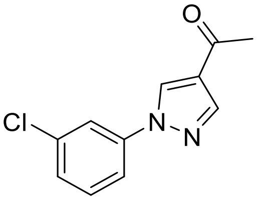

7c

1-(1-(4-chlorophenyl)-1H-pyrazol-4-yl)ethanone **(7a), 1-(1-(2-chlorophenyl)-1H-pyrazol-4-yl)ethenone (7b) and 1-(1-(3-chlorophenyl)-1H-pyrazol-4-yl)ethanone (7c):** The title compounds were prepared from chlorobenzene (2.0 ml), 1-(1H-pyrazol-4-yl)ethanone (0.4 mmol, 44.0 mg) according to general procedure A with an irradiation time of 80 hours. The crude residue was purified by column chromatography on silica gel with an eluent of hexanes to 20% EtOAc/hexanes to yield a white solid in 55% (48.6 mg). The ratio of the mixture was 8:3:1 (*p*:*o*:*m*) as determined by ^{1}H NMR of reaction solution.

7a: ^{1}H NMR (500 MHz, DMSO-d_6) δ 9.24 (s, 1H), 8.20 (s, 1H), 7.97 – 7.94 (m, 2H), 7.62 – 7.60 (m, 2H), 2.47 (s, 3H). ^{13}C NMR (126 MHz, DMSO-d_6, mixture of **a, b and c**) δ 192.2, 192.2, 141.8, 141.4, 138.3, 136.0, 132.0, 131.8, 131.3, 131.0, 130.1, 129.2, 128.9, 128.9, 128.8, 126.0, 125.1, 121.1, 28.5, 17.3.

7b: ^{1}H NMR (500 MHz, DMSO-d_6) δ 8.84 (s, 1H), 8.20 (s, 1H), 7.74 - 7.04 (m, 4H), 2.46 (s, 3H). ^{13}C NMR (126 MHz, DMSO-d_6, mixture of **a, b and c**) δ 192.2, 192.2, 141.8, 141.4, 138.3, 136.0, 132.0, 131.8, 131.3, 131.0, 130.1, 129.2, 128.9, 128.9, 128.8, 126.0, 125.1, 121.1, 28.5, 17.3.

7c: ^{1}H NMR (500 MHz, DMSO-d_6) δ 8.58 (s, 1H), 8.16 (s, 1H), 7.74 - 7.55 (m, 3H), 7.04 (s, 1H), 2.44 (s, 3H). ^{13}C NMR (126 MHz, DMSO-d_6, mixture of **a, b and c**) δ 192.2, 192.2, 141.8, 141.4, 138.3, 136.0, 132.0, 131.8, 131.3, 131.0, 130.1, 129.2, 128.9, 128.9, 128.8, 126.0, 125.1, 121.1, 28.5, 17.3.

MS (DART) exact mass: calculated for (M+H)$^+$:221.0476; found: 221.0487

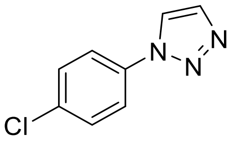

8a

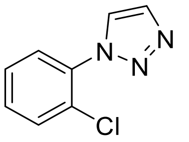

8b

1-(4-chlorophenyl)-1H-1,2,3-triazole **(8a) and 1-(2-chlorophenyl)-1H-1,2,3-triazole (8b):** The title compounds were prepared from chlorobenzene (2.0 ml), 1H-1,2,3-triazole (0.4 mmol, 27.6 mg) according to general procedure A with an irradiation time of 80 hours. The crude residue was purified by column chromatography on silica gel with an eluent of hexanes to 30% EtOAc/hexanes to yield a white solid in 31% (22.3 mg). The ratio of the mixture was 3:1 (*p*:*o*) as determined by ^{1}H NMR of reaction solution.

8a: ^{1}H NMR (500 MHz, Chloroform-*d*) δ 7.98 (d, *J* = 1.1 Hz, 1H), 7.86 (d, *J* = 1.1 Hz, 1H), 7.72 – 7.70 (m, 2H), 7.52 – 7.51 (m, 2H). ^{13}C NMR (126 MHz, Methanol-d_4, mixture of **a and b**) δ 135.7, 134.3, 134.0, 133.0, 131.3, 130.5, 129.7, 127.9, 126.8, 122.8, 121.8.

8b: ^{1}H NMR (500 MHz, Chloroform-*d*) δ 8.01 (d, *J* = 5.0 Hz, 1H), 7.87 (s, 1H), 7.64 - 7.58 (m, 2H), 7.47 – 7.46 (m, 2H). ^{13}C NMR (126 MHz, Methanol-d_4, mixture of **a and b**) δ 135.7, 134.3, 134.0, 133.0, 131.3, 130.5, 129.7, 127.9, 126.8, 122.8, 121.8.

MS (DART) exact mass: calculated for (M+H)$^+$:180.0323; found: 180.0330.

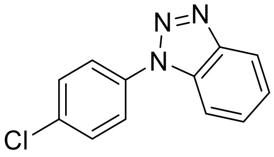

9

1-(4-chlorophenyl)-1H-benzo[d][1,2,3]triazole **(9)**: The title compounds were prepared from chlorobenzene (2.0 ml), 1H-benzo[d][1,2,3]triazole (0.4 mmol, 47.6 mg) according to general procedure A with an irradiation time of 72 hours. The crude residue was purified by column chromatography on silica gel with an eluent of hexanes to 30% EtOAc/hexanes to yield a white solid in 35% (32.2 mg). The ratio of the mixture was 10:1 (*p*:*o*) as determined by ^{1}H NMR of reaction solution.

9: ^{1}H NMR (500 MHz, Chloroform-*d*) δ 8.17 (d, *J* = 8.3 Hz, 1H), 7.80 – 7.70 (m, 3H), 7.64 – 7.54 (m, 3H), 7.48 – 7.44 (m, 1H). ^{13}C NMR (126 MHz, Chloroform-*d*) δ 135.6, 134.5, 132.2, 130.1, 128.6, 124.6, 124.0, 120.5, 110.1.

MS (DART) exact mass: calculated for (M+H)$^+$:230.0480; found:230.0492.

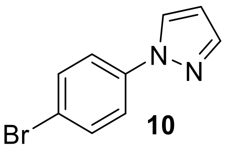

10

***1-(4-bromophenyl)-1H-pyrazole* (10)**: The title compound was prepared from bromobenzene (2.0 mL) and 1H-pyrazole (0.4 mmol, 27.2 mg) according to general procedure A with an irradiation/electrolysis time of 96 hours. The crude residue was purified by column chromatography on silica gel with an eluent of hexanes to 15% EtOAc/hexanes to yield a white solid in 35% (31.2 mg). The ratio of the mixture was 3:1 (*p*:*o*) as determined by ^{1}H NMR of reaction solution.

10: ^{1}H NMR (500 MHz, Chloroform-*d*) δ 7.87 (d, *J* = 2.5 Hz, 1H), 7.72 (d, *J* = 1.7 Hz, 1H), 7.60 – 7.52 (m, 4H), 6.46 (t, *J* = 2.1 Hz, 1H). ^{13}C NMR (126 MHz, Chloroform-*d*) δ 141.4, 139.2, 132.5, 126.6, 120.6, 119.6, 108.1.

MS (DART) exact mass: calculated for $(M+H)^+$:222.9865; found:222.9878.

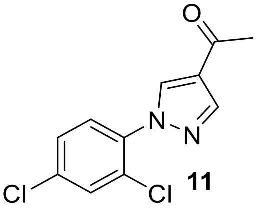

11

***1-(1-(2,4-dichlorophenyl)-1H-pyrazol-4-yl)ethanone* (11)**: The title compounds were prepared from 1,3-dichlorobenzene (2.0 ml), 1-(1H-pyrazol-4-yl)ethanone (0.4 mmol, 44.0 mg) according to general procedure B with an irradiation time of 80 hours. The crude residue was purified by column chromatography on silica gel with an eluent of hexanes to 20% EtOAc/hexanes to yield a white solid in 40% (40.8 mg).

11: ^{1}H NMR (500 MHz, Chloroform-*d*) δ 8.35 (s, 1H), 8.14 (s, 1H), 7.62 – 7.55 (m, 2H), 7.42 (dd, *J* = 8.6, 2.3 Hz, 1H), 2.53 (s, 3H). ^{13}C NMR (126 MHz, Chloroform-*d*) δ 191.9, 141.6, 136.0, 135.3, 133.8, 130.6, 129.1, 128.5, 128.2, 125.3, 28.1.

MS (DART) exact mass: calculated for $(M+H)^+$:255.0086; found:255.0099.

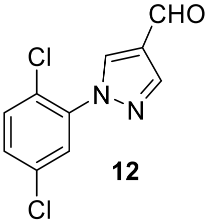

12

***1-(2,5-dichlorophenyl)-1H-pyrazole-4-carbaldehyde* (12)**: The title compounds were prepared from 1,4-dichlorobenzene (8 mmol, 1.176 g), 1H-pyrazole-4-carbaldehyde (0.4 mmol, 38.4 mg) according to general procedure B with an irradiation time of 72 hours. The crude residue was purified by column chromatography on silica gel with an eluent of hexanes to 20% EtOAc/hexanes to yield a light yellow solid in 42% (40.5 mg).

12: ^{1}H NMR (500 MHz, Chloroform-*d*) δ 9.99 (s, 1H), 8.44 (s, 1H), 8.20 (s, 1H), 7.69 – 7.68 (m, 1H), 7.50 (d, *J* = 8.6 Hz, 1H), 7.40 – 7.38 (m, 1H). ^{13}C NMR (126 MHz, Chloroform-*d*) δ 183.9, 135.0, 133.8, 131.8, 130.1, 127.7, 126.2.

MS (DART) exact mass: calculated for $(M+H)^+$:240.9930; found: 240.9941.

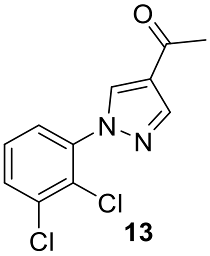

13

1-(1-(2,3-dichlorophenyl)-1H-pyrazol-4-yl)ethanone **(13)**: The title compounds were prepared from 1,2-dichlorobenzene (2.0 ml), 1-(1H-pyrazol-4-yl)ethanone (0.4 mmol, 44.0 mg) according to general procedure B with an irradiation time of 72 hours. The crude residue was purified by column chromatography on silica gel with an eluent of hexanes to 20% EtOAc/hexanes to yield a white solid in 30% (30.6 mg).

13: ^{1}H NMR (500 MHz, Chloroform-*d*) δ 8.36 (s, 1H), 8.09 (s, 1H), 7.94 – 7.82 (m, 1H), 7.56 – 7.56 (m, 2H), 2.51 (s, 3H). ^{13}C NMR (126 MHz, Chloroform-*d*) δ 191.8, 142.8, 138.4, 133.9, 131.7, 131.3, 129.0, 126.2, 121.6, 118.5, 28.1.

MS (DART) exact mass: calculated for $(M+H)^+$:255.0086; found:255.0099.

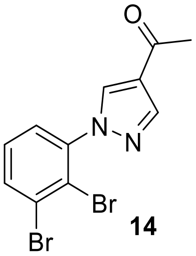

14

1-(4-bromophenyl)-1H-pyrazole **(14)**: The title compounds were prepared from 1,2-dibromobenzene (2.0 ml), 1-(1H-pyrazol-4-yl)ethanone (0.4 mmol, 44.0 mg) according to general procedure B with an irradiation time of 96 hours. The crude residue was purified by column chromatography on silica gel with an eluent of hexanes to 20% EtOAc/hexanes to yield a light yellow solid in 31% (42.7 mg).

14: ^{1}H NMR (500 MHz, Chloroform-*d*) δ 8.39 (s, 1H), 8.12 (s, 1H), 8.07 (d, *J* = 2.6 Hz, 1H), 7.75 (d, *J* = 8.7 Hz, 1H), 7.56 (dd, *J* = 8.7, 2.6 Hz, 1H), 2.53 (s, 3H). ^{13}C NMR (126 MHz, Chloroform-*d*) δ 191.8, 143.1, 142.0, 138.9, 134.4, 129.0, 126.2, 124.6, 123.7, 119.2, 28.1.

MS (DART) exact mass: calculated for $(M+H)^+$:342.9076; found:342.9094.

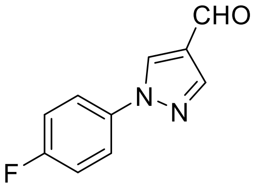

15a

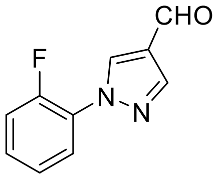

15b

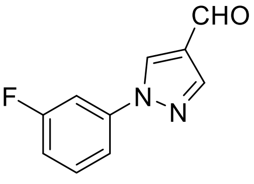

15c

1-(4-fluorophenyl)-1H-pyrazole-4-carbaldehyde **(15a),** ***1-(2-fluorophenyl)-1H-pyrazole-4-carbaldehyde*** **(15b) and** ***1-(3-fluorophenyl)-1H-pyrazole-4-carbaldehyde*** **(15c)**: The title compounds were prepared from fluorobenzene (2.0 mL) and 1H-pyrazole-4-carbaldehyde (0.4 mmol, 38.4 mg) according to general procedure A with an irradiation/electrolysis time of 60 hours. The crude residue was purified by column chromatography on silica gel with an eluent of hexanes to 10% EtOAc/hexanes to yield a colorless oil in 36% yield (27.4 mg). The ratio of the mixture was 5:1:1 (*p*:*o*:*m*) as determined by ^{1}H NMR of reaction solution.

15a: ^{1}H NMR (500 MHz, Chloroform-*d*) δ 9.97 (s, 1H), 8.38 (s, 1H), 8.16 (s, 1H), 7.71 – 7.68 (m, 2H), 7.22 – 7.18 (m, 2H). ^{13}C NMR (126 MHz, Chloroform-*d*, mixture of **a, b and c**) δ 184.0, 184.0, 162.0 (d, *J* = 249.5 Hz), 153.1 (d, *J* = 249.5 Hz), 141.8, 141.7, 141.1, 134.6, 134.5, 123.0, 129.7, 129.3, 129.2, 128.1, 125.8, 125.3, 125.2, 124.6, 121.8 (d, *J* = 8.8 Hz), 119.8, 117.1 (d, *J* = 21.4 Hz).116.7 (d, *J* = 23.9 Hz). ^{19}F NMR (470 MHz, Chloroform-*d*) δ -113.3 (m).

15b: ^{1}H NMR (500 MHz, Chloroform-*d*) δ 9.99 (s, 1H), 8.53 (s, 1H), 8.19 (s, 1H), 7.95 – 7.91 (m, 1H), 7.73 – 7.68 (m, 1H), 7.53 – 7.28 (m, 2H). ^{13}C NMR (126 MHz, Chloroform-*d*, mixture of **a, b and c**) δ 184.0, 184.0, 162.0 (d, *J* = 249.5 Hz), 153.1 (d, *J* = 249.5 Hz), 141.8, 141.7, 141.1, 134.6, 134.5, 123.0, 129.7, 129.3, 129.2, 128.1, 125.8, 125.3, 125.2, 124.6, 121.8 (d, *J* = 8.8 Hz), 119.8, 117.1 (d, *J* = 21.4 Hz).116.7 (d, *J* = 23.9 Hz). ^{19}F NMR (470 MHz, Chloroform-*d*) δ -124.7 (m).

15c: ^{1}H NMR (500 MHz, Chloroform-*d*) δ 9.97 (s, 1H), 8.44 (s, 1H), 8.17 (s, 1H), 7.73 – 7.68 (m, 1H), 7.53 – 7.28 (m, 3H). ^{13}C NMR (126 MHz, Chloroform-*d*, mixture of **a, b and c**) δ 184.0, 184.0, 162.0 (d, *J* = 249.5 Hz), 153.1 (d, *J* = 249.5 Hz), 141.8, 141.7, 141.1, 134.6, 134.5, 123.0, 129.7, 129.3, 129.2, 128.1, 125.8, 125.3, 125.2, 124.6, 121.8 (d, *J* = 8.8 Hz), 119.8, 117.1 (d, *J* = 21.4 Hz).116.7 (d, *J* = 23.9 Hz). ^{19}F NMR (470 MHz, Chloroform-*d*) δ -124.7 (m).

MS (DART) exact mass: calculated for $(M+H)^+$: 191.0615; found: 191.0626.

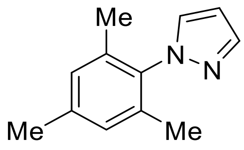

17

***1-mesityl-1H-pyrazole* (17)**: The title compound was prepared from mesitylene (1.4 mmol, 195 µL, 3.5 equiv.) and 1H-pyrazole (0.4 mmol, 27.2 mg) according to general procedure E with an irradiation/electrolysis time of 48 hours. The crude residue was purified by column chromatography on silica gel with an eluent of hexanes to 10% EtOAc/hexanes to yield a colorless oil in 80% yield (59.6 mg).

17: ^{1}H NMR (500 MHz, Chloroform-*d*) δ 7.78 – 7.66 (m, 1H), 7.43 (d, *J* = 2.2 Hz, 1H), 6.94 (s, 2H), 6.43 (s, 1H), 2.33 (s, 3H), 1.97 (s, 6H). ^{13}C NMR (126 MHz, Chloroform-*d*) δ 140.0, 138.7, 137.0, 135.9, 130.8, 128.8, 105.7, 21.1, 17.2.

MS (DART) exact mass: calculated for $(M+H)^+$: 187.1235; found: 187.1239.

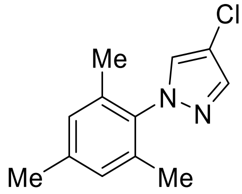

18

***4-Chloro-1-mesityl-1H-pyrazole* (18)**: The title compound was prepared from mesitylene (1.4 mmol, 195 µL, 3.5 equiv.) and 4-chloro-1H-pyrazole (0.4 mmol, 41.0 mg) according to general procedure E with an irradiation/electrolysis time of 48 hours. The crude residue was purified by column chromatography on silica gel with an eluent of hexanes to 10% EtOAc/hexanes to yield a colorless oil in 82% yield (72.4 mg).

18: ^{1}H NMR (500 MHz, Chloroform-*d*) δ 7.64 (s, 1H), 7.42 (s, 1H), 6.94 (s, 2H), 2.33 (s, 3H), 1.98 (s, 6H). ^{13}C NMR (126 MHz, Chloroform-*d*) δ 139.3, 138.6, 136.5, 135.7, 128.9, 128.8, 110.4, 21.1, 17.2.

MS (DART) exact mass: calculated for $(M+H)^+$: 221.0840; found: 221.0852.

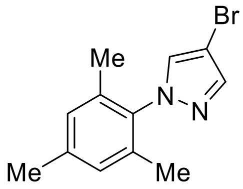

19

***4-Bromo-1-mesityl-1H-pyrazole* (19)**: The title compound was prepared from mesitylene (1.4 mmol, 195 µL, 3.5 equiv) and 4-bromo-1H-pyrazole (0.4 mmol, 58.8 mg) according to general procedure E with an irradiation/electrolysis time of 60 hours. The crude residue was purified by column chromatography on silica gel with an eluent of hexanes to 10% EtOAc/hexanes to yield a colorless oil in 69% yield (73.2 mg).

19: ^{1}H NMR (500 MHz, Chloroform-*d*) δ 7.68 (s, 1H), 7.45 (s, 1H), 6.94 (s, 2H), 2.33 (s, 3H), 1.98 (s, 6H). ^{13}C NMR (126 MHz, Chloroform-*d*) δ 140.7, 139.3, 136.5, 135.7, 131.0, 128.9, 93.5, 21.1, 17.2.

MS (DART) exact mass: calculated for $(M+H)^+$: 265.0335; found:265.0348.

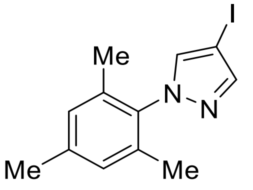

20

***4-Iodo-1-mesityl-1H-pyrazole* (20)**: The title compound was prepared from mesitylene (1.4 mmol, 195 µL, 3.5 equiv) and 4-iodo-1H-pyrazole (0.4 mmol, 77.6 mg) according to general procedure E with an irradiation/electrolysis time of 72 hours. The crude residue was purified by column chromatography on silica gel with an eluent of hexanes to 10% EtOAc/hexanes to yield a colorless oil in 58% yield (72.4 mg).

20: ^{1}H NMR (500 MHz, Chloroform-*d*) δ 7.75 (s, 1H), 7.50 (s, 1H), 6.96 (s, 2H), 2.35 (s, 3H), 1.99 (s, 6H). ^{13}C NMR (126 MHz, Chloroform-*d*) δ 145.2, 139.3, 136.3, 135.7, 135.2, 128.9, 56.6, 21.1, 17.2.

MS (DART) exact mass: calculated for $(M+H)^+$: 313.0196; found: 313.0211.

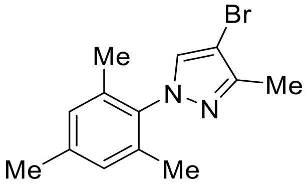

21

***4-Bromo-1-mesityl-3-methyl-1H-pyrazole* (21)**: The title compound was prepared from mesitylene (1.4 mmol, 195 µL, 3.5 equiv.) and 4-bromo-3-methyl-1H-pyrazole (0.4 mmol, 64.4 mg) according to general procedure E with an irradiation/electrolysis time of 72 hours. The crude residue was purified by column chromatography on silica gel with an eluent of hexanes to 15% EtOAc/hexanes to yield a light yellow oil in 83% yield (92.7 mg).

21: ^{1}H NMR (500 MHz, Chloroform-*d*) δ 7.39 (s, 1H), 6.94 (s, 2H), 2.34 (m, 6H), 2.01 (s, 6H). ^{13}C NMR (126 MHz, Chloroform-*d*) δ 148.0, 139.0, 136.6, 135.8, 131.3, 128.8, 94.2, 21.1, 17.3, 12.1.

MS (DART) exact mass: calculated for $(M+H)^+$: 279.0491; found: 279.0506.

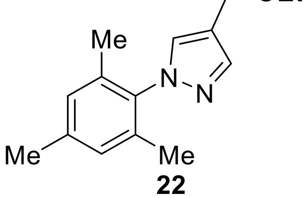

22

***ethyl 1-mesityl-1H-pyrazole-4-carboxylate* (22)**: The title compound was prepared from mesitylene (1.4 mmol, 195 µL, 3.5 equiv) and ethyl 1H-pyrazole-4-carboxylate (0.4 mmol, 56.0 mg) according to general procedure E with an irradiation/electrolysis time of 72 hours. The crude residue was purified by column chromatography on silica gel with an eluent of hexanes to 15% EtOAc/hexanes to yield a light yellow oil in 71% yield (73.4 mg).

22: ^{1}H NMR (500 MHz, Chloroform-*d*) δ 8.11 (s, 1H), 7.92 (s, 1H), 6.94 (s, 2H), 4.32 (q, *J* = 7.1 Hz, 2H), 2.32 (s, 3H), 1.97 (s, 6H), 1.36 (t, *J* = 7.1 Hz, 3H). ^{13}C NMR (126 MHz, Chloroform-*d*) δ 163.2, 141.6, 139.4, 136.1, 135.4, 134.5, 128.9, 115.6, 60.3, 21.1, 17.2, 14.4.

MS (DART) exact mass: calculated for $(M+H)^+$: 259.1441; found: 259.1454.

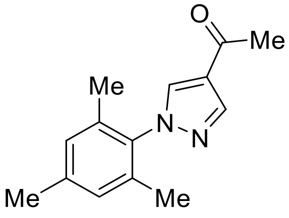

23

1-(1-mesityl-1H-pyrazol-4-yl)ethanone **(23)**: The title compound was prepared from mesitylene (1.4 mmol, 195 µL, 3.5 equiv.) and 1-(1H-pyrazol-4-yl)ethanone (0.4 mmol, 44.0 mg) according to general procedure E with an irradiation/electrolysis time of 72 hours. The crude residue was purified by column chromatography on silica gel with an eluent of hexanes to 15% EtOAc/hexanes to yield a light yellow oil in 75% yield (68.5 mg).

S45: ^{1}H NMR (500 MHz, Chloroform-*d*) δ 8.10 (s, 1H), 7.92 (s, 1H), 6.95 (s, 2H), 2.48 (s, 3H), 2.32 (s, 3H), 1.97 (s, 6H). ^{13}C NMR (126 MHz, Chloroform-*d*) δ 192.3, 141.0, 139.6, 136.0, 135.3, 133.7, 129.0, 124.5, 28.0, 21.1, 17.2.

MS (DART) exact mass: calculated for $(M+H)^+$: 229.1335; found: 229.1349.

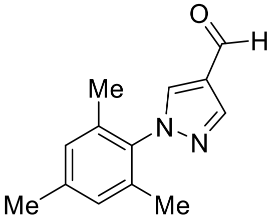

24

1-mesityl-1H-pyrazole-4-carbaldehyde **(24)**: The title compound was prepared from mesitylene (1.4 mmol, 195 µL, 3.5 equiv.) and 1H-pyrazole-4-carbaldehyde (0.4 mmol, 38.4 mg) according to general procedure E with an irradiation/electrolysis time of 60 hours. The crude residue was purified by column chromatography on silica gel with an eluent of hexanes to 10% EtOAc/hexanes to yield a colorless oil in 67% yield (57.4 mg).

24: ^{1}H NMR (500 MHz, Chloroform-*d*) δ 9.97 (d, *J* = 1.8 Hz, 1H), 8.19 (s, 1H), 7.99 (d, *J* = 2.2 Hz, 1H), 6.98 (s, 2H), 2.35 (s, 3H), 2.00 (d, *J* = 2.3 Hz, 6H). ^{13}C NMR (126 MHz, Chloroform-*d*) δ 184.2, 141.2, 139.8, 135.9, 135.2, 134.7, 129.1, 124.7, 21.1, 17.2.

MS (DART) exact mass: calculated for $(M+H)^+$: 215.1179; found: 215.1191.

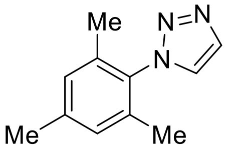

25

1-mesityl-1H-1,2,3-triazole **(25)**: The title compound was prepared from mesitylene (1.4 mmol, 195 µL, 3.5 equiv.) and 1H-1,2,3-triazole (0.4 mmol, 27.6 mg) according to general procedure E with an irradiation/electrolysis time of 72 hours. The crude residue was purified by column chromatography on silica gel with an eluent of hexanes to 15% EtOAc/hexanes to yield a light yellow oil in 65% yield (48.7 mg).

25: ^{1}H NMR (500 MHz, Chloroform-*d*) δ 7.89 (d, *J* = 1.0 Hz, 1H), 7.62 (d, *J* = 1.0 Hz, 1H), 6.99 (s, 2H), 2.35 (s, 3H), 1.94 (s, 6H). ^{13}C NMR (126 MHz, Chloroform-*d*) δ 140.1, 135.1, 133.5, 129.1, 125.5, 21.1, 17.2.

MS (DART) exact mass: calculated for $(M+H)^+$: 188.1182; found:118.1192.

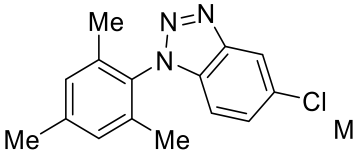

26a

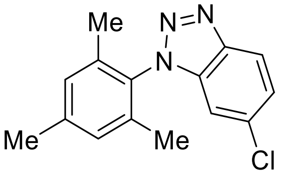

26b

5-chloro-1-mesityl-1H-benzo[d][1,2,3]triazole **(26a) and 6-chloro-1-mesityl-1H-benzo[d][1,2,3]triazole (26b):** The title compounds were prepared from mesitylene (1.4 mmol, 195 µL, 3.5 equiv.), 5-chloro-1H-benzo[d][1,2,3]triazole (0.4 mmol, 61.4 mg) according to general procedure A with an irradiation time of 72 hours. The crude residue was purified by column chromatography on silica gel with an eluent of hexanes to 30% EtOAc/hexanes to yield a light yellow oil in 51% (55.4 mg). The ratio of the mixture was 1:1 (***a***:***b***) as determined by ^{1}H NMR of reaction solution.

26a: ^{1}H NMR (500 MHz, Chloroform-*d*) δ 8.13 (d, *J* = 1.9 Hz, 1H), 7.44 (dd, *J* = 8.7, 1.8 Hz, 1H), 7.14 (d, *J* = 8.8 Hz, 1H), 7.06 (s, 2H), 2.40 (s, 3H), 1.85 (s, 6H). ^{13}C NMR (126 MHz, Chloroform-*d*, mixture of **a and b**) δ 146.1, 144.1, 140.6, 140.6, 136.1, 136.1, 134.5, 132.6, 131.1, 130.0, 129.5, 129.43, 129.0, 125.3, 121.1, 119.5, 110.7, 109.5, 21.2, 17.4, 17.3.

26b: ^{1}H NMR (500 MHz, Chloroform-*d*) δ 8.07 (d, *J* = 8.5 Hz, 1H), 7.38 (dd, *J* = 9.0, 2.0 Hz, 1H), 7.20 (d, *J* = 2.0 Hz, 1H), 7.06 (s, 2H), 2.40 (s, 3H), 1.87 (s, 6H). ^{13}C NMR (126 MHz, Chloroform-*d*, mixture of **a and b**) δ 146.1, 144.1, 140.6, 140.6, 136.1, 136.1, 134.5, 132.6, 131.1, 130.0, 129.5, 129.43, 129.0, 125.3, 121.1, 119.5, 110.7, 109.5, 21.2, 17.4, 17.3.

MS (DART) exact mass: calculated for $(M+H)^+$:272.0949; found: 272.0961.

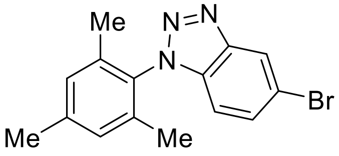

27

5-bromo-1-mesityl-1H-benzo[d][1,2,3]triazole **(27):** The title compounds were prepared from mesitylene (1.4 mmol, 195 µL, 3.5 equiv.), 5-bromo-1H-benzo[d][1,2,3]triazole (0.4 mmol, 79.2 mg) according to general procedure A with an irradiation time of 72 hours. The crude residue was purified by column chromatography on silica gel with an eluent of hexanes to 30% EtOAc/hexanes to yield a white solid in 75% (94.9 mg). The ratio of the mixture was 1:1 (***a***:***b***) as determined by ^{1}H NMR of reaction solution.

27: ^{1}H NMR (500 MHz, Chloroform-*d*) δ 8.32 (d, *J* = 1.6 Hz, 1H), 7.57 (dd, *J* = 8.7, 1.7 Hz, 1H), 7.10 (d, *J* = 8.7 Hz, 1H), 7.06 (s, 2H), 2.40 (s, 3H), 1.86 (s, 6H). ^{13}C NMR (126 MHz, Chloroform-*d*) δ 146.7, 140.6, 136.1, 132.9, 131.4, 131.2, 129.4, 122.8, 117.3, 111.1, 21.2, 17.3.

MS (DART) exact mass: calculated for $(M+H)^+$:316.0444; found: 316.0462.

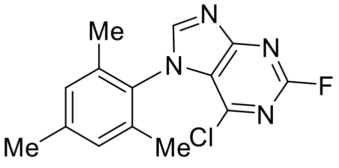

28

6-chloro-2-fluoro-7-mesityl-7H-purine **(28)**: The title compound was prepared from mesitylene (1.4 mmol, 195 µL, 3.5 equiv.) and 6-chloro-2-fluoro-7H-purine (0.4 mmol, 69.0 mg) according to general procedure E with an irradiation/electrolysis time of 72 hours. The crude residue was purified by column chromatography on silica gel with an eluent of hexanes to 30% EtOAc/hexanes to yield a light yellow solid in 50% yield (58.1 mg).

28: ^{1}H NMR (500 MHz, Chloroform-*d*) δ 8.05 (s, 1H), 7.04 (s, 2H), 2.36 (s, 3H), 1.95 (s, 6H). ^{13}C NMR (126 MHz, Chloroform-*d*) δ 157.2 (d, *J* = 221.8 Hz), 153.8 (d, *J* = 16.4 Hz), 153.2 (d, *J* = 16.4 Hz), 146.4 (d, *J* = 3.8 Hz), 140.7, 135.5, 130.0 (d, *J* = 5.0 Hz), 129.7, 128.4, 21.2, 17.7. ^{19}F NMR (470 MHz, Chloroform-*d*) δ -48.55.

MS (DART) exact mass: calculated for $(M+H)^+$: 291.0807; found: 291.0822.

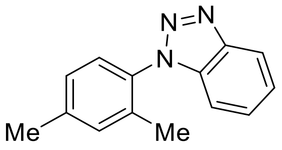

29a

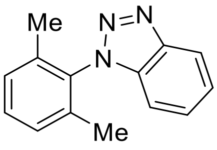

29b

1-(2,4-dimethylphenyl)-1H-benzo[d][1,2,3]triazole **(29a) and 1-(2,6-dimethylphenyl)-1H-benzo[d][1,2,3]triazole (29b):** The title compounds were prepared from m-xylene (2.0 mL) and 1Hbenzo[d][1,2,3]triazole (0.4 mmol, 47.6 mg) according to general procedure E with an irradiation/electrolysis time of 72 hours. The crude residue was purified by column chromatography on silica gel with an eluent of hexanes to 20% EtOAc/hexanes to yield a light yellow solid in 82% yield (73.2 mg). The ratio of the mixture was 6:1 (***a*:*b***) as determined by ^{1}H NMR of reaction solution.

29a: ^{1}H NMR (500 MHz, Chloroform-*d*) δ 8.14 (d, *J* = 8.4 Hz, 1H), 7.59 – 7.45 (m, 1H), 7.42 – 7.39 (m, 1H), 7.34 – 7.32 (m, 1H), 7.27 – 7.25 (m, 2H), 7.20 – 7.18 (m, 1H), 2.44 (s, 3H), 2.07 (s, 3H). ^{13}C NMR (126 MHz, Chloroform-*d*, mixture of **a and b**) δ 145.6, 140.2, 134.9, 134.0, 132.7, 132.3, 127.9, 127.6, 126.7, 124.1, 120.0, 110.2, 21.3, 17.7.

29b: ^{1}H NMR (500 MHz, Chloroform-*d*) δ 8.17 – 8.13 (m, 1H), 7.59 – 7.45 (m, 1H), 7.42 – 7.39 (m, 1H), 7.34 – 7.32 (m, 1H), 7.27 – 7.25 (m, 2H), 7.20 – 7.18 (m, 1H), 1.91 (s, 6H). ^{13}C NMR (126 MHz, Chloroform-*d*, mixture of **a and b**) δ 145.6, 140.2, 134.9, 134.0, 132.7, 132.3, 127.9, 127.6, 126.7, 124.1, 120.0, 110.2, 21.3, 17.7.

MS (DART) exact mass: calculated for (M+H)$^{+}$: 224.1182; found: 224.1193.

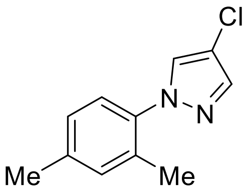

30a

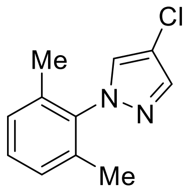

30b

4-chloro-1-(2,4-dimethylphenyl)-1H-pyrazole **(30a) and 4-chloro-1-(2,6-dimethylphenyl)-1H-pyrazole (30b):** The title compounds were prepared from m-xylene (2.0 mL) and 4-chloro-1H-pyrazole (0.4 mmol, 41.0 mg) according to general procedure E with an irradiation/electrolysis time of 72 hours. The crude residue was purified by column chromatography on silica gel with an eluent of hexanes to 10% EtOAc/hexanes to yield a light yellow oil in 87% yield (71.9 mg). The ratio of the mixture was 10:1 (***a*:*b***) as determined by ^{1}H NMR of reaction solution.

30a: ^{1}H NMR (500 MHz, Chloroform-*d*) δ 7.64 (s, 1H), 7.58 (s, 1H), 7.19 (d, *J* = 8.0 Hz, 1H), 7.14 (d, *J* = 1.9 Hz, 1H), 7.10 (dd, *J* = 7.9, 2.0 Hz, 1H), 2.39 (s, 3H), 2.22 (s, 3H). ^{13}C NMR (126 MHz, Chloroform-*d*, mixture of **a and b**) δ 138.9, 138.6, 137.2, 133.4, 132.0, 128.5, 127.3, 125.9, 110.7, 21.1, 17.8.

30b: ^{1}H NMR (500 MHz, Chloroform-*d*) δ 7.68 (d, *J* = 9.0 Hz, 1H), 7.46 (d, *J* = 14.5 Hz, 1H), 7.20 – 7.09 (m, 2H), 6.97 – 6.97 (m, 1H), 2.01 (s, 6H). ^{13}C NMR (126 MHz, Chloroform-*d*, mixture of **a and b**) δ 138.9, 138.6, 137.2, 133.4, 132.0, 128.5, 127.3, 125.9, 110.7, 21.1, 17.8.

MS (DART) exact mass: calculated for (M+H)$^{+}$: 207.0684; found: 207.0695.

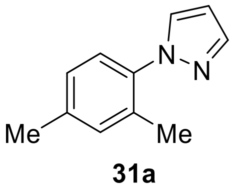

31a

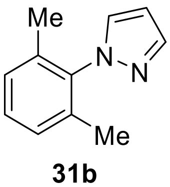

31b

1-(2,4-dimethylphenyl)-1H-pyrazole **(31a) and 1-(2,6-dimethylphenyl)-1H-pyrazole (31b):** The title compounds were prepared from m-xylene (2.0 mL) and 1H-pyrazole (0.4 mmol, 27.2 mg) according to general procedure E with an irradiation/electrolysis time of 72 hours. The crude residue was purified by column chromatography on silica gel with an eluent of hexanes to 10% EtOAc/hexanes to yield a light yellow oil in 71% (48.9 mg). The ratio of the mixture was 11:1 (***a:b***) as determined by ^{1}H NMR of reaction solution.

31a: ^{1}H NMR (500 MHz, Chloroform-*d*) δ 7.73 (s, 1H), 7.59 – 7.58 (m, 1H), 7.23 (d, *J* = 7.8 Hz, 1H), 7.14 (s, 1H), 7.10 (d, *J* = 8.0 Hz, 1H), 6.44 – 6.44 (m, 1H), 2.39 (s, 3H), 2.22 (s, 3H). ^{13}C NMR (126 MHz, Chloroform-*d*, mixture of **a and b**) δ 140.1, 138.3, 137.7, 133.5, 131.8, 130.6, 127.1, 126.0, 106.0, 21.1, 17.9.

31b: ^{1}H NMR (500 MHz, Chloroform-*d*) δ 7.76 (s, 1H), 7.48 – 7.47 (m, 1H), 7.24 – 7.09 (m, 3H), 6.47 (s, 1H), 2.03 (s, 6H). ^{13}C NMR (126 MHz, Chloroform-*d*, mixture of **a and b**) δ 140.1, 138.3, 137.7, 133.5, 131.8, 130.6, 127.1, 126.0, 106.0, 21.1, 17.9.

MS (DART) exact mass: calculated for $(M+H)^+$: 173.1073; found: 173.1083.

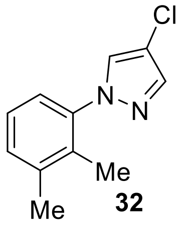

32

4-chloro-1-(2,3-dimethylphenyl)-1H-pyrazole **(32)**: The title compound was prepared from *o*-xylene (2.0 mL) and 4-chloro-1H-pyrazole (0.4 mmol, 41.0 mg) according to general procedure E with an irradiation/electrolysis time of 72 hours. The crude residue was purified by column chromatography on silica gel with an eluent of hexanes to 10% EtOAc/hexanes to yield a colorless oil in 61% yield (50.4 mg).

32: ^{1}H NMR (500 MHz, Chloroform-*d*) δ 7.88 (s, 1H), 7.64 (s, 1H), 7.45 (d, *J* = 2.4 Hz, 1H), 7.34 (dd, *J* = 8.1, 2.5 Hz, 1H), 7.22 (d, *J* = 8.1 Hz, 1H), 2.34 (2, 3H), 2.31 (2, 3H). ^{13}C NMR (126 MHz, Chloroform-*d*) δ 139.1, 138.1, 137.8, 135.6, 130.5, 124.8, 120.4, 116.3, 111.9, 20.0, 19.3.

MS (DART) exact mass: calculated for $(M+H)^+$: 207.0684; found: 207.0694.

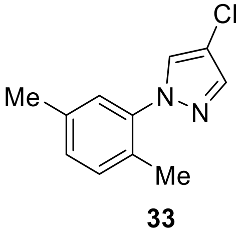

33

4-chloro-1-(2,5-dimethylphenyl)-1H-pyrazole **(33)**: The title compound was prepared from *p*-xylene (2.0 mL) and 4-chloro-1H-pyrazole (0.4 mmol, 41.0 mg) according to general procedure E with an irradiation/electrolysis time of 72 hours. The crude residue was purified by column chromatography on silica gel with an eluent of hexanes to 10% EtOAc/hexanes to yield a colorless oil in 56% yield (46.3 mg).

33: ^{1}H NMR (500 MHz, Chloroform-*d*) δ 7.63 (s, 1H), 7.58 (s, 1H), 7.20 – 7.18 (m, 1H), 7.16 – 7.10 (m, 2H), 2.35 (s, 3H), 2.20 (s, 3H). ^{13}C NMR (126 MHz, Chloroform-*d*) δ 139.3, 138.7, 136.6, 131.2, 130.2, 129.6, 128.4, 126.5, 110.8, 20.7, 17.5.

MS (DART) exact mass: calculated for $(M+H)^+$: 207.0684; found: 207.0696.

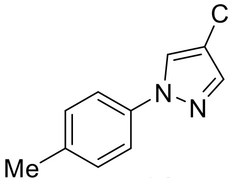

34a

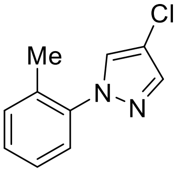

34b

4-chloro-1-(p-tolyl)-1H-pyrazole **(34a) and** ***4-chloro-1-(o-tolyl)-1H-pyrazole*** **(34b)**: The title compounds were prepared from toluene (2.0 ml), 4-chloro-1H-pyrazole (0.4 mmol, 41.0 mg) according to general procedure B with an irradiation time of 72 hours. The crude residue was purified by column chromatography on silica gel with an eluent of hexanes to 10% EtOAc/hexanes to yield a colorless oil in 55% (42.4 mg). The ratio of the mixture was 7:1 (*p*:*o*) as determined by ^{1}H NMR of reaction solution.

34a: ^{1}H NMR (500 MHz, Chloroform-*d*) δ 7.89 (s, 1H), 7.64 (s, 1H), 7.57 – 7.49 (m, 2H), 7.28 – 7.26 (m, 2H), 2.41 (s, 3H). ^{13}C NMR (126 MHz, Chloroform-*d*, mixture of **a and b**) δ 139.3, 139.2, 137.6, 137.0, 130.1, 129.3, 127.81, 124.8, 119.8, 119.0, 112.1, 21.5, 21.0.

34b: ^{1}H NMR (500 MHz, Chloroform-*d*) δ 7.92 (s, 1H), 7.65 (s, 1H), 7.57 – 7.49 (m, 1H), 7.44 – 7.41 (m, 1H), 7.37 – 7.34 (m, 1H), 7.16 – 7.14 (m, 1H), 2.44 (s, 3H). ^{13}C NMR (126 MHz, Chloroform-*d*, mixture of **a and b**) δ 139.3, 139.2, 137.6, 137.0, 130.1, 129.3, 127.81, 124.8, 119.8, 119.0, 112.1, 21.5, 21.0.

MS (DART) exact mass: calculated for $(M+H)^+$:193.0527; found:193.0539.

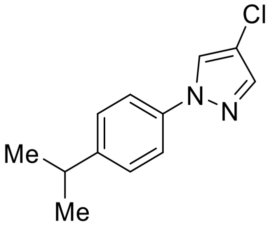

35a

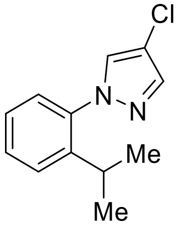

35b

4-chloro-1-(4-isopropylphenyl)-1H-pyrazole **(35a) and** ***4-chloro-1-(2-isopropylphenyl)-1H-pyrazole*** **(35b)**: The title compounds were prepared from cumene (2.0 ml), 4-chloro-1H-pyrazole (0.4 mmol, 41.0 mg) according to general procedure B with an irradiation time of 72 hours. The crude residue was purified by column chromatography on silica gel with an eluent of hexanes to 10% EtOAc/hexanes to yield a colorless oil in 45% (39.7 mg). The ratio of the mixture was 6:1 (*p*:*o*) as determined by ^{1}H NMR of reaction solution.

35a: ^{1}H NMR (500 MHz, Chloroform-*d*) δ 7.89 (s, 1H), 7.65 (s, 1H), 7.57 – 7.55 (m, 2H), 7.34 – 7.32 (m, 2H), 3.02 – 2.93 (m, 1H), 1.30 (d, *J* = 7.2 Hz, 6H). ^{13}C NMR (126 MHz, Chloroform-*d*, mixture of **a and b**) δ 148.0, 139.3, 139.2, 137.8, 129.4, 128.3, 127.5, 126.4, 124.8, 119.1, 116.5, 112.0, 34.2, 33.7, 24.0.

35b: ^{1}H NMR (500 MHz, Chloroform-*d*) δ 7.93 (s, 1H), 7.66 (s, 1H), 7.46 – 7.39 (m, 3H), 7.28 – 7.20 (m, 1H), 3.02 – 2.93 (m, 1H), 1.30 – 1.27 (m, 6H). ^{13}C NMR (126 MHz, Chloroform-*d*, mixture of **a and b**) δ 148.0, 139.3, 139.2, 137.8, 129.4, 128.3, 127.5, 126.4, 124.8, 119.1, 116.5, 112.0, 34.2, 33.7, 24.0.

MS (DART) exact mass: calculated for $(M+H)^+$:221.0840; found: 221.0852.

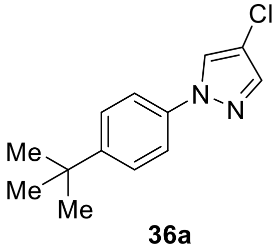

36a

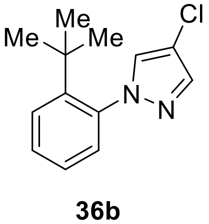

36b

1-(4-(tert-butyl)phenyl)-4-chloro-1H-pyrazole **(36a)** **and** ***1-(2-(tert-butyl)phenyl)-4-chloro-1H-pyrazole*** **(36b)**: The title compounds were prepared from tert-butylbenzene (2.0 ml), 4-chloro-1H-pyrazole (0.4 mmol, 41.0 mg) according to general procedure B with an irradiation time of 72 hours. The crude residue was purified by column chromatography on silica gel with an eluent of hexanes to 10% EtOAc/hexanes to yield a colorless oil in 62% (58.2 mg). The ratio of the mixture was 4:1 (*p*:*o*) as determined by ^{1}H NMR of reaction solution.

36a: ^{1}H NMR (500 MHz, Chloroform-*d*) δ 7.89 (s, 1H), 7.65 (s, 1H), 7.58 – 7.56 (m, 2H), 7.50 – 7.48 (m, 2H), 1.37 (s, 9H). ^{13}C NMR (126 MHz, Chloroform-*d*, mixture of **a and b**) δ 153.2, 150.2, 139.2, 137.8, 137.4, 130.4, 130.2, 129.2, 126.4, 125.1, 124.8, 124.2, 118.7, 116.5, 116.3, 112.1, 34.6, 31.4, 31.3, 31.3.

36b: ^{1}H NMR (500 MHz, Chloroform-*d*) δ 7.93 (s, 1H), 7.70 (s, 1H), 7.76 – 7.76 (m, 1H), 7.42 – 7.40 (m, 2H), 7.29 – 7.28 (m, 1H), 1.39 (s, 9H). ^{13}C NMR (126 MHz, Chloroform-*d*, mixture of **a and b**) δ 153.2, 150.2, 139.2, 137.8, 137.4, 130.4, 130.2, 129.2, 126.4, 125.1, 124.8, 124.2, 118.7, 116.5, 116.3, 112.1, 34.6, 31.4, 31.3, 31.3.

MS (DART) exact mass: calculated for $(M+H)^+$:235.0997; found: 235.1008.

Substratres for Table 4-2 (entries 1-18):

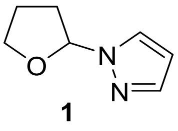

1

1-(tetrahydrofuran-2-yl)-1H-pyrazole **(1)**: The title compound was prepared from tetrahydrofuran (2.0 mL) and 1H-pyrazole (0.4 mmol, 27.2 mg) according to general procedure C with an irradiation/electrolysis time of 36 hours. The crude residue was purified by column chromatography on silica gel with an eluent of hexanes to 30% EtOAc/hexanes to yield a colorless oil in 75% yield (41.5 mg).

1: ^{1}H NMR (500 MHz, Chloroform-*d*) δ 7.55 (s, 2H), 6.27 – 7.26 (m, 1H), 6.00 – 5.98 (m, 1H), 4.14 – 4.09 (m, 1H), 4.00 – 3.96 (m, 1H), 2.63 – 2.57 (m, 1H), 2.36 – 2.29 (m, 1H), 2.21 – 2.15 (m, 1H), 2.07 – 2.00 (m, 1H). ^{13}C NMR (126 MHz, Chloroform-*d*) δ 139.9, 128.0, 105.7, 90.0, 69.2, 31.7, 24.4.

MS (DART) exact mass: calculated for $(M+H)^+$: 139.0866; found: 139.0873.

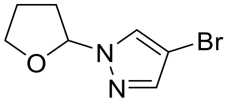

2

4-bromo-1-(tetrahydrofuran-2-yl)-1H-pyrazole **(2)**: The title compound was prepared from tetrahydrofuran (2.0 mL) and 4-bromo-1H-pyrazole (0.4 mmol, 58.8 mg) according to general procedure C with an irradiation/electrolysis time of 36 hours. The crude residue was purified by column chromatography on silica gel with an eluent of hexanes to 40% EtOAc/hexanes to yield a colorless oil in 79% yield (68.6 mg).

2: ^{1}H NMR (500 MHz, Chloroform-*d*) δ 7.59 (s, 1H), 7.49 (s, 1H), 5.94 (dd, *J* = 6.8, 2.4 Hz, 1H), 4.11 – 4.06 (m, 1H), 4.00 – 3.97 (m, 1H), 2.60 – 2.54 (m, 1H), 2.33 – 2.29 (m, 1H), 2.13 – 2.09 (m, 1H), 2.04 – 2.03 (m, 1H). ^{13}C NMR (126 MHz, Chloroform-*d*) δ 140.3, 128.1, 93.4, 90.6, 69.4, 31.7, 24.1.

MS (DART) exact mass: calculated for $(M+H)^+$: 216.9971; found:216.9982.

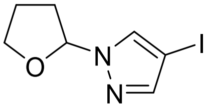

3

4-iodo-1-(tetrahydrofuran-2-yl)-1H-pyrazole **(3)**: The title compound was prepared from tetrahydrofuran (2.0 mL) and 4-iodo-1H-pyrazole (0.4 mmol, 77.6 mg) according to general procedure C with an irradiation/electrolysis time of 36 hours. The crude residue was purified by column chromatography on silica gel with an eluent of hexanes to 40% EtOAc/hexanes to yield a colorless oil in 82% yield (86.6 mg).

3: ^{1}H NMR (500 MHz, Chloroform-*d*) δ 7.59 (s, 1H), 7.51 (s, 1H), 5.94 (dd, *J* = 6.6, 2.4 Hz, 1H), 4.11 – 4.06 (m, 1H), 3.99 – 3.94 (m, 1H), 2.55 – 2.53 (m, 1H), 2.31 – 2.27 (m, 1H), 2.11 – 2.07 (m, 1H), 2.02 – 1.99 (m, 1H). ^{13}C NMR (126 MHz, Chloroform-*d*) δ 144.7, 132.5, 90.5, 69. 5, 56.6, 31.8, 24.1.

MS (DART) exact mass: calculated for $(M+H)^+$: 264.9832; found: 264.9846.

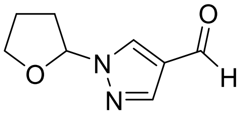

4

1-(tetrahydrofuran-2-yl)-1H-pyrazole-4-carbaldehyde **(4)**: The title compound was prepared from tetrahydrofuran (2.0 mL) and 1H-pyrazole-4-carbaldehyde (0.4 mmol, 38.4 mg) according to general procedure C with an irradiation/electrolysis time of 36 hours. The crude residue was purified by column chromatography on silica gel with an eluent of hexanes to 50% EtOAc/hexanes to yield a white solid in 85% yield (56.5 mg).

4: ^{1}H NMR (500 MHz, Chloroform-*d*) δ 9.83 (s, 1H), 8.09 (s, 1H), 7.96 (s, 1H), 5.98 (dd, *J* = 6.5, 2.1 Hz, 1H), 4.17 – 4.13 (m, 1H), 4.02 – 3.98 (m, 1H), 2.57 – 2.49 (m, 1H), 2.38 – 2.30 (m, 1H), 2.08 – 2.00 (m, 2H). ^{13}C NMR (126 MHz, Chloroform-*d*) δ 184.2, 140.9, 131.5, 124.0, 90.8, 69.8, 32.2, 23.8.

MS (DART) exact mass: calculated for $(M+H)^+$: 167.0815; found: 167.0825.

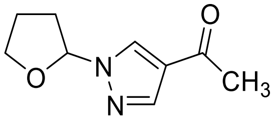

5

1-(1-(tetrahydrofuran-2-yl)-1H-pyrazol-4-yl)ethanone **(5)**: The title compound was prepared from tetrahydrofuran (2.0 mL) and 1-(1H-pyrazol-4-yl)ethanone (0.4 mmol, 44.0 mg) according to general procedure C with an irradiation/electrolysis time of 36 hours. The crude residue was purified by column chromatography on silica gel with an eluent of hexanes to 50% EtOAc/hexanes to yield a white solid in 72% yield (51.9 mg).

5: ^{1}H NMR (500 MHz, Chloroform-*d*) δ 8.07 (s, 1H), 7.95 (s, 1H), 6.00 (dd, *J* = 6.5, 2.3 Hz, 1H), 4.17 – 4.21 (m, 1H), 4.07 – 4.02 (m, 1H), 2.62 – 2.56 (m, 1H), 2.45 (s, 3H), 2.40 – 2.36 (m, 1H), 2.17 – 1.98 (m, 2H). ^{13}C NMR (126 MHz, Chloroform-*d*) δ 192.2, 140.7, 130.4, 123.9, 90.6, 69.7, 32.1, 27.9, 23.9.

MS (DART) exact mass: calculated for $(M+H)^+$: 181.0972; found: 181.0980.

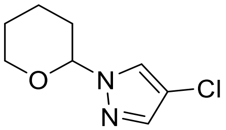

6

4-chloro-1-(tetrahydro-2H-pyran-2-yl)-1H-pyrazole **(6)**: The title compound was prepared from tetrahydro-2H-pyran (2.0 mL) and 4-chloro-1H-pyrazole (0.4 mmol, 41.0 mg) according to general procedure C with an irradiation/electrolysis time of 48 hours. The crude residue was purified by column chromatography on silica gel with an eluent of hexanes to 30% EtOAc/hexanes to yield a light yellow oil in 76% yield (56.7 mg).

6: ^{1}H NMR (500 MHz, Chloroform-*d*) δ 7.59 (s, 1H), 7.46 (s, 1H), 5.31 (dd, *J* = 7.5, 4.5 Hz, 1H), 4.06 – 3.99 (m, 1H), 3.72 – 3.64 (m, 1H), 2.08 – 1.98 (m, 3H), 1.73 – 1.58 (m, 3H). ^{13}C NMR (126 MHz, Chloroform-*d*) δ 137.9, 125.7, 110.7, 88.0, 67.7, 30.3, 24.9, 22.1.

MS (DART) exact mass: calculated for $(M+H)^+$: 187.0633; found: 187.0642.

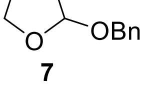

7

2-(benzyloxy)tetrahydrofuran **(7)**: The title compound was prepared from tetrahydrofuran (2.0 mL) and benzyl alcohol (0.4 mmol, 41.6 µL) according to general procedure C with an irradiation/electrolysis time of 24 hours. The crude residue was purified by column chromatography on silica gel with an eluent of hexanes to 30% EtOAc/hexanes to yield a light yellow oil in 55% yield (39.2 mg).

7: ^{1}H NMR (500 MHz, Chloroform-*d*) δ 7.40 – 7.29 (m, 5H), 5.25 (dd, *J* = 4.3, 2.0 Hz, 1H), 4.75 (d, *J* = 11.9 Hz, 1H), 4.50 (d, *J* = 11.8 Hz, 1H), 4.03 – 3.87 (m, 2H), 2.13 – 1.83 (m, 4H). ^{13}C NMR (126 MHz, Chloroform-*d*) δ 138.4, 128.4, 127.9, 127.5, 103.1, 68.8, 67.0, 32.4, 23.5.

MS (DART) exact mass: calculated for $(M+H)^+$: 179.1067; found: 179.1072.

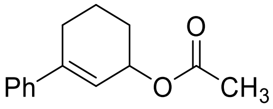

8

3,4,5,6-tetrahydro-[1,1'-biphenyl]-3-yl acetate **(8)**: The title compound was prepared from 1-phenyl-1-cyclohexene (0.4 mmol, 63.3 mg, 63.7 µL) according to general procedure D with an irradiation/electrolysis time of 10 hours. The crude residue was purified by column chromatography on silica gel with an eluent of hexanes to 30% EtOAc/hexanes to yield a colorless oil in 51% yield (44.1 mg).

8: ^{1}H NMR (500 MHz, Chloroform-*d*) δ 7.47 – 7.41 (m, 2H), 7.37 – 7.34 (m, 2H), 7.33 – 7.26 (m, 1H), 6.18 – 6.06 (m, 1H), 5.5. – 5.48 (m, 1H), 2.60 – 2.51 (m, 1H), 2.46 – 2.37 (m, 1H), 2.10 (s, 3H), 2.02 – 1.90 (m, 2H), 1.89 – 1.77 (m, 2H). ^{13}C NMR (126 MHz, Chloroform-*d*) δ 170.9, 142.2, 141.1, 128.3, 127.7, 125.5, 122.3, 69.0, 28.0, 27.4, 21.5, 19.5.

MS (DART) exact mass: calculated for $(M-CH_3CO)^+$: 173.0966; found: 173.0964.

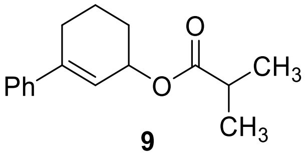

9

3,4,5,6-tetrahydro-[1,1'-biphenyl]-3-yl isobutyrate **(9)**: The title compound was prepared from 1-phenyl-1-cyclohexene (0.4 mmol, 63.3 mg, 63.7 µL) according to general procedure D with an irradiation/electrolysis time of 10 hours. The crude residue was purified by column chromatography on silica gel with an eluent of hexanes to 30% EtOAc/hexanes to yield a colorless oil in 65% yield (63.8 mg).

9: ^{1}H NMR (500 MHz, Chloroform-*d*) δ 7.49 – 7.40 (m, 2H), 7.40 – 7.29 (m, 3H), 6.15 – 6.04 (m, 1H), 5.53 – 5.42 (m, 1H), 2.65 – 2.51 (m, 2H), 2.49 – 2.35 (m, 1H), 2.03 – 1.90 (m, 2H), 1.90 – 1.74 (m, 2H), 1.21 (dd, *J* = 7.0, 2.2 Hz, 6H). ^{13}C NMR (126 MHz, Chloroform-*d*) δ 177.0, 142.0, 141.2, 128.3, 127.6, 125.5, 122.5, 68.6, 34.2, 28.1, 27.4, 19.5, 19.1, 19.0.

MS (DART) exact mass: calculated for $(M-CH_3CO)^+$: 173.0966; found: 173.0968.

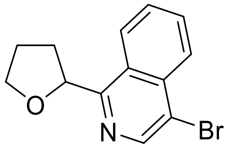

10

***4-bromo-1-(tetrahydrofuran-2-yl)isoquinoline* (10)**: The title compound was prepared from tetrahydrofuran (2.0 mL) and 4-bromoisoquinoline (0.4 mmol, 83.2 mg) according to general procedure B with an irradiation/electrolysis time of 48 hours. The crude residue was purified by column chromatography on silica gel with an eluent of hexanes to 30% EtOAc/hexanes to yield a light yellow oil in 75% yield (83.4 mg).

10: ^{1}H NMR (500 MHz, Chloroform-*d*) δ 8.66 (s, 1H), 8.33 (d, *J* = 8.5 Hz, 1H), 8.17 (d, *J* = 8.4 Hz, 1H), 7.78 – 7.74 (m, 1H), 7.66 – 7.63 (m, 1H), 5.66 (t, *J* = 7.0 Hz, 1H), 4.15 – 4.11 (m, 1H), 4.03 – 3.98 (m, 1H), 2.53 – 2.49 (m, 1H), 2.38 – 2.36 (m, 1H), 2.18 – 2.03 (m, 2H). ^{13}C NMR (126 MHz, Chloroform-*d*) δ 159.2, 143.2, 135.1, 131.1, 128.0, 127.9, 126.6, 125.7, 119.3, 78.8, 69.1, 30.6, 26.1.

MS (DART) exact mass: calculated for $(M+H)^+$: 278.0175; found: 278.0187.

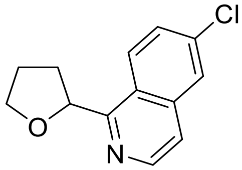

11

***6-Chloro-1-(tetrahydrofuran-2-yl)isoquinoline* (11)**: The title compound was prepared from tetrahydrofuran (2.0 mL) and 6-chloroisoquinoline (0.4 mmol, 65.4 mg) according to general procedure C with an irradiation/electrolysis time of 48 hours. The crude residue was purified by column chromatography on silica gel with an eluent of hexanes to 20% EtOAc/hexanes to yield a colorless oil in 80% yield (74.8 mg).

11: ^{1}H NMR (500 MHz, Chloroform-*d*) δ 8.51 (d, *J* = 5.7 Hz, 1H), 8.34 (d, *J* = 9.0 Hz, 1H), 7.82 (d, *J* = 2.1 Hz, 1H), 7.54 (dd, *J* = 9.0, 2.1 Hz, 1H), 7.50 (d, *J* = 5.7 Hz, 1H), 5.66 (t, *J* = 7.1 Hz, 1H), 4.19 - 4.14 (m, 1H), 4.06 – 4.02 (m, 1H), 2.60 – 2.50 (m, 1H), 2.44 – 2.36 (m, 1H), 2.22 – 2.09 (m, 2H). ^{13}C NMR (126 MHz, Chloroform-*d*) δ 159.8, 142.6, 137.4, 136.1, 128.1, 127.4, 126.0, 124.9, 119.6, 79.3, 69.0, 30.5, 26.1.

MS (DART) exact mass: calculated for $(M+H)^+$: 234.0680; found: 234.0688.

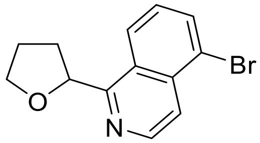

12

***5-Bromo-1-(tetrahydrofuran-2-yl)isoquinoline* (12)**: The title compound was prepared from tetrahydrofuran (2.0 mL) and 5-bromoisoquinoline (0.4 mmol, 83.2 mg) according to general procedure C with an irradiation/electrolysis time of 48 hours. The crude residue was purified by column chromatography on silica gel with an eluent of hexanes to 20% EtOAc/hexanes to yield a colorless oil in 77% yield (85.7 mg).

12: ^{1}H NMR (500 MHz, Chloroform-*d*) δ ^{1}H NMR (500 MHz, Chloroform-*d*) δ 8.60 (d, *J* = 5.9 Hz, 1H), 8.35 (d, *J* = 8.5 Hz, 1H), 8.03 – 7.88 (m, 2H), 7.47 - 7.43 (m, 1H), 5.71 (t, *J* = 7.0 Hz, 1H), 4.18-4.14 (m, 1H), 4.06-4.01 (m, 1H), 2.59-2.54 (m, 1H), 2.42 – 2.38 (m, 1H), 2.19-2.10 (m, 2H). ^{13}C NMR (126 MHz, Chloroform-*d*) δ 160.0, 142.9, 135.6, 133.6, 127.8, 127.4, 125.1, 122.3, 119.4, 79.0, 69.1, 30.6, 26.1.

MS (DART) exact mass: calculated for $(M+H)^+$: 278.0175; found: 278.0186.

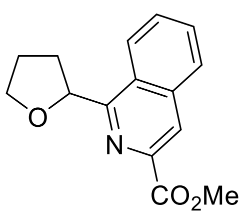

13

***Methyl 1-(tetrahydrofuran-2-yl)isoquinoline-3-carboxylate* (13)**: The title compound was prepared from tetrahydrofuran (2.0 mL) and methyl isoquinoline-3-carboxylate (0.4 mmol, 74.9 mg) according to general procedure C with an irradiation/electrolysis time of 60 hours. The crude residue was purified by column chromatography on silica gel with an eluent of hexanes to 30% EtOAc/hexanes to yield a white solid in 60% yield (61.8 mg).

13: ^{1}H NMR (500 MHz, Chloroform-*d*) δ 8.51 – 8.51 (m, 2H), 7.98 – 7.96 (m, 1H), 7.76 – 7.73 (m, 2H), 5.68 (t, *J* = 7.2 Hz, 1H), 4.22 – 4.14 (m, 1H), 4.07 – 4.04 (m, 4H), 2.76 – 2.67 (m, 1H), 2.47 – 2.39 (m, 1H), 2.27 – 2.11 (m, 2H). ^{13}C NMR (126 MHz, Chloroform-*d*) δ 166.5, 160.0, 140.0, 136.4, 130.5, 129.3, 128.8, 128.2, 126.0, 124.2, 80.5, 69.0, 52.7, 30.2, 26.1.

MS (DART) exact mass: calculated for $(M+H)^+$: 258.1125; found: 258.1135.

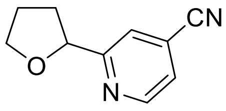

14

***2-(Tetrahydrofuran-2-yl)isonicotinonitrile* (14)**: The title compound was prepared from tetrahydrofuran (2.0 mL) and 4-pyridinecarbonitrile (0.4 mmol, 41.6 mg) according to general procedure C with an irradiation/electrolysis time of 72 hours. The crude residue was purified by column chromatography on silica gel with an eluent of hexanes to 30% EtOAc/hexanes to yield a yellow oil in 56% yield (39.0 mg).

14: ^{1}H NMR (500 MHz, Chloroform-*d*) δ 8.74 (d, *J* = 4.9 Hz, 1H), 7.74 (s, 1H), 7.41 (d, *J* = 4.9 Hz, 1H), 5.08 (t, *J* = 6.7 Hz, 1H), 4.19 – 4.09 (m, 1H), 4.05 – 4.00 (m, 1H), 2.54 – 2.46 (m, 1H), 2.06 – 1.95 (m, 3H). ^{13}C NMR (126 MHz, Chloroform-*d*) δ 165.3, 149.9, 123.4, 121.6, 120.9, 116.8, 80.7, 69.3, 33.1, 25.7.

MS (DART) exact mass: calculated for $(M+H)^+$: 175.0866; found: 175.0873.

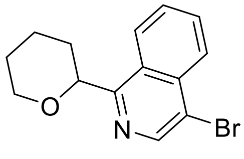

15

4-Bromo-1-(tetrahydro-2H-pyran-2-yl)isoquinoline **(15)**: The title compound was prepared from tetrahydropyran (2.0 mL) and 4-bromoisoquinoline (0.4 mmol, 83.2 mg) according to general procedure C with an irradiation/electrolysis time of 60 hours. The crude residue was purified by column chromatography on silica gel with an eluent of hexanes to 15% EtOAc/hexanes to yield a white solid in 60% yield (70.1 mg).

15: ^{1}H NMR (500 MHz, Chloroform-*d*) δ 8.73 (s, 1H), 8.40 (d, *J* = 8.5 Hz, 1H), 8.22 (d, *J* = 8.5 Hz, 1H), 7.81 (ddd, *J* = 8.4, 6.9, 1.2 Hz, 1H), 7.68 (ddd, *J* = 8.3, 6.8, 1.3 Hz, 1H), 5.16 (dd, *J* = 10.9, 2.3 Hz, 1H), 4.34 – 4.21 (m, 1H), 3.83 – 3.77 (m, 1H), 2.17 – 1.64 (m, 6H). ^{13}C NMR (126 MHz, Chloroform-*d*) δ 159.3, 143.5, 135.2, 131.1, 127.9, 127.4, 126.7, 125.7, 119.3, 79.0, 69.5, 31.0, 25.9, 23.8.

MS (DART) exact mass: calculated for $(M+H)^+$: 292.0332; found: 292.0343.

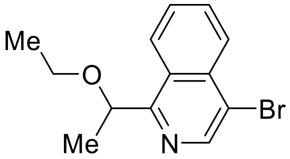

16

4-Bromo-1-(1-ethoxyethyl)isoquinoline **(16)**: The title compound was prepared from diethyl ether (2.0 mL) and 4-bromoisoquinoline (0.4 mmol, 83.2 mg) according to general procedure C with an irradiation/electrolysis time of 72 hours. The crude residue was purified by column chromatography on silica gel with an eluent of hexanes to 15% EtOAc/hexanes to yield a colorless oil in 45% yield (50.4 mg).

16: ^{1}H NMR (500 MHz, Chloroform-*d*) δ 8.74 (d, *J* = 8.6 Hz, 1H), 8.68 (s, 1H), 8.27 – 8.22 (m, 1H), 7.84 – 7.81 (m, 1H), 7.69 – 7.66 (m, 1H), 5.16 (q, *J* = 6.8 Hz, 1H), 3.57 – 3.50 (m, 1H), 3.45 – 3.38 (m, 1H), 1.71 (d, *J* = 6.7 Hz, 3H), 1.21 (t, *J* = 7.0 Hz, 3H). ^{13}C NMR (126 MHz, Chloroform-*d*) δ 161.5, 143.3, 135.3, 131.2, 127.8, 127.4, 126.8, 125.9, 119.3, 79.7, 64.6, 21.6, 15.5.

MS (DART) exact mass: calculated for $(M - EtO)^+$: 233.9918; found: 233.9922.

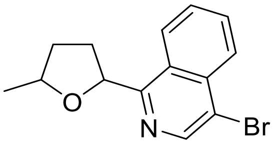

17

***4-Bromo-1-(5-methyltetrahydrofuran-2-yl)isoquinoline* (17)**: The title compound was prepared from 2-methyltetrahydrofuran (2.0 mL) and 4-bromoisoquinoline (0.4 mmol, 83.2 mg) according to general procedure C with an irradiation/electrolysis time of 72 hours. The crude residue was purified by column chromatography on silica gel with an eluent of hexanes to 15% EtOAc/hexanes to yield a white solid (diastereoisomers, d.r. 1.1:1) in 55% yield (64.3 mg).

17: ^{1}H NMR (500 MHz, Chloroform-*d*) δ 8.70 (s, 1H), 8.47 – 8.45 (m, 1H), 8.22 – 8.20 (m, 1H), 7.82 – 7.78 (m, 1H), 7.72 – 7.65 (m, 1H), 5.73 (t, *J* = 7.1 Hz, 1H), 4.45 – 4.27 (m, 1H), 2.69 – 2.56 (m, 1H), 2.49 – 2.19 (m, 2H), 1.81 – 1.72 (m, 1H), 1.39 – 1.37 (d, *J* = 6.1 Hz, 3H). ^{13}C NMR (126 MHz, Chloroform-*d*) δ 159.7, 158.8, 143.3, 143.2, 135.2, 135.1, 131.1, 131.1, 128.2, 128.0, 128.0, 127.9, 126.6, 126.6, 126.1, 125.7, 119.4, 119.2, 79.5, 78.2, 77.0, 76.1, 34.0, 33.2, 31.2, 30.2, 21.4, 21.2.

MS (DART) exact mass: calculated for $(M+H)^+$: 292.0332; found: 292.0341.

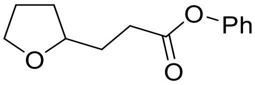

18

***Phenyl 3-(tetrahydrofuran-2-yl)propanoate* (18)**: The title compound was prepared from tetrahydrofuran (2.0 mL) and phenyl acrylate (0.4 mmol, 59.3 mg) according to general procedure D with an irradiation/electrolysis time of 48 hours. The crude residue was purified by column chromatography on silica gel with an eluent of hexanes to 10% EtOAc/hexanes to yield a colorless oil in 53% yield (46.7 mg).

18: ^{1}H NMR (500 MHz, Chloroform-*d*) δ 7.41 - 7.38 (m, 2H), 7.25 – 7.23 (m, 1H), 7.10 (d, *J* = 8.0 Hz, 2H), 3.98 – 3.87 (m, 2H), 3.80 – 3.77 (m, 1H), 2.74 – 2.67 (m, 2H), 2.07 – 1.92 (m, 5H), 1.58 – 1.54 (m, 1H). ^{13}C NMR (126 MHz, Chloroform-*d*) δ 172.2, 150.8, 129.4, 125.7, 121.6, 78.1, 67.8, 31.3, 31.3, 30.7, 25.8.

MS (DART) exact mass: calculated for $(M - PhO)^+$: 127.0759; found: 127.0761.

13. References

1. M. Silvi, C. Verrier, Y. P. Rey, L. Buzzetti, P. Melchiorre, Visible-light excitation of iminium ions enables the enantioselective catalytic β-alkylation of enals. *Nature Chemistry* **9,** 868–873 (2017).

2. E. M. Simmons, J. F. Hartwig, On the Interpretation of Deuterium Kinetic Isotope Effects in C-H Bond Functionalizations by Transition-Metal Complexes. *Angewandte Chemie International Edition* **51,** 3066–3072 (2012).

3. Sheldrick, G. M. *SHELXTL*, an integrated system for solving, refining, and displaying crystal structures from diffraction data; University of Göttingen, Göttingen, Federal Republic of Germany. (1981).

4. Sheldrick, G, M, *SHELXT* – Integrated space-group and crystal-structure determination. *Acta Crystallographica Section A.* **71**, 3-8 (2015).

5. Sheldrick, G, M, A short history of *SHELX*. *Acta Crystallographica Section A.* **64**, 112-122 (2008).

6. F. Neese, The ORCA program system. *Wiley Interdisciplinary Reviews: Computational Molecular Science* **2,** 73–78 (2011).

7. W. Humphrey, A. Dalke, K. Schulten, VMD: Visual molecular dynamics. *Journal of Molecular Graphics* **14,** 33–38 (1996).

8. M. Petersilka, U. J. Gossmann, E. K. U. Gross, Excitation Energies from Time-Dependent Density-Functional Theory. *Physical Review Letters* **76,** 1212–1215 (1996).

9. A. K. Dutta, F. Neese, R. Izsák, Towards a pair natural orbital coupled cluster method for excited states. *The Journal of Chemical Physics* **145,** 034102 (2016).

NMR Spectral Data

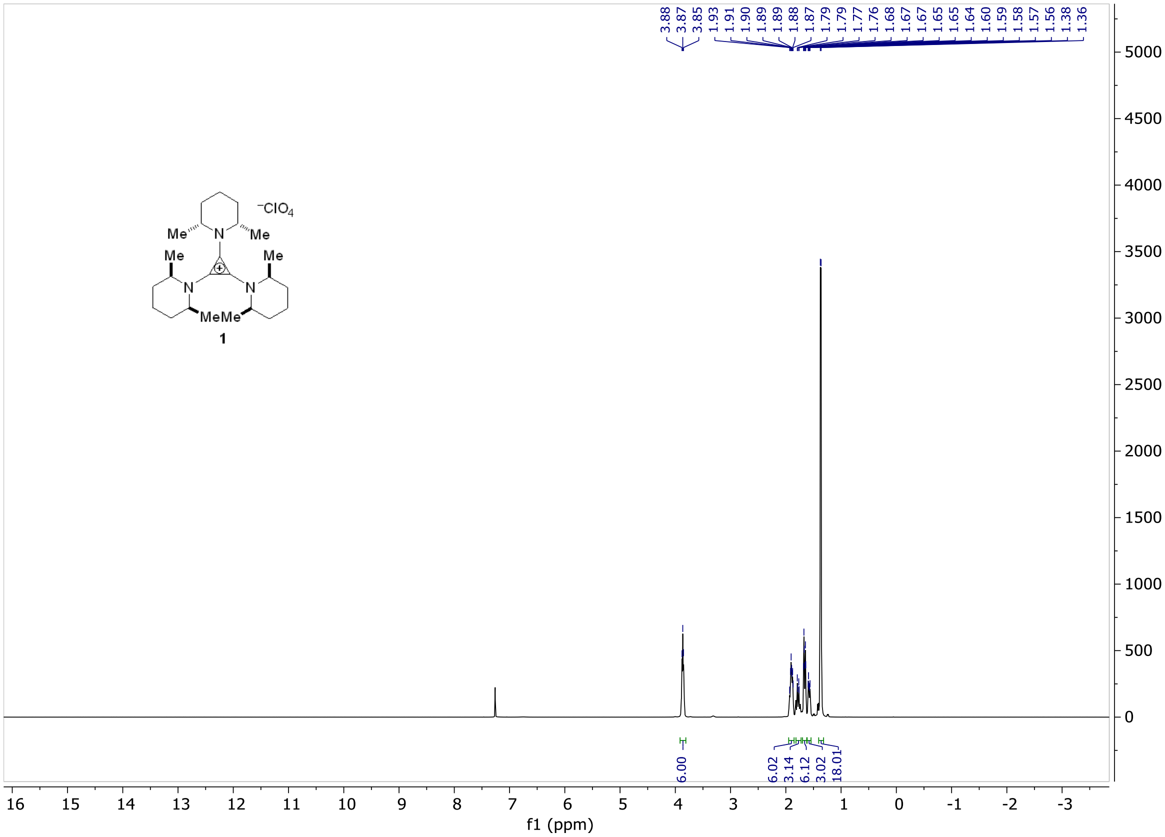

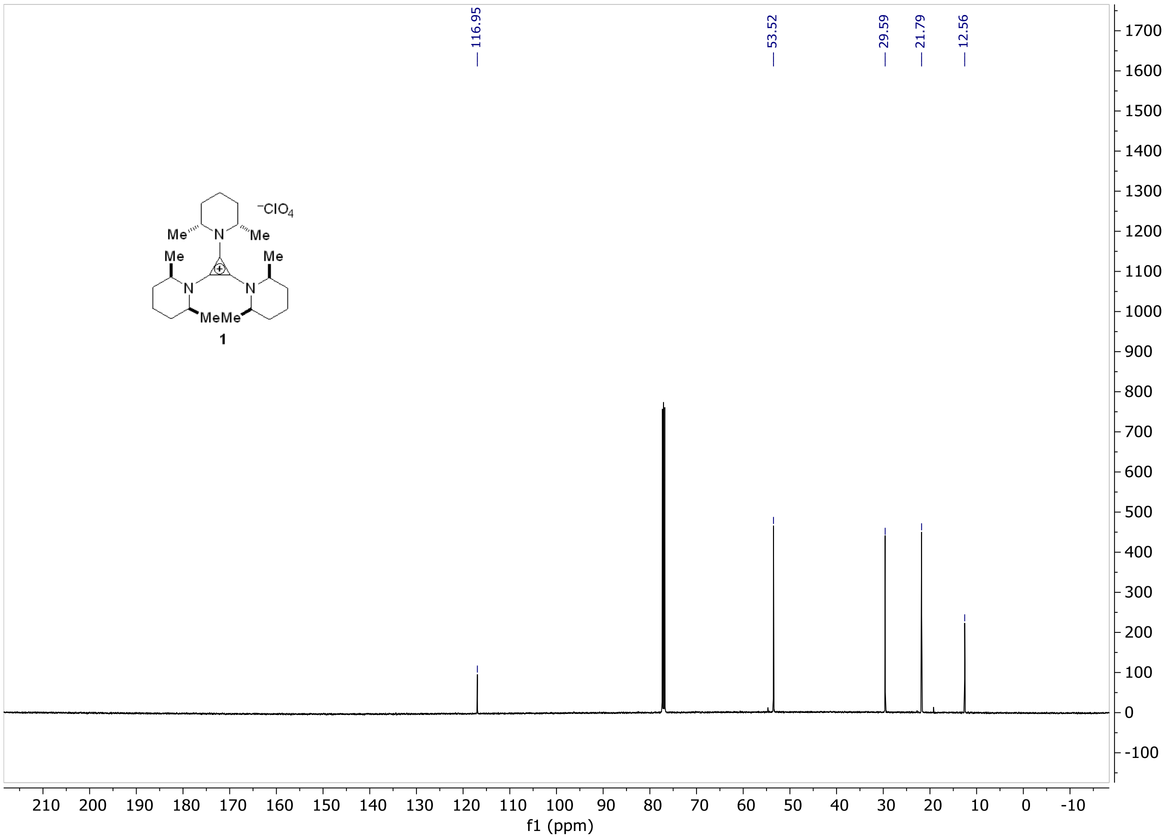

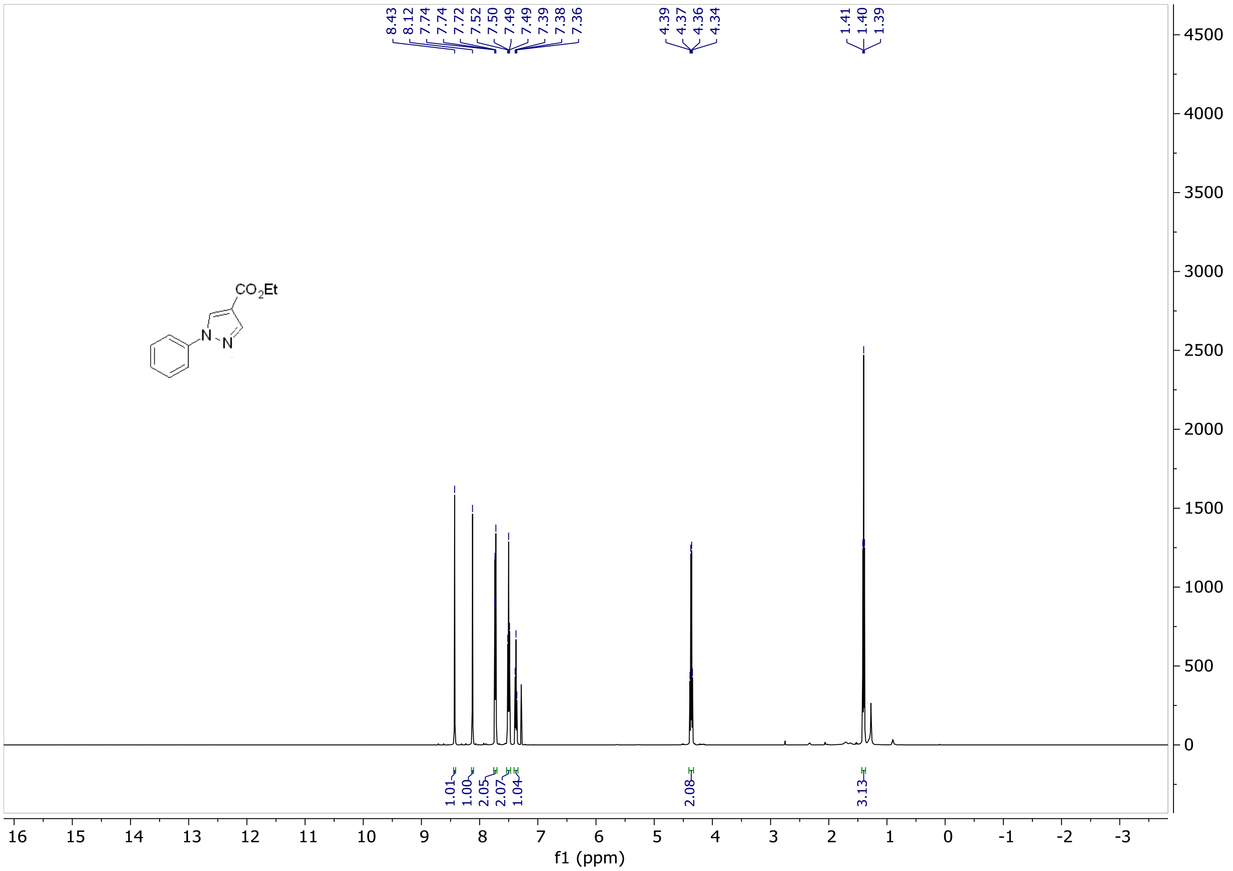
8.43
8.12
7.74
7.74
7.72
7.52
7.50
7.49
7.49
7.39
7.38
7.36
4.39
4.37
4.36
4.34
1.41
1.40
1.39
CO2Et
N
N
1.01
1.00
2.05
2.07
1.04
2.08
3.13
4500
4000
3500
3000
2500
2000
1500
1000
500
0
16 15 14 13 12 11 10 9 8 7 6 5 4 3 2 1 0 -1 -2 -3
f1 (ppm)

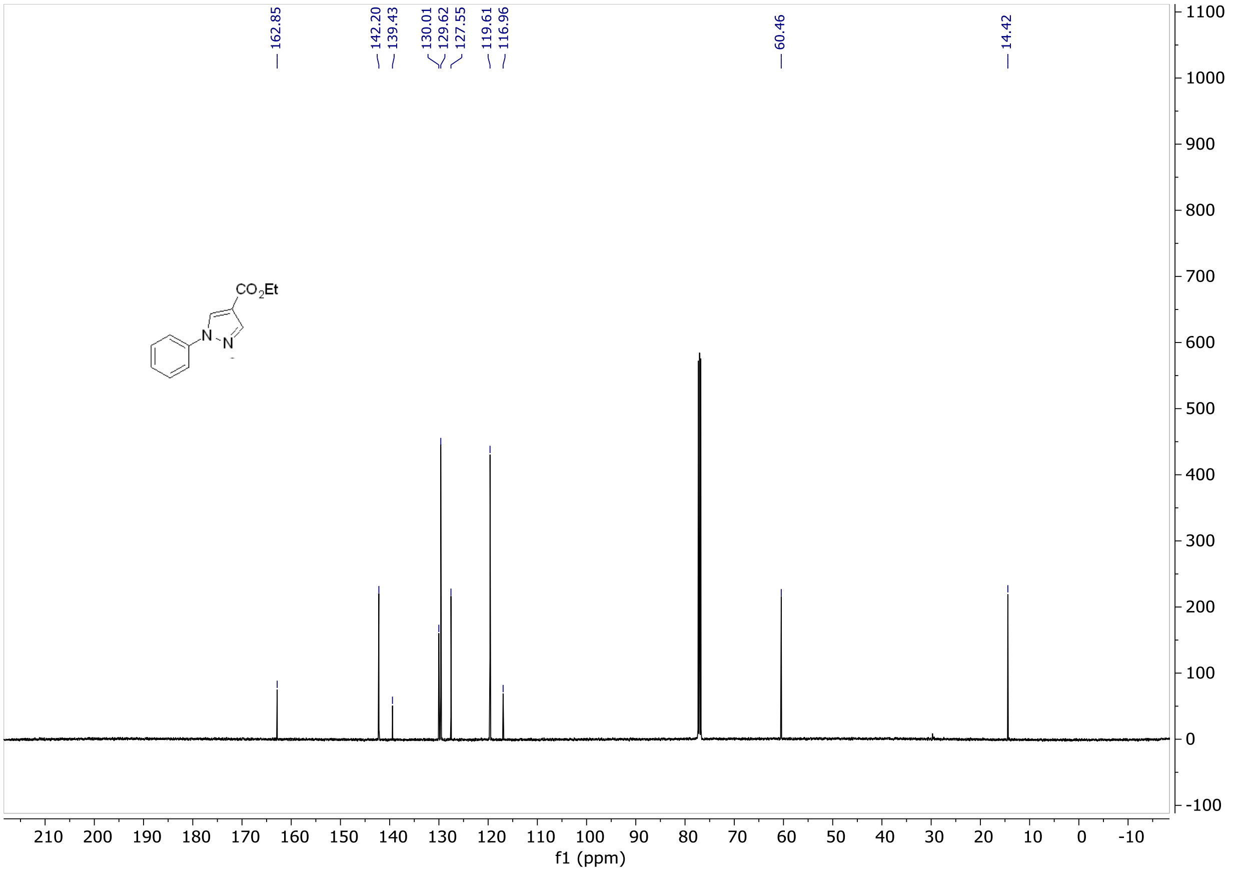
162.85
142.20
139.43
130.01
129.62
127.55
119.61
116.96
60.46
14.42
CO2Et
N
N
1100
1000
900
800
700
600
500
400
300
200
100
0
-100
210 200 190 180 170 160 150 140 130 120 110 100 90 80 70 60 50 40 30 20 10 0 -10
f1 (ppm)

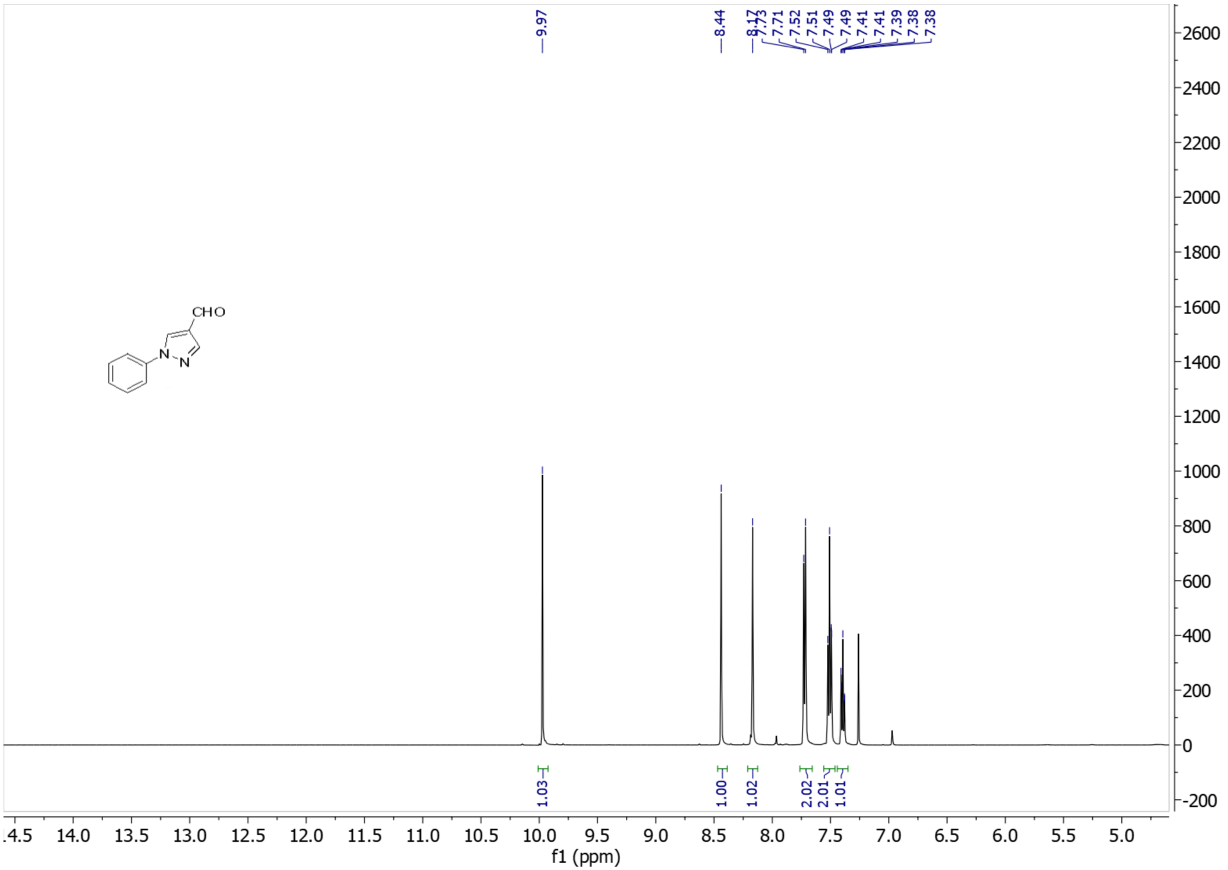
9.97
8.44
8.17
7.73
7.71
7.52
7.51
7.49
7.49
7.41
7.39
7.38
7.38
CHO
N
N
1.03
1.00
1.02
2.02
2.01
1.01
2600
2400
2200
2000
1800
1600
1400
1200
1000
800
600
400
200
0
-200
14.5
14.0
13.5
13.0
12.5
12.0
11.5
11.0
10.5
10.0
9.5
9.0
8.5
8.0
7.5
7.0
6.5
6.0
5.5
5.0
f1 (ppm)

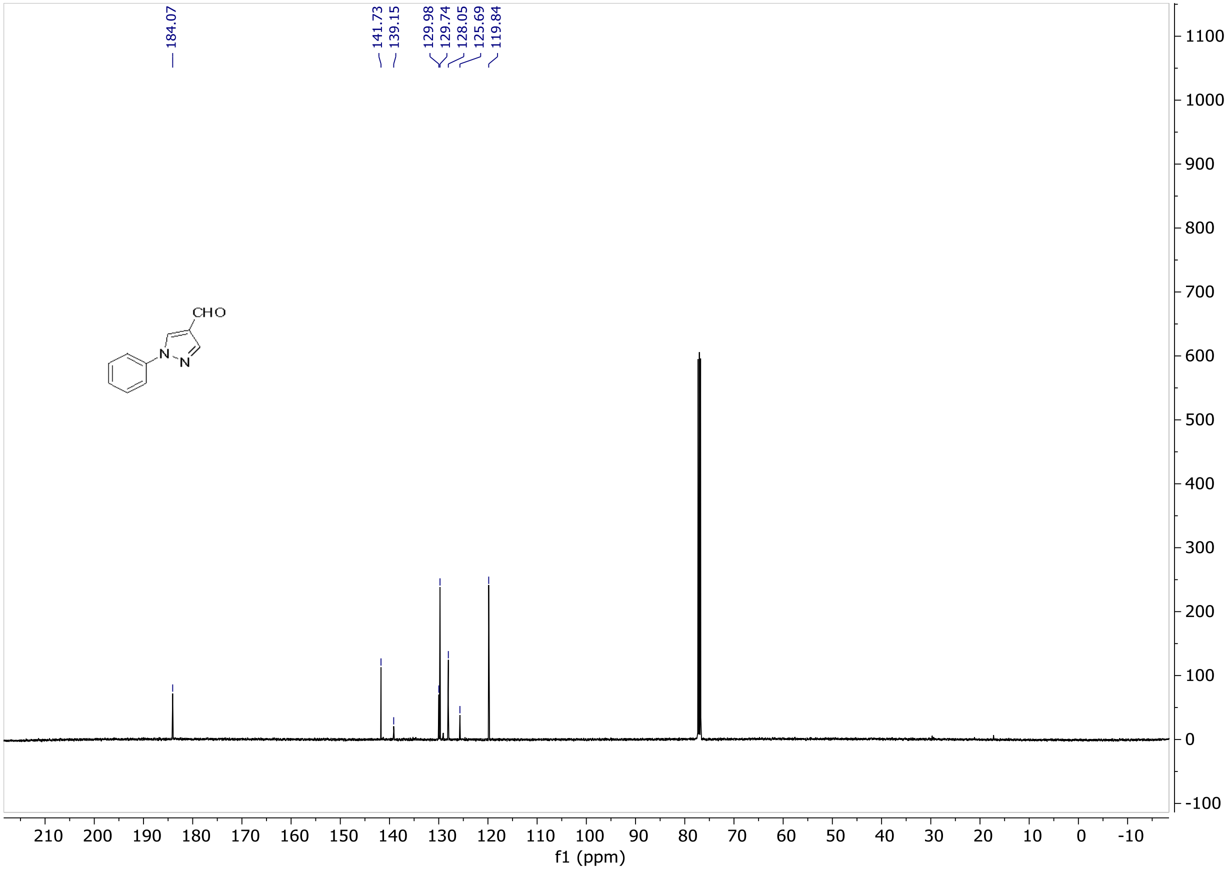
184.07
141.73
139.15
129.98
129.74
128.05
125.69
119.84
CHO
N
N
1100
1000
900
800
700
600
500
400
300
200
100
0
-100
210
200
190
180
170
160
150
140
130
120
110
100
90
80
70
60
50
40
30
20
10
0
-10
f1 (ppm)

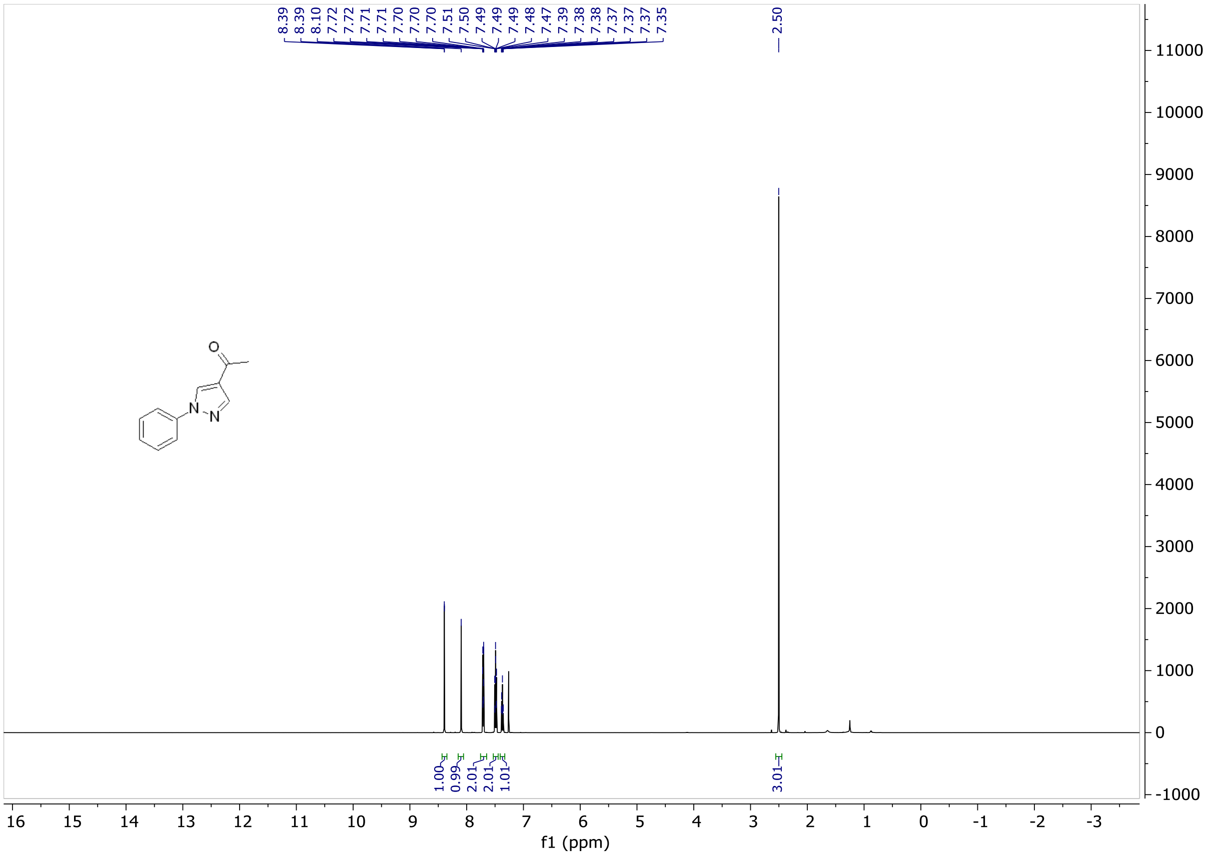
8.39
8.39
8.10
7.72
7.72
7.71
7.71
7.70
7.70
7.70
7.51
7.50
7.49
7.49
7.49
7.48
7.47
7.39
7.38
7.38
7.37
7.37
7.37
7.35
2.50
O
N
N
1.00
0.99
2.01
2.01
1.01
3.01
11000
10000
9000
8000
7000
6000
5000
4000
3000
2000
1000
0
-1000
16 15 14 13 12 11 10 9 8 7 6 5 4 3 2 1 0 -1 -2 -3
f1 (ppm)

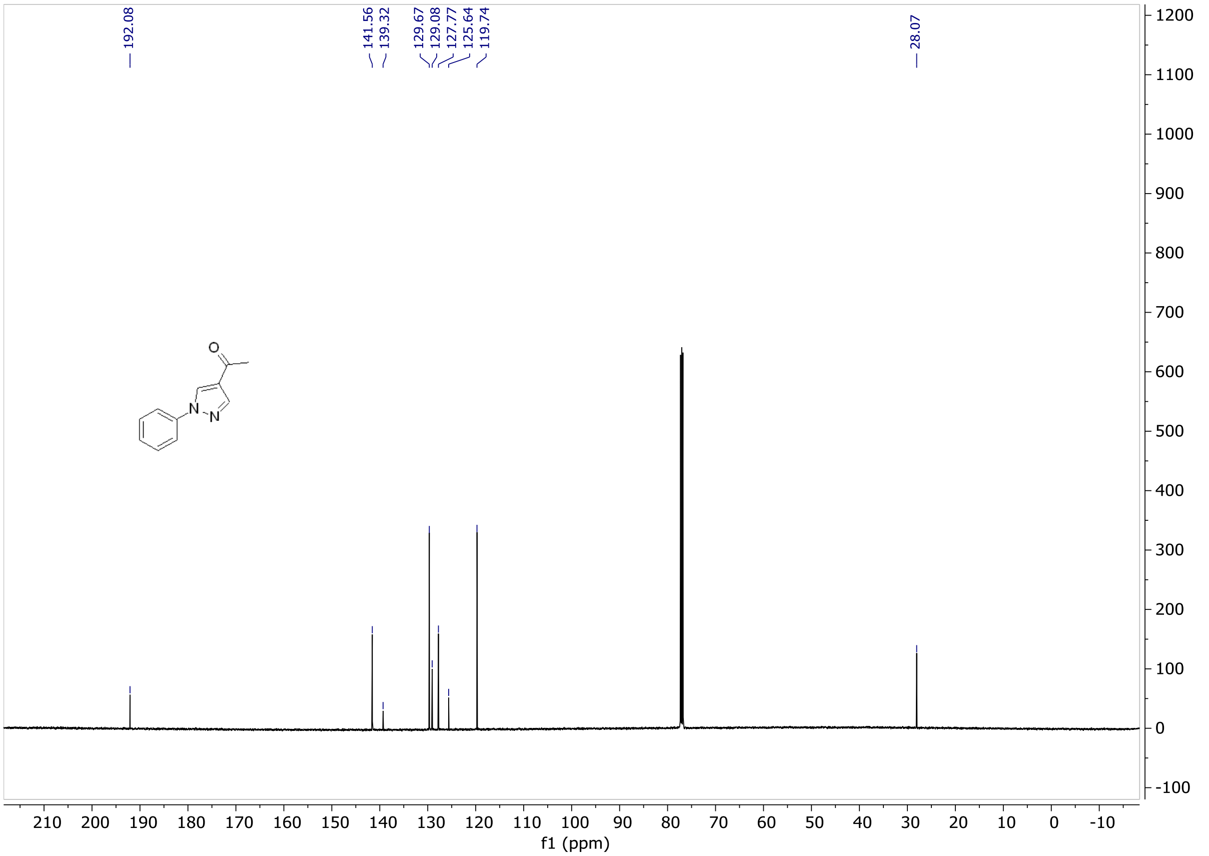
192.08
141.56
139.32
129.67
129.08
127.77
125.64
119.74
28.07
O
N
N
1200
1100
1000
900
800
700
600
500
400
300
200
100
0
-100
210 200 190 180 170 160 150 140 130 120 110 100 90 80 70 60 50 40 30 20 10 0 -10
f1 (ppm)

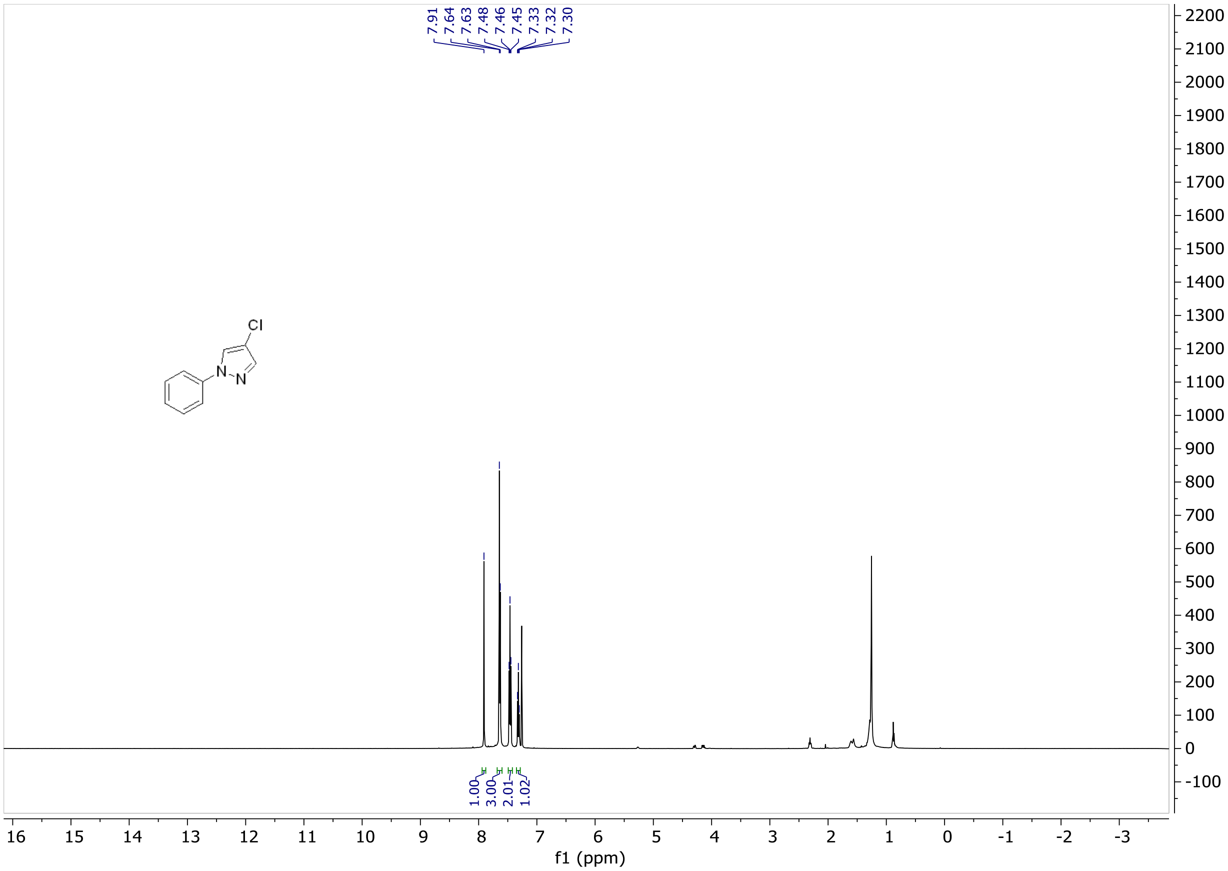
7.91
7.64
7.63
7.48
7.46
7.45
7.33
7.32
7.30
Cl
N
N
1.00
3.00
2.01
1.02
f1 (ppm)

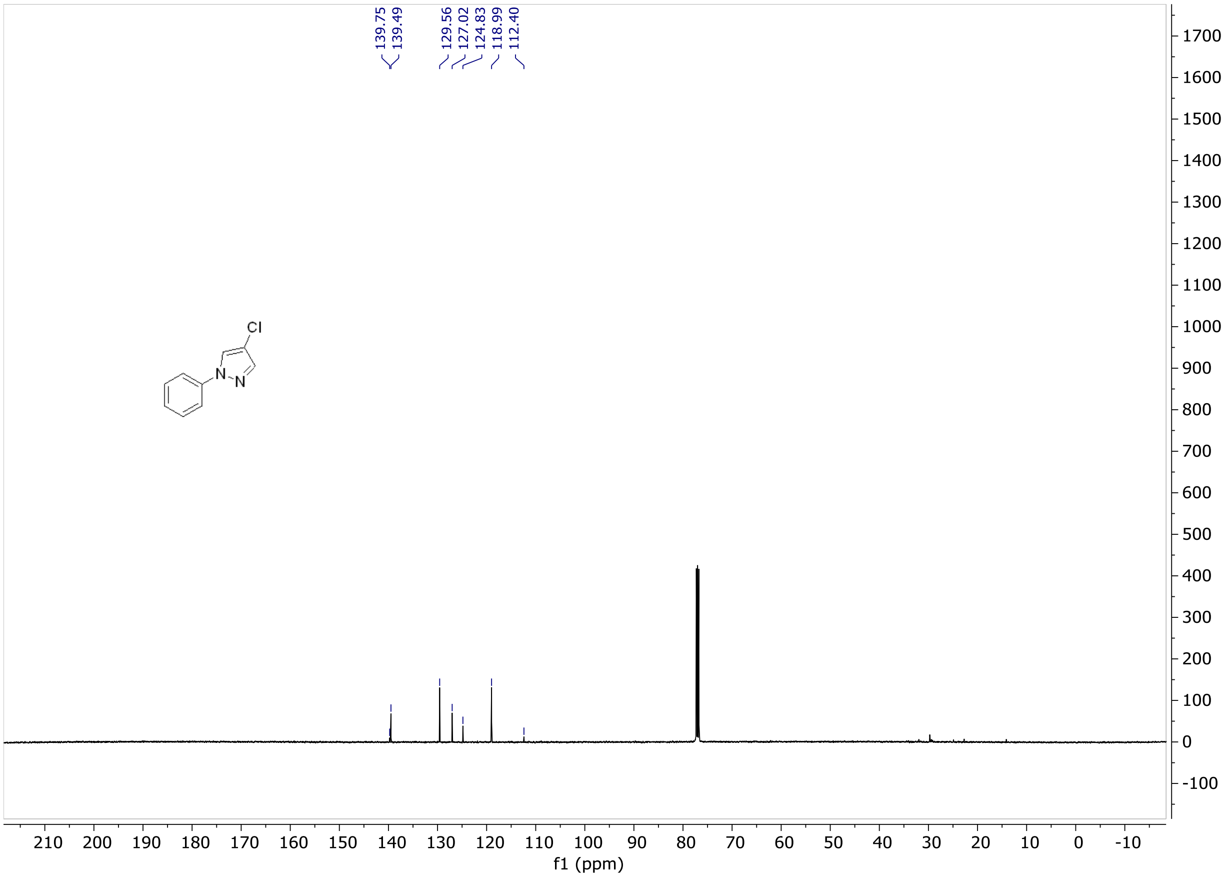
139.75
139.49
129.56
127.02
124.83
118.99
112.40
Cl
N
N
f1 (ppm)

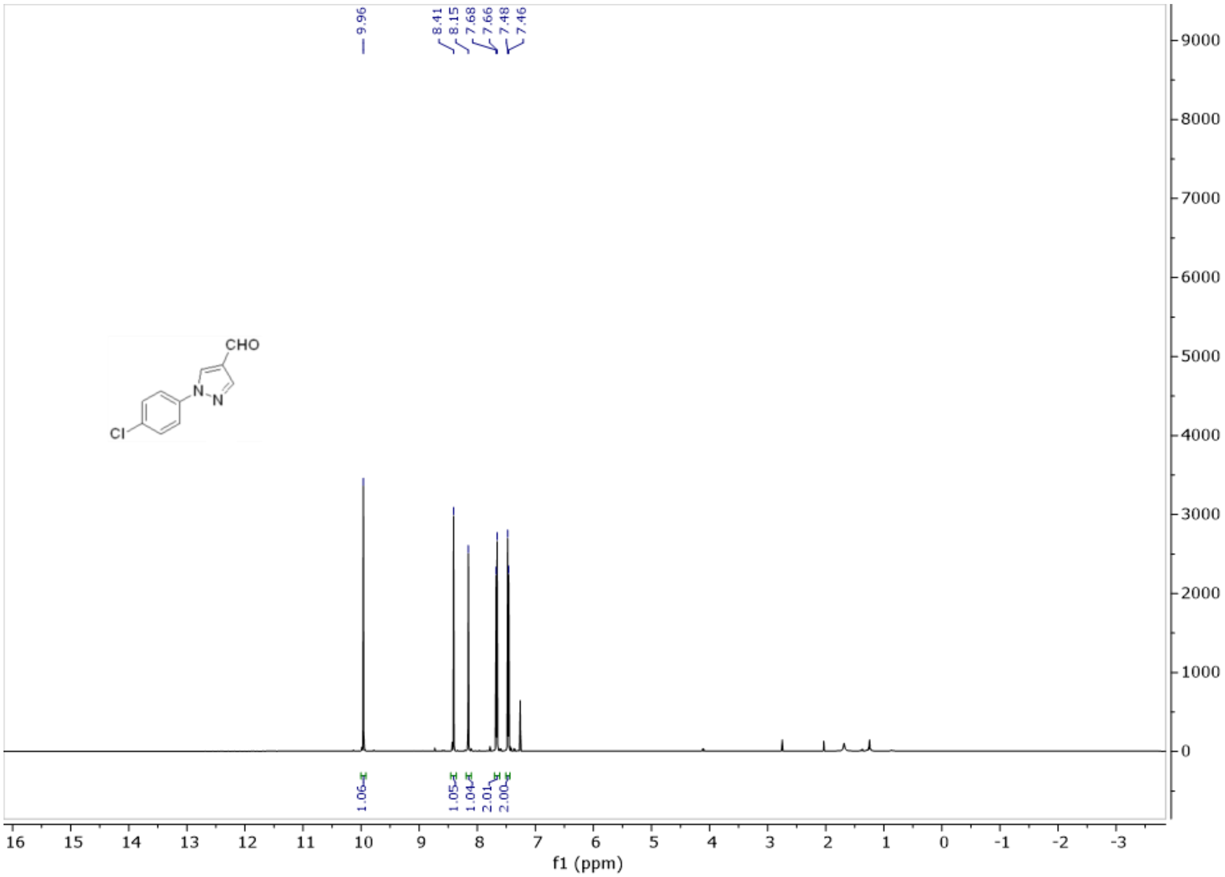
9.96
8.41
8.15
7.68
7.66
7.48
7.46
CHO
N
N
Cl
1.06
1.05
1.04
2.01
2.00
9000
8000
7000
6000
5000
4000
3000
2000
1000
0
16
15
14
13
12
11
10
9
8
7
6
5
4
3
2
1
0
-1
-2
-3
f1 (ppm)

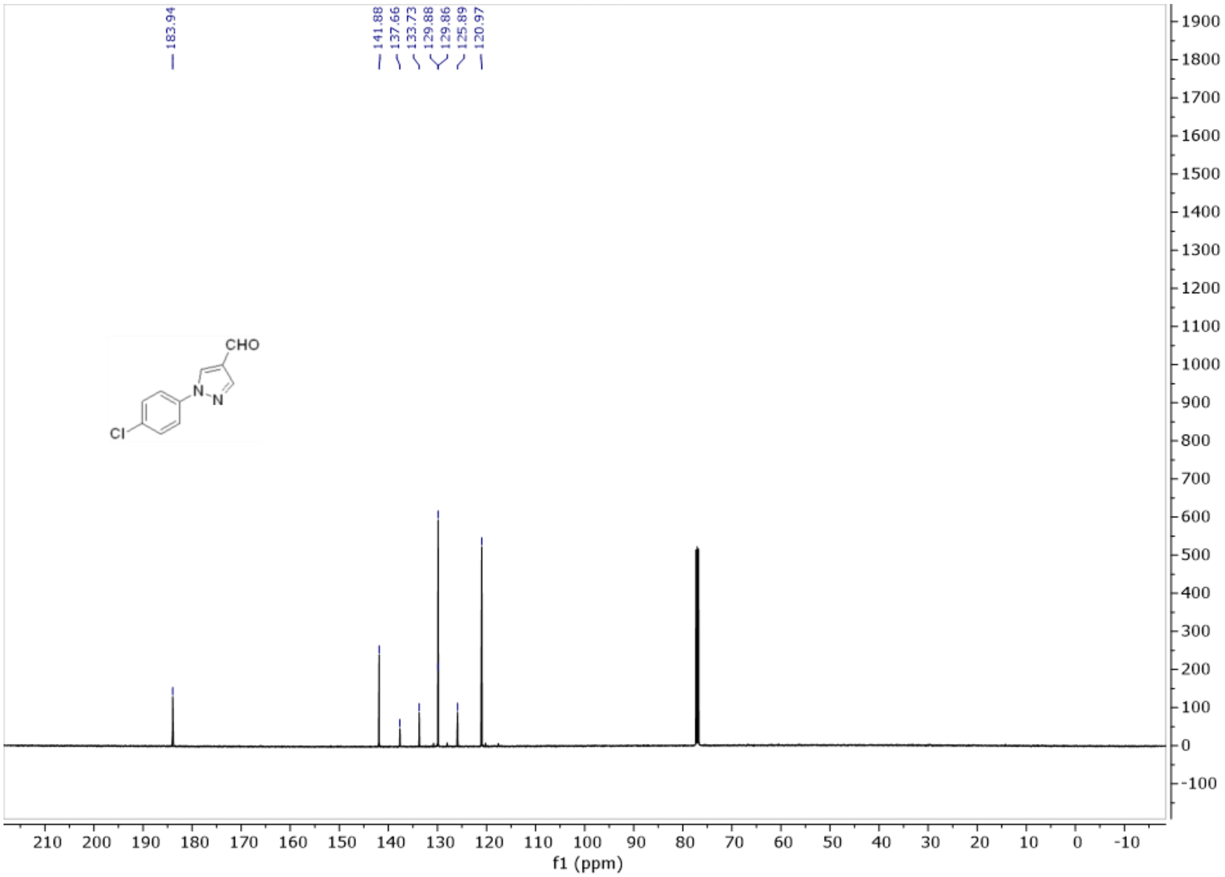
183.94
141.88
137.66
133.73
129.88
129.86
125.89
120.97
CHO
N
N
Cl
1900
1800
1700
1600
1500
1400
1300
1200
1100
1000
900
800
700
600
500
400
300
200
100
0
-100
210
200
190
180
170
160
150
140
130
120
110
100
90
80
70
60
50
40
30
20
10
0
-10
f1 (ppm)

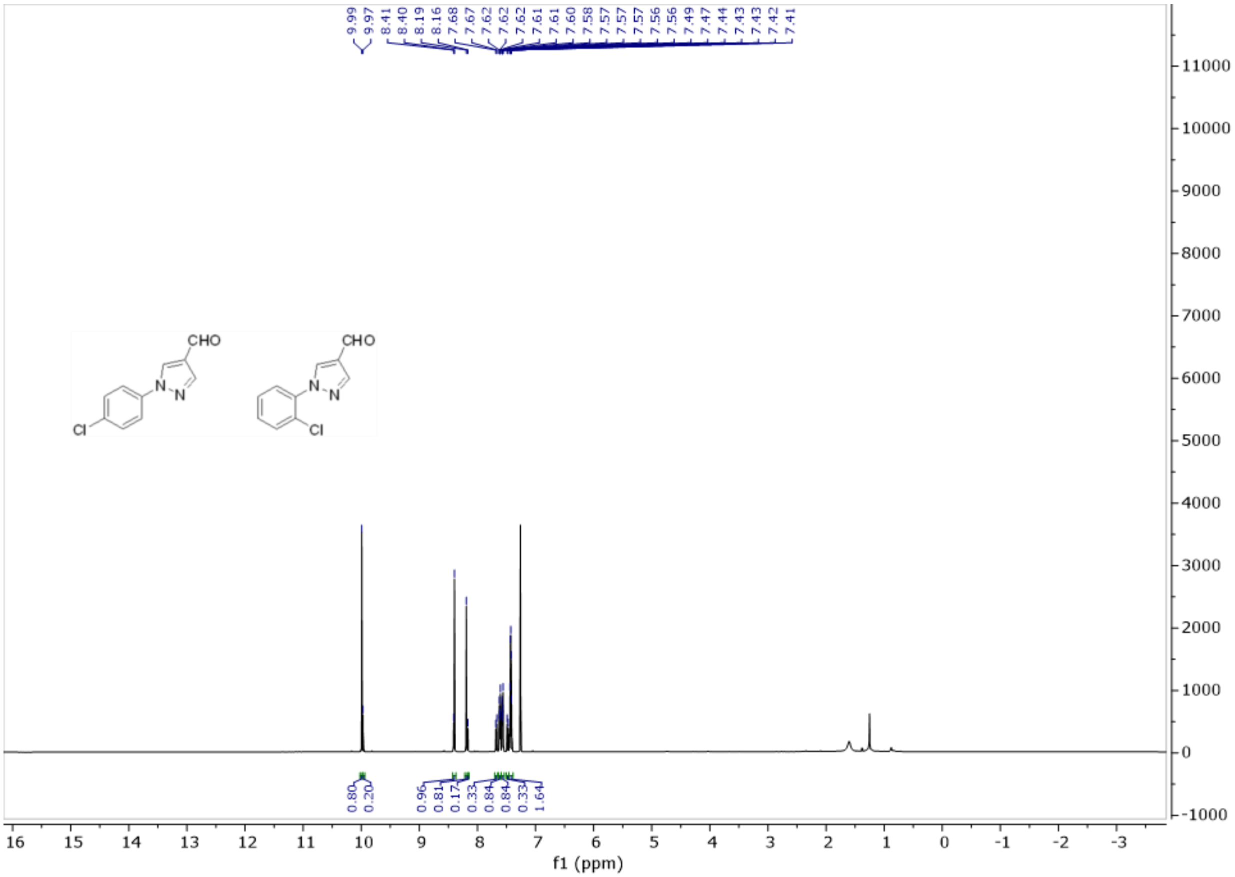
9.99
9.97
8.41
8.40
8.19
8.16
7.68
7.67
7.62
7.62
7.62
7.61
7.61
7.60
7.58
7.57
7.57
7.57
7.56
7.49
7.47
7.44
7.43
7.43
7.42
7.41
CHO
N
N
Cl
CHO
N
N
Cl
0.80
0.20
0.96
0.81
0.17
0.33
0.84
0.84
0.33
1.64
f1 (ppm)

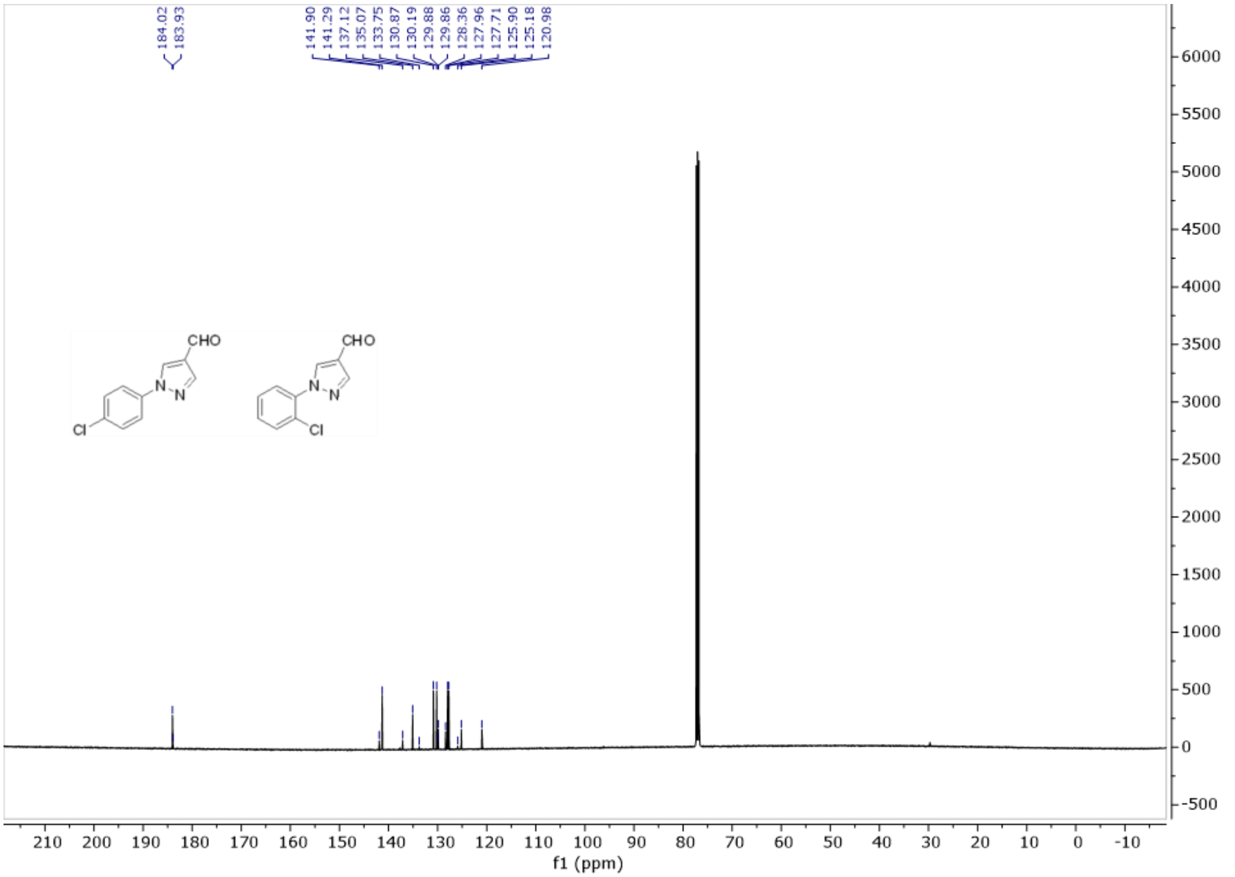
184.02
183.93
141.90
141.29
137.12
135.07
133.75
130.87
130.19
129.88
129.86
128.36
127.96
127.71
125.90
125.18
120.98
CHO
N
N
Cl
CHO
N
N
Cl
f1 (ppm)

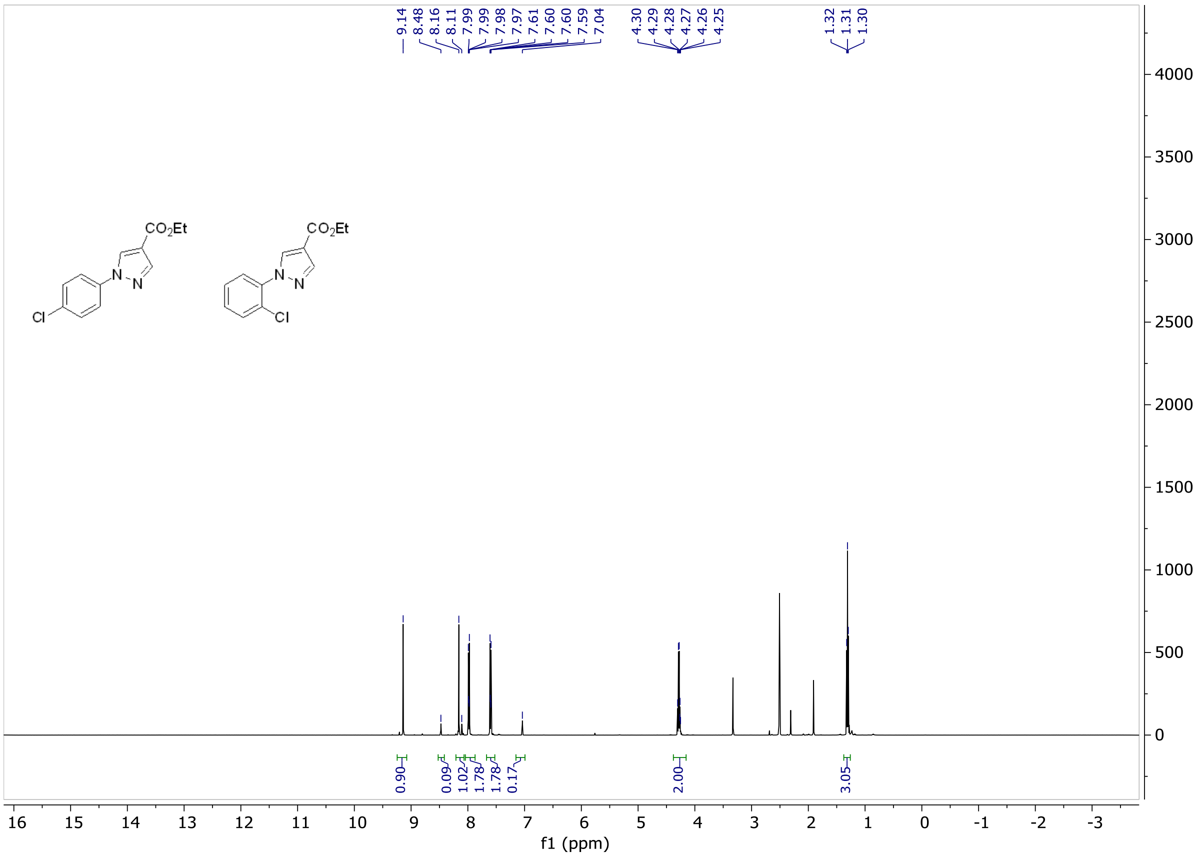
9.14
8.48
8.16
8.11
7.99
7.99
7.98
7.97
7.61
7.60
7.60
7.59
7.04
4.30
4.29
4.28
4.27
4.26
4.25
1.32
1.31
1.30
CO$_2$Et
N
N
Cl
CO$_2$Et
N
N
Cl
0.90
0.09
1.02
1.78
1.78
0.17
2.00
3.05
4000
3500
3000
2500
2000
1500
1000
500
0
16 15 14 13 12 11 10 9 8 7 6 5 4 3 2 1 0 -1 -2 -3
f1 (ppm)

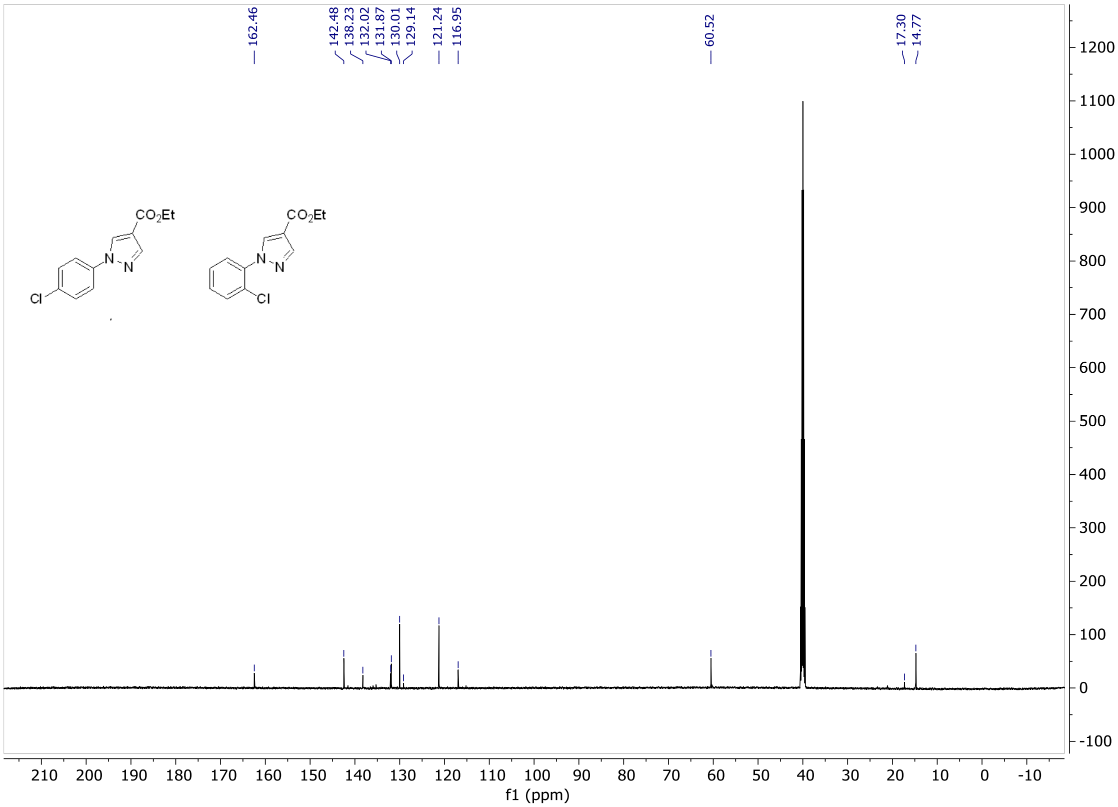
162.46
142.48
138.23
132.02
131.87
130.01
129.14
121.24
116.95
60.52
17.30
14.77
CO$_2$Et
N
N
Cl
CO$_2$Et
N
N
Cl
1200
1100
1000
900
800
700
600
500
400
300
200
100
0
-100
210 200 190 180 170 160 150 140 130 120 110 100 90 80 70 60 50 40 30 20 10 0 -10
f1 (ppm)

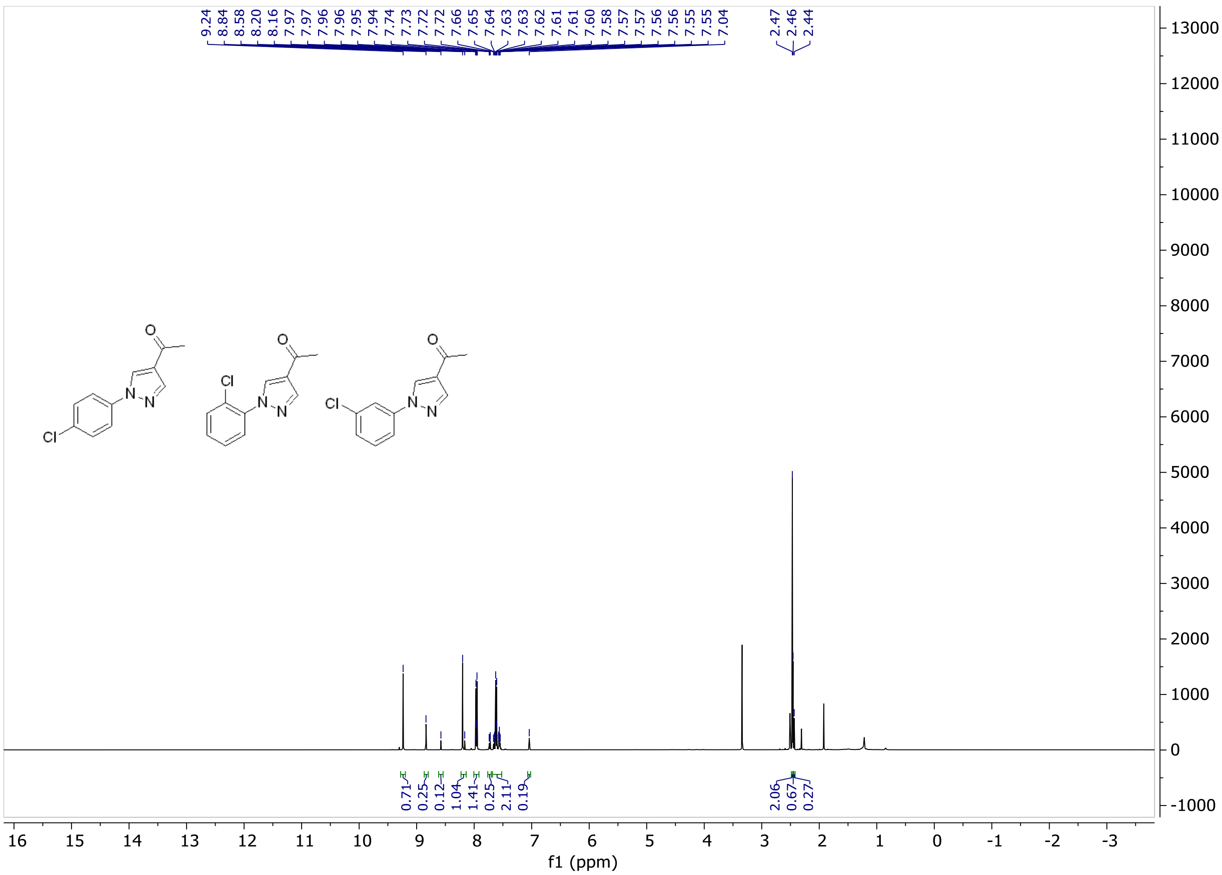

9.24 8.84 8.58 8.20 8.16 7.97 7.97 7.96 7.96 7.95 7.94 7.74 7.73 7.72 7.72 7.66 7.65 7.64 7.63 7.63 7.62 7.61 7.61 7.60 7.58 7.57 7.57 7.56 7.56 7.55 7.55 7.04
2.47 2.46 2.44
O
Cl
N
N
0.71 0.25 0.12 1.04 1.41 0.25 2.11 0.19
2.06 0.67 0.27
13000 12000 11000 10000 9000 8000 7000 6000 5000 4000 3000 2000 1000 0 -1000
16 15 14 13 12 11 10 9 8 7 6 5 4 3 2 1 0 -1 -2 -3
f1 (ppm)

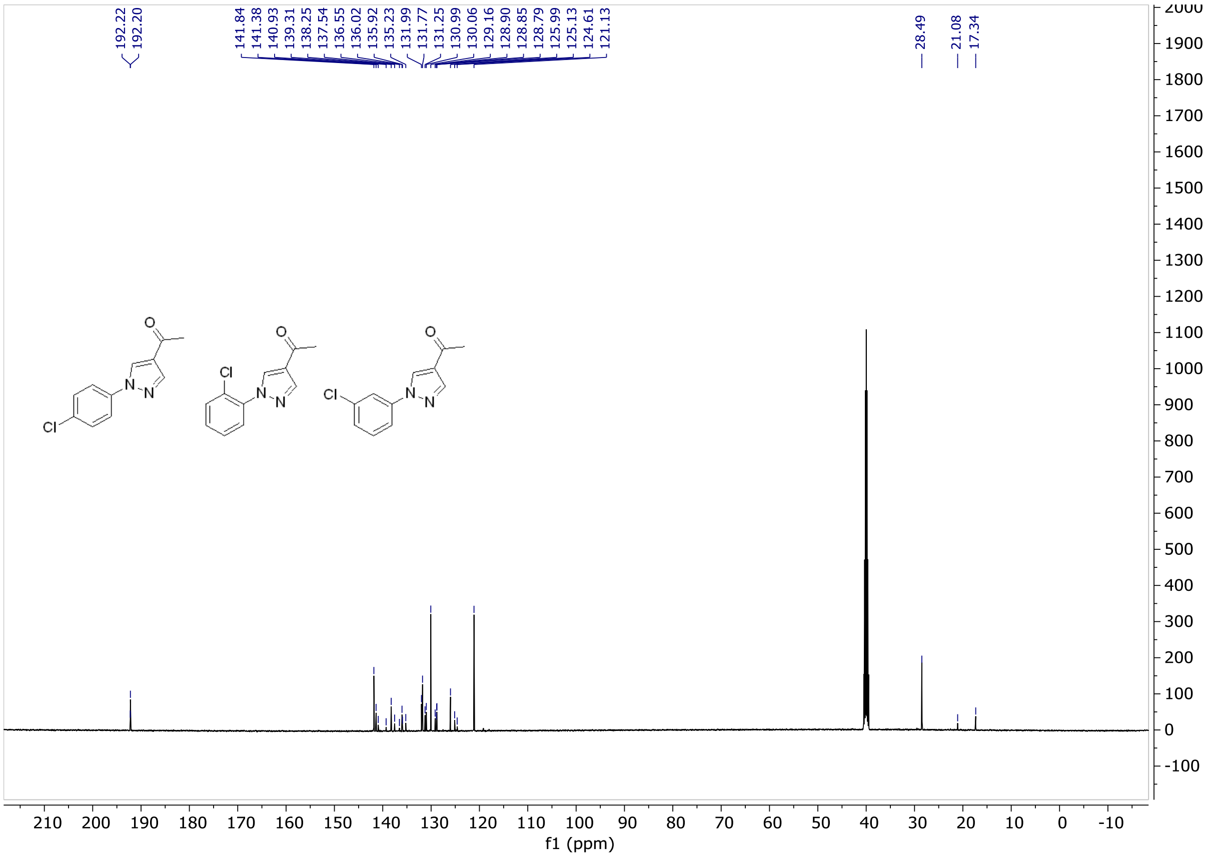

192.22 192.20
141.84 141.38 140.93 139.31 138.25 137.54 136.55 136.02 135.92 135.23 131.99 131.77 131.25 130.99 130.06 129.16 128.90 128.85 128.79 125.99 125.13 124.61 121.13
28.49
21.08
17.34
O
Cl
N
N
2000 1900 1800 1700 1600 1500 1400 1300 1200 1100 1000 900 800 700 600 500 400 300 200 100 0 -100
210 200 190 180 170 160 150 140 130 120 110 100 90 80 70 60 50 40 30 20 10 0 -10
f1 (ppm)

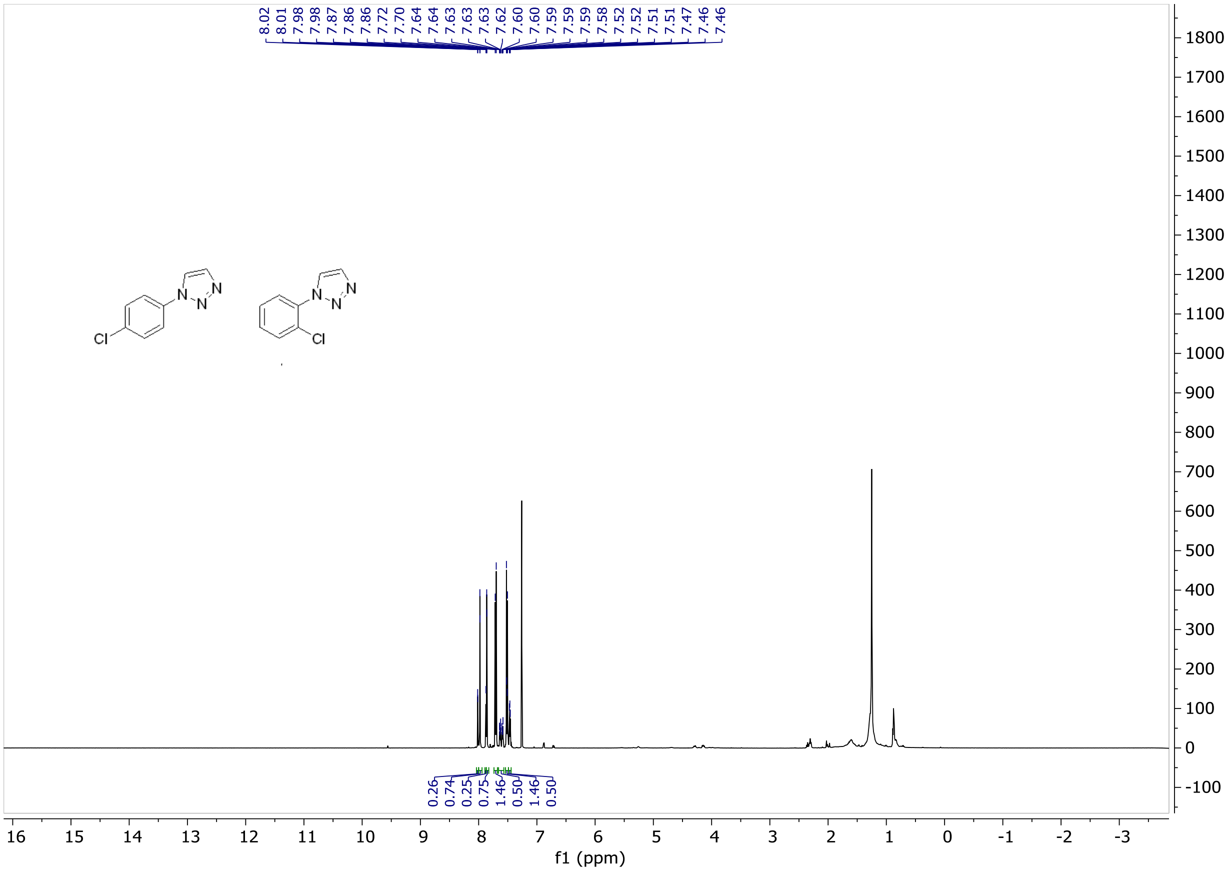
8.02
8.01
7.98
7.98
7.87
7.86
7.86
7.72
7.70
7.64
7.64
7.63
7.63
7.63
7.62
7.60
7.59
7.59
7.59
7.58
7.52
7.52
7.51
7.51
7.47
7.46
7.46
0.26
0.74
0.25
0.75
1.46
0.50
1.46
0.50
Cl
N
N
N
Cl
N
N
N
f1 (ppm)

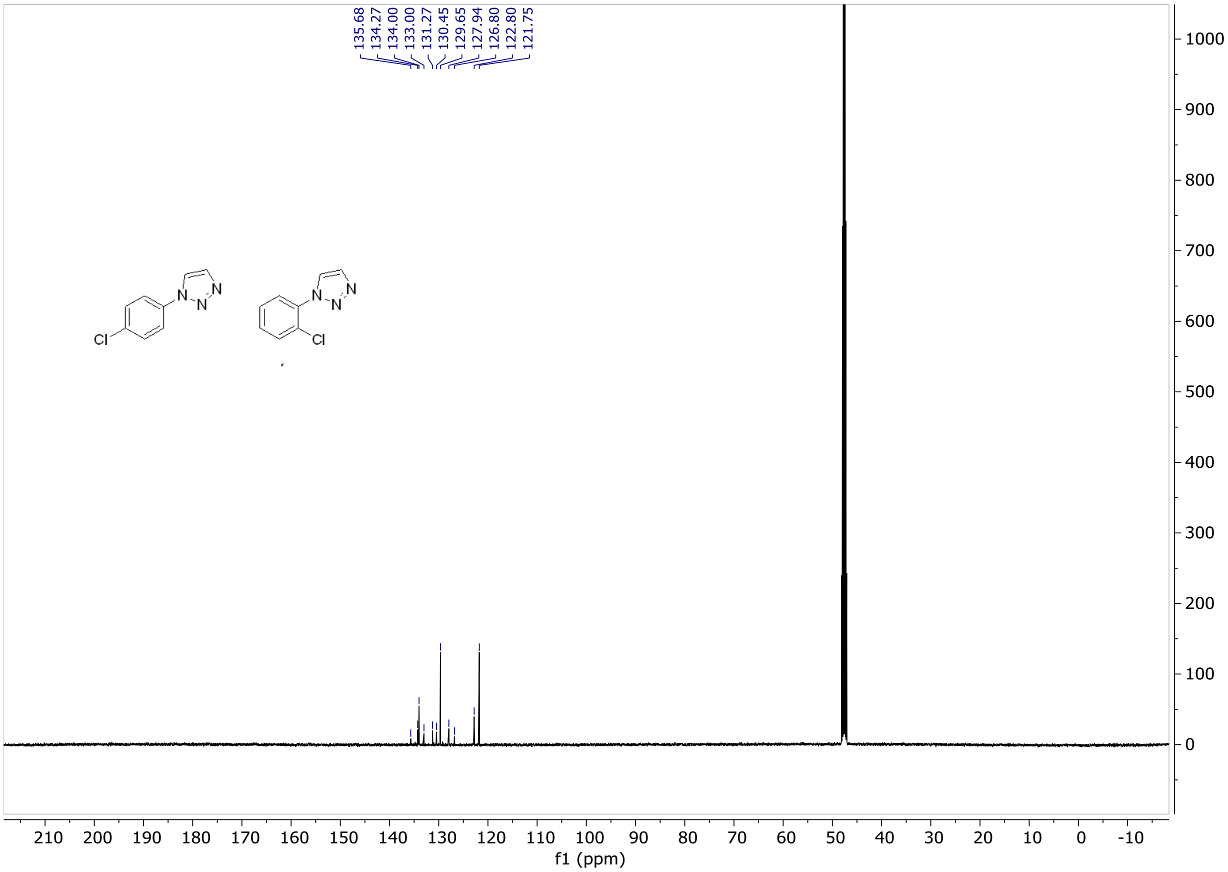
135.68
134.27
134.00
133.00
131.27
130.45
129.65
127.94
126.80
122.80
121.75
Cl
N
N
N
Cl
N
N
N
f1 (ppm)

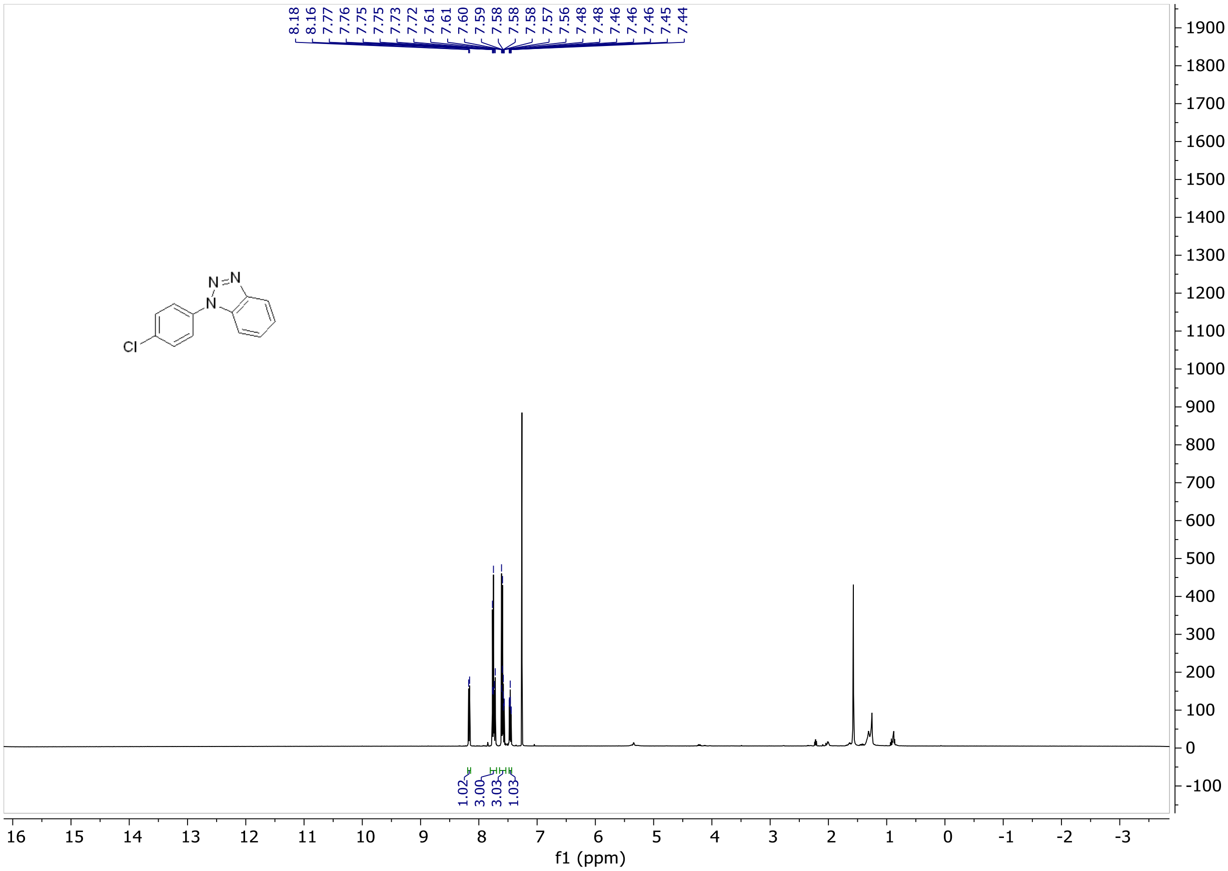
8.18
8.16
7.77
7.76
7.75
7.75
7.73
7.72
7.61
7.61
7.60
7.59
7.58
7.58
7.58
7.58
7.57
7.56
7.48
7.48
7.46
7.46
7.45
7.44
N
N
N
Cl
1.02
3.00
3.03
1.03
1900
1800
1700
1600
1500
1400
1300
1200
1100
1000
900
800
700
600
500
400
300
200
100
0
-100
16 15 14 13 12 11 10 9 8 7 6 5 4 3 2 1 0 -1 -2 -3
f1 (ppm)

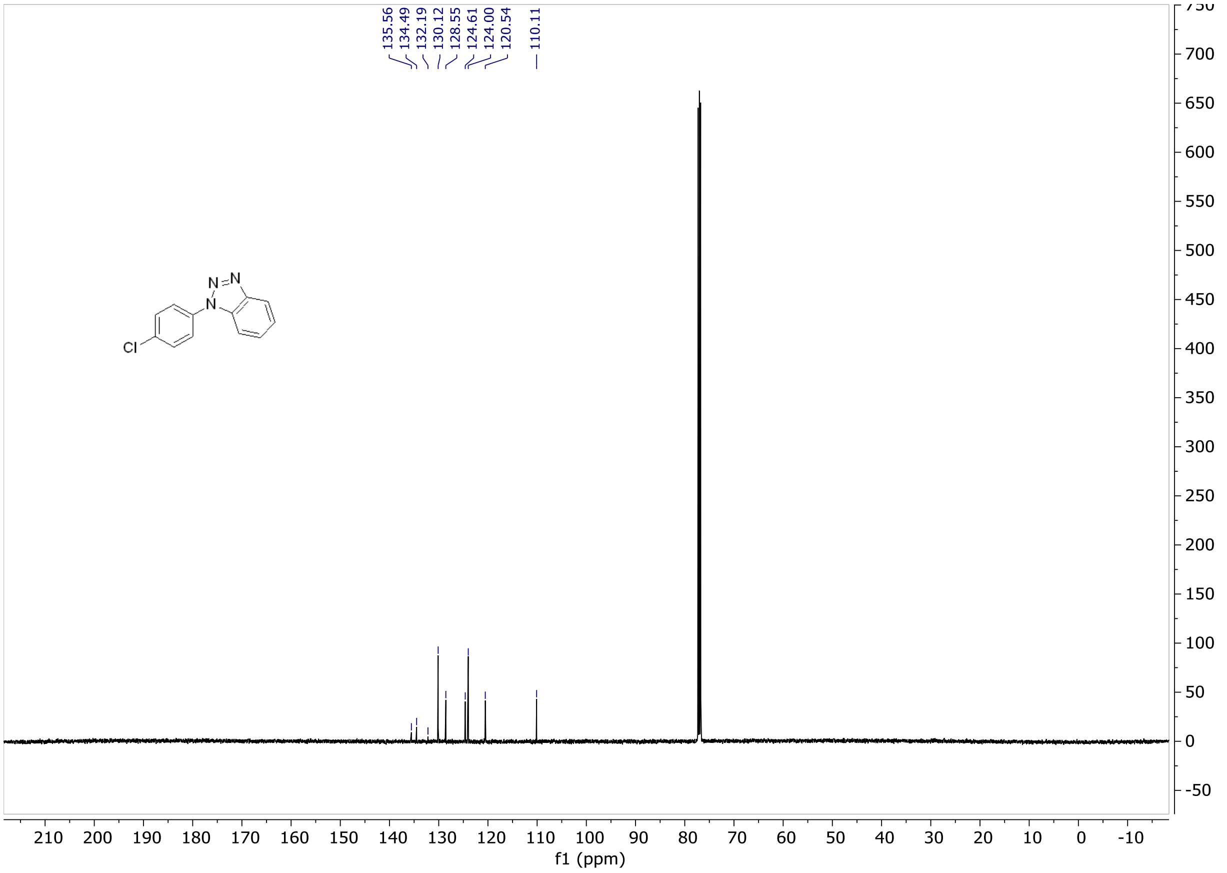
135.56
134.49
132.19
130.12
128.55
124.61
124.00
120.54
110.11
N
N
N
Cl
750
700
650
600
550
500
450
400
350
300
250
200
150
100
50
0
-50
210 200 190 180 170 160 150 140 130 120 110 100 90 80 70 60 50 40 30 20 10 0 -10
f1 (ppm)

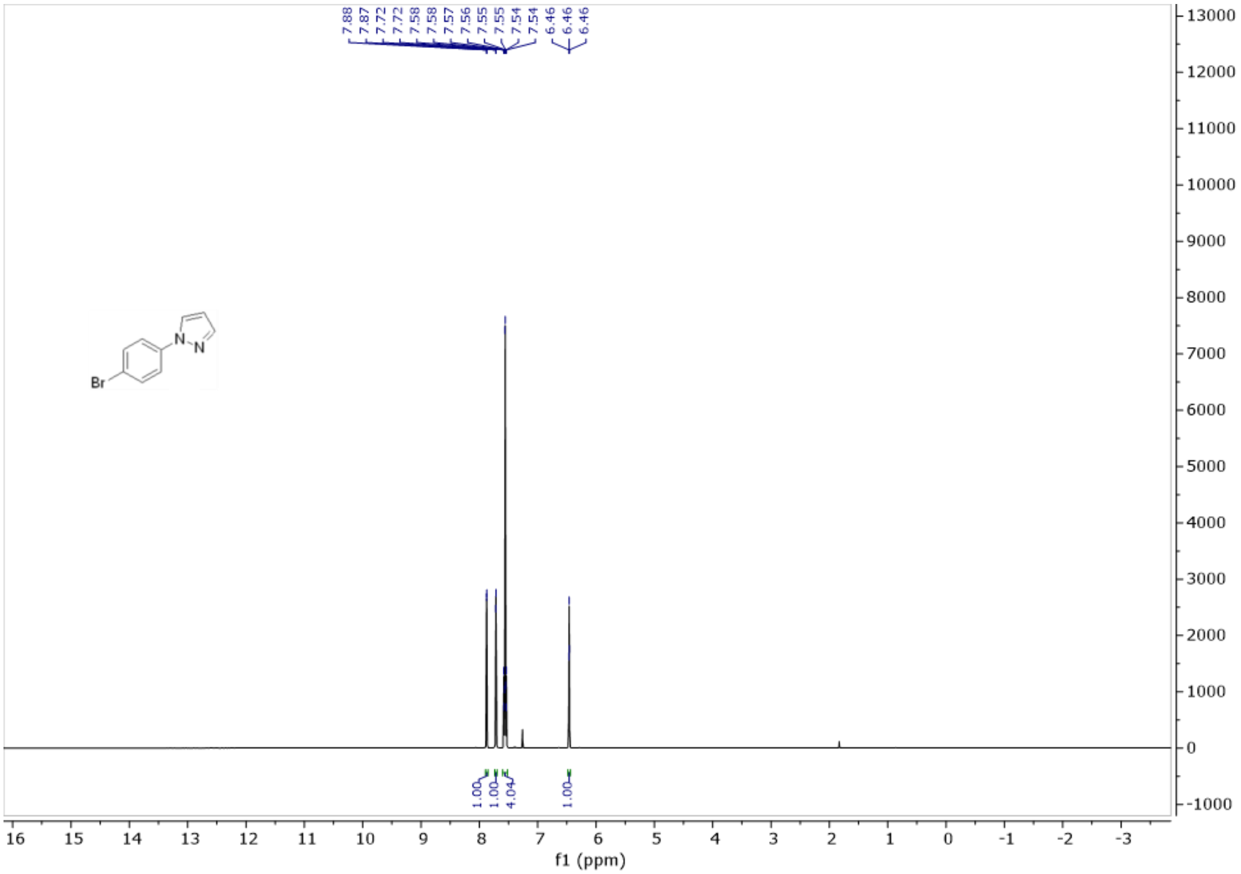
7.88
7.87
7.72
7.72
7.58
7.58
7.57
7.56
7.55
7.55
7.54
7.54
6.46
6.46
6.46
Br
N
N
1.00
1.00
4.04
1.00
13000
12000
11000
10000
9000
8000
7000
6000
5000
4000
3000
2000
1000
0
-1000
16
15
14
13
12
11
10
9
8
7
6
5
4
3
2
1
0
-1
-2
-3
f1 (ppm)

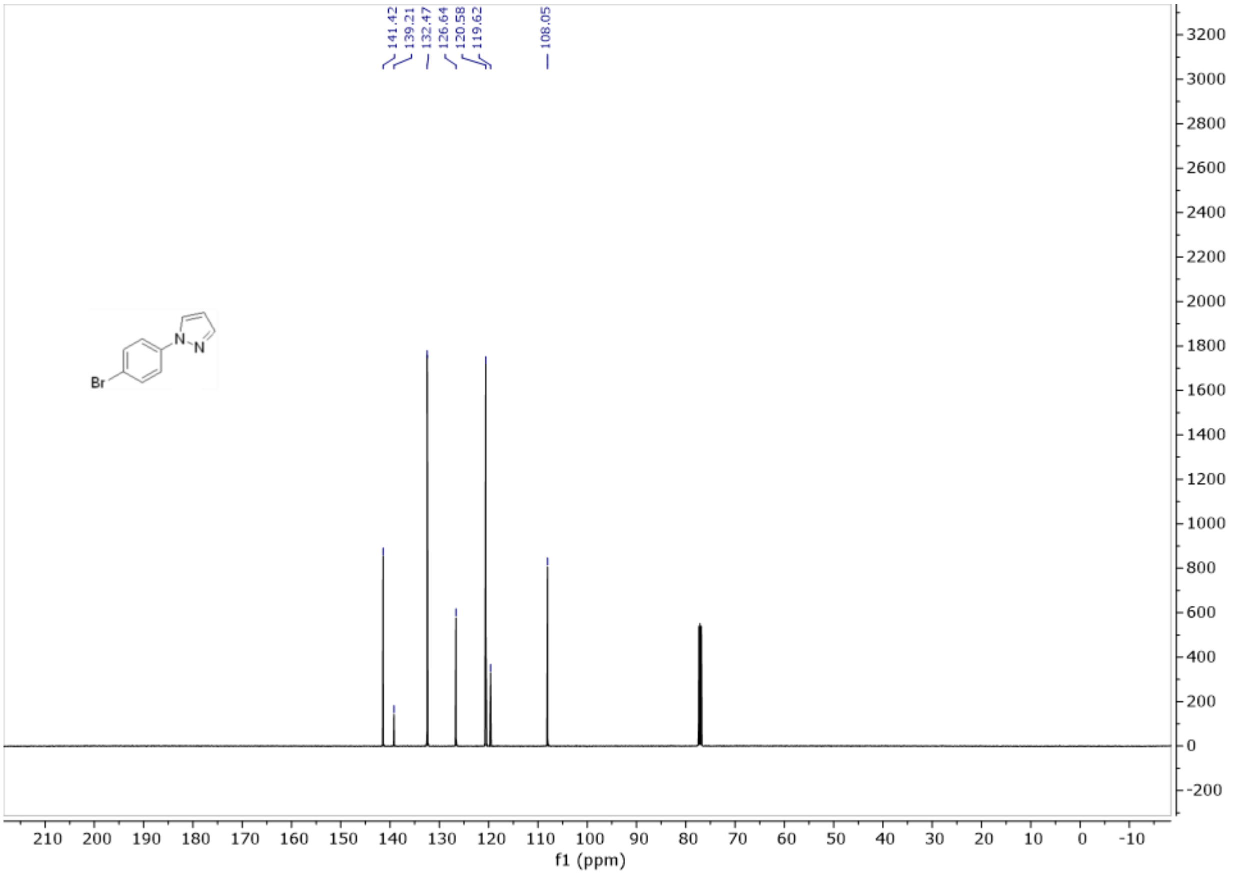
141.42
139.21
132.47
126.64
120.58
119.62
108.05
Br
N
N
3200
3000
2800
2600
2400
2200
2000
1800
1600
1400
1200
1000
800
600
400
200
0
-200
210
200
190
180
170
160
150
140
130
120
110
100
90
80
70
60
50
40
30
20
10
0
-10
f1 (ppm)

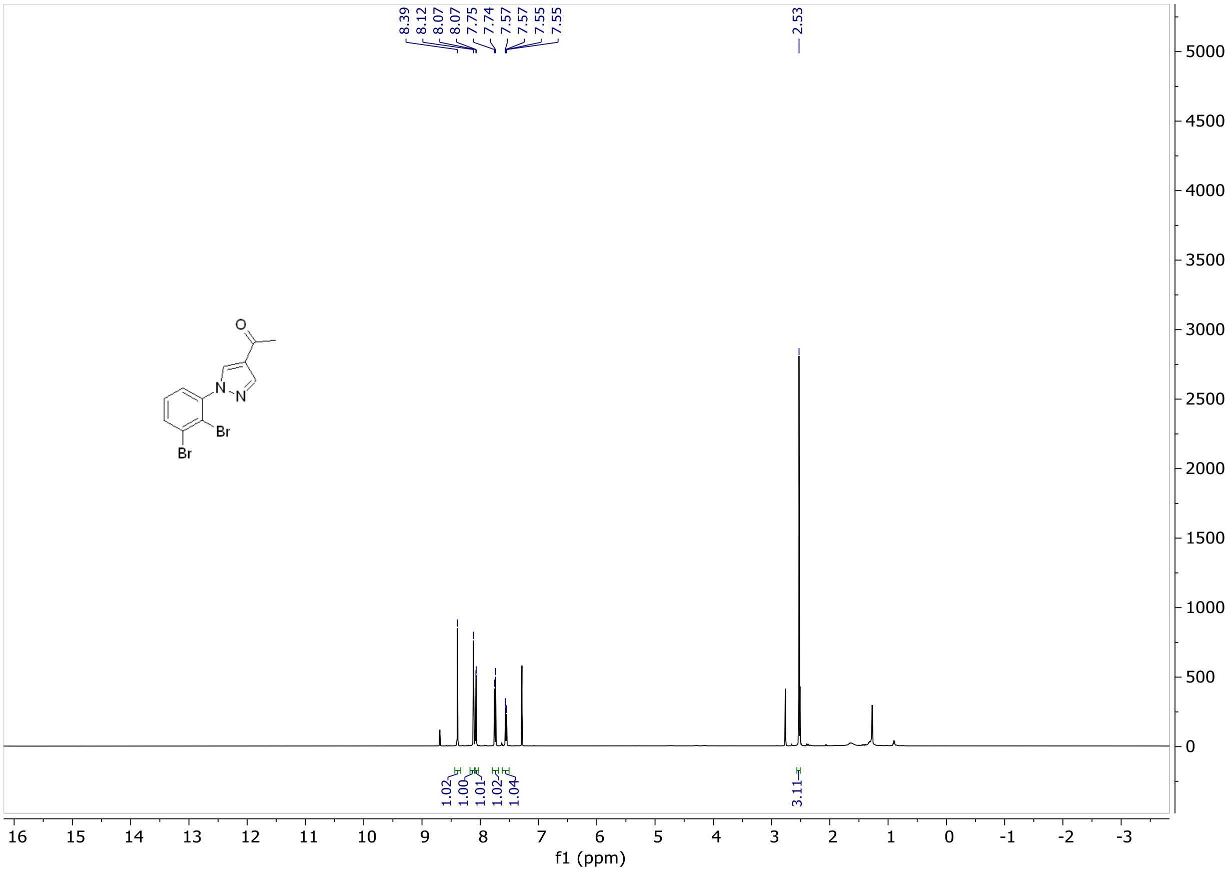
8.39
8.12
8.07
8.07
7.75
7.74
7.57
7.57
7.55
7.55
2.53
O
N
N
Br
Br
1.02
1.00
1.01
1.02
1.04
3.11
16 15 14 13 12 11 10 9 8 7 6 5 4 3 2 1 0 -1 -2 -3
f1 (ppm)
5000 4500 4000 3500 3000 2500 2000 1500 1000 500 0

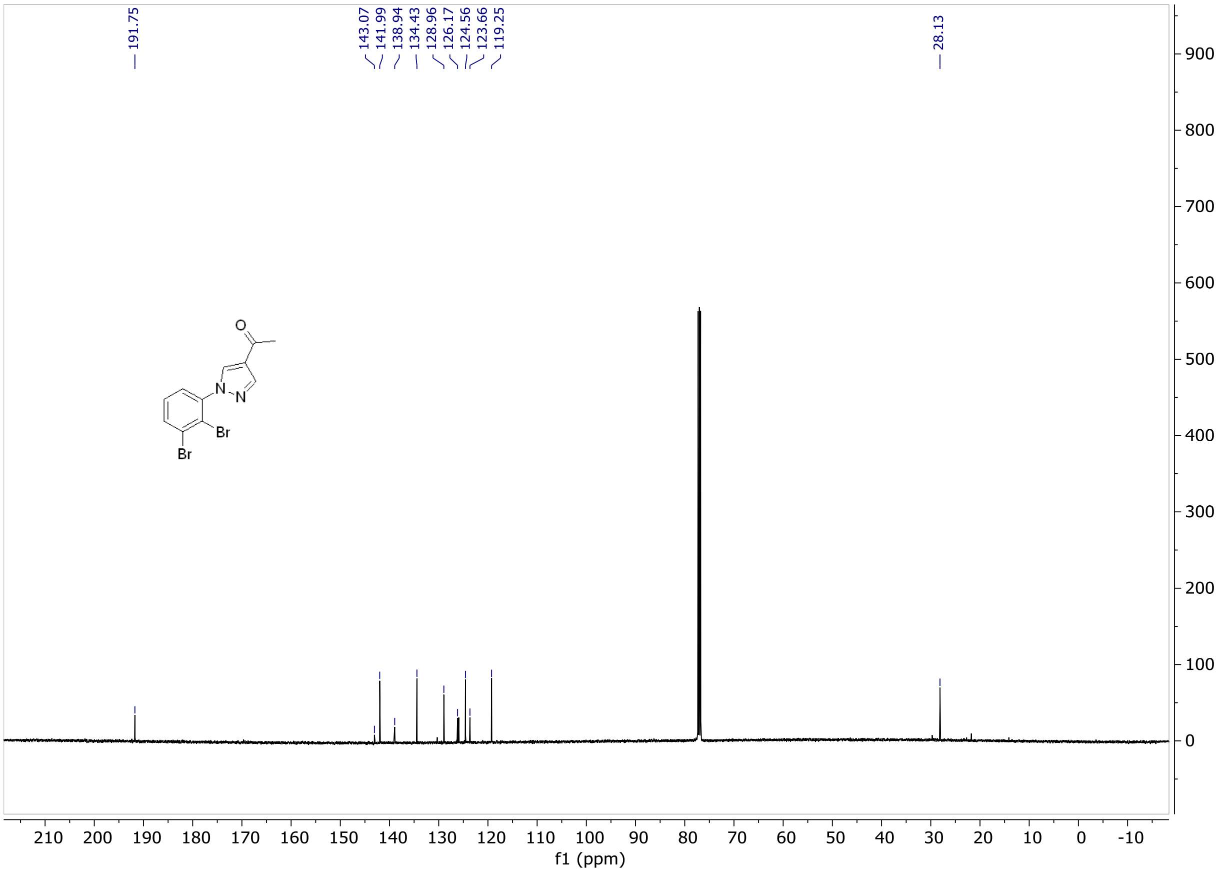
191.75
143.07
141.99
138.94
134.43
128.96
126.17
124.56
123.66
119.25
28.13
O
N
N
Br
Br
210 200 190 180 170 160 150 140 130 120 110 100 90 80 70 60 50 40 30 20 10 0 -10
f1 (ppm)
900 800 700 600 500 400 300 200 100 0

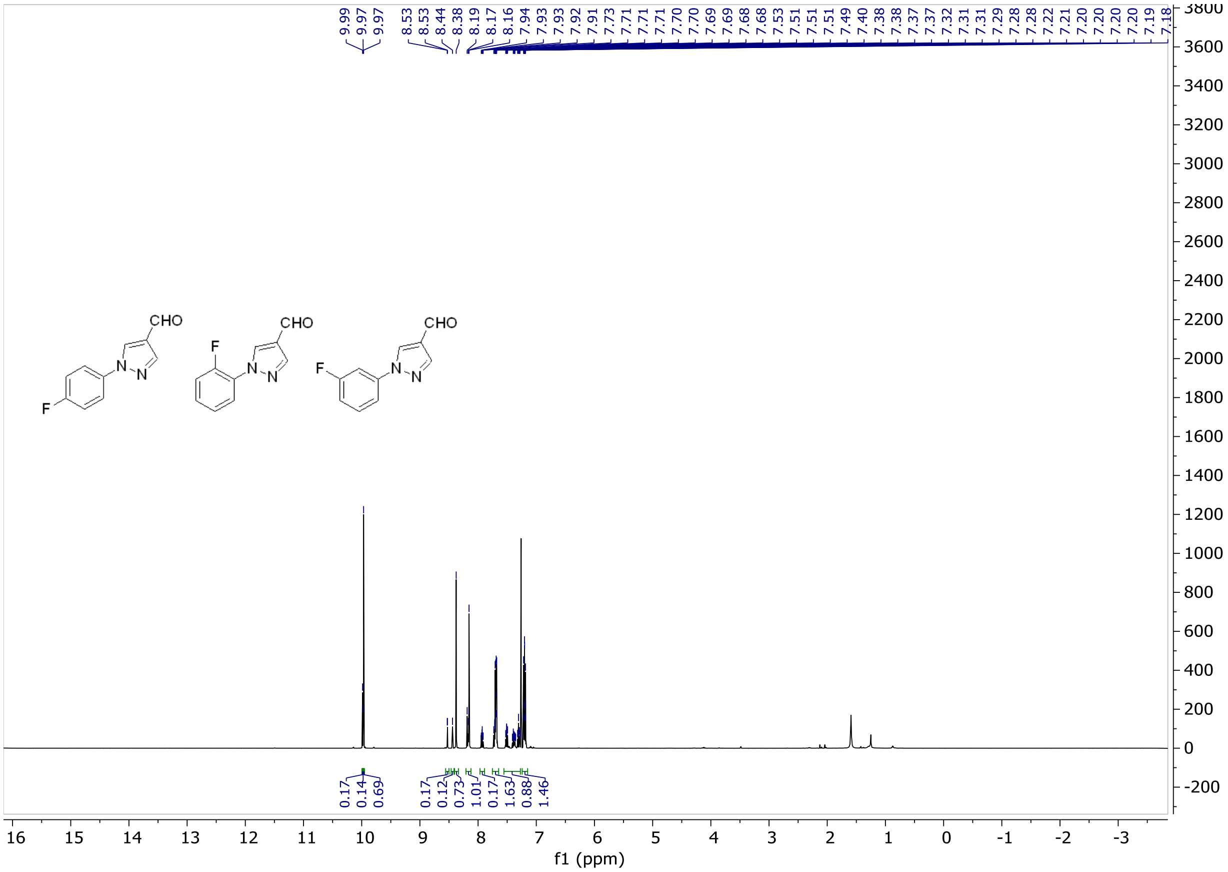

9.99
9.97
9.97
8.53
8.53
8.44
8.38
8.19
8.17
8.16
7.94
7.93
7.93
7.92
7.91
7.73
7.71
7.71
7.71
7.70
7.69
7.69
7.68
7.68
7.53
7.51
7.51
7.51
7.49
7.40
7.38
7.38
7.37
7.37
7.32
7.31
7.31
7.29
7.28
7.28
7.28
7.22
7.21
7.20
7.20
7.20
7.19
7.18
CHO
N
N
F
0.17
0.14
0.69
0.17
0.12
0.73
1.01
0.17
1.63
0.88
1.46
16
15
14
13
12
11
10
9
8
7
6
5
4
3
2
1
0
-1
-2
-3
f1 (ppm)
3800
3600
3400
3200
3000
2800
2600
2400
2200
2000
1800
1600
1400
1200
1000
800
600
400
200
0
-200

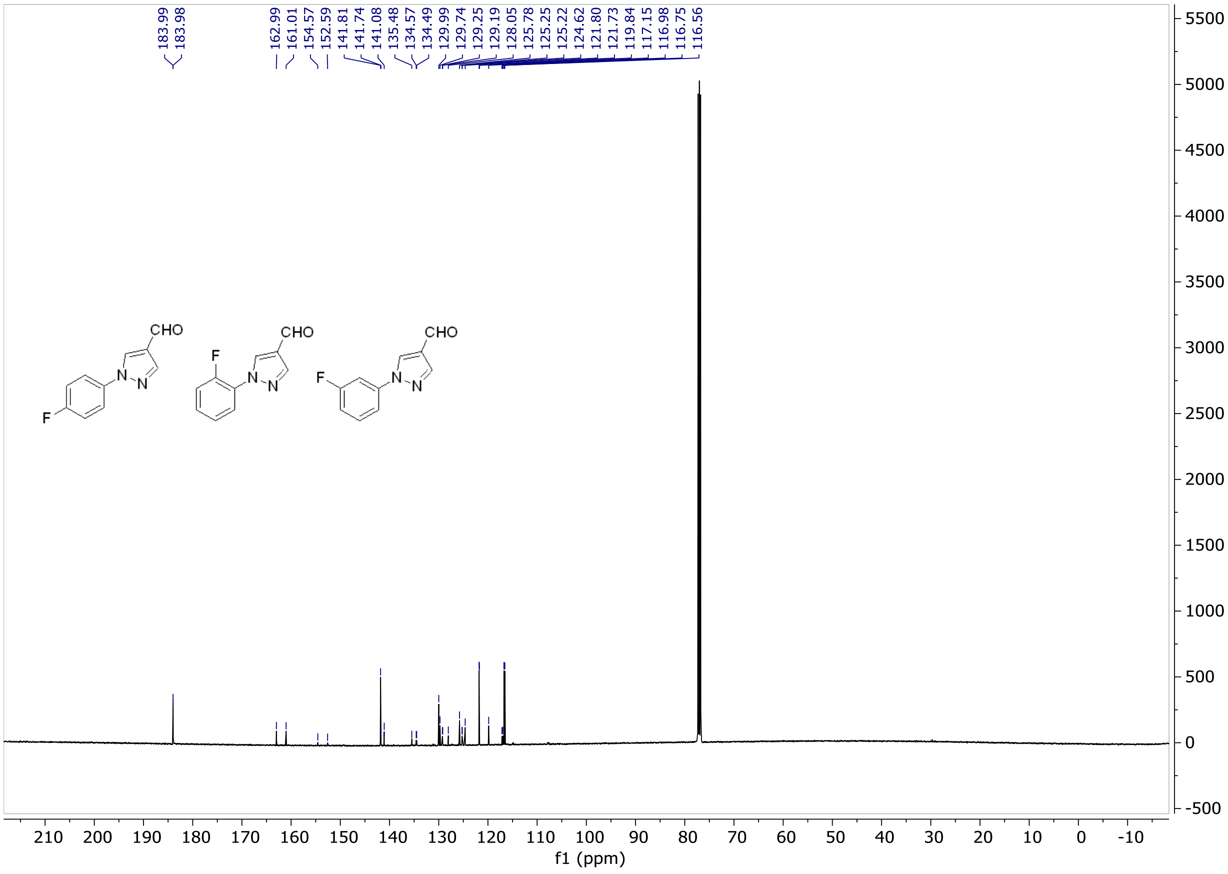

183.99
183.98
162.99
161.01
154.57
152.59
141.81
141.74
141.08
135.48
134.57
134.49
129.99
129.74
129.25
129.19
128.05
125.78
125.25
125.22
124.62
121.80
121.73
119.84
117.15
116.98
116.75
116.56
CHO
N
N
F
210
200
190
180
170
160
150
140
130
120
110
100
90
80
70
60
50
40
30
20
10
0
-10
f1 (ppm)
5500
5000
4500
4000
3500
3000
2500
2000
1500
1000
500
0
-500

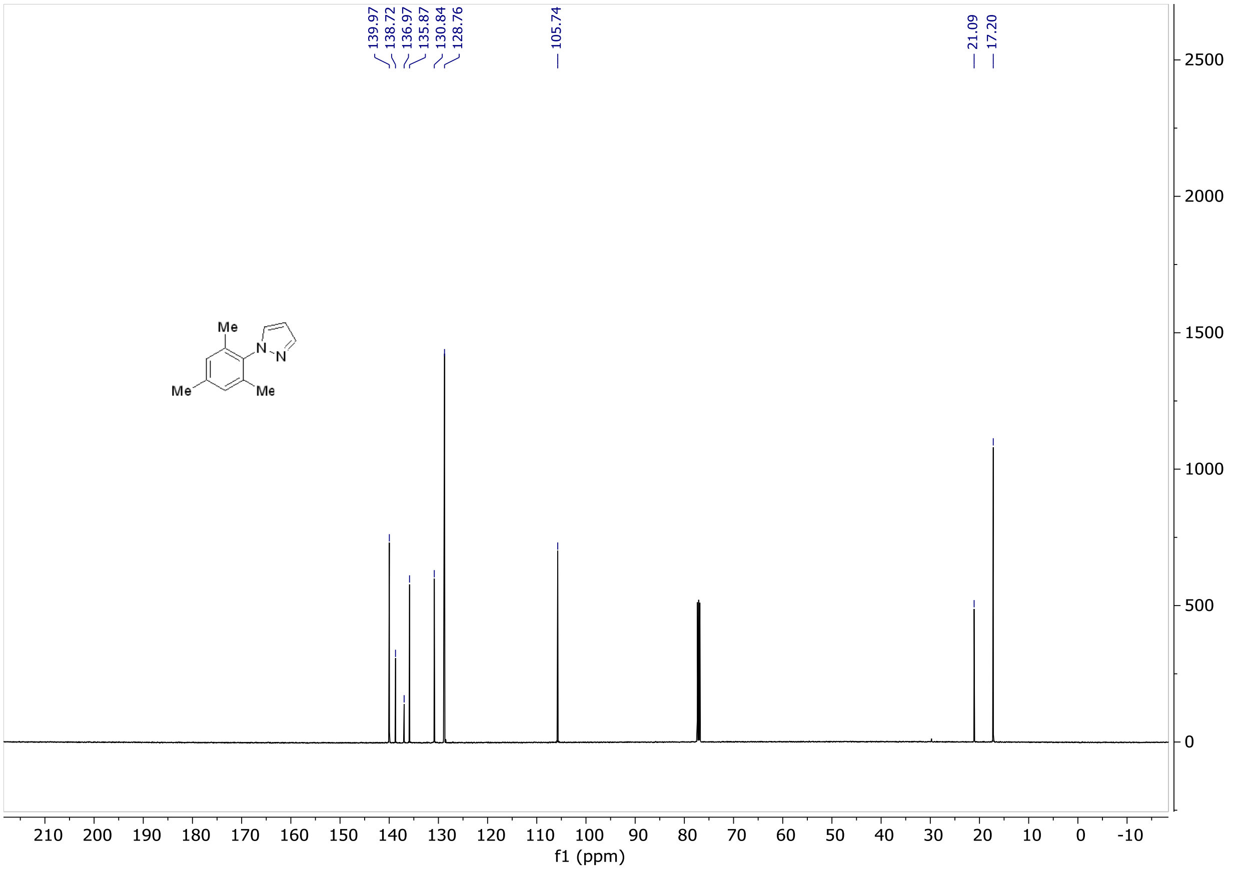

139.97
138.72
136.97
135.87
130.84
128.76
105.74
21.09
17.20
Me
N
N
Me
Me
2500
2000
1500
1000
500
0
210 200 190 180 170 160 150 140 130 120 110 100 90 80 70 60 50 40 30 20 10 0 -10
f1 (ppm)

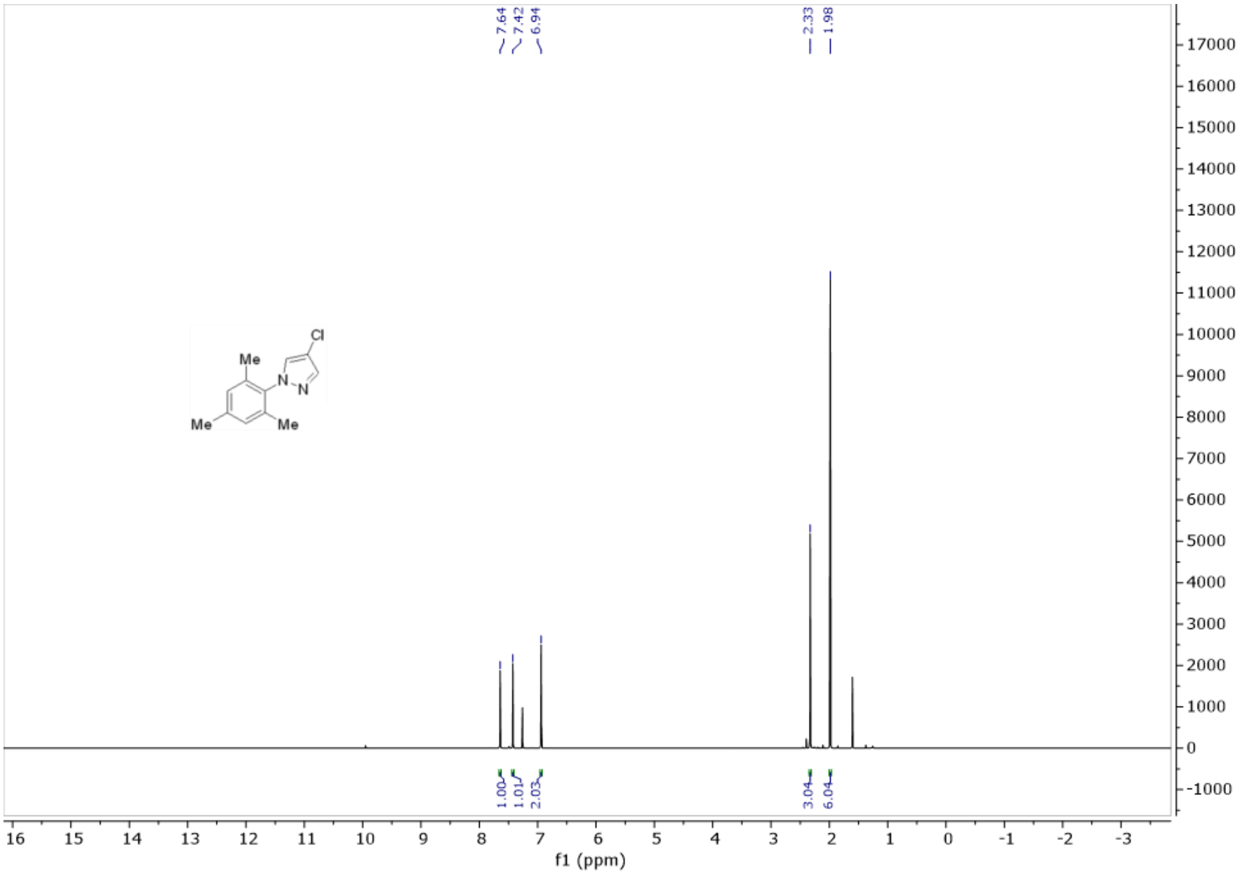

7.64
7.42
6.94
2.33
1.98
Cl
Me
N
N
Me
Me
17000
16000
15000
14000
13000
12000
11000
10000
9000
8000
7000
6000
5000
4000
3000
2000
1000
0
-1000
1.00
1.01
2.03
3.04
6.04
16 15 14 13 12 11 10 9 8 7 6 5 4 3 2 1 0 -1 -2 -3
f1 (ppm)

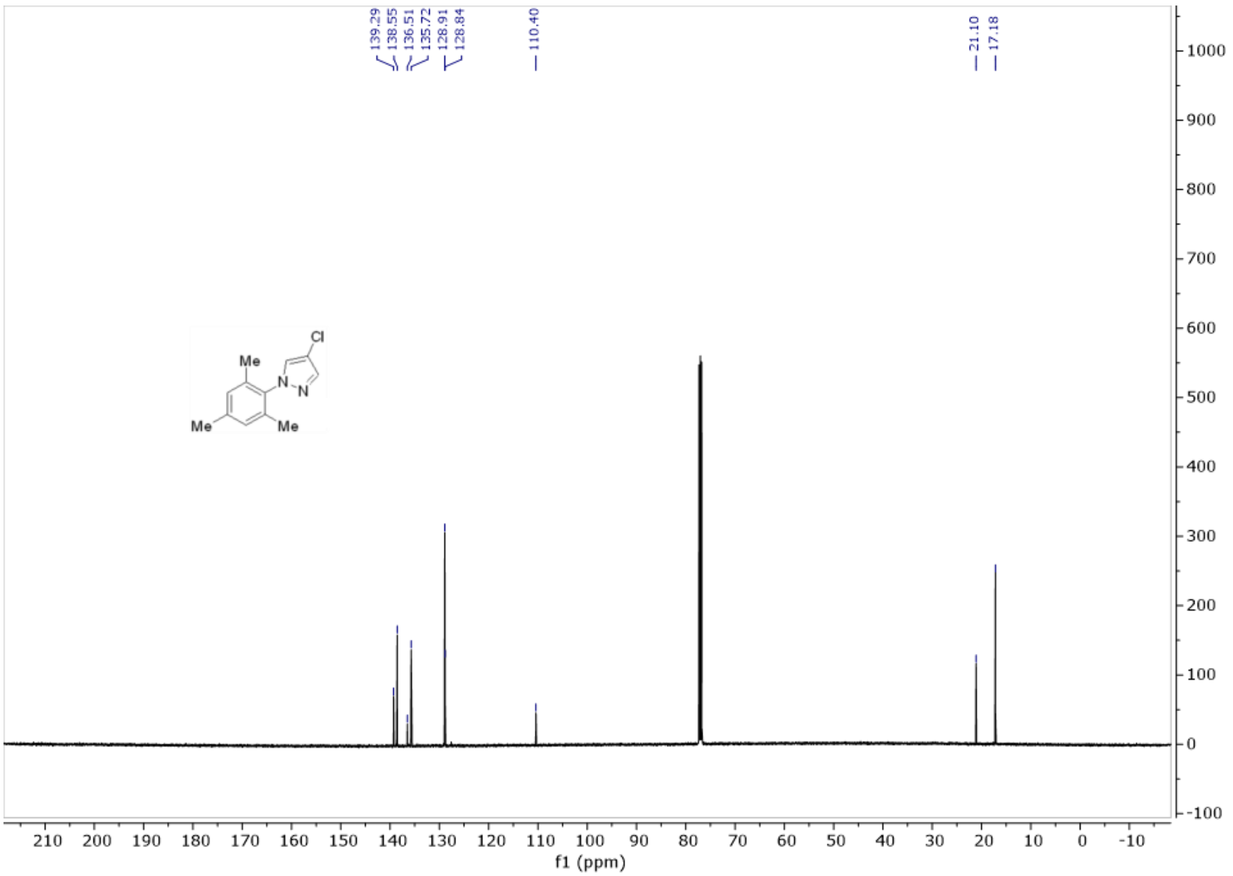
139.29
138.55
136.51
135.72
128.91
128.84
110.40
21.10
17.18
Cl
Me
N
N
Me
Me
1000
900
800
700
600
500
400
300
200
100
0
-100
210 200 190 180 170 160 150 140 130 120 110 100 90 80 70 60 50 40 30 20 10 0 -10
f1 (ppm)

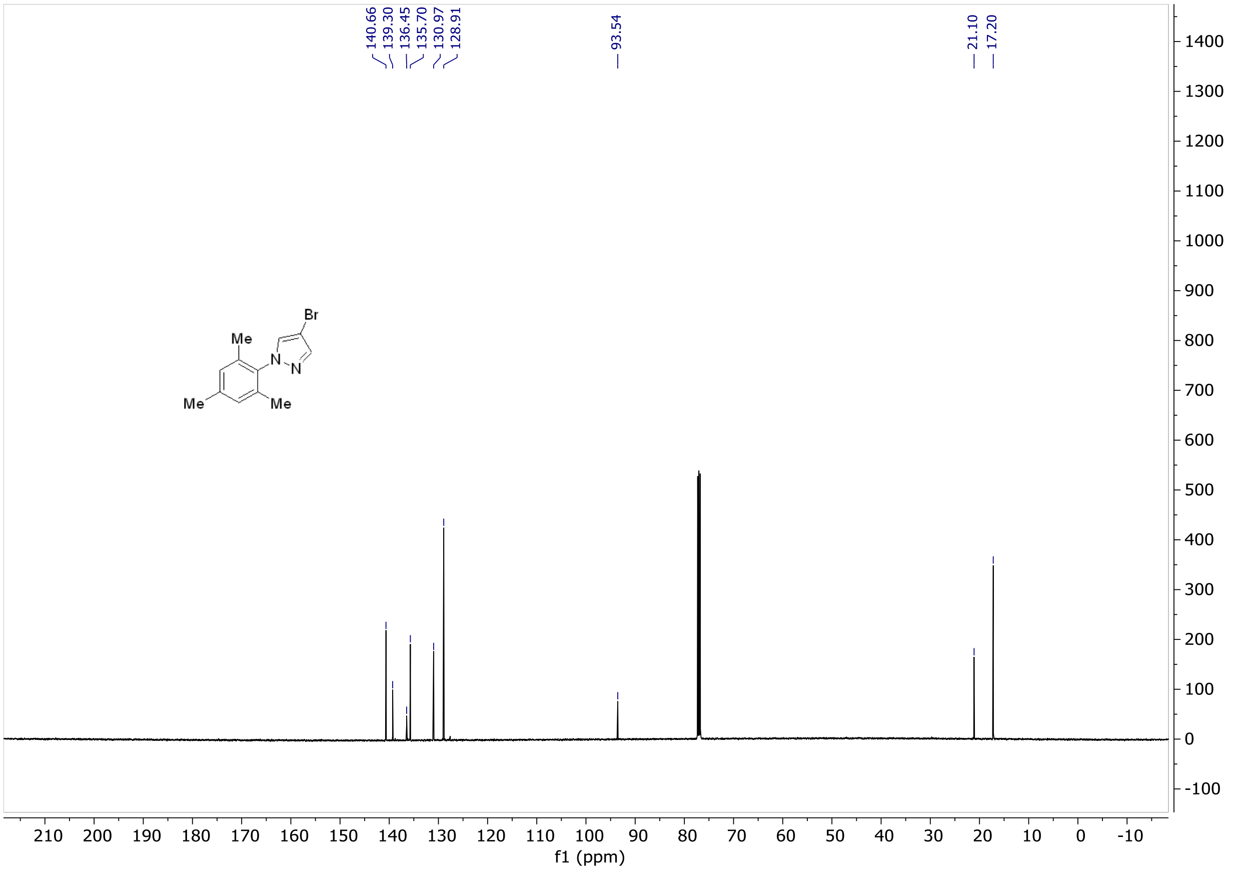
140.66
139.30
136.45
135.70
130.97
128.91
93.54
21.10
17.20
Br
Me
N
N
Me
Me
1400
1300
1200
1100
1000
900
800
700
600
500
400
300
200
100
0
-100
210 200 190 180 170 160 150 140 130 120 110 100 90 80 70 60 50 40 30 20 10 0 -10
f1 (ppm)

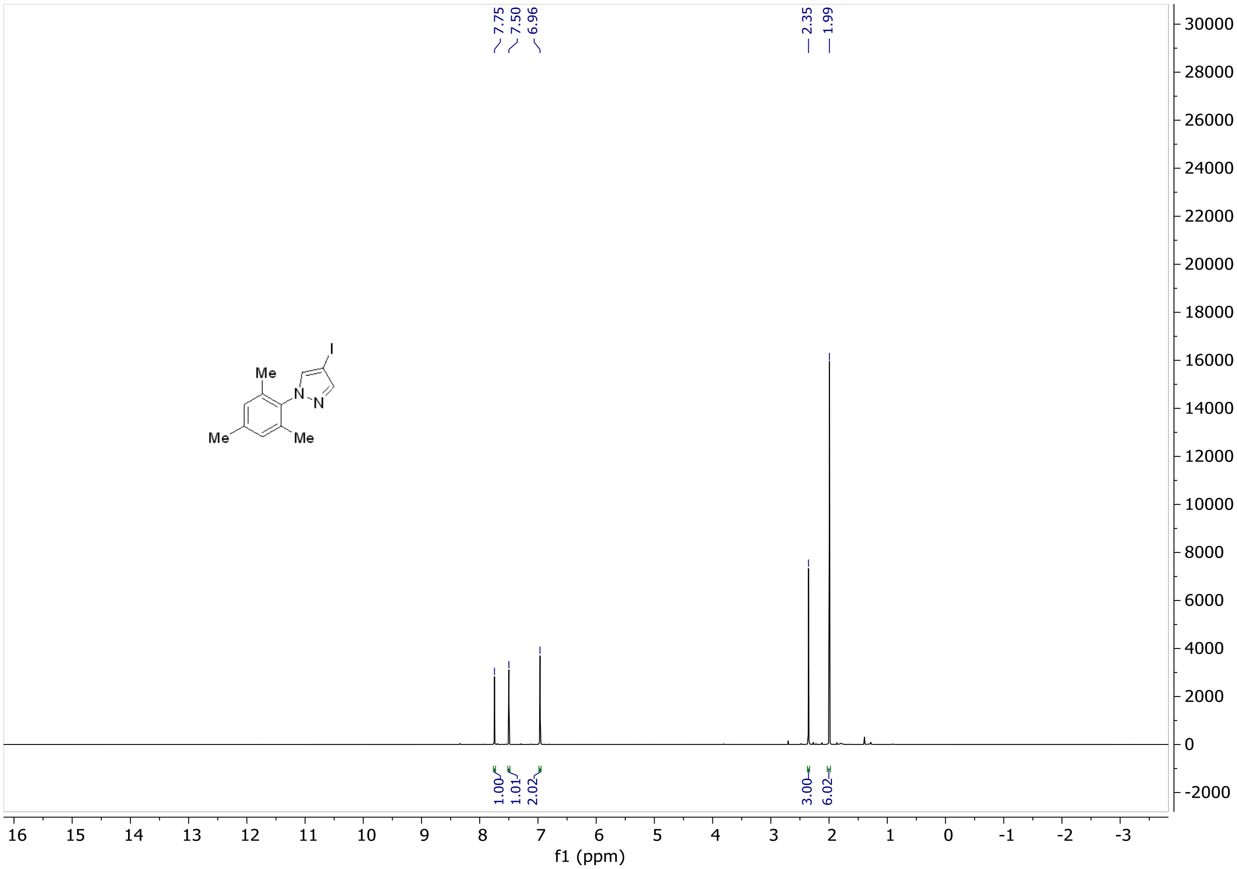
7.75
7.50
6.96
2.35
1.99
1.00
1.01
2.02
3.00
6.02
I
Me
N
N
Me
Me
30000
28000
26000
24000
22000
20000
18000
16000
14000
12000
10000
8000
6000
4000
2000
0
-2000
16 15 14 13 12 11 10 9 8 7 6 5 4 3 2 1 0 -1 -2 -3
f1 (ppm)

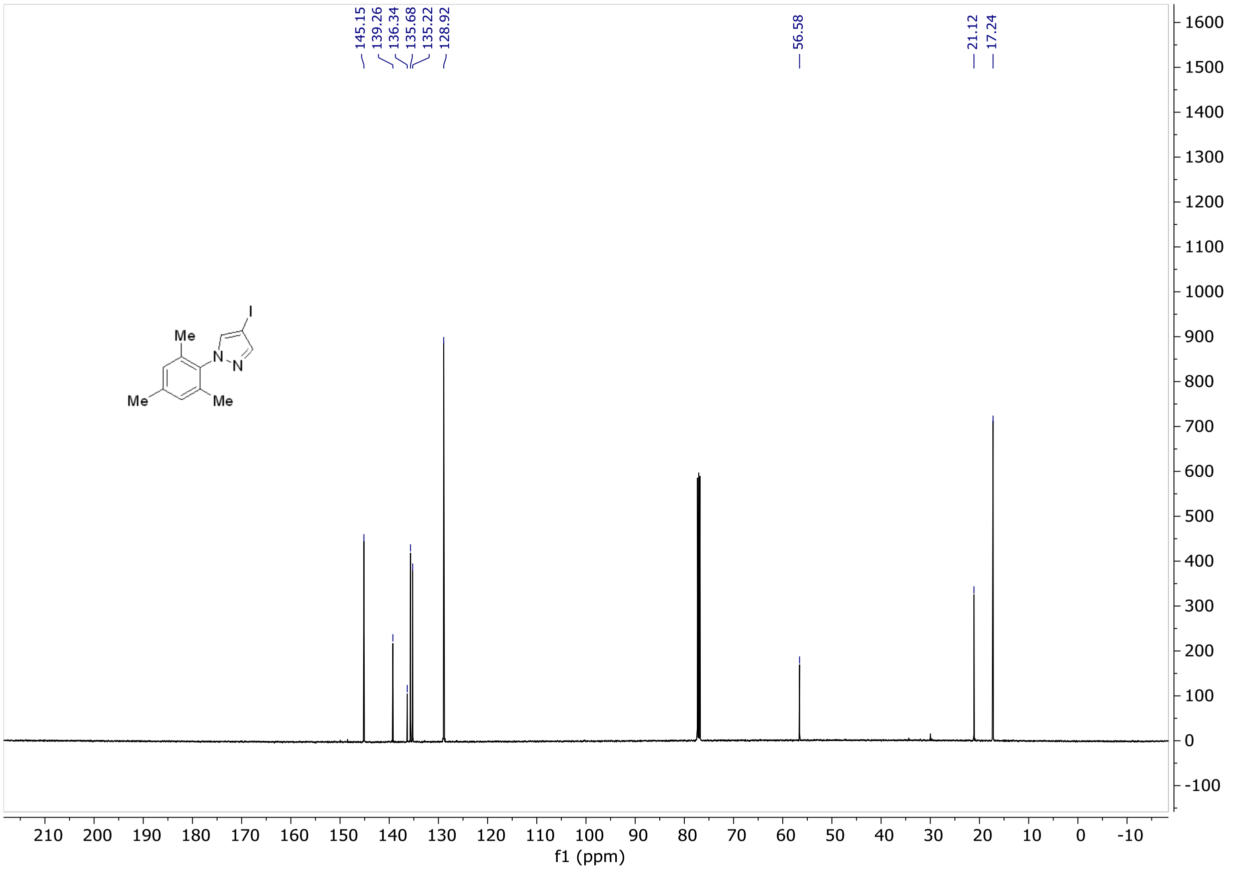
145.15
139.26
136.34
135.68
135.22
128.92
56.58
21.12
17.24
I
Me
N
N
Me
Me
1600
1500
1400
1300
1200
1100
1000
900
800
700
600
500
400
300
200
100
0
-100
210 200 190 180 170 160 150 140 130 120 110 100 90 80 70 60 50 40 30 20 10 0 -10
f1 (ppm)

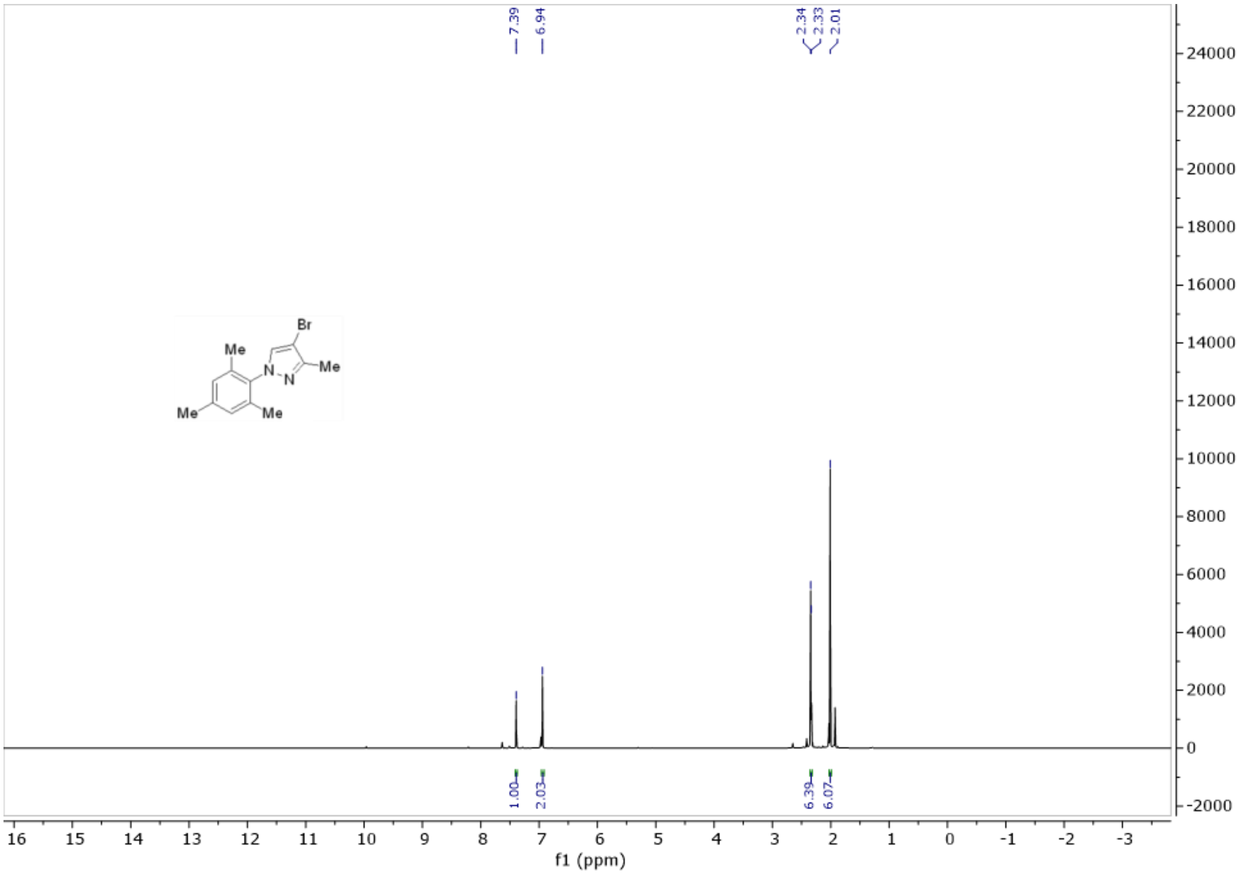
7.39
6.94
2.34
2.33
2.01
Br
Me
N
N
Me
Me
Me
1.00
2.03
6.39
6.07
24000
22000
20000
18000
16000
14000
12000
10000
8000
6000
4000
2000
0
-2000
16 15 14 13 12 11 10 9 8 7 6 5 4 3 2 1 0 -1 -2 -3
f1 (ppm)

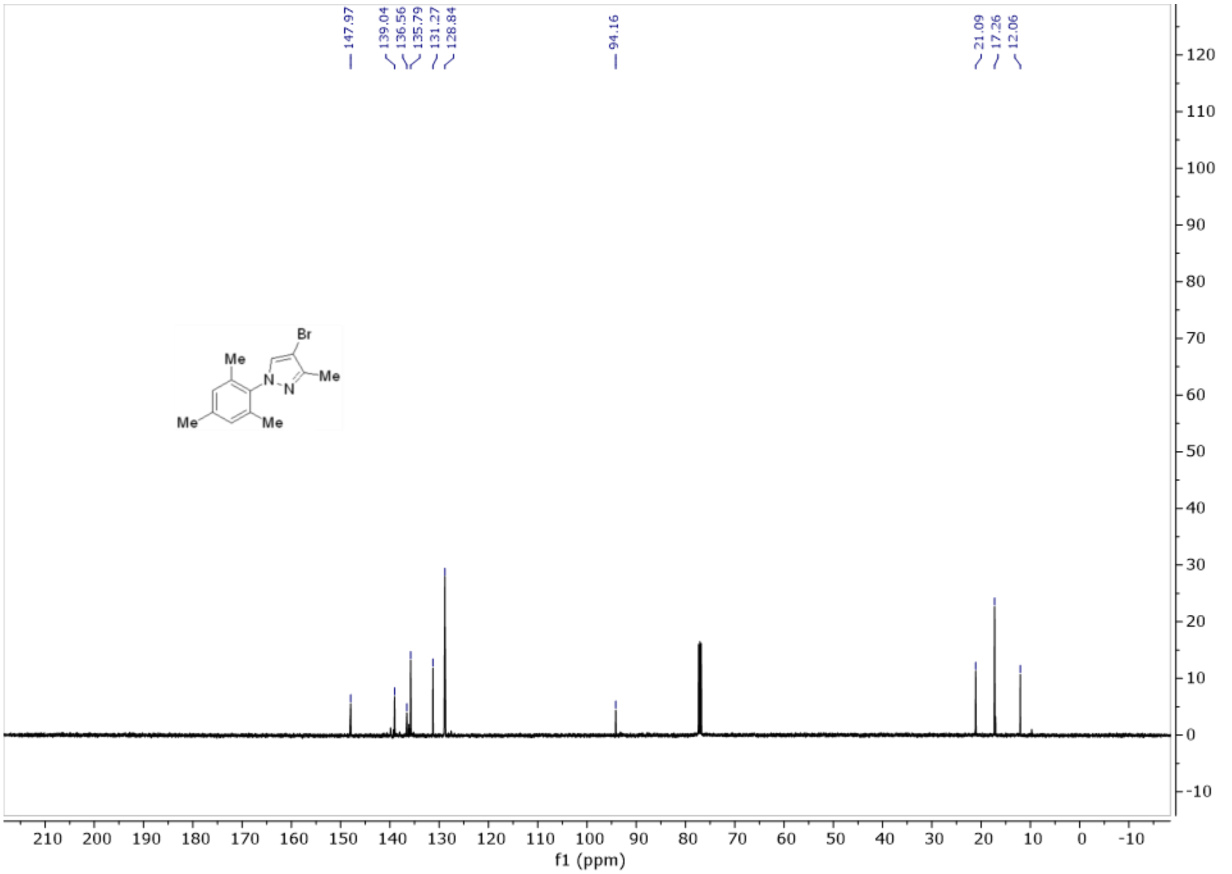
147.97
139.04
136.56
135.79
131.27
128.84
94.16
21.09
17.26
12.06
Br
Me
N
N
Me
Me
Me
120
110
100
90
80
70
60
50
40
30
20
10
0
-10
210 200 190 180 170 160 150 140 130 120 110 100 90 80 70 60 50 40 30 20 10 0 -10
f1 (ppm)

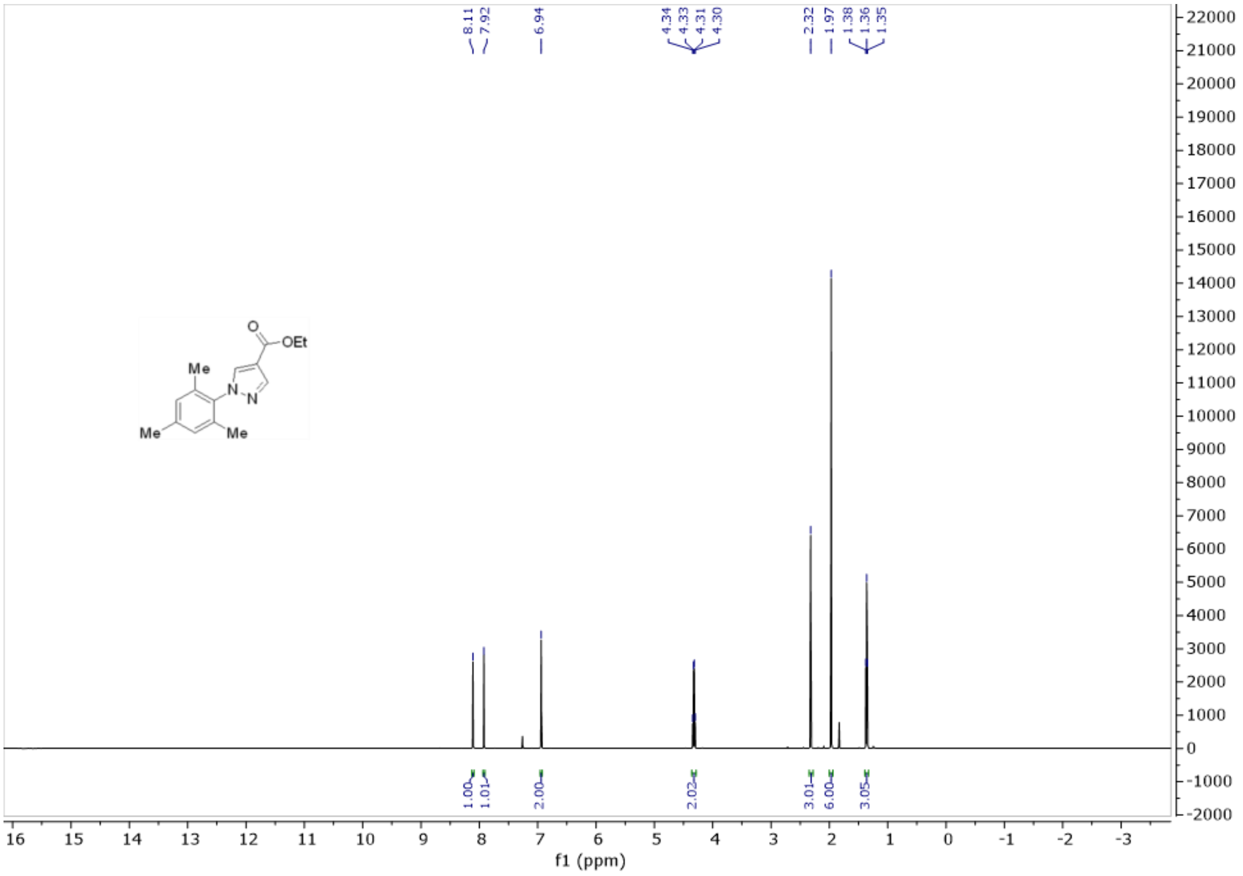

8.11
7.92
6.94
4.34
4.33
4.31
4.30
2.32
1.97
1.38
1.36
1.35
1.00
1.01
2.00
2.02
3.01
6.00
3.05
O
OEt
Me
N
N
Me
Me
22000
21000
20000
19000
18000
17000
16000
15000
14000
13000
12000
11000
10000
9000
8000
7000
6000
5000
4000
3000
2000
1000
0
-1000
-2000
16
15
14
13
12
11
10
9
8
7
6
5
4
3
2
1
0
-1
-2
-3
f1 (ppm)

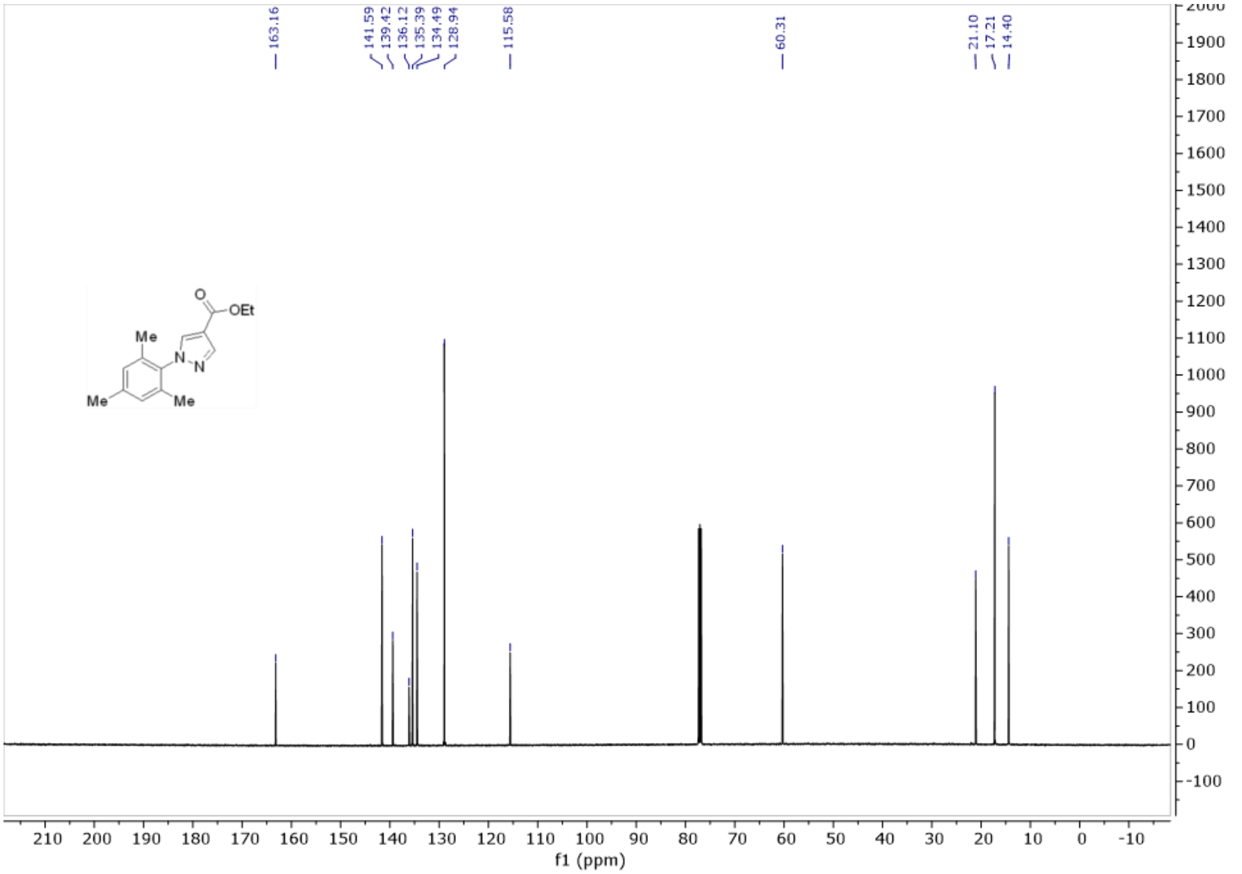

163.16
141.59
139.42
136.12
135.39
134.49
128.94
115.58
60.31
21.10
17.21
14.40
O
OEt
Me
N
N
Me
Me
2000
1900
1800
1700
1600
1500
1400
1300
1200
1100
1000
900
800
700
600
500
400
300
200
100
0
-100
210
200
190
180
170
160
150
140
130
120
110
100
90
80
70
60
50
40
30
20
10
0
-10
f1 (ppm)

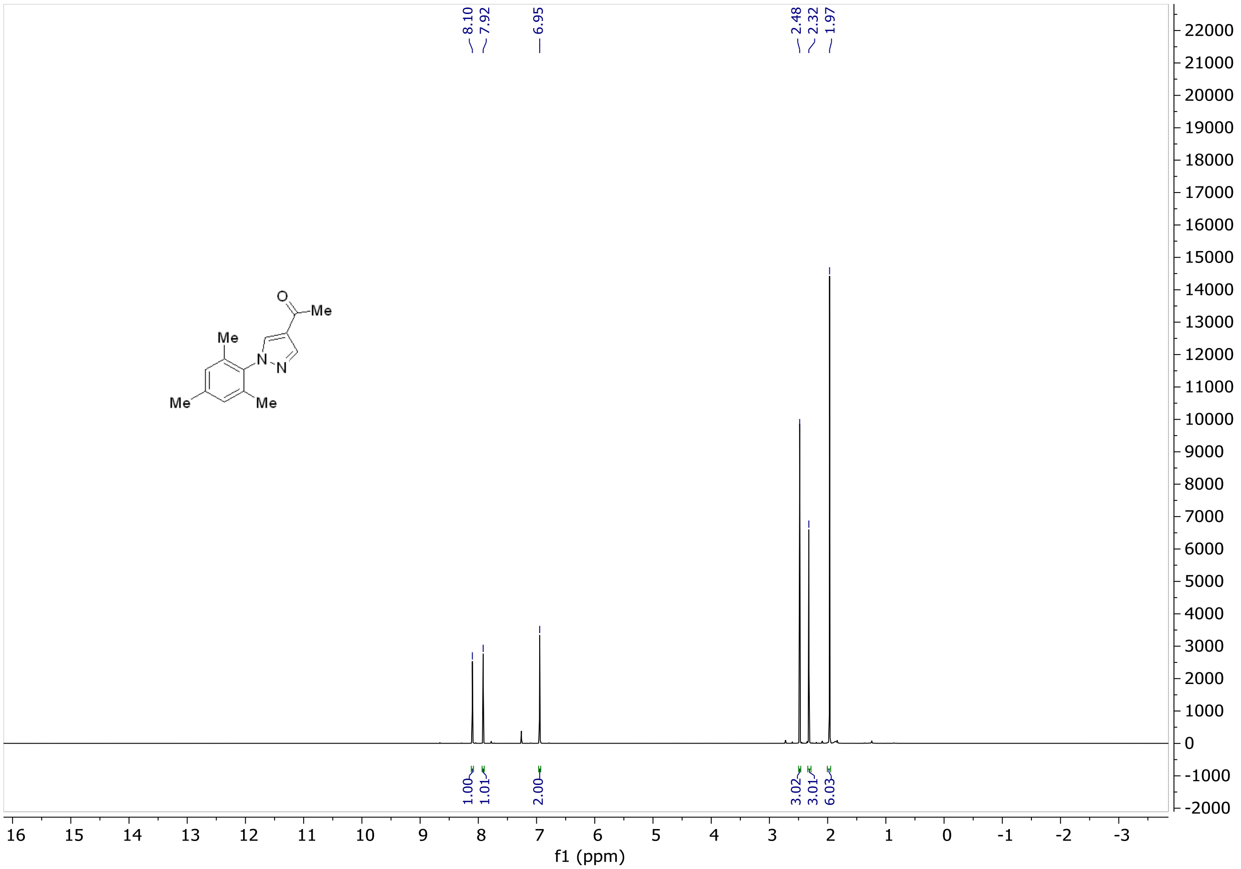
8.10
7.92
6.95
2.48
2.32
1.97
1.00
1.01
2.00
3.02
3.01
6.03
O
Me
Me
N
N
Me
Me
f1 (ppm)

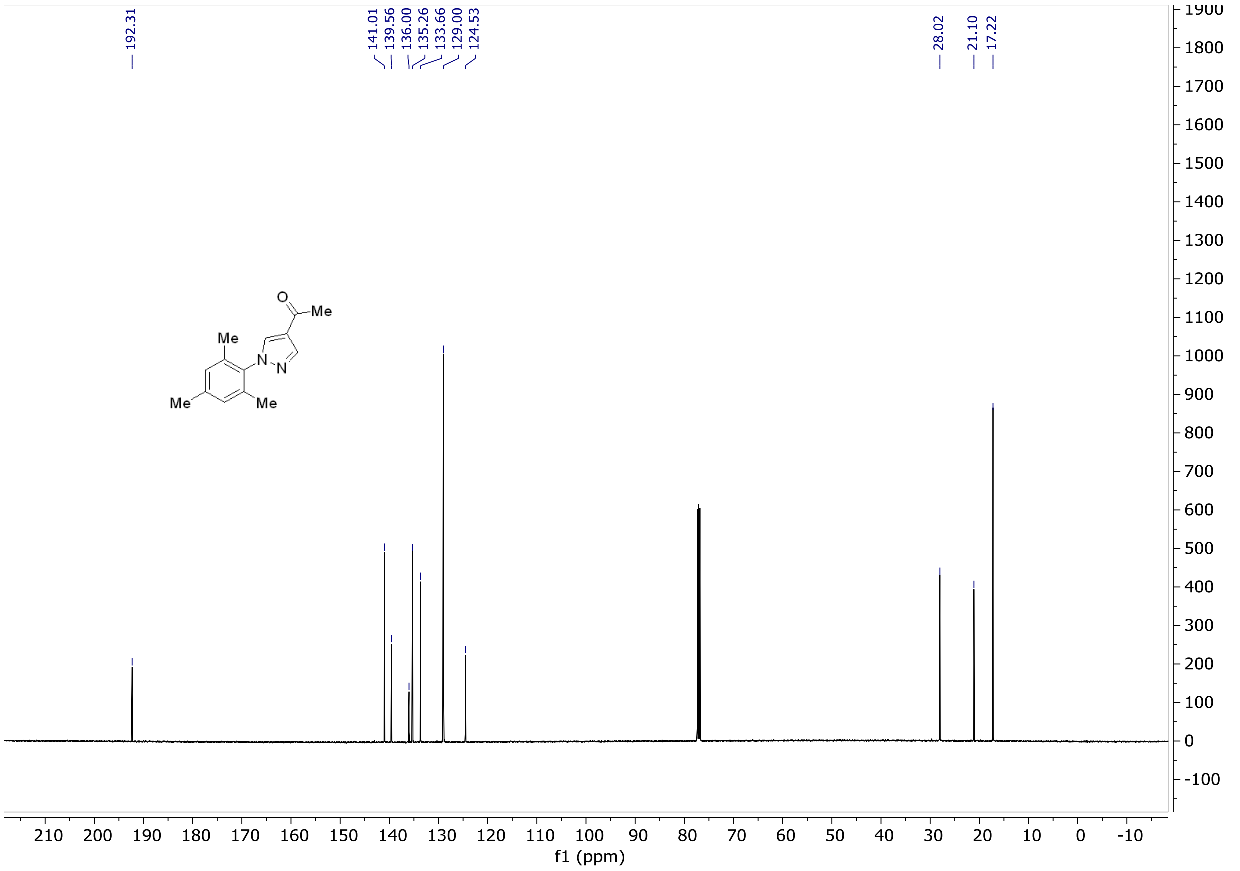
192.31
141.01
139.56
136.00
135.26
133.66
129.00
124.53
28.02
21.10
17.22
O
Me
Me
N
N
Me
Me
f1 (ppm)

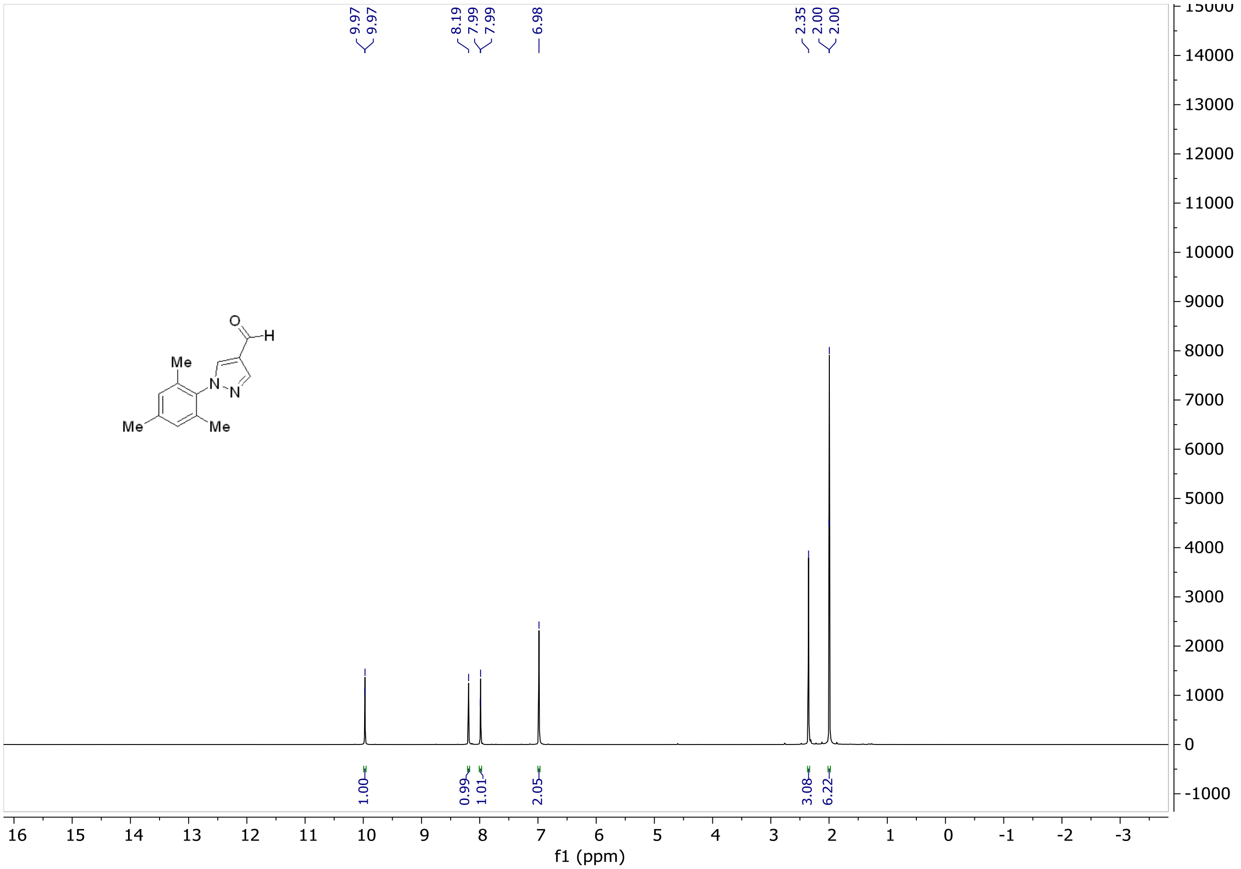

9.97
9.97
8.19
7.99
7.99
6.98
2.35
2.00
2.00
O
H
Me
N
N
Me
Me
1.00
0.99
1.01
2.05
3.08
6.22
16 15 14 13 12 11 10 9 8 7 6 5 4 3 2 1 0 -1 -2 -3
f1 (ppm)
15000
14000
13000
12000
11000
10000
9000
8000
7000
6000
5000
4000
3000
2000
1000
0
-1000

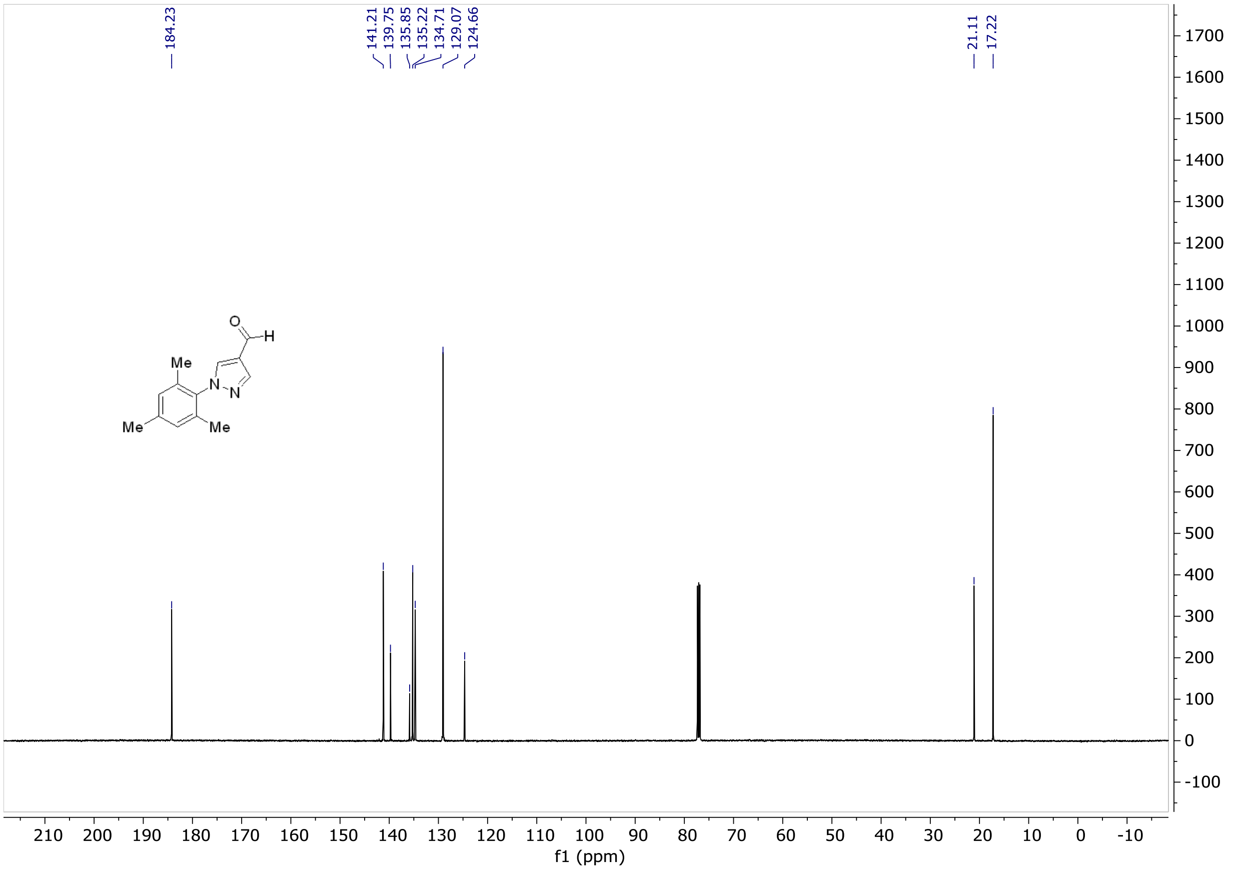

184.23
141.21
139.75
135.85
135.22
134.71
129.07
124.66
21.11
17.22
O
H
Me
N
N
Me
Me
210 200 190 180 170 160 150 140 130 120 110 100 90 80 70 60 50 40 30 20 10 0 -10
f1 (ppm)
1700
1600
1500
1400
1300
1200
1100
1000
900
800
700
600
500
400
300
200
100
0
-100

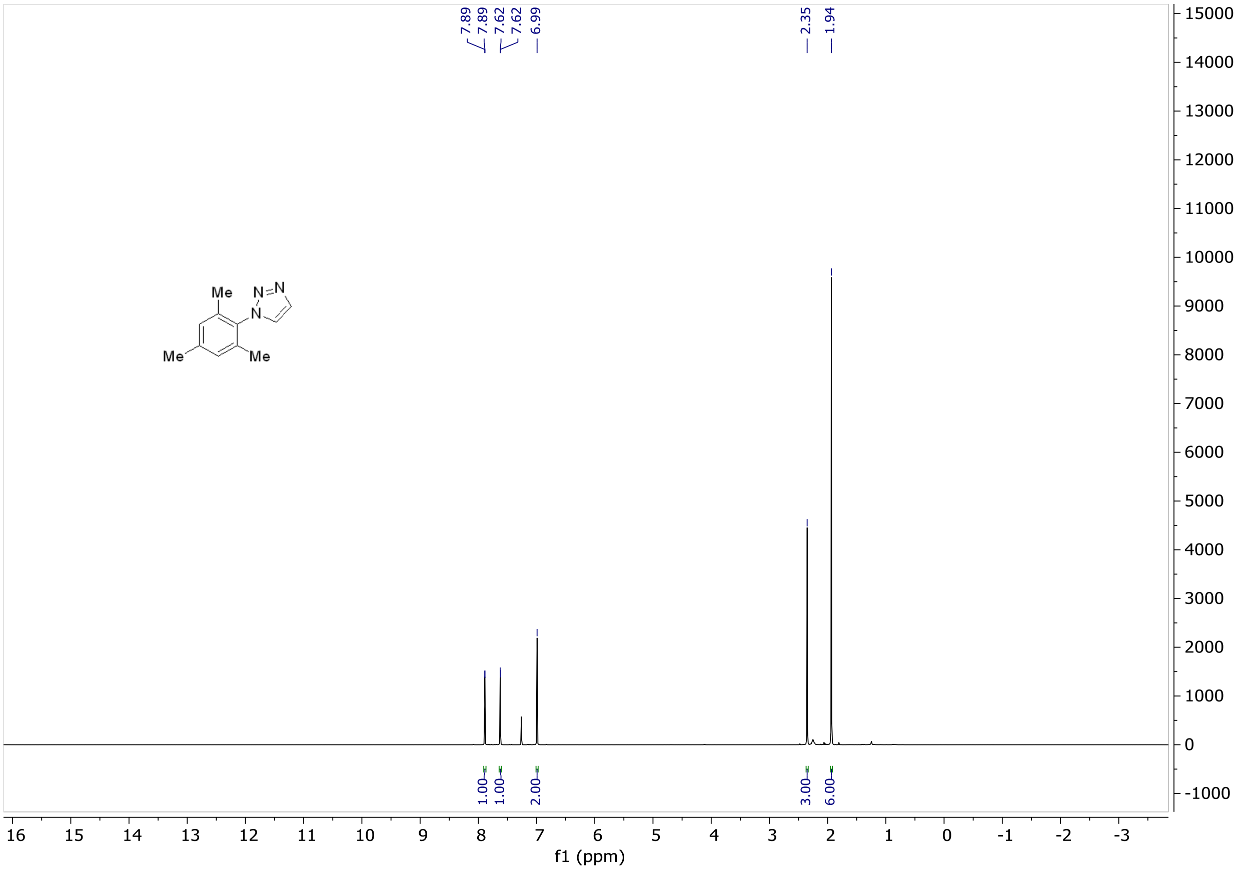

7.89
7.89
7.62
7.62
6.99
2.35
1.94
Me
N
N
N
N
Me
Me
1.00
1.00
2.00
3.00
6.00
15000
14000
13000
12000
11000
10000
9000
8000
7000
6000
5000
4000
3000
2000
1000
0
-1000
16
15
14
13
12
11
10
9
8
7
6
5
4
3
2
1
0
-1
-2
-3
f1 (ppm)

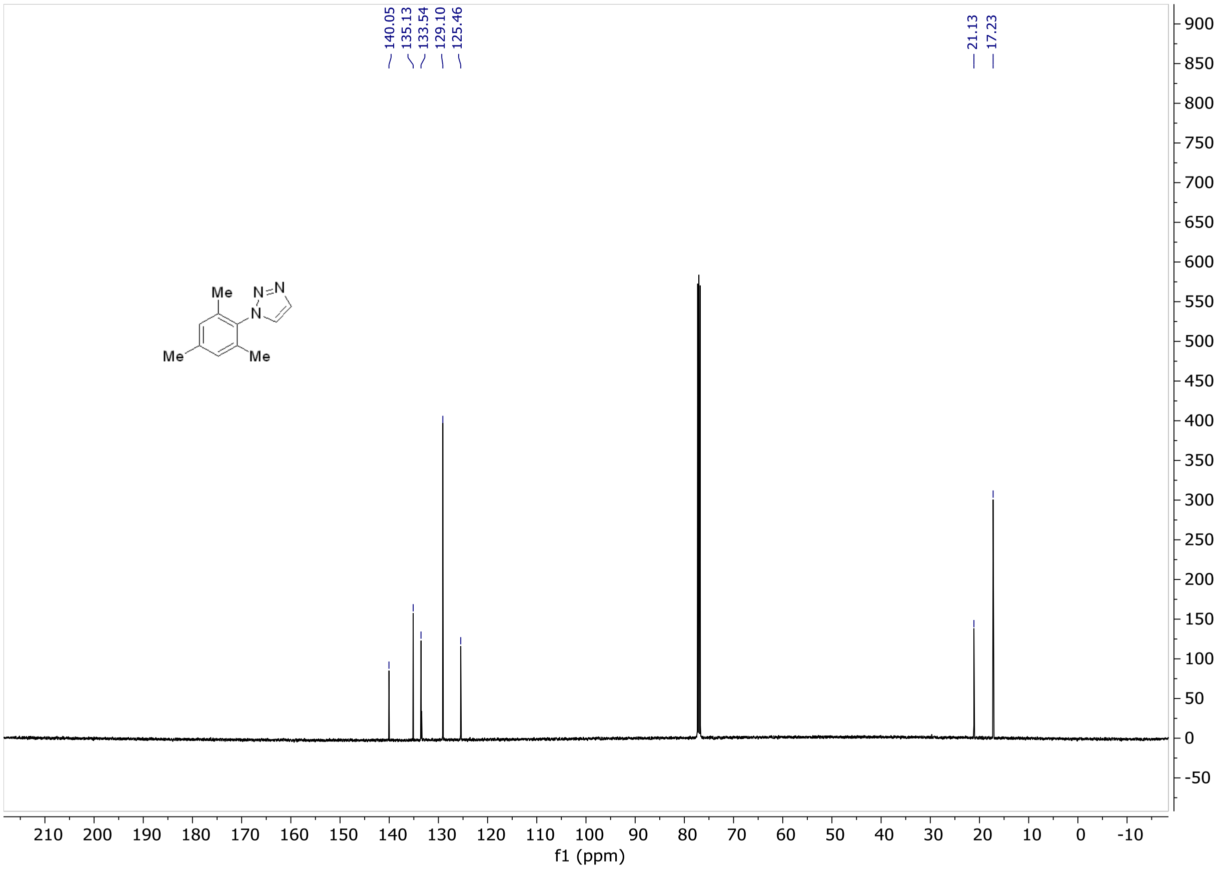

140.05
135.13
133.54
129.10
125.46
21.13
17.23
Me
N
N
N
N
Me
Me
900
850
800
750
700
650
600
550
500
450
400
350
300
250
200
150
100
50
0
-50
210
200
190
180
170
160
150
140
130
120
110
100
90
80
70
60
50
40
30
20
10
0
-10
f1 (ppm)

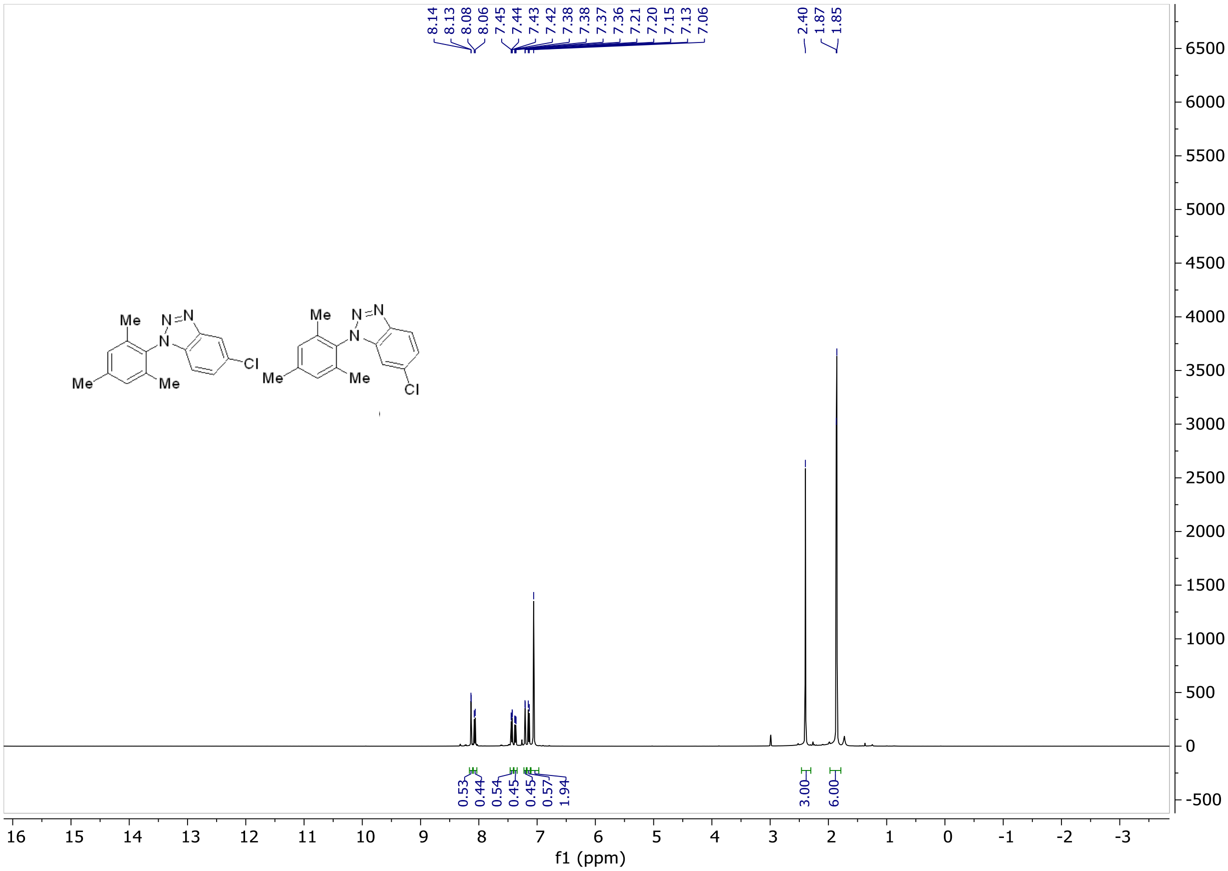
8.14
8.13
8.08
8.06
7.45
7.44
7.43
7.42
7.38
7.38
7.37
7.36
7.21
7.20
7.15
7.13
7.06
2.40
1.87
1.85
Me
N
N=N
N
Me
Me
Cl
Me
N
N=N
N
Me
Me
Cl
0.53
0.44
0.54
0.45
0.45
0.57
1.94
3.00
6.00
6500
6000
5500
5000
4500
4000
3500
3000
2500
2000
1500
1000
500
0
-500
16
15
14
13
12
11
10
9
8
7
6
5
4
3
2
1
0
-1
-2
-3
f1 (ppm)

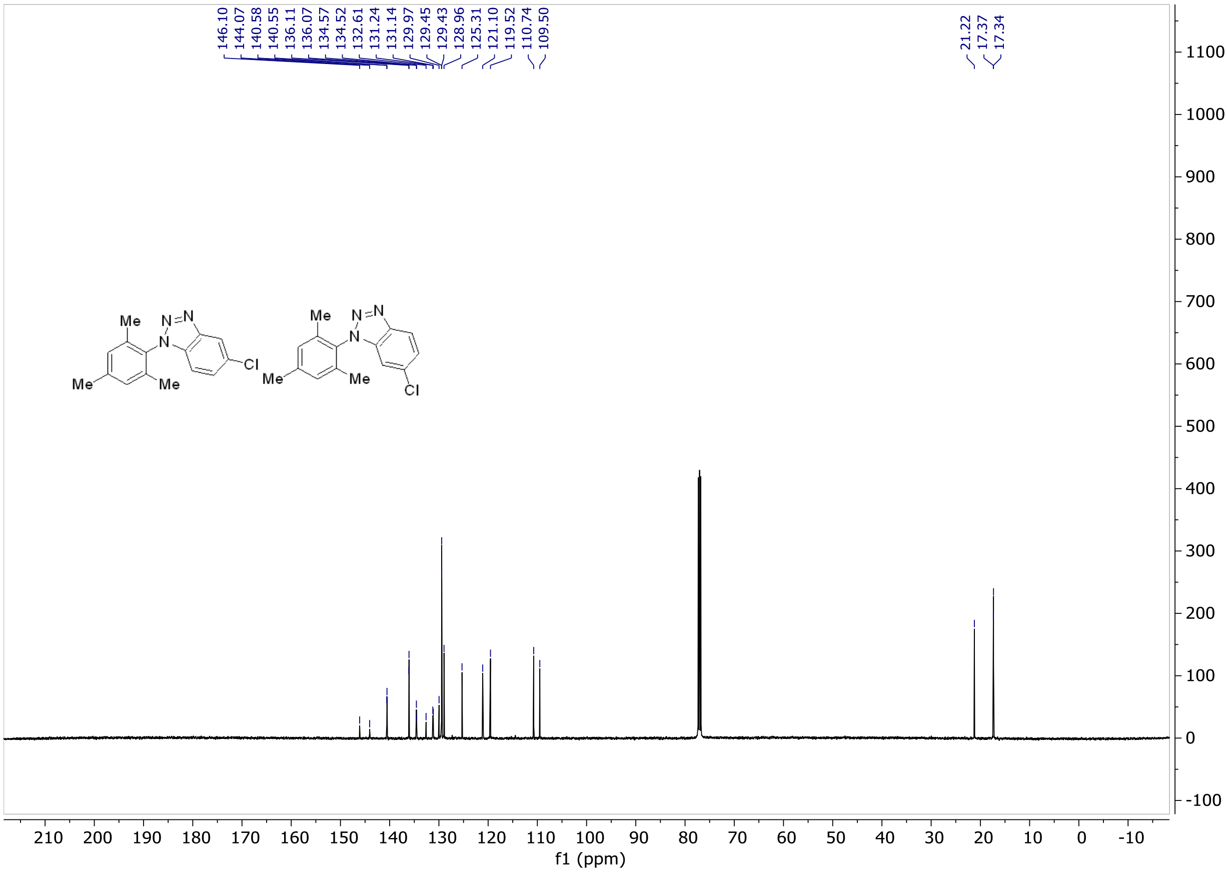
146.10
144.07
140.58
140.55
136.11
136.07
134.57
134.52
132.61
131.24
131.14
129.97
129.45
129.43
128.96
125.31
121.10
119.52
110.74
109.50
21.22
17.37
17.34
Me
N
N=N
N
Me
Me
Cl
Me
N
N=N
N
Me
Me
Cl
1100
1000
900
800
700
600
500
400
300
200
100
0
-100
210
200
190
180
170
160
150
140
130
120
110
100
90
80
70
60
50
40
30
20
10
0
-10
f1 (ppm)

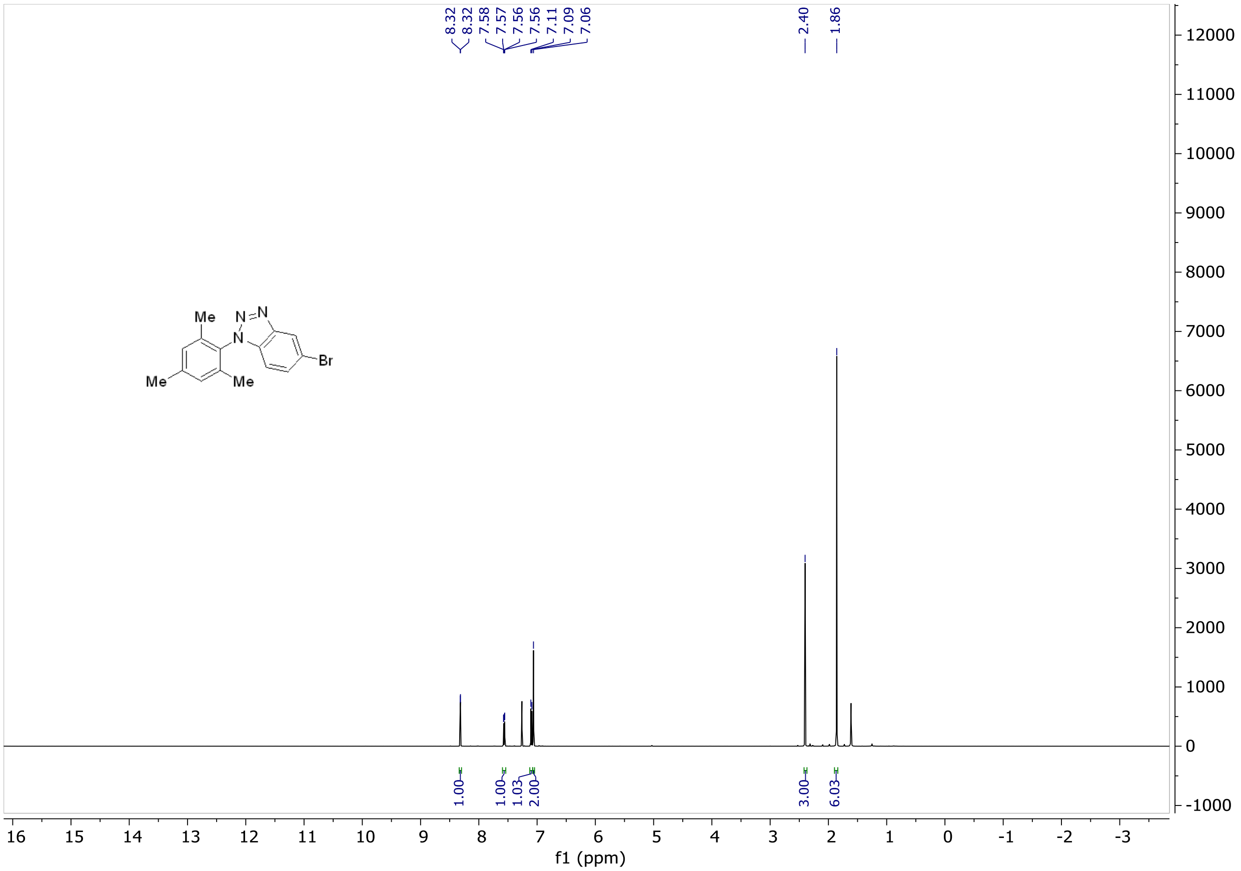
8.32
8.32
7.58
7.57
7.56
7.56
7.11
7.09
7.06
2.40
1.86
Me
N=N
N
Br
Me
Me
1.00
1.00
1.03
2.00
3.00
6.03
12000
11000
10000
9000
8000
7000
6000
5000
4000
3000
2000
1000
0
-1000
16
15
14
13
12
11
10
9
8
7
6
5
4
3
2
1
0
-1
-2
-3
f1 (ppm)

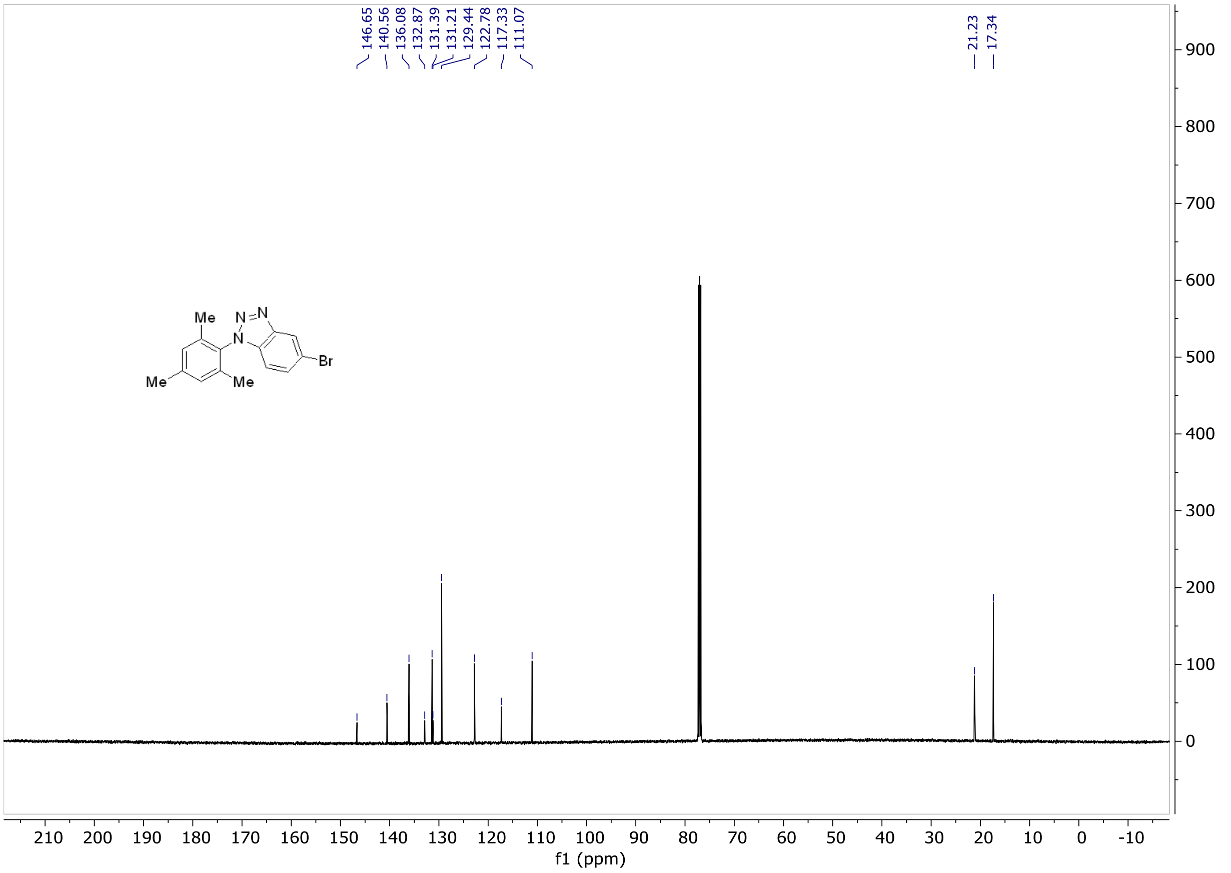
146.65
140.56
136.08
132.87
131.39
131.21
129.44
122.78
117.33
111.07
21.23
17.34
Me
N=N
N
Br
Me
Me
900
800
700
600
500
400
300
200
100
0
210
200
190
180
170
160
150
140
130
120
110
100
90
80
70
60
50
40
30
20
10
0
-10
f1 (ppm)

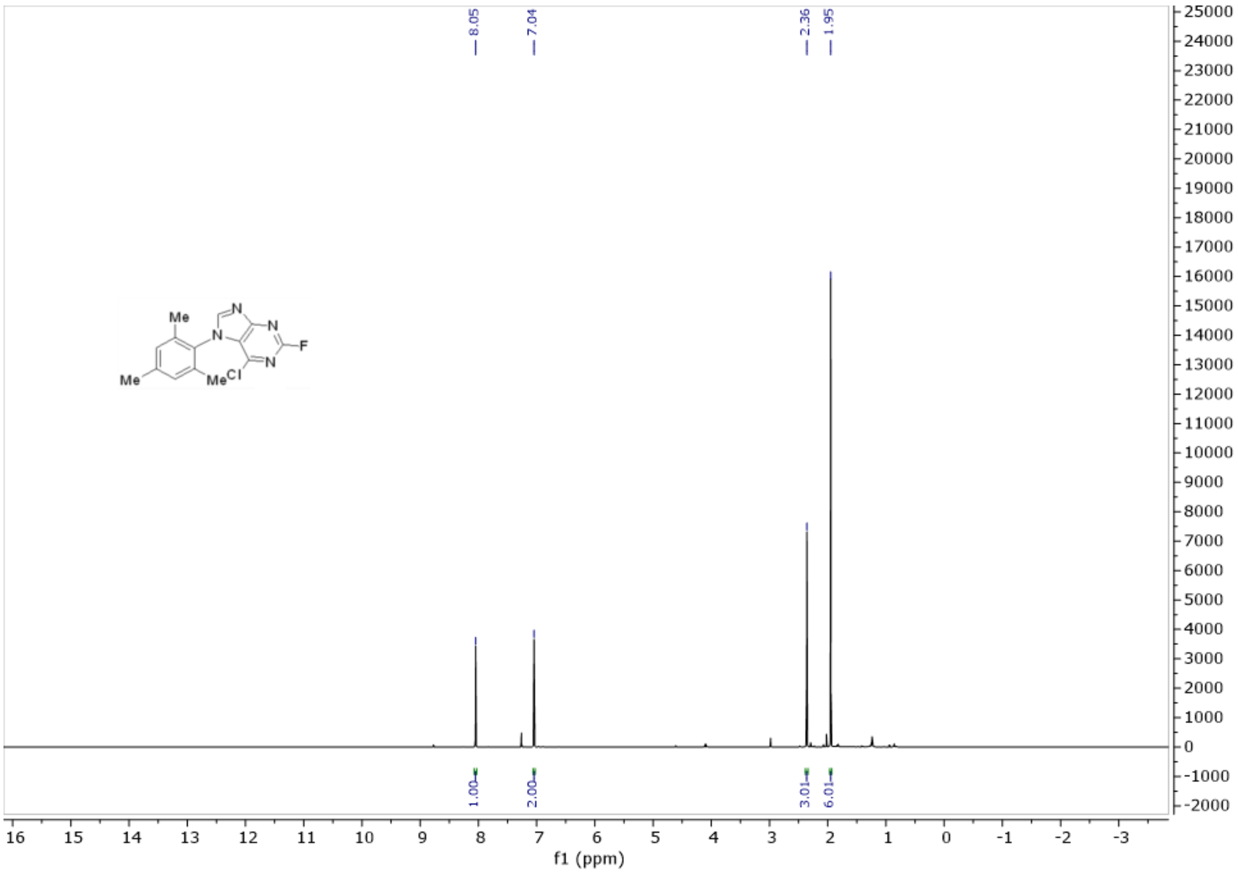
8.05
7.04
2.36
1.95
1.00
2.00
3.01
6.01
Me
Me
Me
N
N
N
N
F
Cl
25000
24000
23000
22000
21000
20000
19000
18000
17000
16000
15000
14000
13000
12000
11000
10000
9000
8000
7000
6000
5000
4000
3000
2000
1000
0
-1000
-2000
16 15 14 13 12 11 10 9 8 7 6 5 4 3 2 1 0 -1 -2 -3
f1 (ppm)

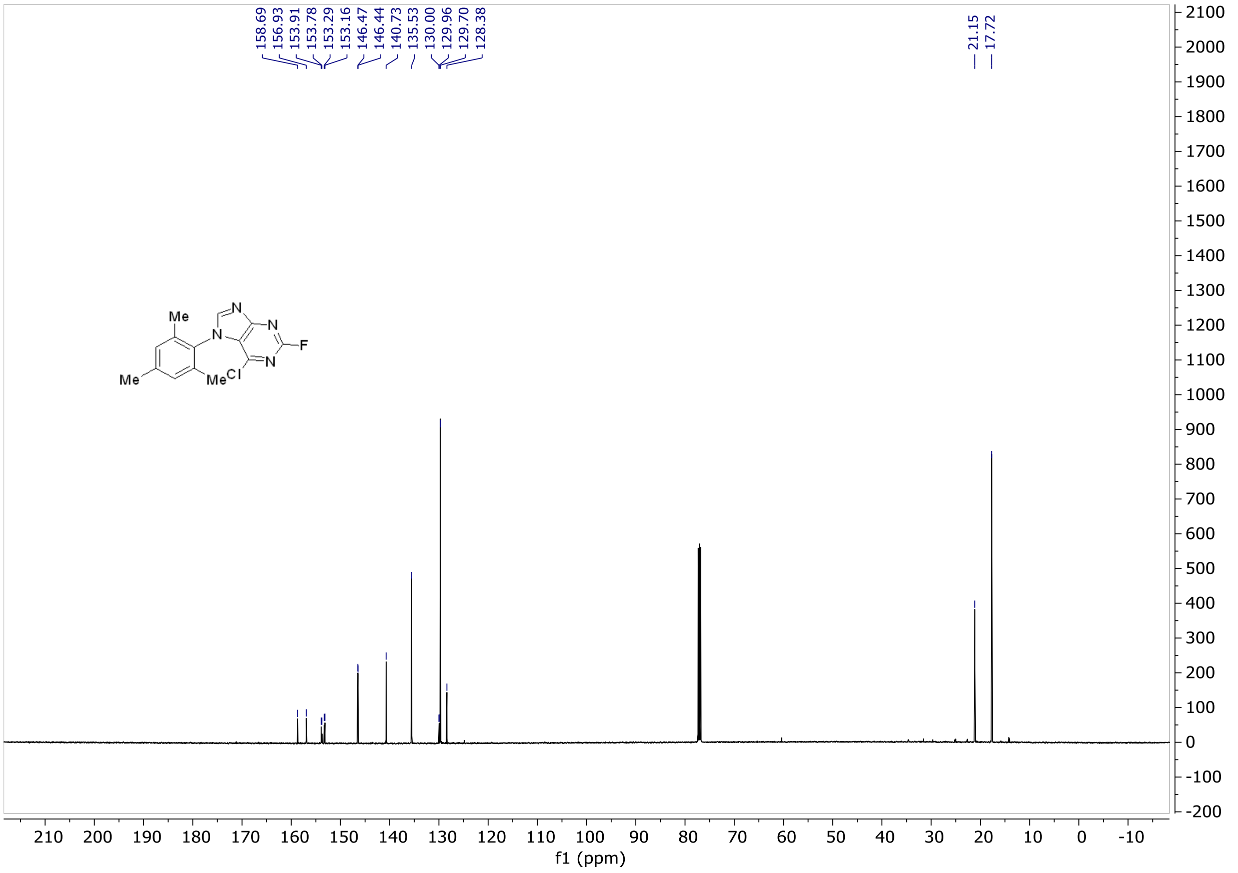
158.69
156.93
153.91
153.78
153.29
153.16
146.47
146.44
140.73
135.53
130.00
129.96
129.70
128.38
21.15
17.72
Me
Me
Me
N
N
N
N
F
Cl
2100
2000
1900
1800
1700
1600
1500
1400
1300
1200
1100
1000
900
800
700
600
500
400
300
200
100
0
-100
-200
210 200 190 180 170 160 150 140 130 120 110 100 90 80 70 60 50 40 30 20 10 0 -10
f1 (ppm)

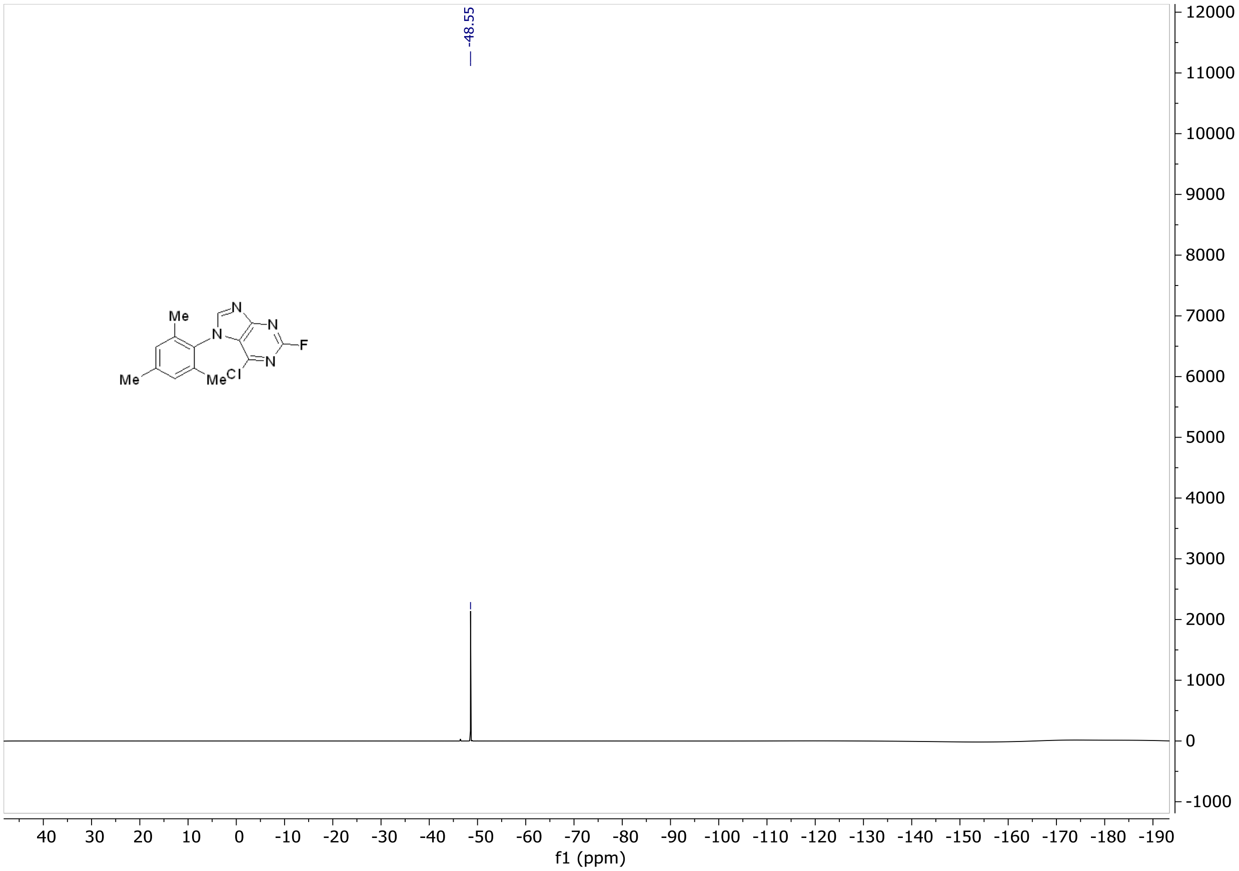
-48.55
Me
N
N
N
F
Me
Me
Cl
N
N
12000
11000
10000
9000
8000
7000
6000
5000
4000
3000
2000
1000
0
-1000
40
30
20
10
0
-10
-20
-30
-40
-50
-60
-70
-80
-90
-100
-110
-120
-130
-140
-150
-160
-170
-180
-190
f1 (ppm)

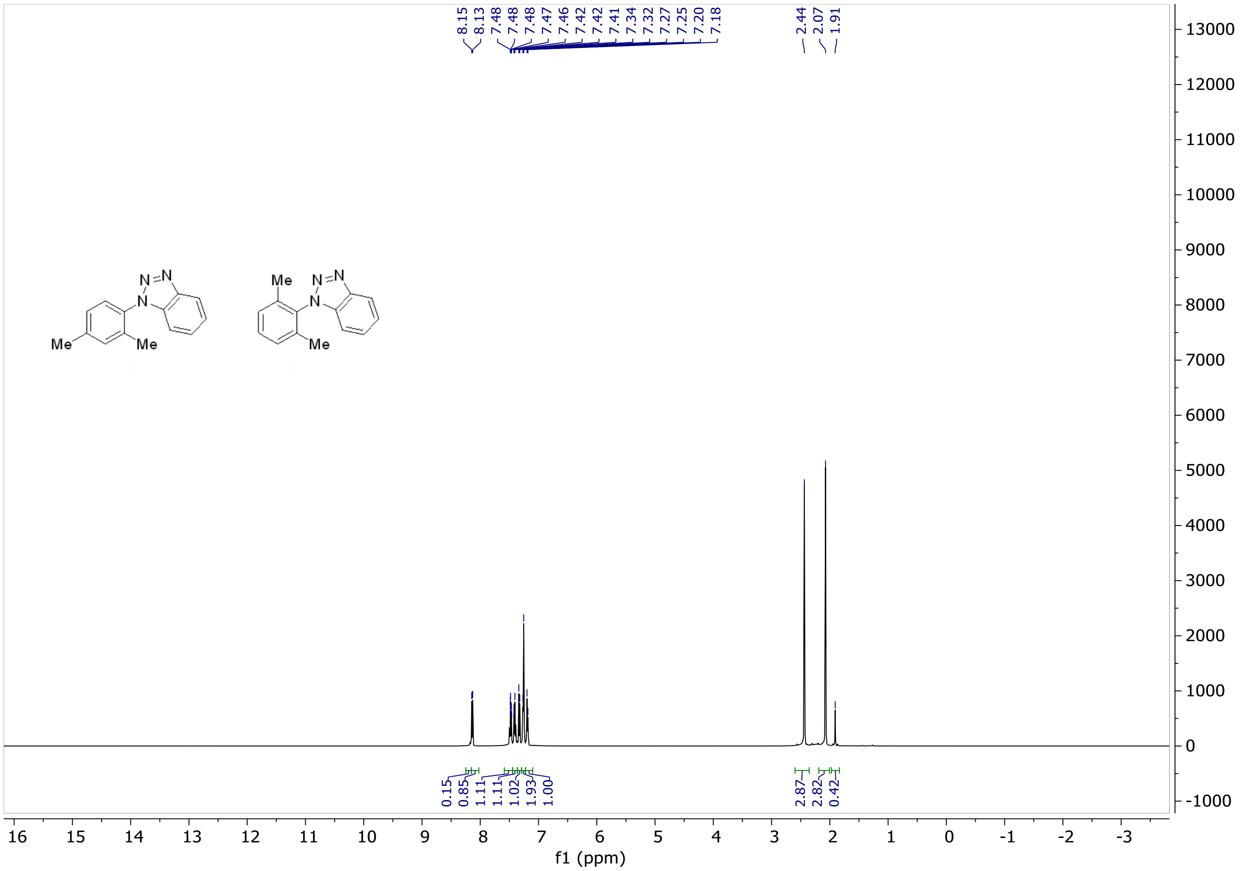
8.15
8.13
7.48
7.48
7.48
7.47
7.46
7.42
7.42
7.41
7.34
7.32
7.27
7.25
7.20
7.18
2.44
2.07
1.91
N=N
N
Me
Me
Me
0.15
0.85
1.11
1.11
1.02
1.93
1.00
2.87
2.82
0.42
f1 (ppm)

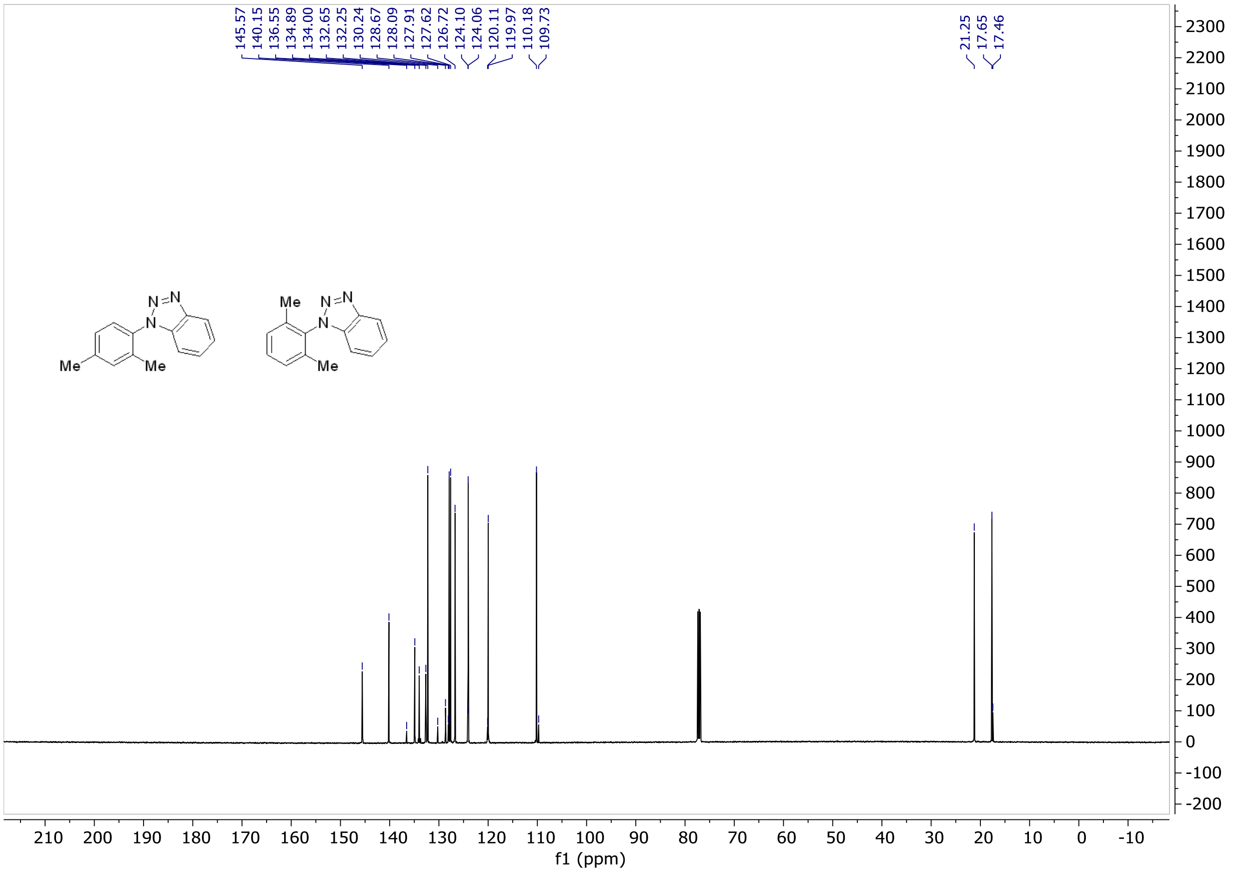
145.57
140.15
136.55
134.89
134.00
132.65
132.25
130.24
128.67
128.09
127.91
127.62
126.72
124.10
124.06
120.11
119.97
110.18
109.73
21.25
17.65
17.46
N=N
N
Me
Me
Me
f1 (ppm)

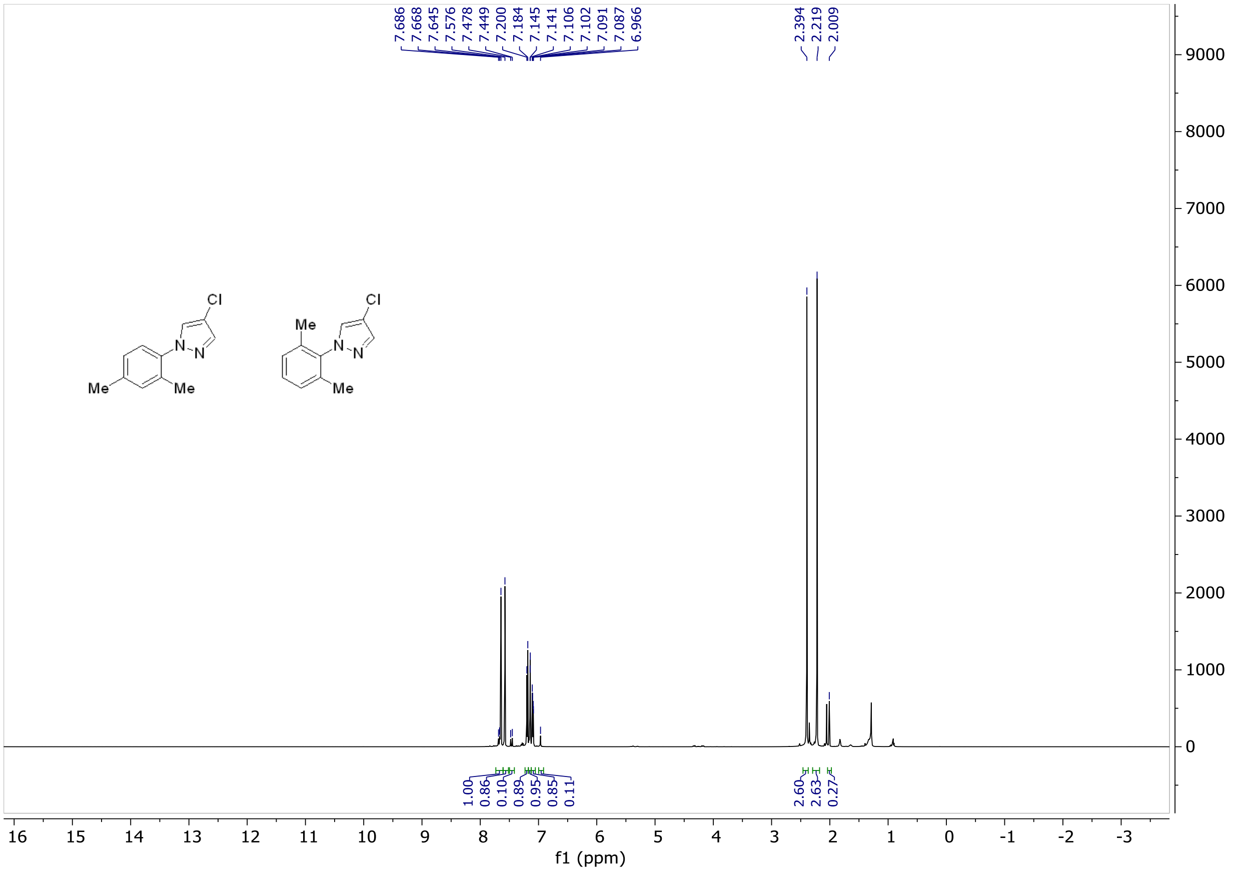
7.686
7.668
7.645
7.576
7.478
7.449
7.200
7.184
7.145
7.141
7.106
7.102
7.091
7.087
6.966
2.394
2.219
2.009
Cl
N
N
Me
Me
Cl
Me
N
N
Me
1.00
0.86
0.10
0.89
0.95
0.85
0.11
2.60
2.63
0.27
9000
8000
7000
6000
5000
4000
3000
2000
1000
0
16
15
14
13
12
11
10
9
8
7
6
5
4
3
2
1
0
-1
-2
-3
f1 (ppm)

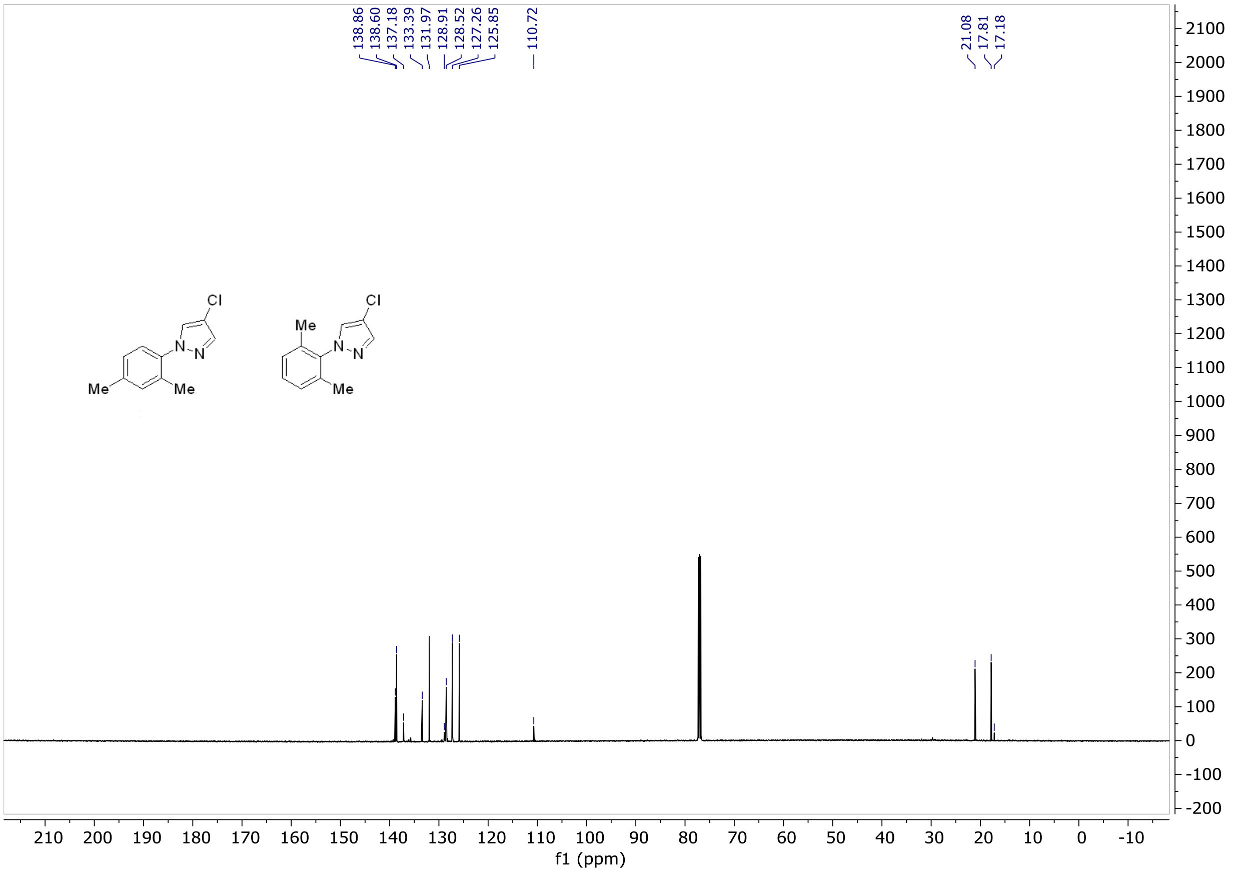
138.86
138.60
137.18
133.39
131.97
128.91
128.52
127.26
125.85
110.72
21.08
17.81
17.18
Cl
N
N
Me
Me
Cl
Me
N
N
Me
2100
2000
1900
1800
1700
1600
1500
1400
1300
1200
1100
1000
900
800
700
600
500
400
300
200
100
0
-100
-200
210
200
190
180
170
160
150
140
130
120
110
100
90
80
70
60
50
40
30
20
10
0
-10
f1 (ppm)

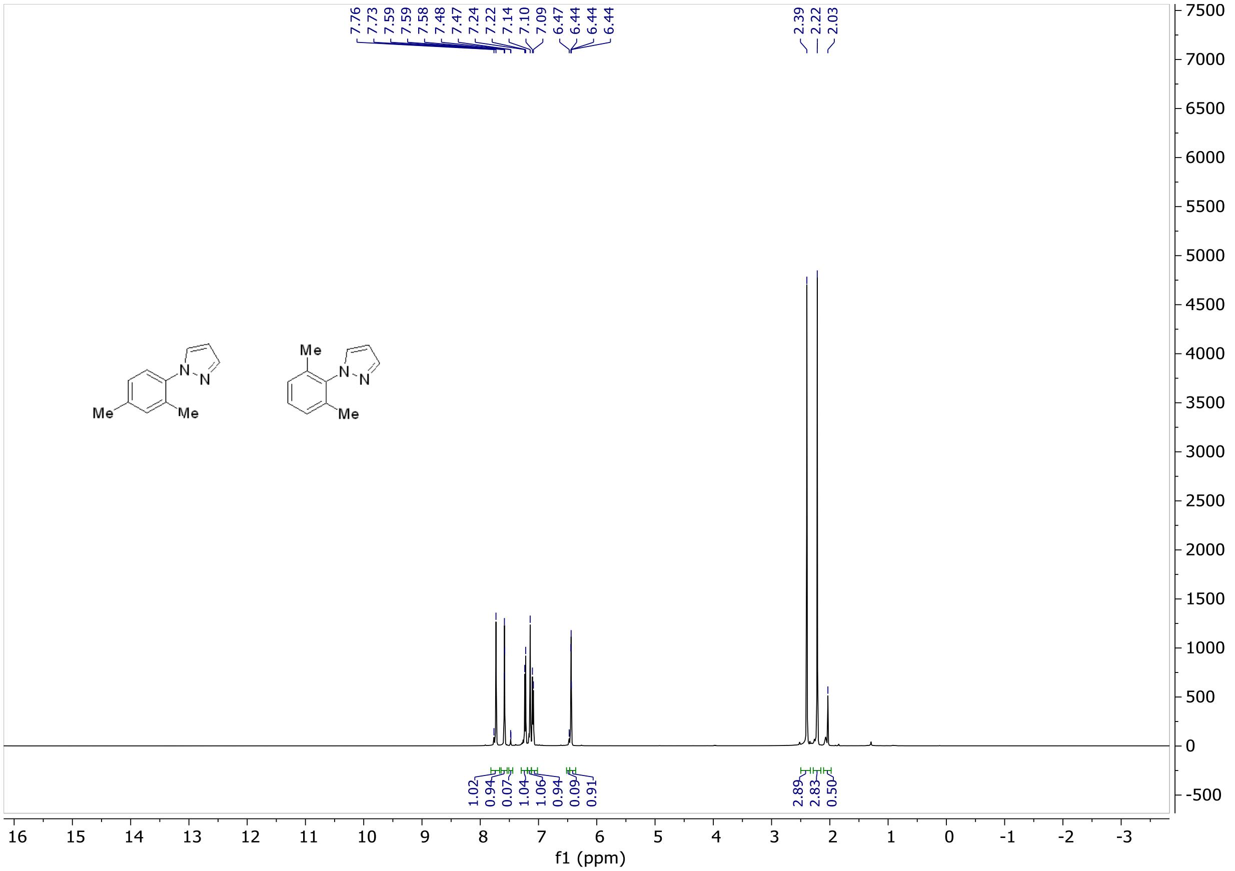
7.76
7.73
7.59
7.59
7.58
7.48
7.47
7.24
7.22
7.14
7.10
7.09
6.47
6.44
6.44
6.44
2.39
2.22
2.03
Me
N
N
Me
Me
Me
N
N
Me
1.02
0.94
0.07
1.04
1.06
0.94
0.09
0.91
2.89
2.83
0.50
16
15
14
13
12
11
10
9
8
7
6
5
4
3
2
1
0
-1
-2
-3
f1 (ppm)
7500
7000
6500
6000
5500
5000
4500
4000
3500
3000
2500
2000
1500
1000
500
0
-500

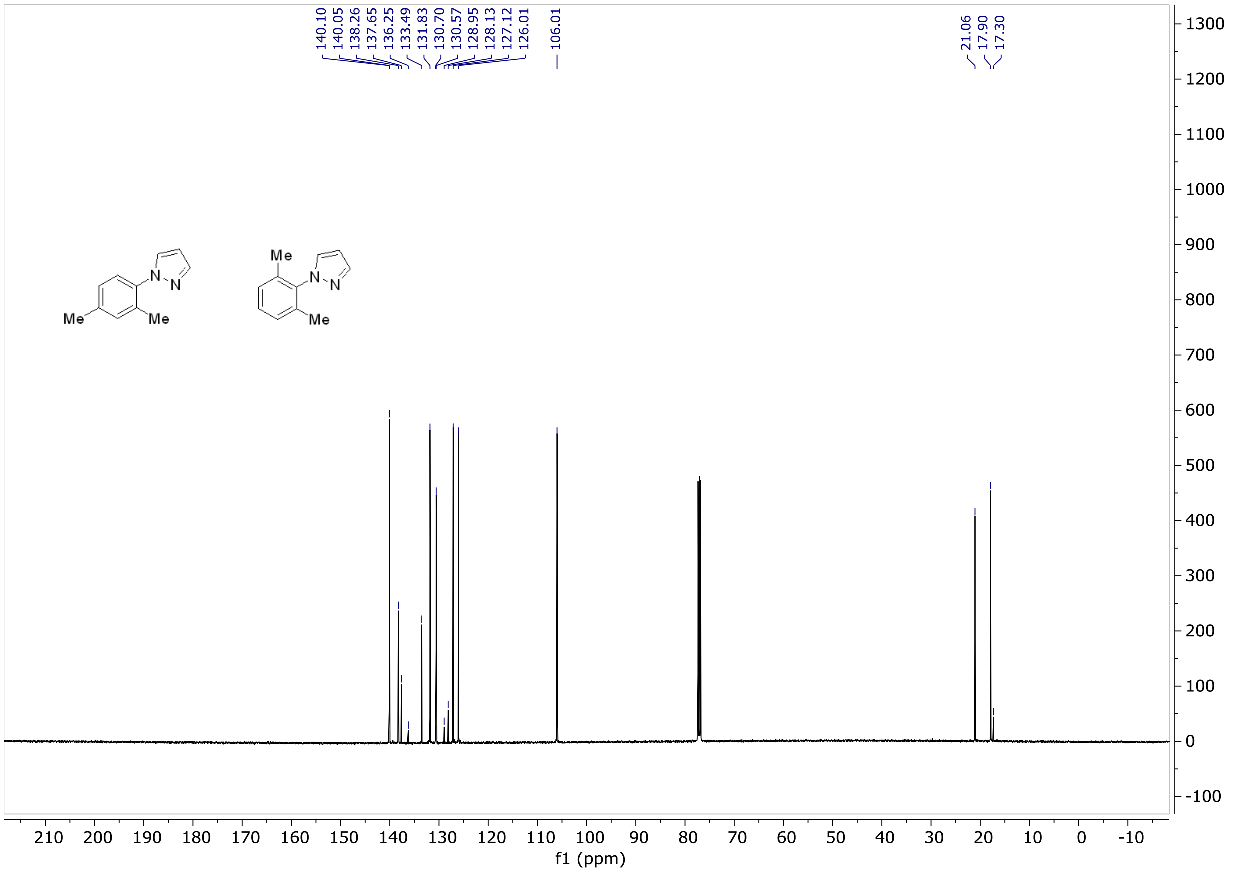
140.10
140.05
138.26
137.65
136.25
133.49
131.83
130.70
130.57
128.95
128.13
127.12
126.01
106.01
21.06
17.90
17.30
Me
N
N
Me
Me
N
N
Me
Me
210
200
190
180
170
160
150
140
130
120
110
100
90
80
70
60
50
40
30
20
10
0
-10
f1 (ppm)
1300
1200
1100
1000
900
800
700
600
500
400
300
200
100
0
-100

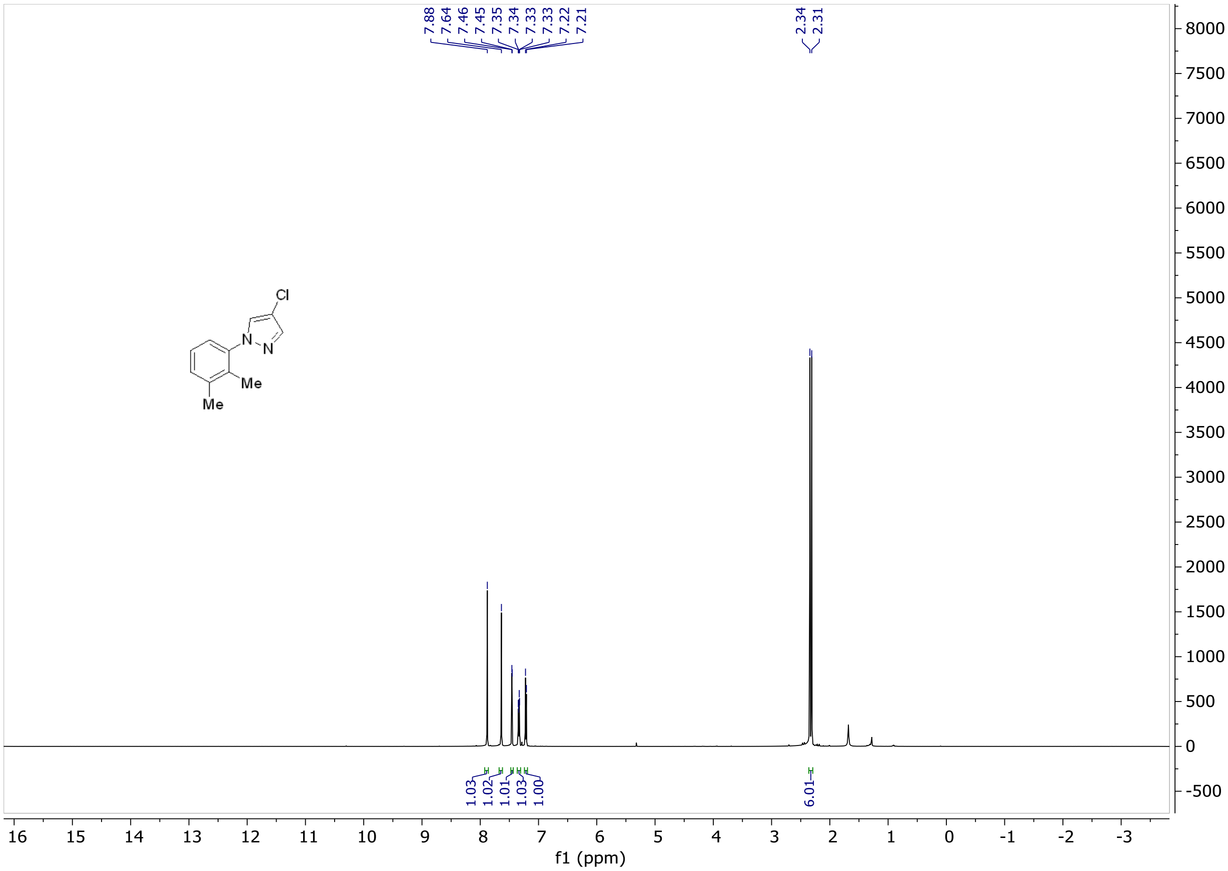
7.88
7.64
7.46
7.45
7.35
7.34
7.33
7.33
7.22
7.21
2.34
2.31
Cl
N
N
Me
Me
1.03
1.02
1.01
1.03
1.00
6.01
8000
7500
7000
6500
6000
5500
5000
4500
4000
3500
3000
2500
2000
1500
1000
500
0
-500
16
15
14
13
12
11
10
9
8
7
6
5
4
3
2
1
0
-1
-2
-3
f1 (ppm)

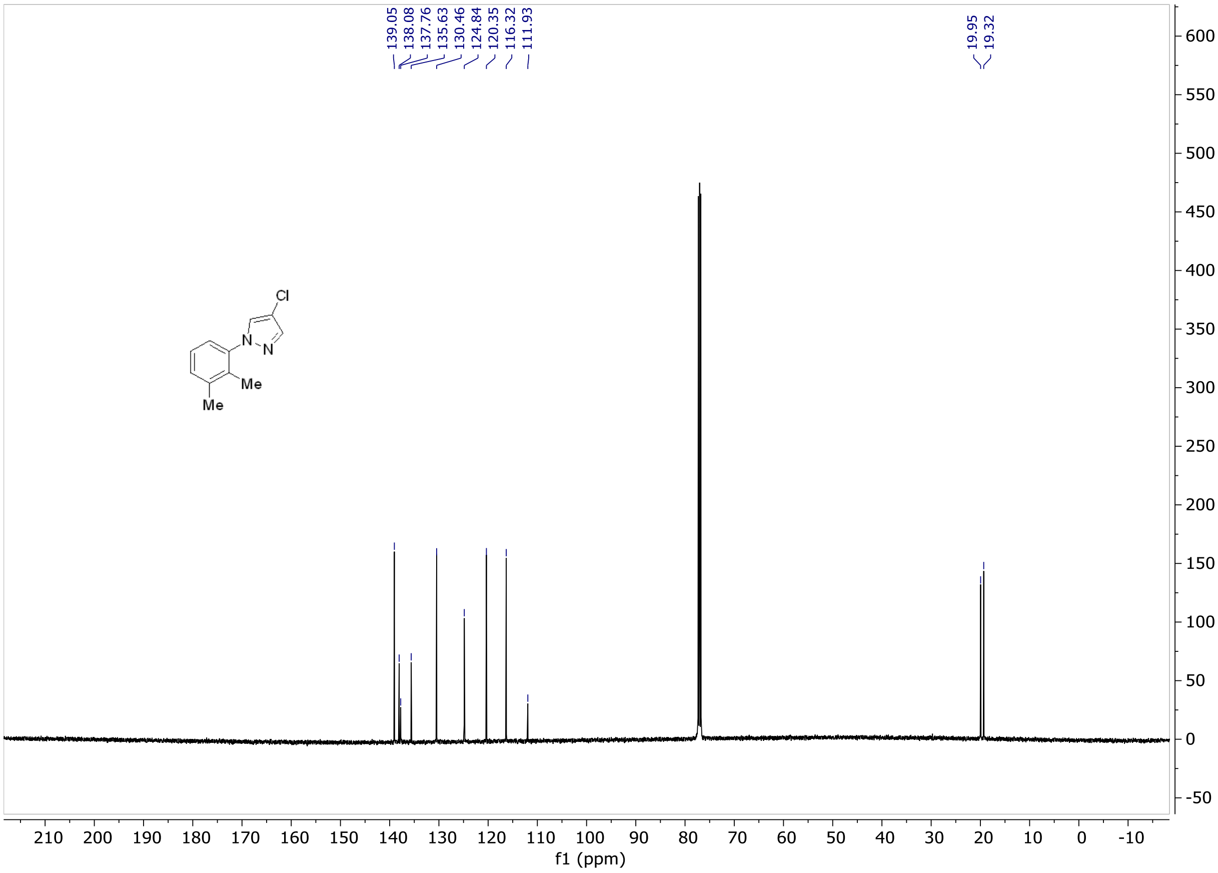
139.05
138.08
137.76
135.63
130.46
124.84
120.35
116.32
111.93
19.95
19.32
Cl
N
N
Me
Me
600
550
500
450
400
350
300
250
200
150
100
50
0
-50
210
200
190
180
170
160
150
140
130
120
110
100
90
80
70
60
50
40
30
20
10
0
-10
f1 (ppm)

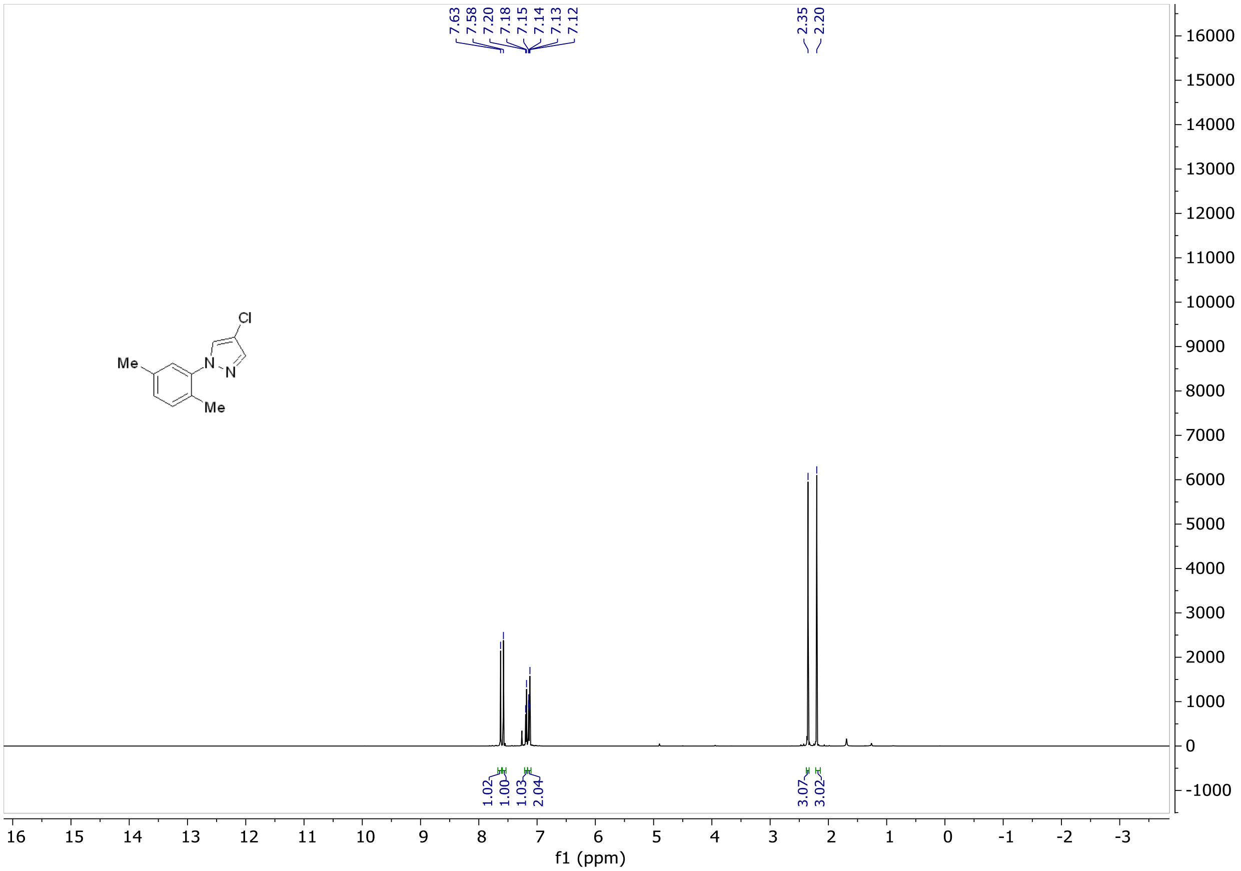
7.63
7.58
7.20
7.18
7.15
7.14
7.13
7.12
2.35
2.20
Cl
N
N
Me
Me
1.02
1.00
1.03
2.04
3.07
3.02
16000
15000
14000
13000
12000
11000
10000
9000
8000
7000
6000
5000
4000
3000
2000
1000
0
-1000
16 15 14 13 12 11 10 9 8 7 6 5 4 3 2 1 0 -1 -2 -3
f1 (ppm)

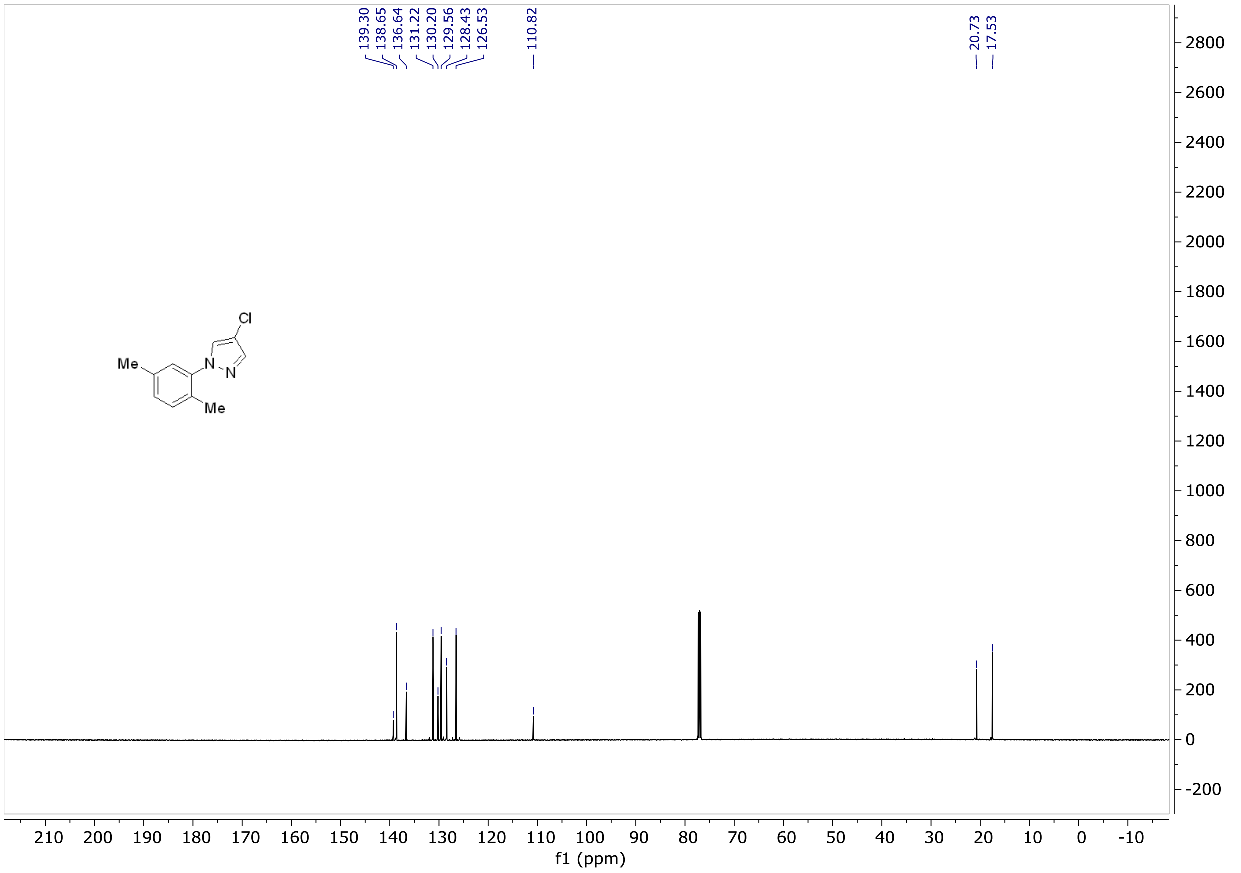
139.30
138.65
136.64
131.22
130.20
129.56
128.43
126.53
110.82
20.73
17.53
Cl
N
N
Me
Me
2800
2600
2400
2200
2000
1800
1600
1400
1200
1000
800
600
400
200
0
-200
210 200 190 180 170 160 150 140 130 120 110 100 90 80 70 60 50 40 30 20 10 0 -10
f1 (ppm)

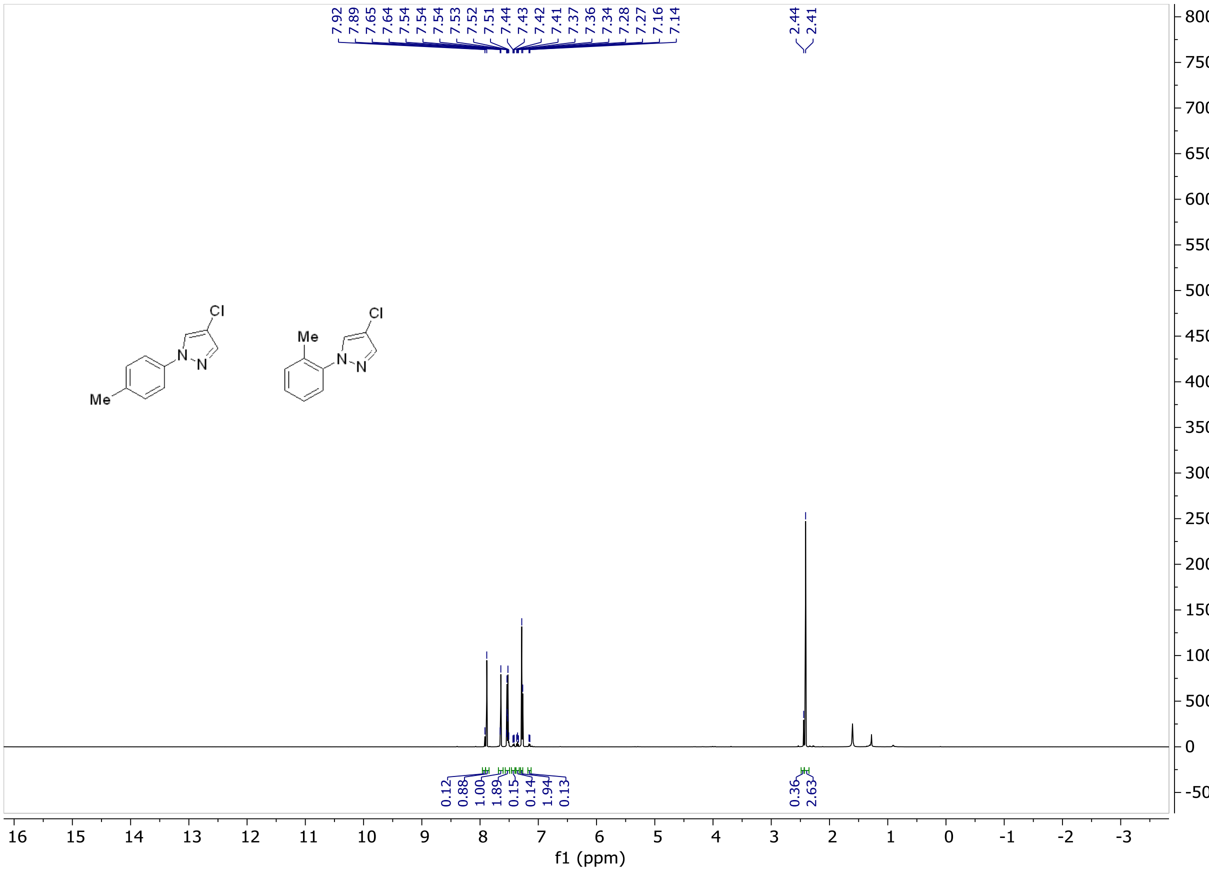
7.92
7.89
7.65
7.64
7.54
7.54
7.53
7.52
7.51
7.44
7.43
7.42
7.41
7.37
7.36
7.34
7.28
7.27
7.16
7.14
2.44
2.41
Cl
N
N
Me
Cl
Me
N
N
0.12
0.88
1.00
1.89
0.15
0.14
1.94
0.13
0.36
2.63
8000
7500
7000
6500
6000
5500
5000
4500
4000
3500
3000
2500
2000
1500
1000
500
0
-500
16
15
14
13
12
11
10
9
8
7
6
5
4
3
2
1
0
-1
-2
-3
f1 (ppm)

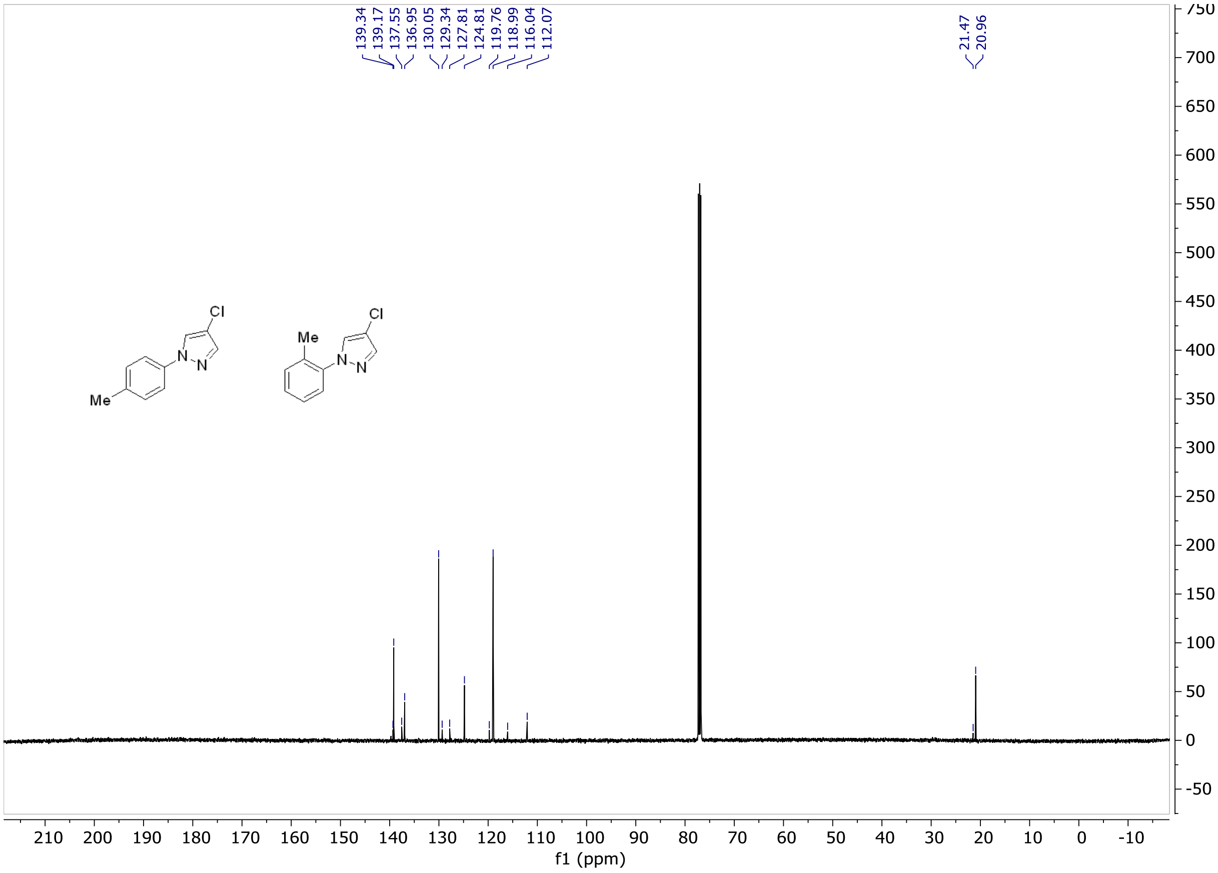
139.34
139.17
137.55
136.95
130.05
129.34
127.81
124.81
119.76
118.99
116.04
112.07
21.47
20.96
Cl
N
N
Me
Cl
Me
N
N
750
700
650
600
550
500
450
400
350
300
250
200
150
100
50
0
-50
210
200
190
180
170
160
150
140
130
120
110
100
90
80
70
60
50
40
30
20
10
0
-10
f1 (ppm)

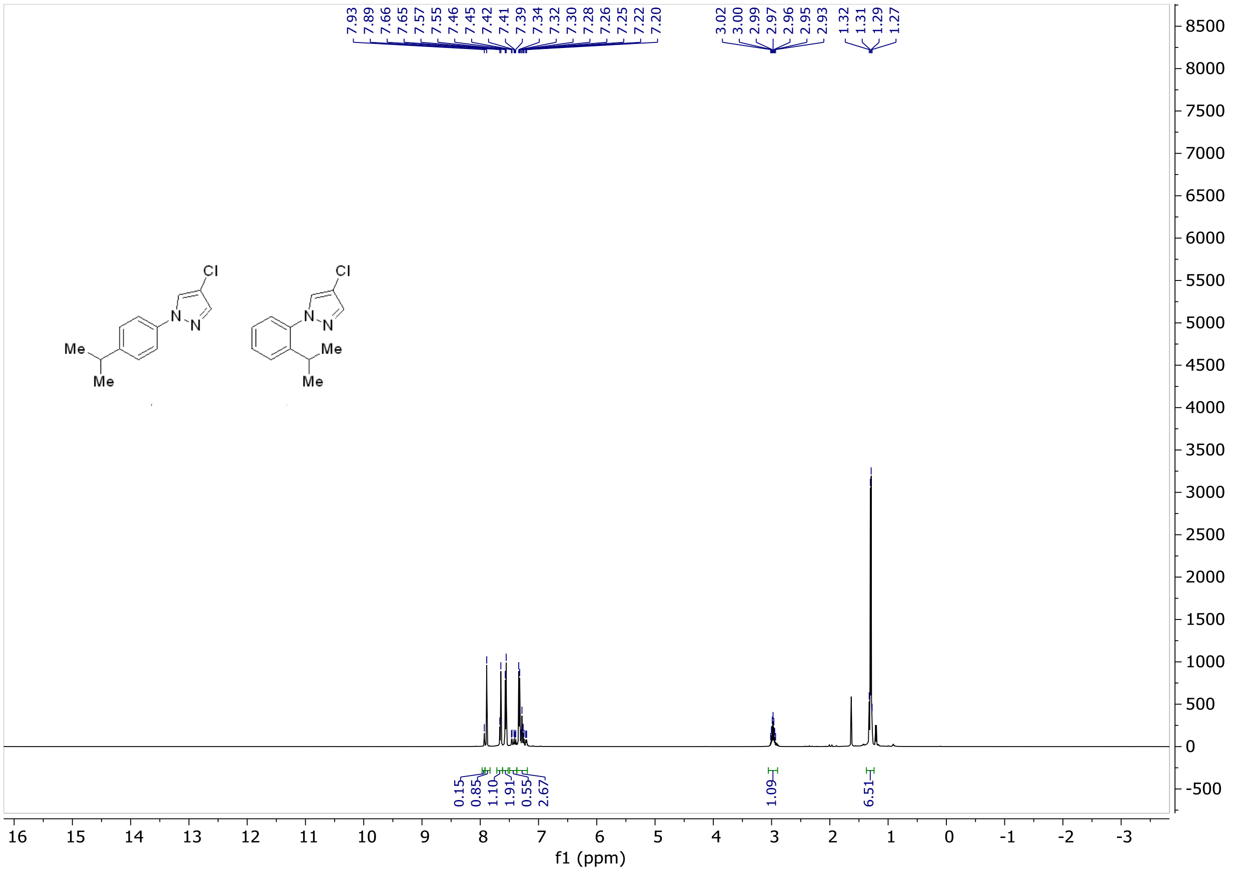
7.93
7.89
7.66
7.65
7.57
7.55
7.46
7.45
7.42
7.41
7.39
7.34
7.32
7.30
7.28
7.26
7.25
7.22
7.20
3.02
3.00
2.99
2.97
2.96
2.95
2.93
1.32
1.31
1.29
1.27
Cl
N
N
Me
Me
Cl
N
N
Me
Me
0.15
0.85
1.10
1.91
0.55
2.67
1.09
6.51
8500
8000
7500
7000
6500
6000
5500
5000
4500
4000
3500
3000
2500
2000
1500
1000
500
0
-500
16
15
14
13
12
11
10
9
8
7
6
5
4
3
2
1
0
-1
-2
-3
f1 (ppm)

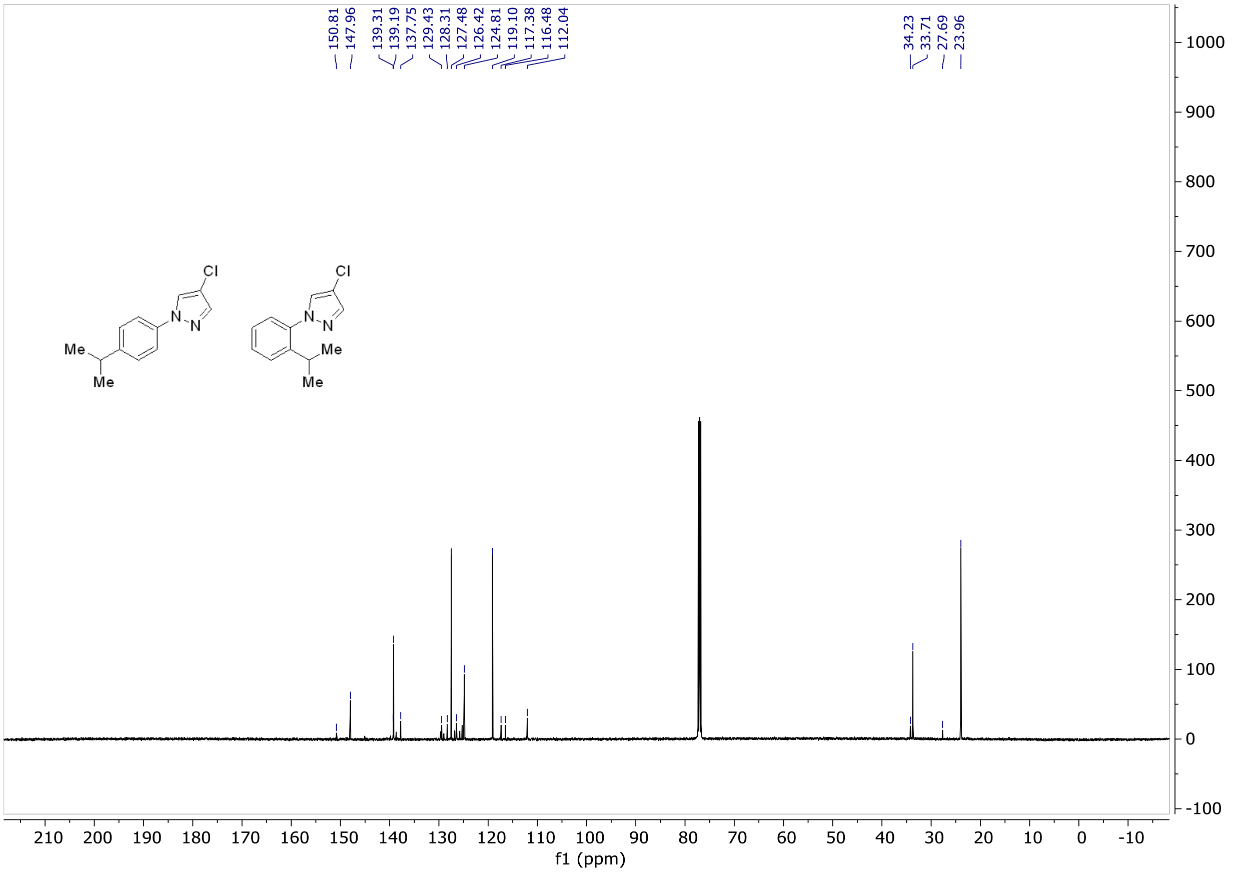
150.81
147.96
139.31
139.19
137.75
129.43
128.31
127.48
126.42
124.81
119.10
117.38
116.48
112.04
34.23
33.71
27.69
23.96
Cl
N
N
Me
Me
Cl
N
N
Me
Me
1000
900
800
700
600
500
400
300
200
100
0
-100
210
200
190
180
170
160
150
140
130
120
110
100
90
80
70
60
50
40
30
20
10
0
-10
f1 (ppm)

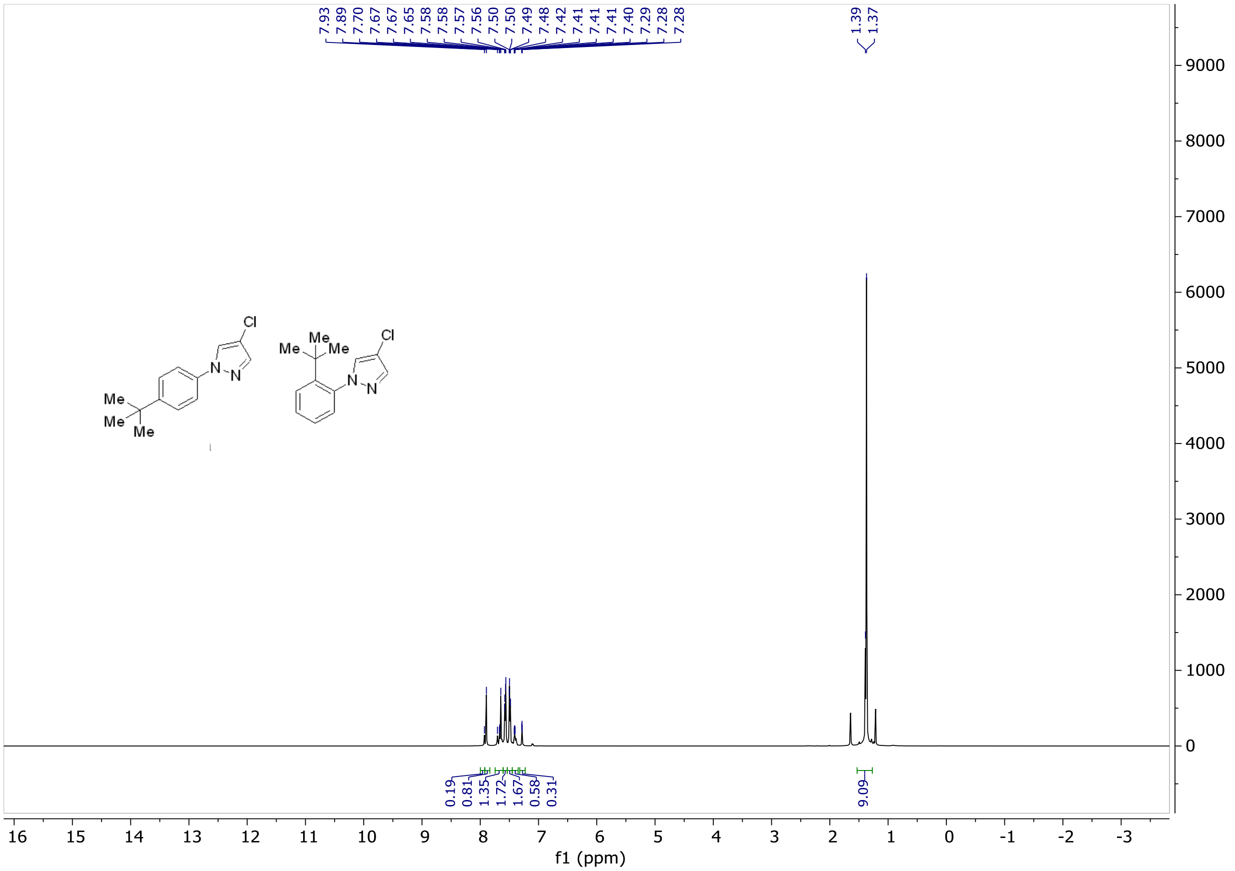
7.93
7.89
7.70
7.67
7.67
7.65
7.58
7.58
7.57
7.56
7.50
7.50
7.49
7.48
7.42
7.41
7.41
7.41
7.40
7.29
7.28
7.28
1.39
1.37
Cl
N
N
Me
Me
Me
Me
Me
Me
Cl
N
N
0.19
0.81
1.35
1.72
1.67
0.58
0.31
9.09
9000
8000
7000
6000
5000
4000
3000
2000
1000
0
16 15 14 13 12 11 10 9 8 7 6 5 4 3 2 1 0 -1 -2 -3
f1 (ppm)

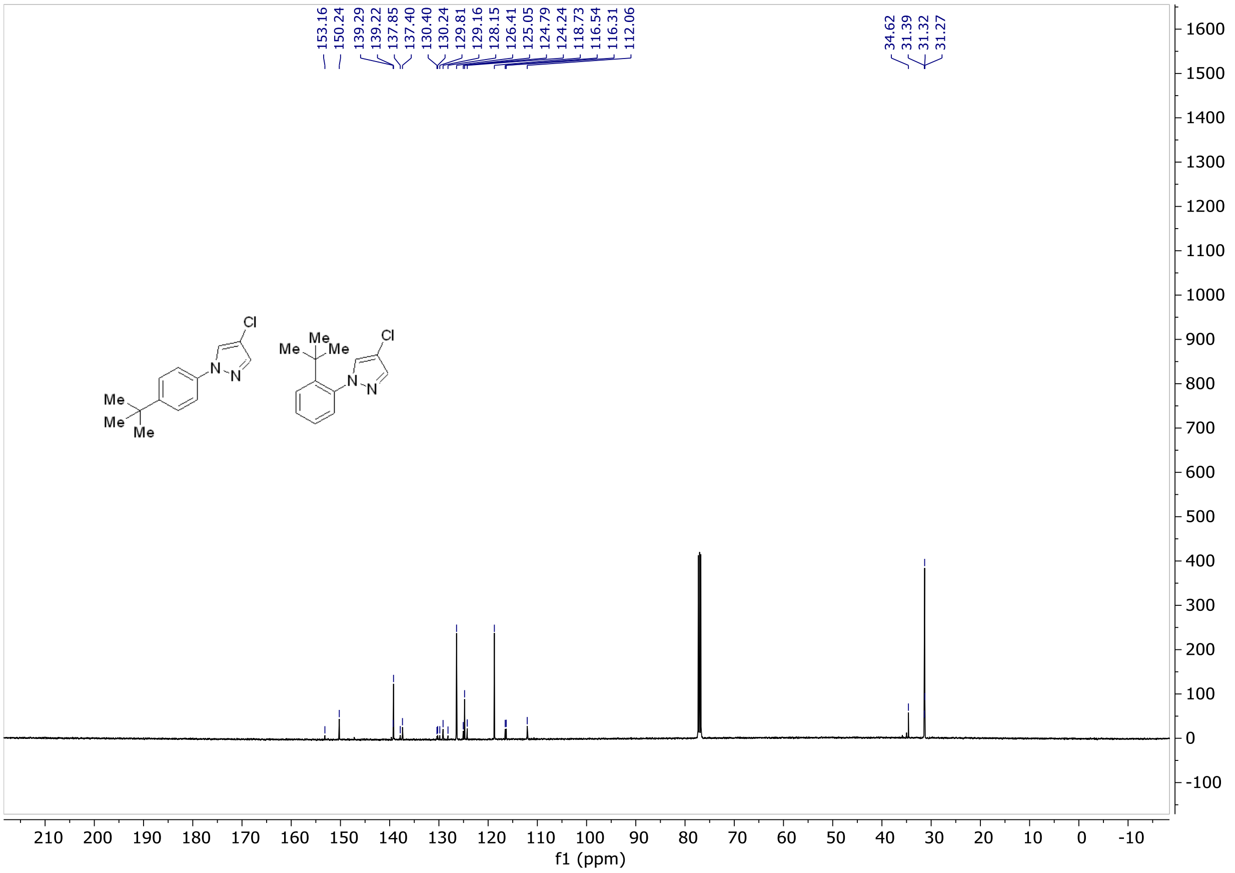
153.16
150.24
139.29
139.22
137.85
137.40
130.40
130.24
129.81
129.16
128.15
126.41
125.05
124.79
124.24
118.73
116.54
116.31
112.06
34.62
31.39
31.32
31.27
Cl
N
N
Me
Me
Me
Me
Me
Me
Cl
N
N
1600
1500
1400
1300
1200
1100
1000
900
800
700
600
500
400
300
200
100
0
-100
210 200 190 180 170 160 150 140 130 120 110 100 90 80 70 60 50 40 30 20 10 0 -10
f1 (ppm)

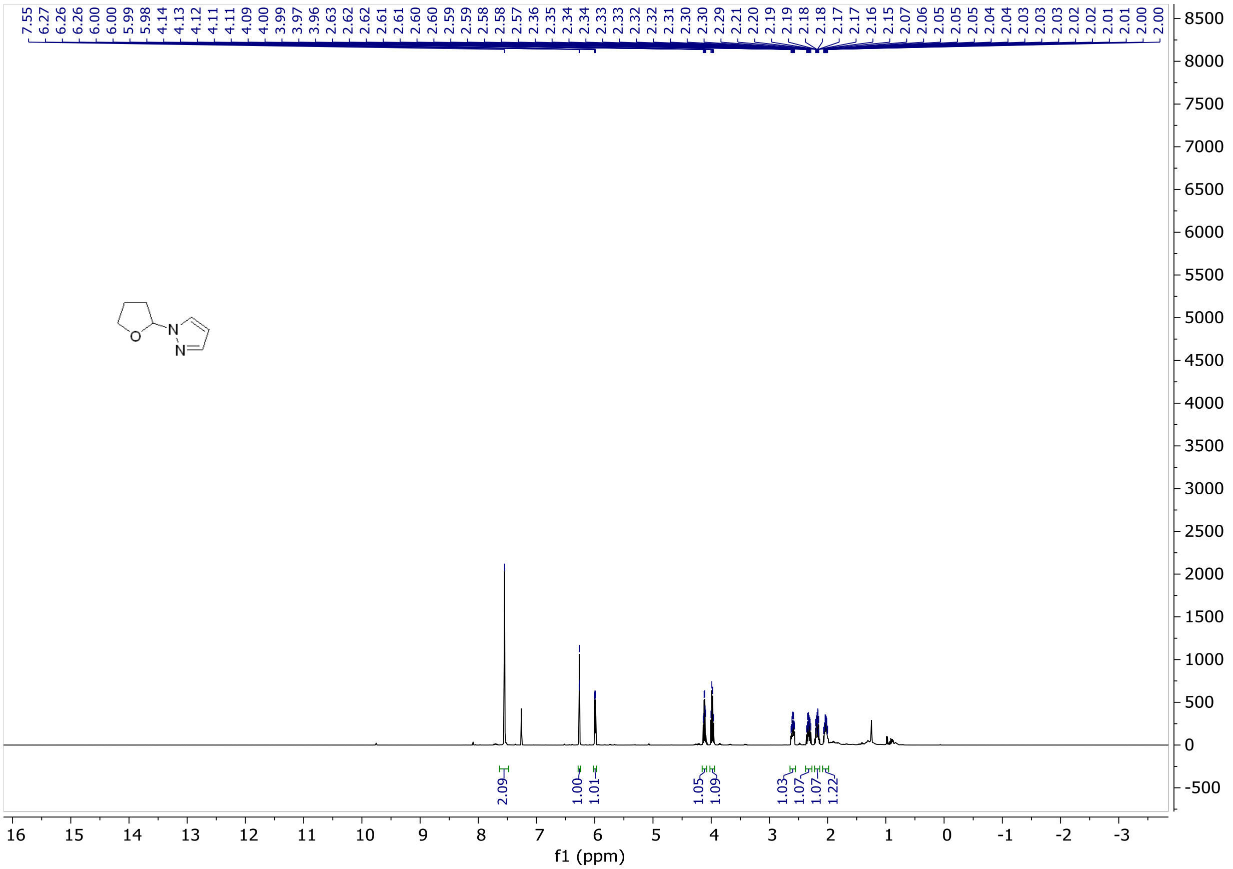
7.55
6.27
6.26
6.26
6.00
6.00
5.99
5.98
4.14
4.13
4.12
4.11
4.11
4.09
4.00
3.99
3.97
3.96
2.63
2.62
2.62
2.61
2.61
2.60
2.59
2.59
2.58
2.57
2.36
2.35
2.34
2.34
2.33
2.33
2.32
2.32
2.31
2.30
2.30
2.29
2.21
2.20
2.19
2.19
2.18
2.18
2.17
2.17
2.16
2.15
2.07
2.06
2.05
2.05
2.05
2.04
2.04
2.03
2.03
2.02
2.02
2.01
2.00
2.00
O
N
N
2.09
1.00
1.01
1.05
1.09
1.03
1.07
1.07
1.22
f1 (ppm)

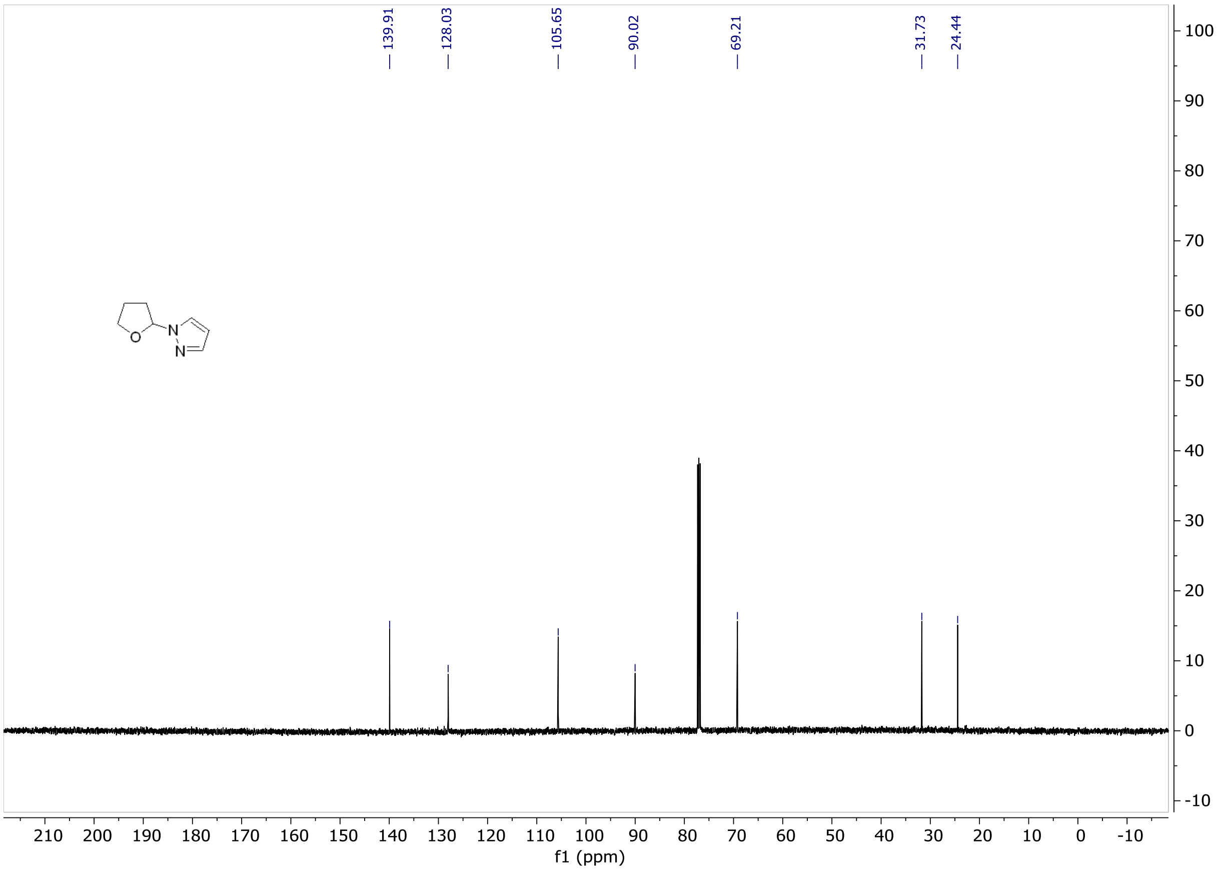
139.91
128.03
105.65
90.02
69.21
31.73
24.44
O
N
N
f1 (ppm)

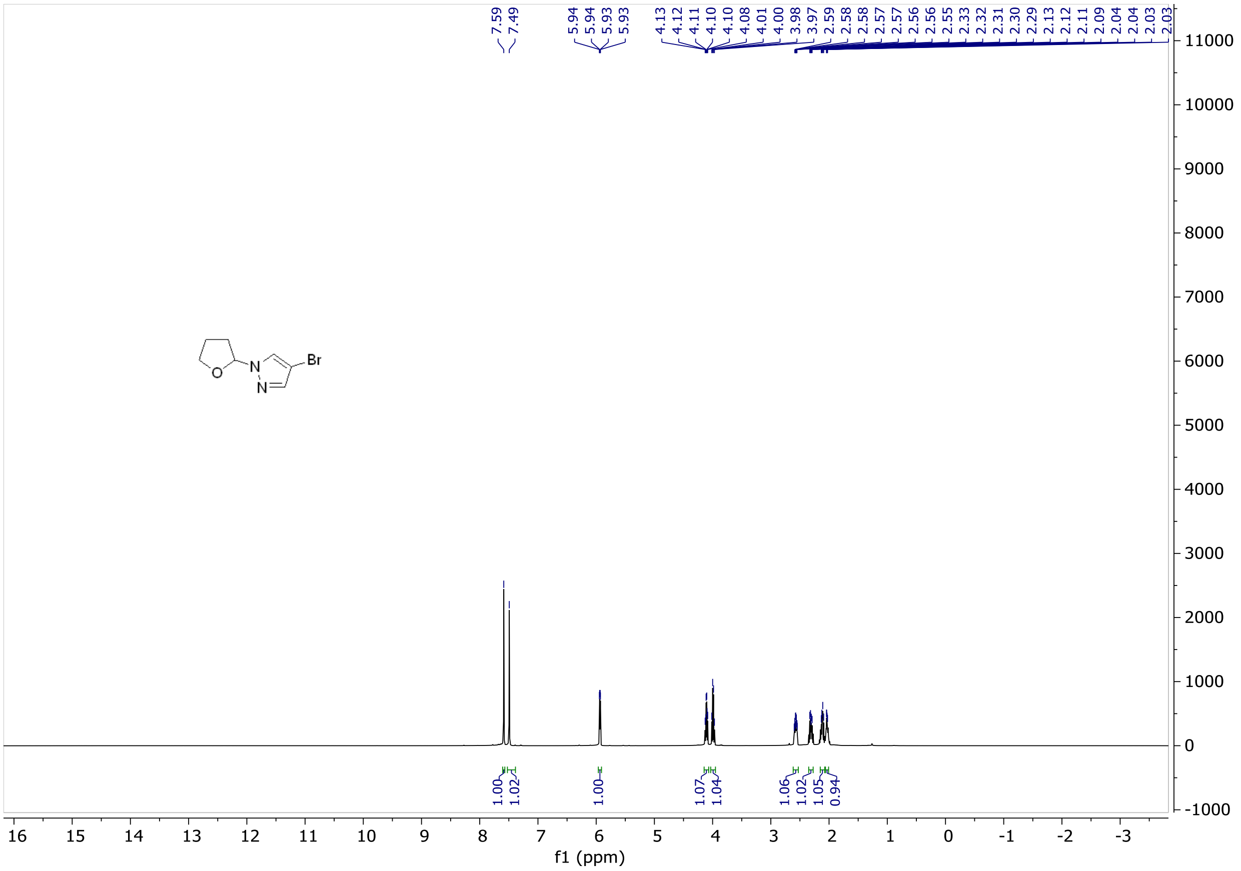
7.59
7.49
5.94
5.94
5.93
5.93
4.13
4.12
4.11
4.10
4.10
4.08
4.01
4.00
3.98
3.97
2.59
2.58
2.58
2.57
2.57
2.56
2.56
2.55
2.33
2.32
2.31
2.30
2.29
2.13
2.12
2.11
2.09
2.04
2.03
2.03
Br
N
N
O
1.00
1.02
1.00
1.07
1.04
1.06
1.02
1.05
0.94
f1 (ppm)

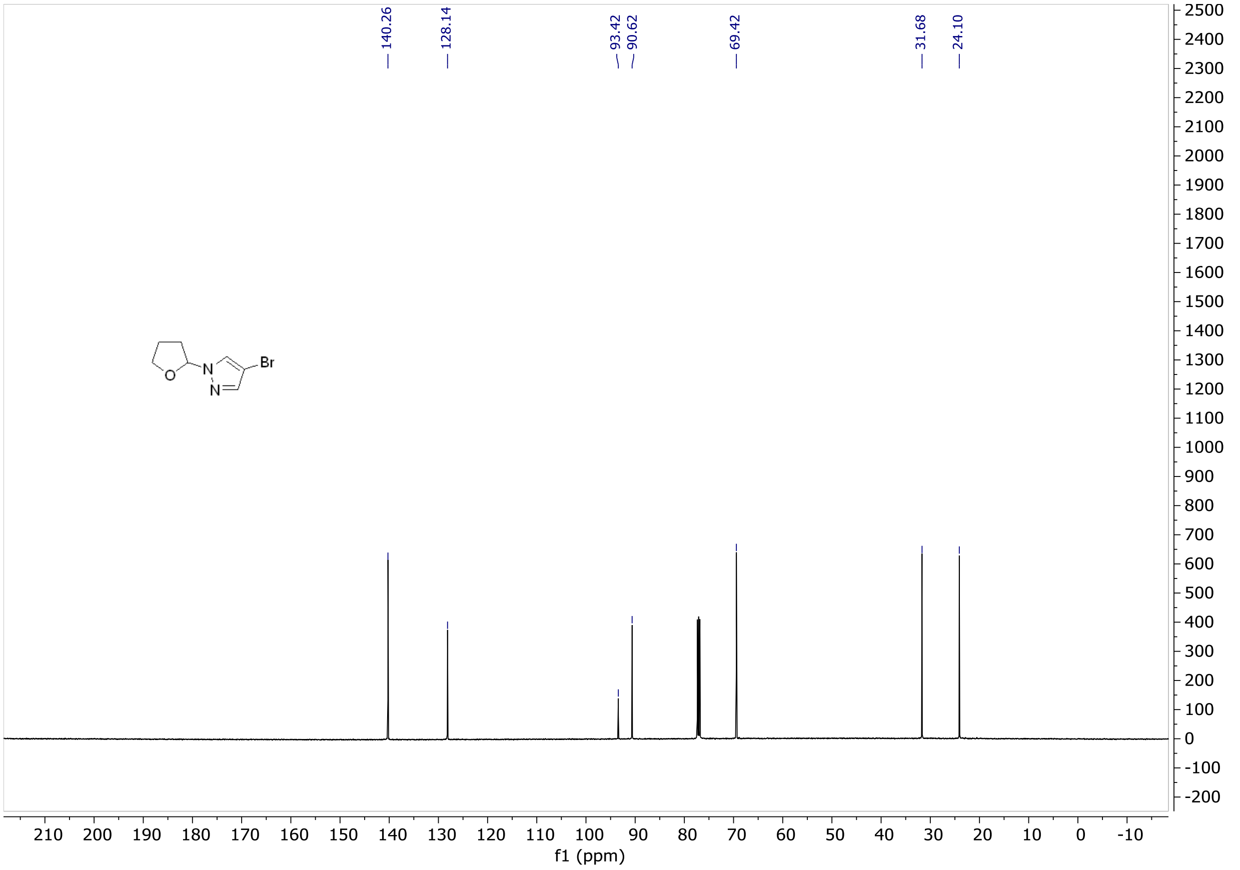
140.26
128.14
93.42
90.62
69.42
31.68
24.10
Br
N
N
O
f1 (ppm)

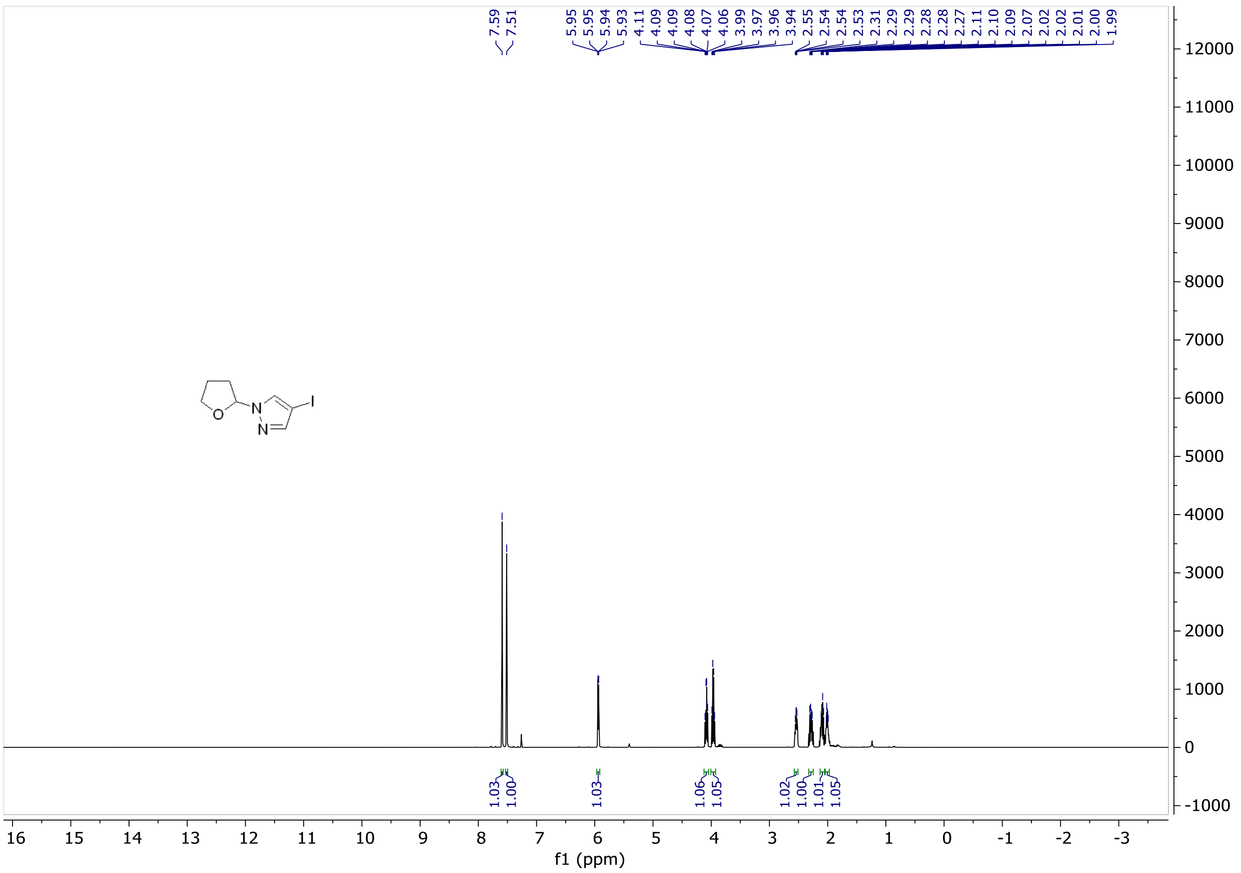
7.59
7.51
5.95
5.95
5.94
5.93
4.11
4.09
4.09
4.08
4.07
4.06
3.99
3.97
3.96
3.94
2.55
2.54
2.54
2.53
2.31
2.29
2.29
2.28
2.28
2.27
2.11
2.10
2.09
2.07
2.02
2.02
2.01
2.00
1.99
1.03
1.00
1.03
1.06
1.05
1.02
1.00
1.01
1.05
N
N
O
I
f1 (ppm)

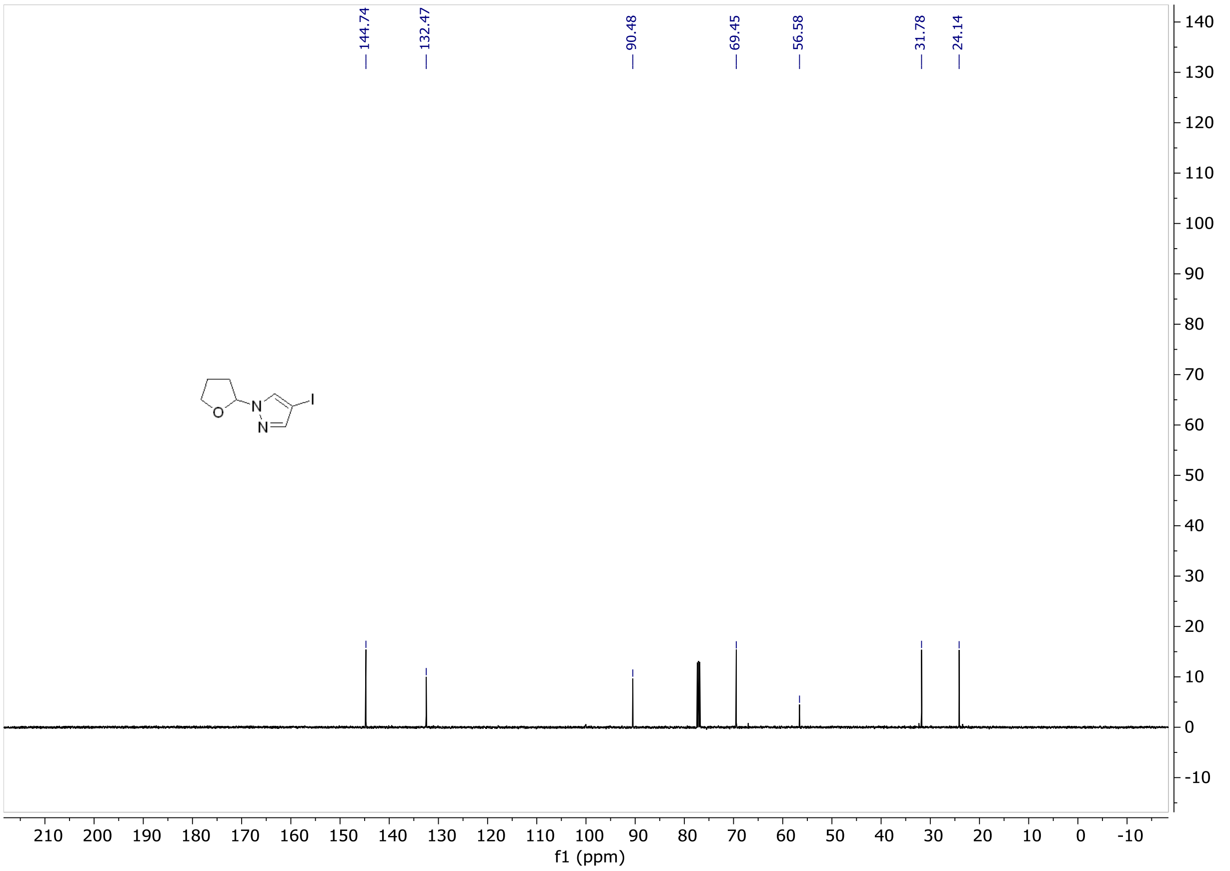
144.74
132.47
90.48
69.45
56.58
31.78
24.14
N
N
O
I
f1 (ppm)

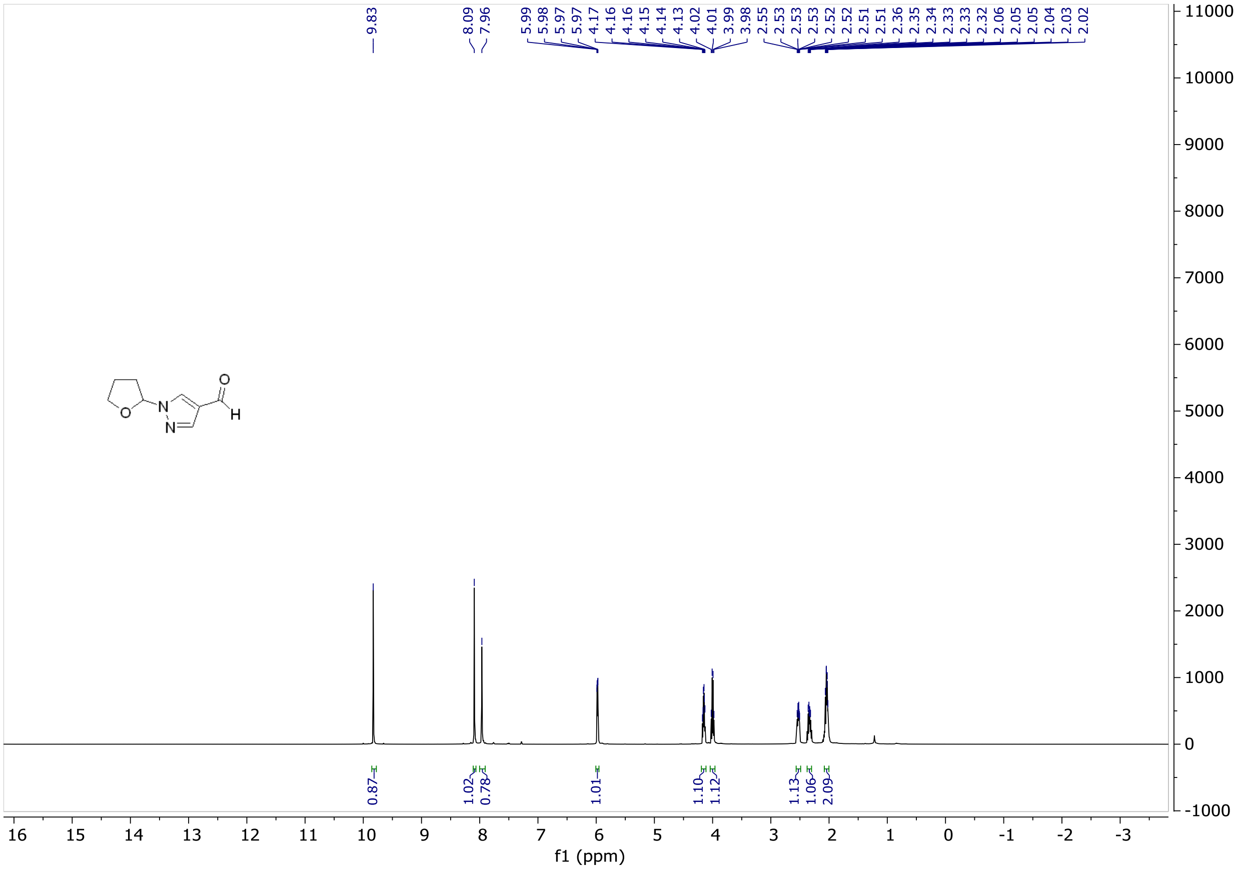
9.83
8.09
7.96
5.99
5.98
5.97
5.97
4.17
4.16
4.16
4.15
4.14
4.13
4.02
4.01
3.99
3.98
2.55
2.53
2.53
2.53
2.52
2.52
2.51
2.51
2.36
2.35
2.34
2.33
2.33
2.32
2.06
2.05
2.05
2.04
2.03
2.02
0.87
1.02
0.78
1.01
1.10
1.12
1.13
1.06
2.09
O
N
N
O
H
f1 (ppm)

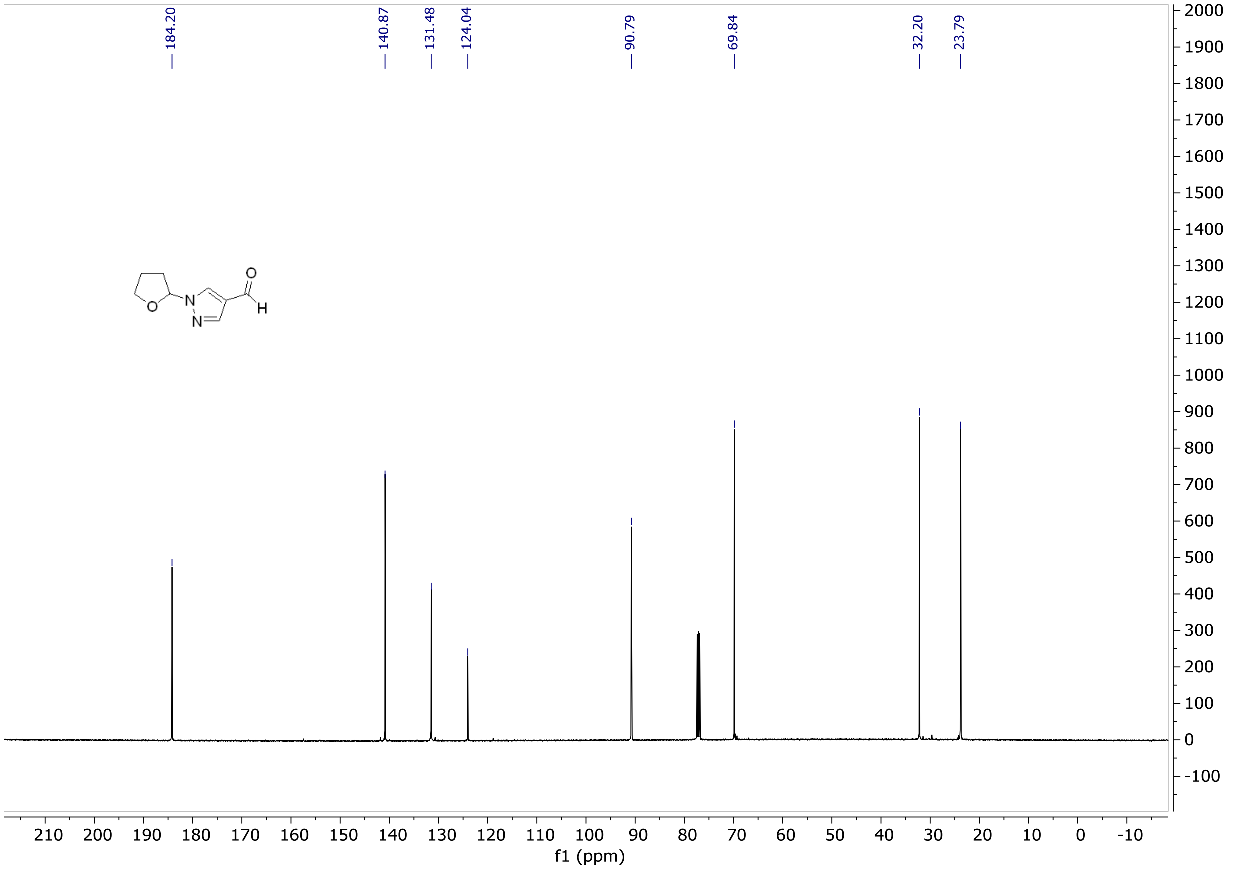
184.20
140.87
131.48
124.04
90.79
69.84
32.20
23.79
O
N
N
O
H
f1 (ppm)

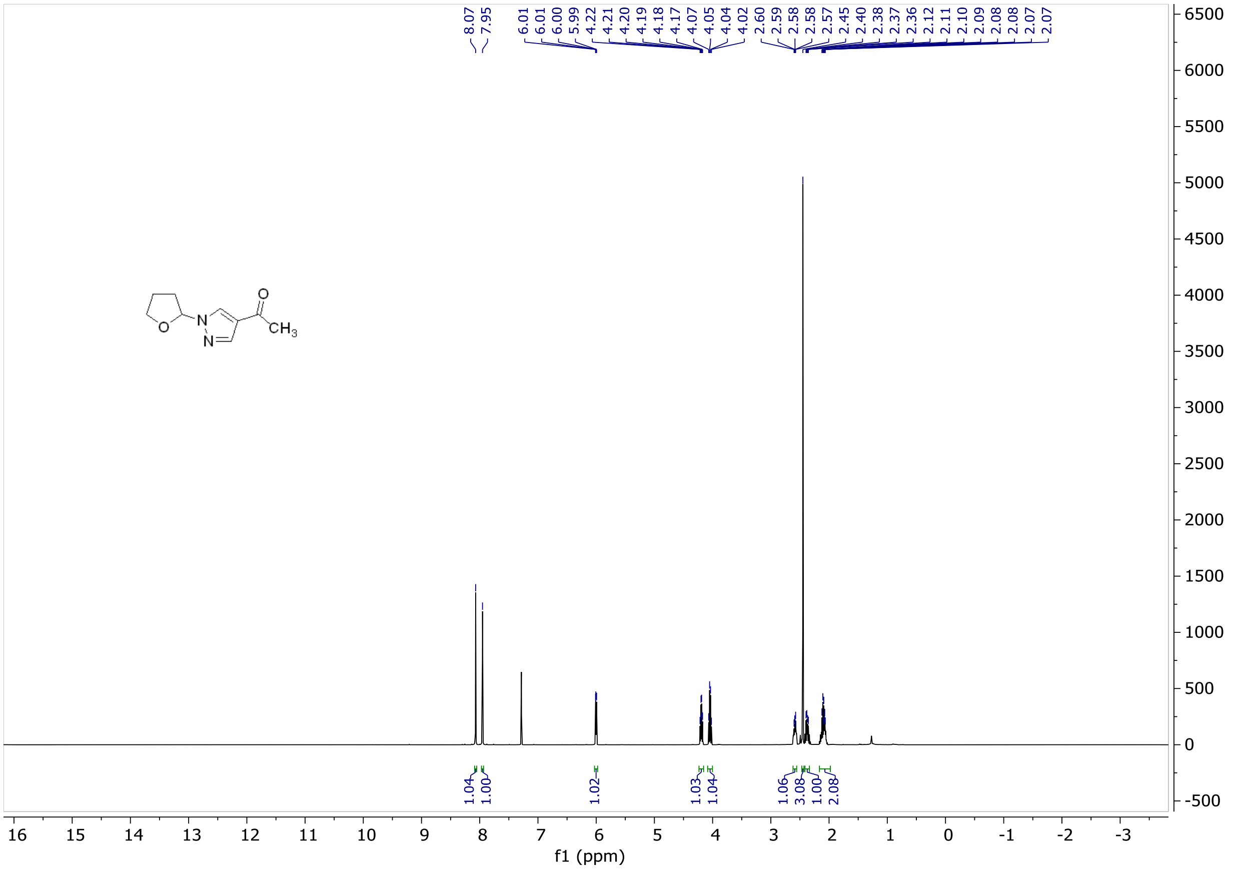
8.07
7.95
6.01
6.01
6.00
5.99
4.22
4.21
4.20
4.19
4.18
4.17
4.07
4.05
4.04
4.02
2.60
2.59
2.58
2.58
2.57
2.45
2.40
2.38
2.37
2.36
2.12
2.11
2.10
2.09
2.08
2.07
2.07
O
N
N
O
CH3
1.04
1.00
1.02
1.03
1.04
1.06
3.08
1.00
2.08
f1 (ppm)

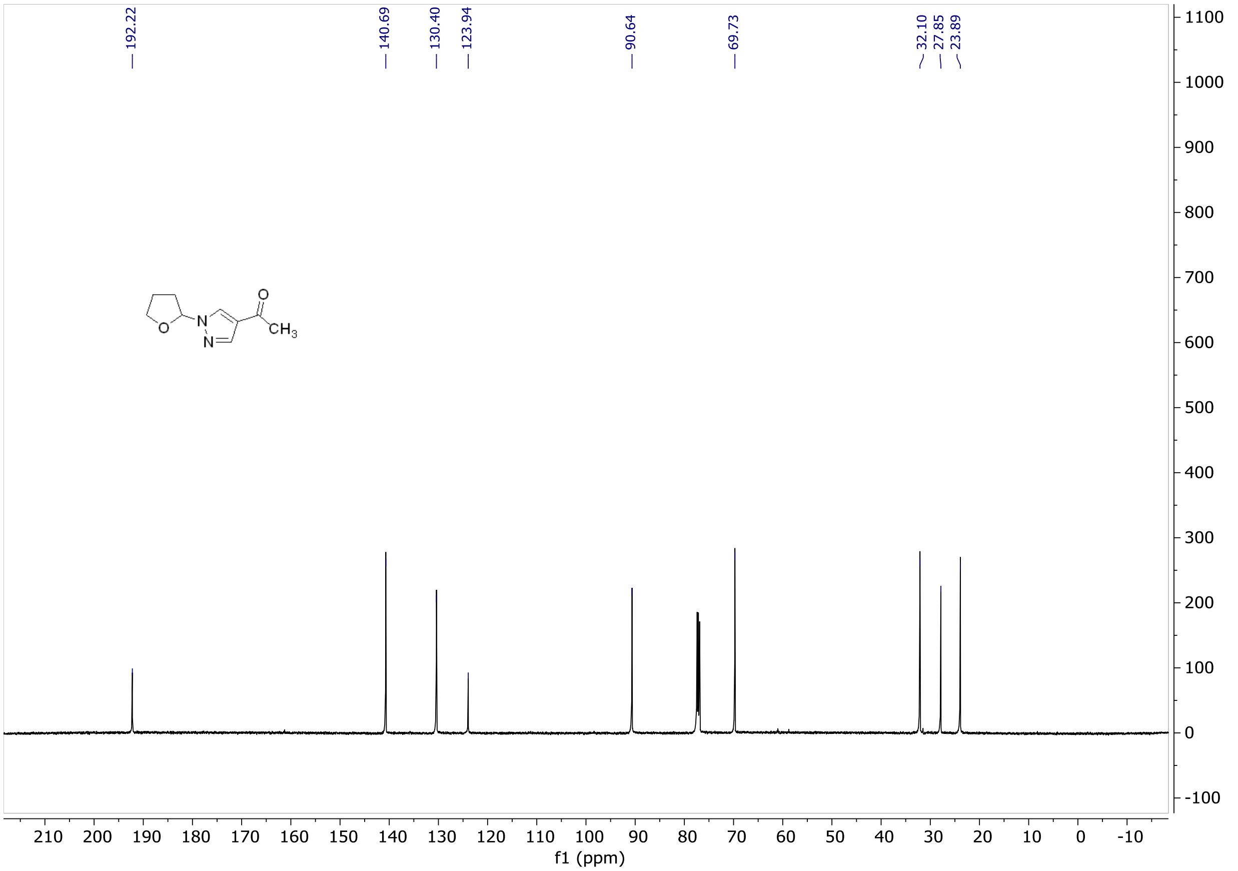
192.22
140.69
130.40
123.94
90.64
69.73
32.10
27.85
23.89
O
N
N
O
CH3
f1 (ppm)

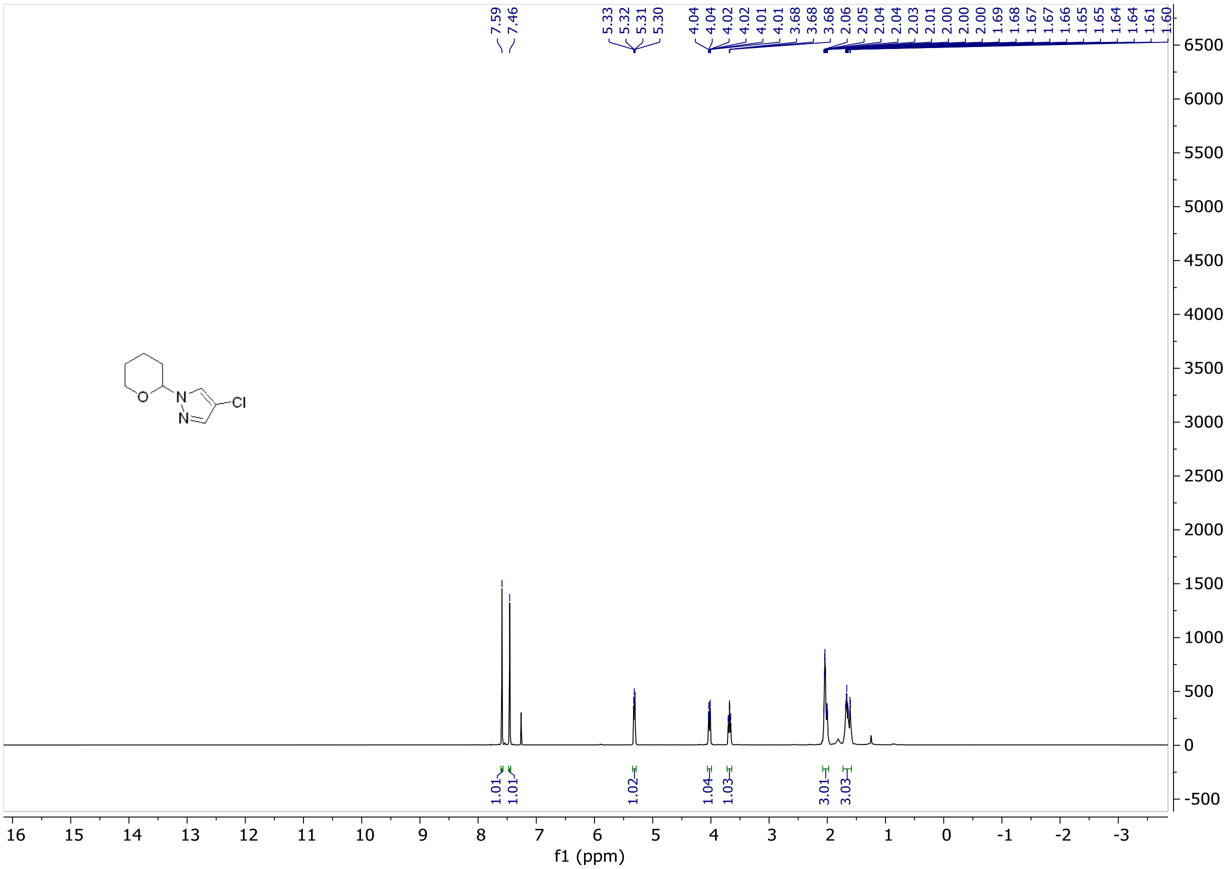
7.59
7.46
5.33
5.32
5.31
5.30
4.04
4.04
4.02
4.02
4.01
4.01
3.68
3.68
3.68
2.06
2.05
2.04
2.04
2.03
2.01
2.00
2.00
2.00
1.69
1.68
1.67
1.67
1.66
1.65
1.65
1.64
1.64
1.61
1.60
O
N
N
Cl
1.01
1.01
1.02
1.04
1.03
3.01
3.03
6500
6000
5500
5000
4500
4000
3500
3000
2500
2000
1500
1000
500
0
-500
16 15 14 13 12 11 10 9 8 7 6 5 4 3 2 1 0 -1 -2 -3
f1 (ppm)

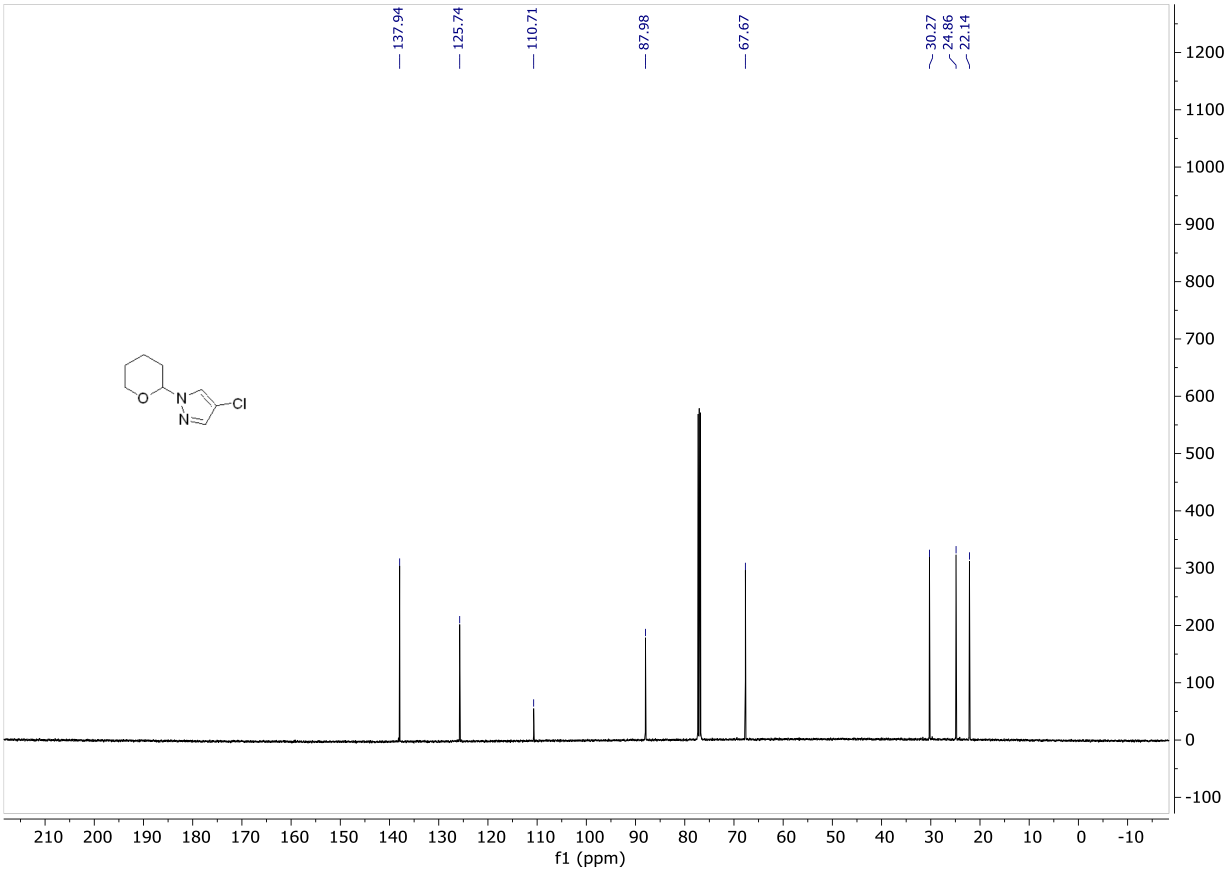
137.94
125.74
110.71
87.98
67.67
30.27
24.86
22.14
O
N
N
Cl
1200
1100
1000
900
800
700
600
500
400
300
200
100
0
-100
210 200 190 180 170 160 150 140 130 120 110 100 90 80 70 60 50 40 30 20 10 0 -10
f1 (ppm)

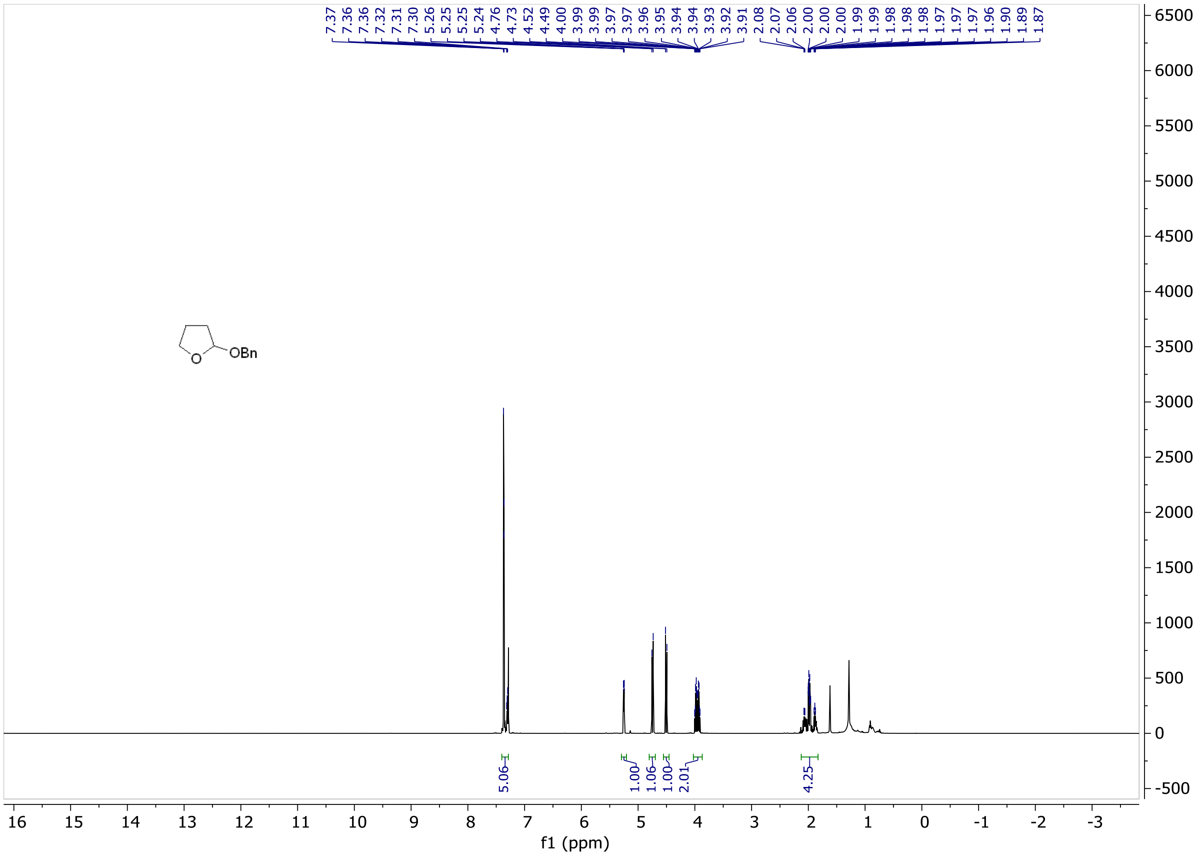
7.37
7.36
7.36
7.32
7.31
7.30
5.26
5.25
5.25
5.24
4.76
4.73
4.52
4.49
4.00
3.99
3.99
3.97
3.97
3.96
3.95
3.94
3.94
3.93
3.92
3.91
2.08
2.07
2.06
2.00
2.00
2.00
1.99
1.99
1.98
1.98
1.98
1.97
1.97
1.97
1.96
1.90
1.89
1.87
O
OBn
5.06
1.00
1.06
1.00
2.01
4.25
f1 (ppm)

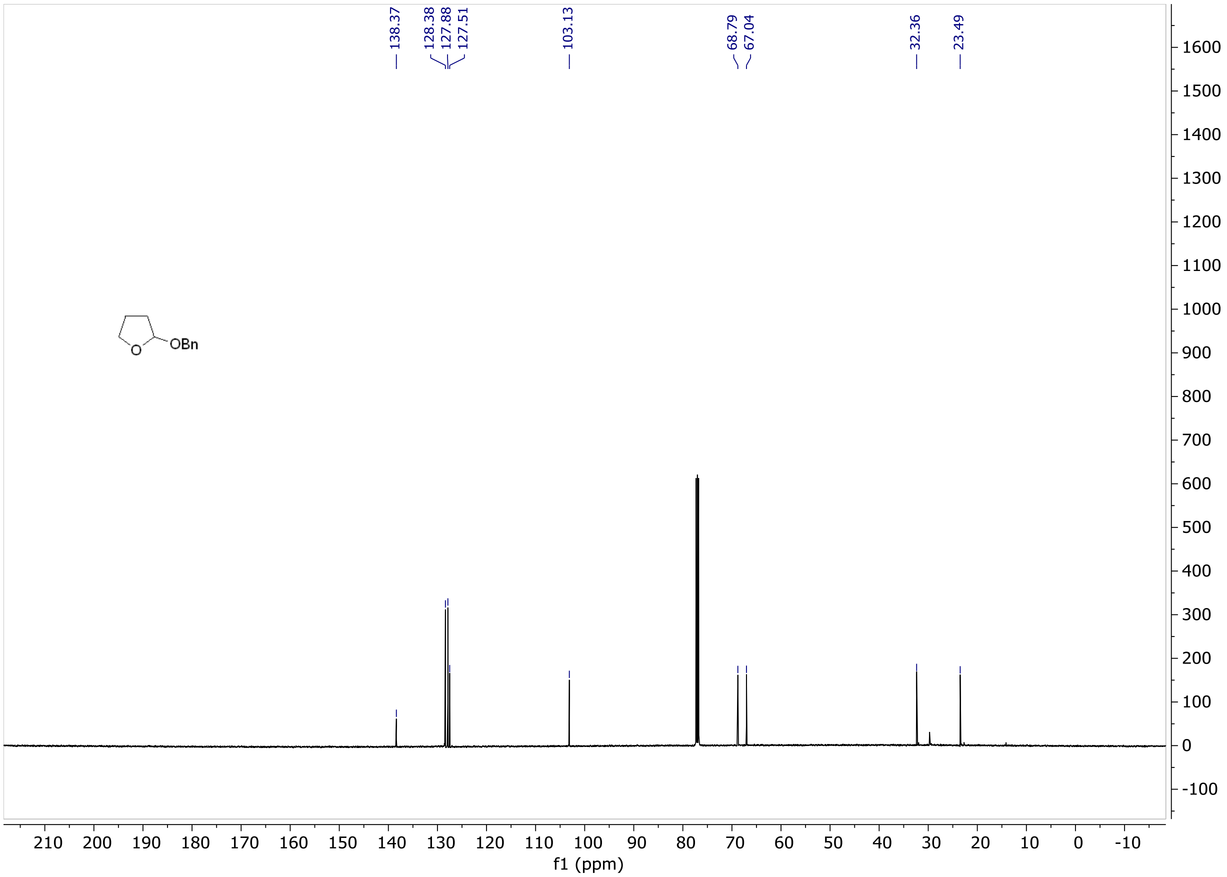
138.37
128.38
127.88
127.51
103.13
68.79
67.04
32.36
23.49
O
OBn
f1 (ppm)

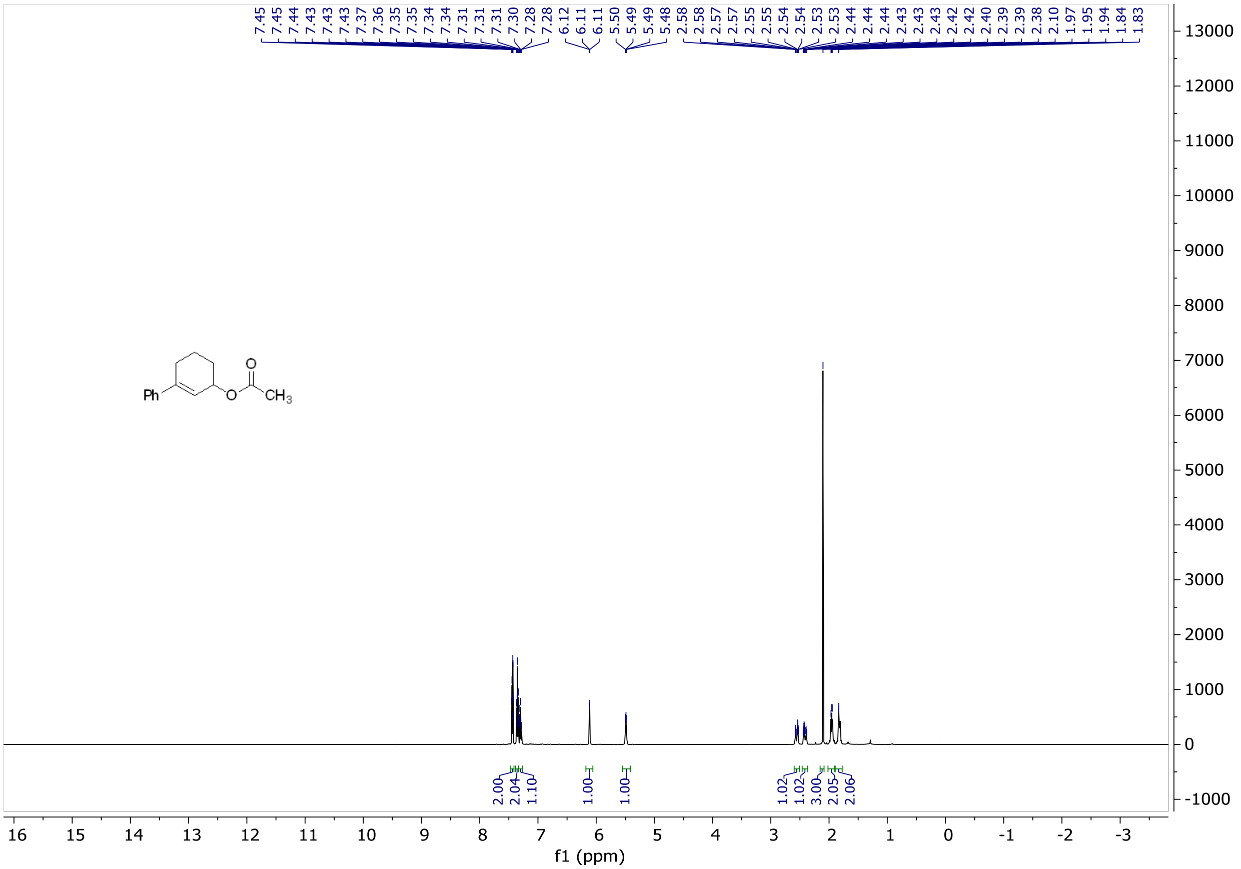
7.45 7.45 7.44 7.43 7.43 7.43 7.37 7.36 7.35 7.35 7.34 7.34 7.31 7.31 7.30 7.28 7.28 6.12 6.11 6.11 5.50 5.49 5.49 5.48 2.58 2.57 2.57 2.55 2.55 2.54 2.54 2.53 2.53 2.44 2.44 2.44 2.44 2.43 2.43 2.43 2.42 2.42 2.40 2.39 2.39 2.38 2.10 1.97 1.95 1.94 1.84 1.83
Ph
O
CH3
2.00
2.04
1.10
1.00
1.00
1.02
1.02
3.00
2.05
2.06
13000
12000
11000
10000
9000
8000
7000
6000
5000
4000
3000
2000
1000
0
-1000
16 15 14 13 12 11 10 9 8 7 6 5 4 3 2 1 0 -1 -2 -3
f1 (ppm)

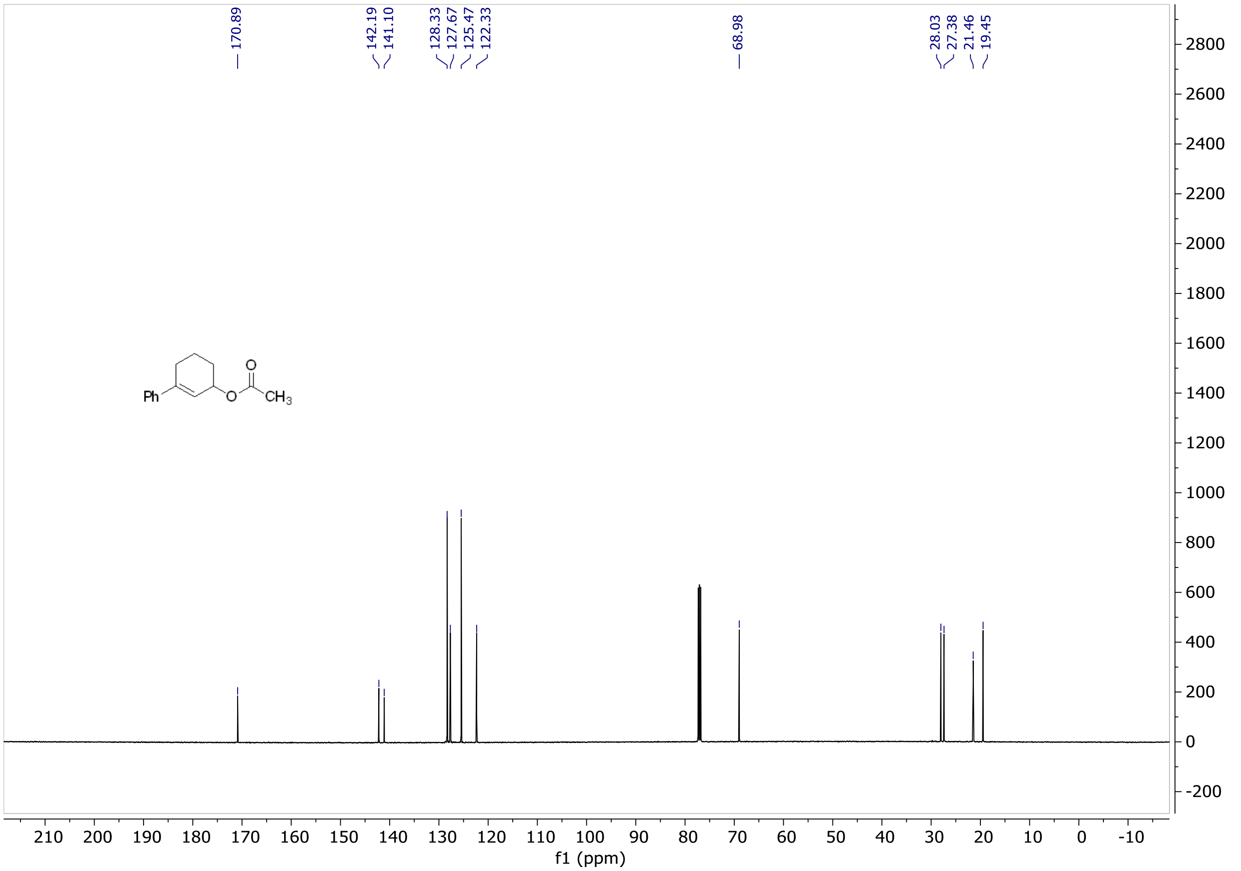
170.89
142.19
141.10
128.33
127.67
125.47
122.33
68.98
28.03
27.38
21.46
19.45
Ph
O
CH3
2800
2600
2400
2200
2000
1800
1600
1400
1200
1000
800
600
400
200
0
-200
210 200 190 180 170 160 150 140 130 120 110 100 90 80 70 60 50 40 30 20 10 0 -10
f1 (ppm)

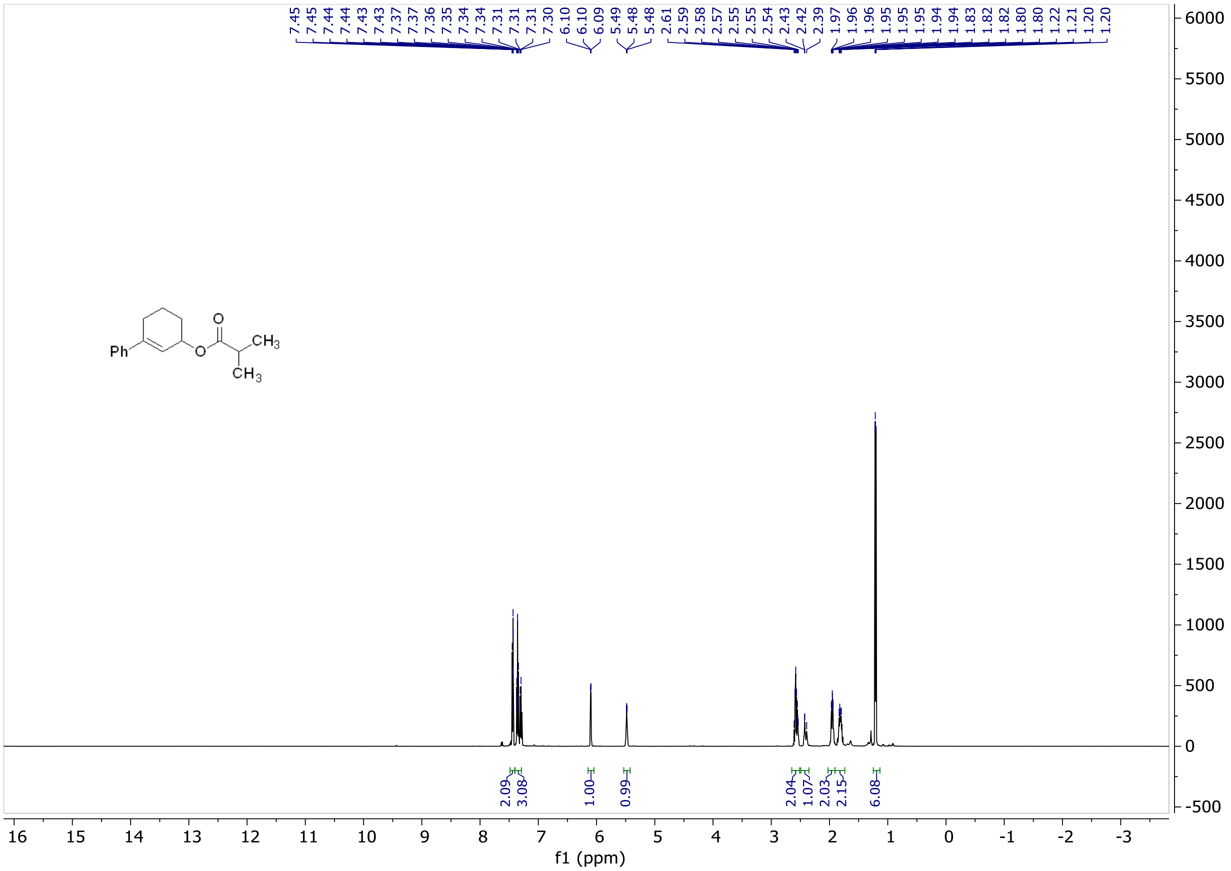
7.45
7.45
7.44
7.43
7.43
7.37
7.37
7.36
7.35
7.34
7.34
7.31
7.31
7.31
7.30
6.10
6.10
6.09
5.49
5.48
5.48
2.61
2.59
2.58
2.57
2.55
2.55
2.54
2.43
2.42
2.39
1.97
1.96
1.96
1.95
1.95
1.95
1.94
1.94
1.83
1.82
1.82
1.80
1.80
1.22
1.21
1.20
1.20
Ph
O
O
CH_3
CH_3
2.09
3.08
1.00
0.99
2.04
1.07
2.03
2.15
6.08
6000
5500
5000
4500
4000
3500
3000
2500
2000
1500
1000
500
0
-500
16
15
14
13
12
11
10
9
8
7
6
5
4
3
2
1
0
-1
-2
-3
f1 (ppm)

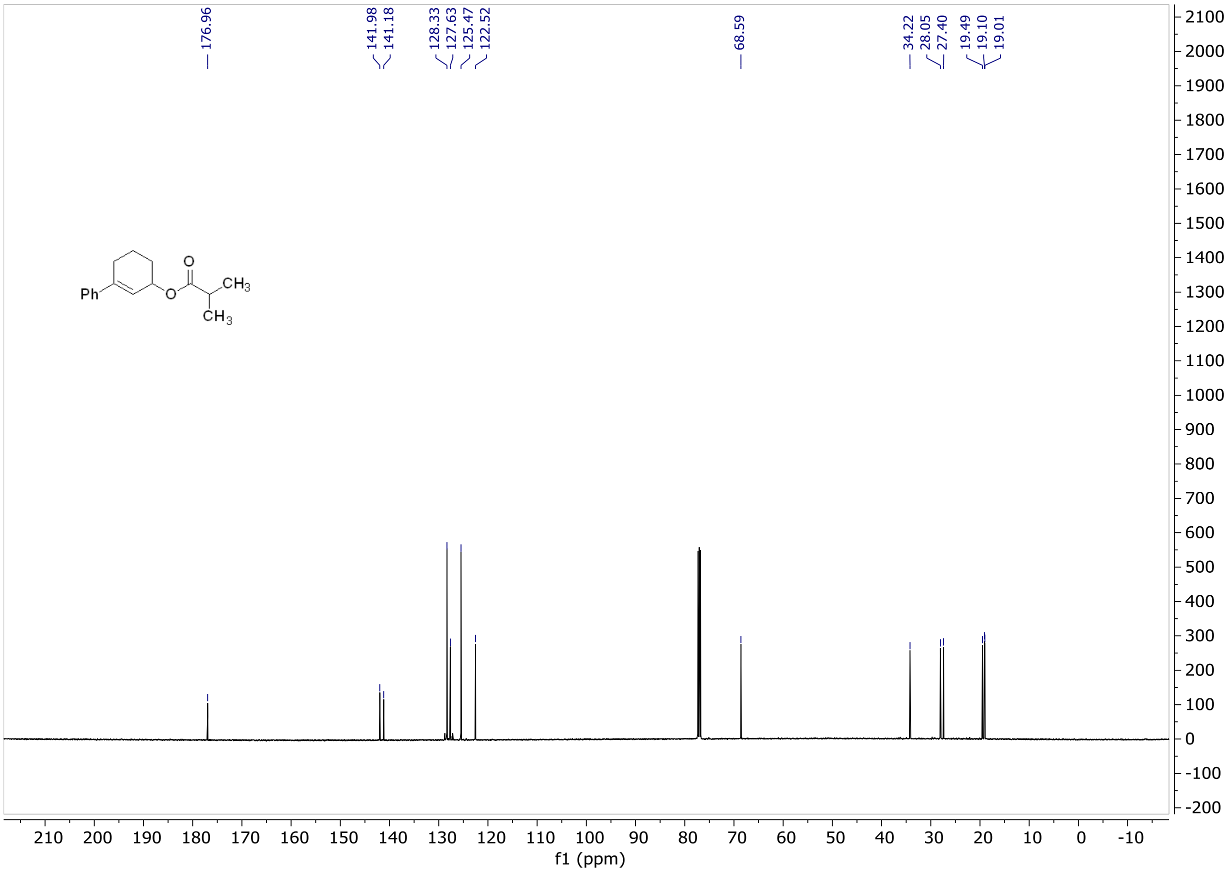
176.96
141.98
141.18
128.33
127.63
125.47
122.52
68.59
34.22
28.05
27.40
19.49
19.10
19.01
Ph
O
O
CH_3
CH_3
2100
2000
1900
1800
1700
1600
1500
1400
1300
1200
1100
1000
900
800
700
600
500
400
300
200
100
0
-100
-200
210
200
190
180
170
160
150
140
130
120
110
100
90
80
70
60
50
40
30
20
10
0
-10
f1 (ppm)

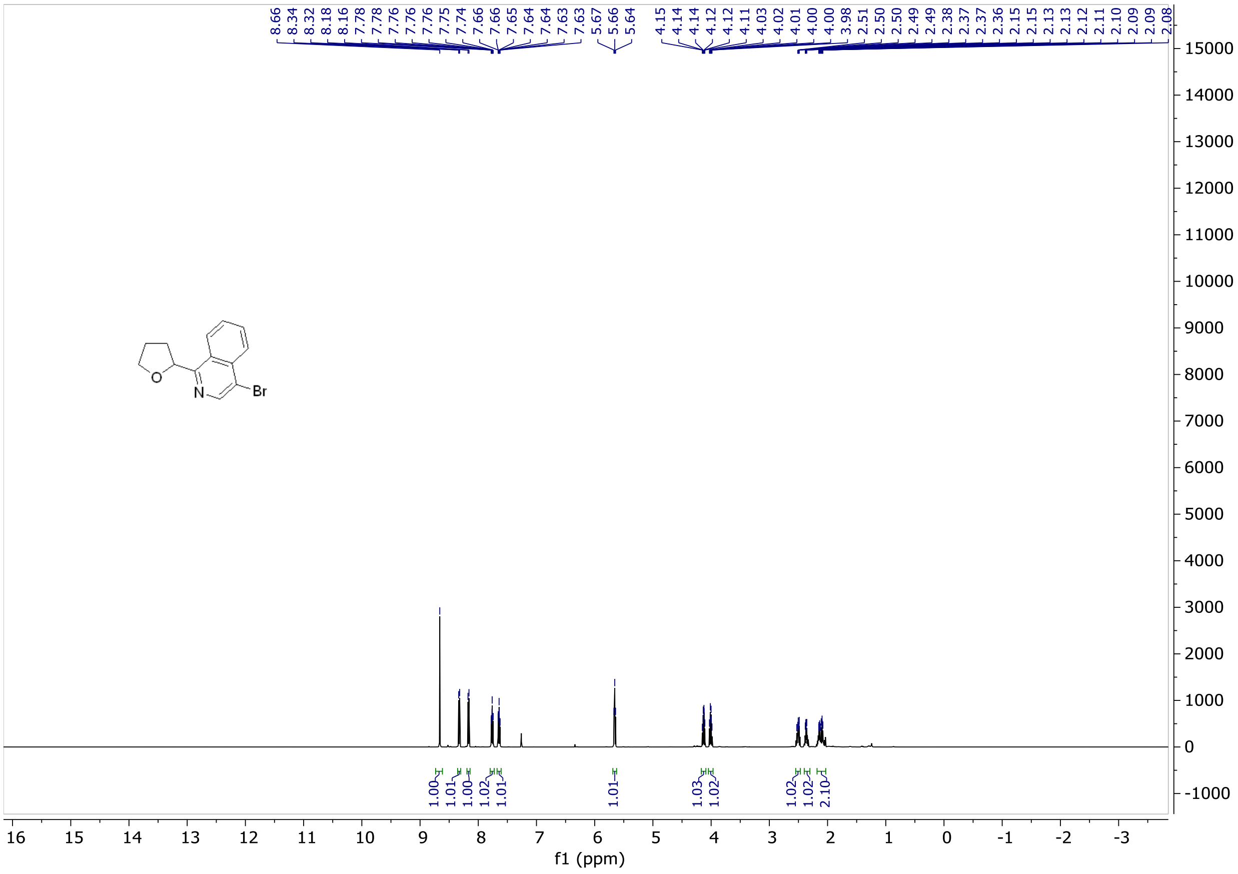
8.66 8.34 8.32 8.18 8.16 7.78 7.78 7.76 7.76 7.75 7.74 7.66 7.66 7.65 7.64 7.64 7.63 7.63 5.67 5.66 5.64 4.15 4.14 4.14 4.12 4.12 4.11 4.03 4.02 4.01 4.00 4.00 3.98 2.51 2.50 2.50 2.49 2.49 2.38 2.37 2.37 2.36 2.15 2.15 2.13 2.12 2.11 2.10 2.09 2.09 2.08
O
N
Br
1.00 1.01 1.00 1.02 1.01 1.01 1.03 1.02 1.02 1.02 2.10
f1 (ppm)

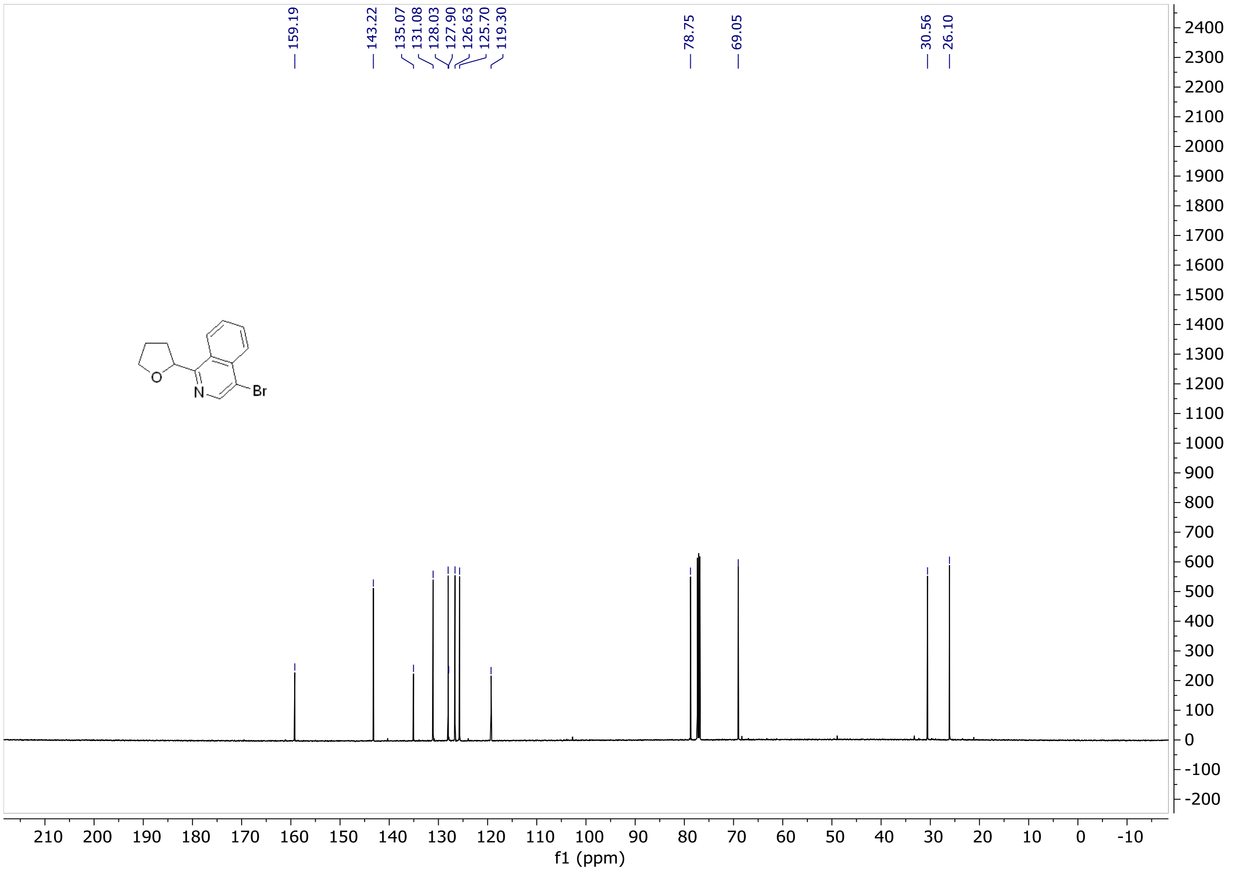
159.19
143.22
135.07 131.08 128.03 127.90 126.63 125.70 119.30
78.75
69.05
30.56
26.10
O
N
Br
f1 (ppm)

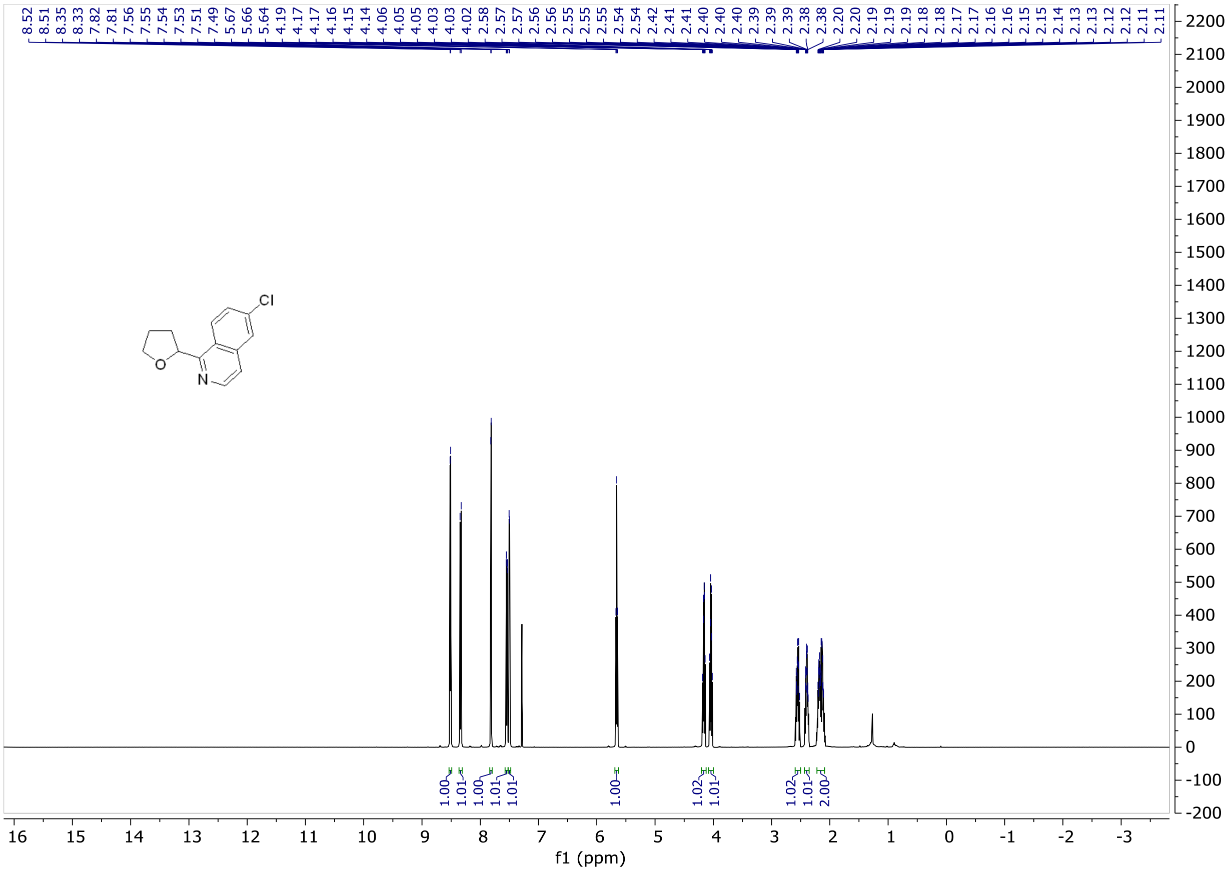
8.52
8.51
8.35
8.33
7.82
7.81
7.56
7.55
7.54
7.53
7.51
7.49
5.67
5.66
5.64
4.19
4.17
4.17
4.16
4.15
4.14
4.06
4.05
4.05
4.03
4.03
4.02
2.58
2.57
2.57
2.56
2.56
2.55
2.55
2.54
2.54
2.42
2.41
2.41
2.40
2.40
2.40
2.39
2.39
2.38
2.38
2.20
2.20
2.19
2.19
2.19
2.18
2.18
2.17
2.17
2.16
2.16
2.15
2.14
2.13
2.13
2.12
2.12
2.11
2.11
Cl
O
N
1.00
1.01
1.00
1.01
1.01
1.00
1.02
1.01
1.02
1.01
2.00
16
15
14
13
12
11
10
9
8
7
6
5
4
3
2
1
0
-1
-2
-3
f1 (ppm)
2200
2100
2000
1900
1800
1700
1600
1500
1400
1300
1200
1100
1000
900
800
700
600
500
400
300
200
100
0
-100
-200

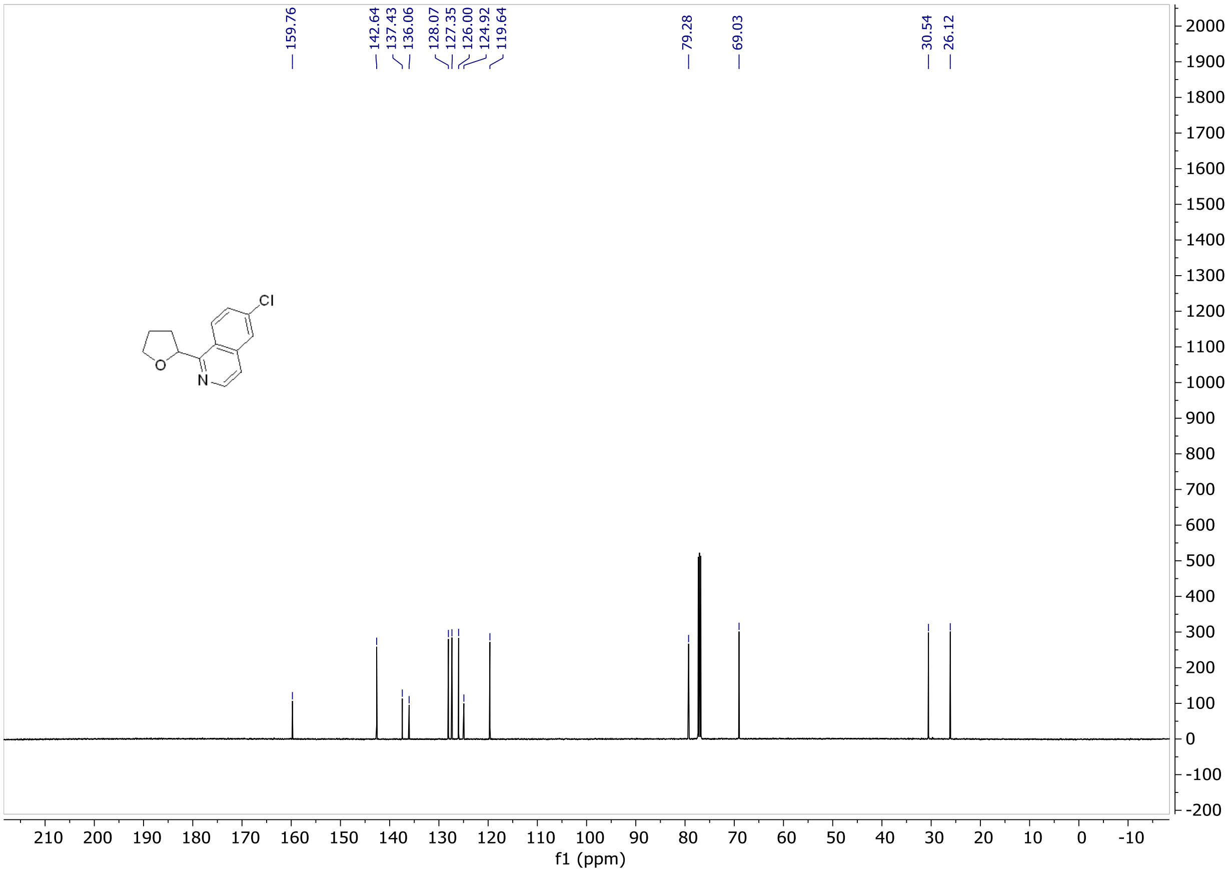
159.76
142.64
137.43
136.06
128.07
127.35
126.00
124.92
119.64
79.28
69.03
30.54
26.12
Cl
O
N
210
200
190
180
170
160
150
140
130
120
110
100
90
80
70
60
50
40
30
20
10
0
-10
f1 (ppm)
2000
1900
1800
1700
1600
1500
1400
1300
1200
1100
1000
900
800
700
600
500
400
300
200
100
0
-100
-200

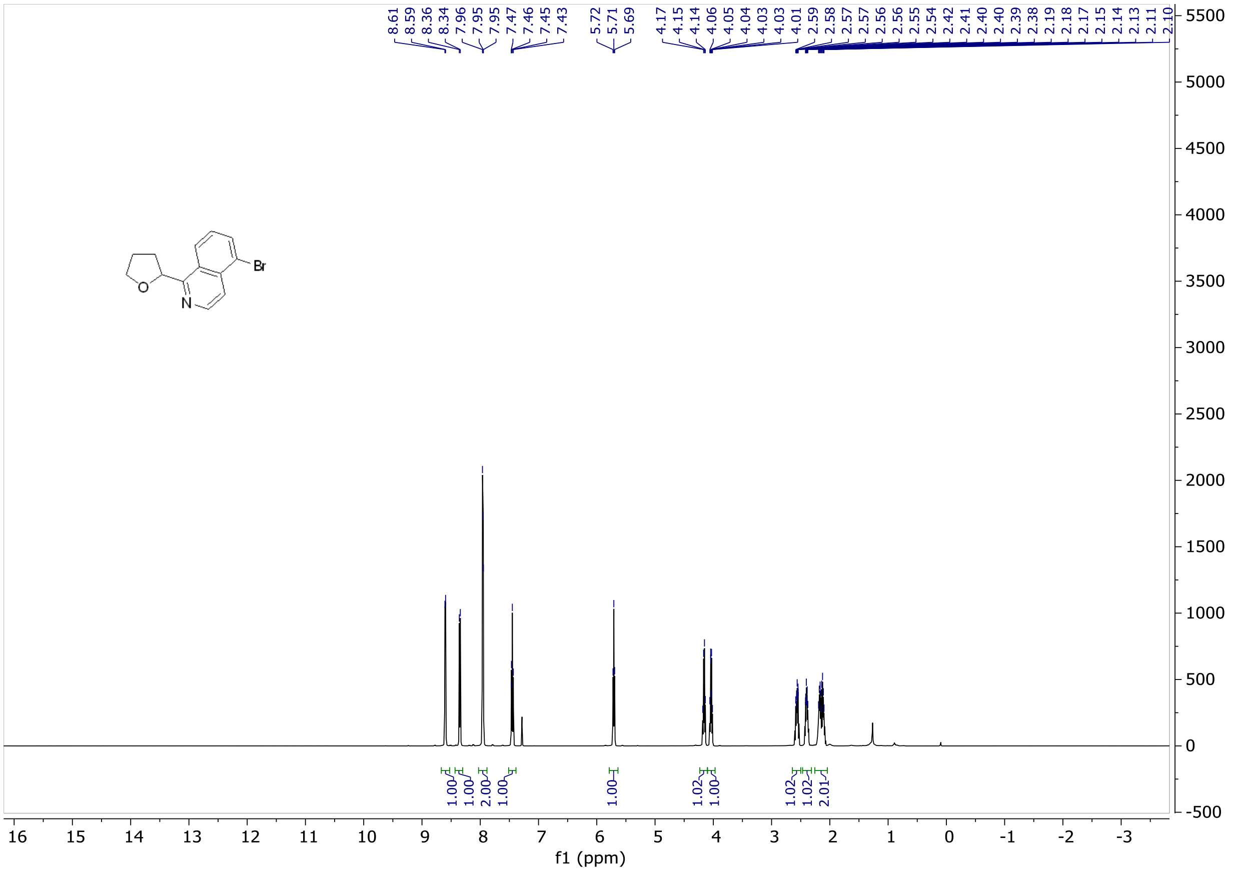
8.61
8.59
8.36
8.34
7.96
7.95
7.95
7.47
7.46
7.45
7.43
5.72
5.71
5.69
4.17
4.15
4.14
4.06
4.05
4.04
4.03
4.03
4.01
2.59
2.58
2.57
2.57
2.56
2.56
2.55
2.54
2.42
2.41
2.40
2.40
2.39
2.38
2.19
2.18
2.17
2.15
2.14
2.13
2.11
2.10
Br
O
N
1.00
1.00
2.00
1.00
1.00
1.02
1.00
1.02
1.02
2.01
16 15 14 13 12 11 10 9 8 7 6 5 4 3 2 1 0 -1 -2 -3
f1 (ppm)
5500 5000 4500 4000 3500 3000 2500 2000 1500 1000 500 0 -500

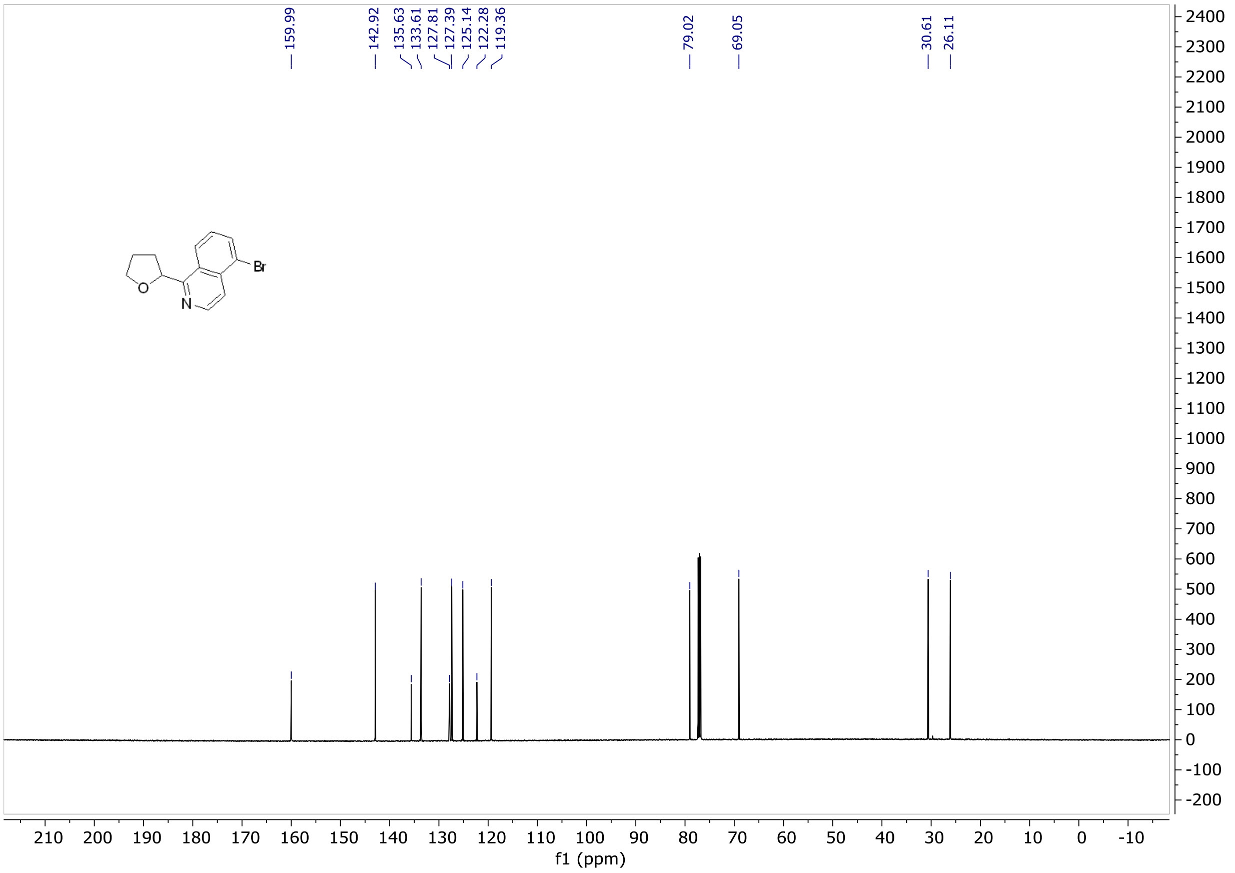
159.99
142.92
135.63
133.61
127.81
127.39
125.14
122.28
119.36
79.02
69.05
30.61
26.11
Br
O
N
210 200 190 180 170 160 150 140 130 120 110 100 90 80 70 60 50 40 30 20 10 0 -10
f1 (ppm)
2400 2300 2200 2100 2000 1900 1800 1700 1600 1500 1400 1300 1200 1100 1000 900 800 700 600 500 400 300 200 100 0 -100 -200

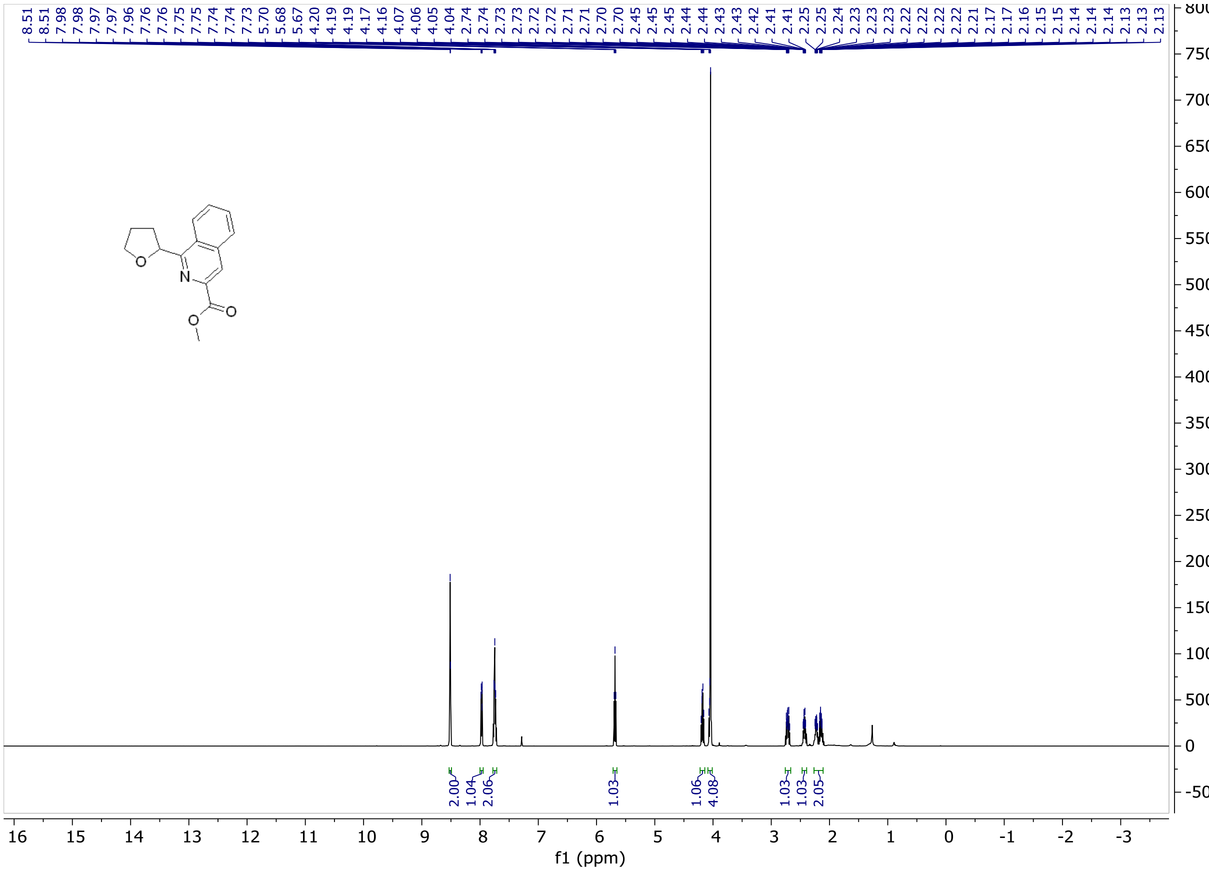
8.51
8.51
7.98
7.98
7.97
7.97
7.96
7.76
7.76
7.75
7.75
7.74
7.74
7.73
5.70
5.68
5.67
4.20
4.19
4.19
4.17
4.16
4.07
4.06
4.05
4.04
2.74
2.74
2.73
2.73
2.72
2.72
2.71
2.71
2.70
2.45
2.45
2.45
2.44
2.44
2.43
2.43
2.42
2.41
2.41
2.25
2.25
2.25
2.24
2.23
2.23
2.23
2.22
2.22
2.22
2.22
2.21
2.17
2.17
2.16
2.15
2.15
2.14
2.14
2.13
2.13
2.13
O
N
O
O
2.00
1.04
2.06
1.03
1.06
4.08
1.03
1.03
2.05
16 15 14 13 12 11 10 9 8 7 6 5 4 3 2 1 0 -1 -2 -3
f1 (ppm)
8000 7500 7000 6500 6000 5500 5000 4500 4000 3500 3000 2500 2000 1500 1000 500 0 -500

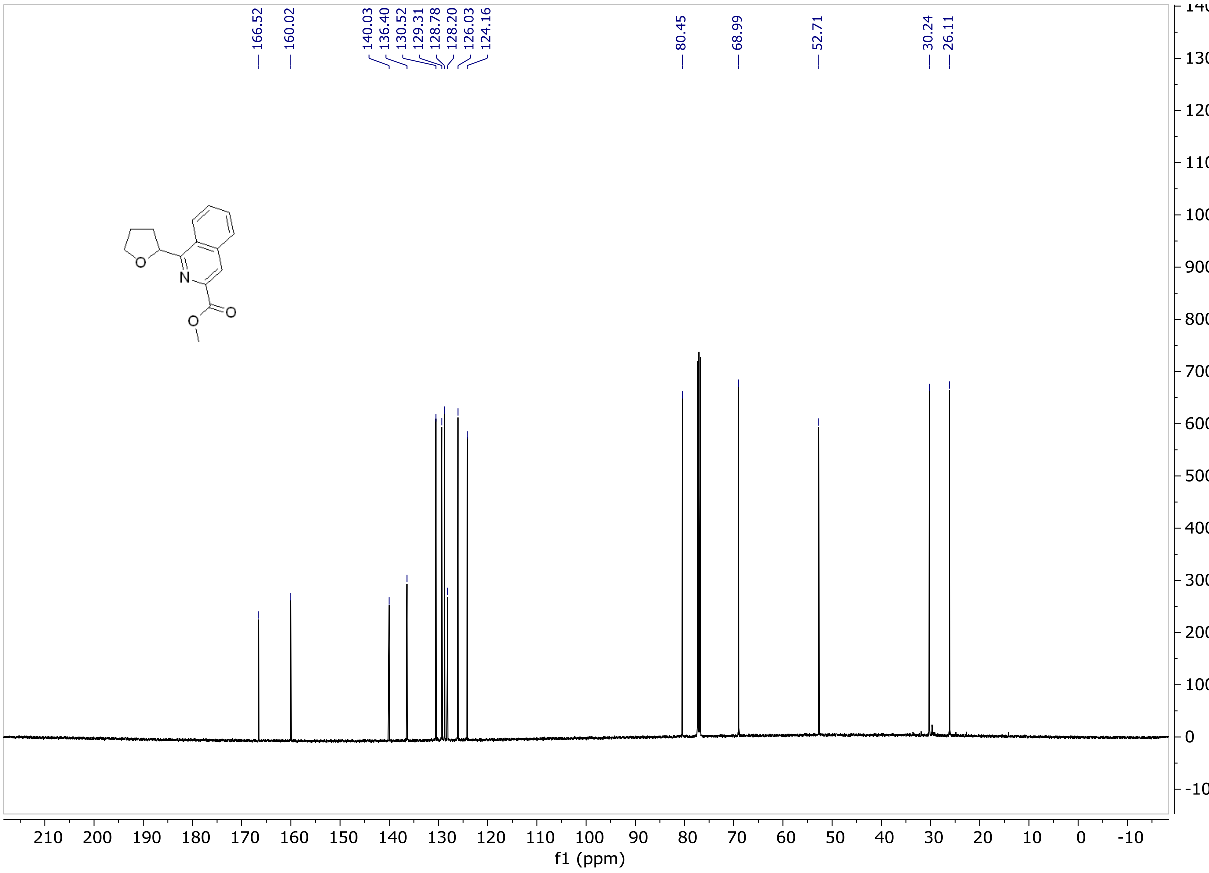
166.52
160.02
140.03
136.40
130.52
129.31
128.78
128.20
126.03
124.16
80.45
68.99
52.71
30.24
26.11
O
N
O
O
210 200 190 180 170 160 150 140 130 120 110 100 90 80 70 60 50 40 30 20 10 0 -10
f1 (ppm)
1400 1300 1200 1100 1000 900 800 700 600 500 400 300 200 100 0 -100

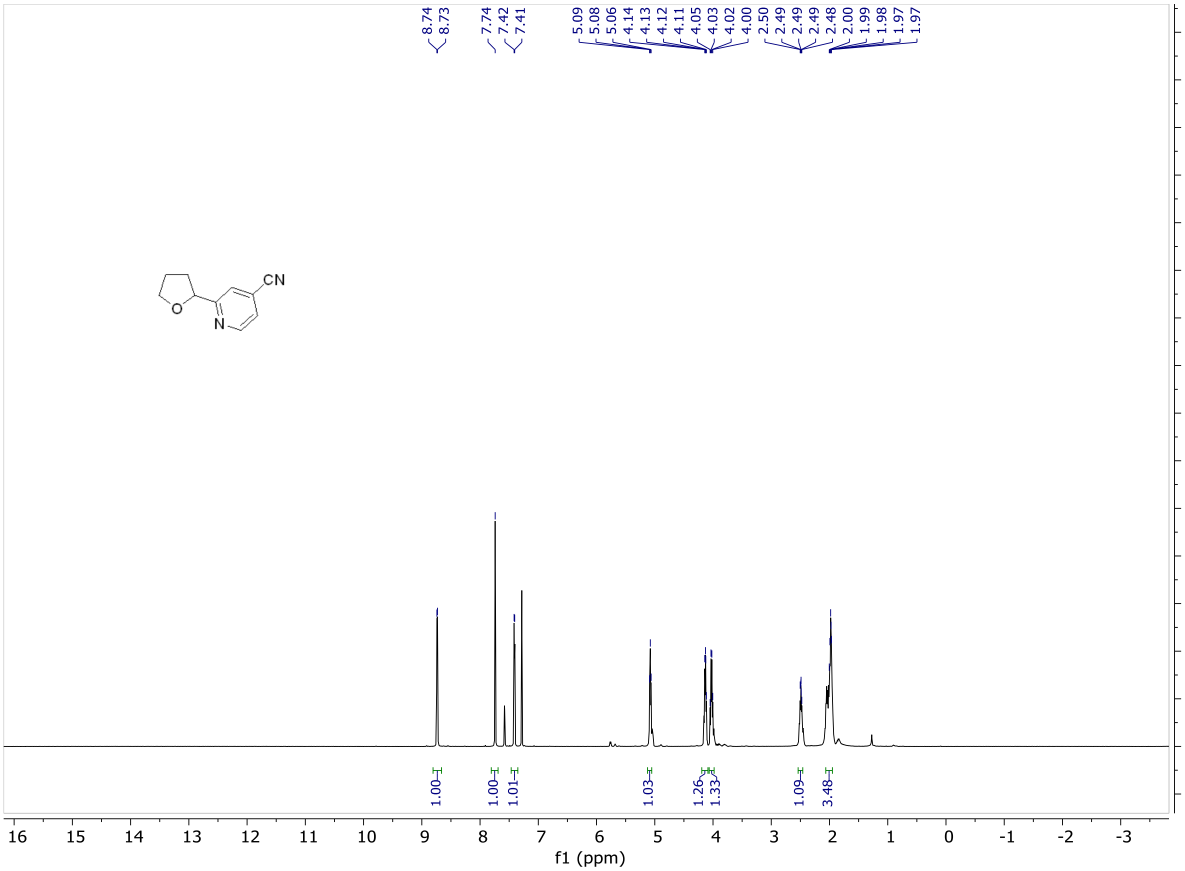
8.74
8.73
7.74
7.42
7.41
5.09
5.08
5.06
4.14
4.13
4.12
4.11
4.05
4.03
4.02
4.00
2.50
2.49
2.49
2.48
2.00
1.99
1.98
1.97
1.97
CN
O
N
1.00
1.00
1.01
1.03
1.26
1.33
1.09
3.48
16 15 14 13 12 11 10 9 8 7 6 5 4 3 2 1 0 -1 -2 -3
f1 (ppm)
1500 1400 1300 1200 1100 1000 900 800 700 600 500 400 300 200 100 0 -100

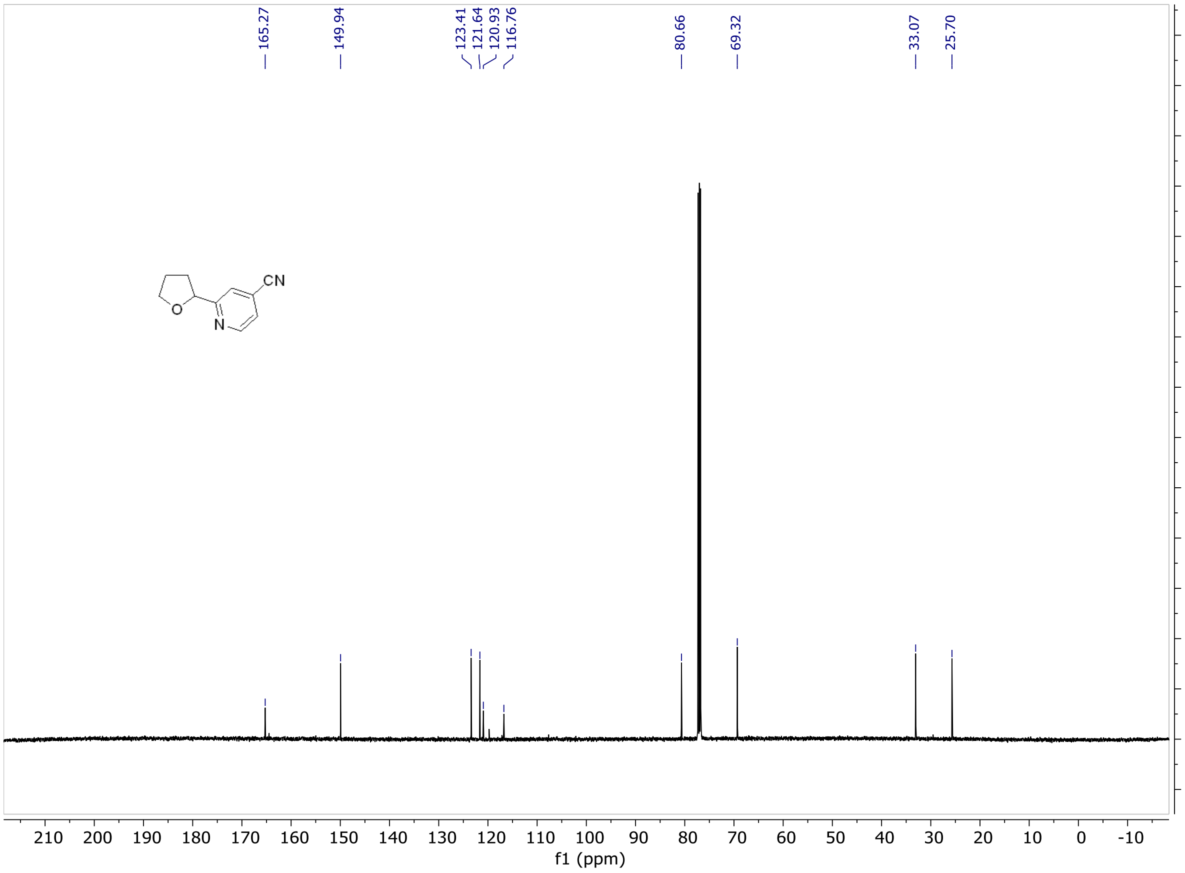
165.27
149.94
123.41
121.64
120.93
116.76
80.66
69.32
33.07
25.70
CN
O
N
210 200 190 180 170 160 150 140 130 120 110 100 90 80 70 60 50 40 30 20 10 0 -10
f1 (ppm)
700 650 600 550 500 450 400 350 300 250 200 150 100 50 0 -50

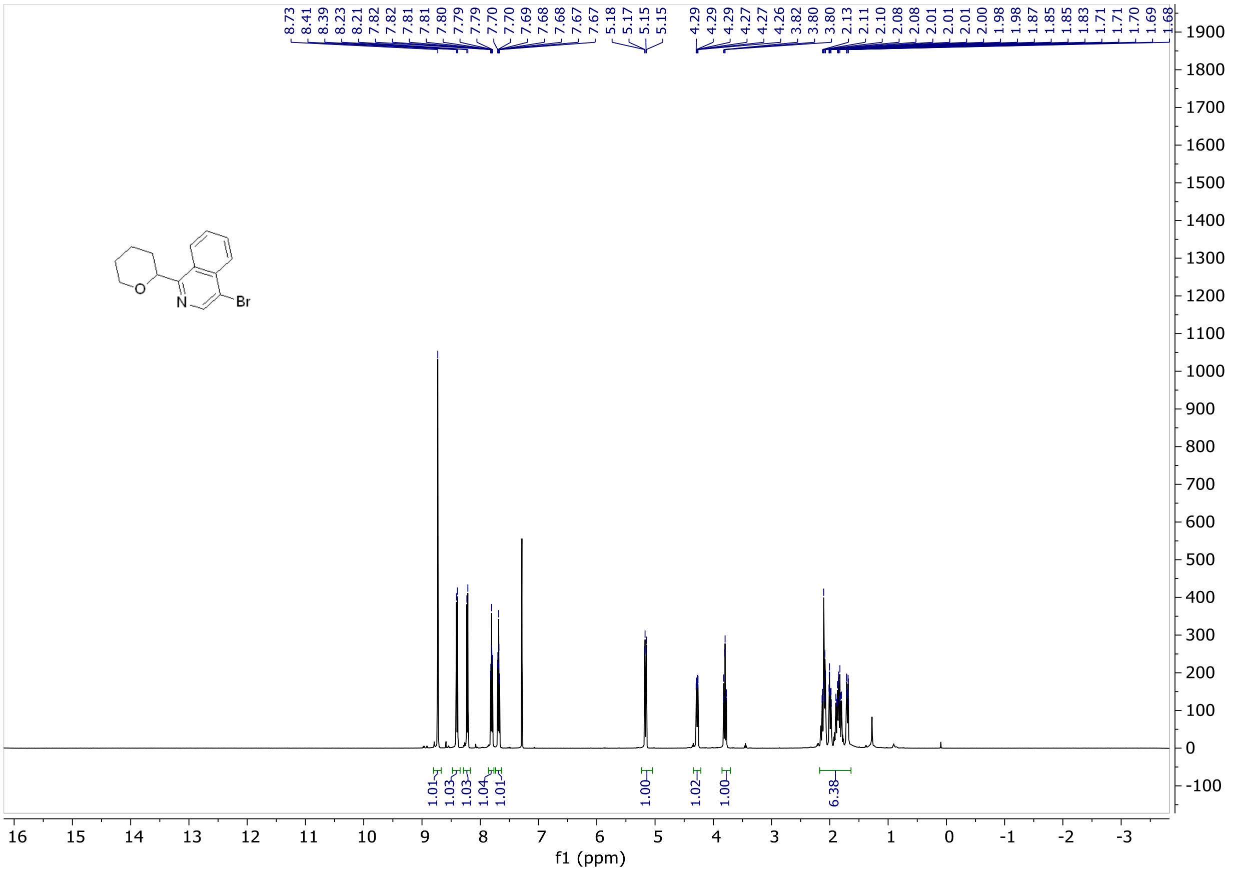
8.73
8.41
8.39
8.23
8.21
7.82
7.82
7.81
7.81
7.80
7.79
7.79
7.70
7.70
7.69
7.68
7.68
7.67
7.67
5.18
5.17
5.15
5.15
4.29
4.29
4.29
4.27
4.27
4.26
3.82
3.80
3.80
2.13
2.11
2.10
2.08
2.08
2.01
2.01
2.01
2.00
1.98
1.98
1.87
1.85
1.85
1.83
1.71
1.71
1.70
1.69
1.68
O
N
Br
1.01
1.03
1.03
1.04
1.01
1.00
1.02
1.00
6.38
16 15 14 13 12 11 10 9 8 7 6 5 4 3 2 1 0 -1 -2 -3
f1 (ppm)
1900 1800 1700 1600 1500 1400 1300 1200 1100 1000 900 800 700 600 500 400 300 200 100 0 -100

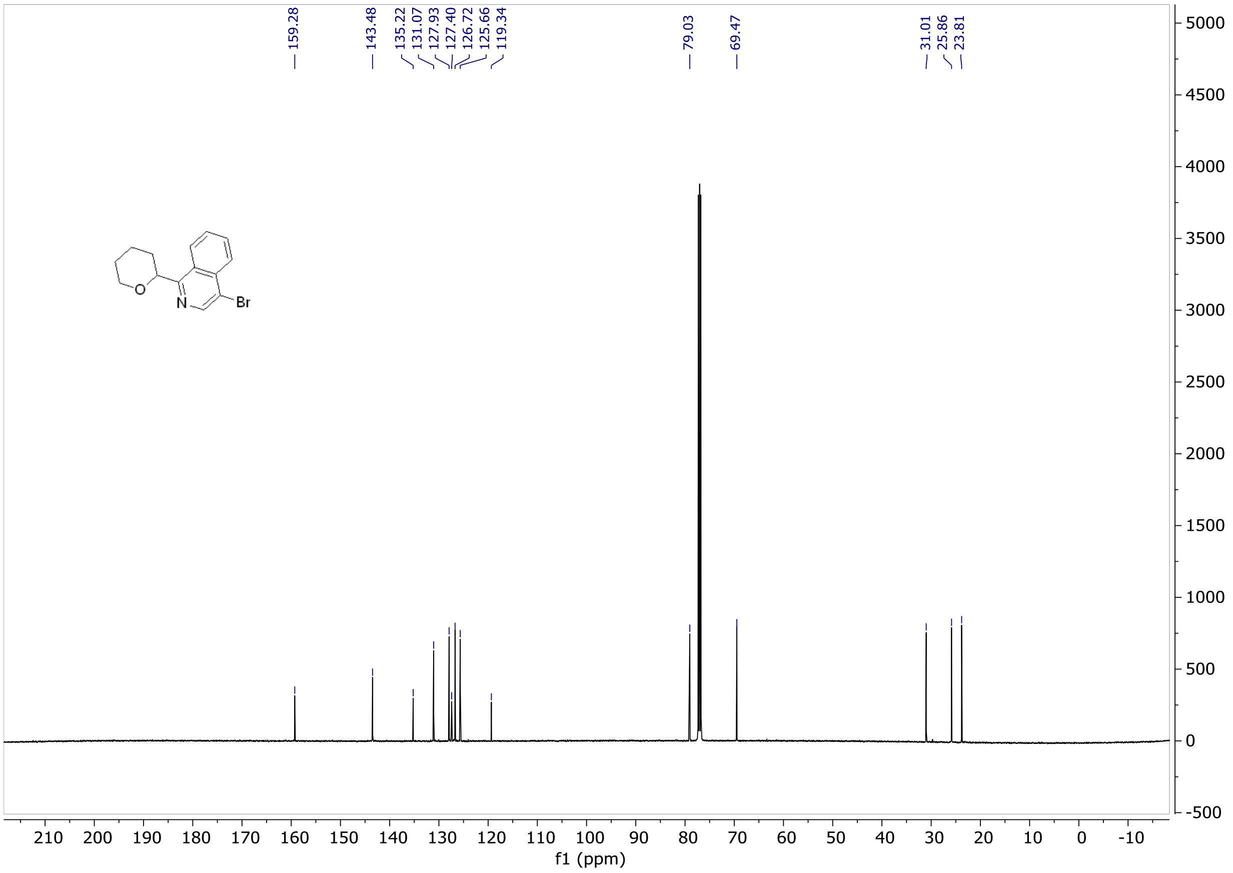
159.28
143.48
135.22
131.07
127.93
127.40
126.72
125.66
119.34
79.03
69.47
31.01
25.86
23.81
O
N
Br
210 200 190 180 170 160 150 140 130 120 110 100 90 80 70 60 50 40 30 20 10 0 -10
f1 (ppm)
5000 4500 4000 3500 3000 2500 2000 1500 1000 500 0 -500

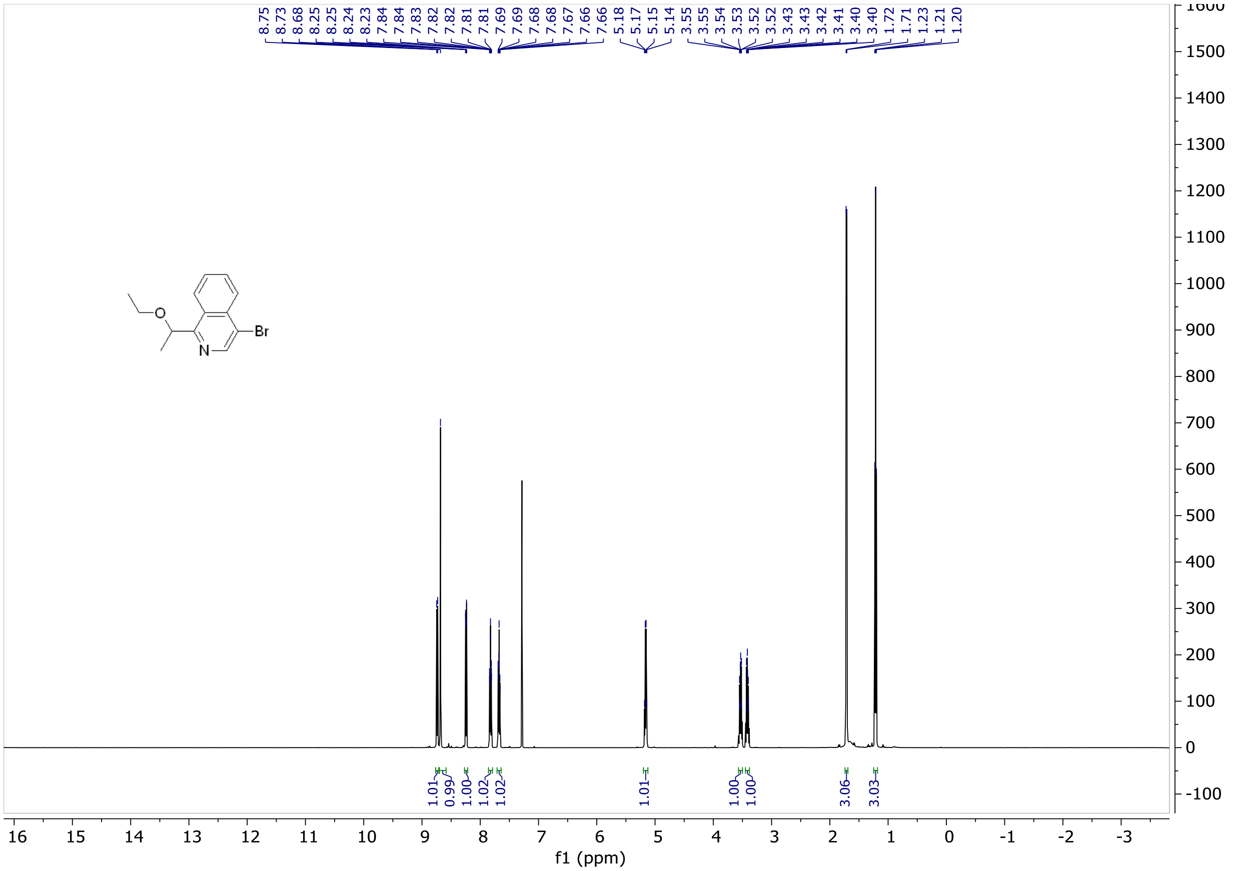

8.75 8.73 8.68 8.25 8.25 8.24 8.23 7.84 7.84 7.83 7.82 7.82 7.81 7.81 7.69 7.69 7.68 7.68 7.67 7.66 7.66 5.18 5.17 5.15 5.14 3.55 3.55 3.54 3.53 3.52 3.52 3.43 3.43 3.42 3.41 3.40 3.40 1.72 1.71 1.23 1.21 1.20
O
N
Br
1.01
0.99
1.00
1.02
1.02
1.01
1.00
1.00
3.06
3.03
16 15 14 13 12 11 10 9 8 7 6 5 4 3 2 1 0 -1 -2 -3
f1 (ppm)
1600 1500 1400 1300 1200 1100 1000 900 800 700 600 500 400 300 200 100 0 -100

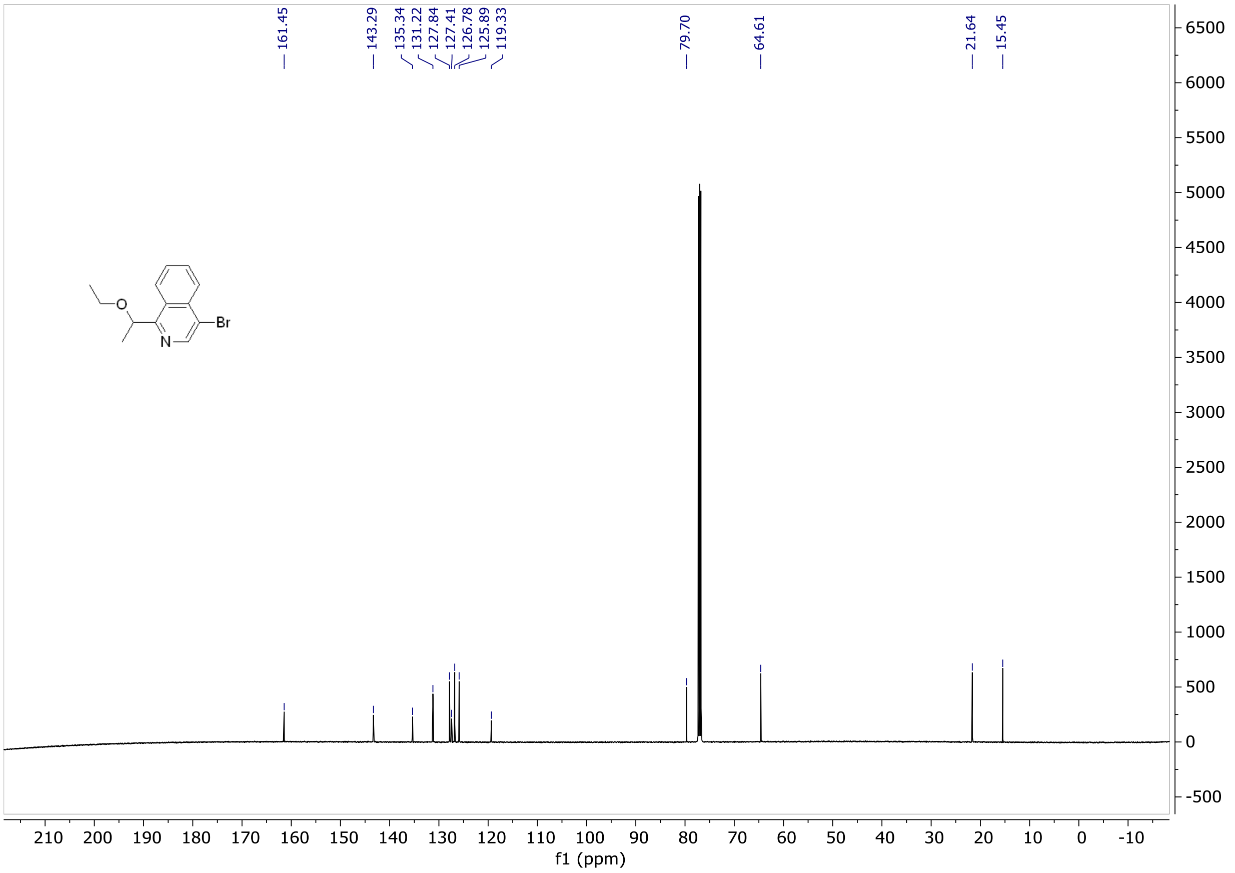

161.45
143.29
135.34 131.22 127.84 127.41 126.78 125.89 119.33
79.70
64.61
21.64
15.45
O
N
Br
210 200 190 180 170 160 150 140 130 120 110 100 90 80 70 60 50 40 30 20 10 0 -10
f1 (ppm)
6500 6000 5500 5000 4500 4000 3500 3000 2500 2000 1500 1000 500 0 -500

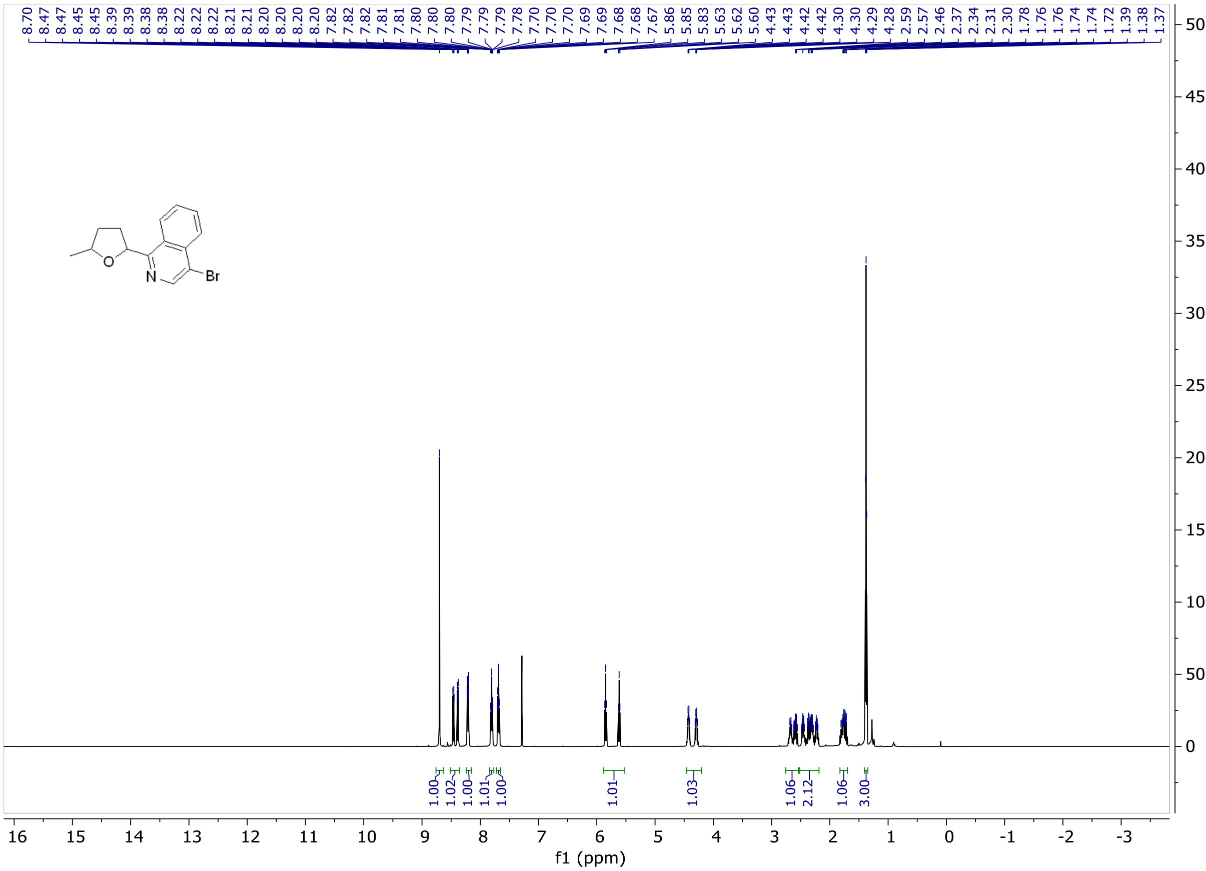
8.70
8.47
8.47
8.45
8.45
8.39
8.39
8.38
8.38
8.22
8.22
8.22
8.21
8.21
8.20
8.20
8.20
8.20
7.82
7.82
7.82
7.81
7.81
7.80
7.80
7.80
7.79
7.79
7.79
7.78
7.70
7.70
7.70
7.69
7.69
7.68
7.68
7.67
5.86
5.85
5.83
5.63
5.62
5.60
4.43
4.43
4.42
4.42
4.30
4.30
4.29
4.28
2.59
2.57
2.46
2.37
2.34
2.31
2.30
1.78
1.76
1.76
1.74
1.74
1.72
1.39
1.38
1.37
O
N
Br
1.00
1.02
1.00
1.01
1.00
1.01
1.03
1.06
2.12
1.06
3.00
16
15
14
13
12
11
10
9
8
7
6
5
4
3
2
1
0
-1
-2
-3
f1 (ppm)
5000
4500
4000
3500
3000
2500
2000
1500
1000
500
0

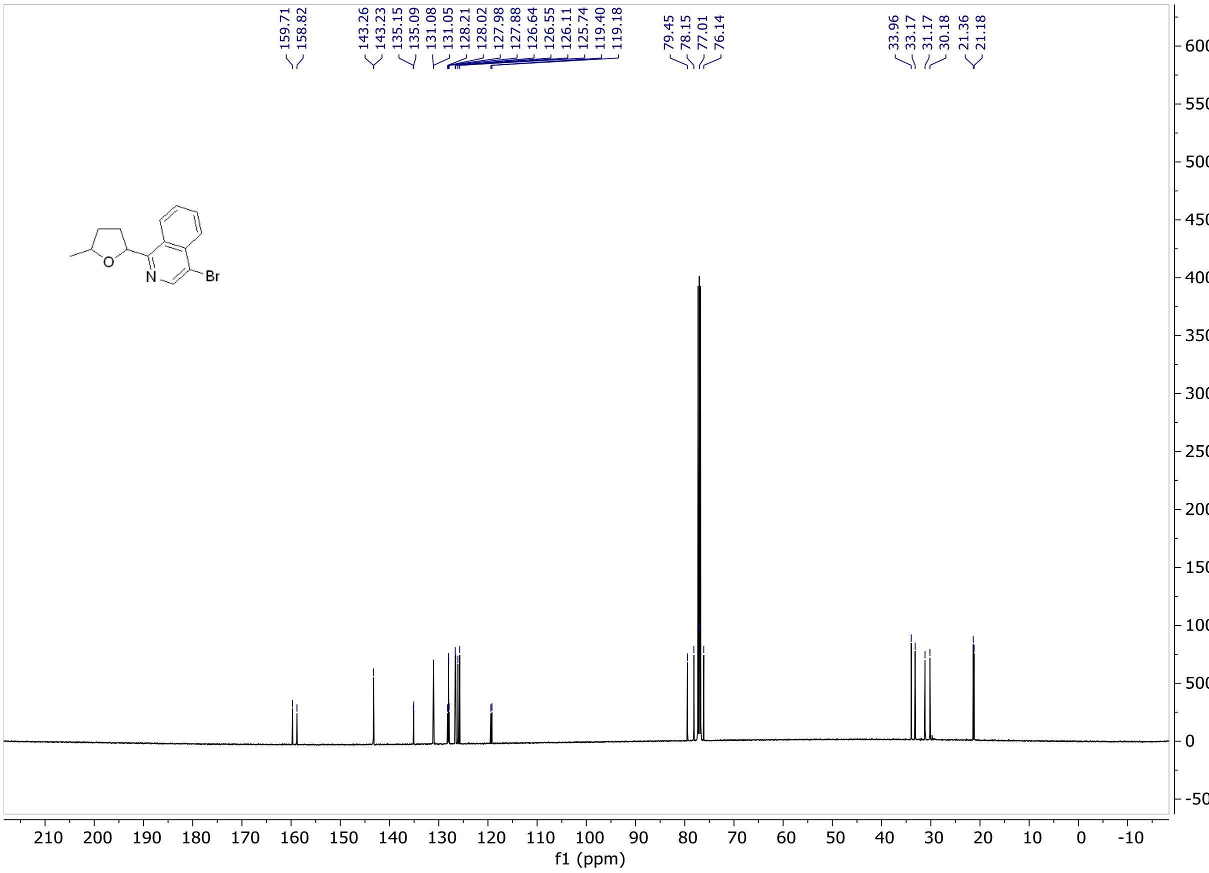
159.71
158.82
143.26
143.23
135.15
135.09
131.08
131.05
128.21
128.02
127.98
127.88
126.64
126.55
126.11
125.74
119.40
119.18
79.45
78.15
77.01
76.14
33.96
33.17
31.17
30.18
21.36
21.18
O
N
Br
210
200
190
180
170
160
150
140
130
120
110
100
90
80
70
60
50
40
30
20
10
0
-10
f1 (ppm)
6000
5500
5000
4500
4000
3500
3000
2500
2000
1500
1000
500
0
-500

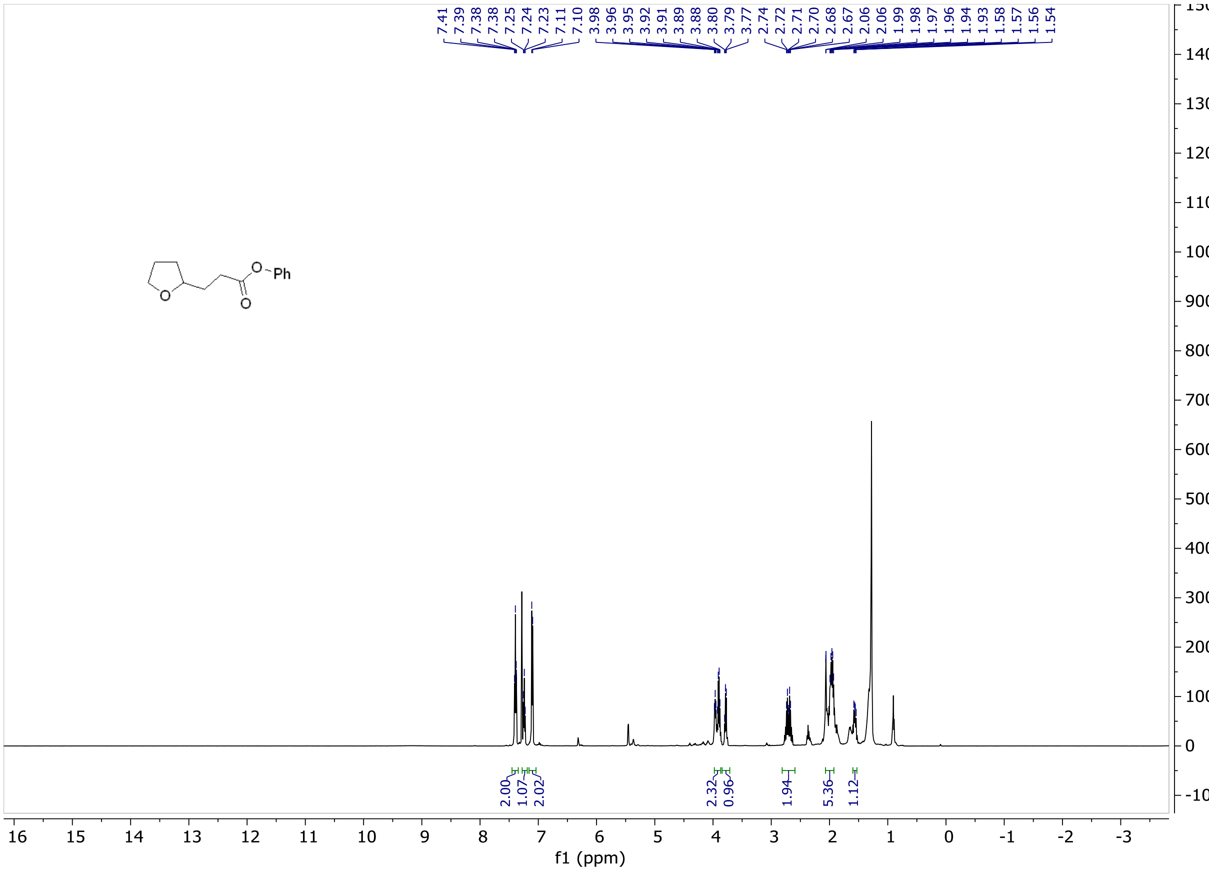
7.41
7.39
7.38
7.38
7.25
7.24
7.23
7.11
7.10
3.98
3.96
3.95
3.92
3.91
3.89
3.88
3.80
3.79
3.77
2.74
2.72
2.71
2.70
2.68
2.67
2.06
2.06
1.99
1.98
1.97
1.96
1.94
1.93
1.58
1.57
1.56
1.54
O
O
O
Ph
2.00
1.07
2.02
2.32
0.96
1.94
5.36
1.12
1500
1400
1300
1200
1100
1000
900
800
700
600
500
400
300
200
100
0
-100
16
15
14
13
12
11
10
9
8
7
6
5
4
3
2
1
0
-1
-2
-3
f1 (ppm)

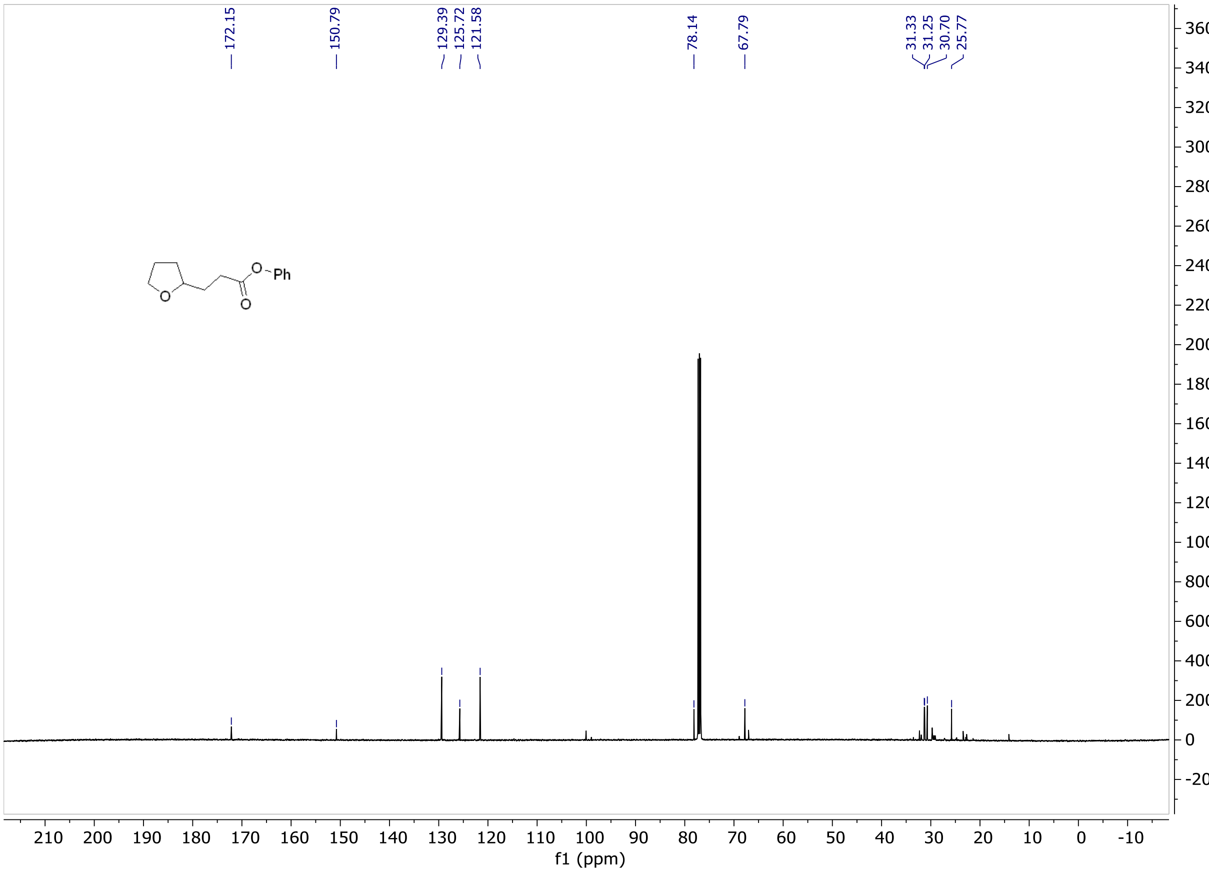
172.15
150.79
129.39
125.72
121.58
78.14
67.79
31.33
31.25
30.70
25.77
O
O
O
Ph
3600
3400
3200
3000
2800
2600
2400
2200
2000
1800
1600
1400
1200
1000
800
600
400
200
0
-200
210
200
190
180
170
160
150
140
130
120
110
100
90
80
70
60
50
40
30
20
10
0
-10
f1 (ppm)